GENERALIZED NON-COHERENT DETECTION

By

Dimitrios Makrakis

A THESIS
SUBMITTED TO THE SCHOOL OF
GRADUATE STUDIES AND RESEARCH
IN PARTIAL FULFILLMENT OF THE REQUIREMENTS
FOR THE DEGREE OF
DOCTOR IN PHILOSOPHY

OTTAWA-CARLETON INSTITUTE FOR ELECTRICAL
ENGINEERING

DEPARTMENT OF ELECTRICAL ENGINEERING
FACULTY OF ENGINEERING
UNIVERSITY OF OTTAWA

National Library
of Canada

Acquisitions and
Bibliographic Services Branch

395 Wellington Street
Ottawa, Ontario
K1A 0N4

Bibliothèque nationale
du Canada

Direction des acquisitions et
des services bibliographiques

395, rue Wellington
Ottawa (Ontario)
K1A 0N4

Your file Votre référence

Our file Notre référence

ISBN 0-612-15647-8

Canada

UNIVERSITÉ D'OTTAWA
UNIVERSITY OF OTTAWA

To

my wife Maria

and

my parents Zoe and Ioannis

your support, love and understanding

are my strength and motivation

ABSTRACT

The objective of this thesis is to introduce new power efficient non-coherent receiver structures for linear (Quadrature Amplitude Modulated and Phase Shift Keyed) as well as Continuous Phase Modulated signals.

A generalized non-coherent detection theory, addressing single or multi-amplitude/phase signals as well as operation in time dispersive channels has been developed. Structures of optimal non-coherent sequence estimators and symbol-by-symbol receivers are proposed. The analysis carried out provides the relation and link between existing non-coherent receivers and the optimal non-coherent detection concept.

Using the framework set by the generalized non-coherent detection theory and applying approximations and reasonable simplifications wherever needed, we were able to propose new families of powerful, yet simple non-coherent receivers. Such receivers are the:

1. *Block Decoders for PSK and CPM signals.* They process the received signal information in a block form. Evaluation of them in both ideal and time dispersive channels has verified considerable gains (as compared to conventional differential receivers), especially when used with trellis coded schemes. The evaluation results have indicated improvements higher than 3 dB when the operation takes place in a Gaussian channel. In a faded channel, the results have shown improvements higher than 7 dB and a reduction in error floors close to one order of magnitude.

2. *Asymptotically optimal decoders for a time dispersive channel and/or multi-amplitude/phase signals.* They have been able to considerably improve the system's performance. When evaluated for uncoded and coded schemes they demonstrated excellent performance. Compared to the conventional differential receiver the results demonstrated improvements in excess of 5 dB. With the introduction of these receivers the extension of non-coherent technology to the power and bandwidth efficient family of the multi-amplitude/phase signals has been made possible.

3. *Combined Squared Envelope and Multiple Differential Detection (recursive) Algorithms.* They process the information provided by the use of a

squared envelope and more than one (multiple) differential receivers in a recursive form. When evaluated with various linear and CPM signals they demonstrated considerable improvements. For white Gaussian noise channels, they achieved gains higher than 9 dB (compared to the conventional differential receiver). In a faded channel they were able to reduce the error floors by more than three orders of magnitude.

4. *Symbol-by-symbol receivers based on phase correction and signal combining controlled by decision feedback.* These receivers achieve their improvements by applying partial (decision directed) intersymbol interference (ISI) cancellation from the phase of the signal and by combining the outputs of more than one differential detector according to the decisions made regarding previous symbols. Evaluations have demonstrated improvements higher than 5 dB.

In all of the above proposed receivers, a particular emphasis has been put on the simplicity factor. Possible efficient implementation scenarios of the receivers using today's digital signal processing technology are discussed in various parts of the present work.

To evaluate the proposed schemes, an analytical framework has been developed. It covers evaluation in AWGN (ideal or time dispersive) as well as faded channels. Through this analysis, new distance expressions (equivalent to the Euclidean distance we encounter in coherent systems) which characterize the performance of the proposed non-coherent receivers have been identified. These distance metrics can be used for the design of improved coded schemes, developed to "match" the characteristics and operation principles of the proposed non-coherent receivers.

ACKNOWLEDGEMENTS

I would like to extend my deepest gratitude to my supervisor, Dr. Kamilo Feher, for trusting my research abilities and allowing me to define and pursue the research objectives of this work. I thank him for his assistance and the financial support he provided me in the initial years of my Ph. D. studies. Furthermore, I would like to thank him for showing me the importance of practicality as an accompaniment to solving analytical problems and for insisting that I include both components in my work.

Through my involvement with the Digital Communications Research Group at the University of Ottawa, I was fortunate to work with Dr. P. T. Mathiopoulos, Dr. K. T. Wu, Dr. J. S. Seo, Dr. I. Sasase, Mr. H. Ohnishi, Dr. D. Hatzinakos, Mr. Y. Tunca, Dr. A. Kucar and Mr. D. Prendergast. I will always have fond memories of our research discussions and our times together.

Dr. P. T. Mathiopoulos of UBC, Dr. K. T. Wu of BNR, J. S. Seo of IDC and Dr. A. Kucar of 4U Communications, were instrumental in critically reading parts of the draft manuscript and made valuable suggestions which improved the presentation of this work. I express a special thanks to Dr. P. T. Mathiopoulos for his assistance in the development and presentation of several sections in the Introductory chapter.

The excellent collaboration I had and continue to have with Dr. P. T. Mathiopoulos and Mr. D. Bouras of the University of British Columbia and Mr. Y. Tunca, formerly with the University of Ottawa, on topics extending from the core of this material is acknowledged sincerely. This collaboration provided me with the rare opportunity to see ideas and concepts developed through this work being transformed from expressions and algorithms on paper to modem prototypes and VLSI chips.

I would like to also express my appreciation to Dr. Vasilios Makios of the University of Patras, Greece and Dr. A. Kontaratos of the Onaseion Heart Institute, Greece. Both professors introduced me to the magic of *transforming ideas and concepts to reality.*

Thanks must also go to the members of my thesis defence committee, Dr. R. Goulet of Sherbrooke University, Dr. W. Steenaart of University of Ottawa, Dr. M. El-Tanany of Carleton University and Dr. A. Sheikh

of Carleton University for the time and effort spent on reading this paper. Their valuable comments helped to improve considerably the presentation of this work.

My wife Maria Ioannou-Makrakis was my vital source of encouragement through this long process. The great support, patience and understanding she showed me during my deep involvement in this work was most valuable. Maria and her family were always ready to assist me in whatever way possible and contribute to my determination. I deeply thank my father Ioannis Makrakis, for being an ideal example of honesty, diligence and devotion. I thank my grandmother Antonia Roussou and my brother Michael for their support and encouragement. My mother Zoe Roussou-Makrakis spent endless hours with me during my early years, shaping me and ensuring that I stay committed to my studies. There is no doubt in my mind that a considerable part of what I have accomplished in this field is the result of the endless support of my parents.

PREFACE

Some of the publications and submissions for publication produced by the work reported in this thesis are the following:

REFEREED PAPERS IN JOURNALS

R-1 D. Makrakis et. al., "Novel Receiver Structures for Systems Using Differential Detection", IEEE Trans. on Vehicular Tech., Vol. VT-36, pp. 71-77, May 1987.

R-2 A. Yongacoglu, D. Makrakis et. al., "Differential Detection of GMSK Using Decision Feedback", IEEE Trans. on Comm., Vol. COM-36, June 1988, pp. 637-649.

R-3 D. Makrakis et. al., "Optimal Non-Coherent Detection of PSK Signals", Electronics Letters, Vol. 26, pp. 398-401, March 15 1990.

R-4 D. Makrakis et. al., "Differential Detection of Correlative Encoded Continuous Phase Modulation Schemes using Decision Feedback", IEE Proc. Part I, Vol.198, Oct. 1991, pp. 473-480.

R-5 D. Makrakis et. al., "Multiple Differential Detection of Continuous Phase Modulation Signals", to appear in the May 1993 issue of the IEEE Transactions on Vehicular Technology (paper consists of 11 pages).

SUBMISSIONS TO REFEREED JOURNALS

RS-1 D. Makrakis et. al., "Generalized Non-Coherent Sequential Detection of PSK Signals. Part I: Optimal and Near Optimal Receivers", submitted for publication to the IEE Proceedings Part I, May 1990 (manuscript consists of 29 pages).

RS-2 D. Makrakis et. al., "Generalized Non-Coherent Sequential Detection of PSK Signals. Part II: Reduced Complexity Decoders", submitted for publication to the IEE Proceedings Part I, May 1990 (manuscript consists of 15 pages).

RS-3 D. Makrakis, "Improved Non-Coherent Receivers. Part I: Evaluation Under Non-Ideal Conditions", submitted for publication to the IEEE Trans. on Communications, May 1991 (manuscript consists of 23 pages).

RS-4 D. Makrakis, "Improved Non-Coherent Receivers . Part II: Optimal and Asymptotically Optimal Decoders in a Time Dispersive Environment", submitted for publication to the IEEE Trans. on Communications, May 1991 (manuscript consists of 21 pages).

RS-5 D. Makrakis, "Trellis Coded Modulations with Improved Non-Coherent Detection for Personal and Mobile Satellite Communications", submitted to the International Journal of Satellite Communications, Nov. 1992 (manuscript consists of 33 pages).

REFEREED PAPERS TO CONFERENCE PROCEEDINGS

C-1 D. Makrakis et. al., "Novel Receiver Structures for Systems Using Differential Detection" Proc. of International Conference on Digital Satellite Communications (ICDSC-7), pp. 631-688, May 1986.

C-2 A. Yongacoglu D. Makrakis et. al., "One-bit Differential Detection of GMSK with Data-Aided Phase Control", Proc. of International Conference on Communications 86, June 1986, Toronto, Ont., pp. 57.8.1-5.

C-3 A. Yongacoglu D. Makrakis et. al., "A New Receiver for the Differential Detection of GMSK", Proc. of Global Communications Conference 86, Dec. 1986, Houston Texas, pp. 29.5.1-6.

C-4 D. Makrakis et. al., "Two-Bit Differential Detection of GMSK with or without Precoding and Using Decision Feedback", Proc. of International Conference on Communications 87, June 1987, Seattle, Wash., pp. 903-908.

C-5 D. Makrakis et. al., "A new Soft Decision Sequential Decoder for the Differential detection of TFM", Proc. of Global Communications Conference 87, Nov. 1987, Tokyo Japan, pp. 8.8. 1-4.

C-6 D. Makrakis et. al., "An Improved Viterbi Decoder for the Differential Detection of Continuous Phase Modulation Schemes", IEEE WESCANEX'88, May 1988, Saskatoon Sask., pp. 78-87.

C-7 D. Makrakis et. al., "A sequential decoder for the Differential Detection of Trellis Coded PSK Signals", Proc. of International Conference on Communications (ICC'88), pp. 1433-1438, June 1988.

C-8 D. Makrakis et. al., "Interleaving for Differential Detection using Multiple Detectors", Proc. of IEEE Vehicular Technology Conference (VTC'88), pp. 267-272, June 1988.

C-9 D. Makrakis et. al., "Trellis Coded Non-Coherent QAM: A New Bandwidth and Power Efficient Scheme", Proc. of IEEE Vehicular Technology Conference (VTC'89), pp. 95-100, April 1989.

C-10 D. Makrakis et. al., "Non-Coherent Multilevel Trellis Coded Continuous Phase Modulation", Proc. of International Conference on Communications (ICC'89), pp. 275-280, June 1989.

C-11 D. Makrakis et. al., "Differential Detection of Correlative Encoded Continuous Phase Modulation Schemes using Decision Feedback", Proc. of International Conference on Communications (ICC'90), June 1990, Atlanta Georgia, pp. 619-625.

C-12 D. Makrakis et. al., "Optimal Non-Coherent Sequential Detection of Trellis Coded Signals in Non-Ideal Channels", Proc. of Global Communications Conference , Dec. 1990, pp. 371-375.

C-13 D. Makrakis et. al., "Optimal Non-Coherent Detection of Multi-Amplitude/Phase Modulations for Mobile and Personal Satellite Communication Systems", Proceedings of International Conference on Digital Satellite Communications (ICDSC-10), Copenhagen, Denmark, pp. 87-94, May 1992.

LIST OF ABBREVIATIONS

ACI	Adjacent Channel Interference
AMP	Amplitude Modulated Pulses
AMPS	Advanced Mobile Phone System
AOD	Asymptotically Optimal Decoder
AWGN	Additive White Gaussian Noise
BD	Block Decoder
BER	Bit Error Rate
BPSK	Binary Phase Shift Keying
CCI	Cochannel Interference
CDMA	Code Division Multiple Access
CONV. ENC.	Convolutional Encoder
CPM	Continuous Phase Modulation
CQPSK	Coherent Quadrature Phase Shift Keying
CWF	Combining With Feedback
DAPC	Data Aided Phase Correction
DBPSK	Differential Binary Phase Shift Keying
DD	Differential Detector
D.E.	Differential Encoder

DMPSK	Differential M-ary Phase Shift Keying
DQPSK	Differential Quadrature Phase Shift Keying
EHF	Extra High Frequencies
FDMA	Frequency Division Multiple Access
FM	Frequency Modulation
GEO	Geostationary Earth Orbit
GMSK	Gaussian Minimum Shift Keying
GPS	Global Positioning System
GHz	Giga Hertz
GTFM	Generalized Tamed Frequency Modulation
HEO	Highly Elliptical Orbit
IC	Ideal Channel
IF	Intermediate Frequencies
ISD	Integrate Sample and Dump
ISI	Intersymbol Interference
LB	Lower Bound
LEO	Low Earth Orbit
LOS	Line Of Sight

MA-MSK	Multi-Amplitude Minimum Shift Keying
MCPSK	M-ary Coherent Phase Shift Keying
MDD	Multiple Differential Detection
MDD/CWF	Multiple Differential Detection with Combining and Decision Feedback
MHz	Mega Hertz
MLRT	Maximum Likelihood Ratio Test
MMSE	Minimum Mean Square Error
MPSK	M-ary Phase Shift Keying
MSAT	Mobile Satellite
MSK	Minimum Shift Keying
NASA	National Aeronautics and Space Administration
NC–MQAM	Non-Coherent M-ary Quadrature Amplitude Modulation
NEC	Non-Redundant Error Correction
pdf	probability density function
PLL	Phase Lock Loop
PSK	Phase Shift Keying
PU	Processing Unit

QPSK	Quadrature Phase Shift Keying
QAM	Quadrature Amplitude Modulation
S-B-S	Symbol-By-Symbol (Receiver)
SEMDD	Squared Envelope & Multiple Differential Detection
SER	Symbol Error Rate
S. M.	Signal Mapper
SNR	Signal-to-Noise Ratio
TCM	Trellis Coded Modulation
TDMA	Dime Division Multiple Access
TFM	Tamed Frequency Modulation
UB	Upper Bound
UHF	Ultra High Frequencies
VCO	Voltage Controlled Oscillator
VHF	Very High Frequencies
VSAT	Very Small Antenna Terminals
WPCS	Wireless Personal Communication Systems
WPDCS	Wireless Personal Digital Communication Systems
ZFE	Zero Forcing Equalization

LIST OF SYMBOLS

$\bar{a}_k^p$	p-bit Information Word.
$\widehat{\bar{a}_k^p}$	Decision of $\bar{a}_k^p$.
$\widehat{\widehat{\bar{a}_\xi^p}}$	Decision of $\bar{a}_k^p$, Produced by the Backward First -Stage Detector.
$\widehat{\widehat{\widehat{\bar{a}_\xi^p}}}$	Decision of $\bar{a}_k^p$, Produced by the Second-Stage Detector.
$\bar{A}$	Information Sequence.
$\alpha_{n,k}^{AMP}$	Complex Gain of the n^{th} Amplitude Modulation Pulse in the Approximation of a CPM Signal through the AMP Decomposition Technique.
$\bar{b}_k^q$	Encoded q-bit word.
$\bar{B}$	Encoded Sequence.
$B_e^{MDD}(\lambda)$	Upper Bound of the Symbol Error Probability of the Truncated Multiple Differential Detection Sequence Estimator.
B_F	Fading Bandwidth.
$B_{[\nu,\zeta]}^Z$	Upper Bound of the Probability of Occurrence of the Error Event $\{\bar{C}(\bar{A}^\zeta) \leftarrow \bar{C}(\bar{A}^\nu)\}$ when the Block Decoder is used (the Signal is MPSK and the Channel is corrupted by AWGN).
$\mathcal{BF}_{[\nu,\zeta]}^Z$	Upper Bound of the Probability of Occurrence of the Error Event $\{\bar{C}(\bar{A}^\zeta) \leftarrow \bar{C}(\bar{A}^\nu)\}$ when the Block Decoder is used (the Signal is MPSK and the

	Channel is corrupted by AWGN and Multipath Fading).
$B^{Z}_{HAO[\nu,\zeta]}$	Upper Bound of the Probability of Occurrence of the Error Event $\{\bar{C}(\bar{A}^{\zeta}) \leftarrow \bar{C}(\bar{A}^{\nu})\}$ when the Asymptotically Optimal Decoder is used (the Signal is MPSK).
$\bar{C}(\bar{A})$	Sequence of Transmitted Symbols.
c_k	k^{th} Transmitted Symbol.
C/I	Carrier to Interference Ratio.
$\underline{\mathcal{C}}^{\bar{S}_l}_{\underline{S}}(k)$	Set Consisting of all $\bar{C}(\bar{A})$ Sequences with $\bar{a}^{p}_{k} = \bar{S}_l$.
$\{\bar{C}(\bar{A}^{\zeta}) \leftarrow \bar{C}(\bar{A}^{\nu})\}$	Error Event Occurring when the Sequence $\bar{C}(\bar{A}^{\nu})$ is Transmitted and the Receiver Decides in Favor of the Sequence $\bar{C}(\bar{A}^{\zeta})$.
d^{H}_{m}	Hamming Distance.
d^{H}_{min}	Minimum Hamming Distance.
$d_l(k)$	Sampled Output of the the Differential Detector with Delay element l Times the Symbol Period.
$d^{I}_{l}(k)$	Real Part of $d_l(k)$.
$d^{Q}_{l}(k)$	Imaginary Part of $d_l(k)$.
$D^{Z}_{[\nu,\zeta]}$	Distance Function which Determines the value of the Probability of the Error Event $\{\bar{C}(\bar{A}^{\zeta}) \leftarrow \bar{C}(\bar{A}^{\nu})\}$ (the Channel is Corrupted by AWGN).
$D^{Z}_{IC[\nu,\zeta]}$	Expression of the Distance Function $D^{Z}_{[\nu,\zeta]}$ when the

	Channel is Ideal.
$E\{\bullet\}$	Average Value of $\bullet$.
$EV_{0\leftarrow\epsilon}$	Event that $\{\bar{C}(\bar{A}^{\epsilon}) \leftarrow \bar{C}(\bar{A}^{0})\}$ occurs.
$\overline{EV}_{0\leftarrow\epsilon}$	Event that $\{\bar{C}(\bar{A}^{\epsilon}) \leftarrow \bar{C}(\bar{A}^{0})\}$ does not occur.
$erfc(\cdot)$	Complimentary Error Function.
f_c	Carrier Frequency.
$f_F(t)$	Multipath Fading Corrupting the Transmitted Signal.
$f_F^I(t)$	Real Part of $f_F(t)$.
$f_F^Q(t)$	Imaginary Part of $f_F(t)$.
$\overline{f_F^I}$	Average of $f_F^I(t)$.
$\overline{f_F^Q}$	Average of $f_F^Q(t)$.
f_k^F	Sample of $f_F(t)$ at $k\,T$.
$f_{ra}^{en}(\cdot)$	Probability Density Function of the Signal Envelope Fluctuation due to Rayleigh Fading.
$f_{ra}^{ph}(\cdot)$	Probability Density Function of the Signal Phase Fluctuation due to Rayleigh Fading.
$f_{ri}^{en}(\cdot)$	Probability Density Function of the Signal Envelope Fluctuation due to Rician Fading.
$f_{ri}^{ph}(\cdot)$	Probability Density Function of the Signal Phase Fluctuation due to Rician Fading.

$f_{Sh}^{en}(\cdot)$	Probability Density Function of the Signal Envelope Fluctuation due to Shadowing.
$f_{co}^{en}(\cdot)$	Probability Density Function of the Signal Envelope Fluctuation due to the Combined Effect of Shadowing and Multipath Fading.
$f_{fl}(\cdot)$	Probability Density Function of the Signal Phase Fluctuation due to the Combined Effect of Shadowing and Multipath Fading.
E_b/N_o	Bit Energy Signal-to-Noise Ratio.
E_S/N_o	Symbol Energy Signal-to-Noise Ratio.
g_k	Information Symbols.
$\bar{G}(\bar{A})$	Sequence of Information Symbols g_k.
$h_c(t)$	Impulse Response of the Channel.
$h_{c,B}(t)$	Baseband Equivalent of the Channel Impulse Response $h_c(t)$.
$H_T(\omega)$	Premodulation Filter.
$h_T(t)$	Impulse Response of the Premodulation Filter $H_T(\omega)$.
$H_R(\omega)$	Frequency Response of the Postdetection Filter.
$h_R(t)$	Impulse Response of the Postdetection Filter.
$H_E(\omega)$	Baseband Frequency Response of the Cascaded Transmitter-Channel Combination.
$h_E(t)$	Baseband Impulse Response of the Cascaded

	Transmitter–Channel Combination.
$H(\omega)$	Baseband Frequency Response of the Cascaded Transmitter, Channel and Receiver Combination.
$h(t)$	Baseband Impulse Response of the Cascaded Transmitter, Channel and Receiver Combination.
h_k	Sample of the Impulse Response $h(t)$ at $k\,T$.
$\bar{h}$	Array Consisting of the h_k Samples.
$h_n^{AMP}(t)$	n^{th} Amplitude Modulation Pulse.
$h_{E,n}^{AMP}(t)$	Convolution Between the n^{th} Amplitude Modulation Pulse $h_n^{AMP}(t)$ and the Baseband Equivalent of the Channel Impulse Response $h_{c,B}(t)$.
$I_0(\cdot)$	Modified Bessel Function of Zero Order.
$\mathcal{J}_k$	Amplitude of the Information Symbol g_k.
$IST(\bar{h}, \bar{C}(\bar{A}))$	Term Accounting the Presence of Intersymbol Interference in the Non-Coherent Detection of a Linear Modulation Signal.
$IST_{CPM}(\bar{C}(\bar{A}), h_{c,B}(t), t)$	Term Accounting the Presence of Intersymbol Interference in the Non-Coherent Detection of a Continuous Phase Modulation Signal.
$Im\{\bullet\}$	Imaginary Part of $\bullet$.
K_F	Power Ratio between the Direct and the Diffused Signal Component (K-factor).
K_r	Power Ratio between the Direct and the Diffused Signal

	Component in dB.
$\mathcal{LB}_{\lambda}^{MDD}$	Lower Bound of $B_e^{MDD}(\lambda)$.
$MST(h_0, \bar{C}(\bar{A}))$	Term Accounting the Multi-Amplitude Nature of a Linearly Modulated Signal in the Non-Coherent Detection Process.
$MST_{CPM}(\bar{C}(\bar{A}), h_{c,B}(t), t)$	Term Accounting the Multi-Amplitude Nature of a Continuous Phase Modulation Signal in the Non-Coherent Detection Process.
$\mathcal{MB}_{HAO[\nu,\zeta]}^{Z}$	Upper Bound of the Probability of Occurrence of the $\{\bar{C}(\bar{A}^{\zeta}) \leftarrow \bar{C}(\bar{A}^{\nu})\}$ Error Event when the Asymptotically Optimal Decoder (for High E_b/N_o) is used (Linearly Modulated Signal with Multi-Amplitude/Phase Constellation).
N_o	One-Sided Power Spectral Density of the Additive White Gaussian Noise.
$n_e(\{\bar{C}(\bar{A}^{\zeta}) \leftarrow \bar{C}(\bar{A}^{\nu})\})$	Number of Symbols in Error Associated with the Error Event $\{\bar{C}(\bar{A}^{\zeta}) \leftarrow \bar{C}(\bar{A}^{\nu})\}$.
$n_w(t)$	Additive White Gaussian Noise Corrupting the Channel.
P_e	Symbol Error Probability of of the Block Decoder.
$P_e^{Coh.(NDE)}$	Probability of Error of the Non-Differentially Encoded Coherent BPSK in a Slow Rayleigh Faded Multipath Channel.
$P_e^{Coh.(DE)}$	Probability of Error of the Differentially Encoded Coherent BPSK in a Slow Rayleigh Faded Multipath Channel.

P_e^{CWF}	Probability of Symbol Error of the Combining With Feedback Receiver.
P_e^{DD}	Probability of Error of the Differential BPSK in a Slow Rayleigh Faded Multipath Channel.
$P_e^{MDD}(\lambda)$	Symbol Error Probability of the Truncated Multiple Differential Detection Sequence Estimator.
P_e^{HAO}	Symbol Error Probability of The Asymptotically Optimal Decoder for MPSK Signals.
$P_e^{[MAD]HAO}$	Symbol Error Probability of The Asymptotically Optimal Decoder for Multi-Amplitude Linearly Modulated Signals.
$\mathcal{P}e_{SBS}^{z}$	Symbol Error Probability of the Asymptotically Optimal Symbol-By-Symbol Receiver.
$P(\{\bar{C}(\bar{A}^{\varsigma}) \leftarrow \bar{C}(\bar{A}^{\nu})\})$	Probability that the Error Event $\{\bar{C}(\bar{A}^{\varsigma}) \leftarrow \bar{C}(\bar{A}^{\nu})\}$ will occur. The Channel is Corrupted by AWGN.
$P_f(\{\bar{C}(\bar{A}^{\varsigma}) \leftarrow \bar{C}(\bar{A}^{\nu})\})$	Probability that the Error Event $\{\bar{C}(\bar{A}^{\varsigma}) \leftarrow \bar{C}(\bar{A}^{\nu})\}$ will occur. The Channel is Corrupted by AWGN and Flat Multipath Fading.
$Q(\cdot)$	Error Function.
$Q_f(\cdot,\cdot)$	Marcum's Q Function.
$\mathcal{Q}_3(\lambda, \bar{y}, \bar{C}(\bar{A}))$	Metric Expression to be Maximized by the Truncated Multiple Differential Detection Sequence Estimator of a MPSK Signal.
$Re\{\bullet\}$	Real Part of $\bullet$.

$R_n(\tau)$	Autocorrelation Function of the additive Gaussian Noise $n(t)$, corrupting the output of the Postdetection Filter $H_R(\omega)$.
R_k^n	Sample of $R_n(\tau)$ at $k\ T$.
$R_F(\tau)$	Autocorrelation Function of $f_F^I(t)$ and $f_F^Q(t)$.
R_k^F	Sample of $R_F(\tau)$ at $k\ T$.
$R_{tr}(\bar{C}(\bar{A}), t)$	Envelope of the Transmitted Signal.
$\bar{S}_i$	i^{th} Combination of $\bar{a}_k^p$.
$s(\bar{C}(\bar{A}), t)$	Input of the Voltage Controlled Oscillator (which produces the CPM Signal).
S_{CW}^Z	Set Consisting of all Possible Codewords $\bar{C}(\bar{A})$.
$S_{\bar{C}(\bar{A}^\nu)}$	Set Consisting of all Codeword Elements of S_{CW}^Z Except $\bar{C}(\bar{A}^\nu)$.
$sgn\{\bullet\}$	Signum of $\bullet$.
t_D	Delay Spread.
$\mathcal{UB}^Z$	Upper Bound of the Symbol Error Probability of the Block Decoder.
$\mathcal{UB}_{app.}^Z$	Approximate Upper Bound of the Symbol Error Probability of the Block Decoder (the Signal is Uncoded MPSK).
$\mathcal{U}_{\mathcal{HAO}}\mathcal{B}^Z$	Upper Bound of the Symbol Error Probability of the Asymptotically Optimal Decoder (the Signal is MPSK).

$\mathcal{U}_{\mathcal{HAO}}B^{Z}_{app.}$	Approximate Upper Bound of the Symbol Error Probability of the Asymptotically Optimal Decoder (the Signal is Uncoded MPSK).
$\mathcal{U}^{MAP}_{\mathcal{HAO}}B^{Z}$	Upper Bound of the Symbol Error Probability of the Asymptotically Optimal Decoder (the Signal is Linearly Modulated with Multi-Amplitude/Phase Constellation).
$\mathcal{U}^{SBS}B$	Upper Bound of the Symbol Error Probability for the Asymptotically Optimal Symbol-By-Symbol Receiver.
$\mathcal{U}B^{MDD}_{\lambda}$	Upper Bound of $B^{MDD}_{e}(\lambda)$.
$x_{FM}(\bar{C}(\bar{A}),t)$	Output of the Voltage Controlled Oscillator.
$x_{FM,B}(\bar{C}(\bar{A}),t)$	Baseband Equivalent of $x_{FM}(\bar{C}(\bar{A}),t)$.
$x_{tr}(\bar{C}(\bar{A}),t)$	Transmitted Signal.
$x_{tr,B}(\bar{C}(\bar{A}),t)$	Signal at the output of the Premodulation Filter.
$x^{app.}_{tr,B}(\bar{C}(\bar{A}),t)$	Approximation of $x_{tr,B}(\bar{C}(\bar{A}),t)$ Using the AMP Decomposition Technique.
$x(\bar{C}(\bar{A}),h_c(t),t)$	Transmitted Signal Distorted by a Time Dispersive Channel.
$x^{app.}(\bar{C}(\bar{A}),h_c(t),t)$	Approximation of $x(\bar{C}(\bar{A}),h_c(t),t)$ Using the AMP Decomposition Technique.
$x_B(\bar{C}(\bar{A}),h_{c,B}(t),t)$	Baseband Equivalent of $x(\bar{C}(\bar{A}),h_c(t),t)$.
$x^{app.}_B(\bar{C}(\bar{A}),h_{c,B}(t),t)$	Approximation of $x_B(\bar{C}(\bar{A}),h_{c,B}(t),t)$ using the AMP Decomposition Technique.
$x_r(t)$	Received Signal.

$y(t)$	Signal at the Output of the Postdetection Filter.
y_k	Sample of the Postdetection Filter Output ($y(t)$) at $k\,T$.
$\bar{y}$	Array Consisting of the y_k Samples.
$\mathcal{Y}_n^{AMP}(t)$	Output of a Postdetection filter matched to $h_{E,n}^{AMP}(t)$.
$\mathcal{Y}_{n,k}^{AMP}$	Sample of $\mathcal{Y}_n^{AMP}(t)$ at $k\,T$.
$\bar{\mathcal{Y}}_n^{AMP}$	Array Consisting of the $\mathcal{Y}_{n,k}^{AMP}$ Samples.
$y^{CPM}(t)$	Signal at the Output of the Postdetection Filter of a Continuous Phase Modulation System.
y_k^{CPM}	Sample of the Postdetection Filter Output ($y^{CPM}(t)$) at $k\,T$.
$\bar{y}_{[Z+\mathcal{L}_c,0]}^{CPM}$	Array Consisting of the y_k^{CPM} Samples.
α_{eb}	Excess Bandwidth of a Nyquist Filter.
$\mathcal{A}_k$	Envelope of a Multi-Amplitude CPM Signal in the [(k T, (K+1)T] Time Interval.
$\delta_K(i)$	*Kroneker delta* Function.
$\Delta\Theta_l(k)$	*modulo* (2π) Difference between the Phases of the Transmitted Symbols c_k and c_{k-l}.
ψ	Initial Carrier Phase.
$\hat{\psi}$	Carrier Phase Estimate, Produced at the Receiver.
θ_k	Phase of the Transmitted Symbol c_k.

ϕ_k	Phase of the Information Symbol g_k.
$\phi_{tr}(\bar{C}(\bar{A}), t)$	Phase of the Information-Carrying Signal.
ω_c	Radian Carrier Frequency.
$\hat{\omega}_c$	Radian Carrier Frequency Estimate, produced at the Receiver.
$\cup$	Union Operator Between Sets.
ρ_e	Amplitude Strength of the Delayed Signal Component (Reflection) in a 2-Ray Multipath Frequency Selective Fading Channel.

$\aleph_{ge}(x_r(t), x_B(\bar{C}(\bar{A}), h_{c,B}(t), t))$	General Metric Expression to be Maximized by the Optimal Non-Coherent Sequence Estimator (the maximization is in respect to $\bar{C}(\bar{A})$).
$\aleph_{OP}^{LMD}(h_0, \bar{h}, \bar{y}, \bar{C}(\bar{A}))$	Metric Expression to be Maximized by the Optimal Non-Coherent Sequence Estimator of a Linearly Modulated Signal.
$\aleph_{OP}^{LMI}(h_0, \bar{y}, \bar{C}(\bar{A}))$	Metric Expression to be Maximized by the Optimal Non-Coherent Sequence Estimator of a QAM Signal when the Channel is Ideal.
$\aleph_{OP}^{PSK}(\bar{h}, \bar{y}, \bar{C}(\bar{A}))$	Metric Expression to be Maximized by the Optimal Non-Coherent Sequence Estimator of a MPSK Signal when the Channel is Time Dispersive.
$\aleph_{LAO}^{LMD}(h_0, \bar{h}, \bar{y}, \bar{C}(\bar{A}))$	Metric Expression to be Maximized by the Asymptotically Optimal Non-Coherent Sequence Estimator (for Low E_b/N_o) of a Linearly Modulated Signal .
$\aleph_{LAO}^{PSK}(\bar{h}, \bar{y}, \bar{C}(\bar{A}))$	Metric Expression to be Maximized by the Asymptotically Optimal Non-Coherent Sequence Estimator (for Low E_b/N_o) of a MPSK Signal when the Channel is Time Dispersive.
$\aleph_{HAO}^{LMD}(h_0, \bar{h}, \bar{y}, \bar{C}(\bar{A}))$	Metric Expression to be Maximized by the Asymptotically Optimal Non-Coherent Sequence Estimator (for High E_b/N_o) of a Linearly Modulated Signal.
$\aleph_{HAO}^{PSK}(\bar{h}, \bar{y}, \bar{C}(\bar{A}))$	Metric Expression to be Maximized by the Asymptotically Optimal Non-Coherent Sequence Estimator (for High E_b/N_o) of

	a MPSK Signal when the Channel is Time Dispersive .
$\aleph_{HAO}^{LMI}(h_0, \bar{y}, \bar{C}(\bar{A}))$	Metric Expression to be Maximized by the Asymptotically Optimal Non-Coherent Sequence Estimator (for High E_b/N_o) of a QAM Signal when the Channel is Ideal.
$\aleph_{IC}(\bar{y}, \bar{C}(\bar{A}))$	Metric Expression to be Maximized by the Optimal Non-Coherent Sequence Estimator of a PSK Signal when the Channel is Ideal.
$\aleph_{IC}^{MDD}(\bar{y}, \bar{C}(\bar{A}))$	Metric Expression to be Maximized by the Multiple Differential Detection Sequence Estimator of a PSK Signal.
$\aleph_{OP}^{CPMD}(\bar{C}(\bar{A}), \mathcal{F}_{[Z-1,0]}^{CPM}(\bar{C}(\bar{A})), h_{c,B}(t), t))$	Metric Expression to be Maximized by the Optimal Non-Coherent Sequence Estimator of a Continuous Phase Modulation Signal. The Channel is Time Dispersive.
$\aleph_{LAO}^{CPMD}(\bar{C}(\bar{A}), \mathcal{F}_{[Z-1,0]}^{CPM}, h_{c,B}(t), t))$	Metric Expression to be Maximized by the Asymptotically Optimal Non-Coherent Sequence Estimator (for Low E_b/N_o)of a Continuous Phase Modulation Signal. The Channel is Time Dispersive.
$\aleph_{HAO}^{CPMD}(\bar{C}(\bar{A}), \mathcal{F}_{[Z-1,0]}^{CPM}, h_{c,B}(t), t))$	Metric Expression to be Maximized by the Asymptotically Optimal Non-Coherent Sequence Estimator (for High E_b/N_o) of a Continuous Phase Modulation Signal. The Channel is Time Dispersive.
$\aleph_{LAO}^{CPMI}(\bar{C}(\bar{A}), \mathcal{F}_{[Z-1,0]}^{CPM}, h_{c,B}(t), t))$	Metric Expression to be Maximized by the Asymptotically Optimal Non-Coherent

Sequence Estimator (for Low E_b/N_o) of a Multi-Amplitude Continuous Phase Modulation Signal . The Channel is Ideal.

$\aleph_{HAO}^{CPMI}(\bar{C}(\bar{A}), \mathcal{F}_{[Z-1,0]}^{CPM}, h_{c,B}(t), t))$ Metric Expression to be Maximized by the Asymptotically Optimal Non-Coherent Sequence Estimator (for High E_b/N_o) of a Multi-Amplitude Continuous Phase Modulation Signal.

$\aleph_{CPIC}(\bar{C}(\bar{A}), \mathcal{F}_{[Z-1,0]}^{CPM}, t))$ Metric Expression to be Maximized by the Optimal Non-Coherent Sequence Estimator (for High E_b/N_o) of a Single-Amplitude Continuous Phase Modulation Signal. The Channel is Ideal.

$\aleph_{LAO_{app.}}^{CPMD}(\bar{\Re}_{E,[0,0]}^{AMP}, \ldots, \bar{\Re}_{E,[0,\mathcal{N}]}^{AMP}, \bar{\Re}_{E,[1,0]}^{AMP}, \ldots, \bar{\Re}_{E,[\mathcal{N},\mathcal{N}]}^{AMP}, \bar{\mathcal{Y}}_0^{AMP}, \ldots, \bar{\mathcal{Y}}_{\mathcal{N}}^{AMP}, \bar{C}(\bar{A}))$

Metric Expression to be Maximized by the Asymptotically Optimal Non-Coherent Sequence Estimator (for Low E_b/N_o) of a Multi-Amplitude Continuous Phase Modulation Signal. The AMP Decomposition has been used. The Channel is Time Dispersive.

$\aleph_{HAO_{appr}}^{CPMD}(\bar{\Re}_{E,[0,0]}^{AMP}, \ldots, \bar{\Re}_{E,[0,\mathcal{N}]}^{AMP}, \bar{\Re}_{E,[1,0]}^{AMP}, \ldots, \bar{\Re}_{E,[\mathcal{N},\mathcal{N}]}^{AMP}, \bar{\mathcal{Y}}_0, \ldots, \bar{\mathcal{Y}}_{\mathcal{N}}, \bar{C}(\bar{A}))$

Metric Expression to be Maximized by the Asymptotically Optimal Non-Coherent Sequence Estimator (for High E_b/N_o) of a Multi-Amplitude Continuous Phase Modulation Signal. The AMP Decomposition has been used. The Channel is Time Dispersive.

$\aleph_{HAO_{appr}}^{CPSD}(\bar{\Re}_{E,[0,0]}^{AMP}, \bar{\mathcal{Y}}_0, \bar{C}(\bar{A}))$ Metric Expression to be Maximized by the Asymptotically Optimal Non-Coherent Sequence

	Estimator(for High E_b/N_o) of a Single-Amplitude Continuous Phase Modulation Signal. The AMP Decomposition has been used. The Channel is Time Dispersive.
$\aleph_{CPIC_{appr}}(\bar{\Re}^{AMP}_{E,[0,0]}, \bar{\mathcal{Y}}_0, \bar{C}(\bar{A}))$	Metric Expression to be Maximized by the Non-Coherent Sequence Estimator (for High E_b/N_o) of a Single-Amplitude Continuous Phase Modulation Signal. The AMP Decomposition has been used. The Channel is Ideal.
$\aleph^{CPM}_{MDD}(\bar{y}^{CPM}_{[Z+\mathcal{L}_c,0]}, \bar{C}(\bar{A}))$	Metric Expression to be Maximized by the Multiple Differential Detection Sequence Estimator of a Continuous Phase Modulation Signal.

Contents

List of Figures

List of Tables

Chapter 1

INTRODUCTION

1.1 WIRELESS PERSONAL DIGITAL COMMUNICATION SYSTEMS

Over the past five years, there has been a spectacular interest in Wireless Personal Digital Communication Systems (WPDCS) (see for example [241] [37], [38], [39], [97], [98], [99]). The premise that wireless personal communications is emerging as a key, wide-sweeping technology that will dramatically impact our society is quickly becoming a reality (see for example [200], [84], [25], [215]). A realization of an integrated WPDCS would make communications truly personal. Anyone would be able to communicate with anybody else anywhere. In the past, wireless communication systems have been extensively used by telecommunication carriers and many other organizations for point–to–point (analog or digital) transmission of voice and data as alternatives to copper wire and coaxial cable [62]. Even today, such wireless communication systems are widely used instead of fiber for some network links [220]. Examples of such well established telecommunication systems include bandwidth efficient point-to-point terrestrial microwave systems [244] as well as various satellite communication systems [213].

Nevertheless, it has become evident that today's wireless telecommunication thrust focuses on the mobile, portable and personal communications market (see for example [241], [37], [38], [39], [97], [98], [99]). In contrast to

the fixed wireless telecommunication systems, mobile wireless communication networks provide their users with the opportunity to travel without restrictions (within the service area) and simultaneously communicate by voice or data with other users (which could also be mobile). Because of the mobility of the users and their freedom from location restrictions, such systems are referred to as Wireless Personal Communication Systems.

Early Wireless Personal Communication Systems include CB radios [24], cordless telephones [24] and cellular telecommunication systems such as the Advanced Mobile Phone System (AMPS) [10] all of which used analog transmission technology. The main disadvantage of these analog telecommunication systems was that they had limited capacity and therefore could not accommodate the increased number of users as well as demand for improved services [24]. Perhaps the most urgent capacity problem the users are facing today, is with the analog cellular systems [100]. This forced the scientific society and industry to a large scale research. As a result, over the last four years, various standards have been proposed for digital cellular radio communications in Europe [88], [170], North America [55], [81] and Japan [81], [197]. By employing digital modulation, these cellular systems offer increased bandwidth efficiency and overall higher system capacity [65]. In addition, they achieve better speech intelligibility for a given carrier–to–interference ratio (C/I) as compared to the equivalent analog ones. The use of digital technology provides the opportunity to apply powerful digital speech coding techniques that further reduce the spectrum occupancy of voice users [81]. Using digital transmission formats, service providers will be able to offer to their customers a great deal of new features such as data service and signal encryption [81]. Also, it makes the integration between different systems, networks and technologies much easier -a key factor for the implementation of a successful (integrated and unified) WPDCS service [194]-[196]. Apart from the cellular radio, other examples of widespread wireless personal communication systems include the Cordless Telephone [82], the Mobile Satellite (MSAT) system [134] and the Global positioning System (GPS) [121].

We close this very brief introduction by quoting Dr. A.J. Viterbi' s opinion: "*it is almost certain that by the end of the century, almost all wireless communication systems will be digital*" [258]. This is our belief also, and thus we will be referring to all the WPCS as Wireless Personal *Digital* Communication Systems.

1.2 MAJOR IMPAIRMENTS OF THE WPDCS CHANNEL

1.2.1 The Multipath Fading Environment

It is well known to all involved with mobile and portable radio communications, that one of the major disturbances encountered in these channels is the presence of multipath fading (see for example [126], [214], [99], [102]).

Propagation in the mobile and portable environment takes place through scattered and/or reflected waves. As a result, the mobile user receives a number of signal replicas arriving through multiple, random propagation paths which vary according to the user's velocity. Due to the randomness of these replicas, the received signal experiences severe envelope fluctuations as well as randomly changing phase shifts [102]. Collectively, the above phenomena create a diffused signal which is referred to as multipath fading. Naturally, the channels in which these phenomena take place are known as multipath fading channels.

Presently, the two forerunners of WPDCS, the cellular radio and mobile-satellite communications service have been planned and operated in the VHF/UHF (400/800 MHz.) bands. However, today there is strong consideration to provide mobile-satellite communications service in the L band (1.2/1.5 GHz). Also, the new and fast growing personal satellite communications field (either in the form of Low Earth Orbit (LEO) [171], [219], Highly Elliptical Orbit (HEO) [54], [105], [221], [11] or Geostationary orbit (GEO) satellite systems) might be serviced in S, C or Ka (17 GHz - 35 GHz) bands. The Ka band might also be used for passenger communications in aeronautical applications. In addition, active research is presently being carried out considering the use of frequencies above 50 GHz to provide wireless intra-building communications. Considering that the effect of multipath fading becomes more destructive at higher frequencies makes us realize that multipath fading will remain as one of the major challenges in the design and implementation of efficient and successful WPDCS.

Depending on whether or not there is a line-of-sight (LOS) direct path between transmitter and the receiver, faded channels can have Rayleigh or

Rician characteristics [174]. For the Rayleigh faded channel (in which a direct path does not exist), the probability density function (pdf) of the faded signal envelope r, follows the Rayleigh distribution, i.e.,

$$f_{ra}^{en}(r) = \begin{cases} \frac{r}{\sigma^2} e^{-\frac{r^2}{2\sigma^2}} & \text{for } r \geq 0 \\ 0 & \text{elsewhere} \end{cases} \tag{1.1}$$

whereas its phase θ is uniformly distributed in the $(-\pi, \pi)$ interval, i.e.,

$$f_{ra}^{ph}(\theta) = \begin{cases} \frac{1}{2\pi} & \text{for } -\pi \leq \theta \leq \pi \\ 0 & \text{elsewhere.} \end{cases} \tag{1.2}$$

On the other hand, in a Rician faded channel, in addition to the diffused signal (Rayleigh fading), there is a direct LOS path. The vector sum of the direct signal with the Rayleigh fading component results in a composite signal with Rician statistics. The pdf of the envelope of such a signal can be mathematically expressed as [242]:

$$f_{ri}(r) = 2r\sqrt{\frac{(1+K_F)}{K_F}} \exp[-K_F - (1+K_F)r^2] I_0(2r\sqrt{K_F(1+K_F)}]) \tag{1.3}$$

where K_F denotes the power ratio between the direct and the diffused signal component, and $I_0(\cdot)$ is the modified Bessel function of zero order [1]. The phase statistics of the Rician fading channel are described by [204]

$$f_{ri}^{ph}(\theta) = \frac{e^{-K_F}}{2\pi} + \frac{\sqrt{K_F}\cos(\theta)\exp(-K_F \sin^2(\theta))}{2\sqrt{\pi}}[2 - \text{erfc}(\sqrt{K_F \cos(\theta)})] \tag{1.4}$$

where erfc$(\cdot)$ denotes the complimentary error function [204]. For both Rayleigh and Rician faded channels, the diffused signal component has a two-sided bandwidth of $2B_F = 2vf_c/c$ where f_c is the carrier frequency, c is the propagation velocity and v the velocity of the user. Depending upon the values of v, as well as on the transmitted symbol rate $1/T$, the fading could be characterized as either fast or slow. B_F is also known as the fading bandwidth or maximum Doppler shift. The power spectral density of the faded signal, depends upon the fading spectrum assumed. Examples of several such spectra can be found in [174].

Depending upon the values of the delay spread, t_D, of the reflected waves, as compared to the symbol duration T, the fading could be *frequency selective* or *frequency non-selective* (which is also known as *flat fading*). Essentially, the effect of the frequency selectivity is to create a fading channel with *variable* time dispersion. For small values of $\frac{t_D}{T}$ (typically < 0.1) it is probably fair to state that fading is frequency non-selective. In practice, flat and frequency selective fading co-exist in the mobile radio applications [216]. Which of the two fading behaviours becomes predominant, depends on the channel bandwidth, frequency band used and the velocity of the user.

1.2.2 Shadowing

Depending on the geographic area of operation, WPDCS systems, in addition to multipath fading, might experience shadowing [138]. Such behaviour is very common in areas with vegetation and/or other obstacles which can absorb a considerable percentage of the signal power. A classic example is the mobile satellite service in vegetated areas with a significant presence of trees [139]. The dynamic behaviour of the shadowing (fade rate, average inter/intra-fade durations etc.) depends strongly on the frequency used, the velocity of the user and the nature of the geographic area.

Through the years, studies conducted [139], modeled the fading behaviour of the signal envelope due to shadowing as a log-normal process, i.e.

$$f_{Sh}^{en}(R) = \frac{1}{R\sqrt{2\pi d_o}} e^{-\frac{(ln(R)-\mu_o)^2}{2d_0}} \tag{1.5}$$

where d_0 and μ_o are the variance and mean of the normal distribution. The pdf of the envelope fluctuation resulting from the combined effect of shadowing and Rayleigh or Rician fading is [136]-[139]:

$$f_{co}^{en}(r) = \frac{r}{b_0\sqrt{2\pi d_0}} \int_0^\infty \frac{}{R} e^{[-\frac{(ln(R)-\mu_o)^2}{2d_0} - \frac{(r^2+R^2)}{2d_0}]} I_0(\frac{rR}{b_o}) dR. \tag{1.6}$$

The pdf of the random phase fluctuation created by the combined shadowing-multipath fading can be approximated as Gaussian [136]-[139], i.e.

$$f_{fl}(\theta) = \frac{1}{\sqrt{2\pi\sigma}} e^{-\frac{(\theta-\eta)^2}{2\sigma^2}} \tag{1.7}$$

where σ and η represent the mean and the standard deviation respectively. The effect of shadowing (as is also the case for multipath fading) already a serious problem in UHF/VHF frequency bands, increases both in terms of depth, slope of attenuation and rate of change (i.e. faster changes and deeper fades) with the increase in signal frequency. This would definitely be a serious threat to WPDCS systems operating in higher frequency bands as is the case for personal satellite communication systems operating in Extra High Frequencies (EHF) such as the Ka band.

1.2.3 The Co-channel Interference (CCI) Environment

In mobile/cellular communication systems, *frequency reuse* is a core concept which can drastically increase the spectrum efficiency. *Frequency reuse* means that the same frequency is repeatedly used by different cells spanned in different geographic locations as shown in Fig. 1.1 [128]. It can be seen that a channel with carrier frequency f_1 is being used in the central cell as well as in the surrounding six cells located at the reuse distance D away from the cell. The co-channels in the six cells would interfere with the central cell, if the signal coverage area of each cell overlaps with that of the others. As a consequence, CCI would occur.

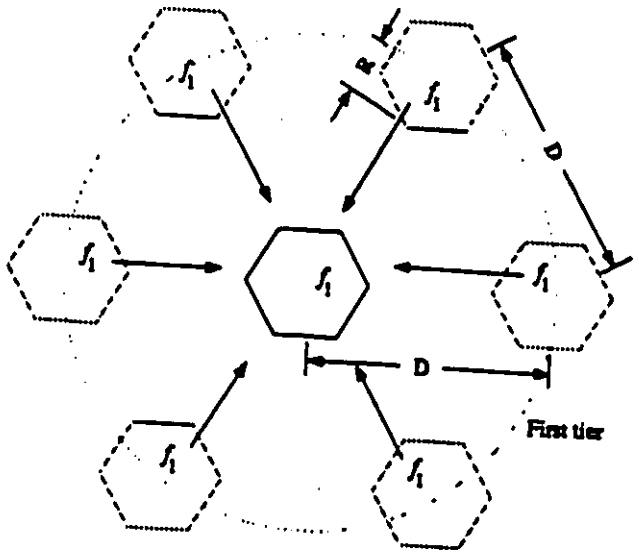

Figure 1.1: Illustration of the frequency reuse concept, and the resulting CCI from the interfering cells.

In general, the carrier-to-interference (C/I) ratio is defined as [128]

$$\mathrm{C/I} = \sum_{k=1}^{K_I} (\frac{D_k}{R})^{\gamma} \tag{1.8}$$

where γ (typically equal to 4 [128]) is the propagation path-loss determined by the actual environment, K_I is the number of cochannel cells in the first tier, R is the cell size determined by the coverage area of the signal strength in each cell, D_k is the distance between the user and the k^{th} interferer and C/I is the receiver carrier-to-interference ratio at the desired mobile receiver. From Fig. 1.1, it can be observed that as the separation distance D increases, the CCI between cells decreases. In turn, the frequency channels are less often reused, which results in a reduction of the spectral efficiency. A compromise is thus required. A crucial factor to make this decision is the power efficiency and resistance to interference that the wireless telecommunication systems are designed to deal with.

1.3 POTENTIAL AND WEAKNESSES OF THE NON-COHERENT TECHNIQUES

Coherent detection requires knowledge of the frequency and phase of the received information signal. This information is generated at the receiver site through processing which is applied on the received signal itself or on separate signals transmitted specifically for this purpose (pilot signals). The frequency/phase estimation is performed by units designed specifically for this purpose, known as carrier recovery circuits. The quality of the frequency/phase estimates produced by the carrier recovery circuits is crucial, since it determines the bit error rate performance of the communication system. In channels controlled by additive white Gaussian noise (AWGN) carrier recovery is able to provide high quality estimates, making coherent detection the most power efficient technique. However, in environments controlled by multipath fading, shadowing, phase noise, Doppler shifts or interference, the well established and extensively used carrier recovery techniques fail to produce highly reliable frequency and phase estimates. Even though the coherent receivers do not have any fundamental limitation, they fail to perform

well when they are used with low quality frequency and phase estimates. As a result, the communication system experiences significant degradations and suffers from high error floors [94], [86], [2], [238] (i.e. increasing the transmitted power does not reduce the BER below a certain value). It is clear that in order to operate efficiently with coherent detection under these impairments, some new more sophisticated and possibly more complex carrier recovery technology is needed. However, higher complexity usually results in higher cost, weight and size which are negative factors in WPDCS applications. Another problem with the coherent detection is the long acquisition time of the carrier recovery circuit [238], [12], [13], [70], [89]. This is a major disadvantage when the transmitted information is sent in bursts (e.g. packet data or voice activated digital speech), as fast acquisition is then needed to maintain high transmission efficiency [226], [122].

The fact that the channels we encounter in WPDCS applications experience the severe disturbances mentioned above led a considerable segment of the scientific society to consider and study non-coherent techniques for possible use in mobile and personal communications. The classical non-coherent detection schemes, in the form of envelope, differential or discriminator detection, are robust to fading [94]. Their acquisition times are shorted and their error floors are lower compared to the coherent system. Also, due to the fact that non-coherent schemes do not require carrier recovery, they achieve better and faster synchronization while maintaining reduced complexity and low implementation cost. At the same time, the length of preamble required by non-coherent systems is shorter, which increases the system capacity.

Another advantage of the non-coherent detection schemes is their suitability for use in spread spectrum communications. Due to their good time acquisition and synchronization properties, the non-coherent detection techniques are popular with direct sequence and frequency hoping spread spectrum systems [228]. These schemes have recently gained considerable popularity [257], and they are strong candidates for future cellular radio systems [127], [79], [212] indoor wireless communications systems [110], [111] as well as VSAT [192], [193], [194] and MSAT [188] applications. It is expected that spread spectrum techniques will be proven even more useful in the new personal communications services.

Even though the classical and well known non-coherent detection schemes

appear very promising for the aforementioned applications, there is still space for improvements in their performance. Because of the nature of the non-coherent detection, they suffer more from Gaussian noise than coherent schemes do. This behaviour becomes more pronounced in coded systems. In Chapter 4 we have presented cases where the coded differentially detected system performs worse than the uncoded differentially detected signal of equal spectral efficiency. The performance losses increase when the non-coherent (e.g. differential) receiver operates in the presence of colored noise or time dispersion [262]-[263]. Such conditions can arise when there is channel distortion (e.g. time dispersion) or in the presence of a narrowband interference. Elimination or even partial reduction of such losses is very beneficial, because this will directly translate to transceivers of reduced size and cost. It should also be pointed out that low power efficiency will lead to low capacity as well as expensive and large size systems, since it can lead to the need for use of larger antennas and power supplies (e.g. batteries) to sustain reliable operation of advanced WPDCS.

Over the last three decades or so, there has been a significant number of publications including textbooks (see for example [7], [214]) and technical papers (see for example [3], [33]-[34], [247], [116]-[120], [174]-[175], [180]-[181], [184], [210]-[211], [222], [230]-[234], [262]-[264], [265], [268]) which dealt with non-coherent detection. Based on the published literature, it is fair to state that so far, the research efforts related to the non-coherent detection have dealt almost exclusively with Phase Shift Keying (PSK) and Continuous Phase Modulation (CPM) signals. In addition, the various receivers proposed and analyzed, can be classified into differential (e.g. [222], [230]-[234], [262]-[264]) and limiter/discriminator (e.g. [33]-[34], [247], [120]) structures. However, it is well known that PSK and CPM signals are not the most appropriate modulation schemes for bandwidth efficient applications, where efficiencies of more than 2 bits-per-second-per-Hz (bps/Hz) are required (the North-American standard for cellular radio ($\frac{\pi}{4}$-QPSK) provides an efficiency of only 1.6 bps/Hz (48 Kbits/sec. in a 30 KHz channel bandwidth); also the modem designed for the MSAT-X experiment has an efficiency of 0.96 bps/Hz [104]). Perhaps, the best known technique to achieve high spectral efficiencies (and as a result increases the overall system capacity) is to employ Quadrature Amplitude Modulation [214], [60]-[63].

As compared to equivalent PSK systems, QAM schemes offer signifi-

cant power efficiency improvements. For example, for spectral efficiencies of 4b/sec/Hz and at a bit error rate (BER) of 10^{-5}, the performance of 16QAM is 5 dB better than an equivalent 16PSK system.

Considering today's wireless telecommunications need for higher spectral efficiency, QAM-type of signals could very well be the most appropriate solution to the congested spectrum problem. Nevertheless, so far, in the open technical literature, QAM-type of signals have not been considered in conjunction with an efficient non-coherent detection scheme. Such an approach is very promising, since it will maintain both, the high bandwidth efficiency and excellent performance of QAM schemes. At the same time it will provide the advantages associated with non-coherent detection which were mentioned earlier. Unfortunately, lack of available technology to apply non-coherent detection in QAM schemes could become a barrier preventing their use in these vital WPDCS services.

1.4 RESEARCH CONTRIBUTIONS OF THIS THESIS

Stimulated by the suitability of the non-coherent detection techniques to WPDCS and encouraged by the realization that there is still room for improvement, we directed our research efforts towards the development and provision of improved non-coherent technology capable to operate reliably and efficiently in the complex environment of the WPDCS channels. However, while in the past most of the work carried out treated the non-coherent schemes independently and without linking them, we have decided to follow another direction and examine the non-coherent detection in a unified fashion. The research tasks performed and the results obtained in this thesis can be summarized as follows.

1. The development of a unified non-coherent detection theory which provides the optimal[1] non-coherent receiver structures both in the symbol-by-symbol and sequence estimation sense. This theory is general enough

[1]The Maximum Likelihood Ratio Test (MLRT) is used through this work as criterion of optimality.

to accommodate the optimal non-coherent detection of linear (i.e. MPSK) and non-linear (i.e. CPM) modulation schemes as well as to include multi-amplitude/phase signals (QAM, Multi-Amplitude MSK (MA-MSK)). The receivers have been developed for ideal and time dispersive channels (material related to these contributions of the thesis has been published in [148]-[155]). It is important to point out that in the past, research on non-coherent detection has been performed rather on an "ad-hoc" approach and no serious effort has been reported in establishing a unified non-coherent detection theory. Through our work, the well-known and extensively analyzed conventional non-coherent detection techniques (e.g. 1 or 2-symbol differential detector and envelope detector) become specific examples of our unified theory.

2. Keeping in mind the importance of practicality and low cost/complexity, (whenever our work led us to complex, impractical structures) we applied reasonable approximations and simplifications which resulted in improved non-coherent receivers with reasonable levels of complexity and with performance close to the performance of the optimal configurations. Such schemes are the development of asymptotically optimal sequence estimators [148] - [155], combined envelope and multiple differential detection algorithms [145]-[148], [152] and simple symbol-by-symbol receivers which are based on decision feedback [161]-[165]. These reduced complexity structures which are applicable to both linear and non-linearly modulated signals resulted in significant performance improvements as compared to the conventional receivers. *In Gaussian channels they provided gains higher than 9 dB . In faded channels the improvements were higher than 11 dB; they also reduced the error floors more than three orders of magnitude.*

3. The development of a general framework for analytical evaluation of the proposed non-coherent receivers in AWGN, time dispersive and faded channels (published in [151]-[155]). The results have demonstrated that some of the proposed receivers asymptotically *achieve the performance of the coherent receiver which has perfect carrier reference and operates in an ideal channel*[2] *(best performance possible). In many cases,*

[2]We define as ideal channel, a channel with flat amplitude and linear phase characteristics, impaired only by additive white Gaussian noise.

the non-coherent receivers practically reach (or come very close to) this performance with very reasonable levels of complexity. As a result of the performance analysis, we were able to identify the non-optimality of the existing coding schemes (when used with the proposed non-coherent technology). We also provided new distance metric expressions (equivalent to the Euclidean distance, characterizing the performance of coherent systems) which can be used for the design of coding techniques appropriate for these non-coherent applications.

1.5 THESIS ORGANIZATION

Including this introductory chapter, this thesis consists of six chapters and 10 Appendixes.

In Chapter 2 an overview of the existing popular transmission and detection, as well as coding techniques, is presented. For the transmission, linear as well as continuous phase modulation signals are considered. For the detection component, coherent and non-coherent (i.e. differential, discriminator and envelope detection) are discussed. In the same chapter, an overview of the trellis coding, its differences and advantages as compared to the traditional coding schemes is also discussed.

Chapter 3 presents the generalized non-coherent detection theory and sets the background for the material covered in the following two chapters. It provides optimal non-coherent (symbol-by-symbol and sequence estimation) receivers in ideal or time dispersive channels both for (single or multi-amplitude/phase) linear and CPM signals.

Chapter 4 deals with linearly modulated signals. The objective of this chapter is to provide feasible receiver structures and present the background material for the analytical evaluation of the proposed schemes (in ideal, time dispersive as well as faded channels). Structures of receivers such as Asymptotically Optimal Decoders (AOD), block decoders, combined squared envelope and multiple differential detectors as well as decision feedback non-coherent symbol-by-symbol receivers are derived and presented. Uncoded as well as trellis coded schemes are considered and evaluated. Distance expressions for the pairwise error events (equivalent to the Euclidean distance

metric characterizing the performance of coherent systems) are provided. Our analytical results have shown that the proposed receivers reach asymptotically the performance of the coherent receiver (with perfect carrier synchronization, i.e. the best performance possible). In reality they reach these levels of performance with relatively simple structures. Evaluations carried out for various coded and uncoded schemes demonstrated *improvements in excess of 5.5 dB* in Gaussian channels. In faded channels we have verified *improvements in excess of 7 dB and reduction in error floors close to one order of magnitude.*

Chapter 5 extends the work of the previous two chapters to CPM signals. Asymptotically optimal (symbol-by-symbol and sequence estimation) receiver structures as well as practical low complexity symbol-by-symbol receivers and sequence estimators are derived and evaluated (both for Gaussian as well as faded channels). Evaluation carried out for these receivers has verified *improvements higher than 9 dB.* Also it has demonstrated the capability of these schemes to reduce the error floors experienced by the CPM signal when operating in a fast faded environment. The results demonstrated *reduction of error floors in excess of three orders of magnitude.*

Chapter 6 summarizes the material covered in this thesis and provides suggestions for further research related to this thesis topic.

Chapter 2

REVIEW OF TRANSMISSION, DETECTION AND CODING TECHNIQUES

This chapter will present an overview of a few major transmission, detection and coding techniques. More emphasis is put on the schemes which are encountered in this thesis.

2.1 TRANSMISSION

In this thesis we encounter two different types of communication systems. One is the class of linearly modulated signals. The other is the family of Continuous Phase Modulation (CPM) signals. The main characteristic of a CPM signal is the phase continuity it exhibits. This enables one to obtain good spectral characteristics, even under constant envelope signaling. It also provides some kind of encoding to the signal, which when appropriately exploited, offers some improvements in bit error rate (BER) performance

[202]. At the same time, the constant envelope nature of the CPM signal makes possible the use of power efficient class-C non-linear amplifiers without suffering from signal distortion or sidelobe regrowth problems due to non-linear amplification.

2.1.1 Linear Modulation

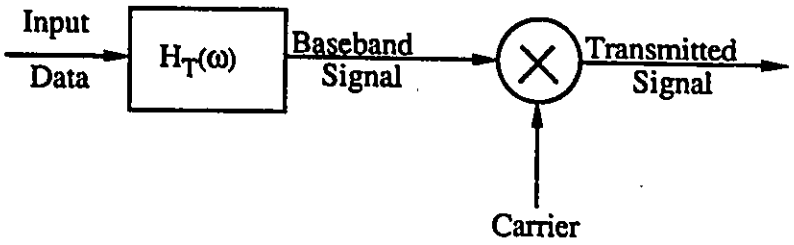

Figure 2.1: Block diagram of the linear transmitter.

The model of the transmitter for a linear modulation scheme is presented in Fig. 2.1. The input to the modulator is a data sequence. The data sequence is passed through a premodulation low pass filter $H_T(\omega)$, in order to obtain the desired spectral shaping. The output of $H_T(\omega)$ is a baseband signal. This signal is transferred to high frequencies, by modulating a carrier signal. The outcome of the modulation is the transmitted signal.

2.1.2 Continuous Phase Modulation

The block diagram of a CPM transmitter is shown in Fig. 2.2. The data sequence enters the premodulation lowpass filter $H_T(\omega)$. The purpose of $H_T(\omega)$ is to shape the data spectrum, in order to control the spectral occupancy of the transmitted signal. At the same time, it affects the power efficiency. Usually, spectrally efficient schemes have inferior power efficiency, and vice

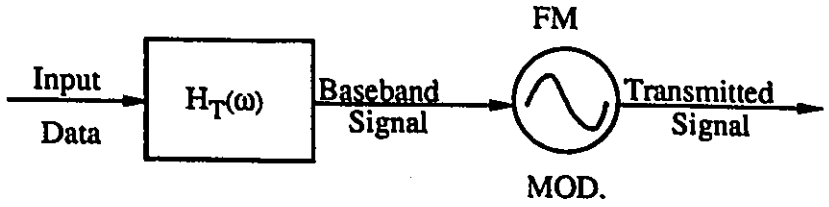

Figure 2.2: Block diagram of the CPM transmitter.

versa. Consequently power efficiency is traded for spectral efficiency. By regulating $H_T(\omega)$, different CPM schemes as Minimum Shift Keying (MSK) [60], Duobinary MSK [12], Gaussian MSK (GMSK) [191], Tamed Frequency Modulation (TFM) [103], Generalized TFM (GTFM) [34], etc. can be obtained. The baseband CPM signal modulates a carrier generated by a Voltage Controlled Oscillator (VCO). The modulation index of the VCO is important because it affects the performance in terms of spectral and power efficiency of the entire system, and in some cases, even the complexity of the receiver.

The block diagram of the CPM transmitter shown in Fig. 2.2 is more of a conceptual one. For implementation purposes, CPM transmitters based on look-up table techniques [33] and use of Digital Signal Processors are more suitable because they offer reduced complexity, reduced cost, higher reliability and flexibility. At the same time, the problems of frequency drifts (experienced by VCOs which lead to the need of feedback control circuits to control the carrier frequency) can be avoided. The disadvantage is that the power spectrum of CPM signals, generated through look-up table techniques, appears with elevated power levels at the sidelobes and a slightly reduced mainlobe. This comes as consequence of the truncation which is applied on the impulse response of the lowpass filter [34]. As a results, the level of the adjacent channel interference increases and some distortion appears on the signal. However, the spectral distortion is usually small enough, that does not create serious degradation to the communication system and the adjacent communication channels.

2.2 DETECTION TECHNIQUES

The digital signals can be detected coherently or non-coherently. In this section, the most popular detection techniques and their properties are reviewed.

2.2.1 Coherent Detection

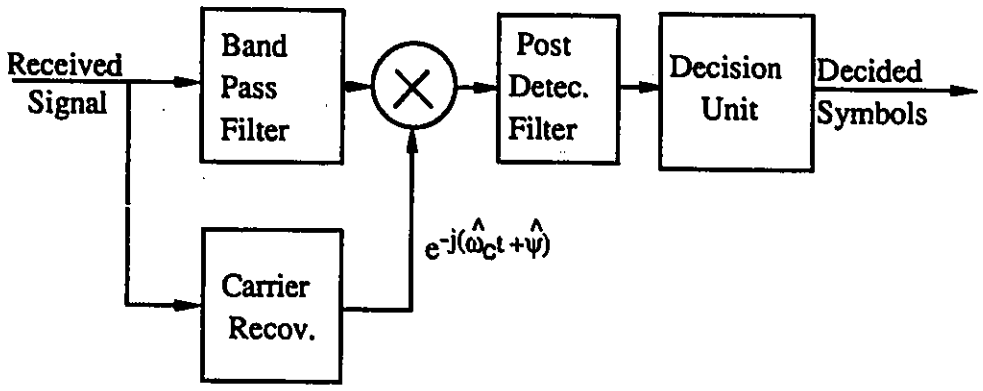

Figure 2.3: Block diagram of the coherent receiver.

The block diagram of a generic coherent detection system is presented in Fig. 2.3. The coherent detector uses an estimate of the carrier as a reference to demodulate the received signal. The carrier estimate is provided through the carrier recovery (CR) unit where $\hat{\omega}_c$, $\hat{\psi}$ are the estimates of the (radian) carrier frequency ω_c and carrier phase ψ respectively. After the signal has been demodulated, it is passed through a post detection filter. After filtering, it is appropriately sampled (usually at the symbol rate) and the samples are fed to the Decision Unit to make the decision regarding the transmitted data.

The coherent detector is ideally suited for operation in additive Gaussian noise controlled channels. However, in faded channels or in the presence of severe phase noise, it is difficult to obtain and maintain a good phase

estimate. The phase error coming from these disturbances generates high error floors [70].

Coherent receivers experience long acquisition times, especially for narrowband signals [238], [13], [14], [70], [89]. One of the methods for generating the carrier estimate is from tones (generated by applying non-linear processing to the received signal) which carry information regarding the carrier. These tones are extracted by using narrowband filters or phase lock loops (PLL) [74]. However, as the signal becomes narrower, the bandwidth of the extraction filter (or the PLL) has to be reduced in order to lower the levels of pattern noise passing through the filter (pattern noise increases with an increase in the spectral efficiency of the system; this forces the need to reduce the bandwidth of the extraction filter in order to maintain a good quality estimate of the carrier). Reduction of the loop bandwidth increases the acquisition time of the filter [74]. This becomes a serious problem when burst transmission is used (e.g. packet data or voice activated digital speech), as fast acquisition is then needed to achieve high transmission efficiency [226], [122].

One way to relax the carrier recovery requirements and improve the Bit Error Rate (BER) performance of the coherent receiver (experiencing adverse phase variations) is to transmit a separate (pilot tone) signal along with the information bearing one. Several such schemes have been described in the literature [178], [260], [272], [144], [43], [16], [41], [229]. Some of these techniques require additional bandwidth, (e.g. [178], [16], [41]), while all of them require more power than the conventional coherent detection.

2.2.2 Non-coherent Detection

In non-coherent detection, the phase coherence requirement is either relaxed or completely removed. Popular non-coherent detection schemes are differential detection [214], discriminator detection [247] and envelope detection [214]. A common characteristic of all these non-coherent detection schemes is that they do not require recovery of the carrier phase. This relaxes the need for complex carrier recovery circuits, and eliminates the problems associated with the carrier recovery (i.e., high error floors, long acquisition times). A brief description of the three aforementioned non-coherent detection tech-

niques follows.

2.2.2.1 Differential Detection

When differential detection is used[1], the information is encoded into the phase change (i.e., the difference) between two successive symbols rather than the absolute phases. At the receiver, the signal is demodulated by generating the phase difference between the successive symbols, or by comparing the phases between two (usually consecutive) received signal samples. The block diagram of the two implementations (generating the phase difference and comparing the phases) are presented in Fig. 2.4 (a), (b) respectively. The signal delay element in the most conventional systems is equal to the symbol period [214]. However, a number of differential receivers with delay elements different than the symbol period have been proposed in the past [8], [230]. The choice of the size of the delay element depends on the modulation format of the signal [230] or the channel behaviour [8]. Successful choice of the delay element may provide improvements, compared to the one-symbol differential detector.

By avoiding the carrier recovery, the differential detector has faster synchronization, usually exhibits lower error floors in flat faded channels and requires less hardware complexity than the coherent detector. Examples of commercially available systems using differential detection can be found in [17], [29], [23]. Differential detection is a good candidate for use in optical communications [223] as well as mobile and portable radio. Differential detection has also a very good possibility to be used in the new North American and Japanese standards of cellular digital radio (the modulation technique is $\pi/4$-QPSK [4], [65], [131], [132], [133], [108]). Also the National Aeronautics and Space Administration (NASA) of U.S.A. has adopted differential detection to be used in its Mobile-Satellite experiment (MSAT-X) project, with the objective to transmit 4800 bits/sec. of digital speech over 5 KHz channels [231], [230], [45], [234], [104].

[1] Differential detection is also often referred to as differentially coherent detection. Differential detection should not be confused with differentially encoded coherent detection. The latter method is a coherent demodulation technique where carrier recovery is mandatory, and the purpose of the differential encoding is only to avoid a phase ambiguity in the recovered carrier.

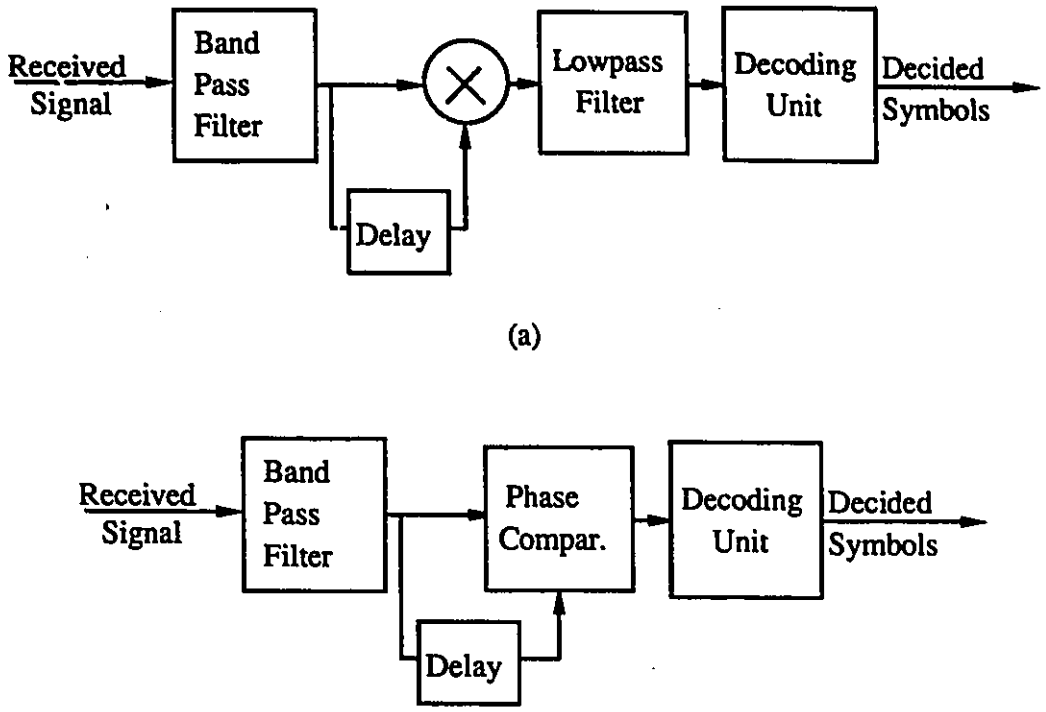

Figure 2.4: Block diagram of the differential receiver. Demodulation by: (a) generating the phase difference through multiplication; (b) comparing the phases between received signal samples.

2.2.2.2 Discriminator Detection

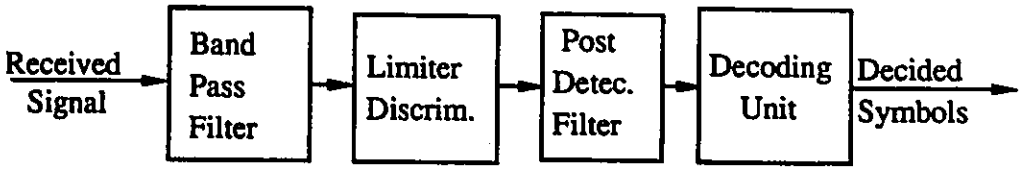

Figure 2.5: Block diagram of the limiter-discriminator detector.

Another form of non-coherent detection is the limiter-discriminator detection [247]. The block diagram of the limiter-discriminator detector is presented in Fig. 2.5. The receiver consists of a (predetection) bandpass filter followed by a limiter-discriminator and a post detection filter. The bandpass filter limits the noise levels, in order to reduce the appearance of "clicks" [208] from the output of the limiter-discriminator. The actual demodulation is performed by the limiter-discriminator circuit. The post detection filter applies the final stage of spectral shaping on the information signal, and reduces the levels of the quadratic noise [124] present at the output of the limiter discriminator. Depending on the characteristics of the transmitted signal, and the performance and complexity requirements, the post detection filter can either be an Integrate Sample and Dump (ISD) circuit [273] or a lowpass filter. The output of the filter is sampled and processed in order to recover the transmitted information.

The discriminator detection is characterized by very low hardware complexity and low error floors (lower than the error floors exhibited by differential detection). Also, its extensive use in the past for analog signal transmission in broadcasting [27], [101], [115], [123], [142], [177], [183], [198], [245], [261] as well as in microwave [20], [62], [66],[67], [68], [80], [248] technology, has made it a well known and well established technique in the communications industry.

Compared to a coherent and differential detector, the discriminator detector is the least sensitive to random FM [126] and frequency offsets [95],

[120], [217], [247], [265]. In flat faded channels it performs considerably better than coherent and fairly better than differential detection. Its weak point is the poor performance in co-channel interference environments [94], [26] (a serious problem in cellular mobile radio). Also, it suffers performance losses when delay distortion appears in the channel [18].

2.2.2.3 Envelope Detection

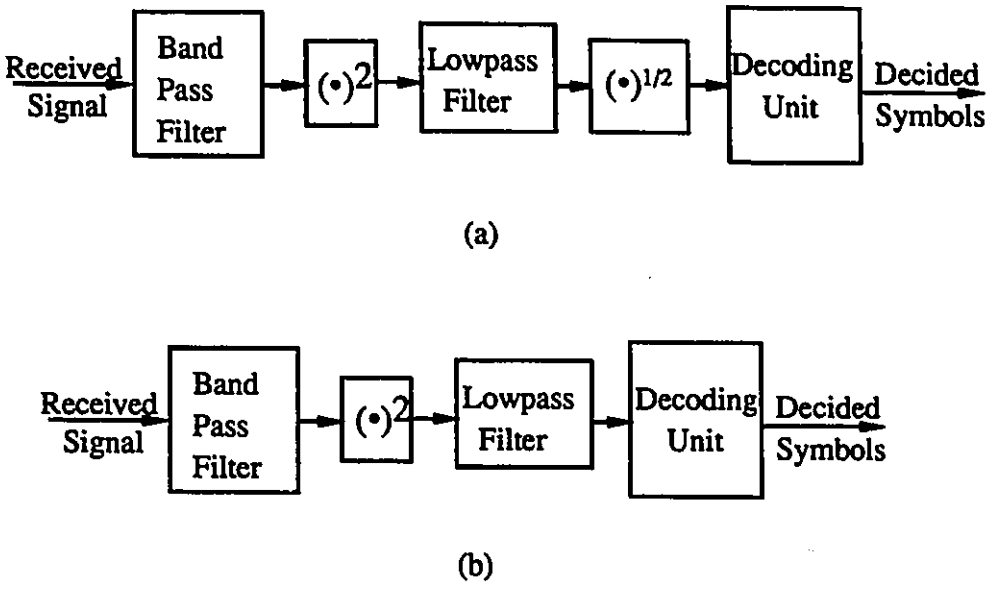

Figure 2.6: Block diagram of the (a) envelope and (b) squared envelope detector.

The block diagrams of the envelope and squared envelope detectors are presented in Fig. 2.6. The envelope and squared envelope detectors decode the information based on the envelope or squared envelope values of the received signal [214]. In a single channel communication system, their performance is identical [214]. They consist of a bandpass filter (which passes the infor-

mation signal and reduces the noise levels), a squaring device followed by a lowpass filter, a square rooting device (needed only for the envelope detector) and the decoding unit. The task of the lowpass filter is to reject the high frequency component from the squared signal and reduce the noise content of the baseband signal before it is used to decide the data sequence.

The technique is simple in terms of implementation (low complexity). Because of its nature, it is relatively insensitive to phase noise, frequency shifts (as for example Doppler shifts [126], [231]) and frequency offsets as compared to coherent and differential detection. Also, it is the least sensitive to multipath fading (especially fast fading), among all the techniques examined in this section. This is clear if we consider that the major problem of fast fading, the error floors, is due to the phase fluctuations to which the envelope detector is absolutely insensitive. In the past, squared envelope detection has been used to develop infrared remote control systems. Also, in indoor wireless applications [19], [76], [77] [78] and in optical communications (in the form of direct detection [109]).

2.3 TRELLIS CODED MODULATION

In this section, a brief description of the trellis coded modulation (TCM) is presented. The principles of TCM, as well as its main differences and advantages over the classical coding schemes is given.

2.3.1 Conventional Coding versus Trellis Coding.

In the conventional communication systems, the functions of modulation and error correction coding are treated separately. The encoders and decoders provide error correction on a discrete channel. The encoder transforms a word of k information bits into one of n bits ($n > k$), introducing a redundancy of $n - k$ bits (k/n rate code). The modulator converts the output of the encoder to an analog waveform, treating all the bits as equiprobable and independent (not a correct assumption since encoding and redundancy have been introduced). At the receiver, the demodulator performs the reverse operation. It makes decisions regarding the transmitted sequence without considering the coded nature, and provides a bit stream to the decoder. The decoder's task is to regenerate the redundant bits of the bit stream and check them with the ones which have been received. If a discrepancy exists, the decoder selects the message sequence which differs in the smallest number of bits from the received ones. Since the decoder operates only on discrete words and decides, based on the number of bits, that each possible transmitted sequence differs from the received one, it is clear that the quality of the code (i.e the performance improvements it offers) can be measured by the Hamming distance d_m^H (the number of bit positions in which two valid encoded sequences differ). The code can correct at least $[\frac{d_{min}^H - 1}{2}]$ codeword errors, where d_{min}^H is the minimum Hamming distance (also called "free Hamming distance") and $[\cdot]$ represents the largest integer number which is smaller than or equal to $\{\cdot\}$. Consequently, when designing a code to be used with a receiver, applying decoding in the conventional sense, (i.e. using hard decision detection prior to the decoding), our effort should be to maximize the minimum Hamming distance for a given degree of complexity.

The insertion of redundant bits in the data stream reduces the information rate of the system. To compensate this, we have two options.

1) Increase the transmission rate when power constraint is present.

2) Enlarge the signal set when bandwidth constraint is present (i.e. make the signal constellation denser).

Unfortunately, the corresponding decrease in noise immunity (created by the denser signal constellation) overcomes most of the potential advantage offered by the coding gain. A characteristic example reflecting this case, is presented in [252], where a 2/3 convolutional code with constraint length 6 and $d^H_{min} = 7$ has actually almost the same performance with the simple uncoded QPSK.

2.3.2 Why is Trellis Coding needed?

The factors limiting the performance of the coded system presented above is the "hard decisions" detection strategy used with the received signal. This jeopardizes useful information. The performance can be improved by applying soft decision decoding. In this case, a set of sufficient statistics (i.e. a set of processed signal samples) is generated. Afterwards, the decoder searches among all code sequences which have been produced by the cascade of encoder and modulator, for the ones with the minimum Euclidean distance from the received signal [251], [252], [253], [73]. This decoding procedure (i.e search over all possible coded sequences) can be performed using the Viterbi algorithm [256],[71], [72],[227]. A brief description of its operation follows.

The decoder stores the path of the most likely state transitions leading up to each possible state. Each path's history is associated with a possible symbol sequence and the corresponding metric represents the distance of the coded sequence from the received signal information (being available up to that point). With each new received symbol, all possible extensions of the stored paths are considered. The algorithm chooses the best of the possible paths (i.e the closest to the received signal information) towards each of the states of the decoder, and discards the rest. Afterwards, the decoder searches back through the path histories and makes the final decision (in practice, the path histories are truncated to a finite length, with minor loss in performance [71], [72]). Today, other families of algorithms such as the stack and M-algorithms [227], [36], [106], [107], [186], [187] have also been used with trellis coded systems. These algorithms trade performance efficiency in

exchange for reduction in complexity.

As mentioned earlier, by applying soft decision decoding, the choice of the transmitted sequence is done based on the minimization of the Euclidean distance. Consequently, when soft decision decoding is applied, our effort should be to develop codes with as large Euclidean distance between the different data sequences, as possible. More specifically, the design criterion in this case should be to develop codes whose minimum distance between information sequences is as large as possible for a given level of complexity. This represents the milestone in the concept of trellis coding, and the designing principle of good trellis codes (for additive white Gaussian noise channels and systems using coherent detection).

The conclusion drawn from the discussion presented in the previous paragraph is that when preservation of bandwidth efficiency is required, the development of the codes should be done on the grounds of maximizing the free Euclidean distance between codewords. Also, the redundancy necessary for coding should be inserted in such a way, that does not generate bandwidth expansion for the system.

The concept of "Euclidean distance" is closely connected to the assignment of the signal points in the constellation, arranged by the modulator. Consequently, since the "Key point" in the code design is the maximization of the "free Euclidean distance", we realize that in trellis coding, the coding and modulation processes should not be treated as independent functions any more, but in unison and as an entity. In the following section, we shall present the basic principles of TCM and see how the assignment of points from the signal constellation to the transmitted symbols (called set partitioning) should be done in order to offer performance improvements.

Ungerboeck, in his pioneering work [251], has concluded that by doubling the number of channel signals, most of the coding gain in terms of channel capacity, can be achieved. Therefore, at the first stages, the effort on trellis coding was concentrated on finding signal sets of size 2^{m+1} for the transmission of m bits per modulation interval. Later on, other works appeared and demonstrated ways to develop combined coding and modulation schemes which achieve high gains with low complexity [271].

2.3.3 The principles of TCM

The approach followed to maximize the free Euclidean distance is based on a mapping rule called "mapping by set partitioning". The mapping follows the successive partitioning of a channel signal set into subsets with increasing minimum subset distances $[\Delta_o < \Delta_1 < \Delta_2, ...]$ between the signal and the subsets. After the selection of a suitable trellis state transition diagram, one has to assign channel signals from the extended signal set to the state transitions, in a way to achieve maximum free Euclidean distance.

The first TCM schemes were developed by Ungerboeck [251]. The development was done in a heuristic manner, and certain rules were developed to assign the channel signals from various subsets to the state transitions. These are the following:

1) When parallel transitions in the trellis diagram exist, they should be associated with points in the constellation which have the maximum Euclidean distance possible between them.

2) Transitions originating from or merging into the same state should be associated with signals at the next subset level in the partition.

3) All available channel signals should occur with equal frequency and with a fair amount of regularity.

In the years that followed Ungerboeck's work as presented in [251], a great deal of work was done on trellis coding. The concept of multidimensional trellis coding [75], [271] was introduced and demonstrated. The multidimensional trellis codes can perform better than 2-dimensional trellis coded schemes, under the same level of complexity. Also, rotationally invariant codes were developed through the years, to relax the carrier recovery requirements [269]-[271] (trellis coded systems are vulnerable to phase errors generated by inaccuracies in the carrier estimate [253]). Later on, in [46] it was shown that the use of asymmetric signal constellations with trellis coded schemes results in performance improvements.

Recently, another important research area in TCM is the development of powerful trellis codes for fading environments. Simon and Divsalar in [233], [234] presented distance expressions which characterize the performance of the trellis coded schemes in fading environments. From their results, it was

made clear that in fading channels, the most important factor influencing the performance is the length of the error events. Taking this into consideration, they proposed trellis codes suitable for fading channels [47]-[50] .

2.3.4 Performance of the Trellis Coded Schemes with Non-Coherent Detection

In Section 2.3.3, it was mentioned that the design criterion for trellis codes was the maximization of the "free" Euclidean distance. This metric is associated with the Viterbi algorithm operating in an additive white Gaussian noise environment. However, the optimality of the Viterbi decoder in the maximum likelihood sense is limited to the case of coherent detection in AWGN controlled environments. When coherent detection is not used or the channel is controlled by other impairments such as fading, interference, etc., the Viterbi decoder does not represent the optimum solution for maximum likelihood sequence estimation. In this case, other metrics provide the optimal solution (in this thesis, the optimal non-coherent sequence estimators have been derived and will be provided in the following chapters (for the non-coherent detection see [148]-[155] ; for the optimal sequence estimation in fast/slow faded channels, see [166], [167]). At the same time, the performance of the coded system is not characterized any more by the "free Euclidean distance" since the statistical behaviour of the noise disturbance is different from being Gaussian (through the research work presented in this thesis, the new distance expressions which characterize the performance of the non-coherent receivers have been identified and presented, see also [151]-[155]). As a result both the trellis encoder as well as the decoder (which are optimized for coherent detection systems operating in AWGN controlled channels) do not represent optimal solutions for the non-coherent detection case[2]. This results in considerable performance losses.

In order to give the reader an idea on how significant these losses can be, we provide the following example. One of the trellis coded modulations which is examined in the fourth chapter of this thesis is an 8PSK 4-state 2/3 rate

[2]Our research results proved this claim; they also identified the distance expressions which should be used in the design of optimal trellis codes for non-coherent detection systems.

trellis code. When coherently detected, this scheme is 1.15 dB superior as compared to coherent uncoded QPSK. However, when differentially detected, it becomes 0.8 dB worse than the uncoded differential QPSK. Differential QPSK is approximately 2.3 dB inferior compared to coherent QPSK. This gives a total of $(1.5 + 2.3 + 0.8) = 4.6$ dB degradation, its only source being the use of differential detection. This amount of performance degradation is serious for power limited applications as the mobile-satellite or personal communications and dictates the need to design new codes which will be able to perform well when they are used with non-coherent detection techniques.

The considerable losses suffered by the trellis coded schemes when non-coherently detected and the need for high power efficiency were one of the driving forces that led to the work which will be presented in the following three chapters. The approach followed resulted in the development of optimal and asymptotically optimal receivers, able to recover the losses suffered by the trellis coded schemes when used with non-coherent detection techniques.

Chapter 3

GENERALIZED NON-COHERENT DETECTION THEORY

3.1 INTRODUCTION

The objective of this chapter is to set the groundwork for the derivation of practical, improved non-coherent receivers, which will be proposed in the next two chapters. First, a generalized non-coherent detection theory will be presented. The structures will be general enough to address linear and Continuous Phase Modulation signals in a unified way. It also extends the notion of optimal non-coherent detection to multi-amplitude/phase signals and to systems operating in time dispersive channels.Through the analysis, the optimal non-coherent sequence estimators and symbol-by-symbol receivers will be presented. In the forthcoming chapters we shall see how these general structures can lead to reasonably complex non-coherent receivers capable of offering considerable gains in performance.

The benefit from this work is twofold. First, the introduction of improved non-coherent receivers to time dispersive channels makes the use of

power efficient non-coherent schemes with WPDCS operating in time dispersive environments possible (examples are the cellular mobile radio, indoor wireless communications etc., see publications [148], [151]-[155]). Also, the introduction of non-coherent detection to spectrally efficient multi-amplitude signals (i.e. Quadrature Amplitude Modulation (QAM) [214]) makes the development of spectrally/power efficient schemes which are also robust to synchronization errors possible (see publications [149], [150], [21]). Such schemes can be used to provide the much needed higher spectral efficiency to applications operating in environments with potential synchronization problems (e.g. mobile-satellite communications, cellular mobile radio etc.).

Some earlier works considering optimal non-coherent detection can be found in [254], [202], [13], [14], [7][1]. In [254], the optimal non-coherent detector for binary communications is given. In [202], the optimal non-coherent symbol-by-symbol receiver for binary CPM signals is presented. In [13], [14], [7], the non-coherent sequence estimator for CPM is provided. However, in these works, there is no consideration of a time dispersive channel behaviour or use of multi-amplitude signals. They are also limited to CPM signals. In the present chapter, the generalized optimal non-coherent detection framework does not only treat linear modulation systems as well, but it also addresses the multi-amplitude phase signals and the time dispersive channels.

The remainder of this chapter will be presented as follows. In Section 3.2, the general model of the communications system is presented and the optimal maximum likelihood receivers both for sequence estimation as well as symbol-by-symbol detection are provided. In Sections 3.3 and 3.4, the results of 3.2 are applied to linear modulation and CPM systems respectively. The highly complex filtering required by the optimal non-coherent CPM receivers, has forced us to consider in section 3.5 an alternative approach for the development of non-coherent receivers, based on signal decomposition using Amplitude Modulated Pulses (AMP) [125]. Through this approach we reach optimal non-coherent receivers for CPM signals, with considerably lower filtering requirements. Section 3.6 concludes the present chapter.

[1] In [254], [13], [14], [7] the concept of the partially coherent detection is treated. Non-coherent detection can be seen as a special case of the partially coherent receiver.

3.2 THE OPTIMAL NON-COHERENT MAXIMUM LIKELIHOOD RECEIVER

3.2.1 Model of the Communication System

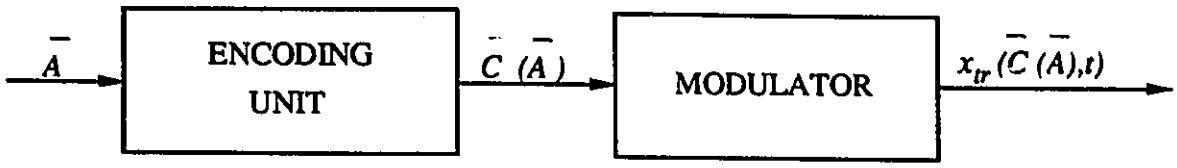

Figure 3.1: Block diagram of the transmitter.

The block diagram of the transmitter for the communication system under consideration is presented in Fig. 3.1. Here we have attempted to provide a generalization of the model, in order to be able to represent the various types of signal formats which will be examined throughout this thesis.

In terms of functionality, the transmitter can be separated into two different parts. The first is the encoding unit and the second one is the modulator. The task of the encoding unit is to translate the information sequence

$$\bar{A} = [\bar{a}_1^p, ..., \bar{a}_{Z-1}^p] \tag{3.1}$$

into a sequence of symbols

$$\bar{C}(\bar{A}) = [c_0, c_1, ..., c_{Z-1}] \tag{3.2}$$

where c_k is of complex nature.

$\bar{a}_k^p$ represents the p-bit word

$$\bar{a}_k^p = [a_k^1, a_k^2, ..., a_k^p] \tag{3.3}$$

with a_k^l being binary ($a_k^l \in \{0,1\}, 1 \leq l \leq p$). The p-bit words $\bar{a}_k^p$ are independent, equiprobable and uncorrelated to each other. Each $\bar{a}_k^p$ word can

have one out of $M_p = 2^p$ different combinations. The i^{th} of these combinations ($0 \leq i \leq M_p - 1$) is represented as

$$\bar{S}_i = [s_1^i, s_2^i ..., s_p^i] \tag{3.4}$$

($s_l \in 0, 1$ and $i = \sum_{\eta=1}^{p} 2^{\eta-1} s_\eta^i$, $0 \leq i \leq M_p$) forming the set $\underline{S}$.

The encoding unit might perform a set of different functions such as convolutional encoding and differential encoding. More descriptive information will be provided in the following sections.

The modulator can be either of linear or FM-type (for the CPM schemes). Its output is the signal $x_{tr}(\bar{C}(\bar{A}), t)$, expressed through the following equation:

$$x_{tr}(\bar{C}(\bar{A}), t) = R_{tr}(\bar{C}(\bar{A}), t) e^{j(\omega_c t + \phi_{tr}(\bar{C}(\bar{A}), t) + \psi)} \tag{3.5}$$

where $R_{tr}(\bar{C}(\bar{A}), t)$ is the envelope of the transmitted signal, ω_c is the carrier frequency, $\phi_{tr}(\bar{C}(\bar{A}), t)$ is the phase of the information-carrying signal and ψ is the initial phase of the modulator.

An alternative way of expressing $x_{tr}(\bar{C}(\bar{A}), t)$ is

$$x_{tr}(\bar{C}(\bar{A}), t) = x_{tr,B}(\bar{C}(\bar{A}), t) e^{j(\omega_c t + \psi)} \tag{3.6}$$

where

$$x_{tr,B}(\bar{C}(\bar{A}), t) = R_{tr}(\bar{C}(\bar{A}), t) e^{j(\phi_{tr}(\bar{C}(\bar{A}), t))}. \tag{3.7}$$

$x_{tr,B}(\bar{C}(\bar{A}), t)$ is the complex baseband representation of the transmitted signal and depends on the signal format used (i.e., PSK, QAM, CPM, etc.).

Since non-coherent detection is considered, ψ is unknown to the receiver, and will be treated as a random variable. In our analysis, we model ψ as uniformly distributed in the $(0, 2\pi)$ interval. Its probability density function $p(\psi)$ is equal to

$$p(\psi) = \begin{cases} \frac{1}{2\pi} & \text{for } 1 \leq \psi \leq 2\pi \\ 0 & \text{elsewhere.} \end{cases} \tag{3.8}$$

This distribution generates the highest uncertainty for the system [214].

3.2.2 Derivation of the Optimal Non-Coherent Receiver

We assume that our channel is corrupted by additive white Gaussian noise (AWGN) with a one-sided power spectral density of N_o. The signal $x_r(t)$ at the input of the receiver can be expressed as:

$$x_r(t) = x(\bar{C}(\bar{A}), h_c(t), t) + n_w(t) = R_r(t)e^{j(\omega_c t + \theta(t))} \tag{3.9}$$

where $n_w(t)$ is the additive white Gaussian noise component and

$$x(\bar{C}(\bar{A}), h_c(t), t) = x_{tr}(\bar{C}(\bar{A}), t) \otimes h_c(t) \tag{3.10}$$

represents the transmitted signal, after it has passed through the channel. $h_c(t)$ is the impulse response of the channel and $\otimes$ defines the convolution operation. $R_r(t)$, $\theta(t)$ are the envelope and phase of $x_r(t)$.

Alternatively, $x(\bar{C}(\bar{A}), h_c(t), t)$ can be expressed as

$$x(\bar{C}(\bar{A}), h_c(t), t) = x_B(\bar{C}(\bar{A}), h_{c,B}(t), t)e^{j(\omega_c t + \psi)} \tag{3.11}$$

with

$$x_B(\bar{C}(\bar{A}), h_{c,B}(t), t) = x_{tr,B}(\bar{C}(\bar{A}), t) \otimes h_{c,B}(t) \tag{3.12}$$

and

$$h_{c,B}(t) = h_c(t)e^{-j\omega_c t} \tag{3.13}$$

being the baseband equivalents of the signal $x(\bar{C}(\bar{A}), t)$ and channel response $h_c(t)$ respectively.

The conditional probability density function (pdf) of $x_r(t)$ conditioned on $x_B(\bar{C}(\bar{A}), h_{c,B}(t), t)$ and ψ, is given by[2]

$$f(x_r(t)/x_B(\bar{C}(\bar{A}), h_{c,B}(t), t), \psi)) =$$

[2]The integral $\int_{t_L}^{t_U} |x_r(t) - x_B(\bar{C}(\bar{A}), h_{c,B}(t), t)e^{j(\omega_c t + \psi)}|^2 dt$ gives the squared Euclidean distance between the received signal $x_r(t)$ and the $x_B(\bar{C}(\bar{A}), h_{c,B}(t), t)$.

$$K_c \exp\{-(\frac{1}{2N_o}\int_{t_L}^{t_U} |x_r(t) - x_B(\bar{C}(\bar{A}), h_{c,B}(t), t)e^{j(\omega_c t+\psi)}|^2 dt)\} =$$

$$K_c \exp\{-(\frac{1}{2N_o}\int_{t_L}^{t_U} |x_r(t)|^2 dt)\} \exp\{-(\frac{1}{2N_o}\int_{t_L}^{t_U} |x_B(\bar{C}(\bar{A}), h_{c,B}(t), t)|^2 dt)\}$$

$$\exp\{\frac{1}{N_o}(\int_{t_L}^{t_U} (x_r(t)x_B^*(\bar{C}(\bar{A}), h_{c,B}(t), t)e^{-j(\omega_c t+\psi)}$$

$$+x_r^*(t)x_B(\bar{C}(\bar{A}), h_{c,B}(t), t)e^{j(\omega_c t+\psi)})dt)\}$$

(3.14)

where K_c is a constant and t_L, t_U represent the limits of the time interval where the transmitted signal appears. Their values depend on the spreading of the signal $x_B(\bar{C}(\bar{A}), h_{c,B}(t), t)$ in the time domain.

$f(x_r(t)/x_B(\bar{C}(\bar{A}), h_{c,B}(t), t))$ can be calculated from Eq.(3.14) through integration, i.e.,

$$f(x_r(t)/x_B(\bar{C}(\bar{A}), h_{c,B}(t), t)) =$$

$$\int_0^{2\pi} f(x_r(t)/x_B(\bar{C}(\bar{A}), h_{c,B}(t), t), \psi)p(\psi)d\psi =$$

$$\frac{1}{2\pi}\int_0^{2\pi} f(x_r(t)/x_B(\bar{C}(\bar{A}), h_{c,B}(t), t), \psi)d\psi. \qquad (3.15)$$

Combining Eq.(3.14), Eq.(3.15), $f(x_r(t)|x_B(\bar{C}(\bar{A}), h_{c,B}(t), t))$ becomes:

$$f(x_r(t)/x_B(\bar{C}(\bar{A}), h_{c,B}(\tau), t)) =$$

$$K_c \exp\{-(\frac{1}{2N_o}(\int_{t_L}^{t_U} |x_r(\tau)|^2 d\tau)\} \exp\{-(\frac{1}{2N_o}(\int_{t_L}^{t_U} |x_B(\bar{C}(\bar{A}), h_{c,B}(t), \tau)|^2 d\tau)\}$$

$$I_0\left(\frac{\left|\int_{t_L}^{t_U}(x_r(t)e^{-j(\omega_c t)})x_B^*(\bar{C}(\bar{A}),h_{c,B}(t),t)dt\right|}{N_o}\right) \tag{3.16}$$

where $I_0(x)$ represents the modified Bessel function of zero order[3]. In Eq. (3.16), the following identity has been used.

$$I_0(2|\epsilon|) = \frac{1}{2\pi}\int_0^{2\pi}\exp\{\epsilon e^{-j\psi} + \epsilon^* e^{j\psi}\}d\psi \tag{3.17}$$

with ϵ representing a complex number.

3.2.2.1 Sequence Estimation

The maximum likelihood sequence estimator should choose as a most likely sequence, the one which maximizes the $f(x_r(t)/x_B(\bar{C}(\bar{A}),h_{c,B}(t),t))$. Since the term $(\int_{t_L}^{t_U}|x_r(t)|^2dt)$ is independent from the transmitted sequence $\bar{C}(\bar{A})$, it can be removed from the decoding process. Considering this, we end up with the following expression (to be maximized):

$$\begin{aligned}&\aleph_{ge}(x_r(t),x_B(\bar{C}(\bar{A}),h_{c,B}(t),t)) = \\ &\exp\{-(\tfrac{1}{2N_o}(\textstyle\int_{t_L}^{t_U}|x_B(\bar{C}(\bar{A}),h_{c,B}(\tau),\tau)|^2d\tau)\} \\ &I_0\left(\frac{\left|\int_{t_L}^{t_U}x_r(\tau)e^{-j(\omega_c\tau)}x^*(\bar{C}(\bar{A}),h_{c,B}(\tau),\tau)d\tau\right|}{N_o}\right).\end{aligned} \tag{3.18}$$

$\aleph_{ge}(x_r(t),x_B(\bar{C}(\bar{A}),h_{c,B}(t),t))$ is the metric of the optimal non-coherent sequence estimator (expressed in general form).

3.2.2.2 Symbol-by-Symbol Detection

Let us assume that we want to decide the information word $\bar{a}_k^p$. As it was mentioned earlier, the bit combination of $\bar{a}_k^p$ generates one of the M_p different elements, members of $\underline{S}$. The optimal symbol-by-symbol receiver is the one that decides according to the following maximization process :

$$\widehat{\bar{a}_k^p} = \bar{S}_l \implies \overset{1\le l\le M_p}{max}\{\sum_{\bar{C}(\bar{A})\in\underline{C}_{\underline{S}}^{\bar{S}_l}(k)} f(x_r(t)/x_B(\bar{C}(\bar{A}),h_{C,B}(t),t))\} \tag{3.19}$$

[3]For the definition of the Bessel function(s) please refer to [1, p.376].

In Eq.(3.19) we take the average over all the $\bar{C}(\bar{A})$ that can result from $\bar{a}_k^p = \bar{S}_l$ regardless of adjacent words. $\Longrightarrow$ stands for *"which gives"*. $\underline{\mathcal{C}}_{\underline{S}}^{S_l}(k)$ represents the set having as members all codewords $\bar{C}(\bar{A})$ which are generated by an information sequence $\bar{A}$ having $\bar{a}_k^p = \bar{S}_l$. $\bar{S}_l$ is one of the bit combinations, the information word $\bar{a}_k^p$ can take. Every set $\underline{\mathcal{C}}_{\underline{S}}^{S_l}(k)$ has a total of $(M_p 2^{Z-2})$ members. $\widehat{\bar{a}_k^p}$ represents decision of $\bar{a}_k^p$. Considering again the independence of $(\int_{t_L}^{t_U} |x_r(t)|^2 dt)$ from $C(\bar{A})$, the decision law expressed in Eq. (3.19) can be restated as follows :

$$\widehat{\bar{a}_k^p} = \bar{S}_l \Longrightarrow \overset{1\le l\le M_p}{\bar{m}\bar{a}x} \{ \sum_{\bar{C}(\bar{A})\in\underline{\mathcal{C}}_{\underline{S}}^{S_l}(k)} \aleph_{ge}(x_r(t), x_B(\bar{C}(\bar{A}), h_{C,B}(t), t)\} \qquad (3.20)$$

In the following sections, the decoding approaches formulated in Eqs. (3.18), (3.20) will be applied to linear modulation systems.

3.3 LINEAR MODULATIONS

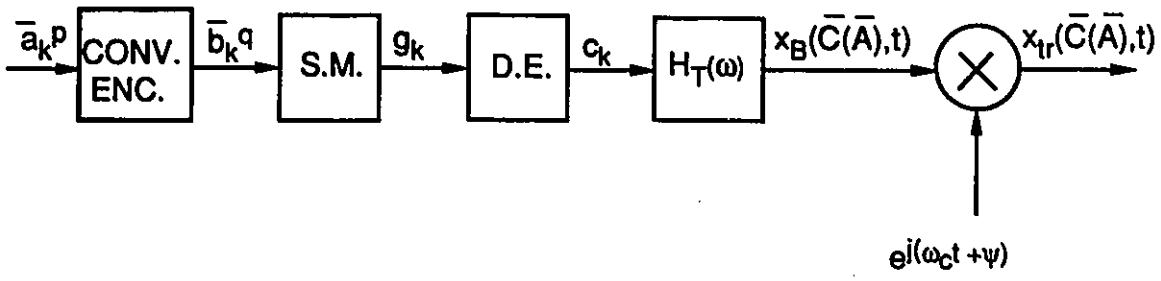

Figure 3.2: Transmitter of a linearly modulated signal.

The model of the transmitter for the case of a linear modulation is presented in Fig. 3.2. Its encoding unit might contain a convolutional encoder (CONV. ENC.), a signal mapper (S. M.) and a differential encoder (D. E.). Input to the convolutional encoder is the sequence $\bar{A}$, (see Eq. (4.100)), while its output is the encoded sequence

$$\bar{B} = [\bar{b}_1^q, ..., \bar{b}_{Z-1}^q] \tag{3.21}$$

with $\bar{b}_k^q$ being the q-bit word

$$\bar{b}_k^q = [b_k^1, b_k^2, ..., b_k^q] \tag{3.22}$$

b_k^ν are binary ($b_k^\nu \in \{0,1\}$, $1 \leq \nu \leq q$). The rate of the code equals p/q. For uncoded systems, $p = q$ and $\bar{a}_k^p = \bar{b}_k^p$.

The sequence $\bar{B}$ enters in the signal mapper, where it is transformed to the sequence of symbols

$$\bar{G}(\bar{A}) = [g_0, g_1, ..., g_{Z-1}] \tag{3.23}$$

g_k has the form:

$$g_k = \mathcal{J}_k e^{j\phi_k} \tag{3.24}$$

where $\mathcal{J}_k$, ϕ_k are the amplitude and phase of g_k respectively.

When PSK formats are considered, $\mathcal{J}_k = 1$. Also, for the PSK systems analyzed in this thesis, we shall consider that ϕ_k are equally spaced phases on the unit circle, in which case, the possible values ϕ_k can have are given by the following equation:

$$\phi_k = \frac{2i\pi}{M} \qquad (i \in \{0, 1, 2, \ldots, M-1\}) \tag{3.25}$$

where M represents the number of points in the PSK constellation (MPSK), $M = 2^q$.

We include in our model the option to apply differential encoding. By differential encoding, the sequence of g_k symbols is transformed into the sequence

$$\bar{C}(\bar{A}) = [c_0, c_1, \ldots, c_{Z-1}] \tag{3.26}$$

which is the output of the differential encoder. The differential encoding process applied is described by the following equation:

$$\begin{aligned} c_k &= |g_k| e^{jArg\{g_k\}} e^{jArg\{c_{k-1}\}} \\ &= \mathcal{J}_k e^{j(\phi_k \oplus \theta_{k-1})} \\ &= \mathcal{J}_k e^{j\theta_k} \end{aligned} \tag{3.27}$$

where θ_k is the phase of c_k. $\oplus$ represents addition in the $mod(2\pi)$ sense. $Arg\{\cdot\}$ stands for *argument of* $\{\cdot\}$. From Eq.(3.27) it can be seen that when differential encoding is applied,

$$\theta_k = \phi_k \oplus \theta_{k-1} \tag{3.28}$$

whereas when differential encoding is absent

$$\theta_k = \phi_k. \tag{3.29}$$

At this point, it is convenient to define the parameter $\Delta\Theta_l(k)$, it being equal to:

$$\Delta\Theta_l(k) = Arg[c_k c_{k-l}^*] = Arg[\mathcal{J}_k \mathcal{J}_{k-l} e^{j(\theta_k \ominus \theta_{k-l})}] = \theta_k \ominus \theta_{k-l} \tag{3.30}$$

where $\ominus$ represents mod (2π) subtraction unless otherwise indicated.

From Eqs.(3.27), (3.29) we have that in the presence of differential encoding,

$$c_k c_{k-l}^* = \mathcal{J}_k \mathcal{J}_{k-l} e^{j(\Delta\Theta_l(k))} = \mathcal{J}_k \mathcal{J}_{k-l} e^{j(\phi_k \oplus \phi_{k-1} \oplus ..... \oplus \phi_{k-l+1})} \tag{3.31}$$

with the result

$$\Delta\Theta_l(k) = \phi_k \oplus \phi_{k-1} \oplus .... \oplus \phi_{k-l+1} \ . \tag{3.32}$$

When differential encoding is absent

$$\Delta\Theta_l(k) = \phi_k \ominus \phi_{k-l} \ . \tag{3.33}$$

The sequence of symbols c_k is fed to the premodulation filter $H_T(\omega)$, whose impulse response is $h_T(t)$. Its output corresponds to $x_{tr,B}(\bar{C}(\bar{A}), t)$ and is equal to:

$$x_{tr,B}(\bar{C}(\bar{A}), t) = \sum_{k=0}^{Z-1} c_k h_T(t - kT). \tag{3.34}$$

$x_{tr,B}(\bar{C}(\bar{A}), t)$ modulates the carrier $e^{j(\omega_c t + \psi)}$. The transmitted signal $x_{tr}(\bar{C}(\bar{A}), t)$ in this case is equal to:

$$x_{tr}(\bar{C}(\bar{A}), t) = (\sum_{k=0}^{Z-1} c_k h_T(t - kT)) e^{j(\omega_c t + \psi)}. \tag{3.35}$$

$x_{tr}(\bar{C}(\bar{A}), t)$, after passing through the channel becomes:

$$x(\bar{C}(\bar{A}), t) = x_{tr}(\bar{C}(\bar{A}), t) \otimes h_c(t) = (\sum_{k=0}^{Z-1} c_k h_E(t - kT)) e^{j(\omega_c t + \psi)} \tag{3.36}$$

with

$$h_E(t) = h_T(t) \otimes h_{c,B}(t) \tag{3.37}$$

representing the overall baseband impulse response of the transmitter and the channel.

3.3.1 Optimal Non-Coherent Sequence Estimation of Linear Modulations

In Eq. (3.18), the two terms which determine the metric quantity $\aleph_{ge}(x_r(t), x_B(\bar{C}(\bar{A}), h_{C,B}(t), t)$ are the:

$$\int_{t_L}^{t_U} |x_B(\bar{C}(\bar{A}), h_{c,B}(t), \tau)|^2 d\tau \tag{3.38}$$

and

$$|\int_{t_L}^{t_U} (x_r(t)e^{-j(\omega_c t)}) x_B^*(\bar{C}(\bar{A}), h_{c,B}(t), t) dt|. \tag{3.39}$$

Using Eqs. (3.11), (3.36),$\int_{-\infty}^{\infty} |x_B(\bar{C}(\bar{A}), h_{c,B}(t), \tau)|^2 d\tau$ becomes:

$$\begin{aligned}
\int_{-\infty}^{\infty} |x_B(\bar{C}(\bar{A}), h_{c,B}(t), \tau)|^2 d\tau &= \int_{-\infty}^{\infty} (\sum_{k=0}^{Z-1} c_k h_E(\tau - kT))(\sum_{l=0}^{Z-1} c_l^* h_E^*(\tau - lT)))d\tau \\
&= \sum_{k=0}^{Z-1} \sum_{l=0}^{Z-1} c_k c_l^* \int_{-\infty}^{\infty} h_E(\tau - kT) h_E^*(\tau - lT) d\tau \\
&= \sum_{k=0}^{Z-1} \sum_{l=0}^{Z-1} c_k c_l^* h_{k-l} \\
&= \sum_{k=1}^{Z-1} \sum_{l=k}^{Z-1} [h_k c_l (c_{l-k}^*) + h_k^* c_l^* c_{l-k}] + h_0 \sum_{k=0}^{Z-1} |c_k|^2.
\end{aligned} \tag{3.40}$$

In Eq. (3.40) the limits of integration $\{t_L, t_U\}$ are set to $\{-\infty, \infty\}$, in order to accommodate the case of band-limited signals,where $h_T(t)$ extends from $-\infty$ to ∞ (and subsequently $h_E(t)$ does the same), spreading the $x_{tr,B}(\bar{C}(\bar{A}), t)$ in the same interval. $h(t)$ is the impulse of the cascaded $H_T(\omega)$, $H_{c,B}(\omega)$ and a filter matched to the combination of $H_T(\omega)$, $H_{c,B}(\omega)$. $h(t)$ is equal to:

$$h(t) = h_E(t) \otimes h_E^*(-t) = \int_{-\infty}^{\infty} h_E(\tau) h_E^*(\tau - t) d\tau \tag{3.41}$$

and $h_k = h(kT)$.

By processing Eq.(3.39), we obtain:

$$\int_{-\infty}^{\infty}(x_r(\tau)e^{-j(\omega_c\tau)})x_B^*(\bar{C}(\bar{A}),h_{c,B}(t),\tau)d\tau$$
$$=\sum_{k=0}^{Z-1}c_k^*\int_{-\infty}^{\infty}(x_r(\tau)e^{-j(\omega_c\tau)})h_E^*(\tau-kT)d\tau=\sum_{k=0}^{Z-1}(y_kc_k^*) \qquad (3.42)$$

where

$$y(t)=\int_{-\infty}^{\infty}(x_r(\tau)e^{-j(\omega_c\tau)})h_E^*(\tau-t)d\tau \qquad (3.43)$$

and $y_k = y(kT)$. $y(t)$ can be derived by demodulating $x_r(t)$ (the process described by the $(x_r(t)e^{-j(\omega_c t)})$ and afterwards passing it through a post detection filter $H_R(\omega)$ matched to $H_E(\omega)$. Notice that for the demodulation process, a carrier replica which is locked only in frequency with the signal carrier is required (phase lock between the signal carrier and the the local estimate is not needed).

$H_E(\omega)$ is the frequency response of $h_E(t)$. In this case,

$$H_R(\omega)=H_E^*(\omega) \quad \text{and} \quad h_R(t)=h_E^*(-t) \qquad (3.44)$$

where $h_R(t)$ is the impulse response of $H_R(\omega)$.

Incorporation of Eqs. (3.40), (3.42) in Eq.(3.18), gives the following expression for $\aleph_{ge}(x_r(t),x_B(\bar{C}(\bar{A}),h_{C,B}(t),t)$:

$$\aleph_{ge}(x_r(t),x_B(\bar{C}(\bar{A}),h_{c,B}(t),t))=\aleph_{OP}^{LMD}(h_0,\bar{h},\bar{y},\bar{C}(\bar{A}))=$$
$$\exp\{-(\tfrac{1}{2N_o}(\textstyle\sum_{k=0}^{Z-1}\sum_{l=0}^{Z-1}c_kc_l^*h_{k-l}\}I_0(\tfrac{|\sum_{k=0}^{Z-1}y_kc_k^*|}{N_o})=$$
$$\exp\{-(\tfrac{1}{2N_o}(h_0\textstyle\sum_{k=0}^{Z-1}|c_k|^2+2\sum_{l=1}^{Z-1}\sum_{k=l}^{Z-1}c_kc_{k-l}^*h_l\}I_0(\tfrac{|\sum_{k=0}^{Z-1}y_kc_k^*|}{N_o})=$$
$$\exp\{-(\tfrac{1}{N_o}(MST(h_0,\bar{C}(\bar{A}))+IST(\bar{h},\bar{C}(\bar{A}))\}I_0(\tfrac{|\sum_{k=0}^{Z-1}y_kc_k^*|}{N_o}) \qquad (3.45)$$

with

$$\bar{y}=[y_0,y_1,...,y_{Z-1}], \qquad (3.46)$$

$$\bar{h}=[h_1,h_2,...,h_{Z-1}], \qquad (3.47)$$

$$MST(h_0, \bar{C}(\bar{A})) = \frac{h_0}{2}(\sum_{k=0}^{Z-1} |c_k|^2) \tag{3.48}$$

and

$$IST(\bar{h}, \bar{C}(\bar{A})) = \sum_{k=1}^{Z-1} \sum_{l=k}^{Z-1} Re\{c_l c_{l-k}^* h_k\} \tag{3.49}$$

Eq.(3.45) is the decoding metric for linear modulation signals (the *LMD* superscript of $\aleph_{OP}^{LMD}(h_0, \bar{h}, \bar{y}, \bar{C}(\bar{A}))$ stands for Linear (modulation), Multi-amplitude (constellation), Distorted (channel)). In Eq.(3.45), $IST(\bar{h}, \bar{C}(\bar{A}))$ accounts for the presence of the ISI while $MST(h_0, \bar{C}(\bar{A}))$ for the multi-amplitude nature of the signal constellation. As we can see, the metric $\aleph_{OP}^{LMD}(h_0, \bar{h}, \bar{y}, \bar{C}(\bar{A}))$ of the optimal sequence estimator requires knowledge of the impulse response $h(t)$. To acquire this information, a channel estimator is needed. Notice that the receiver has to know only the sampled baseband complex impulse response of the channel.

The block diagram of the receiver based on $\aleph_{OP}^{LMD}(h_0, \bar{h}, \bar{y}, \bar{C}(\bar{A}))$ is shown in Fig. 3.3. N_{CW} is the number of $\bar{C}(\bar{A})$ codewords which can be generated by all possible combinations of the information sequence $\bar{A}$. In Fig. 3.4, the block diagram of the i^{th} Processing Unit (PU) is presented. Function of the i^{th} processing unit is to calculate the value of the $\aleph_{OP}^{LMD}(h_0, (\bar{h}, \bar{y}, \bar{C}(\bar{A}^i))$. The c_k^i stands for the value, the symbol c_k has when $\bar{A}^i$ is transmitted. It is to be noted here that the PU computes both, the exponential and modified Bessel function terms of the metric and needs the knowledge of N_o (i.e., E_b/N_o). Development of a decoder implementing complex functions such as exponential and Bessel is unattractive for practical applications (especially when real time implementations are considered) where there is strong demand for low cost and high reliability. In the chapters to follow the general metric expression described by Eq.(3.45) will be used to develop improved non-coherent receivers with lower complexity. It should be mentioned that the non-coherent detection techniques which are covered in this dissertation can be used to develop relatively simple baseband channel impulse response estimators. The estimators do not require knowledge of the carrier phase in order to perform the channel estimation process. These units can be easily made adaptive in order to be able to track possible time variations of the channel impulse response (e.g. when the system operates in a frequency selective fading channel).

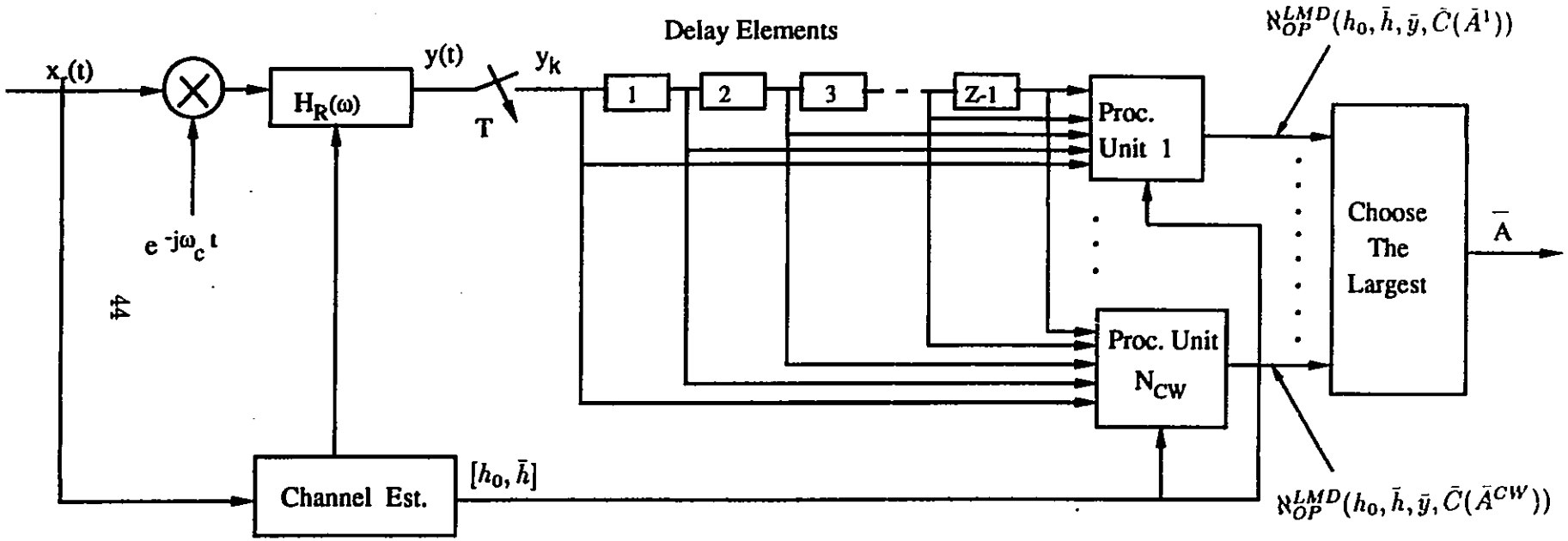

Figure 3.3 Block diagram of the optimal non-coherent sequence estimator for (single/multi-amplitude) linear modulation systems operating in a time dispersive channel.

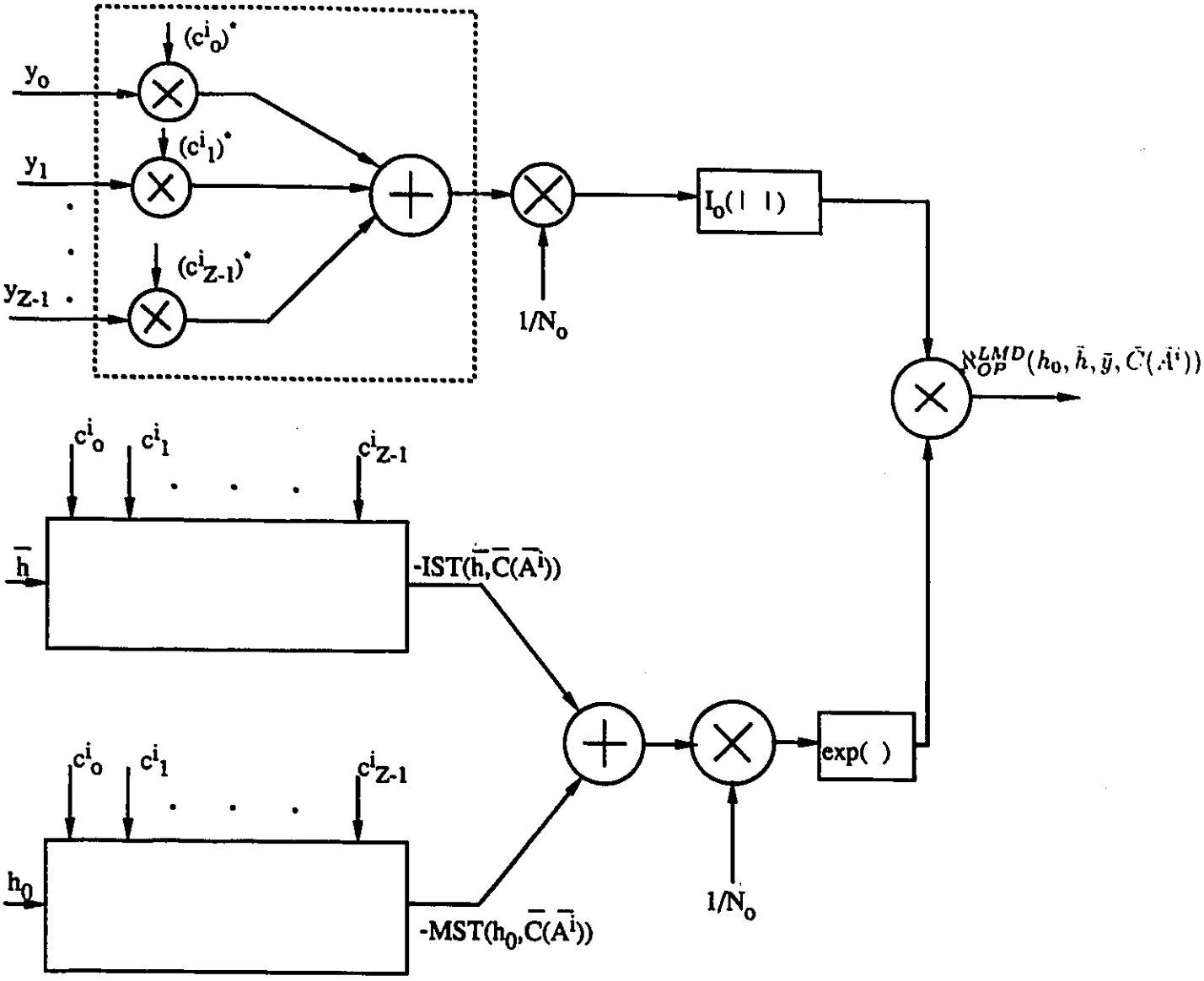

Figure 3.4: i^{th} Processing Unit of the optimal non-coherent sequence estimator for single or multi-amplitude linear modulation systems operating in a time dispersive channel.

3.3.2 Non-Coherent Sequence Estimation of QAM Signals

Eq.(3.45) provides the metric of the optimal non-coherent sequence estimator for a linear modulation signal with single or multi-amplitude/phase constellation, traveling through an ideal or a time dispersive channel. Using it, the design of non-coherent multi-amplitude linear modulation schemes such as non-coherent QAM [149] or multi-amplitude PSK [21] and the development of improved non-coherent receivers for operation in time dispersive channels [151], [152] becomes possible.

When $H_E(\omega)$ has the spectral shaping of a square root Nyquist-I filter, the following identity holds [214]:

$$h_k = \begin{cases} 1 & \text{for } k = 0 \\ 0 & \text{for } k \neq 0. \end{cases} \tag{3.50}$$

Under this assumption, Eq. (3.45) becomes:

$$\aleph_{OP}^{LMI}(h_0, \bar{y}, \bar{C}(\bar{A})) = \exp\{-\frac{(h_0}{2N_o}(\sum_{k=0}^{Z-1} |c_k|^2)\} I_0(\frac{|\sum_{k=0}^{Z-1} y_k c_k^*|}{N_o}) \tag{3.51}$$

or equivalently

$$\aleph_{OP}^{LMI}(h_0, \bar{y}, \bar{C}(\bar{A})) = \exp\{-\frac{1}{2N_o} MST(h_0, \bar{C}(\bar{A}))\} I_0(\frac{|\sum_{k=0}^{Z-1} y_k c_k^*|}{N_o}) \tag{3.52}$$

(LMI stands for Linear (modulations), Multi-amplitude (constellation), Ideal (channel)).

We realize that under Nyquist filtering, the product terms between different symbols c_k and c_l, present in Eq.(3.45), disappear, leaving only the squared values of the symbols (i.e. $|c_k|^2$). The structure of the receiver based on $\aleph_{OP}^{LMI}(h_0, \bar{h}, \bar{y}, \bar{C}(\bar{A}))$ is identical to the one presented in Figs. 3.3, 3.4, with the only difference being that in the PU (see Fig. 3.4), the $IST(\bar{h}, \bar{C}(\bar{A}))$ unit is not needed any more.

3.3.3 Non-Coherent Sequence Estimation of PSK Signals

For PSK signals, the amplitude of the symbols c_k is the same for all possible values c_k can take. Consequently, the amplitudes of the c_k symbols do not convey any information about the transmitted sequence $\bar{C}(\bar{A})$. This allows to simplify Eq.(3.45) furthermore. In Eq.(3.45), all the $(|c_k|^2)$ terms $(0 \leq k \leq Z-1)$ can be eliminated from the argument of the exponential terms as common, and independent from the sequence $\bar{C}(\bar{A})$. This reduces the decoding metric to the following expression:

$$\aleph_{OP}^{PSK}(\bar{h},\bar{y},\bar{C}(\bar{A})) = \exp\{-(\frac{1}{2N_o}(\sum_{k=1}^{Z-1}\sum_{l=k}^{Z-1}(c_l c_{l-k}^* h_k + c_l^* c_{l-k} h_k^*)\} \; I_0(\frac{|\sum_{k=0}^{Z-1} y_k c_k^*|}{N_o}) \tag{3.53}$$

When the first Nyquist criterion [214] is also satisfied, the decoding metric is further simplified (through Eq.(3.50)) and it reduces to the maximization of the modified Bessel function term:

$$\aleph_{OP}^{PSK}(\bar{h},\bar{y},\bar{C}(\bar{A})) = I_0(\frac{|\sum_{k=0}^{Z-1} y_k c_k^*|}{N_o}) \tag{3.54}$$

As a reminder, the decoder based on Eq.(3.54) is optimal only for PSK signals in an ideal channel and with equal apportioning of the Nyquist filter between transmitter-receiver.

3.3.4 Optimal Non-Coherent Symbol-by-Symbol Detection of Linear Modulations

From Eqs.(3.20) , (3.45) we have the following expression as decision law of the optimal non-coherent symbol-by-symbol receiver for linearly modulated signals:

$$\widehat{\bar{\alpha}}_k^p = \bar{S}_i \implies \max^{1\leq i\leq M_p} \{\mathcal{F}_k(h_0,\bar{h},\bar{y},\bar{S}_i)\} \tag{3.55}$$

where

$$\mathcal{F}_k(h_0, \bar{h}, \bar{y}, \bar{S}_i) = \sum_{\bar{C}(\bar{A}) \in \underline{C}_{\underline{S}}^{\bar{S}_i}(k)}$$

$$\exp\{-\frac{1}{2N_o}(h_0 \sum_{k=0}^{Z-1} |c_k|^2 + \sum_{k=1}^{Z-1} \sum_{l=k}^{Z-1} [c_l c_{l-k}^* h_k + c_k^* c_{l-k} h_k^*])\} I_0(\frac{|\sum_{k=0}^{Z-1} y_k c_k^*|}{N_o})\}. \tag{3.56}$$

Under equally apportioned Nyquist filtering Eq.(3.55) becomes

$$\widehat{\bar{\alpha}_k^p} = \bar{S}_i \implies \overset{1 \le i \le M_p}{max} \{ \sum_{\bar{C}(\bar{A}) \in \underline{C}_{\underline{S}}^{\bar{S}_i}(k)} \exp\{-(\frac{h_0}{2N_o}(\sum_{k=0}^{Z-1} |c_k|^2)\} I_0(\frac{|\sum_{k=0}^{Z-1} y_k c_k^*|}{N_o})\}. \tag{3.57}$$

For PSK signals (where $|c_k|$ is constant) Eq. (3.55) can be further simplified leading to

$$\widehat{\bar{\alpha}_k^p} = \bar{S}_i \implies \overset{1 \le l \le M_p}{max} \{ \sum_{\bar{C}(\bar{A}) \in \underline{C}_{\underline{S}}^{\bar{S}_i}(k)} \exp\{-\frac{1}{2N_o}(\sum_{k=1}^{Z-1} \sum_{l=k}^{Z-1} [c_l c_{l-k}^* h_k + c_l^* c_{l-k} h_{k-l}^*])\} I_0(\frac{|\sum_{k=0}^{Z-1} y_k c_k^*|}{N_o})\}. \tag{3.58}$$

For equally apportioned Nyquist filtering, and operation in ideal channel, where $h_i = 0 \ \forall \ i \neq 0$ (see Eq. (3.50)) Eq. (3.58) can be further simplified, leading to the following decision law :

$$\widehat{\bar{\alpha}_k^p} = \bar{S}_l \implies \overset{1 \le i \le M_p}{max} \{ \sum_{\bar{C}(\bar{A}) \in \underline{C}_{\underline{S}}^{\bar{S}_i}(k)} I_0(\frac{|\sum_{k=0}^{Z-1} y_k c_k^*|}{N_o})\}. \tag{3.59}$$

A conceptual block diagram of the receiver is presented in Fig. 3.5. In this figure, the boxes indicated as Proc. Unit $\{i, l\}$ $(1 \leq l \leq M_p 2^{(Z-2)})$ represent the set of processing units required to calculate $\mathcal{F}_k(\bar{h}, \bar{y}, \bar{S}_i)$ as is indicated by Eq.(3.56) (for a conceptual diagram presenting the structure of a processing unit, please refer to Fig. 3.4). Improved structures of practical receivers based on the metrics described by Eqs. (3.53), (3.54), (3.55), (3.58), and (3.59) will be presented in Chapter 4.

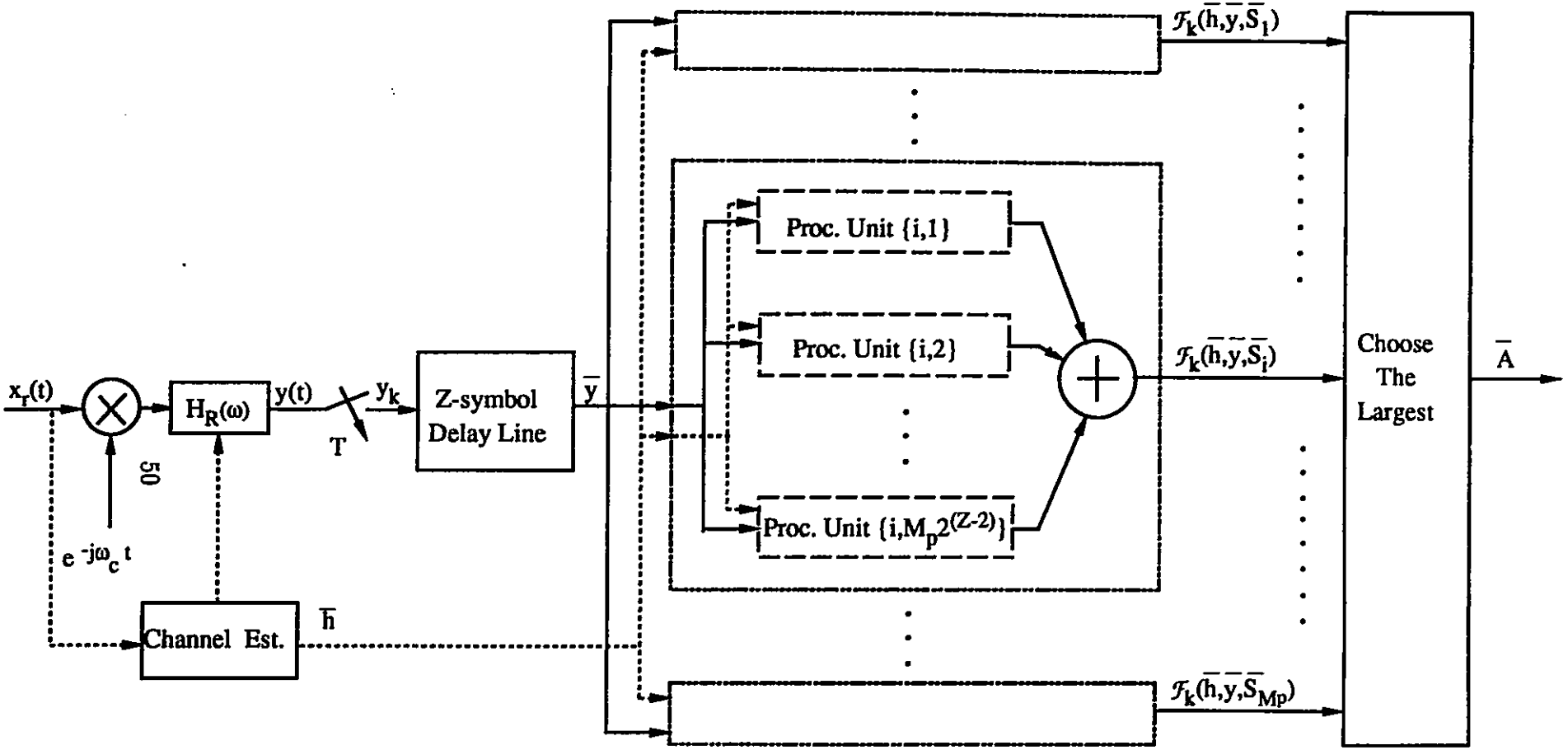

Figure 3.5: Block diagram of the optimal non-coherent symbol-by-symbol receiver operating in a time dispersive environment.

3.4 CONTINUOUS PHASE MODULATION

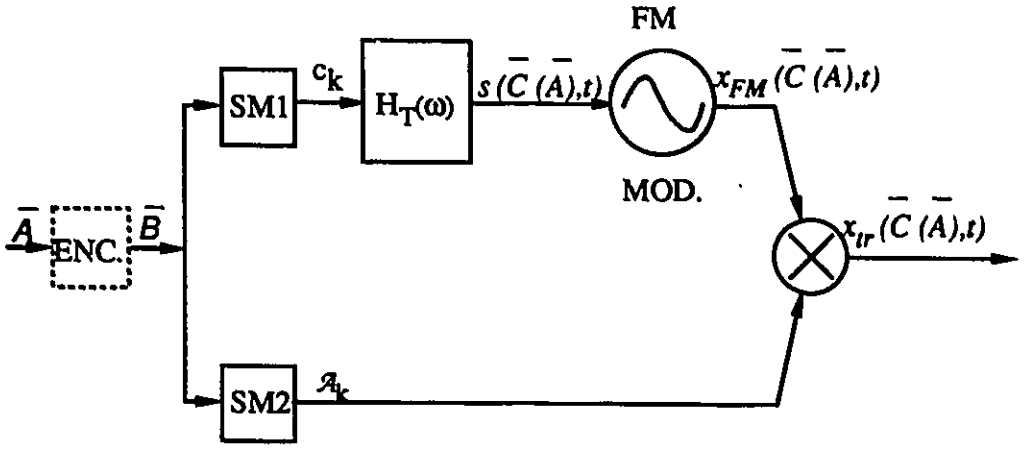

Figure 3.6: Block diagram of the CPM transmitter.

The conceptual block diagram of the CPM transmitter is presented in Fig. 3.6. As in the linear modulations, the information sequence $\bar{A}$ enters the encoder, producing the coded sequence $\bar{B}$ (see Eq. (3.21)). $\bar{B}$ consists of the q-bit coded words $\bar{b}_k = [b_k^1, b_k^2, ..., b_k^q]$. From the q different bits b_k^i $(1 \leq i \leq q)$ which form $\bar{b}_k$, the first Π_1 $(1 \leq \Pi_1 \leq q)$ enter the upper signal mapper (SM1) and they are mapped to a multi-amplitude symbol $c_k = \pm i_{\frac{1}{2^{\Pi_1}-1}}$ where $1 \leq i \leq 2^{\Pi_1-1}$. The rest $(\Pi_2(= \mathrm{q}-\Pi_1))$ of them enter in the lower part (SM2) and they are mapped to a positive valued symbol $\mathcal{A}_k$. The number of possible values $\mathcal{A}_k$ can have is $2^{q-\Pi_1}$. For single amplitude CPM signals, always $\mathcal{A}_k = 1$.

The outputs of the signal mapper c_k act as input to the premodulation filter $H_T(\omega)$. Its output $s(\bar{C}(\bar{A}),t)$ is equal to

$$s(\bar{C}(\bar{A}),t) = \sum_{k=0}^{Z-1} c_k h_T(t-kT). \tag{3.60}$$

We assume that the impulse response of $H_T(\omega)$ is practically zero outside the $(0, LT)$ interval, and can be truncated, i.e.,

$$h_T(t) \approx 0 \quad \text{for} \quad t < 0 \quad \text{and} \quad t > LT. \tag{3.61}$$

$s(\bar{C}(\bar{A}), t)$ goes through an FM modulator (FM MOD). Its output $x_{FM}(\bar{C}(\bar{A}), t)$ equals:

$$x_{FM}(\bar{C}(\bar{A}), t) = x_{FM,B}(\bar{C}(\bar{A}), t)e^{j(\omega_c t+\psi)} \tag{3.62}$$

with

$$x_{FM,B}(\bar{C}(\bar{A}), t) = e^{j(\phi_{tr}(\bar{C}(\bar{A}),t))}. \tag{3.63}$$

$\phi_{tr}(\bar{C}(\bar{A}), t)$ is the information carrying phase, being equal to:

$$\phi_{tr}(\bar{C}(\bar{A}), t) = 2\pi m_h \sum_{k=0}^{Z-1} c_k \int_0^{max\{0,t-kT\}} h_T(\tau)d\tau \tag{3.64}$$

with m_h representing the modulation index of the FM modulator.

$x_{FM}(\bar{C}(\bar{A}), t)$ is multiplied[4] with the signal $\mathcal{A}(t)$, producing the transmitted signal

$$x_{tr}(\bar{C}(\bar{A}), t) = x_{tr,B}(\bar{C}(\bar{A}), t)e^{j(\omega_c t+\psi)} \tag{3.65}$$

with

$$x_{tr,B}(\bar{C}(\bar{A}), t) = \mathcal{A}(t)e^{j(\phi_{tr}(\bar{C}(\bar{A}),t))}. \tag{3.66}$$

$\mathcal{A}(t)$ is defined as follows:

$$\mathcal{A}(t) = \sum_{k=0}^{Z-1} \mathcal{A}_k p(t - kT) \tag{3.67}$$

with

$$p(t) = \begin{cases} 1 & \text{for } 0 \leq t \leq T \\ 0 & \text{elsewhere.} \end{cases} \tag{3.68}$$

[4]In practice, such multiplication is not needed. The output of the SM2 can simply control the levels of the power amplifier or switch between two different power amplifiers in order to generate the multi-level nature of the signal.

$\phi_{tr}(\bar{C}(\bar{A}),t)$ can be written as :

$$\phi_{tr}(\bar{C}(\bar{A}),t)=\sum_{k=0}^{\lceil\frac{t}{T}\rceil-1}c_k\vartheta_0^{\lceil\frac{t}{T}\rceil-k}+\sum_{l=0}^{L}c_{\lceil\frac{t}{T}\rceil-l}\varphi_l(t-\lceil\frac{t}{T}\rceil T) \tag{3.69}$$

where $\lceil x\rceil$ represents the largest integer, smaller than or equal to x. Also,

$$\vartheta_{\xi_1}^{\xi_2}=2\pi m_h\int_{\xi_1 T}^{\xi_2 T}h_T(\tau)d\tau. \tag{3.70}$$

ξ_1, ξ_2 are integers with $\xi_1\leq\xi_2$.

$$\varphi_l(t)=\begin{cases}2\pi m_h\int_{lT}^{t-(\lceil\frac{t}{T}\rceil-l)T}h_T(\tau)d\tau & \text{for } 0\leq t\leq T\\ 0 & \text{elsewhere.}\end{cases} \tag{3.71}$$

Through Eqs. (3.69) to (3.71), $\phi_{tr}(\bar{C}(\bar{A}),t)$ can be expressed as follows:

$$\phi_{tr}(\bar{C}(\bar{A}),t)=\beta_1(\bar{\varphi}_0^{\lceil\frac{t}{T}\rceil-1}(\bar{C}(\bar{A})))+\beta_2(t,\bar{\varphi}_{\lceil\frac{t}{T}\rceil-L+1}^{\lceil\frac{t}{T}\rceil}(\bar{C}(\bar{A}))) \tag{3.72}$$

with

$$\beta_1(\bar{\varphi}_0^{\lceil\frac{t}{T}\rceil-1}(\bar{C}(\bar{A})))=\sum_{k=0}^{\lceil\frac{t}{T}\rceil-1}c_k\vartheta_0^{\lceil\frac{t}{T}\rceil-k} \tag{3.73}$$

$$\beta_2(t,\bar{\varphi}_{\lceil\frac{t}{T}\rceil-L+1}^{\lceil\frac{t}{T}\rceil}(\bar{A}))=\sum_{l=0}^{L-1}c_{\lceil\frac{t}{T}\rceil-l}\varphi_l(t-\lceil\frac{t}{T}\rceil T) \tag{3.74}$$

and

$$\bar{\varphi}_{\zeta_1}^{\zeta_2}(\bar{C}(\bar{A}))=[c_{\zeta_1},c_{\zeta_1+1},.....,c_{\zeta_2}]. \tag{3.75}$$

ζ_1, ζ_2 are integers, with $0\leq\zeta_1\leq\zeta_2\leq Z-1$.

Eqs. (3.72) to (3.74) indicate that $\phi_{tr}(\bar{C}(\bar{A}),t)$ consists of two terms. The first (i.e., $\beta_1(\bar{\varphi}_0^{\lceil\frac{t}{T}\rceil-1}(\bar{C}(\bar{A})))$) does not change within the $(\lceil\frac{t}{T}\rceil T,(\lceil\frac{t}{T}\rceil+1)T)$ interval. The second one ($\beta_2(t,\bar{\varphi}_{\lceil\frac{t}{T}\rceil-L+1}^{\lceil\frac{t}{T}\rceil}(\bar{C}(\bar{A})))$ changes with the time. This

partitioning of the phase is useful in the analysis which will follow and will lead to the formulation of the new receivers.

The signal $x_{tr}(\bar{C}(\bar{A}),t)$, passing through the channel, is transformed into $x(\bar{C}(\bar{A}),h_c(t),t)$. In this case $x(\bar{C}(\bar{A}),h_c(t),t)$ is equal to

$$x(\bar{C}(\bar{A}),h_c(t),t) \;= x_{tr}(\bar{C}(\bar{A}),t)\otimes h_c(t) \;= x_B(\bar{C}(\bar{A}),h_{c,B}(t),t)e^{j(\omega_c t+\psi)} \tag{3.76}$$

with $x_B(\bar{C}(\bar{A}),h_{c,B}(t),t)$ representing the baseband equivalent of $x(\bar{C}(\bar{A}),$ $h_c(t),t)$. For CPM signals $x_B(\bar{C}(\bar{A}),h_{c,B}(t),t)$ equals:

$$\begin{aligned}
& x_B(\bar{C}(\bar{A}),h_{c,B}(t),t) = x_{tr,B}(\bar{C}(\bar{A}),t)\otimes h_{C,B}(t) = \\
&= \sum_{k=0}^{Z-1} e^{j\beta_1(\bar{\rho}_0^{\lceil \frac{k}{T}\rceil -1}(\bar{C}(\bar{A})))}(\mathcal{A}_k(e^{j\beta_2(t,\bar{\rho}^{\lceil \frac{k}{T}\rceil}_{\lceil \frac{k}{T}\rceil -L+1}(\bar{C}(\bar{A})))}p(t-kT))\otimes h_{c,B}(t)) = \\
&= \sum_{k=0}^{Z-1} e^{j\beta_1(\bar{\rho}_0^{k-1}(\bar{C}(\bar{A})))}(\mathcal{A}_k(e^{j\beta_2(t,\bar{\rho}^{k}_{k-L+1}(\bar{C}(\bar{A})))}p(t))\otimes h_{c,B}(t-kT)).
\end{aligned} \tag{3.77}$$

$x(\bar{C}(\bar{A}),h_c(t),t)$ is corrupted by the white Gaussian noise term $n_w(t)$. The outcome $x_r(t)$ is the input to the receiver. The optimal maximum likelihood sequence estimator can be derived from Eq. (3.18). The optimal symbol-by-symbol receiver can be described from Eq.(3.20). For the CPM signals, the two key quantities associated with Eqs.(3.18), (3.20) (described by Eqs. (3.38), (3.39)) become:

$$\begin{aligned}
&\int_{-\infty}^{+\infty} |x_B(\bar{C}(\bar{A}),h_{c,B}(t),\tau)|^2 d\tau = \\
&= \int_{-\infty}^{+\infty} |(\sum_{k=0}^{Z-1} e^{-j\beta_1(\bar{\rho}_0^{k-1}(\bar{C}(\bar{A})))}\mathcal{A}_k(e^{j\beta_2(t,\bar{\rho}^{k}_{k-L+1}(\bar{C}(\bar{A})))}p(t))\otimes h_{c,B}(t-kT))|^2 dt \\
&= \sum_{k=0}^{Z-1}|J_{k,0}|^2 + \sum_{k=1}^{Z-1}\sum_{l=1}^{k}(e^{-j\Delta_l\beta_1(k,\bar{\rho}^{k}_{k-l-L+1}(\bar{C}(\bar{A})))}J_{k,l} \\
&+e^{j\Delta_l\beta_1(k,\bar{\rho}^{k}_{k-l-L+1}(\bar{C}(\bar{A})))}J^*_{k,l})
\end{aligned} \tag{3.78}$$

with

$$J_{k,l} \;=\; \int_{-\infty}^{+\infty}(\mathcal{A}_k(e^{j\beta_2(t,\bar{\rho}^{k}_{k-L+1}(\bar{C}(\bar{A})))}p(t))\otimes h_{c,B}(t-kT))dt$$

$$\int_{-\infty}^{\infty}(\mathcal{A}_k(e^{-j\beta_2(t,\bar{\rho}_{k-l-L+1}^{k-l}(\bar{C}(\bar{A})))}p(t))\otimes h_{c,B}(t-(k-l)T)dt \tag{3.79}$$

and

$$\begin{aligned}\Delta_l\beta_1(k,\rho_{k-l-L+1}^{k-1}(\bar{C}(\bar{A}))) &= \beta_1(\bar{\rho}_0^{k-1}(\bar{C}(\bar{A})))-\beta_1(\bar{\rho}_0^{k-l-1}(\bar{C}(\bar{A})))\\ &= \sum_{\nu=1}^{l}c_{k-\nu}\vartheta_0^k+\sum_{\nu=l+1}^{L+l}c_{k-\nu}\vartheta_{\nu-l}^{\nu}.\end{aligned} \tag{3.80}$$

In Eq.(3.80), l represents a non-negative integer smaller than k ($0\leq l\leq k-1$). At this point, we consider two cases:

1. when the channel is distortionless ($h_{c,B}(t)=\delta(t)$[5], with $\delta(t)$ representing the delta function) and
2. when $L=1$ (i.e., $h_T(t)$ is non-zero only in the $(0,T)$ interval).

In the first case,

$$\{\mathcal{A}_k(e^{j\beta_2(t,\bar{\rho}_{k-L+1}^{k}(\bar{C}(\bar{A})))}p(t))\otimes h_{c,B}(t-kT)\}=\mathcal{A}_k e^{j\beta_2(t,\bar{\rho}_{k-L+1}^{k}(\bar{C}(\bar{A})))}p(t-kT). \tag{3.81}$$

Use of Eq. (3.81) in Eq. (3.79), gives:

$$J_{k,l}=\begin{cases}\mathcal{A}_k & \text{for } l=0\\ 0 & \text{for } l\geq 0.\end{cases} \tag{3.82}$$

This results to

$$\int_{-\infty}^{+\infty}|x_B(\bar{C}(\bar{A}),\delta(t),t)|^2dt=\sum_{k=0}^{Z-1}(\mathcal{A}_k)^2 \tag{3.83}$$

[5]The $h_{c,B}(t)=\delta(t)$ (implying flat amplitude and phase characteristics over the entire bandwidth), guarantees distortionless conditions for CPM signals whose bandwidth theoretically extends from $-\infty$ to ∞. However, in practice, the spectral occupation of CPM signals extend over a finite length bandwidth, and distortionless conditions held only over this bandwidth are enough to guarantee practically undistorted signals.

and for single amplitude CPM signals ($\mathcal{A}_k = 1$)

$$\int_{-\infty}^{+\infty} |x_B(\bar{C}(\bar{A}), \delta(t), t)|^2 dt = Z. \tag{3.84}$$

In the second case (where $L = 1$)[6],

$$\begin{aligned} J_{k,l} &= \int_{-\infty}^{+\infty} (\mathcal{A}_k(e^{j\beta_2(t,c_k)}p(t)) \otimes h_{c,B}(t - kT))dt \\ &\quad \int_{-\infty}^{\infty} (\mathcal{A}_k(e^{-j\beta_2(t,c_l)}p(t)) \otimes h_{c,B}(t - (k-l)T))dt. \end{aligned} \tag{3.85}$$

The term expressed in Eq. (3.39), for the CPM format becomes:

$$\begin{aligned} &|\int_{-\infty}^{+\infty} (x_r(t)e^{-j\omega_c t})x_B^*(\bar{C}(\bar{A}), h_{c,B}(t), t)dt| \\ &= |\sum_{k=0}^{Z-1} e^{-j\beta_1(\bar{\varphi}_0^{k-1}(\bar{C}(\bar{A})))} F_k(x_r(t), \bar{\varphi}_{k-L+1}^k(\bar{C}(\bar{A})))| \end{aligned} \tag{3.86}$$

where

$$\begin{aligned} &F_k(x_r(t), \bar{\varphi}_{k-L+1}^k(\bar{C}(\bar{A}))) = \\ &\int_{-\infty}^{+\infty} (x_r(t)e^{-j\omega_c t})(\mathcal{A}_k(e^{-j\beta_2(t,\bar{\varphi}_{k-L+1}^k(\bar{C}(\bar{A})))}p(t)) \otimes h_{c,B}(t - kT))dt \end{aligned} \tag{3.87}$$

3.4.1 Optimal Non-Coherent Sequence Estimation

Based on Eqs.(3.18), (3.78), (3.86), the optimal maximum likelihood sequence estimator should choose the sequence $\bar{C}(\bar{A})$ which maximizes the

$$\aleph_{ge}(x_r(t), x_B(\bar{C}(\bar{A}), h_{c,B}(t), t)) = \aleph_{OP}^{CPMD}(\bar{C}(\bar{A}), \mathcal{F}_{[Z-1,0]}^{CPM}(\bar{C}(\bar{A})), h_{c,B}(t), t)) =$$

$$\exp\{-\frac{1}{2N_0}(\sum_{k=0}^{Z-1} |J_{k,0}|^2 + \sum_{k=1}^{Z-1}\sum_{l=1}^{k} (e^{-j\Delta_l\beta_1(k,\bar{\varphi}_{k-l}^k(\bar{C}(\bar{A})))} J_{k,l}$$

[6] $\bar{\varphi}_{k-1}^k(\bar{C}(\bar{A})) = [c_k]$.

$$+(e^{j\Delta_l\beta_1(k,\bar{\varphi}^k_{k-l}(\bar{C}(\bar{A})))}J^*_{k,l}))\}$$
$$I_0(\frac{|\sum_{k=0}^{Z-1}F_k(x_r(t),\bar{\varphi}^k_{k-L+1}(\bar{C}(\bar{A})))(e^{-j\beta_1(\bar{\varphi}^{k-1}_0(\bar{C}(\bar{A})))})|}{N_0})$$

(3.88)

where

$$\mathcal{F}^{CPM}_{[m,m_1]}(\bar{C}(\bar{A})) = [F_{m_1}(x_r(t),\bar{\varphi}^k_{k-L+1}(\bar{C}(\bar{A}))),\ldots,F_m(x_r(t),\bar{\varphi}^k_{k-L+1}(\bar{C}(\bar{A})))].$$

(3.89)

(η_1, η_2 are integers with $\eta_1 \leq \eta_2$) *CPMD* stands for Continuous Phase (modulation), Multi-amplitude (signal), Distorted (channel)). Equivalently, Eq.(3.88) can be expressed as:

$$\aleph^{CPMD}_{OP}(\bar{C}(\bar{A}),\mathcal{F}^{CPM}_{[m,m_1]}(\bar{C}(\bar{A})),h_{c,B}(t),t)) =$$
$$\exp\{-\frac{1}{N_0}(ISM_{CPM}(\bar{C}(\bar{A}),h_{c,B}(t),t) + IST_{CPM}(\bar{C}(\bar{A}),h_{c,B}(t),t)\}$$
$$I_0(\frac{|\sum_{k=0}^{Z-1}F_k(x_r(t),\bar{\varphi}^k_{k-L+1}(\bar{C}(\bar{A})))(e^{-j\beta_1(\bar{\varphi}^{k-1}_0(\bar{C}(\bar{A})))})|}{N_0}).$$

(3.90)

$$MST_{CPM}(\bar{C}(\bar{A}),h_{c,B}(t),t) = \frac{1}{2}\sum_{k=0}^{Z-1}|J_{k,0}|^2 \tag{3.91}$$

and

$$IST_{CPM}(\bar{C}(\bar{A}),h_{c,B}(t),t) = \sum_{k=1}^{Z-1}\sum_{l=1}^{k}Re\{e^{-j\Delta_l\beta_1(k,\bar{\varphi}^k_{k-l}(\bar{C}(\bar{A})))}J_{k,l}\}$$

(3.92)

For the case of a distortionless channel, the metric becomes:

$$\aleph_{OP}^{CPMD}(\bar{C}(\bar{A}), \mathcal{F}_{[Z-1,0]}^{CPM}, \delta(t), t)) \;=\; \exp\{-\frac{1}{2N_0}(\sum_{k=0}^{Z-1} \mathcal{A}_k^2)\}$$

$$I_0(\frac{|\sum_{k=0}^{Z-1} F_k(x_r(t), \bar{\varphi}_{k-L+1}^k(\bar{C}(\bar{A})))(e^{-j\beta_1(\bar{\varphi}_0^{k-1}(\bar{C}(\bar{A})))}|}{N_0}) \tag{3.93}$$

For the derivation of Eq.(3.93), Eqs.(3.82), Eq.(3.88) have been used. When distortionless channel conditions are met and the signal is single-amplitude, the argument of the exponential term is independent from the transmitted information sequence (and equal to Z, see Eq.(3.86)). This permits its elimination from the maximization process, leaving only the modified Bessel function term

$$I_0(\frac{|\sum_{k=0}^{Z-1} F_k(x_r(t), \bar{\varphi}_{k-L+1}^k(\bar{C}(\bar{A})))(e^{-j\beta_1(\bar{\varphi}_0^{k-1}(\bar{C}(\bar{A})))})|}{N_0}). \tag{3.94}$$

3.4.2 Optimal Non-Coherent Symbol-by-Symbol Detection of CPM Signals

Using Eq. (3.20) with Eq. (3.93), we end up with the following expression as decision law for the optimal symbol-by-symbol receiver :

$$\widehat{\bar{a}_k^p} = \bar{S}_i \implies \overset{1\le l\le M_p}{\bar{m}ax} \{ \sum_{\bar{C}(\bar{A})\in\underline{C}_{\underline{S}}^{S_i}(k)} \exp\{-\frac{1}{2N_0}(\sum_{k=0}^{Z-1} |J_{k,0}|^2$$

$$+ \sum_{k=1}^{Z-1}\sum_{l=1}^{k}(e^{-j\Delta_l\beta_1(k,\bar{\varphi}_{k-l}^k(\bar{C}(\bar{A})))} J_{k,l} + e^{j\Delta_l\beta_1(k,\bar{\varphi}_{k-l}^k(\bar{C}(\bar{A})))} J_{k,l}^*))\}$$

$$I_0(\frac{|\sum_{k=0}^{Z-1} F_k(x_r(t), \bar{\varphi}_{k-L+1}^k(\bar{C}(\bar{A})))(e^{-j\beta_1(\bar{\varphi}_0^{k-1}(\bar{C}(\bar{A})))}|}{N_0})\}. \tag{3.95}$$

For ideal channel the decision law becomes:

$$\widehat{\bar{a}_k^p} = \bar{S}_l \implies \overset{1\le l\le M_p}{max} \{ \sum_{\bar{C}(\bar{A})\in \underline{\underline{C}}_{\underline{S}}^{S_l}(k)} \exp\{-\frac{1}{2N_0}(\sum_{k=0}^{Z-1}|J_{k,0}|^2)\}$$

$$I_0(\frac{|\sum_{k=0}^{Z-1} F_k(x_r(t), \bar{\varphi}_{k-L+1}^k(\bar{C}(\bar{A})))(e^{-j\beta_1(\bar{\varphi}_0^{k-1}(\bar{C}(\bar{A})))})|}{N_0})\}. \tag{3.96}$$

For single-amplitude signals it is furthermore simplified (using Eq. (3.78)), becoming:

$$\widehat{\bar{a}_k^p} = \bar{S}_l \Longrightarrow \overset{1\le l\le M_p}{max} \{ \sum_{\bar{C}(\bar{A})\in \underline{\underline{C}}_{\underline{S}}^{S_l}(k)}$$

$$I_0(\frac{|\sum_{k=0}^{Z-1} F_k(x_r(t), \bar{\varphi}_{k-L+1}^k(\bar{C}(\bar{A})))(e^{-j\beta_1(\bar{\varphi}_0^{k-1}(\bar{C}(\bar{A})))})|}{N_0})\}. \tag{3.97}$$

In Chapter 5, the decision laws presented here will be used for the derivation of lower complexity receiver structures.

3.4.2.1 Implementation of the Optimal Non-Coherent Receiver for CPM Signals

In order to carry out the maximization process described by Eq.(3.93) or (3.95), the quantities $F_k(x_r(t), \bar{\varphi}_{k-L+1}^k(\bar{C}(\bar{A})))$, $(0 \le k \le Z-1)$ have to be provided to the sequence estimator or symbol-by-symbol receiver, for all possible combinations of the sequence $\bar{C}(\bar{A})$. For the calculation of the $F_k(x_r(t), \bar{\varphi}_{k-L+1}^k(\bar{C}(\bar{A})))$ parameters, first $x_r(t)$ has to be demodulated to baseband (the operation being described by the $(x_r(t)e^{-j\omega_c t})$. Afterwards, the baseband signal has to pass through a bank of η_c^L different correlate/integrate units. The function of the i^{th} (from a total of η_c^L) correlator, is

$$U_{cor}^i(t, \bar{\gamma}_i^L) = (e^{j(\beta_2(t,\bar{\gamma}_i^L)}p(t)) \otimes h_{c,B}(t) \tag{3.98}$$

with $1 \leq i \leq \eta_c^L$ and

$$\bar{\gamma}_i^L = [\gamma_1^i, \gamma_2^i, ..., \gamma_L^i]. \tag{3.99}$$

γ_ν^i $(1 \leq \nu \leq L)$ are numbers which take values from the same alphabet as the one used for c_k. The η_c^L different arrays $\bar{\gamma}_i^L$, provide a complete set of all possible combinations $\gamma_1^i, \gamma_2^i, .., \gamma_L^i$ can generate.

The k^{th} output $(0 \leq k \leq Z-1)$ of the i^{th} correlate/integrate unit equals:

$$B_{cor}^i(k, x_r(t), U_{cor}^i(t, \bar{\gamma}_i^L)) = \int_{-\infty}^{\infty} (x_r(t)e^{-j(\omega_c t)}) U_{cor}^i(t - kT, \bar{\gamma}_i^L) dt$$

$$= \int_{-\infty}^{\infty} (x_r(t)e^{-j(\omega_c t)})(e^{-j(\beta_2(t,\bar{\gamma}_i^L))} p(t)) \otimes h_{c,B}(t - kT) dt. \tag{3.100}$$

Due to the complex nature of $(x_r(t)e^{-j\omega_c t})$ and the functions $U_{cor}^i(t, \bar{\gamma}_i^L)$, four (4) multiplications, two (2) additions and two (2) integrations are required to be performed in each single correlate/integrate unit (for every instant kT) in order to provide the $B_{cor}^i(k, x_r(t), U_{cor}^i(t, \bar{\gamma}_i^L))$. Consequently, the number of operations required in total are $4\eta_c^L$ multiplications, $2\eta_c^L$ additions/subtractions and $2\eta_c^L$ integrations.

Instead of the correlator/integrator implementation presented in the previous paragraphs, a "filter-bank" implementation can be followed. The filter replacing the i^{th} correlator/integrator should have an impulse response equal to

$$h_{f-b}^i(t, \bar{\gamma}_i^L) = (e^{j(\beta_2(-t,\bar{\gamma}_i^L))} p(-t)) \otimes h_{c,B}(-t). \tag{3.101}$$

A total of η_c^L filters are required by the filter bank. It can be verified that the output of the i^{th} filter at kT is equal to:

$$\begin{aligned} E_{f-b}^i(k, x_r(t), h_{f-b}^i(t, \bar{\gamma}_i^L)) &= \int_{-\infty}^{\infty} (x_r(t)e^{-j(\omega_c t)}) h_{f-b}^i(kT - t, \bar{\gamma}_i^L) dt \\ &= \int_{-\infty}^{\infty} (x_r(t)e^{-j(\omega_c t)})(e^{-j(\beta_2(t,\bar{\gamma}_i^L))} p(t)) \otimes h_{c,B}(t - kT) dt. \end{aligned} \tag{3.102}$$

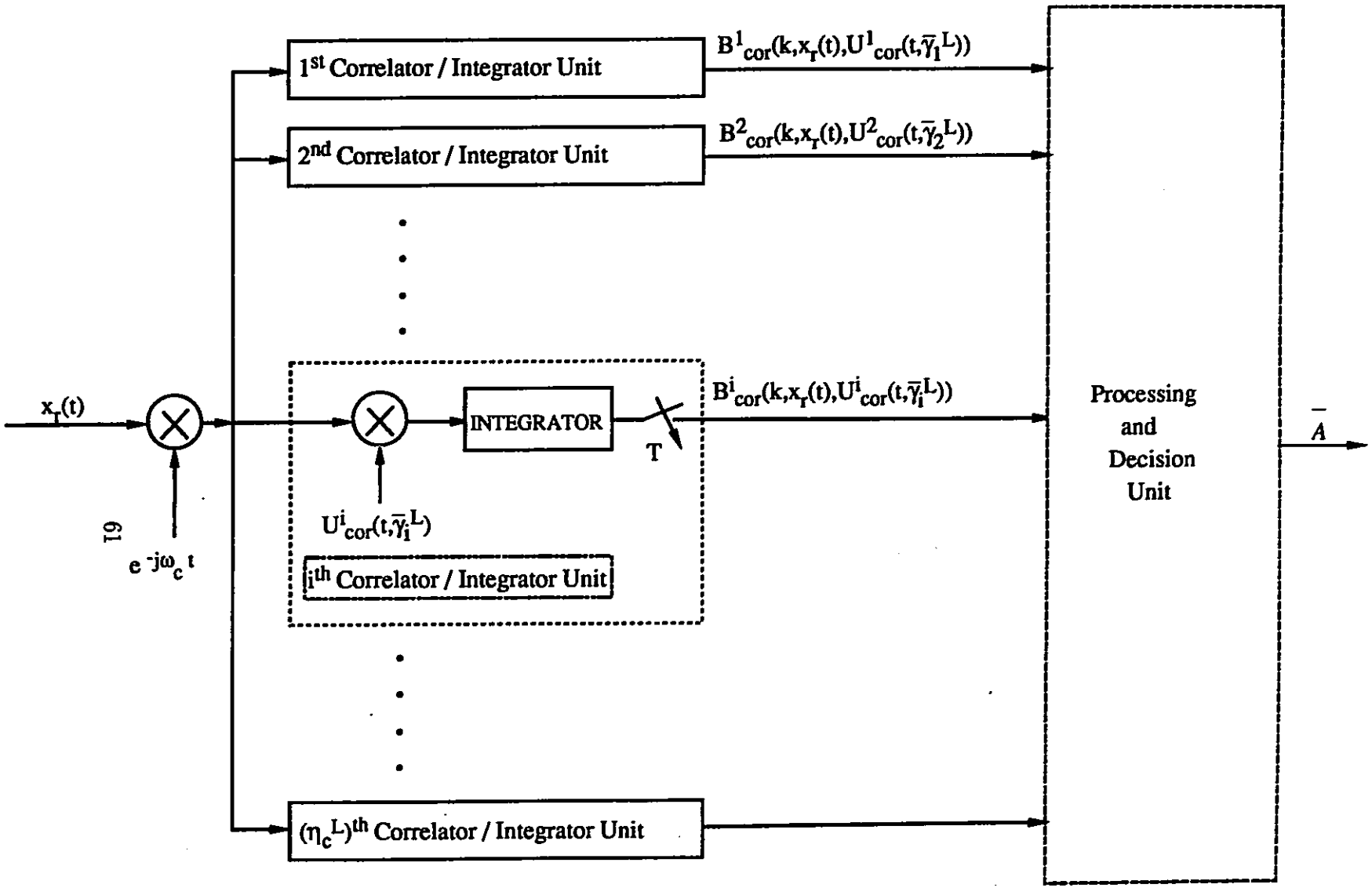

Figure 3.7: Block diagram of the Optimal Non-Coherent CPM Sequence Estimator, based on the Correlator / Integrator implementation.

Equivalently, $E^i_{f-b}(k, x_r(t), h^i_{f-b}(t, \bar{\gamma}^L_i))$ can be expressed as:

$$\begin{aligned} E^i_{f-b}(k, x_r(t), h^i_{f-b}(t, \bar{\gamma}^L_i)) &= [\int_{-\infty}^{\infty} Re\{(x_r(t)e^{-j(\omega_c t)})\} Re\{h^i_{f-b}(kT-t, \bar{\gamma}^L_i)\} dt \\ &+ \int_{-\infty}^{\infty} Im\{(x_r(t)e^{-j(\omega_c t)})\} Im\{h^i_{f-b}(kT-t, \bar{\gamma}^L_i)\} dt] \\ &+ j[\int_{-\infty}^{\infty} Re\{(x_r(t)e^{-j(\omega_c t)})\} Im\{h^i_{f-b}(kT-t, \bar{\gamma}^L_i)\} dt \\ &- \int_{-\infty}^{\infty} Im\{(x_r(t)e^{-j(\omega_c t)})\} Re\{h^i_{f-b}(kT-t, \bar{\gamma}^L_i)\} dt]. \end{aligned} \tag{3.103}$$

where $Re\{\cdot\}$ and $Im\{\cdot\}$ represent real and imaginary terms of $\{\cdot\}$.

From Eq. (3.98), (3.101), it is clear that

$$E^i_{f-b}(k, x_r(t), h^i_{f-b}(t, \bar{\gamma}^L_i)) = B^i_{cor}(k, x_r(t), U^i_{cor}(t, \bar{\gamma}^L_i)). \tag{3.104}$$

Due to the complex nature of $(x_r(t)e^{-j(\omega_c t)})$, $h^i_{f-b}(t, \bar{\gamma}^L_i)$ four (4) different filters and filtering processes are required to provide the (complex) output $E^i_{f-b}(k, x_r(t), h_{f-b}(t, \bar{\gamma}^L_i))$. This can clearly be seen from Eq. (3.103). The total number of filters required by the "filter-bank" is equal to $4\eta^L_c$.

Both approaches described above are complex, especially for spectrally efficient CPM schemes and/or transmission through dispersive channels with long memory. The main source of complexity is the larger number of filters (or correlators/integrators) required to satisfy the filtering requirements. In the following section, we shall see how non-coherent CPM receivers with lower filtering requirements can be reached.

3.5 NON-COHERENT CPM RECEIVERS WITH REDUCED POST DETECTION FILTERING REQUIREMENTS

In the previous section, the optimal non-coherent detection of CPM signals was examined. The results revealed structures requiring the use of a filter bank at the post detection filtering stage. The size of the filter bank depends on the length of the premodulation filter impulse response $h_T(t)$, the channel impulse response $h_{c,B}(t)$ and the size of the alphabet from which the symbols c_k take values. For M-ary and/or spectrally efficient CPM signals (where the impulse response of the premodulation filter $H_T(\omega)$ expands over more than one symbol periods) the size of the filter bank becomes large, making the use of the examined receivers in practical applications impossible. In the following paragraphs we shall see how the filtering requirements can be relieved which may lead to more practical schemes.

In the past, a number of contributions appeared in the literature (see [6], [87], [90], [125], [205], [218]). The CPM signals are expressed as the sum of a finite number of time limited Amplitude Modulation Pulses (AMP decomposition). These contributions demonstrated that even though for an exact representation of the CPM waveform, a large number of such amplitude modulation pulses might be required, in reality, for a number of popular CPM signals, a small number of them (i.e. one or two of them) is enough to give an accurate representation of the CPM signal.

Using the AMP decomposition, the CPM (baseband) signal can be expressed as:

$$x_{tr,B}(\bar{C}(\bar{A}),t) = \sum_{k=0}^{Z-1} \mathcal{A}_k \sum_{n=0}^{2^{L+\Pi_1-1}} \alpha_{n,k}^{AMP} h_n^{AMP}(t-kT) \qquad (3.105)$$

where $h_n^{AMP}(t)$ are the AMP pulses mentioned above and $\alpha_{n,k}^{AMP}$ are unit amplitude ($|\alpha_{n,k}^{AMP}| = 1$) complex terms providing the phases with which the various $h_n^{AMP}(t)$ appear in order to construct the CPM waveform. The $h_n^{AMP}(t)$ pulses are of time limited nature, the longest having a duration equal to $(L+1)T$, the shortest a duration equal to T. As can be seen by Eq.(3.105), the total number of $h_n^{AMP}(t)$ pulses required to provide an exact

reconstruction of the CPM waveform is equal to $2^{L+\amalg_1-1}$ (we remind the reader that L is the length of the symbol periods over which $h_T(t)$ extends and $2^{\amalg_1}$ is the number of values the M-ary c_k symbol can take; for binary CPM $\amalg_1 = 1$). However, $x_{tr,B}(\bar{C}(\bar{A}),t)$ can be very accurately approximated by a small number of terms (i.e $(\mathcal{N}+1)$ of them, where $\mathcal{N}$ is integer and $0 \leq \mathcal{N} \leq (2^{L+\amalg_1-1}-1)$). This leads to the following approximation of $x_{tr,B}(\bar{C}(\bar{A}),t)$:

$$x_{tr,B}^{app.}(\bar{C}(\bar{A}),t) = \sum_{k=0}^{Z-1} \mathcal{A}_k \sum_{n=0}^{\mathcal{N}} \alpha_{n,k}^{AMP} h_n^{AMP}(t-kT). \tag{3.106}$$

In Eq.(3.76) the expression of the transmitted CPM signal $x_{tr,B}(\bar{C}(\bar{A}),t)$ (after it has passed through the channel) is given. The outcome of the time dispersion (if present) is the signal $x(\bar{C}(\bar{A}),h_c(t),t)$. Using the approximation described by Eq.(3.106), $x(\bar{C}(\bar{A}),h_c(t),t)$ can be approximated by the :

$$x^{app.}(\bar{C}(\bar{A}),h_c(t),t) \;= x_{tr}^{app.}(\bar{C}(\bar{A}),t) \otimes h_c(t) \;= x_B^{app.}(\bar{C}(\bar{A}),h_{c,B}(t),t)e^{j(\omega_c t+\psi)} \tag{3.107}$$

with

$$x_B^{app.}(\bar{C}(\bar{A}),h_{c,B}(t),t) = \sum_{k=0}^{Z-1} \mathcal{A}_k \sum_{n=0}^{\mathcal{N}} \alpha_{n,k}^{AMP} h_{E,n}^{AMP}(t-kT) \tag{3.108}$$

and

$$h_{E,n}^{AMP}(t) = h_n^{AMP}(t) \otimes h_{c,B}(t). \tag{3.109}$$

In order to define the structure of the non-coherent receiver which will be based on the approximate expression of the CPM signal formats, the $\{\int_{-\infty}^{+\infty} |x_B^{app.}(\bar{C}(\bar{A}),h_{c,B}(t),\tau)|^2 d\tau\}$, $\{\int_{-\infty}^{+\infty}(x_r(t)e^{-j\omega_c t})(x_B^{app.}(\bar{C}(\bar{A}),h_{c,B}(t),t))^* dt\}$ are required. The expressions for these two terms are:

$$\int_{-\infty}^{+\infty} |x_B^{app.}(\bar{C}(\bar{A}),h_{c,B}(t),\tau)|^2 d\tau = \sum_{k=0}^{Z-1} (\mathcal{A}_k)^2 \sum_{n_1=0}^{\mathcal{N}} \sum_{n_2=0}^{\mathcal{N}} \alpha_{n_1,k}^{AMP} (\alpha_{n_2,k}^{AMP})^* \Re_{E,[n_1,n_2]}^{AMP}(0)$$

$$+ \sum_{k=1}^{Z-1} \sum_{l=k}^{Z-1} \mathcal{A}_l \mathcal{A}_{l-k} \sum_{n_1=0}^{\mathcal{N}} \sum_{n_2=0}^{\mathcal{N}} [\alpha_{n_1,l}^{AMP} (\alpha_{n_2,l-k}^{AMP})^* \Re_{E,[n_1,n_2]}^{AMP}(k)$$

$$+\alpha^{AMP}_{n_2,l-k}(\alpha^{AMP}_{n_1,l})^*(\Re^{AMP}_{E,[n_1,n_2]}(k))^*] \tag{3.110}$$

with

$$\Re^{AMP}_{E,[n_1,n_2]}(k) = h^{AMP}_{E,n_1}(t) \otimes (h^{AMP}_{E,n_2}(t-kT))^* = \int_{-\infty}^{\infty} h^{AMP}_{E,n_1}(\tau)(h^{AMP}_{E,n_2}(t-kT-\tau))^* d\tau \tag{3.111}$$

and

$$\begin{aligned} \int_{-\infty}^{+\infty}(x_r(t)e^{-j\omega_c t})(x_B^{app.}(\bar{C}(\bar{A}),h_{c,B}(t),t))^* dt &= \sum_{k=0}^{Z-1}\mathcal{A}_k\sum_{n=0}^{\mathcal{N}}(\alpha^{AMP}_{n,k})^* \\ \int_{-\infty}^{+\infty}(x_r(t)e^{-j\omega_c t})(h^{AMP}_{E,n}(t-kT))^* dt &= \sum_{k=0}^{Z-1}\mathcal{A}_k\sum_{n=0}^{\mathcal{N}}\mathcal{Y}^{AMP}_{n,k}(\alpha^{AMP}_{n,k})^*. \end{aligned} \tag{3.112}$$

$\mathcal{Y}^{AMP}_{n,k} = \mathcal{Y}^{AMP}_n(kT)$ where

$$\mathcal{Y}^{AMP}_n(t) = \int_{-\infty}^{+\infty}(x_r(\tau)e^{-j\omega_c\tau})(h^{AMP}_{E,n}(\tau-t))^* d\tau. \tag{3.113}$$

$\mathcal{Y}^{AMP}_n(t)$ is the output of a post detection filter matched to $h^{AMP}_{E,n}(t)$, having the demodulated signal $(x_r(t)e^{-j\omega_c t})$ as input.

3.5.1 Maximum Likelihood Sequence Estimation

The metric of the optimal non-coherent sequence estimator has been given in Eq.(3.18). By replacing $\{\int_{-\infty}^{+\infty}|x_B(\bar{C}(\bar{A}),h_{c,B}(t),\tau)|^2 d\tau\}$ and $\{\int_{-\infty}^{+\infty}(x_r(t)e^{-j\omega_c t})(x_B(\bar{C}(\bar{A}),h_{c,B}(\tau),t))^* dt\}$ in Eq.(3.18) with the terms $\{\int_{-\infty}^{+\infty}|x_B^{app.}(\bar{C}(\bar{A}),h_{c,B}(t),\tau)|^2 d\tau\}$ (Eq.(3.110)) and $\{\int_{-\infty}^{+\infty}(x_r(t)e^{-j\omega_c t})(x_B^{app.}(\bar{C}(\bar{A}),h_{c,B}(\tau),t))^* dt\}$ (Eq.(3.112)) respectively, we end up with the following form:

$$\aleph^{CPMD}_{OP_{app.}}(\bar{\Re}^{PAM}_{E,[0,0]},\bar{\Re}^{PAM}_{E,[0,1]},\ldots,\bar{\Re}^{PAM}_{E,[0,\mathcal{N}]},\bar{\Re}^{PAM}_{E,[1,0]},\bar{\mathcal{Y}}^{AMP}_0,\bar{\mathcal{Y}}^{AMP}_1,\ldots,\bar{\mathcal{Y}}^{AMP}_{\mathcal{N}},\bar{C}(\bar{A})) =$$

$$\exp\{-\frac{1}{2N_o}[\sum_{k=0}^{Z-1}(\mathcal{A}_k)^2\sum_{n_1=0}^{\mathcal{N}}\sum_{n_2=0}^{\mathcal{N}}\alpha_{n_1,k}^{AMP}(\alpha_{n_2,k}^{AMP})^*\Re_{E,[n_1,n_2]}^{AMP}(0)$$

$$+\sum_{k=1}^{Z-1}\sum_{l=k}^{Z-1}\mathcal{A}_l\mathcal{A}_{l-k}\sum_{n_1=0}^{\mathcal{N}}\sum_{n_2=0}^{\mathcal{N}}[\alpha_{n_1,l}^{AMP}(\alpha_{n_2,l-k}^{AMP})^*$$

$$\Re_{E,[n_1,n_2]}^{AMP}(k)+\alpha_{n_2,l-k}^{AMP}(\alpha_{n_1,l}^{AMP})^*(\Re_{E,[n_1,n_2]}^{AMP}(k))^*]]\}$$

$$I_0(\frac{|\sum_{k=0}^{Z-1}\mathcal{A}_k\sum_{n=0}^{\mathcal{N}}\mathcal{Y}_{n,k}^{AMP}(\alpha_{n,k}^{AMP})^*|}{N_o})$$

(3.114)

where

$$\bar{\Re}_{E,[i,l]}^{AMP}=[\Re_{E,[i,l]}^{AMP}(0),\Re_{E,[i,l]}^{AMP}(1),\ldots,\Re_{E,[i,l]}^{AMP}(Z-1)] \tag{3.115}$$

(i,l are integers, $0\le i,l\le\mathcal{N}$) and

$$\bar{\mathcal{Y}}_i^{AMP}=[\mathcal{Y}_{i,0}^{AMP},\mathcal{Y}_{i,1}^{AMP},\ldots,\mathcal{Y}_{i,Z-1}^{AMP}] \tag{3.116}$$

(i integer, $0\le i\le\mathcal{N}$).

For many (especially binary) CPM signals, it has been shown ([6], [87], [90], [125], [205]) that practically only one pulse, the $h_0^{AMP}(t)$ of duration $((L+1)T)$ is enough to very accurately describe the CPM signal. Setting $\mathcal{N}=0$ in Eq.(3.114) we get:

$$\aleph_{OP_{app.}}^{CPMD}(\bar{\Re}_{E,[0,0]}^{AMP},\bar{\mathcal{Y}}_0^{AMP},\bar{C}(\bar{A}))\;=\;\exp\{-\frac{1}{2N_o}[\sum_{k=0}^{Z-1}(\mathcal{A}_k)^2\Re_{E,[0,0]}^{AMP}(0)$$

$$+\sum_{k=1}^{Z-1}\sum_{l=k}^{Z-1}\mathcal{A}_l\mathcal{A}_{l-k}[\alpha_{0,l}^{AMP}(\alpha_{0,l-k}^{AMP})^*\Re_{E,[0,0]}^{AMP}(k)+\alpha_{0,l-k}^{AMP}(\alpha_{0,l}^{AMP})^*(\Re_{E,[0,0]}^{AMP}(k))^*]]\}$$

$$I_0(\frac{|\sum_{k=0}^{Z-1}\mathcal{A}_k\mathcal{Y}_{0,k}^{AMP}(\alpha_{0,k}^{AMP})^*|}{N_o}). \tag{3.117}$$

(in Eq.(3.117) the $|\alpha_{0,k}^{AMP}| = 1$ has been used). Comparing Eq.(3.45) with Eq.(3.117) we see the similarities between the non-coherent sequence estimation of a CPM signal approximated through the AMP decomposition and of a linear modulation signal. Considerable simplifications in complexity have been achieved, since the entire filter bank (requiring the use of 2^{L+u_1-1} individual filters) has been replaced by a single filter (the $h_0^{AMP}(t)$).

3.5.2 Symbol-by-Symbol Detection

The decision law of the optimal non-coherent symbol-by-symbol receiver has been given in Eq.(3.19). Using the expressions provided in Eqs.(3.110), (3.112) with Eq.(3.19), we end up with the following expression:

$$\widehat{\bar{a}_k^p} = \bar{S}_l \implies \overset{1\le l\le M_p}{\bar{max}} \{ \sum_{\bar{C}(\bar{A})\in\underline{C}_{\underline{S}}^{S_l}(k)} \aleph_{OP_{appr}}^{CPMD}(\bar{\Re}_{E,[0,0]}^{AMP},\ldots,\bar{\Re}_{E,[0,\mathcal{N}]}^{AMP},\bar{\Re}_{E,[1,0]}^{AMP},\ldots,$$

$$\bar{\Re}_{E,[\mathcal{N},\mathcal{N}]}^{AMP},\bar{\mathcal{Y}}_0^{AMP},\bar{\mathcal{Y}}_1^{AMP},\ldots,\bar{\mathcal{Y}}_{\mathcal{N}}^{AMP},\bar{C}(\bar{A}))\} \tag{3.118}$$

or equivalently

$$\widehat{\bar{a}_k^p} = \bar{S}_l \implies \overset{1\le l\le M_p}{\bar{max}} \{ \sum_{\bar{C}(\bar{A})\in\underline{C}_{\underline{S}}^{S_l}(k)} \exp\{-\frac{1}{2N_o}[\sum_{k=0}^{Z-1}(\mathcal{A}_k)^2 \sum_{n_1=0}^{\mathcal{N}}\sum_{n_2=0}^{\mathcal{N}}$$

$$\alpha_{n_1,k}^{AMP}(\alpha_{n_2,k}^{AMP})^*\Re_{E,[n_1,n_2]}^{AMP}(0) + \sum_{k=1}^{Z-1}\sum_{l=k}^{Z-1}\mathcal{A}_l\mathcal{A}_{l-k}\sum_{n_1=0}^{\mathcal{N}}\sum_{n_2=0}^{\mathcal{N}}[\alpha_{n_1,l}^{AMP}(\alpha_{n_2,l-k}^{AMP})^*$$

$$\Re_{E,[n_1,n_2]}^{AMP}(k) + \alpha_{n_2,l-k}^{AMP}(\alpha_{n_1,l}^{AMP})^*(\Re_{E,[n_1,n_2]}^{AMP}(k))^*]]\}$$

$$I_0(\frac{|\sum_{k=0}^{Z-1}\mathcal{A}_k\sum_{n=0}^{\mathcal{N}}\mathcal{Y}_{n,k}^{AMP}(\alpha_{n,k}^{AMP})^*|}{N_o})\}. \tag{3.119}$$

For $\mathcal{N} = 0$ (i.e. only one pulse is used to represent the CPM signal)

$$\widehat{\bar{a}_k^p} = \bar{S}_l \implies \overset{1\le l\le M_p}{max} \{ \sum_{\bar{C}(\bar{A})\in \underline{\underline{C}}_{\underline{S}}^{S_l}(k)} \exp\{-\frac{1}{2N_o}[\sum_{k=0}^{Z-1}(\mathcal{A}_k)^2\alpha_{0,k}^{AMP}(\alpha_{0,k}^{AMP})^*$$

$$\Re_{E,[0,0]}^{AMP}(0) + \sum_{k=1}^{Z-1}\sum_{l=k}^{Z-1}\mathcal{A}_l\mathcal{A}_{l-k}[\alpha_{0,l}^{AMP}(\alpha_{0,l-k}^{AMP})^*\Re_{E,[0,0]}^{AMP}(k)$$

$$+\alpha_{0,l-k}^{AMP}(\alpha_{0,l}^{AMP})^*(\Re_{E,[0,0]}^{AMP}(k))^*]]\}I_0(\frac{|\sum_{k=0}^{Z-1}\mathcal{A}_k\mathcal{Y}_{0,k}^{AMP}(\alpha_{0,k}^{AMP})^*|}{N_o})\}. \quad (3.120)$$

3.6 Conclusions

This Chapter presented the fundamentals of a generalized theory regarding non-coherent detection. Both sequence estimation and symbol-by-symbol detection were addressed. The theory is general enough to include the cases of ideal as well as time dispersive channels and single or multi-amplitude/phase signals. For the CPM signals, an alternative approach has also been pursued, aimed at the development of improved non-coherent receivers (for CPM signals) with reduced filtering requirements. The presented theoretical frame work is used in the following two chapters towards the development of practical and improved structures of non-coherent receivers.

Chapter 4

NON-COHERENT RECEIVERS FOR LINEAR MODULATIONS

4.1 INTRODUCTION

In Chapter 3, a generalized non-coherent detection theory was presented and the structures of the optimal sequence estimator and symbol-by-symbol receiver for linear modulations and CPM signals was given. Although the material presented in Chapter 3 has provided some new information on the subject of the non-coherent detection, it is of limited use for the design of practical communication systems. The presented metrics consist of products between exponential and modified Bessel functions. Also, as it was mentioned in subsections 3.3.2, 3.3.4 (see Figs. 3.3, 3.5) the receivers need to know the channel impulse response and the operating E_b/N_o point. This requires use of channel estimators, signal power and noise power estimators. A receiver which implements such complex mathematical functions and includes channel estimation, signal power and noise power estimation units is difficult and costly. In many applications, cost, complexity and size are limiting factors. For these applications it would have been useful if reduced complexity structures were proposed. The main objective of the present (4^{th}) and following (5^{th}) chapters is to cover this area for linear modulation and

CPM signals respectively. Starting with the material of Chapter 3 we will reach reduced complexity structures which can be implemented with today's technology.

The rest of this chapter will be presented as follows. In section 4.2 asymptotically optimal decoders for low/high values of the E_b/N_o and operation in time dispersive channels with multi-amplitude/phase signals are presented. In section 4.3 the special case of ideal channel with equal Nyquist filter apportioning is examined. The outcome gives simpler structures compared to those proposed for the dispersive channel case. This gives us the initiative to examine and describe in subsection 4.3.3 how these simplified receivers can be modified in order to be used in the dispersive channel. In section 4.4 an alternative structure of the non-coherent receiver is presented. It provides a better insight regarding the nature and the operation of the non-coherent receiver. The structure processes simultaneously the outputs of a squared envelope and more than one (multiple) differential detector [145]-[148], [151]-[156]. Possible scenarios for implementation of the receiver either in IF or in baseband form are also discussed. It is shown how the improved non-coherent structures can be built by using the simple and cost-effective squared envelope and one-symbol differential detector as building blocks and acquire the rest of the needed information by properly processing the outputs of these two units. As a result, the proposed receivers inherit the advantages of the classical non-coherent detectors (simplicity, cost effectiveness, fast synchronization etc.) while at the same time provide significant performance improvements.

Sections 4.5 to 4.8 deal with the evaluation of the proposed sequence estimators by analytical means (and in some cases by Monte Carlo simulations). Upper bound expressions of the pairwise error event probabilities are presented. These expressions are used in the union bound [227] [256] [214] to provide upper bounds of the system's performance. The evaluations have been conducted for ideal, time dispersive and faded channels and have been performed for coded/uncoded, PSK and QAM signals. *The analysis and the results have demonstrated that the proposed receivers are capable of (asymptotically) reaching the performance of the coherent receiver with perfect carrier synchronization, operating in ideal channel (best performance possible).* Some of the proposed structures are capable to achieve these performance levels with reasonable levels of complexity. The evaluations establish the superiority of the new structures as compared to the conventional

(and widely used) differential receiver. *Our performance results have shown improvements in excess of 5 dB in Gaussian channels. In faded channels the evaluations have shown improvements higher than 7 dB and reduction of error floors close to one order of magnitude.* Through the performance analysis we have identified the distance expressions which characterize the performance of the proposed receivers (equivalent to the Euclidean distance we meet in coherent systems). These distance metrics can be used to design improved coded schemes, for the non-coherent receivers under consideration.

In section 4.9 ways to design reduced complexity sequence estimators operating on long data sequences are presented. These reduced complexity structures are evaluated by analytical means and computer simulations.

Section 4.10 deals with asymptotically optimal symbol-by-symbol (S-B-S) receivers. The receivers are evaluated by analytical means. Section 4.11 introduces reduced complexity S-B-S receivers based on multiple differential detection and the use of signal combining techniques controlled by decision feedback.

Before closing this introductory section, we would like to mention that the notion of detecting PSK signals by using multiple received signal observables is not new [237]. P. E. K. Chow, P. H. Ho [30] and later on Samejima et. al. [225] and Masamura et. al. [172] applied this notion (on BPSK, QPSK and MSK respectively) in the form of an error correction scheme processing hard decisions provided by the outputs of more than one differential detector, called *"Non-Redundant Error Correction"* (NEC). Today, additional work reported in [173], [266] has proven the technique advantageous for use in time dispersive and interference controlled environments.

Our work has been published in various journals and conferences as early as 1986 [146], [145], [147], [148]. In 1989 we also proposed the use of multiple differential detection to Quadrature Amplitude Modulations [149] and Multi-Amplitude MSK (MA-MSK) signals [150]. As a summary we would say that compared to the Non-Redundant Error Correction technique reported in the past, the present work has the following fundamental differences and contributions: i) the multiple differential detection has been developed and used in a soft decision decoding form, ii) its link to the optimal non-coherent detection has been discovered iii) it has been shown that (combined with envelope detection) its use can be extended to multi-amplitude/phase signals and/or

time dispersive environments and iv) we have set the analytical framework for the evaluation of the proposed soft decision multiple differential receivers. Also, while the Non-Redundant Error Correction schemes have been applied only on uncoded signals, our work has made the extension of multiple differential detection to trellis coded signals possible. Our evaluation results have shown that with trellis coded signals, the improvements offered by the multiple differential detection are considerably higher from the gains achieved when the improved non-coherent receivers are used with uncoded signals.

Recently, other authors came with similar receiver structures verifying our results published in earlier years [52], [53]. In terms of content, their work has limitations compared to the analysis presented in this thesis. Their approach does not allow consideration of dispersive channel, neither does it allow the possibility of applying multiple differential detection to multi-amplitude/phase signals. These limitations extend into both the receiver design and the performance evaluation, where we have been able to address time dispersion, use of the non-coherent receivers with multi-amplitude phase signal constellations and operation in channels corrupted by colored noise.

4.2 ASYMPTOTICALLY OPTIMAL SEQUENCE ESTIMATION IN TIME DISPERSIVE CHANNELS

The objective of the work to be covered in this section is to provide lower complexity non-coherent sequence estimators for linear modulation systems operating in a time dispersive channel. In the following paragraph, two approximations of the optimal non-coherent decoder[1] will be provided, one for low E_b/N_o and the other for high E_b/N_o values.

4.2.1 Low E_b/N_o

The exponential and modified Bessel functions can be expressed through the following time series expansion [236]:

$$e^x = 1 + x + \frac{x^2}{2!} + \frac{x^3}{3!} + \cdots = \sum_{l=0}^{\infty} \frac{x^l}{l!} \tag{4.1}$$

$$I_o(x) = 1 + \frac{x^2}{2^2} + \frac{x^4}{2^2 4^2} + \frac{x^6}{2^2 4^2 6^2} + \ldots = \sum_{i=0}^{\infty} \frac{x^{2i}}{2^{2i}(i!)^2} \tag{4.2}$$

Using these formulas with Eq.(3.53), truncating all the terms where $\frac{1}{N_o}$ appear with power higher than two and eliminating all the terms which are independent from the considered sequence $\bar{C}(\bar{A})$, we end up with the following metric expression (to be maximized):

$$\begin{aligned} \aleph_{LAO}^{LMD}(h_0, \bar{h}, \bar{y}, \bar{C}(\bar{A})) \;=\; & -[MST(h_0, \bar{C}(\bar{A})) + IST(\bar{h}, \bar{C}(\bar{A}))] \\ & + \frac{(MST(h_0, \bar{C}(\bar{A})) + IST(\bar{h}, \bar{C}(\bar{A})))^2}{2N_o} \\ & + \frac{|\sum_{k=0}^{z-1} y_k (c_k)^*|^2}{4N_o}. \end{aligned} \tag{4.3}$$

[1] In the text, the reader will encounter the term (non-coherent) decoder. It is used with the meaning "(non-coherent) sequence estimator", unless otherwise indicated.

(LAO stands for Low (E_b/N_o), Asymptotically Optimal (decoder)). For the definition of $MST(h_0, \bar{C}(\bar{A}))$, $IST(\bar{h}, \bar{C}(\bar{A}))$, please refer to Eqs.(3.48), (3.49) in the third Chapter.

For PSK signals, Eq.(4.3) becomes:

$$\aleph_{LAO}^{PSK}(\bar{h}, \bar{y}, \bar{C}(\bar{A})) = -IST(\bar{h}, \bar{C}(\bar{A})) + \frac{IST^2(\bar{h}, \bar{C}(\bar{A}))}{2N_o} + \frac{|\sum_{k=0}^{z-1} y_k(c_k)^*|^2}{4N_o}. \quad (4.4)$$

As E_b/N_o becomes smaller (i.e. $N_o \to \infty \implies \frac{E_b}{N_o} \to 0$), the strength of the two squared terms present in the metric becomes weaker. This leaves the $-[MST(h_0, \bar{C}(\bar{A})) + IST(\bar{h}, \bar{C}(\bar{A}))]$ term to dominate the decision (a term totally independent from the received signal samples y_k). This results in a decision law independent from the received signal. Regardless of what the received signal is, the decoder will always decode the sequence(s) which happens to provide the minimum value for $(MST(h_0, \bar{C}(\bar{A})) + IST(\bar{h}, \bar{C}(\bar{A})))$. From the discussion presented above, we come to the following conclusion: *For the non-coherent sequence estimation at low E_b/N_o in time dispersive channels and/or with multi-amplitude/phase signals, the decision is dominated by the ISI components and the symbols of lower energy content. As the $\frac{E_b}{N_o} \to 0$, the decision becomes gradually more and more independent from the received signal.*
To the best of our knowledge such a behaviour of the non-coherent receiver is being identified for the first time in the literature. This represents a key difference as compared to the coherent detection where the received signal is always present in the detection process, regardless of the operating E_b/N_o, the characteristics of the channel and the signal constellation.

4.2.2 High E_b/N_o

For high E_b/N_o, a considerable simplification of the decoding metric can be achieved by utilizing the following approximation of the modified Bessel function [1]:

$$I_o(|z|) \simeq \frac{1}{\sqrt{2\pi|z|}} e^{|z|} \quad \text{for} \quad |z| > 6.8 \tag{4.5}$$

In Appendix A it has been shown that use of the above approximation in the metric described by Eq.(3.53) leads to the following expression:

$$\begin{aligned} \aleph_{HAO}^{LMD}(h_0, \bar{h}, \bar{y}, \bar{C}(\bar{A})) &= -(\frac{1}{2}h_0(\sum_{k=0}^{Z-1}|c_k|^2) + \sum_{l=1}^{Z-1}\sum_{k=l}^{Z-1} Re\{h_l c_k c_{k-l}^*\}) \\ &\quad + |\sum_{k=0}^{Z-1} y_k c_k^*| \end{aligned} \tag{4.6}$$

or equivalently

$$\begin{aligned} \aleph_{HAO}^{LMD}(h_0, \bar{h}, \bar{y}, \bar{C}(\bar{A})) &= -(MST(h_0, \bar{C}(\bar{A})) + IST(\bar{h}, \bar{C}(\bar{A}))) \\ &\quad + |\sum_{k=0}^{Z-1} y_k c_k^*| \end{aligned} \tag{4.7}$$

(HAO stands for High (E_b/N_o), Asymptotically Optimal (decoder)). For PSK signals the metric is simplified to:

$$\aleph_{HAO}^{PSK}(\bar{h}, \bar{y}, \bar{C}(\bar{A})) = -(\sum_{l=1}^{Z-1}\sum_{k=l}^{Z-1} Re\{h_l c_k c_{k-l}^*\}) + |\sum_{k=0}^{Z-1} y_k c_k^*| \,, \tag{4.8}$$

or equivalently

$$\aleph_{HAO}^{PSK}(\bar{h}, \bar{y}, \bar{C}(\bar{A})) = -IST(\bar{h}, \bar{C}(\bar{A})) + |\sum_{k=0}^{Z-1} y_k c_k^*| \,. \tag{4.9}$$

The structure of the receiver based on $\aleph_{HAO}^{LMD}(h_0, \bar{h}, \bar{y}, \bar{C}(\bar{A}))$ is presented in Fig. 4.1 and the block diagram of the processing unit implementing

$\aleph_{HAO}^{LMD}(h_0, \bar{h}, \bar{y}, \bar{C}(\bar{A}))$ in Fig. 4.2. The first observation is that in this case, the exponential and Bessel functions have disappeared, along with the need to provide scaling according to the operating E_b/N_o. These eliminations represent considerable reduction in complexity. However, at the receiver, knowledge of the channel impulse response is required, consequently a channel estimator has to be incorporated into its structure. Due to the asymptotically optimal nature of the decoder (sequence estimator) described by $\aleph_{HAO}^{LMD}(h_0, \bar{h}, \bar{y}, \bar{C}(\bar{A}))$, we shall be referring to this structure from now on as **Asymptotically Optimal Decoder (AOD).**

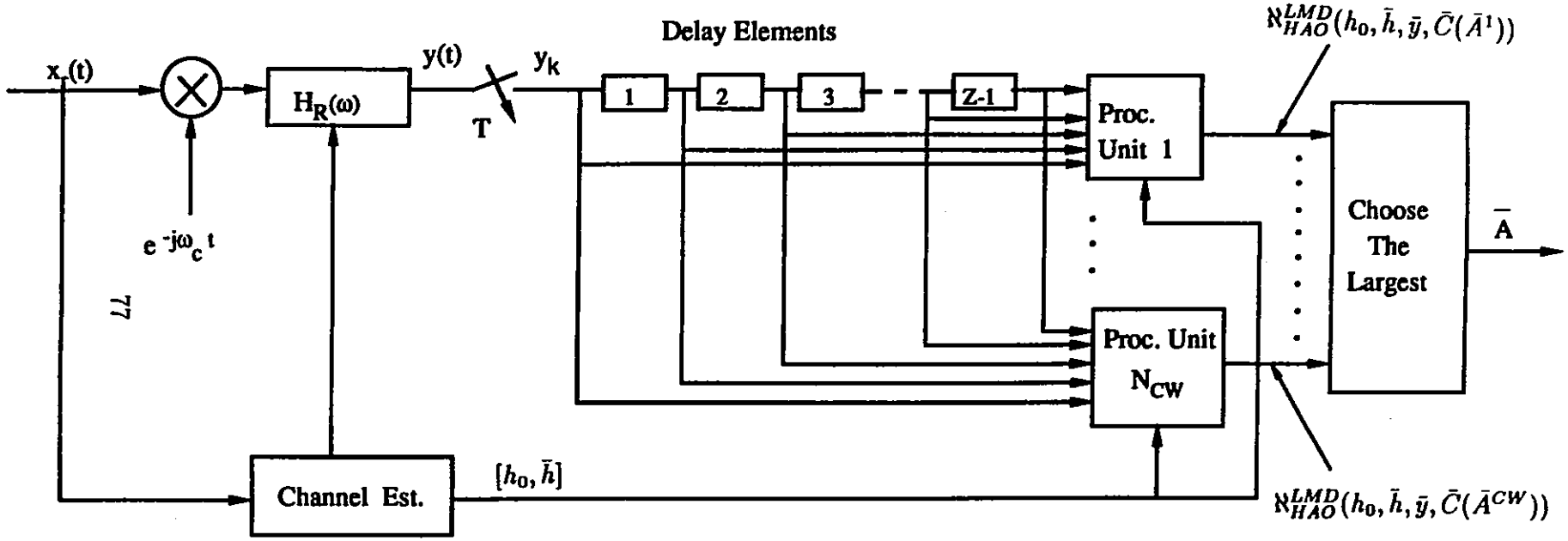

Figure 4.1 Block diagram of the asymptotically optimal non-coherent sequence estimator operating in a time dispersive environment.

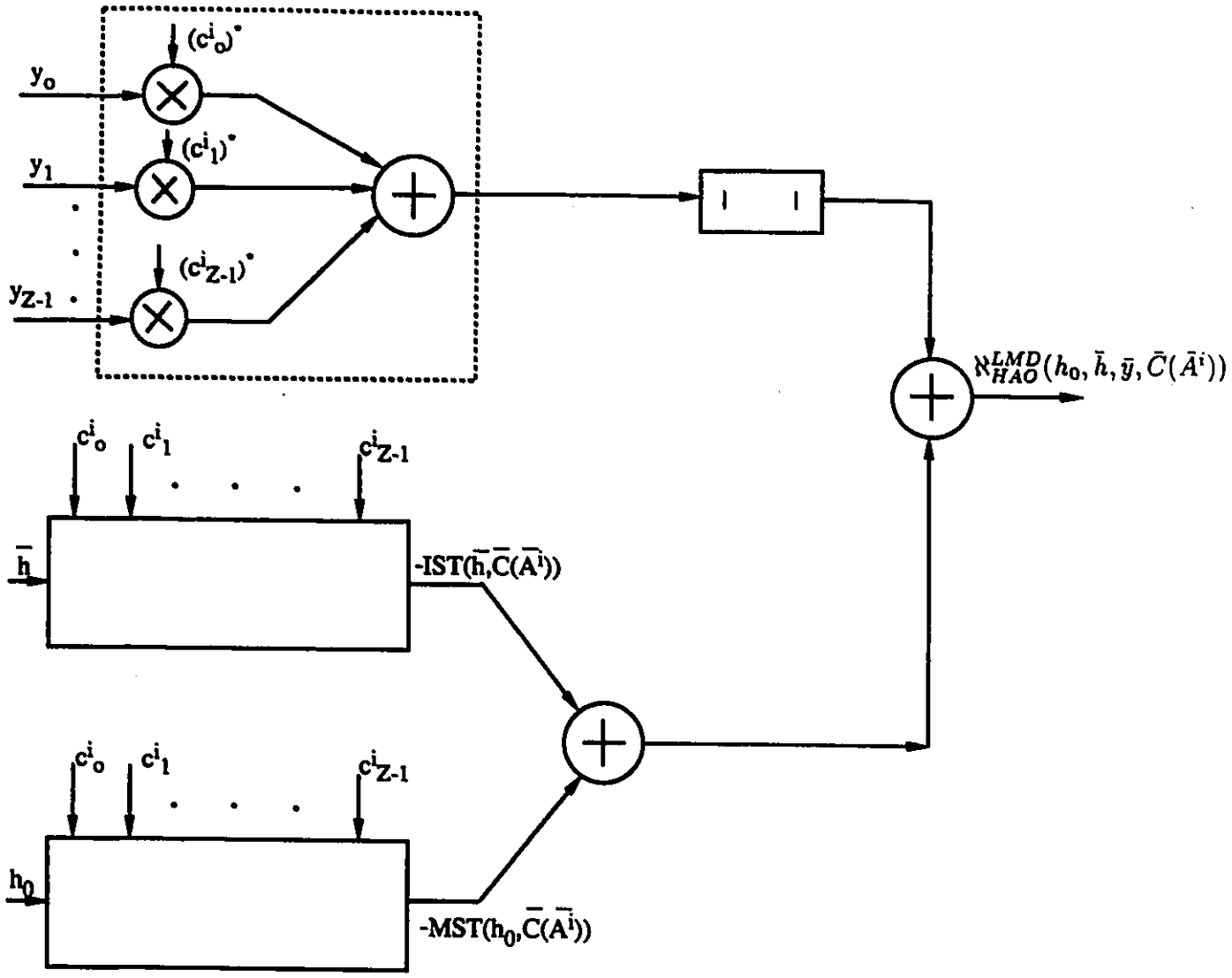

Figure 4.2: i^{th} Processing Unit of the asymptotically optimal non-coherent sequence estimator operating in a time dispersive environment.

4.3 SEQUENCE ESTIMATION IN IDEAL CHANNEL WITH EQUALLY NYQUIST FILTER APPORTIONED SYSTEMS

4.3.1 Multi-Amplitude/Phase Signals

When a Multi-amplitude/phase signal is used, the metric of the asymptotically optimal decoder can be readily derived from Eq.(4.5) by setting $IST(\bar{h}, \bar{C}(\bar{A})) = 0$. The metric expression is:

$$\aleph_{HAO}^{LMI}(h_0, \bar{y}, \bar{C}(\bar{A})) = -MST(h_0, \bar{C}(\bar{A})) + |\sum_{k=0}^{Z-1} y_k c_k^*| \tag{4.10}$$

(*LMI* stands for Linear (modulation) Multi-amplitude (signal) Ideal (channel)) or equivalently

$$\aleph_{HAO}^{LMI}(h_0, \bar{y}, \bar{C}(\bar{A})) = -\frac{1}{2}h_0(\sum_{k=0}^{Z-1}|c_k|^2) + |\sum_{k=0}^{Z-1} y_k c_k^*| \,. \tag{4.11}$$

4.3.2 Phase Shift Keying Signals

The metric of the optimal non-coherent sequence estimator corresponding to a PSK signal has been presented in Eq.(3.54). The metric depends on a zero order modified Bessel function only. Considering the monotonically increasing nature of the modified Bessel function, we can carry on the maximization of its argument rather than the Bessel function itself. This leads to the following metric:

$$\aleph_{IC}(\bar{y}, \bar{C}(\bar{A})) = |\sum_{k=0}^{Z-1} y_k c_k^*|. \tag{4.12}$$

$\aleph_{IC}(\bar{y}, \bar{C}(\bar{A}))$ is valid for any value of the E_b/N_o we are operating at.

As we observe, the sequence estimator processes the received signal samples as a block entity. We shall be calling this sequence estimator as **Block Decoder (BD)**. The block diagram of the receiver is presented in Fig. 4.3 and the processing unit implementing $\aleph_{IC}(\bar{y}, \bar{C}(\bar{A}))$ in Fig. 4.4.

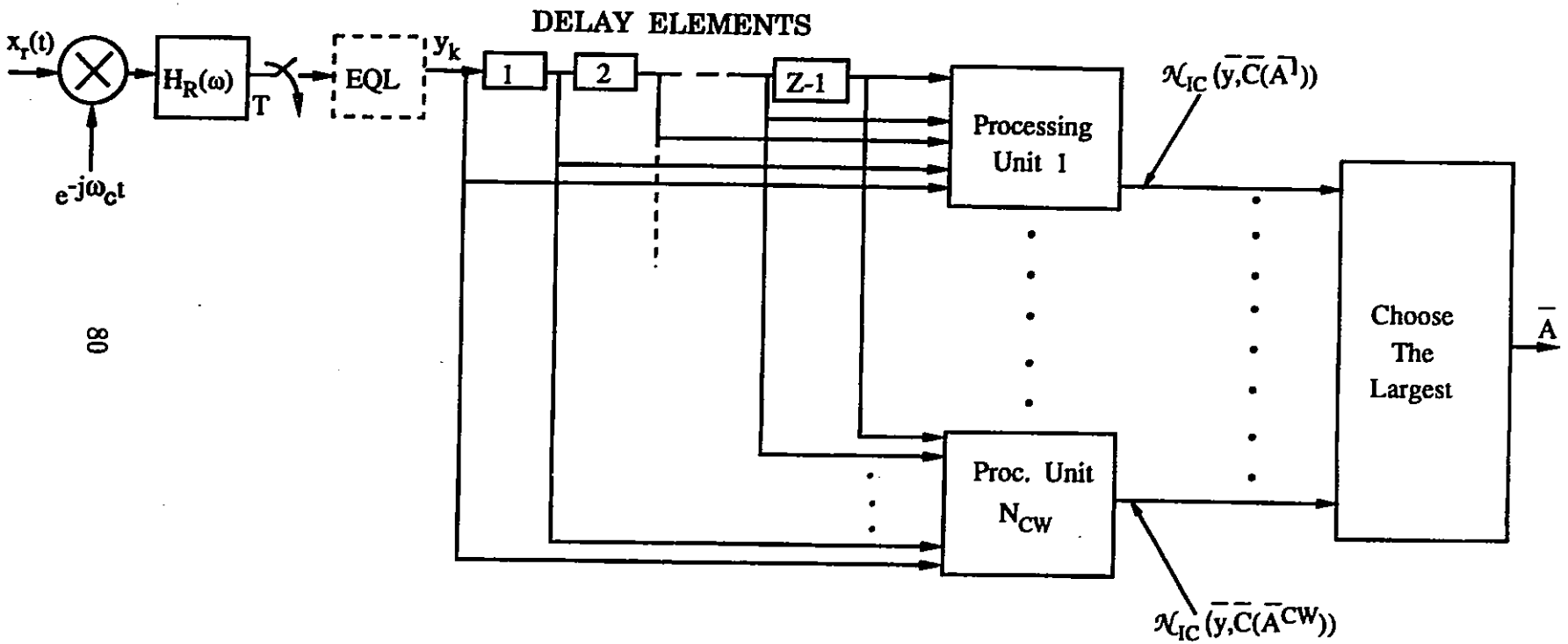

Fig. 4.3 Block diagram of the non-coherent Block Decoder.

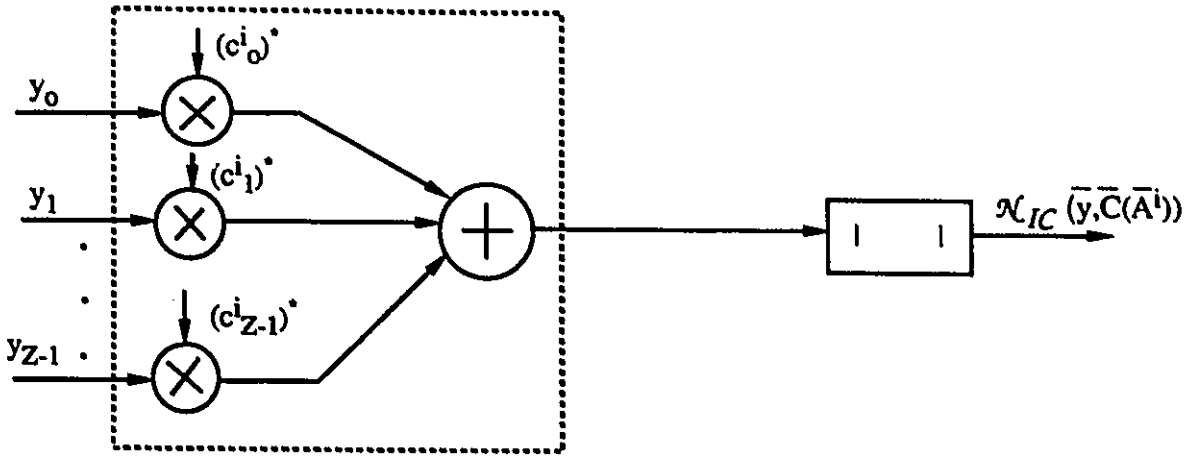

Figure 4.4: i^{th} Processing Unit of non-coherent Block Decoder.

The block decoder has lower complexity levels from both the optimal and asymptotically optimal decoders examined before. However we remind the reader that this structure is optimal only for PSK signals under ideal channel/equal Nyquist filter apportioning.

4.3.3 Use of the Block Decoder in a Time Dispersive Channel and/or with Non-Equally Nyquist Filter Apportioned Systems

The lower complexity levels of the block decoder leads to the natural question: "What penalty in performance would the system pay if the use of the block decoder was to be extended to the non-ideal channel/non-equal apportioning cases?". This question will be answered in this section. Suggestions and approaches of how to reduce the losses and develop power efficient schemes will also be provided.

The analysis presented up to this point has indicated that the demodulated received signal $(x_r(t)e^{-j\omega_c t})$ should be processed by a post detection

filter $H_R(\omega)$ matched to $H_E(\omega)$. However when $H_E(\omega)$ does not have the spectral shaping of a square root Nyquist I filter, the use at the receiver of a filter matched to $H_E(\omega)$ would result in an overall impulse response $h(t)$ which introduces ISI. When the optimal or asymptotically optimal decoder (see Eqs.(3.53), (4.6)) is used, the ISI is taken into consideration during detection through the use of the $IST(\bar{h}, \bar{C}(\bar{A}))$ term. However, when the $\aleph_{IC}(\bar{y}, \bar{C}(\bar{A}))$ is used, the presence of ISI is not reflected anywhere (we remind the reader that under ideal channel/equal Nyquist filter conditions for which $\aleph_{IC}(\bar{y}, \bar{C}(\bar{A}))$ has been derived, ISI is not present).

In order to avoid the considerable degradation from excessive strength of ISI, the matched filter requirement forced on the post detection filtering process ($H_R(\omega)$) has to be relaxed. The post detection filtering should be shaped appropriately so as to suppress the ISI. This can be done by using equalization. The two most popular equalization techniques are the zero forcing equalization (ZFE) [124] and the minimum mean square error (MMSE) equalization [124]. In the first case, the post detection filter-equalizer is chosen such as to completely compensate the ISI [4]. In the ZFE case,

$$y_k = e^{j(\phi_k + \psi)} + n_k. \tag{4.13}$$

Also it can be proven [124] that the autocorrelation between the noise terms n_k equals

$$R_i^n = E\{n_k n_{k-i}^*\} = \frac{1}{2\pi} \int_{-\infty}^{\infty} \frac{1}{|H_E(\omega)|^2} e^{j\omega kT} d\omega. \tag{4.14}$$

The non-equal apportioning of the Nyquist filter between transmitter and receiver belongs to ZFE. In this case, the premodulation filter $H_T(\omega)$ is equal to

$$H_T(\omega) = [H_{NYQ}(\omega)]^{\epsilon} \tag{4.15}$$

where $H(\omega)$ is the spectral shaping of a square root Nyquist I filter, and $0 \leq \epsilon \leq 1$. At the receiver

$$H_R(\omega) = [H_{NYQ}(\omega)]^{1-\epsilon} \tag{4.16}$$

[4] ZFE is advantageous when $H_E(\omega)$ does not contain strong nulls in its spectrum. When this is the case, the equalizer is forced to provide high gains at those frequencies where the nulls appear (in order to compensate them). This increases the levels of noise power and results in serious performance degradation [124].

so that $H_T(\omega)$, $H_R(\omega)$ when cascaded, provide the spectral shaping of the Nyquist I filter (we are assuming that the channel is ideal). From Eq.(4.14), we can easily verify that for this case

$$R_i^n = \frac{1}{2\pi}\int_{-\infty}^{\infty} |H_{NYQ}(\omega)|^{2(1-\epsilon)} e^{j\omega kT} d\omega. \tag{4.17}$$

The use of non-equal apportioning is associated with the desire to have reduced complexity at the transmitter or receiver. A frequently encountered example is the case of broadcasting applications, where it is preferable to put the full apportioning at the transmitter and use a simple low cost filter at the receiver [239]. This approach provides cost efficient receiver units for the large number of users.

In the MMSE, the attempt is to minimize the overall disturbance (i.e. ISI and Gaussian noise). In this case there is some ISI left, and the received signal samples y_k can be expressed as

$$y_k = e^{j\phi} \sum_{l=-l_l}^{l_u} c_{k-l} h_l + n_k \tag{4.18}$$

l_l, l_u being no-negative integers. The expressions which are to be used to upper bound the performance of the block decoder are capable of including the effect of both ISI and noise correlation on the performance (for detailed derivation see Appendix B). Consequently, they provide the ability to evaluate a receiver with either ZFE or MMSE.

4.4 AN ALTERNATIVE STRUCTURE OF THE NON-COHERENT RECEIVER

The analysis carried out to this point has provided structures which are quite different and seem unrelated to the known classical non-coherent detection schemes. However, it is logical to expect some relation between them and the receivers proposed in this work. The objective of the present section is to provide this link between the proposed receivers and familiar non-coherent detection techniques.

4.4.1 A Combined Squared Envelope and Multiple Differential Detection Structure

The starting point for providing the alternative metric expression is to formulate the expression for the square of $\aleph_{IC}(\bar{y}, \bar{C}(\bar{A}))$, $(\aleph_{IC}^{SQ}(\bar{y}, \bar{C}(\bar{A})))$ i.e.

$$\begin{aligned}\aleph_{IC}^{SQ}(\bar{y}, \bar{C}(\bar{A})) &= \sum_{k=0}^{Z-1} |y_k|^2|c_k|^2 + 2\sum_{k=1}^{Z-1}\sum_{l=1}^{k} Re\{(y_k y_{k-l}^*)\}(c_k c_{k-l}^*)^*\} \\ &= \sum_{k=0}^{Z-1} |y_k|^2|c_k|^2 + 2\sum_{k=1}^{Z-1}\sum_{l=1}^{k}[Re\{(y_k y_{k-l}^*)\}Re\{(c_k c_{k-l}^*)\} + \\ &\qquad Im\{(y_k y_{k-l}^*)\}Im\{(c_k c_{k-l}^*)\}] \\ &= (\Xi^E(\bar{y}) + 2\Xi_1^D(\bar{y}, \bar{C}(\bar{A}))) \qquad (4.19)\end{aligned}$$

with

$$\Xi^E(\bar{y}) = \sum_{k=0}^{Z-1} |y_k|^2|c_k|^2 \qquad (4.20)$$

and

$$\Xi_1^D(\bar{y}, \bar{C}(\bar{A})) = \sum_{k=1}^{Z-1}\sum_{l=1}^{k}[Re\{(y_k y_{k-l}^*)\}Re\{(c_k c_{k-l}^*)\} + Im\{(y_k y_{k-l}^*)\}Im\{(c_k c_{k-l}^*)\}] \,. \qquad (4.21)$$

The $|y_k|^2$ are squares of the envelopes of the signal samples y_k. They can be provided at the output of a squared envelope detector. Defining the terms

$$d_l(k) = y_k y_{k-l}^*, \quad d_l^I(k) = Re\{(y_k y_{k-l}^*)\}, \quad d_l^Q(k) = I_m\{(y_k y_{k-l}^*)\}, \qquad (4.22)$$

recalling that (see Eq.(3.30))

$$\Delta\Theta_l(k) = Arg[c_k c_{k-l}^*] = Arg[\mathcal{J}_k \mathcal{J}_{k-l} e^{j(\theta_k \ominus \theta_{k-l})}] = \theta_k \ominus \theta_{k-l} \qquad (4.23)$$

and placing them in Eq. (4.21), we get the following expression for $\Xi_1^D(\bar{y}, \bar{C}(\bar{A}))$:

$$\Xi_1^D(\bar{y}, \bar{C}(\bar{A})) = \sum_{k=0}^{Z-1} \mathcal{J}_k \sum_{l=1}^{k} \mathcal{J}_{k-l}[d_l^I(k)\cos(\Delta\Theta_l(k)) + d_l^Q(k)\sin(\Delta\Theta_l(k))].$$

(4.24)

We remind the reader that $\mathcal{J}_k = |c_k|$. When differential encoding is used at the transmitter

$$c_k c_{k-l}^* = \mathcal{J}_k \mathcal{J}_{k-l} e^{j(\Delta\Theta_l(k))} = \mathcal{J}_k \mathcal{J}_{k-l} e^{j(\phi_k \oplus \phi_{k-1} \oplus ..... \oplus \phi_{k-l+1})} \tag{4.25}$$

(see Eq.(3.31)) and

$$\Delta\Theta_l(k) = \phi_k \oplus \phi_{k-1} \oplus .... \oplus \phi_{k-l+1} \tag{4.26}$$

(see Eq.(3.32)). If differential encoding is absent,

$$\Delta\Theta_l(k) = \theta_k \ominus \theta_{k-l} = \phi_k \ominus \phi_{k-l} \tag{4.27}$$

(see Eq.(3.33)).

The term $d_l(k)$ is the product between the signal sample y_k and the complex conjugate of the y_{k-l} sample, received lT seconds before. This operation represents differential detection, with the differential detector having a delay element equal to lT. From Eq.(4.24) we realize that the optimal non-coherent sequence estimator requires the use and processes the output of a large number of differential detectors (a total of $Z-1$), their delay elements being integer multiples of the symbol period T. Because of the squared envelope and the multiple differential detectors required, we have named this approach **Squared Envelope & Multiple Differential Detection (SEMDD)**[2].

Introducing the expression of $[\aleph_{IC}^{SQ}(\bar{y}, \bar{C}(\bar{A}))]$ in Eqs.(3.45), (4.7), (4.12) they become:

$$\begin{aligned}
\aleph_{OP}^{LMD}(h_0, \bar{h}, \bar{y}, \bar{C}(\bar{A})) &= \exp\{-\frac{1}{N_o}(\frac{1}{2}MST(h_0, \bar{C}(\bar{A})) + IST(\bar{h}, \bar{C}(\bar{A})))\} \\
&\quad I_0(\frac{[\Xi^E(\bar{y}) + 2\Xi_1^D(\bar{y}, \bar{C}(\bar{A}))]^{\frac{1}{2}}}{N_o}) \\
&= \exp\{-\frac{1}{N_o}(\frac{1}{2}(\sum_{k=0}^{Z-1} \mathcal{J}_k^2) + \sum_{l=1}^{Z-1}\sum_{k=l}^{Z-1} \mathcal{J}_k \mathcal{J}_{k-l} Re\{h_l e^{j\Delta\Theta_l(k)}\})\}
\end{aligned}$$

[2]Considering that $y_k y_{k-l}^*$ is equal to $|y_k|^2$ when $l = 0$, we can visualize the squared envelope detector as a differential detector having delay element equal to zero. Consequently, the receiver can be viewed as a generalized multiple differential receiver with Z differential detectors and the delays starting from 0 up to $(Z-1)T$.

$$I_o\left(\frac{\left[\sum_{k=0}^{Z-1}|y_k|^2\mathcal{J}_k^2+2\sum_{k=1}^{Z-1}\mathcal{J}_k\sum_{l=1}^{k}\mathcal{J}_{k-l}(d_l^I(k)\cos(\Delta\Theta_l(k))+d_l^Q(k)\sin(\Delta\Theta_l(k)))\right]^{\frac{1}{2}}}{N_o}\right)$$

(4.28)

$$\begin{aligned}
\aleph_{HAO}^{LMD}(h_0,\bar{h},\bar{y},\bar{C}(\bar{A})) &= -\left(\frac{1}{2}MST(h_0,\bar{C}(\bar{A}))+IST(\bar{h},\bar{y},\bar{C}(\bar{A}))\right) \\
&+ \left[\Xi^E(\bar{y})+2\Xi_1^D(\bar{y},\bar{C}(\bar{A}))\right]^{\frac{1}{2}} \\
&= -\left(\left(\frac{1}{2}\left(\sum_{k=0}^{Z-1}\mathcal{J}_k^2\right)+\sum_{l=1}^{Z-1}\sum_{k=l}^{Z-1}Re\{h_l e^{j\Delta\Theta_l(k)}\}+\left[\sum_{k=0}^{Z-1}|y_k|^2\mathcal{J}_k^2\right.\right.\right. \\
&+ \left.\left.\left. 2\sum_{k=1}^{Z-1}\mathcal{J}_k\sum_{l=1}^{k}\mathcal{J}_{k-l}[d_l^I(k)\cos(\Delta\Theta_l(k))+d_l^Q(k)\sin(\Delta\Theta_l(k))\right]^{\frac{1}{2}}\right.\right.\right. .
\end{aligned}$$

(4.29)

For PSK signals ($\mathcal{J}_k = 1$), the metrics described by Eqs.(4.28), (4.31) become:

$$\begin{aligned}
\aleph_{OP}^{PSK}(\bar{h},\bar{y},\bar{C}(\bar{A})) &= \exp\{-\frac{1}{N_o}(IST(\bar{h},\bar{C}(\bar{A})))\} \\
&\quad I_0\left(\frac{\left[\Xi^E(\bar{y})+2\Xi_1^D(\bar{y},\bar{C}(\bar{A}))\right]^{\frac{1}{2}}}{N_o}\right) \\
&= \exp\{-\frac{1}{N_o}\left(\sum_{l=1}^{Z-1}\sum_{k=l}^{Z-1}Re\{h_l e^{j\Delta\Theta_l(k)}\}\right)\}
\end{aligned}$$

$$I_o\left(\frac{\left[\sum_{k=0}^{Z-1}|y_k|^2+2\sum_{k=1}^{Z-1}\sum_{l=1}^{k}(d_l^I(k)\cos(\Delta\Theta_l(k))+d_l^Q(k)\sin(\Delta\Theta_l(k)))\right]^{\frac{1}{2}}}{N_o}\right)$$

(4.30)

$$\begin{aligned}
\aleph_{HAO}^{PSK}(\bar{h},\bar{y},\bar{C}(\bar{A})) &= -(IST(\bar{h},\bar{y},\bar{C}(\bar{A})))\} + \left[\Xi^E(\bar{y})+2\Xi_1^D(\bar{y},\bar{C}(\bar{A}))\right]^{\frac{1}{2}} \\
&= -\left(\sum_{l=1}^{Z-1}\sum_{k=l}^{Z-1}Re\{h_l e^{j\Delta\Theta_l(k)}\}+\left[\sum_{k=0}^{Z-1}|y_k|^2+\right.\right. \\
&\quad \left.\left. 2\sum_{k=1}^{Z-1}\sum_{l=1}^{k}[d_l^I(k)\cos(\Delta\Theta_l(k))+d_l^Q(k)\sin(\Delta\Theta_l(k))]^{\frac{1}{2}}\right.\right. .
\end{aligned}$$

(4.31)

As it can be seen, both squared envelope as well as the multiple differential detectors are necessary for the decoder.

Regarding the third metric corresponding to the block decoder, expressed in Eq.(4.12) we have:

$$\begin{aligned}\aleph_{IC}(\bar{y},\bar{C}(\bar{A})) &= [\Xi^{E}(\bar{y})+2\Xi_{1}^{D}(\bar{y},\bar{C}(\bar{A}))]^{\frac{1}{2}} \\ &= [\sum_{k=0}^{Z-1}|y_k|^2+2\sum_{k=0}^{Z-1}\sum_{l=1}^{k} \\ &\quad [d_l^I(k)\cos(\Delta\Theta_l(k))+d_l^Q(k)\sin(\Delta\Theta_l(k))]^{\frac{1}{2}} .\end{aligned} \tag{4.32}$$

Considering that maximization of $\aleph_{IC}(\bar{y},\bar{C}(\bar{A}))$ is equivalent to the maximization of its square $\aleph_{IC}^{SQ}(\bar{y},\bar{C}(\bar{A}))$ and using the fact that $\Xi^{E}(\bar{y})$ is common and independent from the sequence $\bar{C}(\bar{A})$, we obtain the following equivalent metric expression (to be maximized):

$$\begin{aligned}\aleph_{IC}^{MDD}(\bar{y},\bar{C}(\bar{A})) &= \Xi_{1}^{D}(\bar{y},\bar{C}(\bar{A})) \\ &= \sum_{k=1}^{Z-1}\sum_{l=1}^{k}[d_l^I(k)\cos(\Delta\Theta_l(k))+d_l^Q(k)\sin(\Delta\Theta_l(k))] .\end{aligned} \tag{4.33}$$

As we see, the decoder requires only the multiple differential detection terms, while the squared envelope detector is not needed any more. We remind the reader that this metric is optimal when dealing with ideal channel and equal Nyquist filter apportioning.

The material given in this section has accomplished two things. It provided the link connecting the various optimal or asymptotically optimal non-coherent receivers to the classic non-coherent detection techniques. The squared envelope and differential detector can be seen as the building blocks which construct the advanced non-coherent detection techniques proposed and examined in this thesis. Also, the possibility of constructing the improved non-coherent receivers by using the simple and cost efficient squared envelope and multiple differential detectors is beneficial for the implementation of the proposed schemes.

4.4.2 An Intuitive Explanation on how SEMDD works

The following is an explanation on how SEMDD works. The squared envelope detector provides information regarding the amount of received signal energy in every symbol period. This allows the receiver to distinguish between information signals with variable energy levels per symbol period. Signals with variable energy levels per symbol period occur when multi-amplitude modulations are used (as for example QAM or multi-amplitude PSK), or the channel is time dispersive. When such inequality in the energy levels does not exist, the squared envelope detector is not needed. This is why it disappears from the metric expression of Eq.(4.33) which deals with PSK signals transmitted through an ideal channel.

The multiple differential detectors extract the information associated with the phase of the transmitted signal. Since we are dealing with non-coherent detection (the initial phase ψ is unknown to the receiver), the information associated with the signal phase is carried in phase differences rather than absolute phase values. From Eqs.(4.26), (4.27) it can be clearly seen that when multiple differential detection is used, the information phases ϕ_k appear at the output of more than one differential detectors. From Eq.(4.26) we also see that differential detectors with delay elements higher than the symbol period (T) apply a self-encoding process to the information phases ϕ_k. The receiver uses this extra information for ϕ_k (coming from the use of multiple differential detectors) in a process that can be seen as signal combining. This increases the signal to noise ratio and makes the decision more reliable.

4.4.3 Implementation of the SEMDD

The implementation of the squared envelope and multiple differential detection can be applied in IF or baseband form. The two different approaches are presented in Figs. 4.5 and 4.6. In the first case, the detectors provide the $|y_k|^2$ and $d_l^I(k)$, $d_l^Q(k)$ signal samples by processing the received signal while still in the IF frequencies [3] . In the second case, the received signal is first

[3]When IF implementation is used, the carrier frequencies f_c should be a multiple of the symbol rate ($\frac{1}{T}$). In the opposite case, phase offsets will appear in the outputs of the differential detectors which will inevitably deteriorate the performance.

demodulated and afterwards it is processed by the squared envelope and the differential detectors.

Both approaches (i.e. IF or baseband) have their advantages and disadvantages. The choice between the two of them should be made according to the nature and operational environment and the characteristics of the particular application. More discussion about the advantages and disadvantages of each technique will follow.

An alternative (and equivalent) expression of $\Xi_1^D(\bar{y}, \bar{C}(\bar{A}))$ is the

$$\Xi_2^D(\bar{y}, \bar{C}(\bar{A})) = \sum_{i=0}^{Z-1} Re\{y_k(\zeta_k^k)^*\} \tag{4.34}$$

with

$$\zeta_k^l = \sum_{i=1}^{l-1} y_{k-i}\{c_k c_{k-i}^*\}. \tag{4.35}$$

Integration of Eq.(4.23) into Eq.(4.35) gives:

$$\zeta_k^l = \{\sum_{i=0}^{l-1} y_{k-i}\mathcal{J}_k\mathcal{J}_{k-i}e^{j\Delta\Theta_i(k)}\} \tag{4.36}$$

with $\Delta\Theta_i(k)$ being as defined in Eq.(4.23) ($\mathcal{J}_k = |c_k|$). The metric of Eq.(4.34) represents an alternative and sometimes more suitable expression for recursive implementation of the decoder, when baseband differential detection is used.

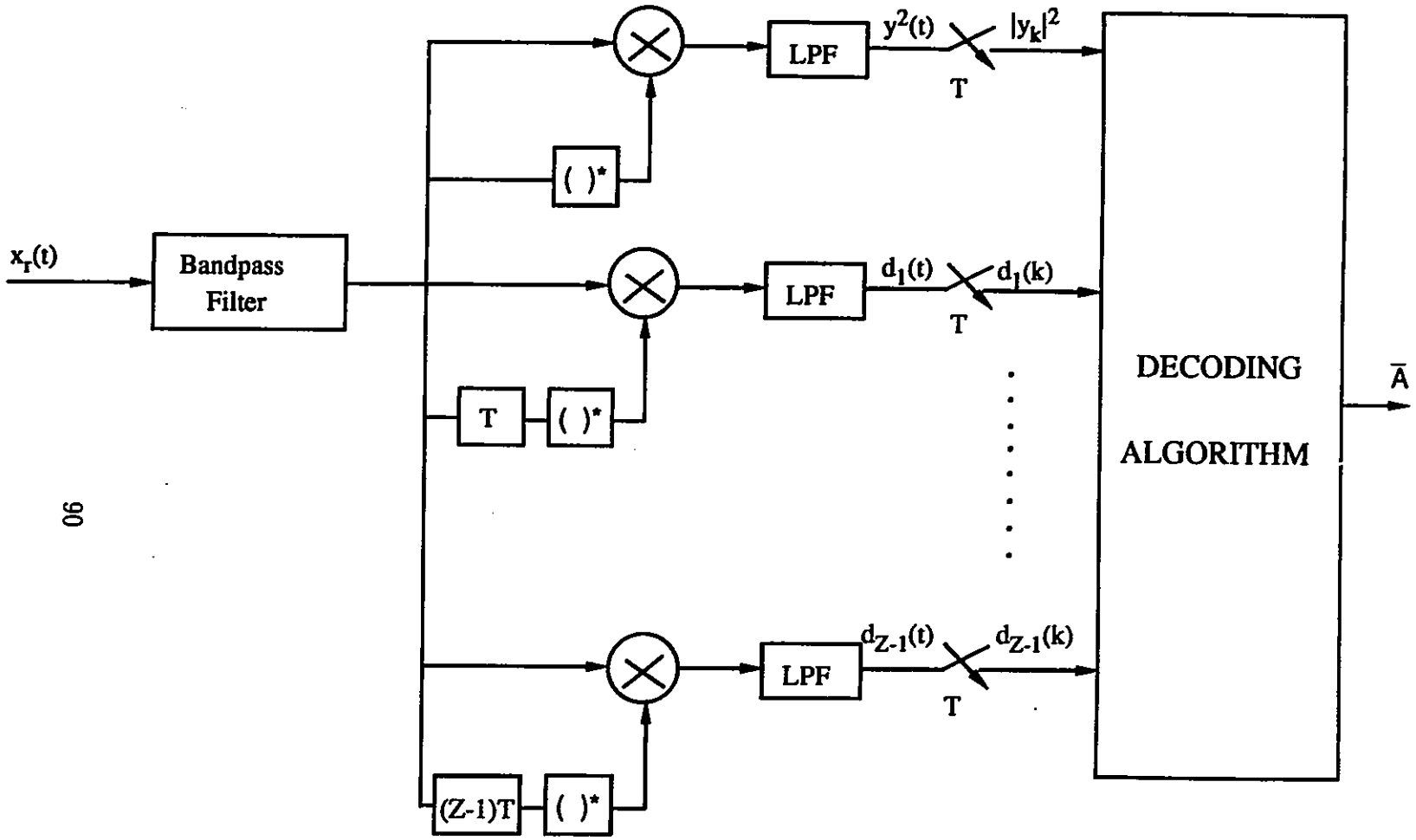

Figure 4.5 IF implementation of the Squared Envelope and Multiple Differential Detection non-coherent receiver.

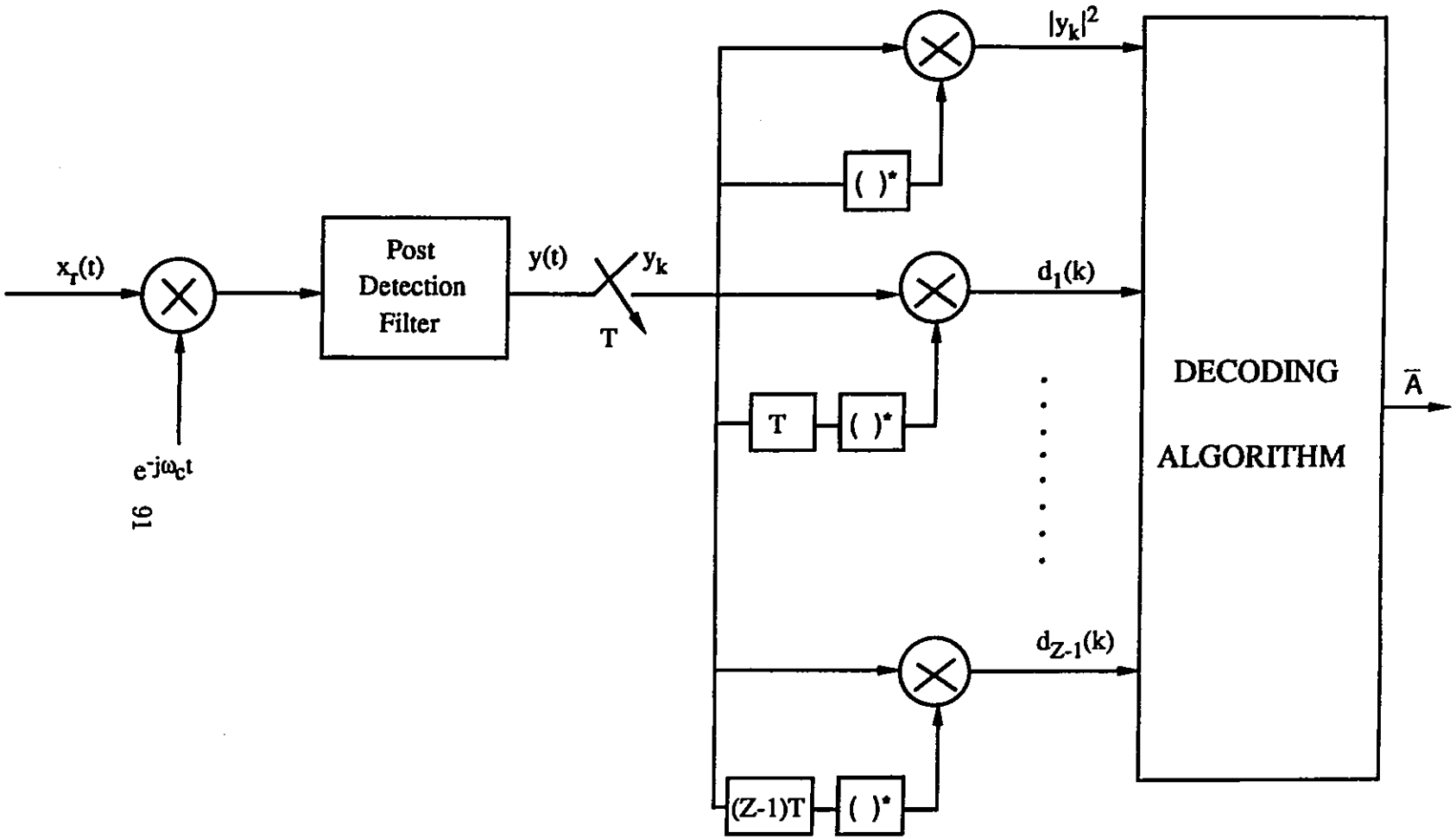

Figure 4.6 Baseband implementation of the Squared Envelope and Multiple Differential Detection non-coherent receiver.

When baseband implementation is used, the demodulating signal has to be generated locally at the receiver site. One way of accomplishing this is to use a pilot[4] or use a preamble. Another method is to generate a reference signal by non-linearly processing the received (information carrying) signal. The first scenario has the disadvantage that valuable resources (as power and bandwidth) are used to transmit the pilot or preamble signal. This results in loss of capacity. For the preamble case it also results in delays in the decoding process, since the receiver has first to process the preamble and afterwards deal with the recovery of the transmitted information.

The non-linear processing scenario also has some serious drawbacks. The carrier recovery circuits require some time until they lock in frequency with the input signal. This problem becomes worse for systems of higher spectral efficiency, since in this case narrower filters (having longer acquisition times) are required.

Since the IF implementation of the squared envelope and the differential detector does not require any locally generated carrier, it avoids all the above mentioned problems. It has fast acquisition times and allows fast recovery of the transmitted information. It also does not suffer from any loss in capacity, since it does not require the use of lengthy preambles. However, the carrier frequency should be chosen properly. The carrier frequency f_c should be a multiple of the symbol rate ($\frac{1}{T}$). In the opposite case, phase offsets will appear at the outputs of the differential detectors. These offsets will inevitably deteriorate the performance.

Use of multiple differential detection requires the use of more than one differential detectors. The first reaction to this is that IF implementation has a definite disadvantage in multiple differential detection structures, since

[4]If every communication channel is provided with its pilot signal for synchronization, it could be more appropriate to use coherent detection. However, in relatively fast faded channels, the bandwidth and power which are used by the pilot, is a large percentage of the power and bandwidth allocated to the information signal. Since pilot signals do not carry data, their use lowers the capacity of the network. An approach which can reduce the size of this loss, is to use the same pilot signal for the synchronization of more than one communication channels. In this multiple channel approach, the pilot signal can not provide information for the initial phase of every individual communication channel which it services. Absence of phase information brings the non-coherent detection concept into the picture as a strong alternative to coherent detection.

it would require the use of a multiple number of IF circuits. However, there is a simple solution to this problem which will be presented in the following paragraphs.

The output of the l-symbol differential detector $d_l(k)$ can be expressed as follows:

$$\begin{aligned} d_l(k) &= y_k y_{k-l}^* = y_k \frac{\Pi_{i=1}^{l-1}|y_{k-i}|^2}{\Pi_{i=1}^{l-1}|y_{k-i}|^2} y_{k-l}^* \\ &= \frac{\Pi_{i=0}^{l-1} d_1(k-i)}{\Pi_{i=1}^{l-1}|y_{k-i}|^2} = d_1(k)\Pi_{i=1}^{l-1}\frac{d_1(k-i)}{|y_{k-i}|^2}. \end{aligned} \tag{4.37}$$

The output $d_l(k)$ of the l-symbol differential detector can be generated by multiplying l consecutive output of the 1-symbol differential detector ($d_1(k)$ to $d_1(k-l+1)$) and normalize the outcome by dividing it with $l-1$ consecutive values of the envelope detector ($|y_{k-1}|^2$ to $|y_{k-l+1}|^2$).

The conclusion from the above discussion is that the multiple differential receiver can be built by using only (and applying processing on) the outputs of an IF differential and an IF squared envelope detector. The block diagram of the SEMDD following this IF implementation approach is shown in Fig. 4.7.

Summarizing we can say that through the material covered in the present section, we have established the connection between the improved non-coherent receivers and the classical and simple non-coherent techniques of envelope and (IF or baseband) differential detection. This does not only provide a better understanding regarding the nature and operation of the advanced receivers, but also makes possible an implementation of these structures by using simple non-coherent receivers as building blocks. As a result, the proposed receivers inherit the advantages of the classical non-coherent detectors (simplicity, cost efficiency, fast synchronization etc.) while at the same time (as will be shown in the following section) they provide significant performance improvements.

One should notice that the multiple differential receivers proposed and analyzed in the present section require the use and process the outputs of $Z-1$ differential detectors for a sequence of Z symbols. Since the complexity of the receiver in processing load increases exponentially with the increase

in the value of Z, it might become prohibitively high for long transmitted sequences. In one of the following sections we shall discuss how the SEMDD can be modified, in order to resolve this problem.

We should mention that regardless of the implementation approach we choose to use (see Figs. 4.5, 4.6, 4.7) the decoding algorithm always remains the same. Also, the performance of the communication system is unaffected from this choice. In terms of cost effectiveness and complexity, we are in favor of the third approach (see Fig. 4.7). This preference is based on the fact that this implementation does not require demodulation and keeps the complexity of the IF circuitry to a minimal, by using a small amount of additional digital signal processing.

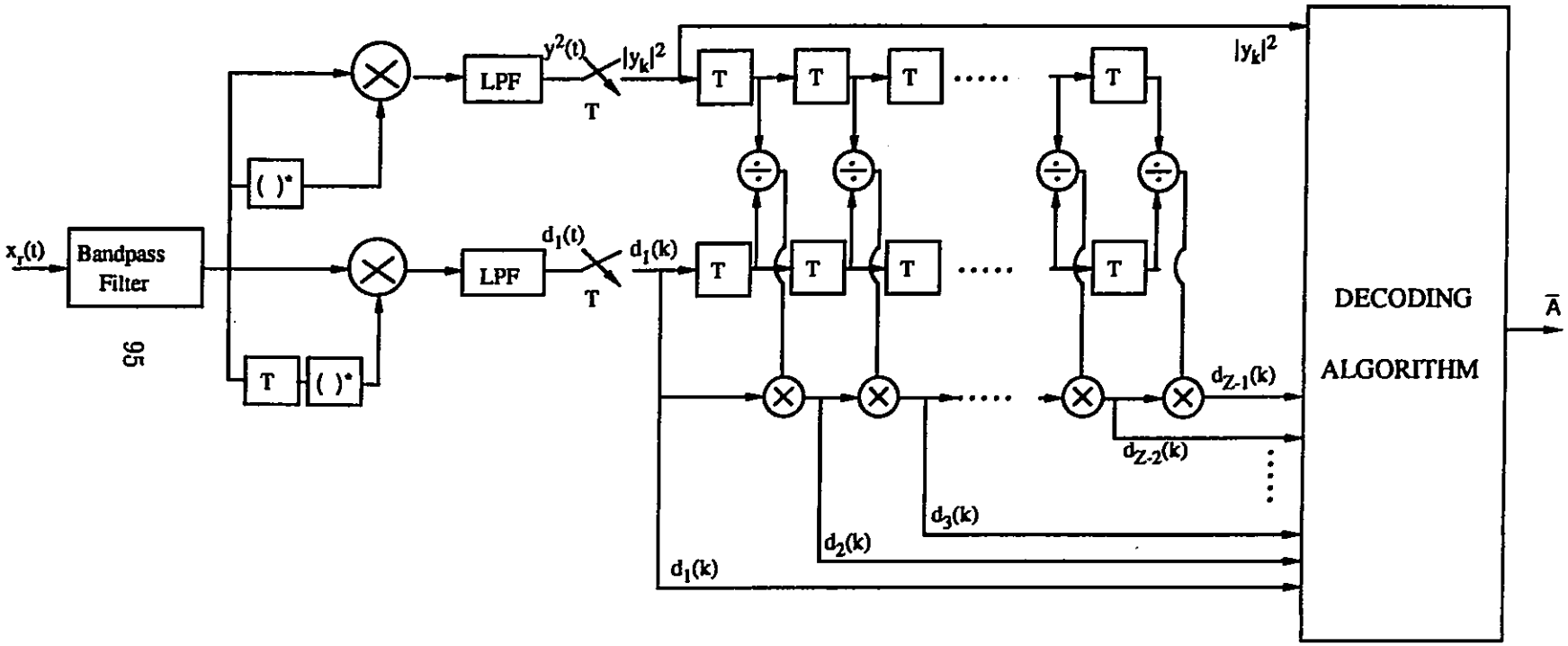

Figure 4.7 Alternative IF implementation of the Squared Envelope and Multiple Differential Detection non-coherent receiver. Only the squared envelope (SE) and one-symbol differential detector (DD) are implemeted in IF form. The rest of the differential detectors are implemented through signal processing applied on the outputs of the two IF non-coherent units (SE & DD).

4.5 PERFORMANCE EVALUATION OF THE NON-COHERENT BLOCK DECODER IN A GAUSSIAN CHANNEL

In the present section, the block decoder described in section 4.3 is evaluated with uncoded and trellis coded signals. The results are based on upper performance bounds. The uncoded schemes evaluated are BPSK, QPSK, 8PSK and 16PSK.

Three trellis coded schemes have been considered. One uses QPSK and the other two use 8PSK constellation. The convolutional codes used are :

[Code A]

[4-state, 1/2 coding rate used with 4–PSK]

$$\bar{b}_k^2 = [b_k^1 = a_k^1 \bigoplus a_{k-2}^1, b_k^2 = a_{k-1}^1]$$

[Code B]

[4-state, 2/3 coding rate used with 8PSK]

$$\bar{b}_k^3 = [b_k^1 = a_k^1 \bigoplus a_{k-2}^1, b_k^2 = a_{k-1}^1, b_k^3 = a_k^2]$$

[Code C]

[4-state, 2/3 coding rate used with 8PSK]

$$\bar{b}_k^3 = [b_k^1 = a_k^1 \bigoplus a_{k-2}^2, b_k^2 = a_{k-1}^2 \bigoplus a_k^2, b_k^3 = a_{k-1}^2]$$

where $\bigoplus$ represents *modulo 2* addition. Codes A and B are optimal trellis codes (under the Euclidean distance criterion). Of the two codes used with 8PSK, code B has parallel transitions in the trellis diagram. The state transition diagrams of the three codes are shown in Figs. 4.8, 4.9 and 4.10.

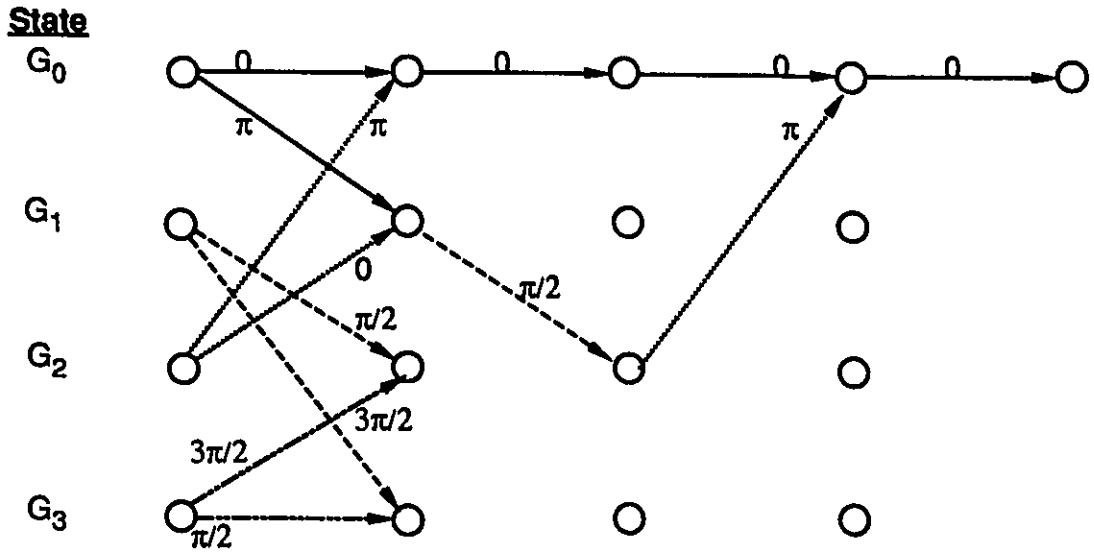

Figure 4.8: State-transition diagram of Code A. On the branches the values of the information phases ϕ_k corresponding to the various transitions are indicated.

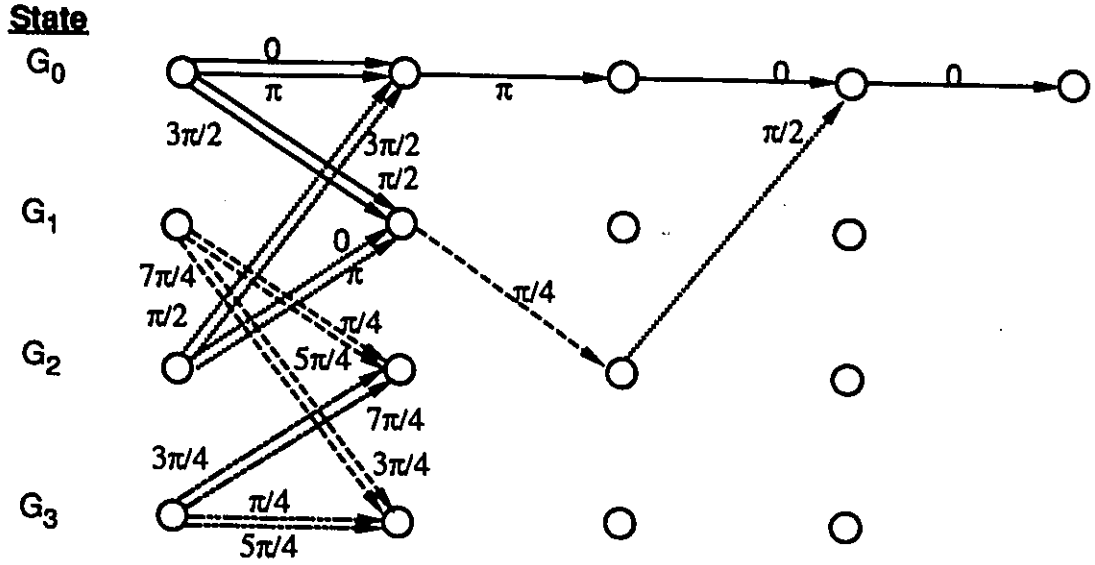

Figure 4.9: State-transition diagram of Code B. On the branches the values of the information phases ϕ_k corresponding to the various transitions are indicated.

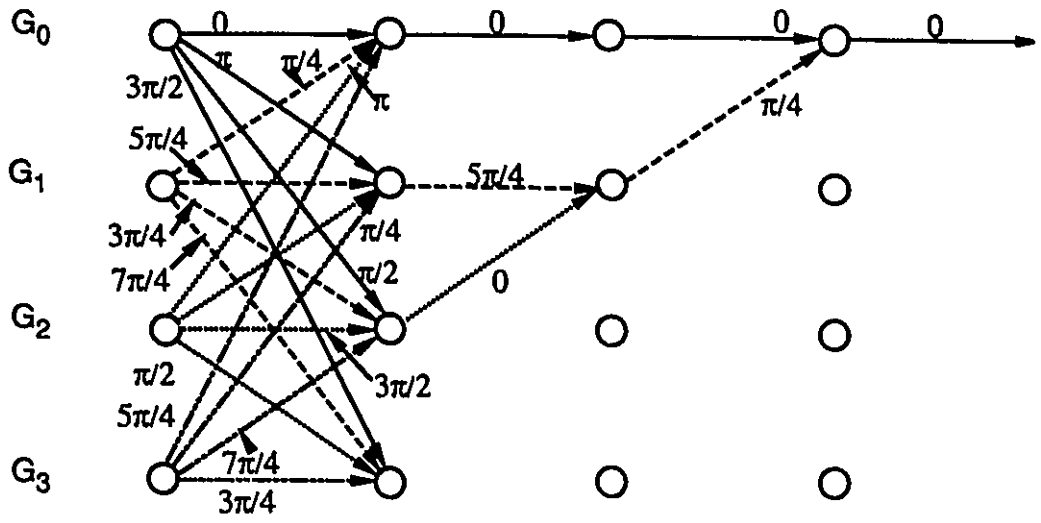

Figure 4.10: State-transition diagram of Code C. On the branches the values of the information phases ϕ_k corresponding to the various transitions are indicated.

4.5.1 Performance Bounds of the Non-Coherent Block Decoder

The starting point is to determine the probability of deciding in favor of an information sequence $\bar{A}^{\zeta}$, when a sequence $\bar{A}^{\nu}$ has been transmitted. This pairwise error event will be represented as $\{\bar{C}(\bar{A}^{\zeta}) \leftarrow \bar{C}(\bar{A}^{\nu})\}$, while the probability of its occurrence as $P(\{\bar{C}(\bar{A}^{\zeta}) \leftarrow \bar{C}(\bar{A}^{\nu})\})$.

4.5.1.1 Upper Bound of the Pairwise Error Probability

In Appendix B we have shown that for the Gaussian noise channel, the pairwise error probability $P(\{\bar{C}(\bar{A}^{\zeta}) \leftarrow \bar{C}(\bar{A}^{\nu})\})$ can be upper bounded by $B^{Z}_{[\nu,\zeta]}$ (i.e. $P(\{\bar{C}(\bar{A}^{\zeta}) \leftarrow \bar{C}(\bar{A}^{\nu})\}) \leq B^{Z}_{[\nu,\zeta]}$), which is equal to

$$B^{Z}_{[\nu,\zeta]} = \frac{1}{2}[\Lambda(\bar{C}(\bar{A}^{\nu}), \bar{C}(\bar{A}^{\zeta}))] \exp\{-\frac{1}{\sigma_n^2}\frac{|\alpha_{[\nu,\zeta]} - \beta_{[\nu,\zeta]}|^2}{2}\}. \tag{4.38}$$

$$\left\{ \begin{array}{c} \alpha_{[\nu,\zeta]} \\ \beta_{[\nu,\zeta]} \end{array} \right\} = [\frac{1}{v_{\nu\nu} + v_{\nu\zeta}}(\frac{|\bar{E}^{\nu}_{\nu}|^2 + |\bar{E}^{\nu}_{\zeta}|^2 - 2Re\{(\bar{E}^{\nu}_{\nu})^{*}\bar{E}^{\nu}_{\zeta}\gamma_{\nu\zeta}\}}{1 - |\gamma_{\nu\zeta}|^2} \mp \frac{|\bar{E}^{\nu}_{\nu}|^2 - |\bar{E}^{\nu}_{\zeta}|^2}{\sqrt{1 - |\gamma_{\nu\zeta}|^2}})]^{\frac{1}{2}} \tag{4.39}$$

and

$$\Lambda(\bar{C}(\bar{A}^{\nu}), \bar{C}(\bar{A}^{\zeta})) = \begin{cases} 1 & \text{for } \alpha_{[\nu,\zeta]} = 0 \\ [1 - \frac{v_{\nu\nu} - v_{\nu\zeta}}{[(v_{\nu\nu}+v_{\nu\zeta})^2 - 4|v^{c}_{\nu\zeta}|^2]^{\frac{1}{2}}}] \frac{1}{\sqrt{2\pi\frac{1}{\sigma_n^2}\alpha_{[\nu,\zeta]}\beta_{[\nu,\zeta]}}} & \text{for } \alpha_{[\nu,\zeta]} \neq 0. \end{cases} \tag{4.40}$$

The $\bar{E}^{\nu}_{\nu}$, $\bar{E}^{\nu}_{\zeta}$, $v_{\nu\nu}$, $v_{\nu\zeta}$, $\gamma_{\nu\zeta}$ appearing in Eqs.(4.39), (4.40) are described in Eqs.(B.4), (B.5), (B.8), (B.9) and (B.12) of Appendix B respectively.

The analysis leading to Eqs.(4.38) - (4.40) considers the presence of ISI in the received signal samples y_k, as well as the presence of correlation between the noise terms n_k which corrupt y_k. This allows the evaluation of the block decoder with time dispersive channels and/or non-equally apportioned systems.

In Eq.(4.38), the $\exp\{-\frac{1}{\sigma_n^2}\frac{|\alpha_{[\nu,\zeta]}-\beta_{[\nu,\zeta]}|^2}{2}\}$ is the dominant term and determines the value of the error bound ($B^Z_{[\nu,\zeta]}$ becomes smaller as $(\alpha_{[\nu,\zeta]}-\beta_{[\nu,\zeta]})^2$ becomes larger). We define the

$$D^Z_{[\nu,\zeta]} = \frac{|\alpha_{[\nu,\zeta]}-\beta_{[\nu,\zeta]}|^2}{2} \tag{4.41}$$

to provide a distance metric for the non-coherent receiver, equivalent to the Euclidean distance used for the coherently detected signals.

When the signal samples y_k are free from ISI and the noise terms n_k (corrupting y_k) are uncorrelated with each other ($E\{n_k n_{k-l}\} = 0 \ \forall \ l \neq 0$), $D^Z_{[\nu,\zeta]}$ (now represented as $D^Z_{IC[\nu,\zeta]}$) becomes equal to

$$D^Z_{IC[\nu,\zeta]} = [Z - |\sum_{k=0}^{Z-1} c_k^\nu (c_k^\zeta)^*|]. \tag{4.42}$$

Also, $\Lambda(\bar{C}(\bar{A}^\nu), \bar{C}(\bar{A}^\zeta))$ becomes

$$\Lambda_{IC}(\bar{C}(\bar{A}^\nu), \bar{C}(\bar{A}^\zeta)) = \begin{cases} 1 & \text{for } \sum_{k=0}^{Z-1} c_k^\nu (c_k^\zeta)^* = 0 \\ \\ \frac{1}{\sqrt{2\pi}} \frac{1}{\sqrt{\frac{1}{\sigma_n^2}}} \frac{\sqrt{2}}{\sqrt{|\sum_{k=0}^{Z-1} c_k^\nu (c_k^\zeta)^*|}} & \text{for } \sum_{k=0}^{Z-1} c_k^\nu (c_k^\zeta)^* \neq 0. \end{cases} \tag{4.43}$$

The use of Eqs.(4.42), (4.43) in Eq.(4.38) leads to

$$B^Z_{[\nu,\zeta]} = \frac{1}{2}[\Lambda_{IC}(\bar{C}(\bar{A}^\nu), \bar{C}(\bar{A}^\zeta))] \exp\{-\frac{1}{2\sigma_n^2}(Z - |\sum_{k=0}^{Z-1} c_k^\nu (c_k^\zeta)^*|)\} . \tag{4.44}$$

When ISI and correlation between the n_k noise components are absent, it is easy to verify from Eqs.(4.42) to (4.44) that opposite error events

$\{\bar{C}(\bar{A}^{\zeta}) \leftarrow \bar{C}(\bar{A}^{\nu})\}$, $\{\bar{C}(\bar{A}^{\nu}) \leftarrow \bar{C}(\bar{A}^{\zeta})\}$ have equal distances ($D^Z_{IC[\nu,\zeta]} = D^Z_{IC[\zeta,\nu]}$) and upper bounds of pairwise error probability ($B^Z_{[\nu,\zeta]} = B^Z_{[\zeta,\nu]}$). However, when ISI or correlation between the noise terms n_k are present, these equations might not hold (generally speaking, $D^Z_{[\nu,\zeta]} \neq D^Z_{[\zeta,\nu]}$ and $B^Z_{[\nu,\zeta]} \neq B^Z_{[\zeta,\nu]}$). This is due to the fact that the various parameters $\bar{E}^{\nu}_{\zeta}$, $\bar{E}^{\nu}_{\nu}$, $v_{\nu\nu}$, $v_{\zeta\zeta}$, $v_{\nu\zeta}$, $v_{\zeta\nu}$ $v^c_{\nu\zeta}$, $v^c_{\zeta\nu}$ (see Eqs.(B.4), (B.5), (B.8), (B.9)), which influence the values of the pairwise error bounds $B^Z_{[\nu,\zeta]}$ $B^Z_{[\zeta,\nu]}$, depend on the entire sequences $C(\bar{A}^{\nu})$, $C(\bar{A}^{\zeta})$ rather than the segments where these two sequences are in divergence (i.e. $c^{\nu}_k \neq c^{\zeta}_k$). This creates inequality in the values of $\{\bar{E}^{\nu}_{\nu}, \bar{E}^{\zeta}_{\zeta}\}$, $\{\bar{E}^{\nu}_{\zeta}, \bar{E}^{\zeta}_{\nu}\}$, $\{v_{\nu\nu}, v_{\zeta\zeta}\}$ which are responsible for this asymmetric behaviour. The appearance of this behaviour is not surprising. A similar case can be found in [262]-[264]. The results reported in [262]-[264] demonstrated that the presence of ISI and/or noise correlation creates unequal probabilities for the various symbols to be in error when the (conventional) differential detector is used. As we see, similar behaviour appears with the non-coherent block decoders.

4.5.2 Upper Bound of the Performance

By using the concept of the Union Bound, the following inequality holds:

$$\begin{aligned} P_e &\leq \frac{1}{(Z-L_c-1)}\frac{1}{2^{(Z-L_c-1)p}} \\ &\quad \sum_{\bar{C}(\bar{A}^{\nu})\in S^Z_{CW}} \sum_{\bar{C}(\bar{A}^{\zeta})\in S_{\bar{C}(\bar{A}^{\nu})}} n_e(\{\bar{C}(\bar{A}^{\zeta}) \leftarrow \bar{C}(\bar{A}^{\nu})\}) P(\{\bar{C}(\bar{A}^{\zeta}) \leftarrow \bar{C}(\bar{A}^{\nu})\} \\ &\leq \mathcal{UB}^Z \end{aligned} \tag{4.45}$$

where P_e represents the symbol error probability of the system and

$$\begin{aligned} \mathcal{UB}^Z &= \frac{1}{(Z-L_c-1)}\frac{1}{2^{(Z-L_c-1)p}} \\ &\quad \sum_{\bar{C}(\bar{A}^{\nu})\in S^Z_{CW}} \sum_{\bar{C}(\bar{A}^{\zeta})\in S_{\bar{C}(\bar{A}^{\nu})}} n_e(\{\bar{C}(\bar{A}^{\zeta}) \leftarrow \bar{C}(\bar{A}^{\nu})\}) B^Z_{[\nu,\zeta]}. \end{aligned} \tag{4.46}$$

L_c is the constraint length of the code (for uncoded schemes $L_c = 0$). S^Z_{CW} represents the set of all possible codewords with length Z (a total of $2^{(Z-L_c-1)p}$) and $S_{\bar{C}(\bar{A}^\nu)}$ represents the set which has as members all the codeword elements of S^Z_{CW} except for $\bar{C}(\bar{A}^\nu)$. Also, $n_e(\{\bar{C}(\bar{A}^\varsigma) \leftarrow \bar{C}(\bar{A}^\nu)\})$ represents the number of symbol errors associated with the error event $\{\bar{C}(\bar{A}^\varsigma) \leftarrow \bar{C}(\bar{A}^\nu)\}$.

In some cases, the following equality might hold[5]:

$$\frac{1}{(Z-L_c-1)} \sum_{\bar{C}(\bar{A}^\varsigma) \in S^Z_{\bar{C}(\bar{A}^\nu)}} n_e(\{\bar{C}(\bar{A}^\varsigma) \leftarrow \bar{C}(\bar{A}^\nu)\}) B^Z_{[\nu,\varsigma]}$$

$$=$$

$$\frac{1}{(Z-L_c-1)} \sum_{\bar{C}(\bar{A}^\iota) \in S^Z_{\bar{C}(\bar{A}^\xi)}} n_e(\{\bar{C}(\bar{A}^\iota) \leftarrow \bar{C}(\bar{A}^\xi)\}) B^Z_{[\xi,\iota]}$$

$$\forall \quad \bar{C}(\bar{A}^\nu), \bar{C}(\bar{A}^\xi) \in S^Z_{CW} \, . \tag{4.47}$$

When the condition, described by Eq.(4.47) holds, the work required to calculate the values of $\mathcal{U}B^Z$ is reduced, since use of Eq.(4.47) in Eq.(4.45) gives the following expression:

$$P_e \leq \mathcal{U}B^Z = \frac{1}{(Z-L_c-1)} \sum_{\bar{C}(\bar{A}^\varsigma) \in S_{\bar{C}(\bar{A}^\nu)}} n_e(\{\bar{C}(\bar{A}^\varsigma) \leftarrow \bar{C}(\bar{A}^\nu)\}) B^Z_{[\nu,\varsigma]}$$

(4.48)

[5]One case where this equality holds is for a MPSK system which uses equal apportioning of the Nyquist I filter between transmitter - receiver and operates in an ideal channel. However, if coded modulations are used and/or if the channel is distorted and/or if the signal constellation is of multi-amplitude nature (for example QAM) this equality does not hold.

where $\bar{C}(\bar{A}^{\nu})$ can be any sequence member of $S^{Z}_{\bar{C}W}$. The right part of Eq.(4.48) actually upper bounds (it is the union bound of) the probability of $C(\bar{A}^{\nu})$ to be in error. The message conveyed from Eq.(4.48) is that in order to calculate the upper bound of the error performance, it is enough to calculate the union bound for the error probability of one of the possible codewords. The obvious advantage is that the numerical calculations required in Eq.(4.48) is only $\frac{1}{2(Z-L_c-1)p}$ the processing needed by Eq.(4.46).

4.5.3 Performance of Coded Signals In Ideal Channel and Equal Apportioning

The SER performance curves for the codes A, B, C are displayed in Figs. 4.11 to 4.16. The curves correspond to values of $Z = 5, 7, 10, 12$. Results for both, non-differentially encoded (Figs. 4.11, 4.13, 4.15, the curves are labeled as Z= (NDE)) and differentially encoded (Figs. 4.12, 4.14, 4.16 the curves are labeled as Z= (DE)) signals are reported. In each figure, the SER curve of the system which uses the same code and employes a conventional receiver, is included[6]. It is based on Monte Carlo simulations and is labelled in the figures as (Con.Rec.)[7]. The curve of the uncoded differentially detected signal of equal spectral efficiency is also included (DBPSK for code A and DQPSK for codes B and C).

In Tables 4.1 , 4.2 we summarize the improvements offered by the block decoder over the conventional differential receiver as a function of the codeword length Z. The values listed in Table 4.1 correspond to a non-differentially encoded signal. Table 4.2 gives the results for the differentially encoded case. The comparison is made for a SER=10^{-4}. In the following two tables (Table 4.3 and Table 4.4), we list the gains offered by the coded schemes (when

[6]For coded systems, we consider as conventional differential receiver the Viterbi decoder [256] (optimal for coherent systems operating in an additive white Gaussian noise environment) which processes the output of a one-symbol delay differential detector. For uncoded signals, the term conventional differential receiver refers to the one-symbol differential detector.

[7]For values of SER below 10^{-4}, the simulations have to either run for an unreasonably long period of time in order to provide reliable results, or the estimated SER performance value will be of small confidence. We have avoided displaying such low confidence results in our figures.

decoded by the block decoder) as compared to the uncoded differentially detected signals of equal spectral efficiency.

Table 4.1: Gains versus codeword length Z, offered by the Block Decoder. The comparison is with the conventional differential receiver. Differential encoding is not used. The reported gains correspond to SER=10^{-4}.

		GAINS (dB)		
		Code A	Code B	Code C
Z	5	1.5	2.6	2.2
	7	2.2	2.8	2.7
	10	2.8	2.8	3
	12	3	3.7	3

Table 4.2: Gains versus codeword length Z, offered by the Block Decoder. The comparison is with the conventional differential receiver. Differential encoding is used. The reported gains correspond to SER=10^{-4}.

		GAINS (dB)		
		Code A	Code B	Code C
Z	5	2.2	2.8	0.5
	7	2.5	2.8	0.8
	10	2.8	3.5	1.7
	12	3	3.9	1.3

Table 4.3: Gains versus codeword length Z, offered by the Block Decoder. The comparison is with the differentially detected signal of equal spectral efficiency (DBPSK for Code A, DQPSK for Codes B & C). Differential encoding is not used.

		GAINS (dB)		
		Code A	Code B	Code C
Z	5	2.3	3.4	0.5
	7	2.8	3.2	0.8
	10	3.8	4	1.1
	12	4.2	5.5	1.3

Table 4.4: Gains versus codeword length Z, offered by the Block Decoder. The comparison is with the differentially detected signal of equal spectral efficiency (DBPSK for Code A, DQPSK for Codes B & C). Differential encoding is used.

		GAINS (dB)		
		Code A	Code B	Code C
Z	5	3.3	3.5	1.5
	7	3.7	4.2	1.9
	10	4	5	2.1
	12	4.2	5.5	2.3

The results plotted in the curves and summarized in the tables demonstrate significant improvements. Compared to the conventional differential receiver, the block decoder achieves improvements close to 4 dB. Compared to the performance of an uncoded differentially detected signal of equal spectral efficiency, the coded schemes, used with the block decoder, provide gains higher than 5 dB.

It is interesting to notice that when the Codes A, B, & C are used with conventional differential receivers, they have poor performance. All the coded schemes are inferior to the differentially uncoded systems of equal spectral efficiency for low values of E_b/N_o. At higher E_b/N_o, there is a crossover between the curve of the coded and the uncoded system. As the E_b/N_o increases beyond the crossover point, the coded schemes show some minor advantage as compared to the uncoded ones. For code A the crossover occurs at a SER higher than 10^{-2} and it is not shown in the curves displayed in Figs. 4.11, 4.12. For Code B, the crossover occurs at a SER between 10^{-2} and 10^{-3} (see Figs. 4.13, 4.14). *Code C remains inferior compared to uncoded DQPSK for SER as low as* 10^{-4}. It is expected that a crossover between the curves will occur at a SER lower than 10^{-5}. Since these codes have asymptotic gains of 3.9 dB (Code A) 3 dB (Code B) and 1.15 dB (Code C) when coherently detected, it is obvious that the conventional differential receiver is the cause of the poor performance. On the contrary, the results listed in Tables 4.3 and 4.4 demonstrate that the block decoder recovers the losses created by the use of conventional differential detection and achieves practically the same performance with the coherent system.

The performance degradations suffered by the conventional differential receiver are due to the nature of the processing which the differential detector applies. The receiver applies a signal multiplication to generate the phase differential between signal samples received one symbol period apart. This introduces correlation between the noise components corrupting consecutive outputs of the differential detector. This mechanism is known to generate double errors (i.e two consecutive erroneous decisions) with uncoded differential systems[8][199] [224] [235]. It is known that correlated signal impairments are harmful to the performance of sequence estimators such as the Viterbi

[8]For a more detailed description of this mechanism please refer to subsection 4.8 of this chapter.

decoder. The noise correlation existing between noise components which corrupt consecutive output samples of the differential detector, is the source of the performance losses experienced by the conventional differential receiver. The effect of this noise correlation is stronger at low E_b/N_o values. As the E_b/N_o increases, the effect of the noise correlation decreases. For uncoded differential systems, this is seen as a reduction at the rate of double symbol error occurrence. For the coded schemes, it is seen as an improvement in the relative performance of the coded scheme as compared to the uncoded one. This creates the crossover of the curves and finally gives the coded system some small advantage over the uncoded one.

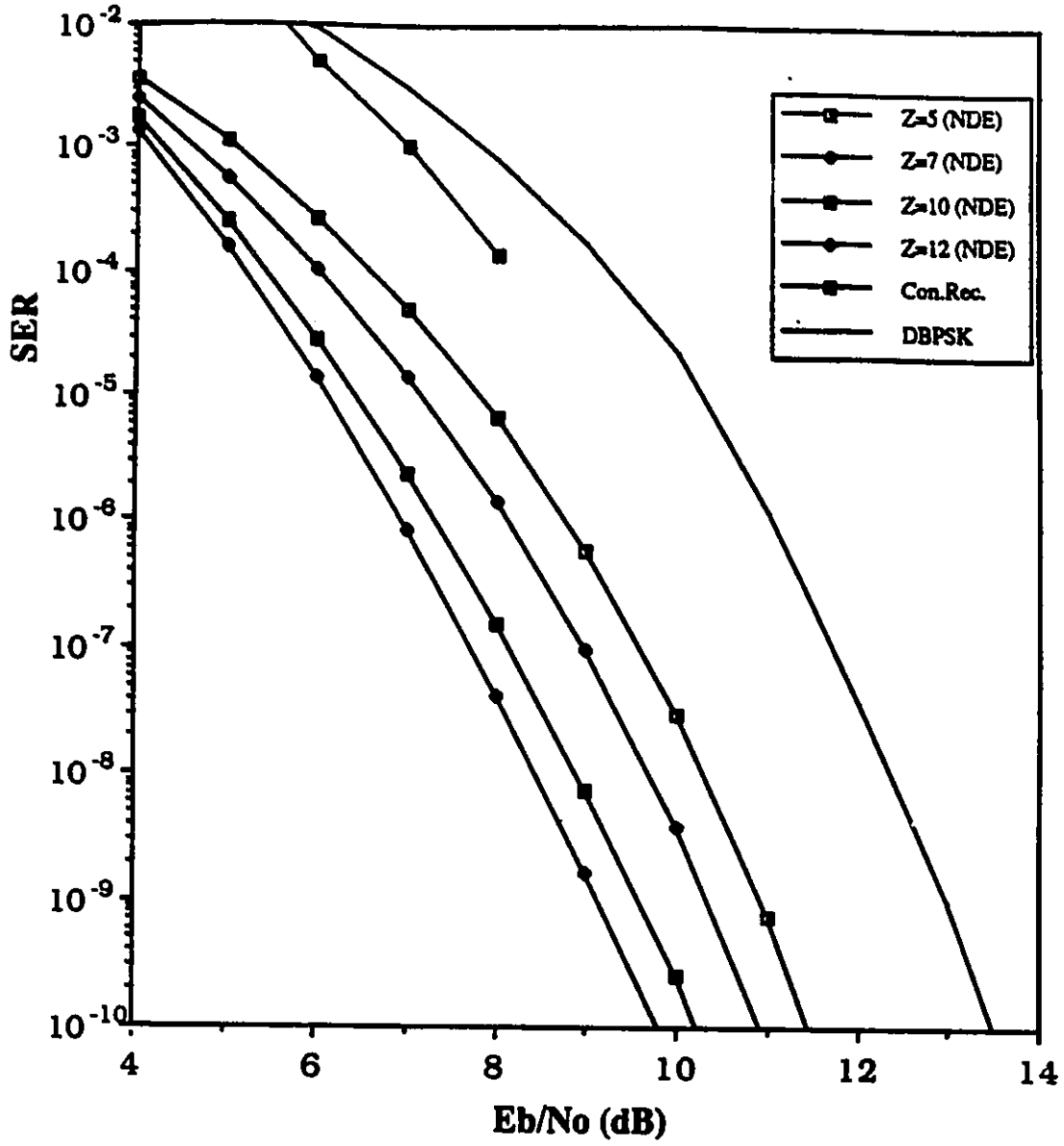

Figure 4.11: SER curves of code A (QPSK constellation) without differential encoding. The channel is assumed ideal. The Nyquist filter is equally apportioned between transmitter-receiver.

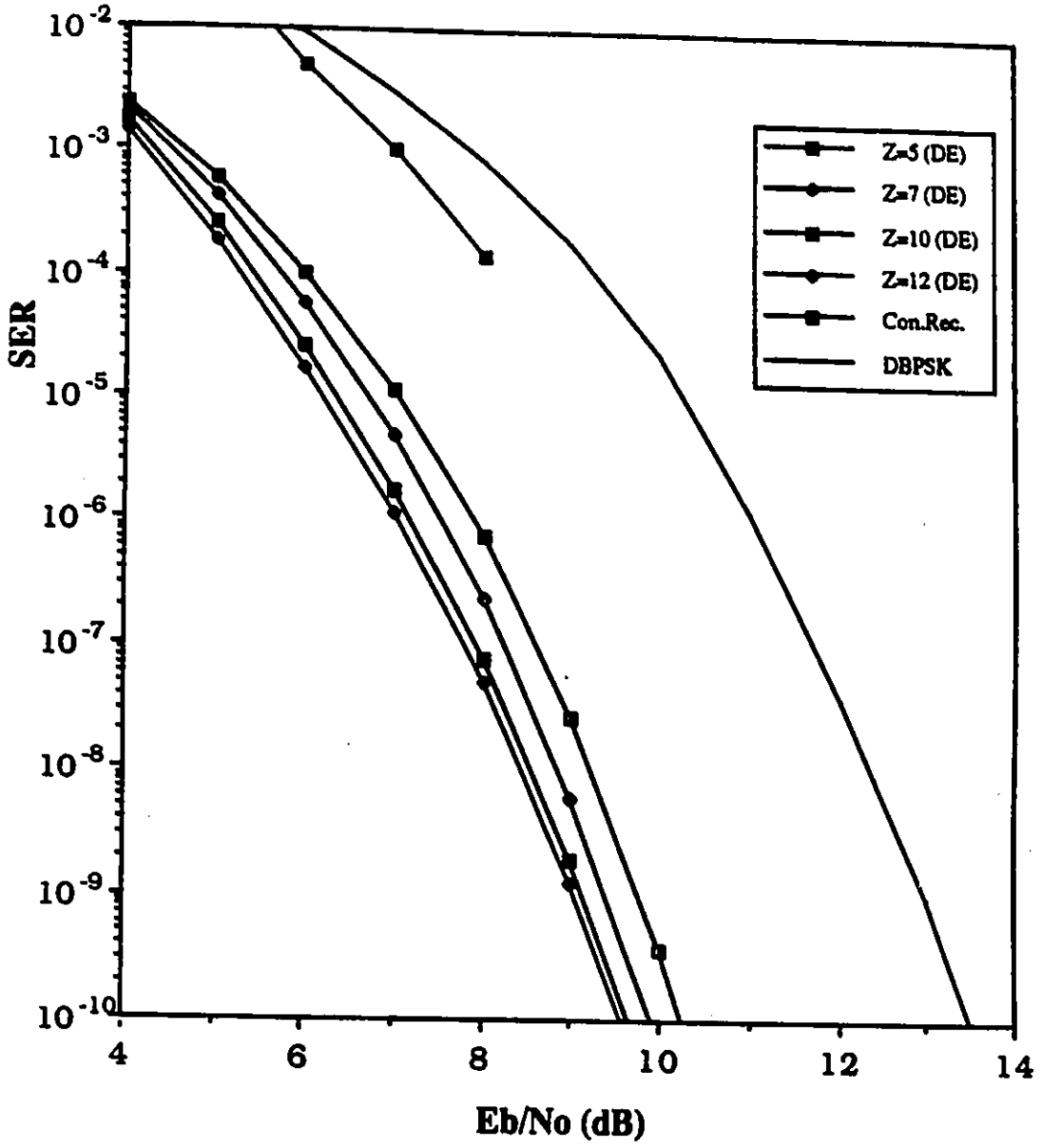

Figure 4.12: SER curves of code A (QPSK constellation) with differential encoding. The channel is assumed ideal. The Nyquist filter is equally apportioned between transmitter-receiver.

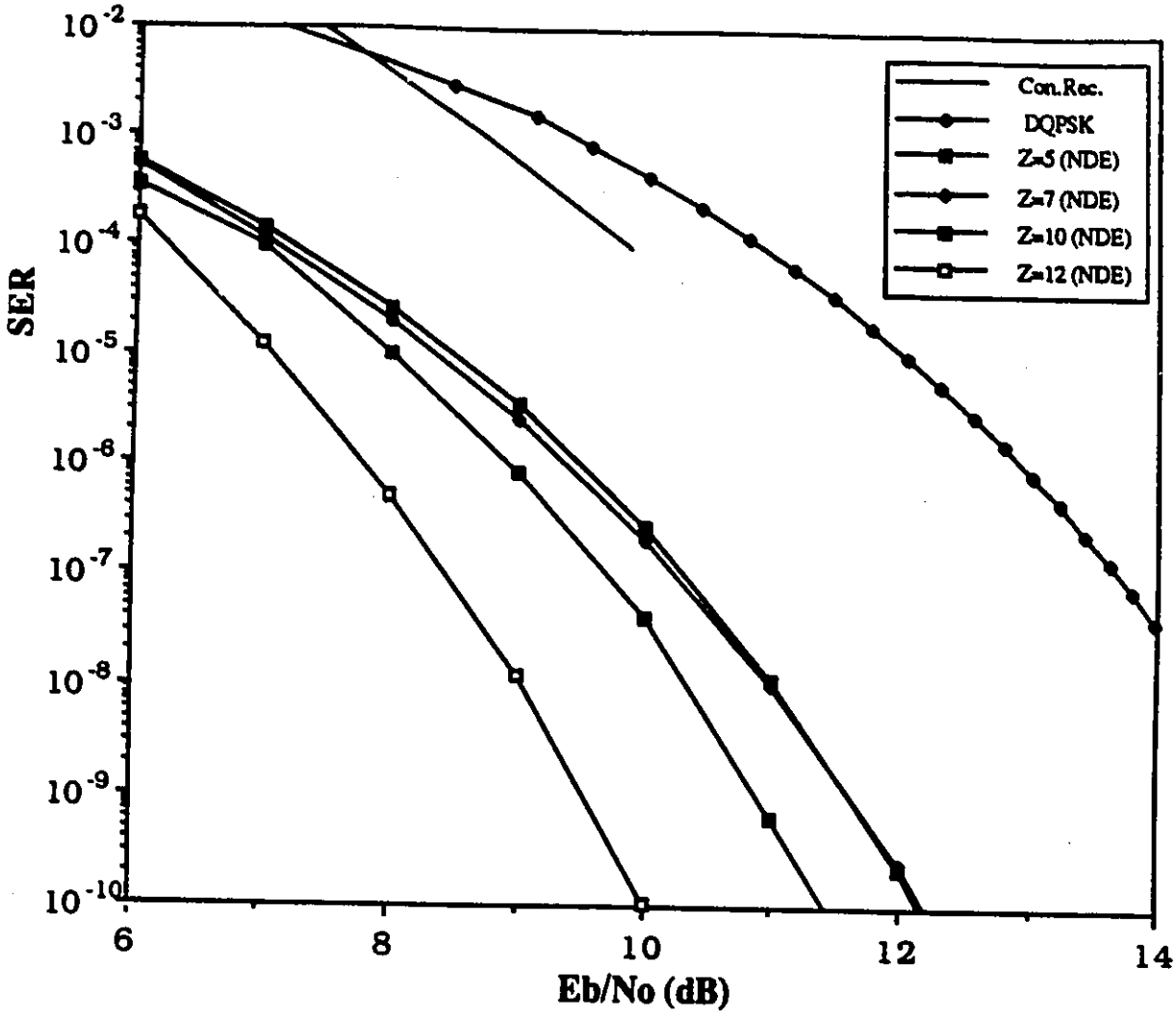

Figure 4.13: SER curves of code B (8PSK constellation) without differential encoding. The channel is assumed ideal. The Nyquist filter is equally apportioned between transmitter-receiver.

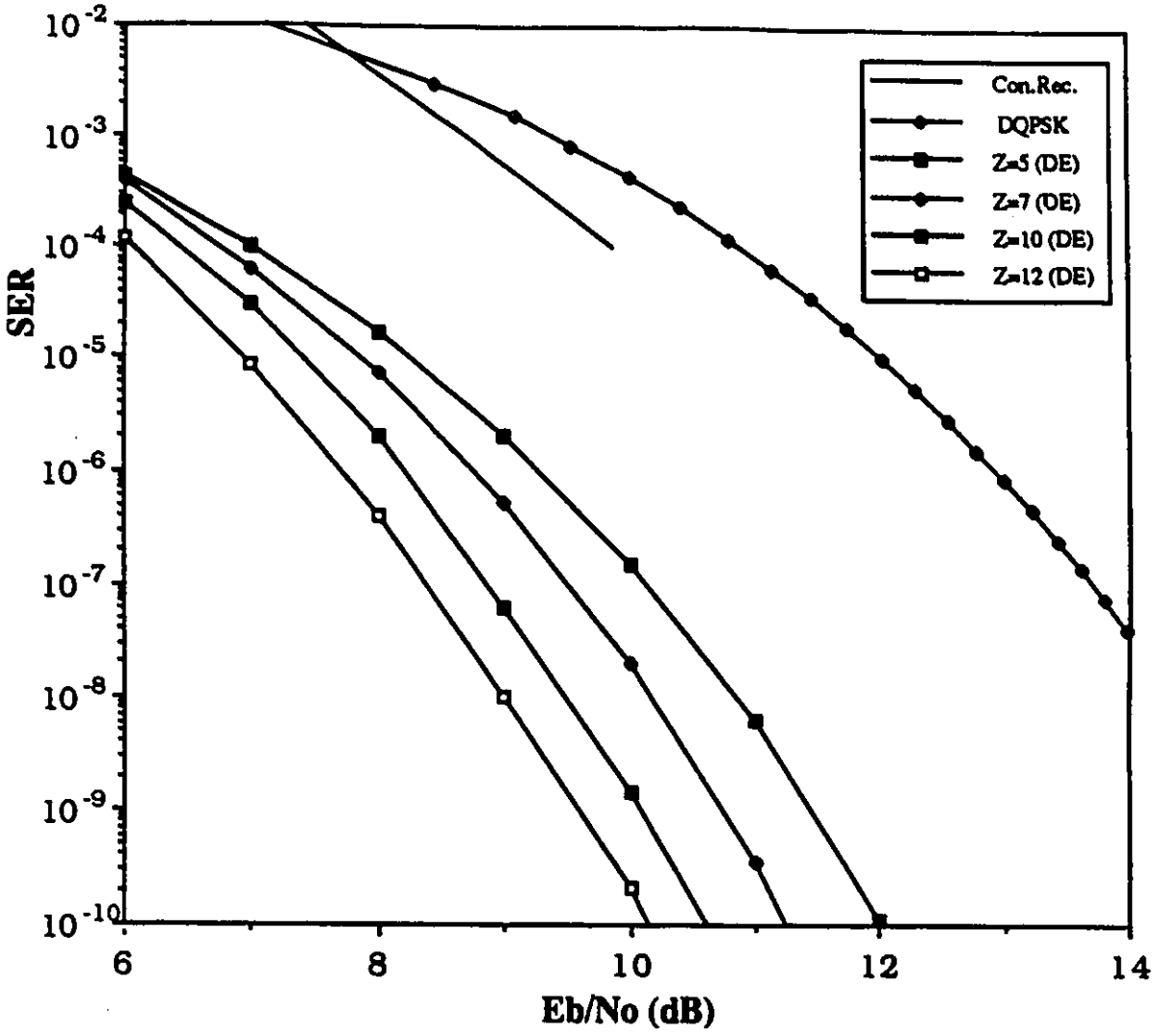

Figure 4.14: SER curves of code B (8PSK constellation) with differential encoding. The channel is assumed ideal. The Nyquist filter is equally apportioned between transmitter-receiver.

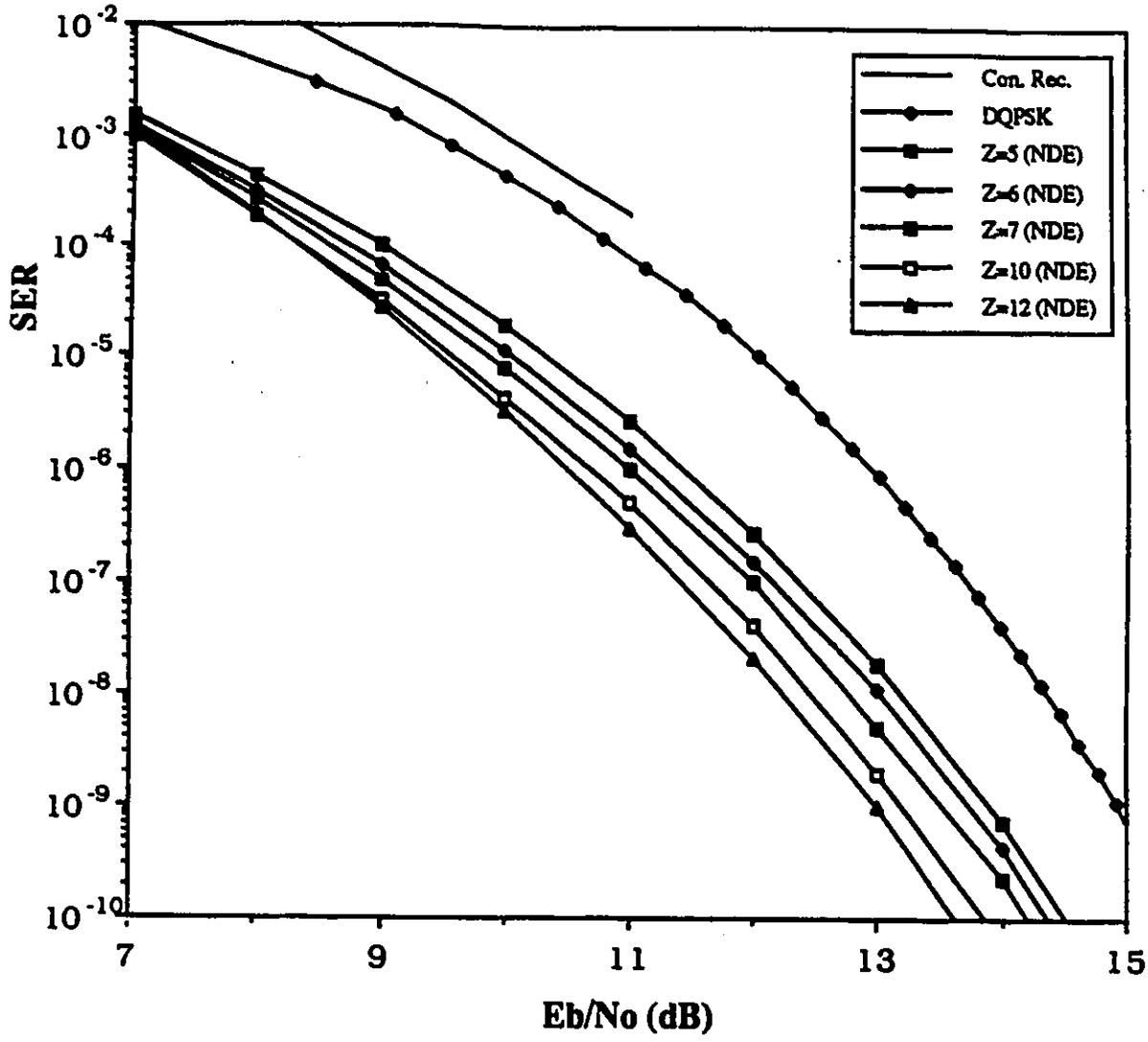

Figure 4.15: SER curves of code C (8PSK constellation) without differential encoding. The channel is assumed ideal. The Nyquist filter is equally apportioned between transmitter-receiver.

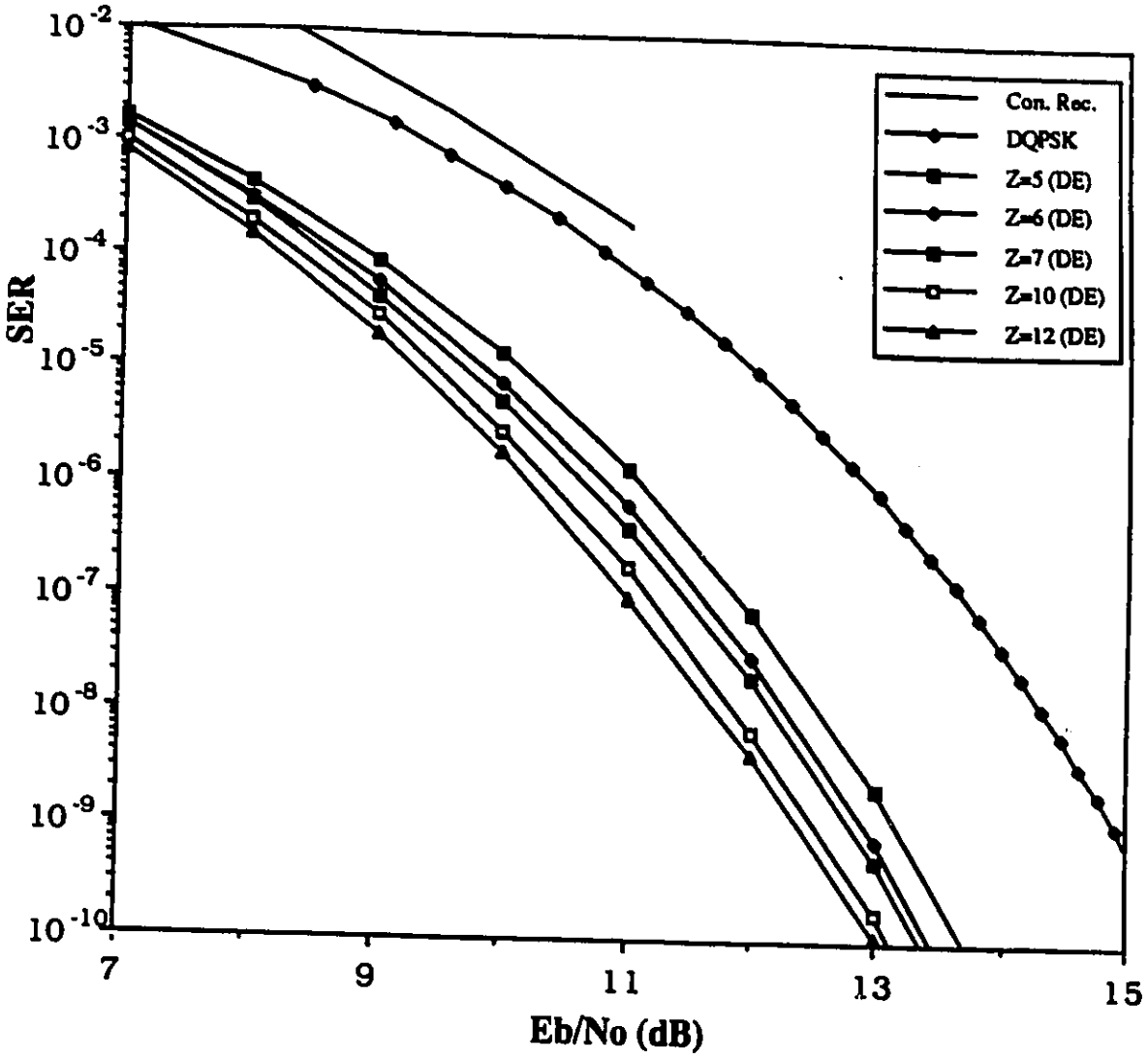

Figure 4.16: SER curves of code C (8PSK constellation) with differential encoding. The channel is assumed ideal. The Nyquist filter is equally apportioned between transmitter-receiver.

4.5.4 Comments and Observations On the Performance of the Coded Non-Coherent Systems

The gains achieved by the trellis coded and non-coherent block decoded schemes over the uncoded differentially detected systems (of same spectral efficiency) are higher compared to the improvements offered by the same codes (coherently detected) over the uncoded coherent systems. For example, while Code A in the coherent case has an asymptotic gain of 3.98 dB over the uncoded BPSK, the same code has a gain of 4.2 dB over differential BPSK. Similarly, while Codes B & C have an asymptotic gain of 3 dB and 1.15 dB over coherent QPSK (CQPSK), their distance from DQPSK is 5.5 dB and 2.3 dB respectively (see Table 4.3). This increase in improvement is due to the use of more sophisticated receivers. In addition to the coding gain, the improvements offered by the block decoder (as compared to the conventional differential detector) are added.

An interesting observation is that in all three cases, the differentially encoded schemes outperform the non-differentially encoded ones. Considering that codes A and B are optimal (i.e. achieve the maximum Euclidean distance for a given level of complexity) leads to the conclusion that *the presently available trellis codes (designed under the maximization of the Euclidean distance criterion), do not constitute optimal solution for the considered non-coherent schemes*[9]. Instead, other codes designed on the principles of maximizing the metric of Eq.(4.42) are needed.

In section 4.5.2 it was mentioned that when the condition described by Eq.(4.47) is satisfied, the upper performance bound can be calculated by using the formula described by Eq.(4.48) rather than Eq.(4.46). The condition of Eq.(4.47) is satisfied in coherent coded systems with linear convolutional codes. The three codes examined in this work satisfy this condition when used in coherent systems. However, we have found that all examined codes, when non-coherently detected, do not satisfy this condition any more. This has forced us to use Eq.(4.46) rather than the more computationally efficient expression of Eq.(4.48). To understand the reason why this is happening, we give the following example from Code A (non-differentially encoded) and

[9]The non-optimality of these codes is due to the non-linear processing applied by the proposed non-coherent receivers.

$Z = 10$. From all the sequences, members of $S_{\bar{C}(\bar{A}^\nu)}$, the sequence which gives the smallest distance with

$$\bar{C}(\bar{A}^\nu) = [\ c_0^\nu = 1,\ c_1^\nu = -1, c_2^\nu = j, c_3^\nu = -1, c_4^\nu = 1, c_5^\nu = 1,\ c_6^\nu = 1,\ c_7^\nu = -1, c_8^\nu = j, c_9^\nu = -1]$$

is the

$$\bar{C}(\bar{A}^\zeta) = [\ c_0^\zeta = 1,\ c_1^\zeta = 1, c_2^\zeta = -1, c_3^\zeta = -j, c_4^\zeta = j, c_5^\zeta = j,\ c_6^\zeta = j,\ c_7^\zeta = -j, c_8^\zeta = -1, c_9^\zeta = 1],$$

this distance being equal to $D^{10}_{IC[\nu,\zeta]} = 1.465$. However, the sequence

$$\bar{C}(\bar{A}^\xi) = [\ c_0^\xi = 1,\ c_1^\xi = 1, c_2^\xi = -1, c_3^\nu = j, c_4^\xi = 1, c_5^\xi = j,\ c_6^\xi = 1,\ c_7^\xi = -1, c_8^\xi = j, c_9^\xi = -1]$$

forms minimum distance with the sequence

$$\bar{C}(\bar{A}^\eta) = [\ c_0^\eta = 1,\ c_1^\eta = -1, c_2^\eta = -j, c_3^\eta = -j, c_4^\eta = -1, c_5^\eta = -1,\ c_6^\eta = -j,\ c_7^\eta = -j, c_8^\eta = -1, c_9^\eta = 1]$$

and $D^{10}_{IC[\xi,\eta]} = 2.765$. There is no sequence $\bar{C}(\bar{A}^\lambda) \in S_{\bar{C}(\bar{A}^\nu)}$ forming distance $D^{10}_{IC[\xi,\lambda]} = D^{10}_{IC[\nu,\zeta]} = 1.465$. Since $D^{10}_{IC[\nu,\zeta]}$, $D^{10}_{IC[\xi,\lambda]}$ are minimum distances for $\bar{C}(\bar{A}^\xi)$, $\bar{C}(\bar{A}^\nu)$, they will dominate the error performance of these two sequences. Since $D^{10}_{IC[\nu,\zeta]} < D^{10}_{IC[\xi,\lambda]}$, errors involving $\bar{C}(\bar{A}^\nu)$ will be appearing more frequently than errors involving $\bar{C}(\bar{A}^\xi)$. Consequently, the error probability of $\bar{C}(\bar{A}^\nu)$ is higher than the error probability of $\bar{C}(\bar{A}^\xi)$. This violates the equality of Eq.(4.47).

In section 4.5.1.1 we mentioned that when the received signal samples y_k are free from ISI and the noise terms corrupting y_k are uncorrelated, opposite error events $\{\bar{C}(\bar{A}^\zeta) \leftarrow \bar{C}(\bar{A}^\nu)\}$, $\{\bar{C}(\bar{A}^\nu) \leftarrow \bar{C}(\bar{A}^\zeta)\}$ have equal distances and probabilities of occurrence. However, when these conditions are not met, even opposite error events can have different distances. This is an extra reason for Eq.(4.47) not to hold.

An interesting point is that *the distance* $D^Z_{IC[\mu,\lambda]}$ *between two sequences* $\bar{C}(\bar{A}^\mu)$, $\bar{C}(\bar{A}^\lambda)$ *does not depend only on the symbols* c_k^μ, c_k^λ, *where the two*

sequences happen to be in divergence ($c_k^\mu \neq c_k^\lambda$), *but on the entire sequence.* As an example, let us refer again to Code A (non-differentially encoded case) and consider the sequences

$$\bar{C}(\bar{A}^\mu) = [\ \ c_0^\mu = 1,\ \ c_1^\mu = 1, c_2^\mu = 1, c_3^\mu = 1, \ldots, c_{Z-1}^\mu = 1],$$

$$\begin{aligned}\bar{C}(\bar{A}^\lambda) \ &= \ [c_0^\lambda = 1, c_1^\lambda = -1, c_2^\lambda = -j, c_3^\lambda = -j, c_4^\lambda = -1, c_5^\lambda = 1,\\ &\qquad c_6^\lambda = 1, c_7^\lambda = 1, c_8^\lambda = 1, \ldots, c_{Z-1}^\lambda = 1].\end{aligned}$$

The paths of these two sequences diverge initially at $k = 1$ and re-emerge at $k = 4$. The expression of $D^Z_{IC[\mu,\lambda]} = Z - |(Z-6) + 2j|$. For $Z = 5$, $D^5_{IC[\mu,\lambda]} = 1.382$ whereas for $Z = 10$, $D^{10}_{IC[\mu,\lambda]} = 2.765$. The distance $D^Z_{IC[\mu,\lambda]}$ changes with Z. The greater Z is, the larger the distance becomes (and the smaller the error probability of the error event becomes as well). On the contrary, in coherent systems, the (Euclidean) distance depends only on the segments where the two sequences have unequal symbols. The length of the sequence has no effect on the performance (we always refer to coded schemes where all the codewords initiate from a common state and end at a common state). As a result of this behaviour, dominant error events do not depend only on the code but also on the length of the codeword. As an example, we consider code B (non-differentially encoded case). For $Z = 3l + 1$ (l integer, $1 \leq l \leq 3$) minimum distance is formed between the sequences

$$\bar{C}(\bar{A}^\nu) \ = \ [c_0^\nu = 1, c_1^\nu = 1, c_2^\nu = 1, \ldots, c_{Z-1}^\nu = 1],$$

and

$$\begin{aligned}\bar{C}(\bar{A}^\zeta) = [\quad c_0^\zeta \ &= 1, c_1^\zeta = e^{j\frac{\pi}{2}}, c_2^\zeta = e^{j\frac{\pi}{4}}, c_3^\zeta = e^{j\frac{\pi}{2}}, c_4^\zeta = e^{j\frac{\pi}{2}},\\ c_5^\zeta \ &= e^{j\frac{\pi}{2}}, \ldots, c_{Z-6}^\zeta = e^{j\frac{\pi}{2}}, c_{Z-5}^\zeta = e^{j\frac{\pi}{2}},\\ c_{Z-4}^\zeta \ &= e^{j\frac{\pi}{4}}, c_{Z-3}^\zeta = e^{j\frac{\pi}{2}}, c_{Z-2}^\zeta = e^{j\frac{\pi}{2}}, c_{Z-1}^\zeta = e^{j\frac{\pi}{4}}]\end{aligned}$$

with $D^Z_{IC[\nu,\zeta]} = (Z - |1 + \pm 2jL + (L+1)e^{\pm j\frac{\pi}{4}})|)$. In Fig. 4.17, the paths of two such sequences are displayed ($l = 1$, $Z = 4$). On the various branches, the phases of the symbols c_k^ν, c_k^ζ are also indicated.

When $Z = 2l + 2$ (l integer, $1 \leq l \leq 3$) minimum distance is formed between the sequences

$$\bar{C}(\bar{A}^\nu) = [c_0^\nu = 1, c_1^\nu = 1, c_2^\nu = 1, \ldots, c_{Z-1}^\nu = 1],$$

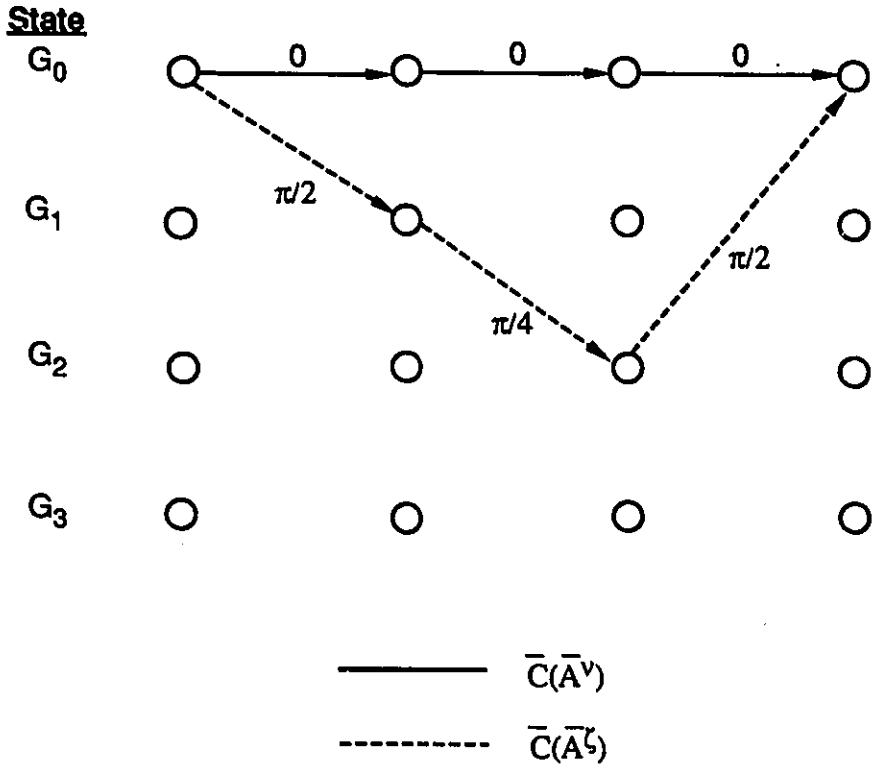

Figure 4.17: Sequences forming a minimum distance error event when Code B (NDE) is used and $Z = 4$ ($l = 1$).

$$\bar{C}(\bar{A}^{\zeta}) = [\quad \begin{aligned} c_0^{\zeta} &= 1, c_1^{\zeta} = e^{j\frac{\pi}{2}}, c_2^{\zeta} = e^{j\frac{\pi}{4}}, c_3^{\zeta} = e^{j\frac{\pi}{2}}, c_4^{\zeta} = e^{j\frac{\pi}{2}}, \\ c_5^{\zeta} &= e^{j\frac{\pi}{2}}, \ldots, c_{Z-6}^{\zeta} = e^{j\frac{\pi}{2}}, \ldots c_{Z-6}^{\zeta} = e^{j\frac{\pi}{2}}, c_{Z-5}^{\zeta} = e^{j\frac{\pi}{4}}, \\ c_{Z-4}^{\zeta} &= e^{j\frac{\pi}{2}}, c_{Z-3}^{\zeta} = e^{j\frac{\pi}{2}}, c_{Z-2}^{\zeta} = e^{j\frac{\pi}{4}}, c_{Z-1}^{\zeta} = 1] \end{aligned}$$

with $D^Z_{IC[\nu,\zeta]} = (Z - |2 + l(\pm 2j + e^{\pm j\frac{\pi}{4}})|)$. In Fig. 4.18 we display the paths corresponding to such an error event when $Z = 5$ ($l = 2$).

Finally for $Z = 3l + 3$ (l integer, $1 \leq l \leq 3$) minimum distance is formed between the sequences

$$\bar{C}(\bar{A}^{\nu}) = [c_0^{\nu} = 1, c_1^{\nu} = 1, c_2^{\nu} = e^{j\frac{\pi}{2}}, c_3^{\nu} = e^{j\frac{\pi}{4}}, c_4^{\nu} = e^{j\frac{\pi}{2}}, c_5^{\nu} = 1, \ldots, c_{Z-1}^{\nu} = 1]$$

and

$$\bar{C}(\bar{A}^{\zeta}) = [\quad \begin{aligned} c_0^{\zeta} &= 1, c_1^{\zeta} = e^{j\frac{\pi}{2}}, c_2^{\zeta} = e^{j\frac{\pi}{4}}, c_3^{\zeta} = e^{j\frac{\pi}{2}}, \\ c_4^{\zeta} &= e^{j\frac{\pi}{2}}, c_5^{\zeta} = e^{j\frac{\pi}{2}}, \ldots, c_{Z-6}^{\zeta} = e^{j\frac{\pi}{2}}, c_{Z-5}^{\zeta} = e^{j\frac{\pi}{4}}, c_{Z-4}^{\zeta} = e^{j\frac{\pi}{2}}, \\ c_{Z-3}^{\zeta} &= e^{j\frac{\pi}{2}}, c_{Z-2}^{\zeta} = e^{j\frac{\pi}{4}}, c_{Z-1}^{\zeta} = 1] \end{aligned}$$

with $D^Z_{IC[\nu,\zeta]} = (Z - |2 \pm 2jL \pm (L+1)e^{\pm j\frac{\pi}{4}}|)$. The paths of such an error event with $Z = 6$ ($l = 3$) are displayed in Fig. 4.19.

When $Z > 12$, the patterns of the most dominant error events change completely. Most dominant error events are formed by pairs of sequences $\bar{C}(\bar{A}^{\nu})$, $\bar{C}(\bar{A}^{\zeta})$ described as follows:

$$[c_0^{\zeta} = c_0^{\nu}, c_1^{\zeta} = c_1^{\nu}, \ldots c_{k-1}^{\zeta} = c_{k-1}^{\nu}, c_k^{\zeta} = c_k^{\nu} e^{-j\pi}, c_{k+1}^{\zeta} = c_{k+1}^{\nu}, \ldots c_{Z-1}^{\zeta} = c_{Z-1}^{\nu}]$$

($1 \leq k \leq Z-1$). The two sequences differ only in one symbol, and these unequal symbols have opposite polarity. The distance between such sequences is $D^Z_{IC[\nu,\zeta]} = 2$. In Fig. 4.20 we present the paths of two sequences forming such an error event. In all transitions with the exception of one, the two paths overlap with each other. For the transition where there is not overlapping, the paths go through two branches parallel to each other.

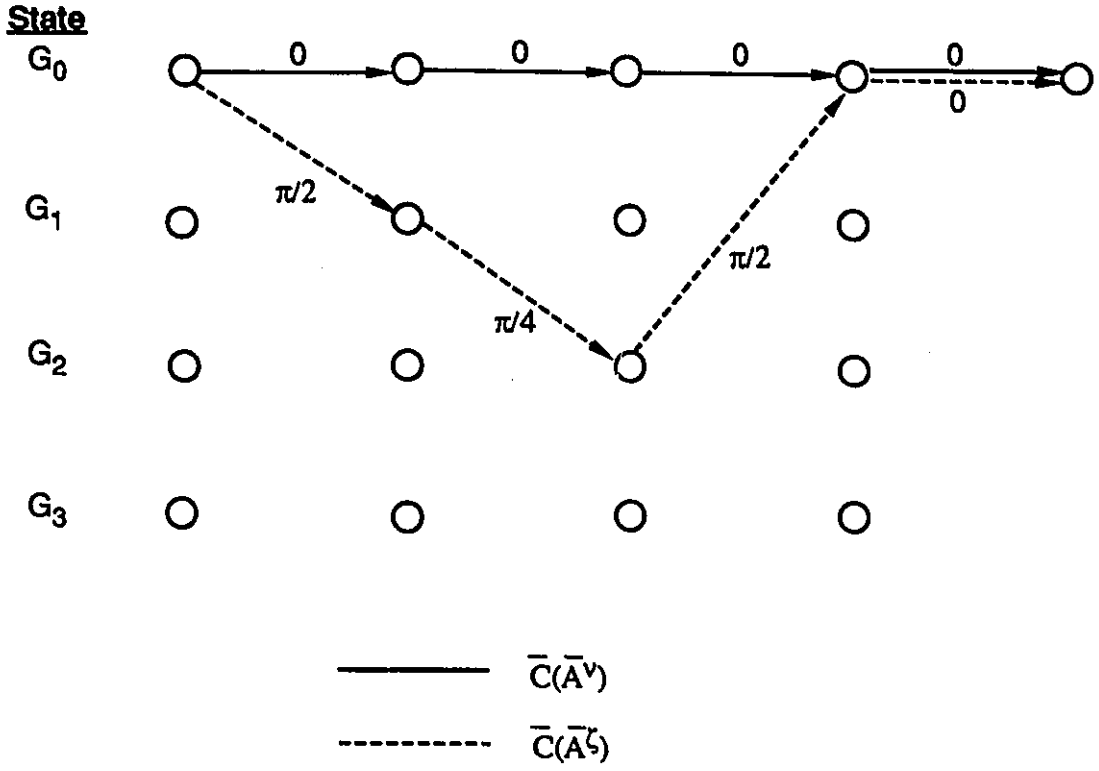

Figure 4.18: Sequences forming a minimum distance error event when Code B (NDE) is used and $Z = 5$ ($l = 1$).

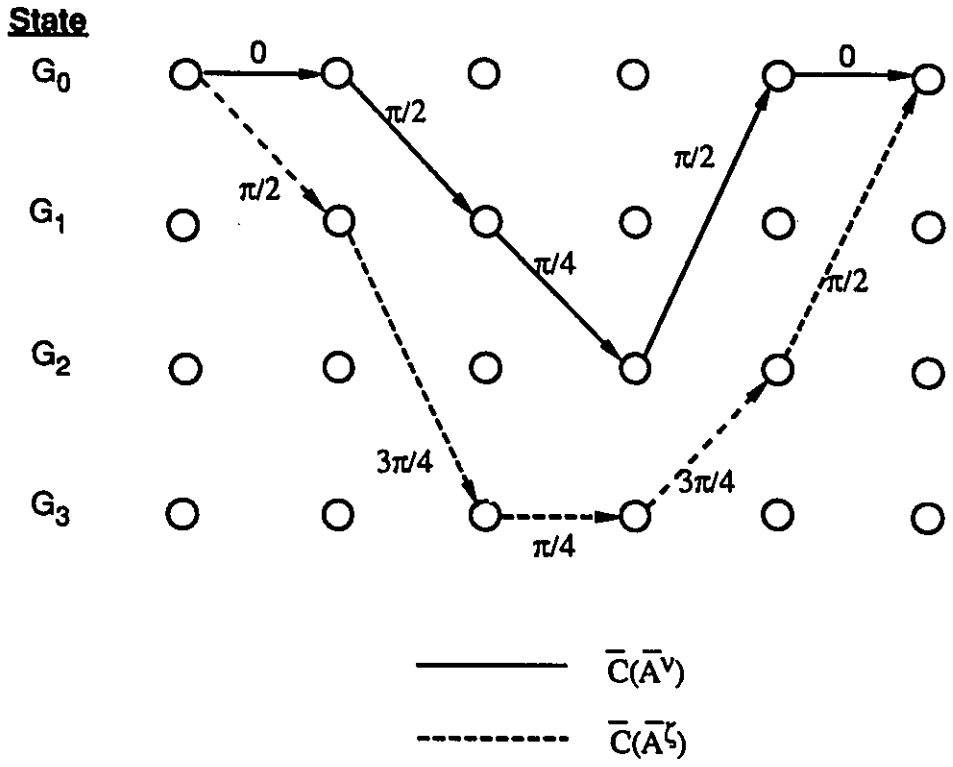

Figure 4.19: Sequences forming a minimum distance error event when Code B (NDE) is used and $Z = 6$ ($l = 1$).

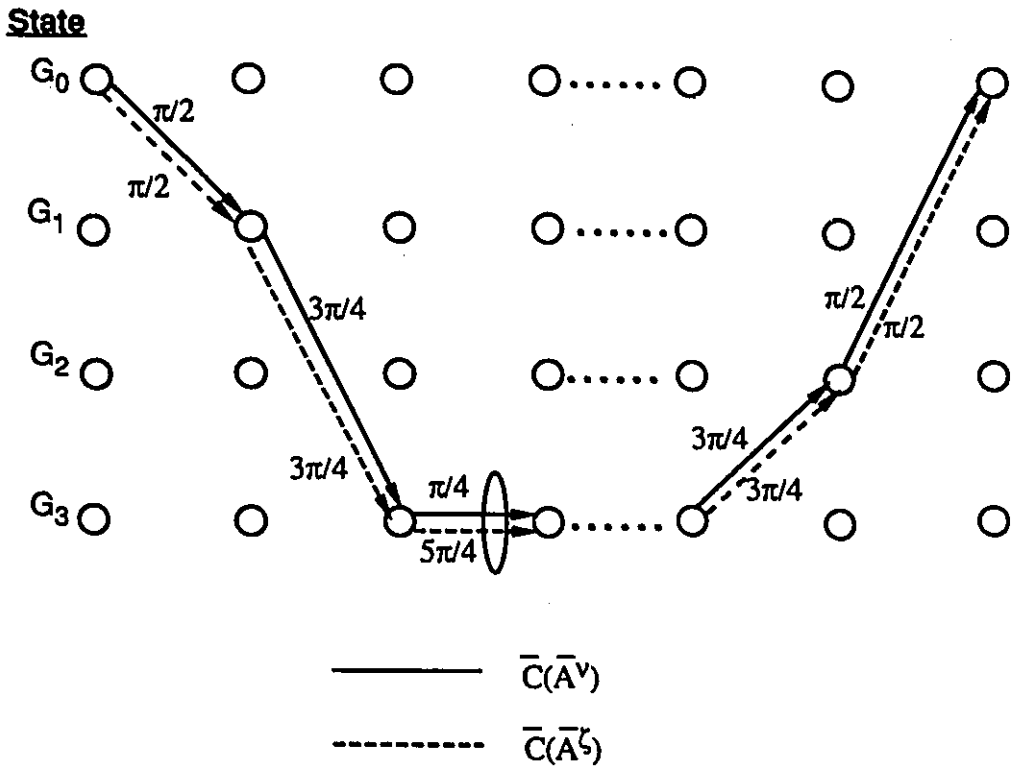

Figure 4.20: Sequences forming a minimum distance error event when Code B (NDE) is used and $Z > 12$ ($l > 3$).

The previous example has shown us that *with the change in Z, there is a dramatic change in the patterns of pairs of sequences which form dominant error events. Such behaviour is not encountered in coherent detection. In coherently systems, the distance of the error event depends strictly on the segments where the two sequences appear with unequal symbols.*

To further demonstrate how strong the interaction between code and length of codeword is, we give the following example. Up to this point, we have restricted all codewords to re-emerge at the same stage. Now, we go one step further and we consider the case where the various codewords, instead of being forced to re-emerge at $(Z-1)T$, are forced to re-emerge at $(Z-2)T$. Below we compare the performance between these two cases (re-emergence at $(Z-2)T$ and re-emergence at $(Z-1)T$). To distinguish between them, we shall be calling the configuration having re-emergence at $(Z-2)T$ *restricted* and the other re-emerging at $(Z-1)T$ *unrestricted.*

In Figs. 4.21, 4.22 we display the curves corresponding to restricted and unrestricted configurations of Code C with $Z = 5, 6, 7$. Both non-differentially encoded (Fig. 4.21) and differentially encoded (Fig. 4.22) systems are considered. The curves of the restricted configurations are identified in the figures as (Z= (NDE or DE)RES). For the unrestricted configurations the various curves are identified as (Z= (NDE or DE)).

In Table 4.5 we summarize the improvements offered by the restricted configurations as compared to the non-restricted ones. When differential encoding is not present, the improvements become higher than 1.5 dB. For the differentially encoded schemes, the restricted configurations remain superior, however their advantage is quite small (0.2 dB).

The identification of dominant error events (i.e. those having the highest probability to occur) has been proven useful in coherent detection. Since it characterizes the performance for high E_b/N_o, it provides the opportunity to have an easy and relatively reliable performance estimate without the need to resort to more complex forms of analysis. We attempted to come up with a systematic approach leading to the identification of dominant error events for the examined non-coherently detected systems. Unfortunately, our effort was not successful. The interaction between the memory of the coded signal (created by the use of coding) and the memory of the block decoder (it is equal to the codeword length) makes the task difficult. In order to identify

Table 4.5: Gains offered by the restricted over the unrestricted configurations versus the codeword length (Z) (Code C is used).

		GAINS (dB)	
		(NDE)	(DE)
Z	5	1.3	0.2
	6	1.5	0.2
	7	1.5	0.2

dominant error events, we had to resort to computer searching techniques. To make the performance estimation even more difficult, we found that even knowledge of dominant error events is not adequate to allow reliable estimation of the performance. Very frequently, the number of sequences forming dominant error events is small compared to the entire population of possible codewords ($2^{(Z-L_c-1)p}$). Since in the union bound, the error probability of every sequence is divided by the number of possible codewords (for large values of $2^{(Z-L_c-1)p}$), their contribution in the error bound can be orders of magnitude smaller from what it is projected by $B^Z_{IC[\nu,\zeta]}$. To clarify this point, we provide the following example from Code C (non-differentially encoded case). For $Z = 7$ this code has minimum distance equal to $D^7_{IC[\nu,\zeta]} = 0.5858$ and the corresponding $B^Z_{IC[\nu,\zeta]}$ at 15 dB is $B^Z_{IC[\nu,\zeta]} = 1.58 \times 10^{-10}$. However, out of all the pairs formed between codewords, only four of them have this distance value. The contribution of these error events in the error probability performance equals to $\frac{2\times4}{2^{10}} B^Z_{IC[\nu,\zeta]} = 7.810^{-3} \times 1.5810^{-10} = 1.23 \times 10^{-12}$ (the value given by the union bound is 2.54×10^{-12}). If the judgement was to be based on the value of $B^Z_{IC[\nu,\zeta]} = 1.58 \times 10^{-10}$, we would have ended up making two orders of magnitude error in the value of SER. Equivalently, we would have underestimated the performance of the system by (approximately) 1 dB.

Summarizing the main points of the above discussion, we state the following:

1. The trellis codes, designed for coherently detected signals and optimized under the Euclidean distance criterion, do not constitute optimal

solutions for the proposed non-coherent schemes. Instead, new coding schemes are required. Their design should be based on the optimization of the new distance expressions presented in the present section, since they determine the performance of the proposed receivers.

2. The improvements which the coded and block decoded schemes obtain, over the uncoded differentially detected signals of equal spectral efficiency, are higher in comparison to the gains provided by the same codes (coherently detected) over their coherent uncoded counterparts.

3. The probabilities of the pairwise error events strongly depend on the size of the codewords. This behaviour is not met in coherent systems.

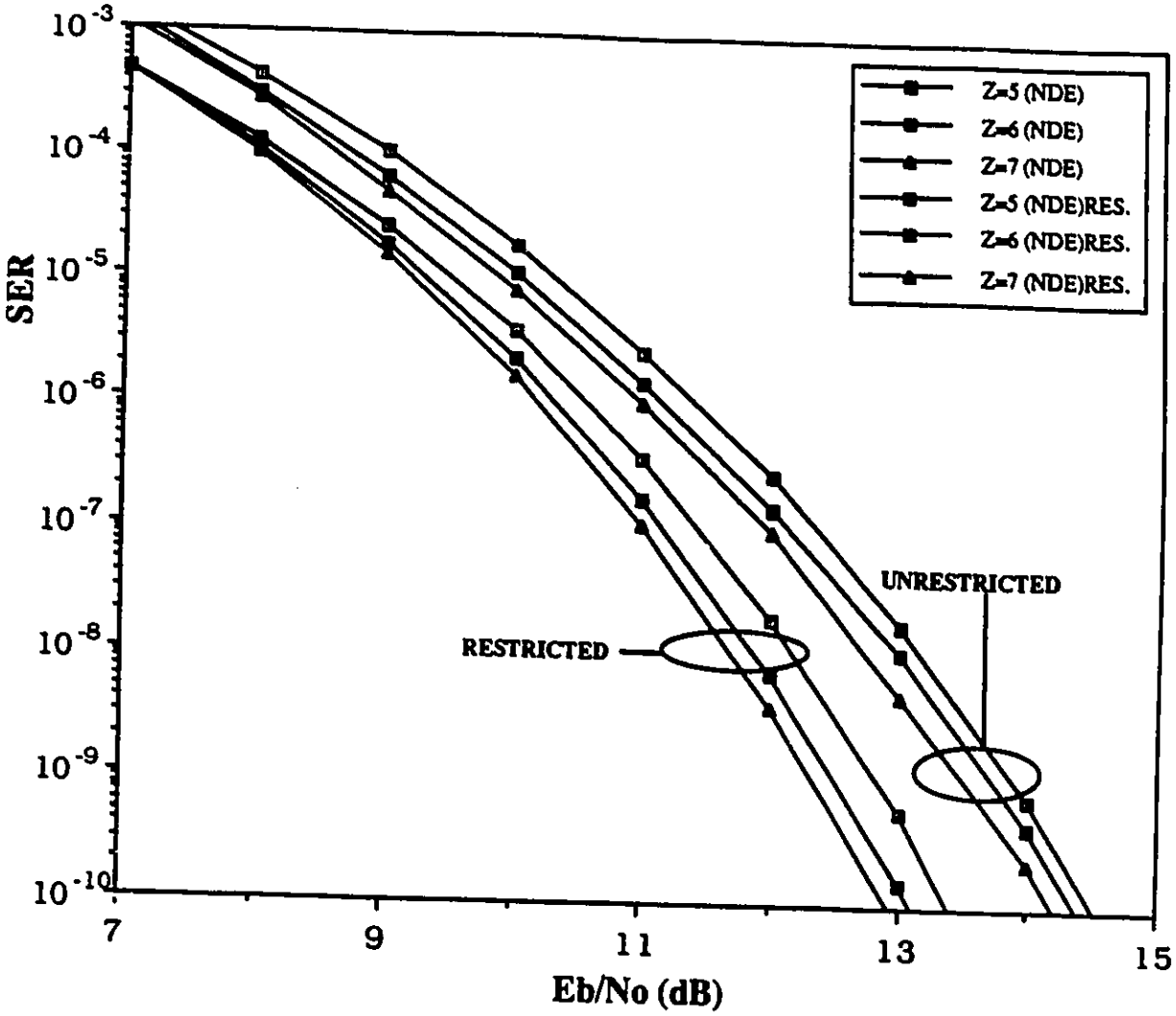

Figure 4.21: SER curves of code C (without differential encoding) corresponding to restricted and unrestricted configurations. The channel is assumed ideal. The Nyquist filter is equally apportioned between transmitter-receiver.

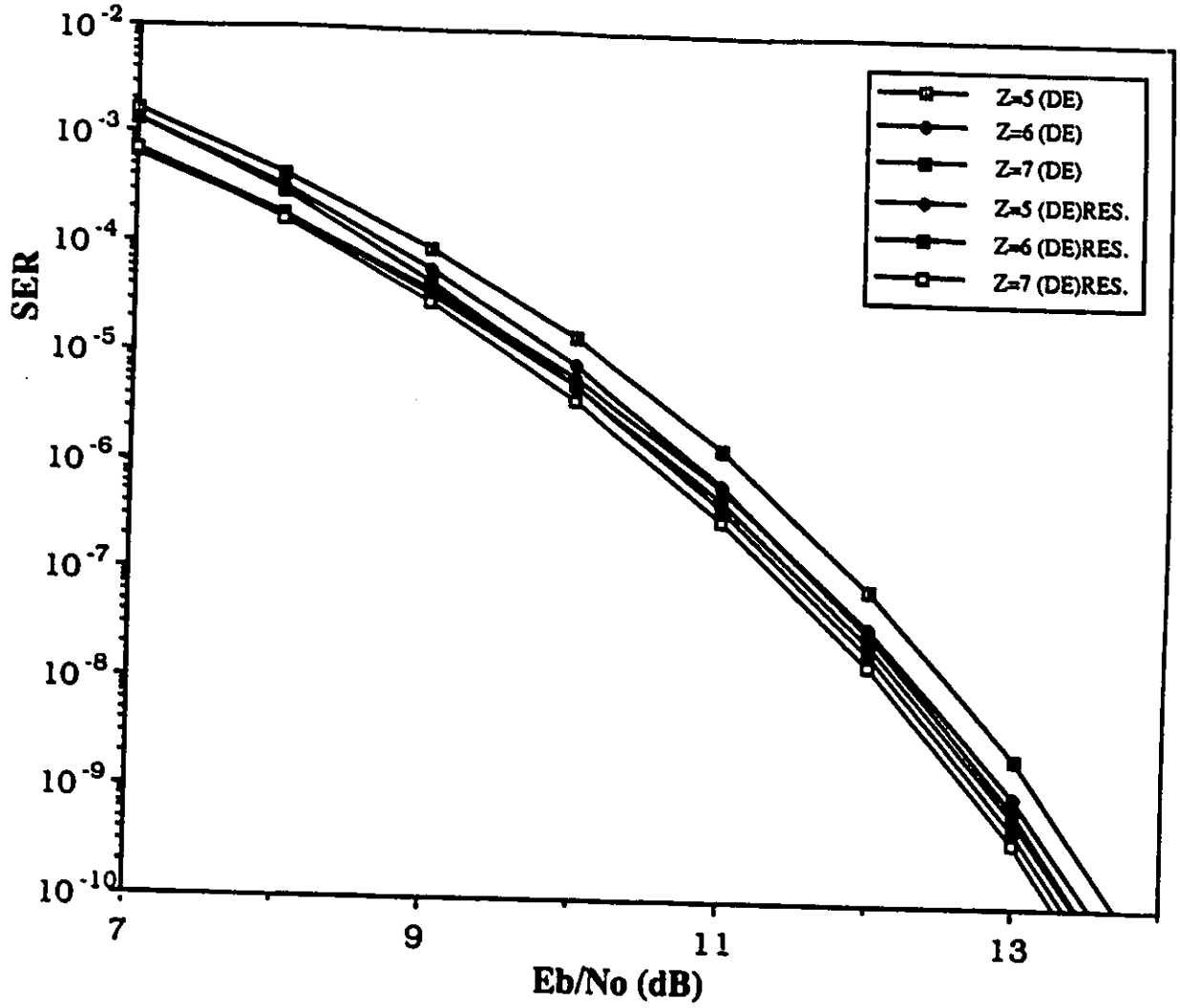

Figure 4.22: SER curves of code C (with differential encoding) corresponding to restricted and unrestricted configurations. The channel is assumed ideal. The Nyquist filter is equally apportioned between transmitter-receiver.

4.5.5 Performance of Uncoded Signals in Ideal Channel and with Equal Nyquist Filter Apportioning Systems

In Appendix C it has been shown that for uncoded MPSK signals, Eq.(4.47) holds. This allows the use of Eq.(4.48) for the calculation of the union bound $\mathcal{UB}^Z$, instead of the (computationally complex) Eq.(4.46). In Appendix C it has been proven that for the uncoded MPSK signals, the union bound has the following expression:

$$\mathcal{UB}^Z = \frac{1}{Z-1}\frac{1}{2}\frac{1}{\sqrt{\sigma_n^2}} \underbrace{\sum_{i_1=0}^{M-1}\sum_{i_2=0}^{M-1}\cdots\sum_{i_{Z-1}=0}^{M-1}}_{i_1+i_2+\ldots+i_{Z-1}\neq 0} \left(\sum_{l=1}^{Z-1}\delta_f(i_l)\right)\Upsilon(i_0,i_1,\ldots,i_{Z-1})$$

$$\exp\left\{-\frac{1}{2\sigma_n^2}\left[Z-\left|1+\sum_{k=1}^{Z-1}\exp\left[-j\frac{2\pi}{M}(i_1\oplus i_2\oplus\cdots\oplus i_k)_{mod(M)}\right]\right|\right]\right\} \quad (4.49)$$

with

$$\Upsilon(i_0,i_1,\ldots,i_{Z-1}) =$$

$$\begin{cases} 1 & \text{for } \sum_{k=0}^{Z-1} \\ & \exp\{-j\frac{2\pi}{M}(i_0\oplus\cdots\oplus i_k)_{mod(M)}\}=0 \\ \dfrac{\sqrt{\frac{\sigma_n^2}{2\pi}}\sqrt{2}}{\sqrt{\left|\sum_{k=0}^{Z-1}\exp\{-j\frac{2\pi}{M}(i_0\oplus\cdots\oplus i_k)_{mod(M)}\}\right|}} & \text{for } \sum_{k=0}^{Z-1} \\ & \exp\{-j\frac{2\pi}{M}(i_0\oplus\cdots\oplus i_k)_{mod(M)}\}\neq 0 \end{cases} \quad (4.50)$$

and

$$\delta_f(x) = \begin{cases} 0 & \text{for } x=0 \\ 1 & \text{for } x\neq 0 \end{cases} \quad (4.51)$$

($\delta_f(x)$ should not be confused with the delta function $\delta(x)$ which is zero for $x\neq 0$ and goes to infinity at $x=0$).

In Eqs.(4.49), (4.50) the $(i_0 \oplus i_1 \oplus ... \oplus i_l)_{mod(M)}$ symbolizes addition in the modulo(M) sense (M is a positive integer). For BPSK, QPSK, 8PSK, and 16PSK, $\frac{1}{\sigma_n^2}$ equals $\frac{E_b}{N_o}$, $\frac{2E_b}{N_o}$, $\frac{3E_b}{N_o}$, and $\frac{4E_b}{N_o}$ respectively.

The importance of easy identification of the dominant error events has been discussed earlier. We also explained why for coded systems, this identification is a very tedious task. However, for uncoded signals the situation is different. The uncoded signal does not have the memory present in the coded case. This simplifies the problem, making the identification of such events possible (for details see Appendix D) and leads to the development of a simpler (and computationally more efficient) performance bound ($\mathcal{UB}^Z_{app.}$). The full analysis leading to the derivation of $\mathcal{UB}^Z_{app.}$ is provided in Appendix D. Here we present the final expression:

$$\mathcal{UB}^Z_{app.} = \frac{1}{Z-1}\frac{1}{2}\sum_{m=1}^{Z-1} N_e^B(M,m)\varphi_{PSK}(M,m)$$
$$\exp\{-\frac{1}{2\sigma_n^2}(Z - \sqrt{Z^2+2m^2-2Zm+2(Z-m)m\cos(\frac{2\pi}{M})}\} \quad (4.52)$$

with

$$\varphi_{PSK}(M,m) = \begin{cases} 1 & \text{when} \quad M = 2 \\ & \text{and } m = \frac{Z-1}{2} \\ \frac{1}{\sqrt{2\pi}}\frac{1}{\sqrt{\frac{1}{\sigma_n^2}}}\frac{\sqrt{2}}{\sqrt{Z^2+2m^2-2Zm+2(Z-m)m\cos(\frac{2\pi}{M})}} & \text{elsewhere} \end{cases} \quad (4.53)$$

and

$$N_e^B(M,m) = \begin{cases} [1+\delta_f(log_2(M)-1)] & \\ [2m\begin{pmatrix} Z-2 \\ m \end{pmatrix} + (2m-1)\begin{pmatrix} Z-2 \\ m-1 \end{pmatrix}] & \text{for } m \le \lceil\frac{Z-1}{2}\rceil \\ [1+\delta_f(log_2(M)-1)] & \\ (Z-1)[\begin{pmatrix} Z-2 \\ m \end{pmatrix} + \begin{pmatrix} Z-2 \\ m-1 \end{pmatrix}] & \text{for } m > \lceil\frac{Z-1}{2}\rceil. \end{cases}$$

$\left(\begin{pmatrix} k \\ j \end{pmatrix} = \frac{(k)!}{j!(k-j)!}\right.$ and $\lceil x \rceil$ represents the largest integer, smaller or equal to x). A brief description on how the approximate bound has been derived, follows.

Two sequences (for example $\bar{C}(\bar{A}^{\nu})$, $\bar{C}(\bar{A}^{\zeta})$) of length Z can differ at most at $Z-1$ symbols. For the sequence $\bar{C}(\bar{A}^{\nu})$, we generate $Z-1$ different sets $\underline{GR}_m^{Z,\nu}$ $(1 \leq m \leq Z-1)$. $\underline{GR}_m^{Z,\nu}$ has as members all sequences $\bar{C}(\bar{A}^{\zeta})$ which happen to have m symbols $c_k^{\zeta} \neq c_k^{\nu}$ $(1 \leq k \leq Z-1)$. For each set $\underline{GR}_m^{Z,\nu}$, an upper bound for $n_e(\{\bar{C}(\bar{A}^{\zeta}) \leftarrow \bar{C}(\bar{A}^{\nu})\})$ is derived (see Eq.(D.16)). This bound is represented as $n_e^b(m)$. Also, the minimum distance $D^Z_{[\nu,\zeta]}$ between the sequences, elements of $\underline{GR}_m^{Z,\nu}$ and $\bar{C}(\bar{A}^{\nu})$ is found ($D^Z_{min_{\underline{GR}_m^{Z,\nu}}}$, see Eq.(D.20)). All elements of $\underline{GR}_m^{Z,\nu}$, having distance $D^Z_{[\nu,\zeta]} = D^Z_{min_{\underline{GR}_m^{Z,\nu}}}$, form the subset $\underline{G^{\cup}_{min} R}_m^{Z,\nu}$. The pairwise error bound $B^Z_{[\nu,\zeta]}$ of these elements (i.e the members of $\underline{G^{\cup}_{min} R}_m^{Z,\nu}$) together with $n_e^b(m)$ are used to provide the approximate upper bound $\mathcal{UB}^Z_{app}$ (see Eqs.(D.21), (D.24)). It is worth mentioning that the calculation of $\mathcal{UB}^Z_{app.}$ requires only $\frac{Z-1}{M_p^{Z-1}-1}$ of the calculations needed for $\mathcal{UB}^Z$. For large Z and M, this is quite a difference. From now on, in order to distinguish $\mathcal{UB}^Z$ and $\mathcal{UB}^Z_{app.}$, we shall be referring to them as *exact* and *approximate* bounds respectively.

In order to provide a clear picture of the accuracy offered by the approximate bound, we have plotted the SER versus E_b/N_o using both $\mathcal{UB}^Z$ and $\mathcal{UB}^Z_{app.}$ for BPSK (Figs. 4.23, 4.24), QPSK (Figs. 4.25, 4.26), 8PSK (Figs. 4.27, 4.28) and 16PSK (Figs. 4.29, 4.30). The displayed curves correspond to the conventional differential detector (DD) and the block decoder with $Z=4$ and $Z=7$ (the curves are identified as (Z= , Ex.Bound) and (Z= ,Ap.Bound)).

The $Z=7$ case achieves practically the same performance as the coherently detected system which uses perfect carrier phase reference. Comparison between these curves, provides us with the following conclusions: i) $\mathcal{UB}^Z_{app.}$ is capable to very accurately characterize the SER performance for the symbol error rates of interest (i.e., SER $\leq 10^{-2}$). ii) Z=4 is adequate to achieve practically all the available improvement. For the BPSK, the improvement

Table 4.6: Gains offered by the Block Decoder as a function of the sequence length Z. The comparison is with the conventional differential detector.

		GAINS (dB)			
		BPSK	QPSK	8PSK	16PSK
Z	4	0.2	1.6	1.6	1.6
	7	0.4	2	2	2

is 0.2 dB, while for the QPSK, 8PSK and 16PSK it is close to 1.6 dB (comparison is between the conventional differential detector and the $Z = 4$ block decoder). For $Z = 7$, this improvement becomes 2 dB.

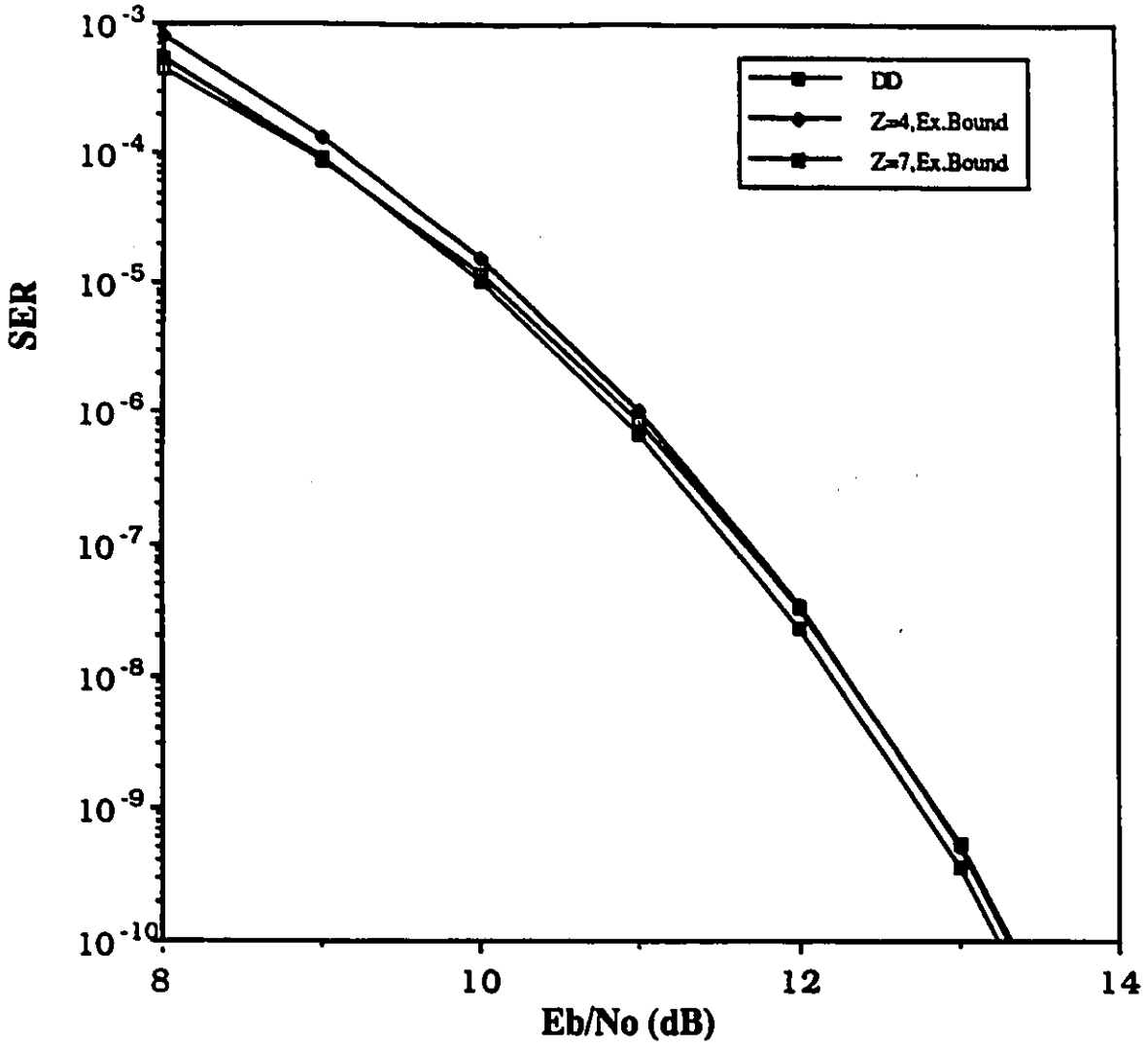

Figure 4.23: SER performance curves of BPSK in ideal channel with equal Nyquist filter apportioning. The curves corresponding to the block decoder are based on the exact bound.

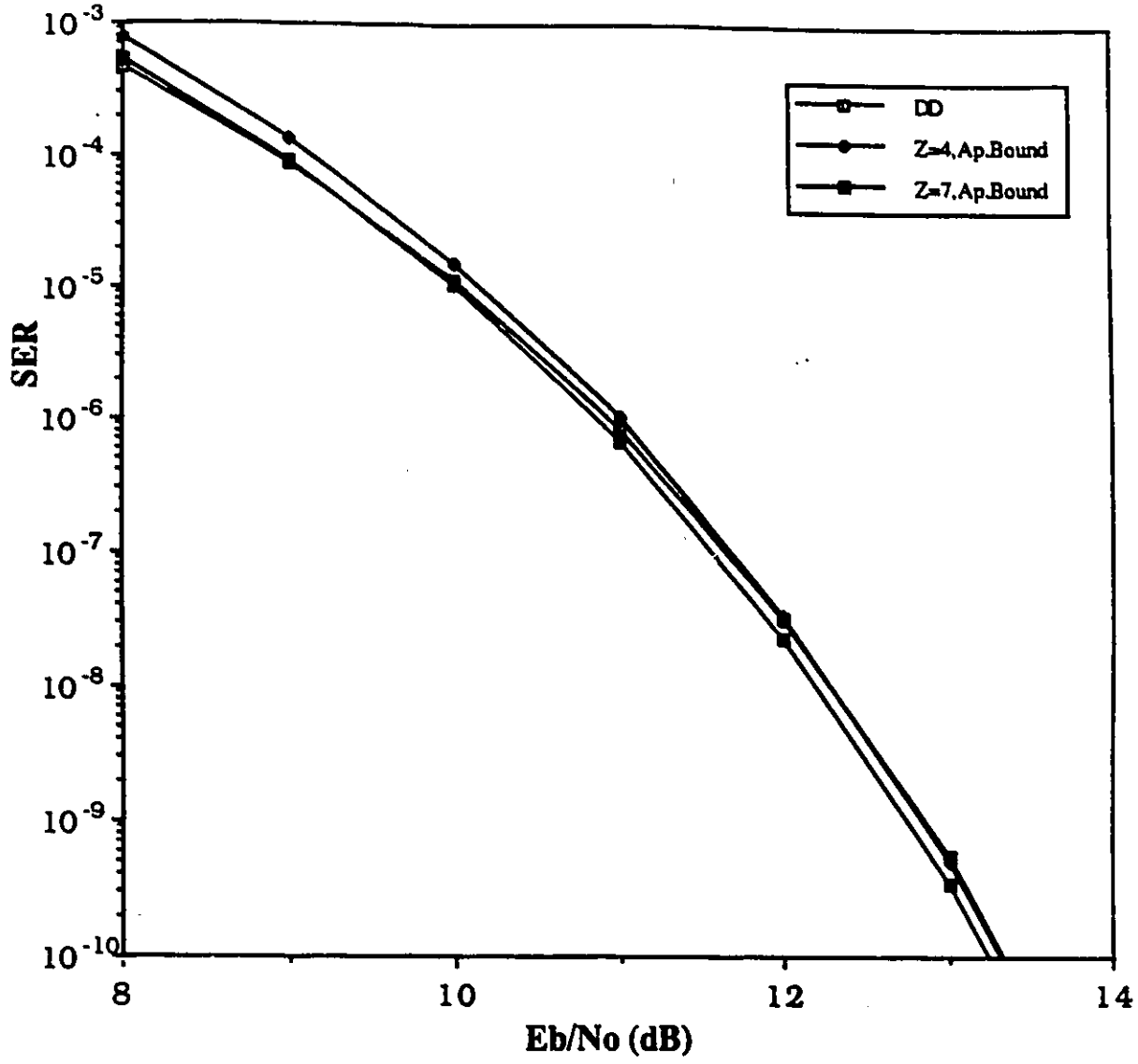

Figure 4.24: SER performance curves of BPSK in ideal channel with equal Nyquist filter apportioning. The curves corresponding to the block decoder are based on the approximate bound.

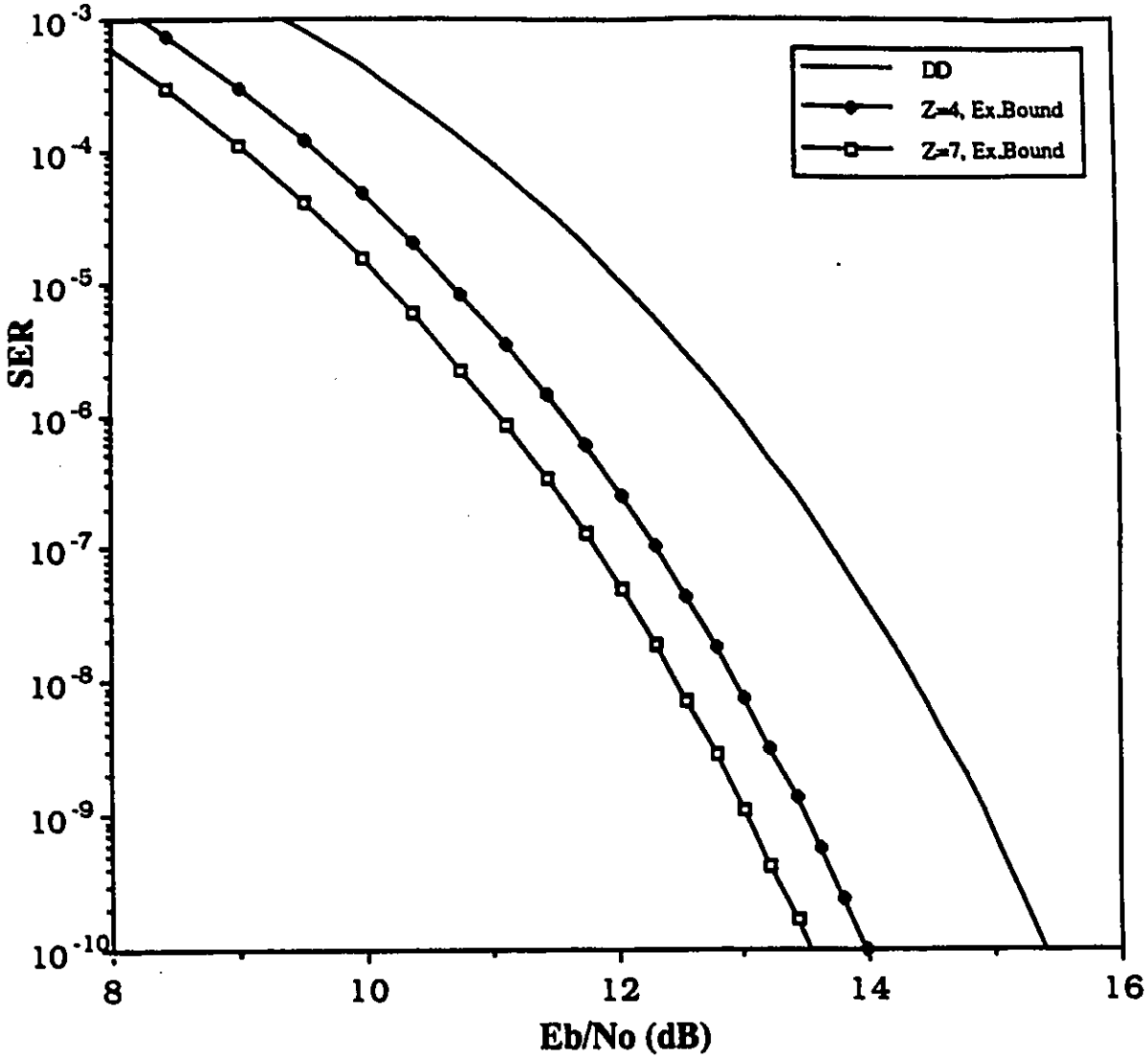

Figure 4.25: SER performance curves of QPSK in ideal channel with equal Nyquist filter apportioning. The curves corresponding to the block decoder are based on the exact bound.

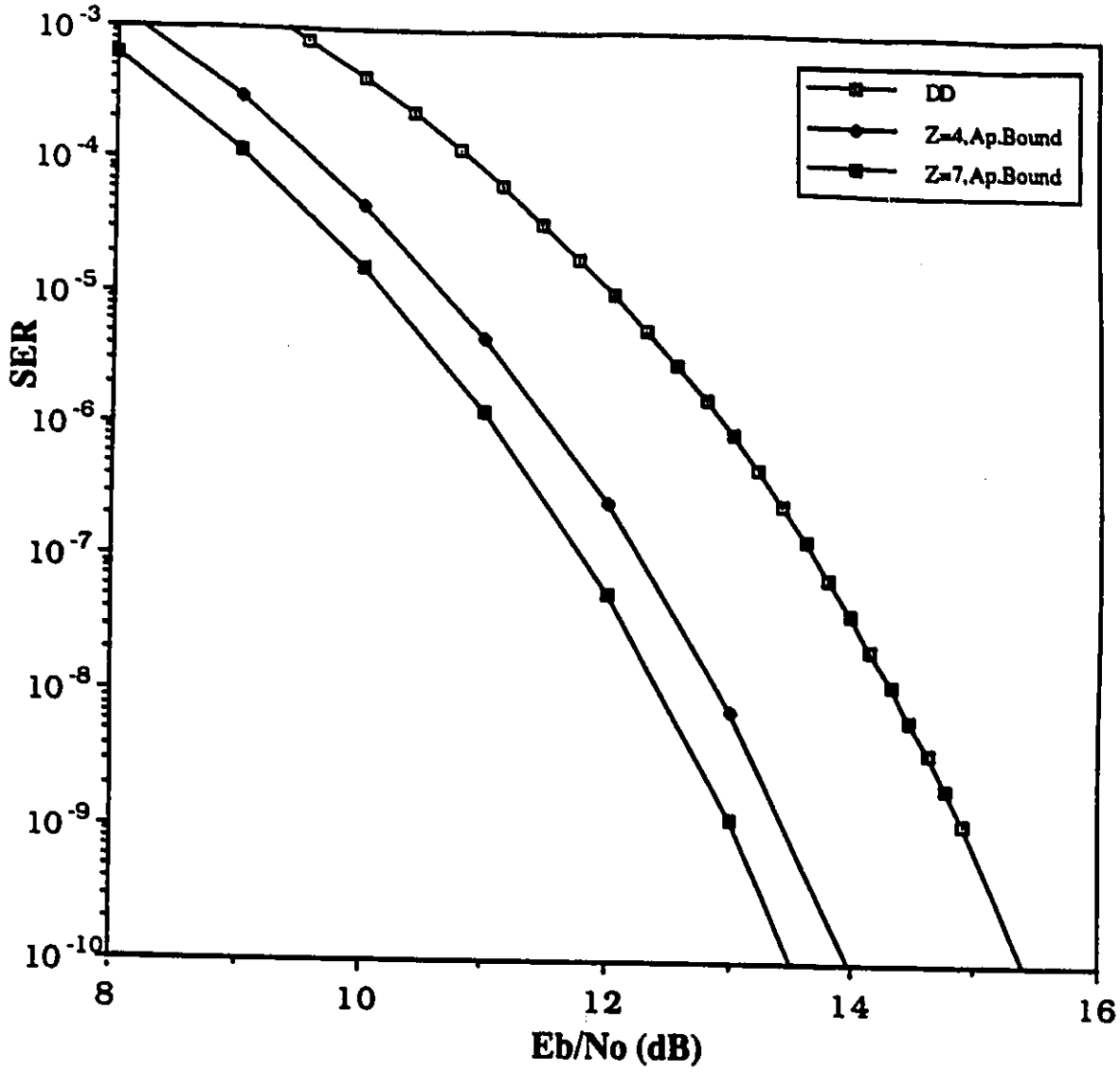

Figure 4.26: SER performance curves of QPSK in ideal channel with equal Nyquist filter apportioning. The curves corresponding to the block decoder are based on the approximate bound.

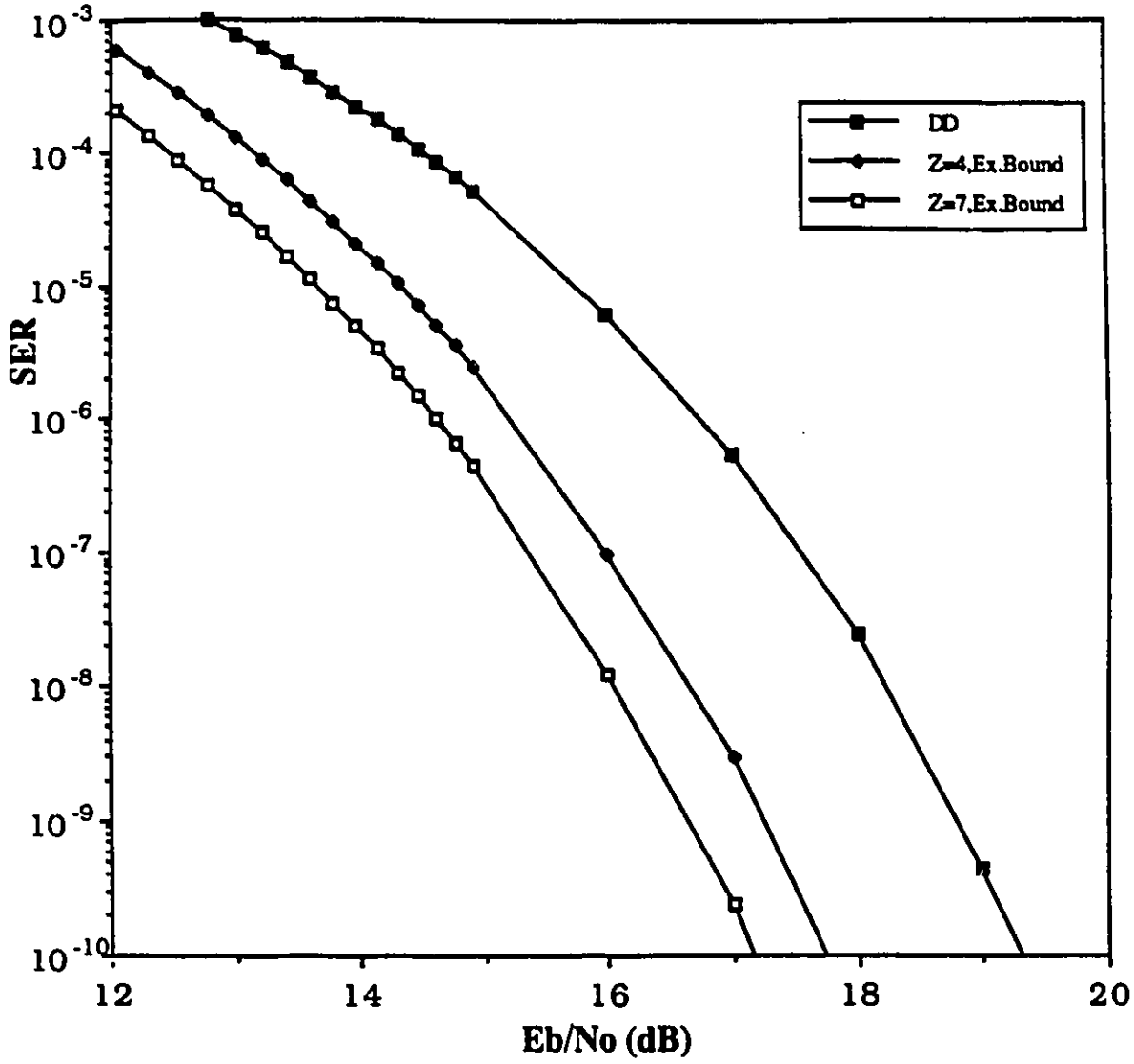

Figure 4.27: SER performance curves of 8PSK in ideal channel with equal Nyquist filter apportioning. The curves corresponding to the block decoder are based on the exact bound.

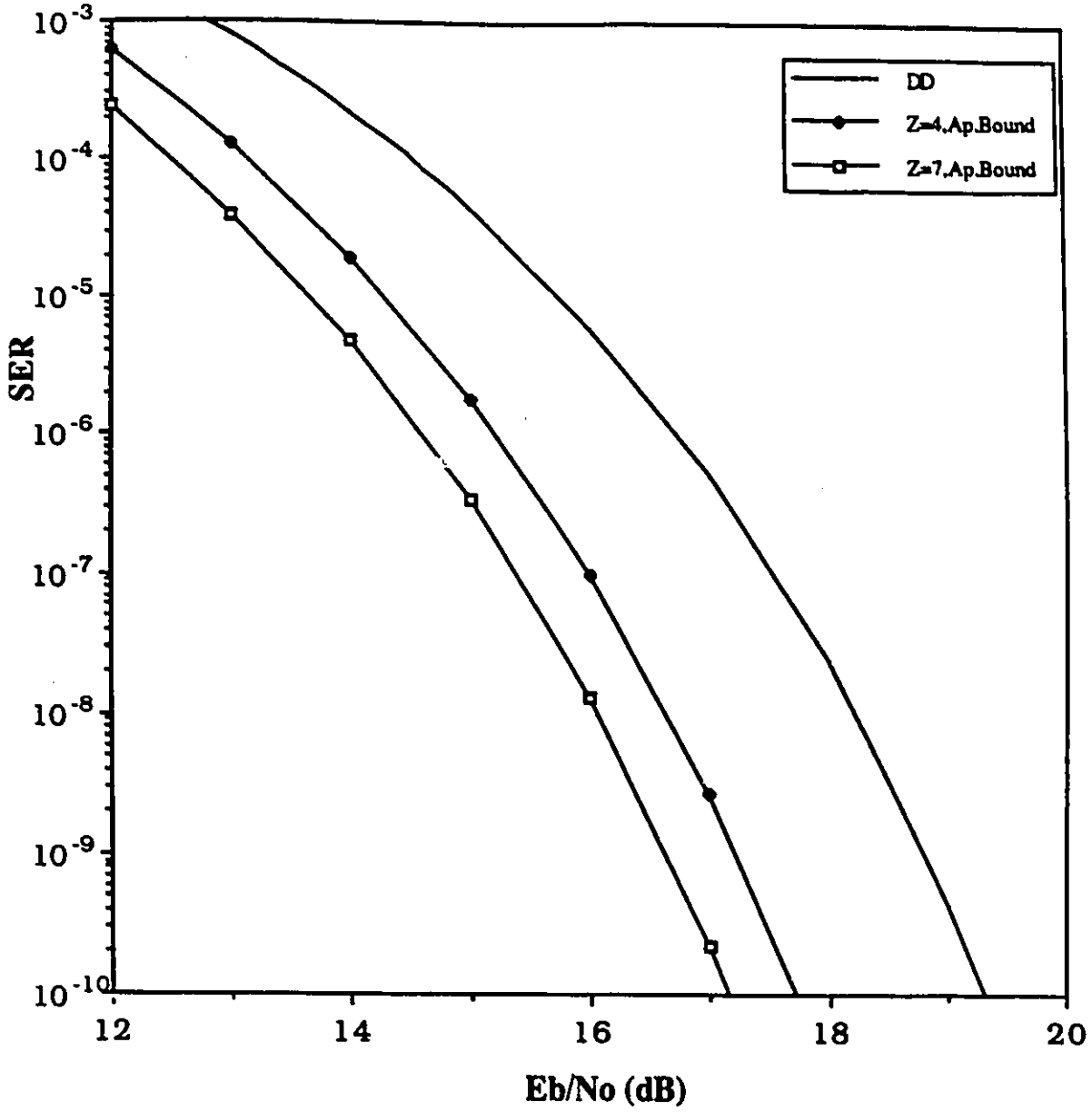

Figure 4.28: SER performance curves of 8PSK in ideal channel with equal Nyquist filter apportioning. The curves corresponding to the block decoder are based on the approximate bound.

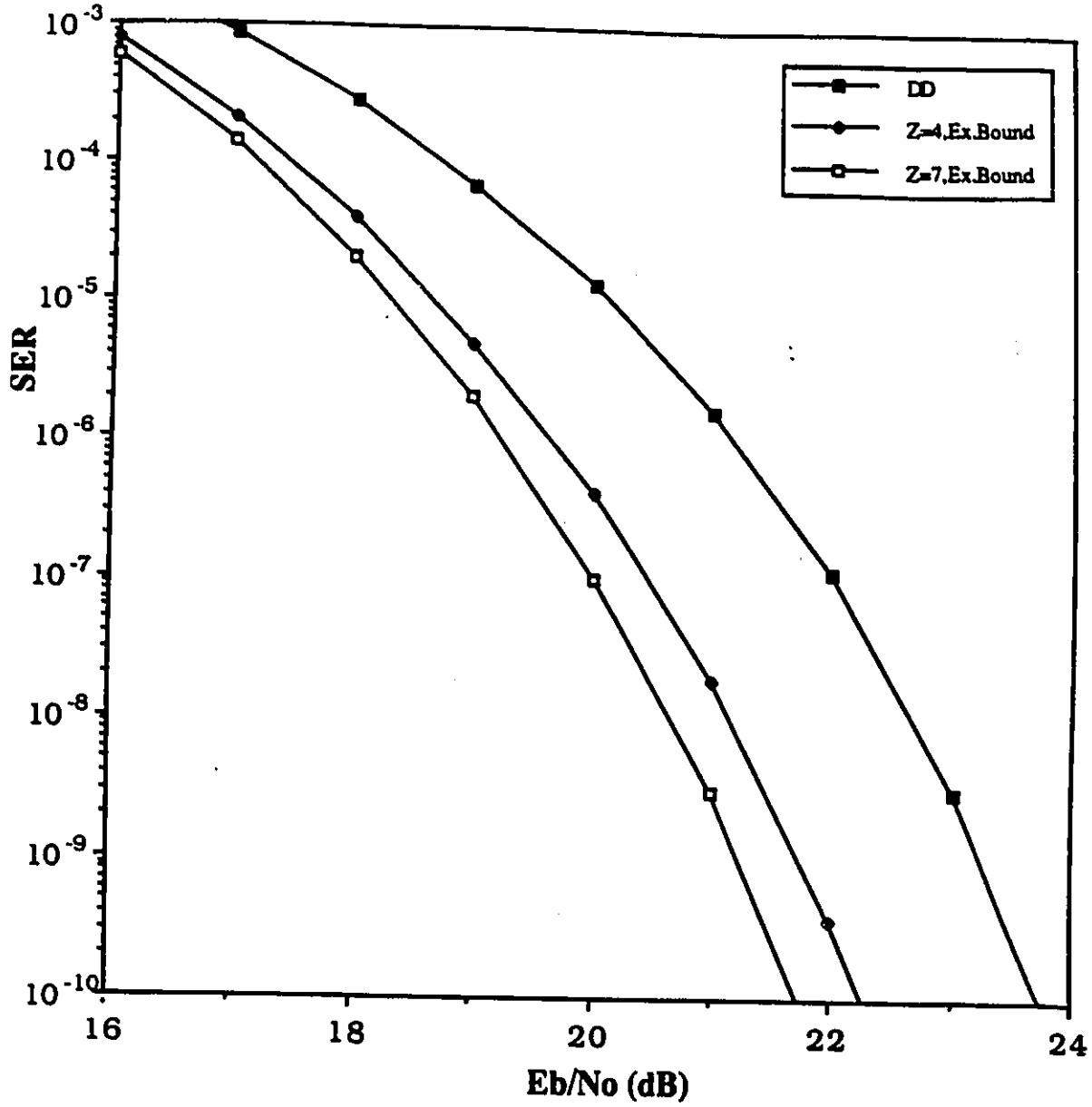

Figure 4.29: SER performance curves of 16PSK in ideal channel with equal Nyquist filter apportioning. The curves corresponding to the block decoder are based on the exact bound.

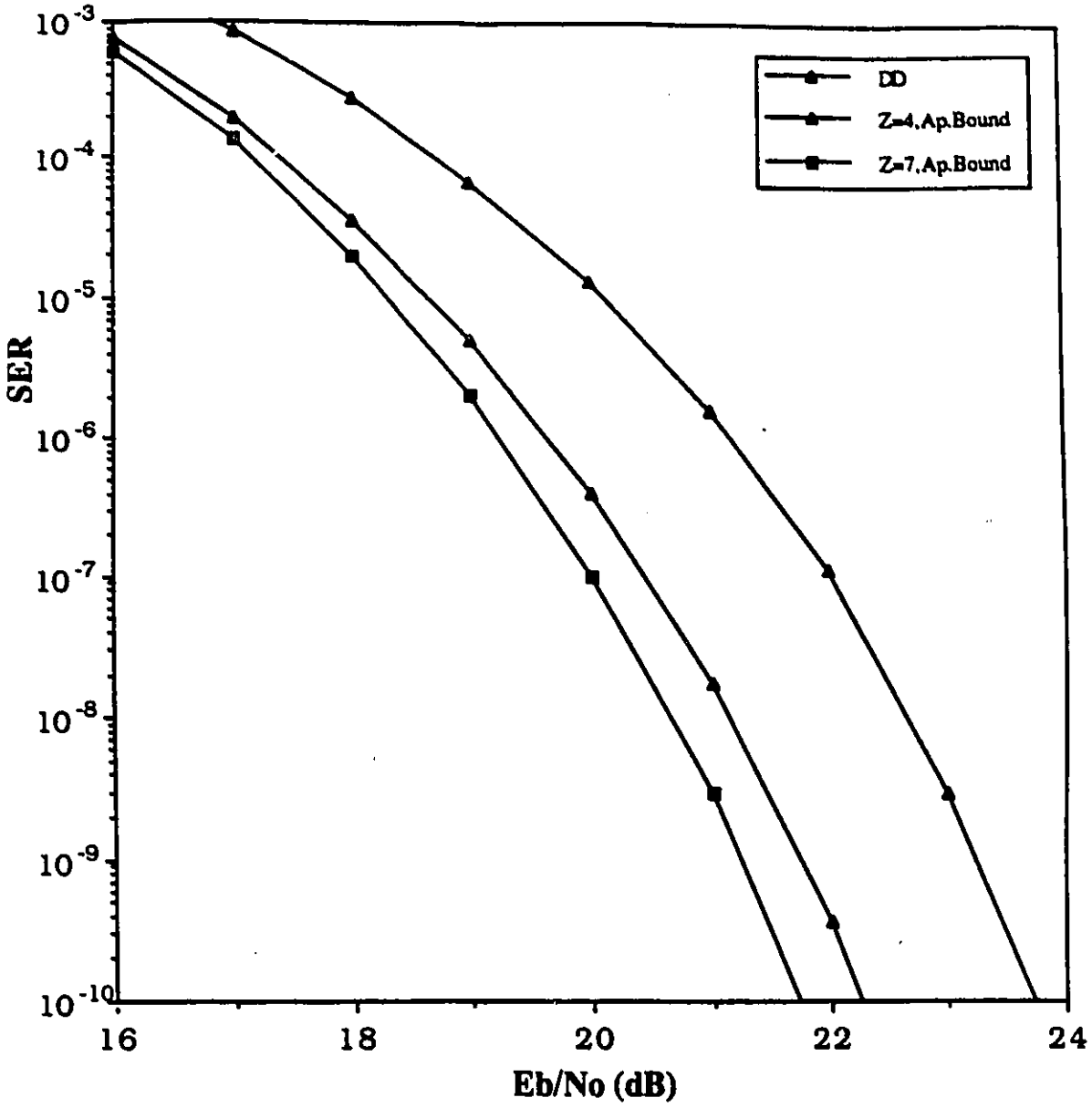

Figure 4.30: SER performance curves of 16PSK in ideal channel with equal Nyquist filter apportioning. The curves corresponding to the block decoder are based on the approximate bound.

4.5.6 Evaluation of PSK Signals with Unequally Nyquist Filter Apportioned Systems

A raised cosine Nyquist I filter is used at the transmitter, whereas at the receiver, an ideal brickwall post detection filter is employed. The noise power passing through the filter and the correlation properties of the noise corrupting the signal samples y_k (processed by the block decoder) depend on the excess bandwidth α_{eb} and can be calculated from Eq.(4.17). The noise power and noise correlation properties are needed for the calculation of $B^Z_{[\nu,\zeta]}$ (see Appendix B). Below we provide results for an excess bandwidth $\alpha_{eb} = 0.5$.

4.5.6.1 Coded Signals

We have evaluated Code A. The results are presented in Figs.(4.31) (non-differentially encoded) and (4.32) (differentially encoded). The displayed curves correspond to block lengths $Z = 5, 7, 10, 12$. The presented curves are labelled as (Z= (NDE-UA)) (non-differentially encoded case) and (Z= (DE-UA)) (differentially encoded case). We also display the SER curves of the conventional differential receiver used with the same code (Con.Rec.(UA)) and the DBPSK (DBPSK(UA)).

In Tables 4.7, 4.8 we have summarized the relative performance of the block decoder versus Z as it compares to the conventional differential receiver and the uncoded DBPSK. Comparing Figs. 4.31, 4.32 with Figs, 4.11, 4.12 which correspond to the equal apportioning case, leads us to the conclusion that the configurations of the block decoder suffer a loss of 2 dB as compared to the equal apportioning case. Its relative performance with the conventional differential receiver remains in the same range. Compared to the uncoded DBPSK, the advantage of the block decoder has been reduced by 0.5 dB compared to the gains it achieved when the apportioning had been split equally between transmitter-receiver.

Table 4.7: Gains versus codeword length Z, offered by the Block Decoder. The comparison is with the conventional differential receiver. The reported gains correspond to SER=10^{-4}. The channel is assumed ideal and full apportioning has been put at the transmitter ($a_{eb} = 0.5$).

		GAINS (dB)	
		(NDE)	(DE)
Z	5	2	2.5
	7	2.6	2.8
	10	3	3.3
	12	3.3	3.3

Table 4.8: Gains versus codeword length Z, offered by the Block Decoder. The comparison is with DBPSK. The channel is assumed ideal and full apportioning has been put at the transmitter ($a_{eb} = 0.5$).

		GAINS (dB)	
		(NDE)	(DE)
Z	5	2.1	2.8
	7	2..9	3.3
	10	3.5	3.7
	12	3.7	3.7

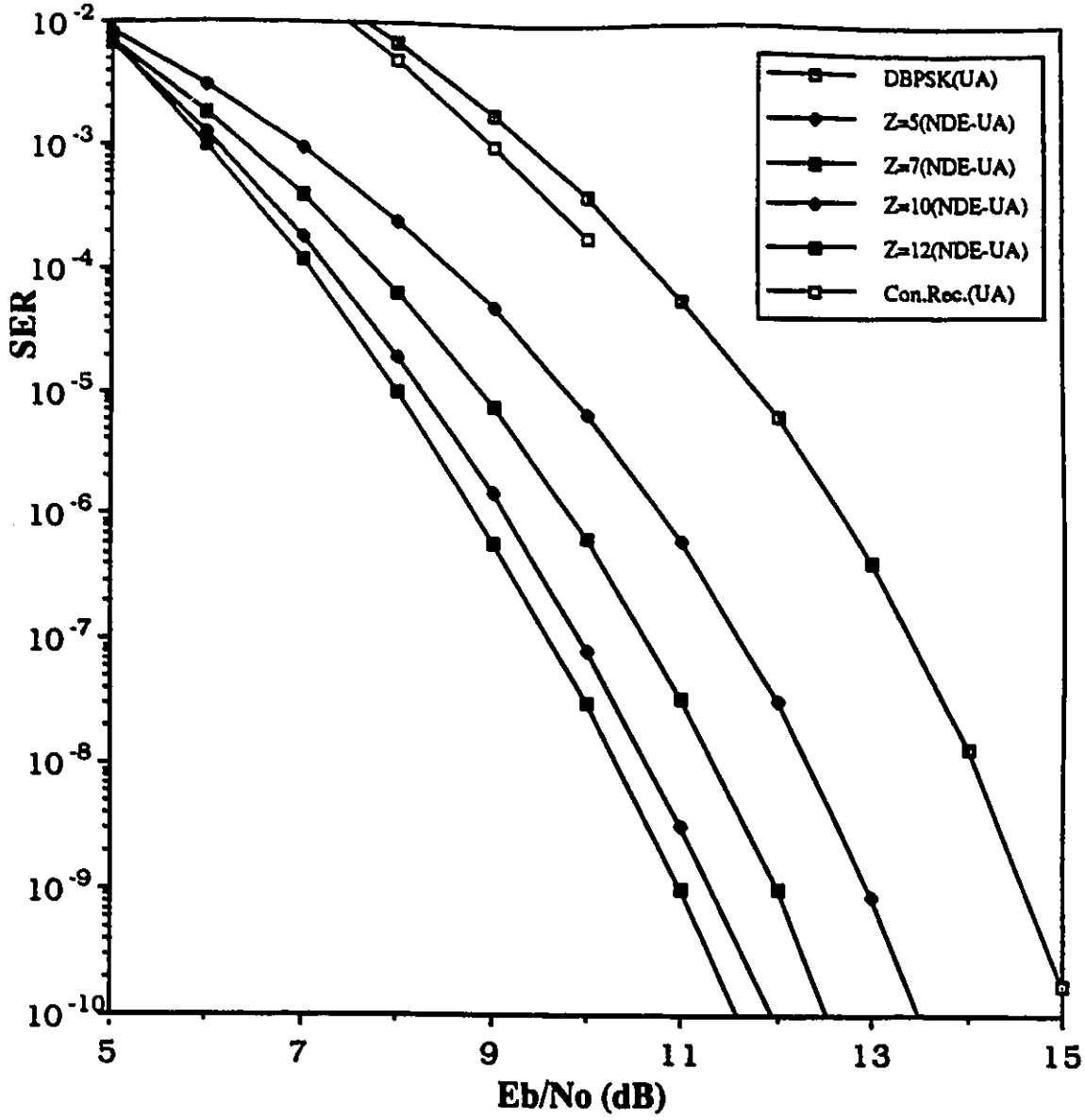

Figure 4.31: SER curves of code A (QPSK constellation) without differential encoding. The channel is assumed ideal and full apportioning has been put at the transmitter ($a_{eb} = 0.5$).

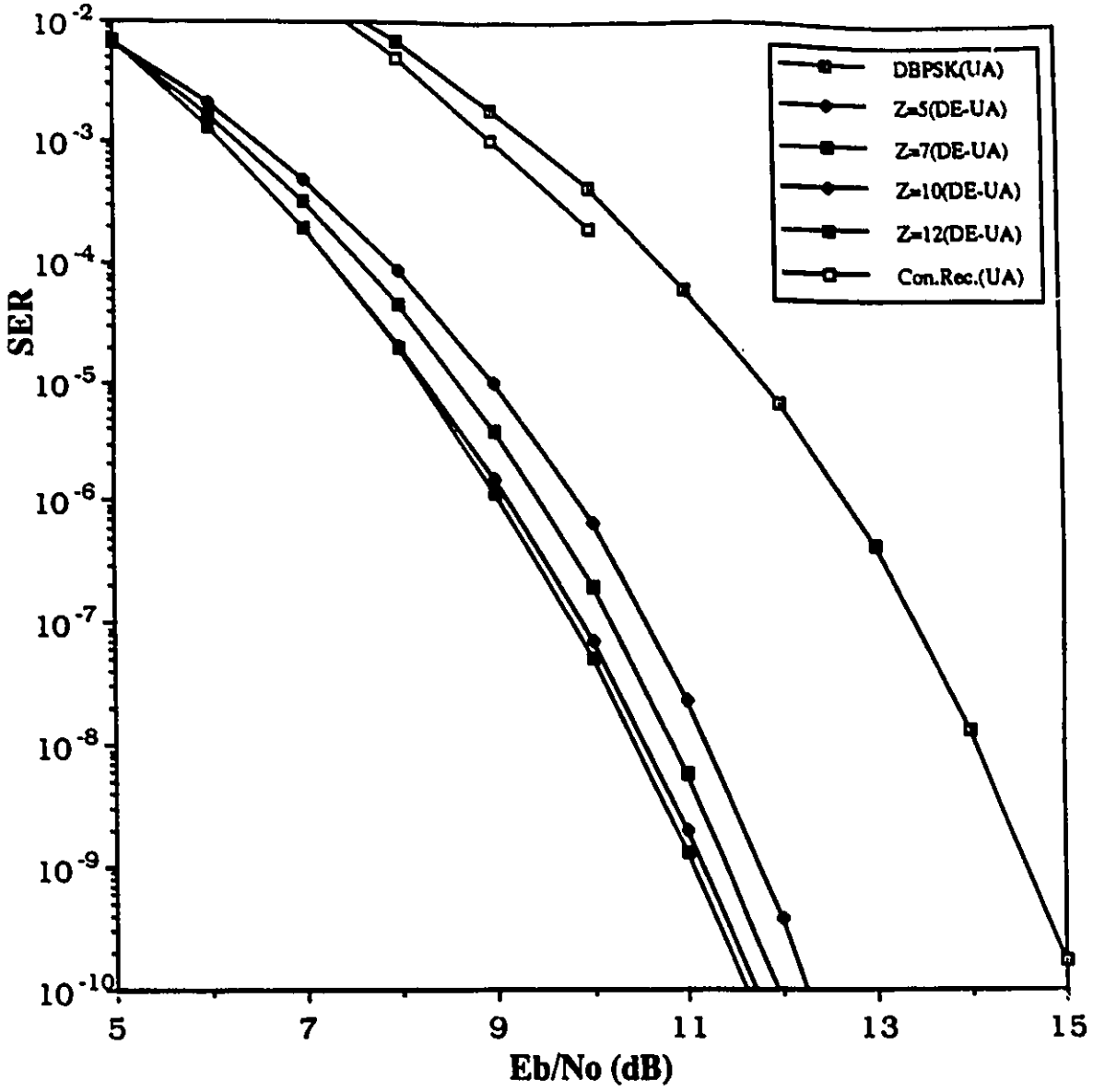

Figure 4.32: SER curves of code A (QPSK constellation) with differential encoding. The channel is assumed ideal and full apportioning has been put at the transmitter ($a_{eb} = 0.5$).

4.5.6.2 Uncoded Signals

The SER curves are presented in Figs. 4.33 (QPSK), 4.34(8PSK) and 4.35 (16PSK). In these figures, the curves of the conventional differential detector (DD) and the $Z = 4$ block decoder are displayed for both, equal and unequal apportioning. For the $Z = 4$ block decoder with non-equal apportioning, two curves are provided. One represents values calculated through the use of the exact bound, while the second is the outcome of the approximate bound. The displayed curves show that the approximate bound is capable of very accurately characterizing the performance of the system. These results confirm the ability of the approximate bound to accurately characterize the performance of the receivers even when the noise exhibits colored behaviour. Regarding the performance of the differential detector and $Z = 4$ block decoder as compared to the equal apportioning case, it seems that both of them suffer approximately the same degradation (as result of using non-equal apportioning) which is close to 2 dB. The relative distance in performance between the two receivers (DD and $Z = 4$ BD) remains practically the same as with equal apportioning which is a 1.6 dB superiority of the $Z = 4$ BD as compared to DD.

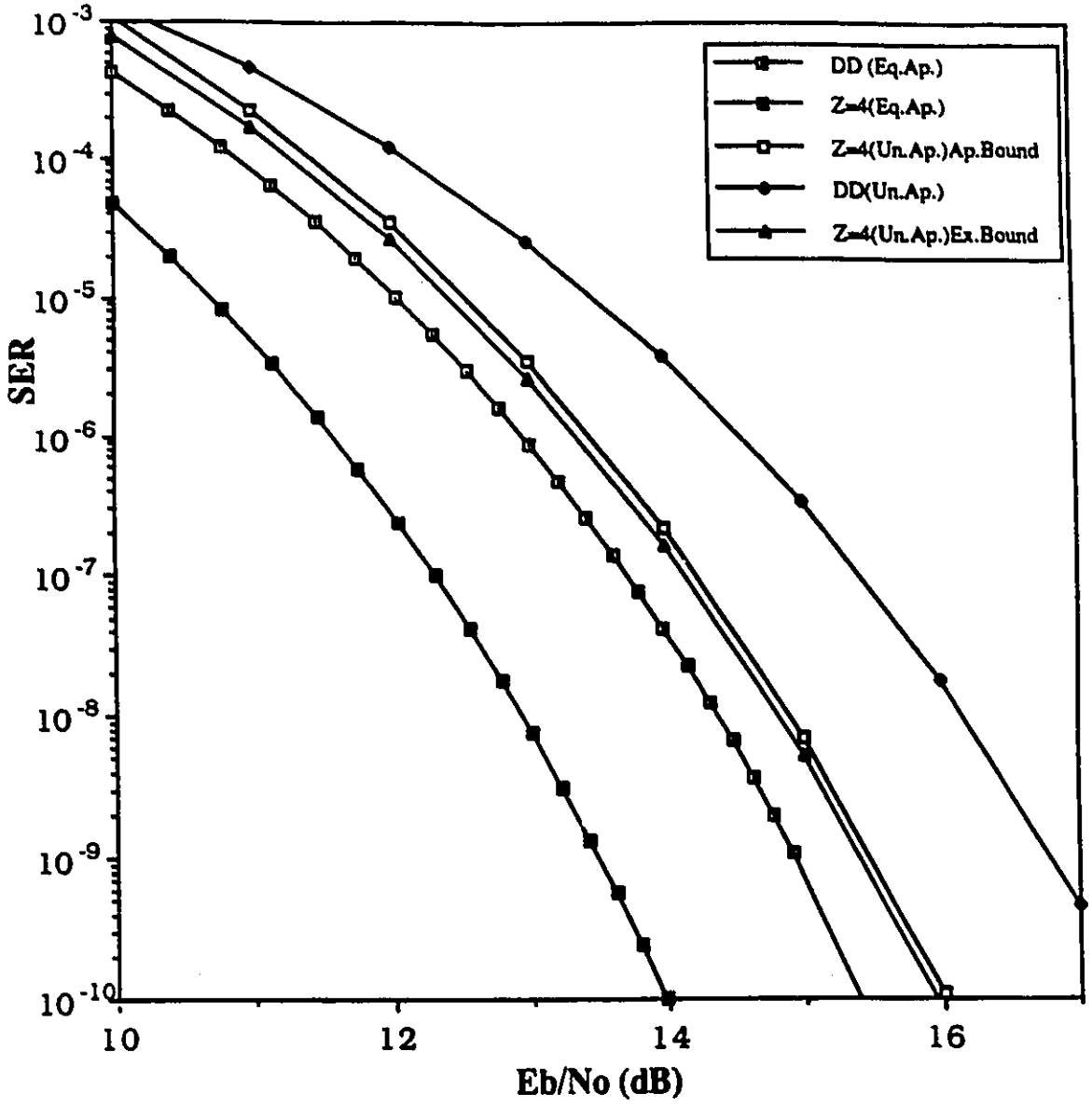

Figure 4.33: SER performance curves of QPSK with full apportioning at the transmitter. The excess bandwidth $a_{eb} = 0.5$.

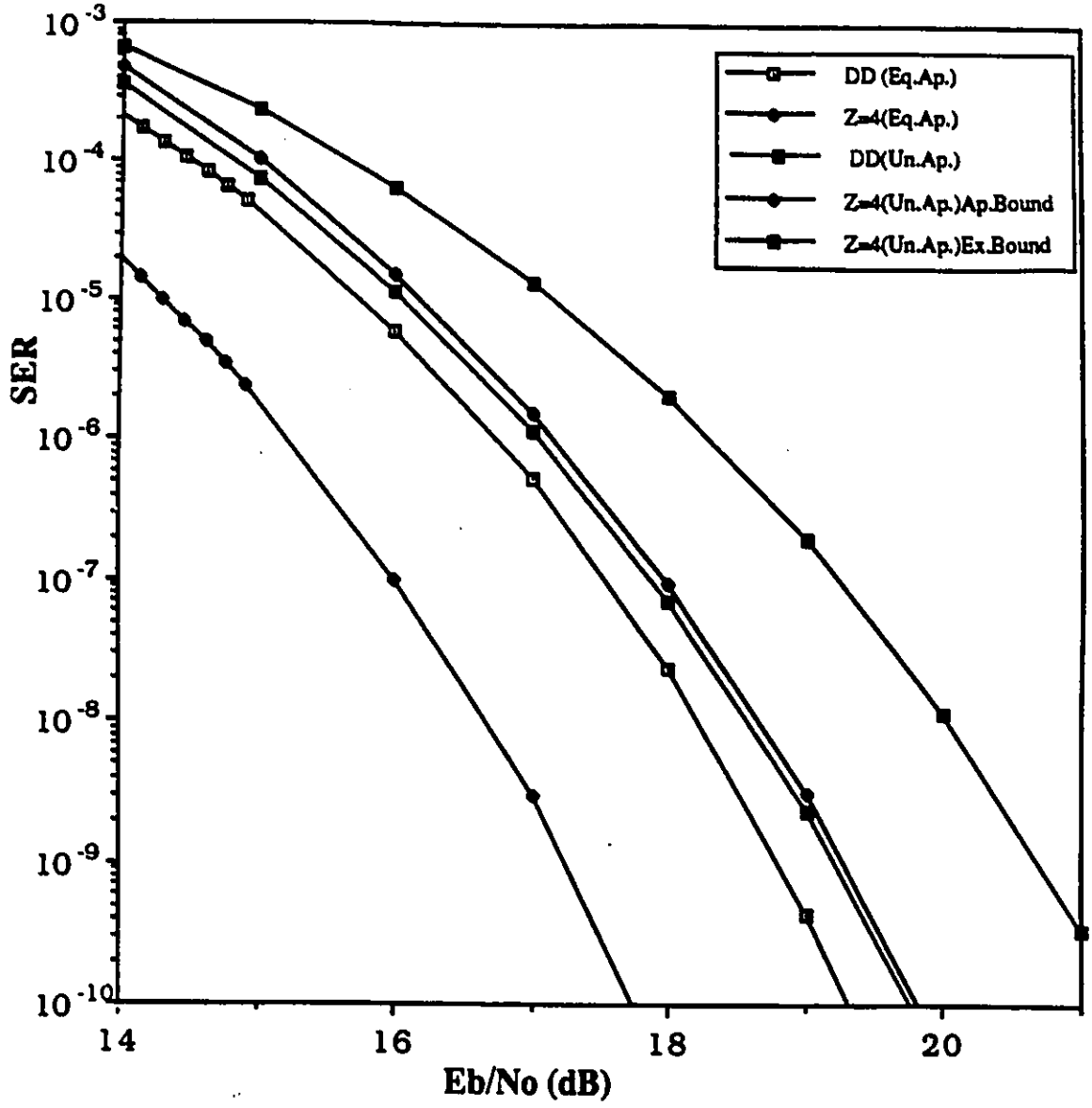

Figure 4.34: SER performance curves of 8PSK with full apportioning at the transmitter. The excess bandwidth $a_{eb} = 0.5$.

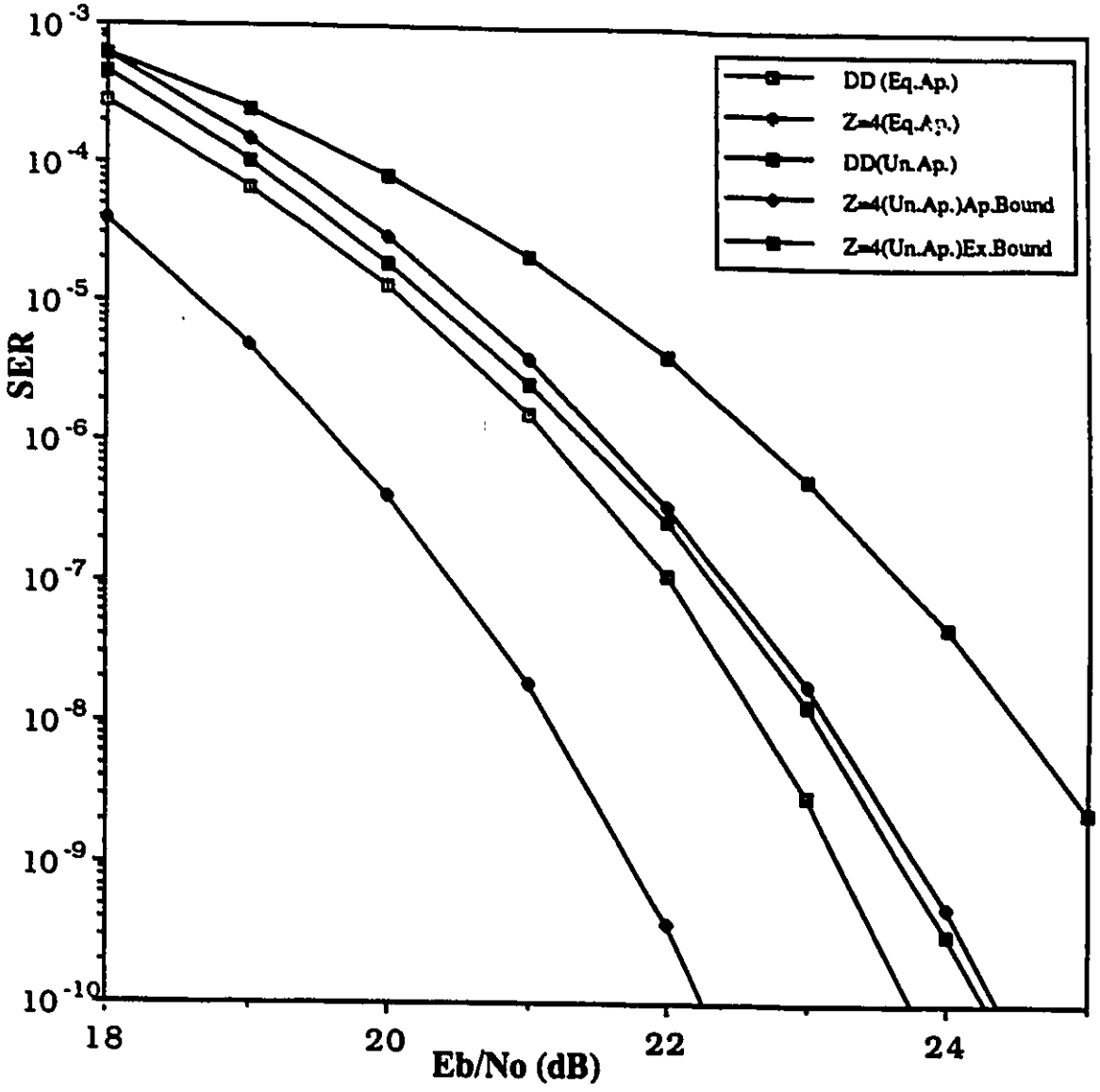

Figure 4.35: SER performance curves of 16PSK with full apportioning at the transmitter. The excess bandwidth $a_{eb} = 0.5$.

4.5.7 Block Decoding of PSK Signals in a Time Dispersive Channel

We consider a two-ray multipath channel. The receiver is reached from the main signal component and a delayed (due to a reflection) version of itself. The received signal can be expressed as:

$$\begin{aligned} x_r(t) &= x_{tr}(t) + \rho_e x_{tr}(t - t_D) + n_w(t) \\ &= [x_B(\bar{C}(\bar{A}), t) + \rho_e e^{-j\omega_c t_D} x_B(\bar{C}(\bar{A}), t - t_D)] e^{j\omega_c t} + n_w(t). \end{aligned} \tag{4.55}$$

t_D is the delay spread and ρ_e regulates the strength of the delayed signal (a positive real number). This is quite a common case in wireless communication channels (i.e. cellular mobile radio, indoor wireless communications etc.) and becomes a source of significant performance degradations. In our analysis, we consider $\rho_e = 0.5$ and $t_D = T$. We also assume that $mod_{2\pi}(\omega_c T) = \pm\pi (\rightarrow e^{-j\omega_c T} = -1)$[10]. The premodulation filter $H_T(\omega)$ is a square root raised cosine with excess bandwidth $\alpha_{eb} = 0.3$.

4.5.7.1 Uncoded Signals

The uncoded QPSK, 8PSK and 16PSK are evaluated. In Figs. 4.36, 4.37, 4.38, the curves for the following configurations are displayed: i) the exact bounds of the $Z = 7$ and $Z = 4$ block decoders (Z= (IC.Eq.Ap.Ex.Bo.) and the conventional differential detector
(DD(IC.Eq.Ap.)) under equal apportioning and ideal channel conditions; ii) the approximate bounds of the $Z = 18, 7, 4$ decoders (Z= (Equal.Ap.Bo.)), iii) the exact bound of the $Z = 4$ decoder (Z=4(Equal.Ex.Bo.)) and iv) the

[10]This section intends to provide the means for the analytical evaluation and access the potential of the proposed receivers in a time dispersive environment. In order to avoid unnecessary complexity, we use a relatively simple example of a time dispersive channel. The material described in the rest of this section can be used to evaluate these receivers with more accurate models of time dispersive wireless personal communication channels, such as the channels we meet in cellular radio and indoor wireless communication environments.

differential detector (DD(Equal.)). The configurations listed under {ii), iii) iv)} are used with zero forcing equalization. For the QPSK, the curves of the $Z = 4$ block decoder (Z=4(Non-Equal.)) and the differential detector (DD(Non-Equal.)) corresponding to a receiver without equalization (i.e. the post detection filter is a square root raised cosine filter) are presented as well. For 8PSK and 16PSK, these last curves are not displayed. The eye diagram at the output of the post detection filter $H_R(\omega)$ is closed and the performance is very poor (outside the range of SER values displayed in the figures).

In Table 4.9 the improvements offered by the block decoder as compared to the differential detector are summarized.

Table 4.9: Gains offered by the Block Decoder versus the sequence length Z. The comparison is with the conventional differential detector.

		GAINS (dB)		
		QPSK	8PSK	16PSK
Z	4	1.6	1.6	1.6
	7	2.4	2.7	2.7
	18	2.7	3.4	3.4

The first conclusion drawn, by comparing the exact and approximate bounds for the $Z = 4$ block decoder, is that the approximate bound is perfectly capable of very accurately estimating the performance of the proposed sequence estimators. The curves of the two bounds are very close and for high E_b/N_o they practically overlap. Also, the approximate bound upper bounds the exact bound.

Comparing the curves corresponding to the ideal and distorted channel (with the use of equalizer at the receiver), we conclude that the degradations suffered by the three MPSK schemes due to the time dispersive nature of the channel are almost the same. The conventional differential detector loses 3.4 dB. This is the case for the $Z = 4$ block decoder as well. However, for higher values of Z, the degradation becomes smaller. For $Z = 7$, the degradation due to the distorted nature of the channel, becomes 2.8 dB and for $Z = 18$ 2.2 dB. The $Z = 18$ decoder reaches the performance of the coherent receiver which uses the same channel equalization strategy and has perfect knowledge

of the carrier phase. The $Z = 18$ receiver achieves an improvement of 2.7 dB for QPSK and 3.4 dB for 8PSK, 16PSK, compared to the conventional differential detector. For $Z = 7$, the improvements are 2.4 dB (QPSK) and 2.7 dB (8PSK, 16PSK). A reminder, under ideal conditions, the improvement offered by the $Z = 7$ decoder (compared to the conventional differential detector) was 2 dB. Also, in the ideal channel, the distance between $Z = 7$ and $Z = 4$ decoders was only 0.4 dB. Now it becomes 1 dB (QPSK) and 1.4 dB (8PSK, 16PSK). We realize that use of block decoders, processing larger blocks of symbols, provides higher improvements when the channel experiences time dispersion.

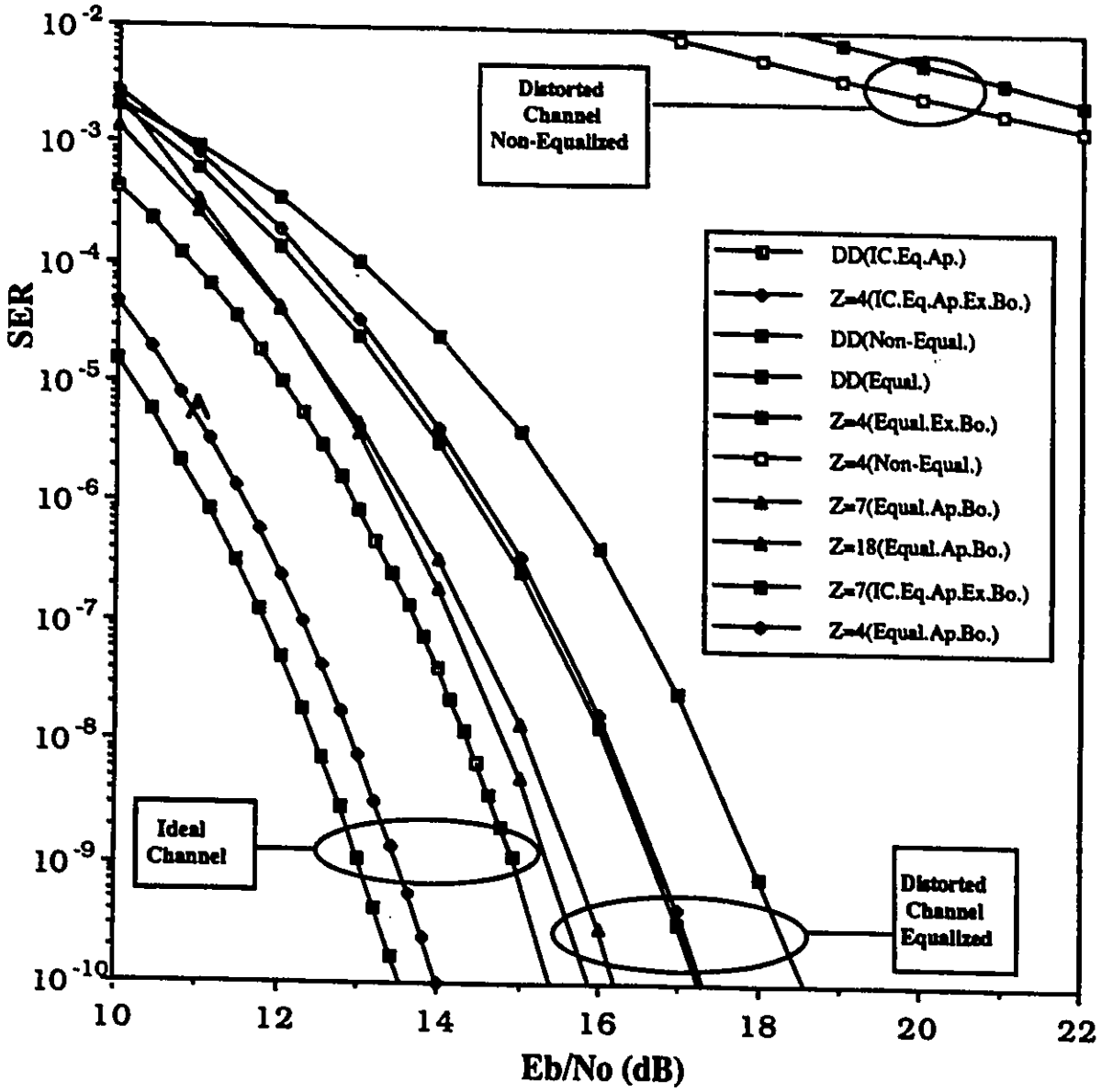

Figure 4.36: SER performance curves of non-coherently detected QPSK in the time dispersive channel. The results correspond to the block decoder and the one-symbol differential detector. When equalized, the receiver uses a zero forcing equalizer to suppress the ISI. For reference, curves corresponding to the ideal channel are displayed as well.

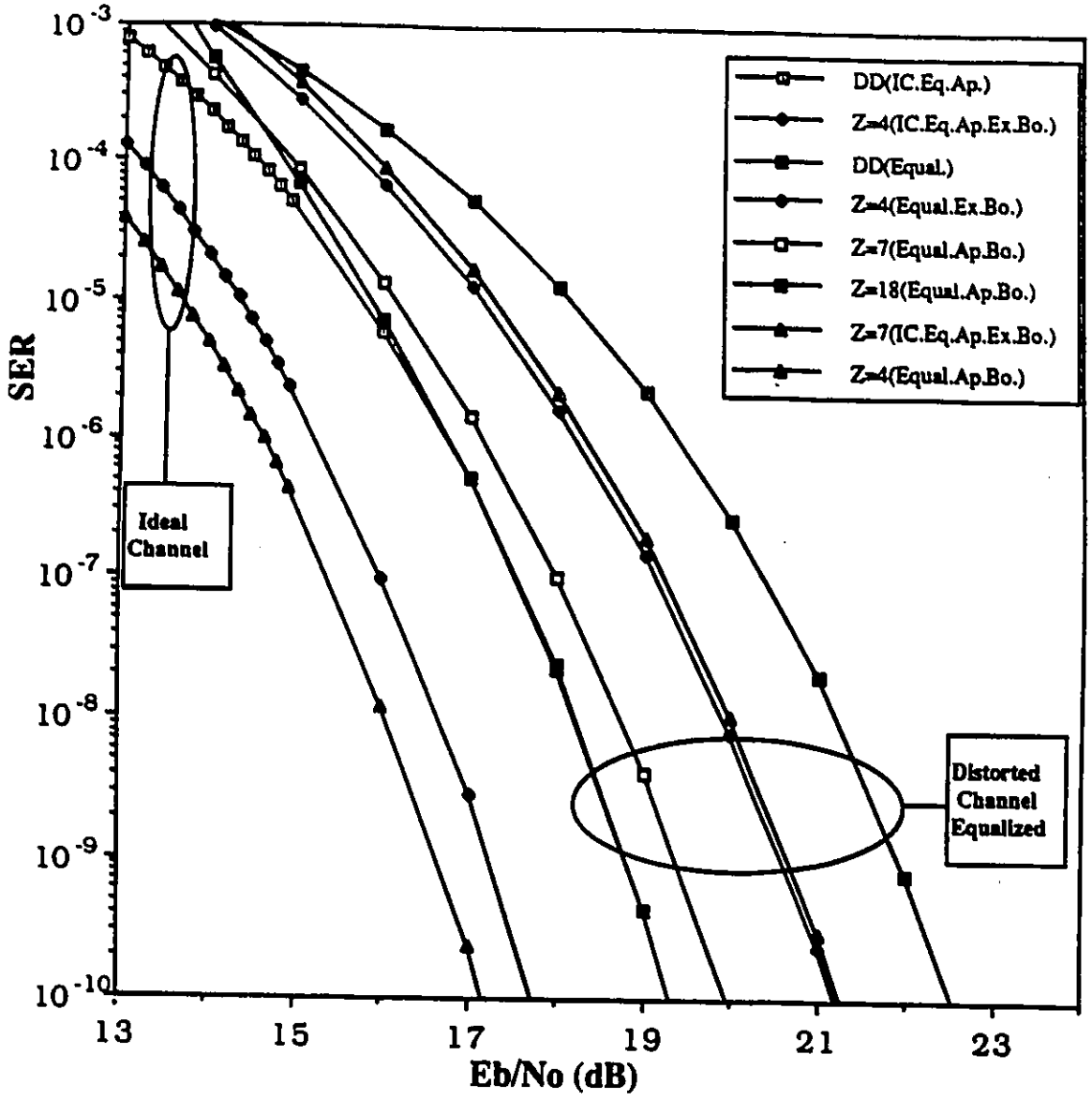

Figure 4.37: SER performance curves of non-coherently detected 8PSK in the time dispersive channel. The results correspond to the block decoder and the one-symbol differential detector. When equalized, the receiver uses a zero forcing equalizer to suppress the ISI. For reference, curves corresponding to the ideal channel are displayed as well.

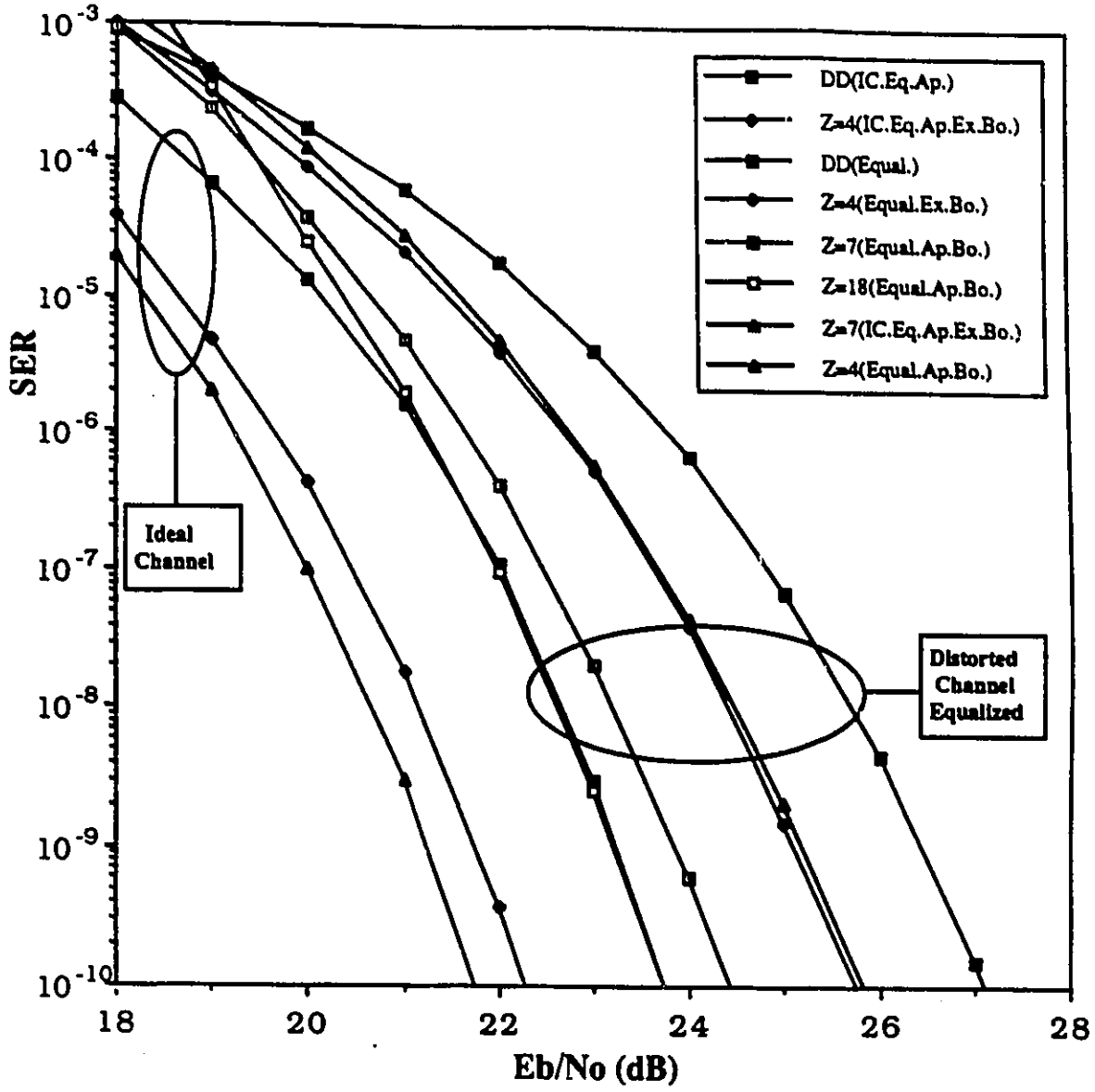

Figure 4.38: SER performance curves of non-coherently detected 16PSK in the time dispersive channel. The results correspond to the block decoder and the one-symbol differential detector. When equalized, the receiver uses a zero forcing equalizer to suppress the ISI. For reference, curves corresponding to the ideal channel are displayed as well.

4.5.7.2 Coded Signals

Code A has been evaluated for operation in the dispersive channel. At the receiver, a zero forcing equalizer is used to compensate the ISI. The results are presented in Figs. 4.44 (no differential encoding), 4.45 (differential encoding). The displayed curves correspond to the block decoder with $Z = 5, 7, 10, 12$ (Z= (NDE or DE)EQ.) the conventional differential receiver (Con.Rec.(EQ.)) and the uncoded DBPSK (DBPSK(EQ.)). In Table 4.10 we list the improvements offered by the block decoder when compared to the conventional differential receiver. In Table 4.11 the block decoder is compared to the uncoded DBPSK. The block decoder is capable of offering improvements as high as 3.2 dB and 2.7 dB as compared to the conventional differential receiver and uncoded DBPSK respectively. Comparing these gains with the improvements the block decoder achieved in ideal channel (see tables 4.1 to 4.4), we find that they remain at the same levels in respect to the conventional differential receiver (differential detector and Viterbi decoder); however, the improvement regarding DBPSK has dropped 1.2 dB. Also, the distance in the performance (of the block decoder) between the differentially and non-differentially encoded cases for $Z = 5$ has been reduced from 0.7 dB to 0.2 dB.

Table 4.10: Gains offered by the Block Decoder versus the codeword length Z. Code A is used. At the receiver, a zero forcing equalizer is used to eliminate the ISI. The comparison is with the conventional differential receiver (the comparison corresponds to SER=10^{-4}).

		GAINS (dB)	
		NDE	DE
Z	5	2.2	2.5
	7	2.8	3
	10	3.2	3.2
	12	3.2	3.2

Table 4.11: Gains offered by the block decoder versus the codeword length Z. Code A is used. At the receiver, a zero forcing equalizer is used to eliminate the ISI. The comparison is with the uncoded DBPSK.

		GAINS (dB)	
		NDE	DE
Z	5	1.8	2
	7	2.2	2.5
	10	2.8	2.8
	12	2.9	2.9

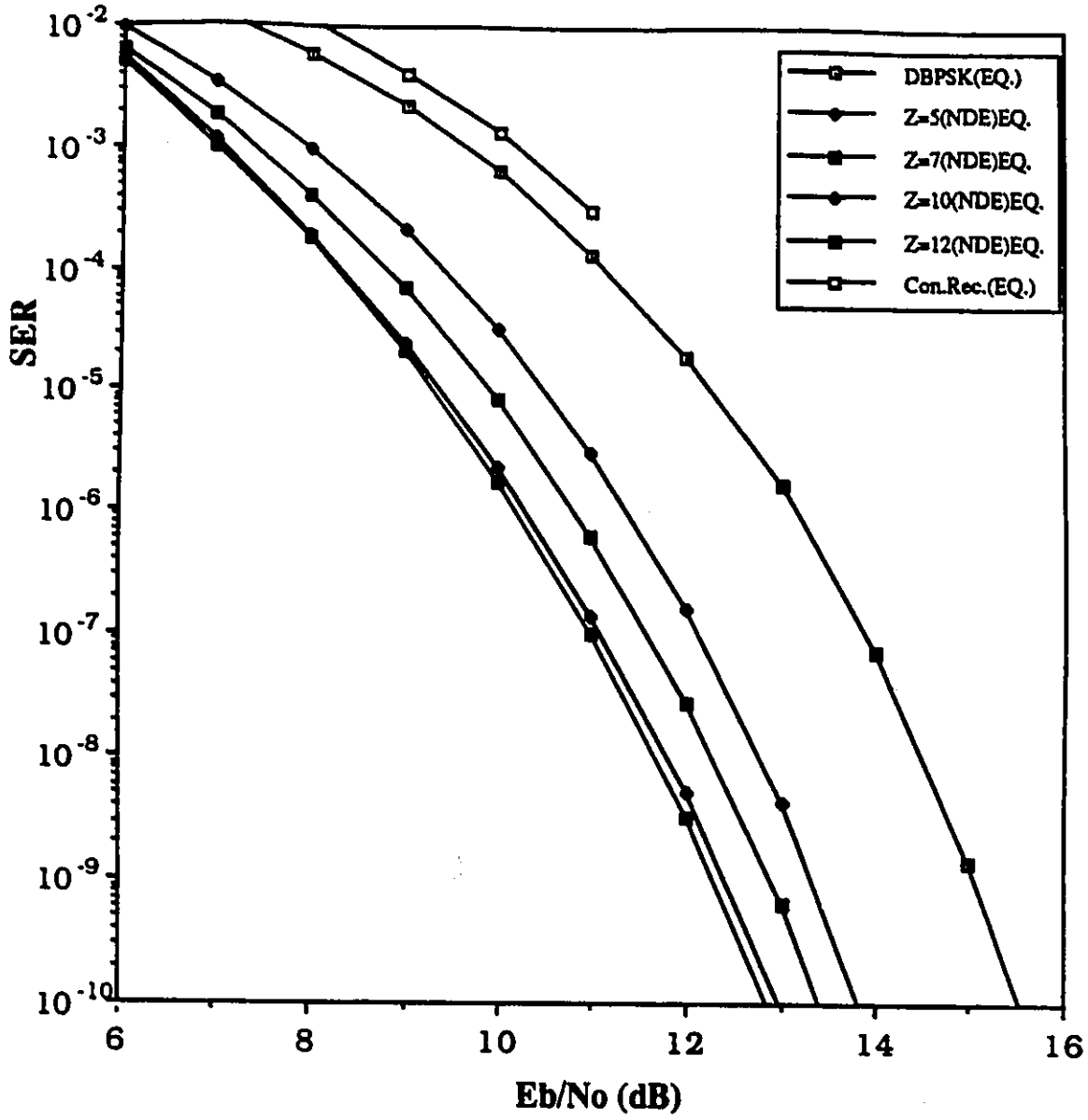

Figure 4.39: SER performance curves of code A (non differentially encoded) in the time dispersive channel. The results correspond to various non-coherent receiver configurations. A zero forcing equalizer is used to suppress the ISI.

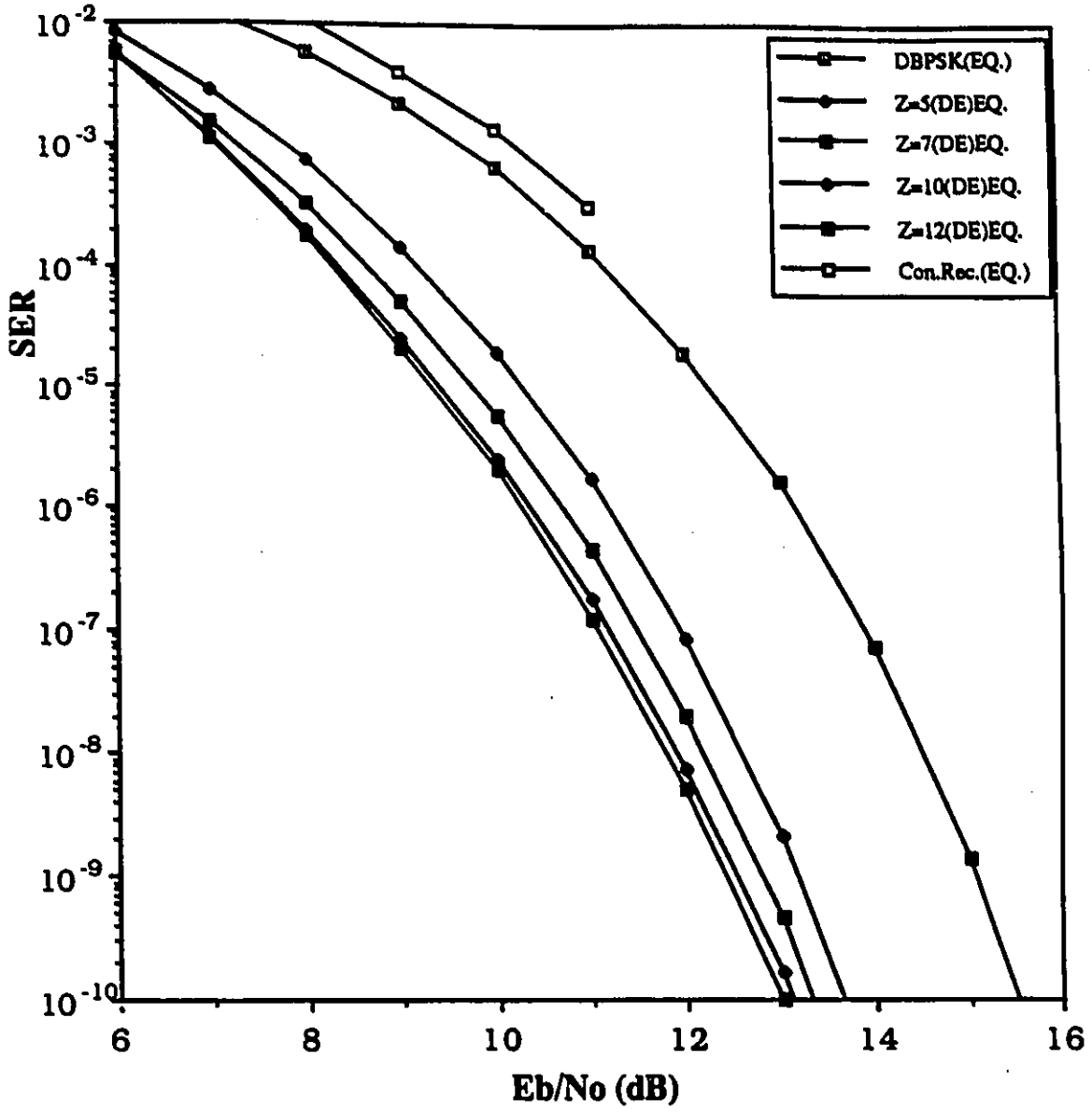

Figure 4.40: SER performance curves of code A (differentially encoded) in the time dispersive channel. The results correspond to various non-coherent receiver configurations. A zero forcing equalizer is used to suppress the ISI.

4.6 PERFORMANCE ANALYSIS OF THE NON-COHERENT ASYMPTOTICALLY OPTIMAL DECODER WITH MPSK SIGNALS

The union bound will be used to upper bound the performance of the asymptotically optimal block decoder. However, the bound of the pair wise error event probability for the asymptotically optimal decoder is different. In the following paragraphs, a brief description of this bound will be provided. Its detailed description and derivation is given in Appendix F.

4.6.1 Upper Bound of the Pairwise Error Probability for the Non-Coherent Asymptotically Optimal Decoder

The upper bound $B^Z_{HAO[\nu,\zeta]}$ of the error probability corresponding to the error event $\{\bar{C}(\bar{A}^\zeta) \leftarrow \bar{C}(\bar{A}^\nu)\}$ (when the asymptotically optimal decoder is used) is given by the following expression:

$$B^Z_{HAO[\nu,\zeta]} = \begin{cases} B^Z_{PW[\nu,\zeta]} & \text{for } \mathcal{D}^{\zeta,\nu}_Z(\bar{h}) \geq 0 \\ B^Z_{PW[\nu,\zeta]} + Q(\frac{\overline{E\mathcal{D}}^{\nu,\star}_{\nu,\zeta}(h_0,\bar{h})}{\sigma_{\nu,\nu}}) & \text{for } \mathcal{D}^{\zeta,\nu}_Z(\bar{h}) < 0 \end{cases} \tag{4.56}$$

with

$$Q(x) = \frac{1}{\sqrt{2\pi}} \int_x^\infty \exp\{-\frac{u^2}{2}\} du, \tag{4.57}$$

$$\mathcal{D}^{\zeta,\nu}_Z(\bar{h}) \quad = \quad IST(\bar{h}, \bar{C}(\bar{A}^\zeta)) - IST(\bar{h}, \bar{C}(\bar{A}^\nu)). \tag{4.58}$$

Also,

$$\overline{E\mathcal{D}}^{\nu,\star}_{\nu,\zeta}(h_0, \bar{h}) = Zh_0 + \sum_{l=1}^{Z-1} \sum_{k=l}^{Z-1} [Re\{h_l c^\zeta_k (c^\zeta_{k-l})^*\} + Re\{h_l c^\nu_k (c^\nu_{k-l})^*\}] \tag{4.59}$$

and

$$B^{Z}_{PW[\nu,\zeta]} = \frac{1}{2}[\Lambda_{PW}(\bar{C}(\bar{A}^{\nu}), \bar{C}(\bar{A}^{\zeta}))] \exp\{-\frac{1}{\sigma_n^2}\frac{(\alpha_{PW[\nu,\zeta]} - \beta_{PW[\nu,\zeta]})^2}{2}\} \quad (4.60)$$

with

$$\Lambda_{PW}(\bar{C}(\bar{A}^{\nu}), \bar{C}(\bar{A}^{\zeta})) = \begin{cases} 1 & \text{for } \alpha_{PW[\nu,\zeta]} = 0 \\ [1 - \frac{v_{\nu\nu} - v_{\nu\zeta}}{[(v_{\nu\nu}+v_{\nu\zeta})^2 - 4|v^c_{\nu\zeta}|^2]^{\frac{1}{2}}}] & \\ \frac{1}{\sqrt{2\pi\frac{1}{\sigma_n^2}\alpha_{PW[\nu,\zeta]}\beta_{PW[\nu,\zeta]}}} & \text{for } \alpha_{PW[\nu,\zeta]} \neq 0 \end{cases} \quad (4.61)$$

and

$$\begin{Bmatrix} \alpha_{PW[\nu,\zeta]} \\ \beta_{PW[\nu,\zeta]} \end{Bmatrix} = [\frac{1}{v_{\nu\nu} + v_{\nu\zeta}}(\frac{|\overline{E\mathcal{D}}^{\nu,*}_{\nu,\zeta}(h_0, \bar{h})|^2 + |\bar{E}^{\nu,*}_{\zeta}|^2 - 2Re\{(\overline{E\mathcal{D}}^{\nu,*}_{\nu,\zeta}(h_0, \bar{h}))^* \bar{E}^{\nu,*}_{\zeta}\gamma_{\nu\zeta}\}}{1 - |\gamma_{\nu\zeta}|^2}$$
$$\mp \frac{|\overline{E\mathcal{D}}^{\nu,*}_{\nu,\zeta}(h_0, \bar{h})|^2 - |\bar{E}^{\nu}_{\zeta}|^2}{\sqrt{1 - |\gamma_{\nu\zeta}|^2}})]^{\frac{1}{2}}. \quad (4.62)$$

(4.63)

$$\bar{E}^{\nu,*}_{\zeta} = h_0 \sum_{k=0}^{Z-1} c^{\nu}_{k}(c^{\zeta}_{k})^* + 2\sum_{l=1}^{Z-1}\sum_{k=l}^{Z-1} h_l[c^{\nu}_{k}(c^{\zeta}_{k-l})^* + (c^{\zeta}_{k})^* c^{\nu}_{k-l}] \quad (4.64)$$

(see Eqs.(F.6), (F.12), (F.17) to (F.19) in Appendix F).

For the definitions of $v_{\nu\nu}$, $v_{\nu\zeta}$, $v^c_{\nu\zeta}$, $\gamma^c_{\nu\zeta}$, see Eqs.(B.8), (B.9) and (B.12) in Appendix B.

4.6.2 Upper Performance Bound of Symbol Error Probability.

Following again the concept of the Union Bound, we have:

$$P_e^{HAO} \leq \frac{1}{(Z-L_c-1)}\frac{1}{2^{(Z-L_c-1)p}} \sum_{\bar{C}(\bar{A}^\nu)\in S_{CW}^Z} \sum_{\bar{C}(\bar{A}^\varsigma)\in S_{\bar{C}(\bar{A}^\nu)}} n_e(\{\bar{C}(\bar{A}^\varsigma)\leftarrow\bar{C}(\bar{A}^\nu)\})P_{HAO}(\{\bar{C}(\bar{A}^\varsigma)\leftarrow\bar{C}(\bar{A}^\nu)\})$$
$$\leq \mathcal{U}_{HAO}\mathcal{B}^Z \tag{4.65}$$

where $P_{HAO}(\{\bar{C}(\bar{A}^\varsigma)\leftarrow\bar{C}(\bar{A}^\nu)\})$ is the pairwise probability of the error event $\{\bar{C}(\bar{A}^\varsigma)\leftarrow\bar{C}(\bar{A}^\nu)\}$ and P_e^{HAO} is the overall symbol error probability when the asymptotically optimal decoder (based on $\aleph_{HAO}^{PSK}(\bar{h},\bar{y},\bar{C}(\bar{A}))$) is used. Also,

$$\mathcal{U}_{HAO}\mathcal{B}^Z = \frac{1}{2^{(Z-L_c-1)p}} \sum_{\{\bar{C}(\bar{A}^\nu)\in S_{CW}^Z\}} P_{HAO}B^{Z,\nu}, \tag{4.66}$$

with

$$P_{HAO}B^{Z,\nu} = \frac{1}{Z-L_c-1} \sum_{\{\bar{C}(\bar{A}^\varsigma)\in S_{\bar{C}(\bar{A}^\nu)}\}} n_e(\{\bar{C}(\bar{A}^\varsigma)\leftarrow\bar{C}(\bar{A}^\nu)\})B_{HAO[\nu,\varsigma]}^Z. \tag{4.67}$$

We remind the reader that S_{CW}^Z represents the set which includes all the possible sequences of length Z (a total of $2^{(Z-L_c-1)p}$) and $S_{\bar{C}(\bar{A}^\nu)}$ is the set which has as members all the elements of S_{CW}^Z except $\bar{C}(\bar{A}^\nu)$. Also, $n_e(\{\bar{C}(\bar{A}^\varsigma)\leftarrow\bar{C}(\bar{A}^\nu)\})$ is the number of symbols in error, associated with the error event $\{\bar{C}(\bar{A}^\varsigma)\leftarrow\bar{C}(\bar{A}^\nu)\}$.

For the uncoded systems, the evaluation can be performed by using the approximate bound described in Section 4.2.5 (detailed description of this approach can be found in Appendix D).

The approximate bound $\mathcal{U}_{AO}\mathcal{B}_{app.}^Z$ is calculated as follows:

$$\mathcal{U}_{HAO}\mathcal{B}_{app.}^Z = \frac{1}{2^{(Z-1)p}} \sum_{\{\bar{C}(\bar{A}^\nu)\ \in\ S_{CW}^Z\}} P_{HAO}B_{app.}^{Z,\nu} \tag{4.68}$$

with

$$P_{HAO}B_{app.}^{Z,\nu} = \frac{1}{Z-1}\Big(\sum_{m=1}^{\lceil\frac{Z-1}{2}\rceil} 2m\Big[\sum_{\{\bar{C}(\bar{A}^\zeta)\ \in\ \underline{G^2_{min}R^{Z,\nu}_m}\}} B^Z_{HAO[\nu,\zeta]}\Big] + (2m-1)\Big[\sum_{\{\bar{C}(\bar{A}^\zeta)\ \in\ \underline{G^1_{min}R^{Z,\nu}_m}\}} B^Z_{HAO[\nu,\zeta]}\Big]\Big) + (Z-1)\Big(\sum_{m=\lceil\frac{Z-1}{2}\rceil+1}^{Z-1}\Big[\sum_{\{\bar{C}(\bar{A}^\zeta)\ \in\ \underline{G^\cup_{min}R^{Z,\nu}_m}\}} B^Z_{HAO[\nu,\zeta]}\Big]\Big) \quad (4.69)$$

(for the definitions of $\underline{G^\cup_{min}R^{Z,\nu}_m}$, $\underline{G^1_{min}R^{Z,\nu}_m}$, $\underline{G^2_{min}R^{Z,\nu}_m}$ see Appendix D). $\lceil\cdot\rceil$ represents the largest integer, smaller or equal to $\{\cdot\}$. As it was mentioned in subsection 4.5.2, the approximate bound requires only $\frac{Z-1}{M_p^{Z-1}-1}$ of the processing needed by the exact bound. For large Z and M, this is quite a difference in computational complexity.

4.6.3 Performance Evaluation Results

We use the channel model described in Eq.(4.55). $\rho_e = 0.5$, $t_D = T$, $mod_{2\pi}(\omega_c T) = \pm\pi$ and the premodulation filter is a square root raised cosine with excess bandwidth $\alpha_{eb} = 0.3$.

4.6.3.1 Uncoded Signals

In Figs. 4.41, 4.42, 4.43, the following SER curves are displayed: i) the exact bound of the $Z = 7$ block decoder used with an equally apportioned system operating in ideal channel (Z=7(IC.Eq.Ap.Ex.Bo.)). Its performance is practically identical to the coherent system; ii) the Z=18 (approximate bound) block decoder operating in the time dispersive channel, used with a receiver applying zero forcing equalization (Z=18(Equal.Ap.Bo.)), iii) the $Z = 18$ (approximate bound), $Z = 7$ (approximate bound) and $Z = 4$ (approximate bound) asymptotically optimal decoder (Z= (AOD.Ap.Bo.)); iv) the $Z = 4$ (exact bound) asymptotically optimal decoder (Z=4(AOD.Ex.Bo.)); v) the conventional differential detector used with a zero forcing equalized receiver (DD(Equal.)).

In Table 4.12 we summarize the improvements offered by the asymptotically optimal decoder versus the sequence length Z. In Table 4.13 the asymptotically optimal decoder and the block decoder are compared. The comparison is done between receivers processing sequences of equal size (Z).

The curves drawn for the asymptotically optimal decoder with $Z = 4$ demonstrate the high accuracy of the approximate bound. Also, for $Z = 18$, the asymptotically optimal decoder practically reaches the performance levels of the coherent receiver (with perfect carrier phase reference) operating in ideal channel[11]. Comparison between the curves of the asymptotically optimal decoder and block decoder (used with equalization), demonstrates the superiority of the asymptotically optimal receiver which for $Z = 4$ outperforms the block decoder by 1.6 dB, for $Z = 7$ by 2 dB and for $Z = 18$, 2.2 dB. It is interesting to notice that the asymptotically optimal decoder with $Z = 4$ is more powerful than the block decoder with $Z = 18$ and at the same time requires less processing as compared to the $Z = 18$ block decoder (roughly 2^{14} times less). Compared to the performance of the conventional differential receiver, the asymptotically optimal decoder provides improvements of 5.2 dB for QPSK and higher than 5.5 dB for 8PSK, 16PSK. The improvements reported above become even higher when more severe distortion is present at the channel.

[11] A similar case is met in the case of Partial Response Signals [274] , where when Viterbi decoding is used, the receiver is capable of recovering almost all the losses due to ISI [114] and the performance becomes almost as good as that of the ideal Pulse Amplitude Modulation Signals (PAM) [214].

Table 4.12: Gains offered by the proposed Asymptotically Optimal Decoder versus the sequence length Z. The comparison is with the conventional differential detector.

		GAINS (dB)		
		QPSK	8PSK	16PSK
Z	4	3.1	3.1	3.1
	7	4.4	4.7	4.7
	18	4.9	5.5	5.5

Table 4.13: Gains offered by the Asymptotically Optimal Decoder as compared to the Block Decoder, used with equalization. The comparison is between decoders processing sequences of equal length (Z).

		GAINS (dB)		
		QPSK	8PSK	16PSK
Z	4	1.8	1.8	1.6
	7	2	2	2
	18	2.2	2.2	2.2

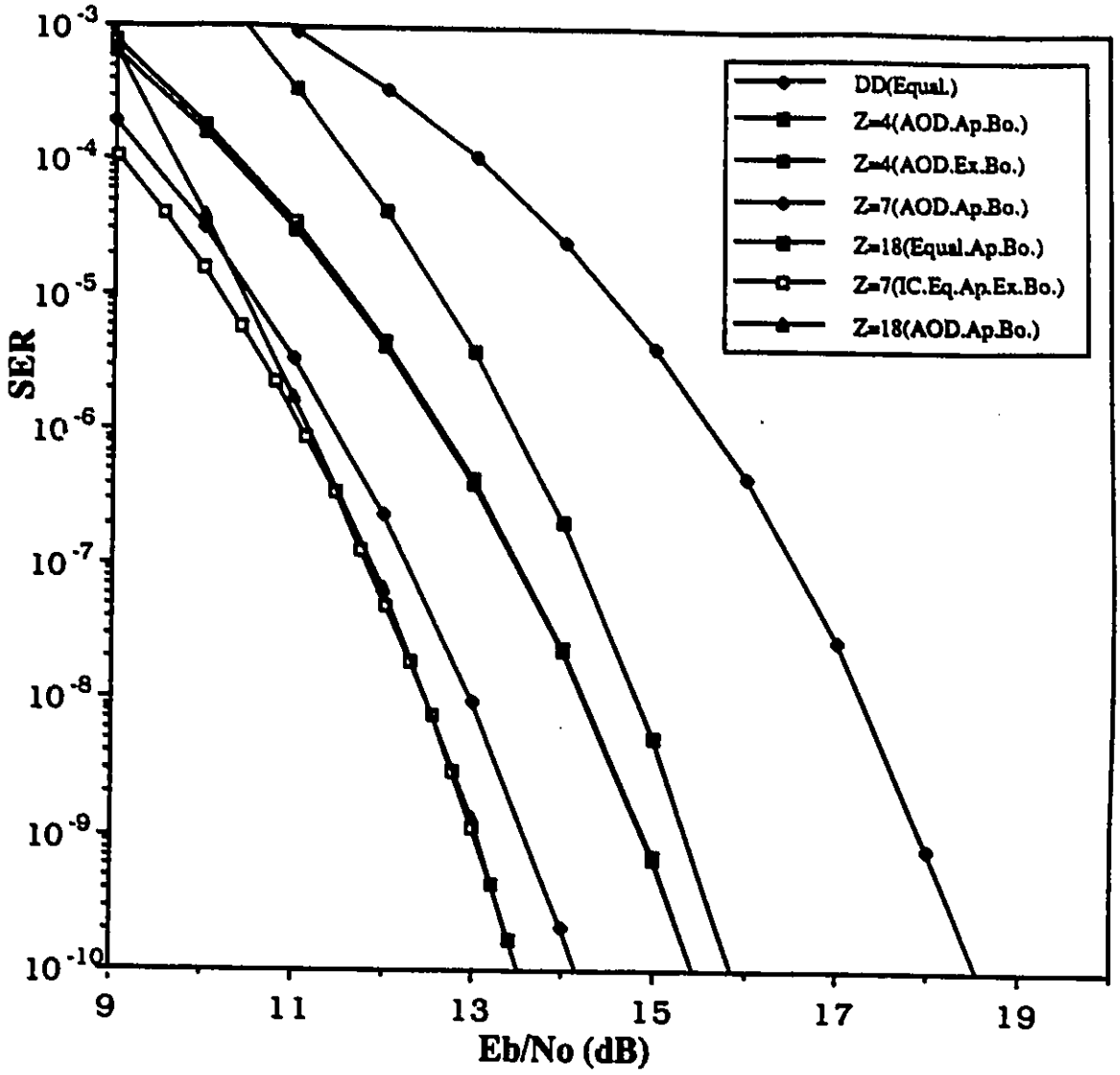

Figure 4.41: SER performance curves of non-coherently detected QPSK in the time dispersive channel. The evaluated structures use either the asymptotically optimal decoder, the block decoder or the conventional one-symbol delay differential detector. The last two are used with zero forcing equalization. For reference, curves corresponding to the ideal channel/equal filter apportioning are also included.

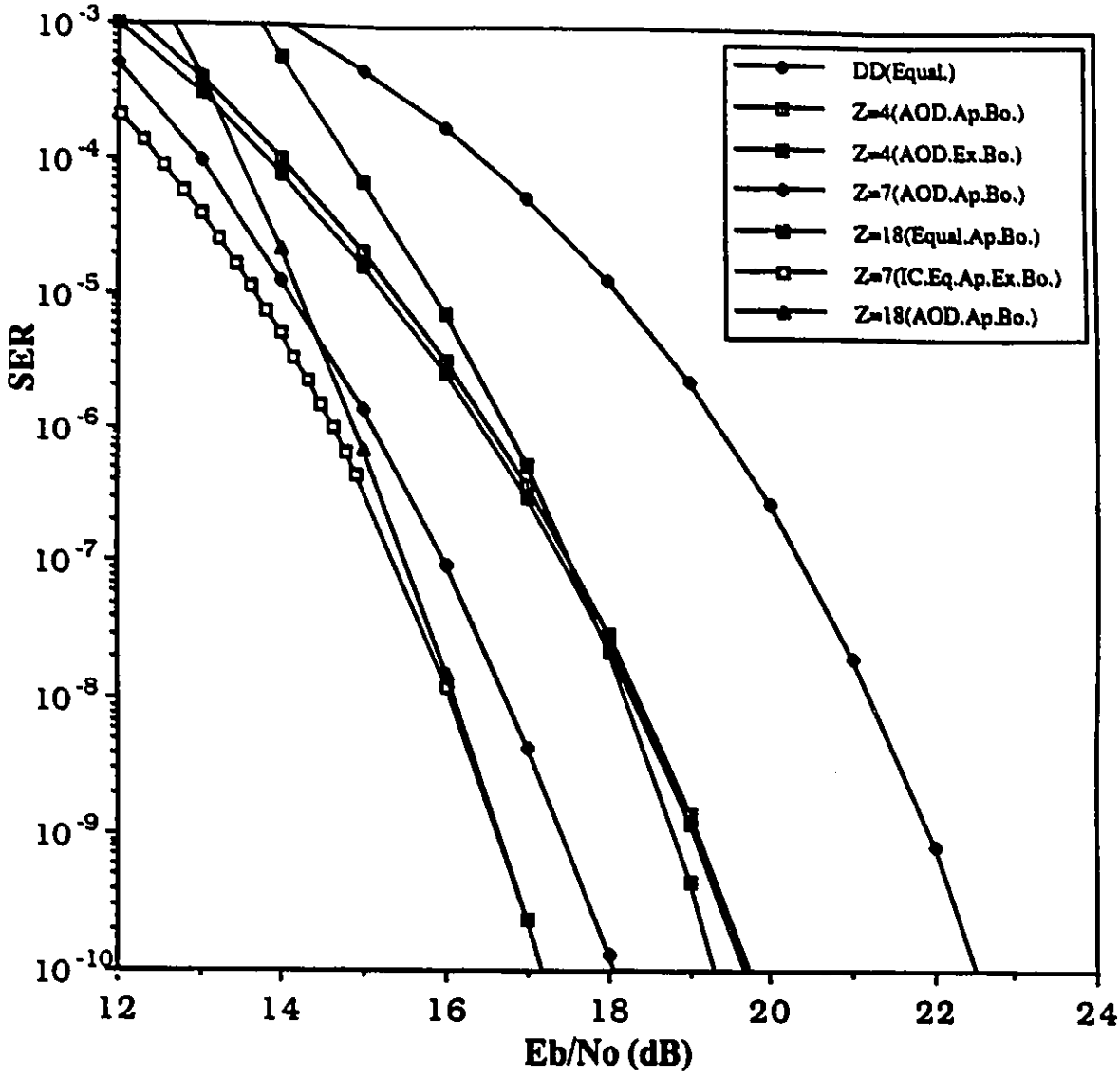

Figure 4.42: SER performance curves of non-coherently detected 8PSK in the time dispersive channel. The evaluated structures use either the asymptotically optimal decoder, the block decoder or the conventional one symbol delay differential detector. The last two are used with zero forcing equalization. For reference, curves corresponding to the ideal channel/equal filter apportioning are also included.

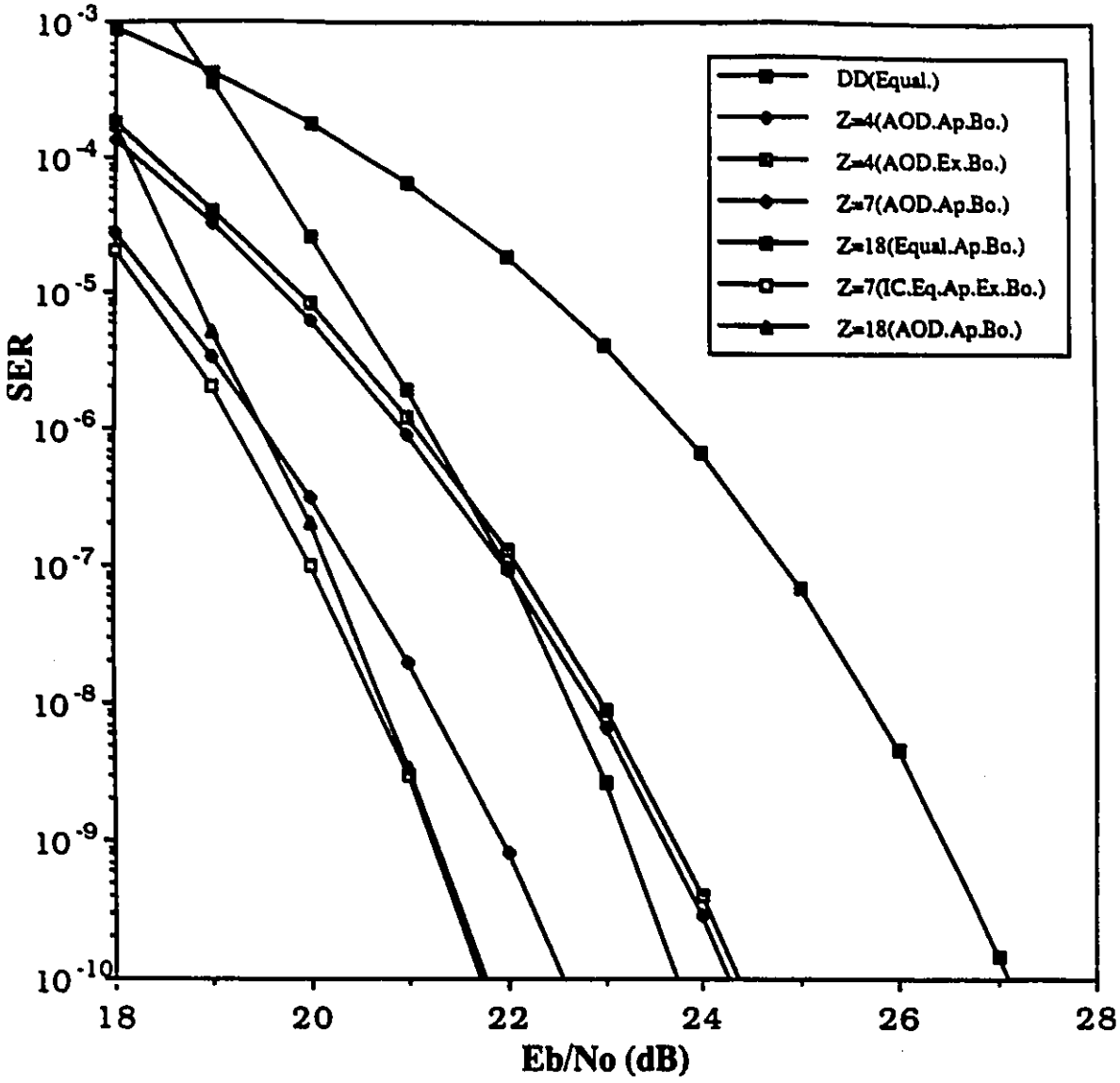

Figure 4.43: SER performance curves of non-coherently detected 16PSK in the time dispersive channel. The evaluated structures use either the asymptotically optimal decoder, the block decoder or the conventional one symbol delay differential detector. The last two are used with zero forcing equalization. For reference, curves corresponding to the ideal channel/equal filter apportioning are also included.

4.6.3.2 Coded Signals

Code A has been evaluated for operation in the dispersive channel. The results are presented in Figs. 4.44, 4.45. Fig. 4.44 provides results for the non-differentially encoded case whereas the results of Fig. 4.45 correspond to a differentially encoded system. The displayed curves are: i) the Z=5, 7, 10, 12 asymptotically optimal decoder (Z= (NDE or DE)AOD), ii) the Z=12 block decoder operating in ideal channel/equal Nyquist filter apportioning (Z=12(NDE or DE)IC.Eq.Ap.), iii) the conventional differential receiver used with a zero forcing equalizer (Con.Rec.(EQ.)) and the uncoded DBPSK also used with a zero forcing equalization (DBPSK(EQ.)).

In Tables 4.14, 4.15 we list the improvements offered by the asymptotically optimal decoder as compared to the conventional differential receiver and the uncoded DBPSK respectively (both of the last two configurations are used with a zero forcing equalizer). The results demonstrate that the asymptotically optimal decoder offers improvements as high as 5.6 dB and 5.5 dB compared to conventional differential receiver and uncoded DBPSK respectively. Note that the conventional differential receiver has worse performance than the uncoded DBPSK. Comparing the improvements to the gains achieved when operating in ideal channel, we find that its advantage has increased by 2.5 dB.

Table 4.14: Gains offered by the Asymptotically Optimal Decoder versus the codeword length Z. Code A is used. The comparison is with the conventional differential receiver (the comparison corresponds to a SER=10^{-4}).

		GAINS (dB)	
		NDE	DE
Z	5	4.6	5
	7	5	5.2
	10	5.5	5.6
	12	5.6	5.6

In Table 4.16 we summarize the improvements offered by the asymptotically optimal decoder as compared to the block decoder of equal length (Z).

Table 4.15: Gains offered by the Asymptotically Optimal Decoder versus the codeword length Z. Code A is used. The comparison is with the uncoded DBPSK.

		GAINS (dB)	
		NDE	DE
Z	5	4.2	4.6
	7	4.5	5
	10	5.2	5.2
	12	5.5	5.5

We see that there is a more than 2 dB improvement between the two receivers. Notice that the $Z = 5$ asymptotically optimal decoder has a superiority of 1.2 dB (NDE) and 1.7 dB (DE) compared to the $Z = 12$ block decoder (NDE or DE). Keeping in mind that at the same time the $Z = 5$ asymptotically optimal decoder has a complexity in processing load (roughly) 2^7 times lower than the $Z = 12$ block decoder, we realize how powerful the asymptotically optimal decoder can be in a severely distorted channel.

Table 4.16: Gains offered by the Asymptotically Optimal Decoder as compared to the Block Decoder, used with equalization. The comparison is between decoders processing codewords of equal length (Z).

		GAINS (dB)	
		NDE	DE
Z	5	2.5	2.5
	7	2.1	2.3
	10	2.3	2.3
	12	2.3	2.3

One interesting point is that for the uncoded schemes the asymptotically optimal decoder was capable of recovering all the performance loss created by the time dispersive nature of the channel (and practically reach identical performance as that of the coherent receiver operating in an ideal AWGN channel); however, this did not happen in the case of coded signals. There is a 1 dB distance between what the asymptotically optimal decoder achieved in the distorted channel and the performance in the ideal channel. The reason for this loss is the following. In the distorted channel case, the ISI present in the channel, acts as an additional encoding mechanism, superimposed on the original code. This modifies the distance metrics. The signal carries the "coding" applied by cascading the convolutional encoder, the differential encoder (if present) and the ISI. The "code" resulting from the cascading of these three encoding processes (we call it *super code*) has minimum distances (Euclidean for the coherent systems, $D^Z_{HAO[\nu,\zeta]}$ for the asymptotically optimal decoder and $D^Z_{[\nu,\zeta]}$ for the block decoder) which are smaller as compared to the ideal channel case. This results in inferior performance. In order to regain the lost performance, *the design of new codes matching the dispersive behaviour of the channel and the non-coherent nature of the receiver are needed. Their design should be based on the maximization of the distance metrics* $D^Z_{[\nu,\zeta]}$ *(for the block decoder) and* $D^Z_{HAO[\nu,\zeta]}$ *(for the asymptotically optimal decoder).*

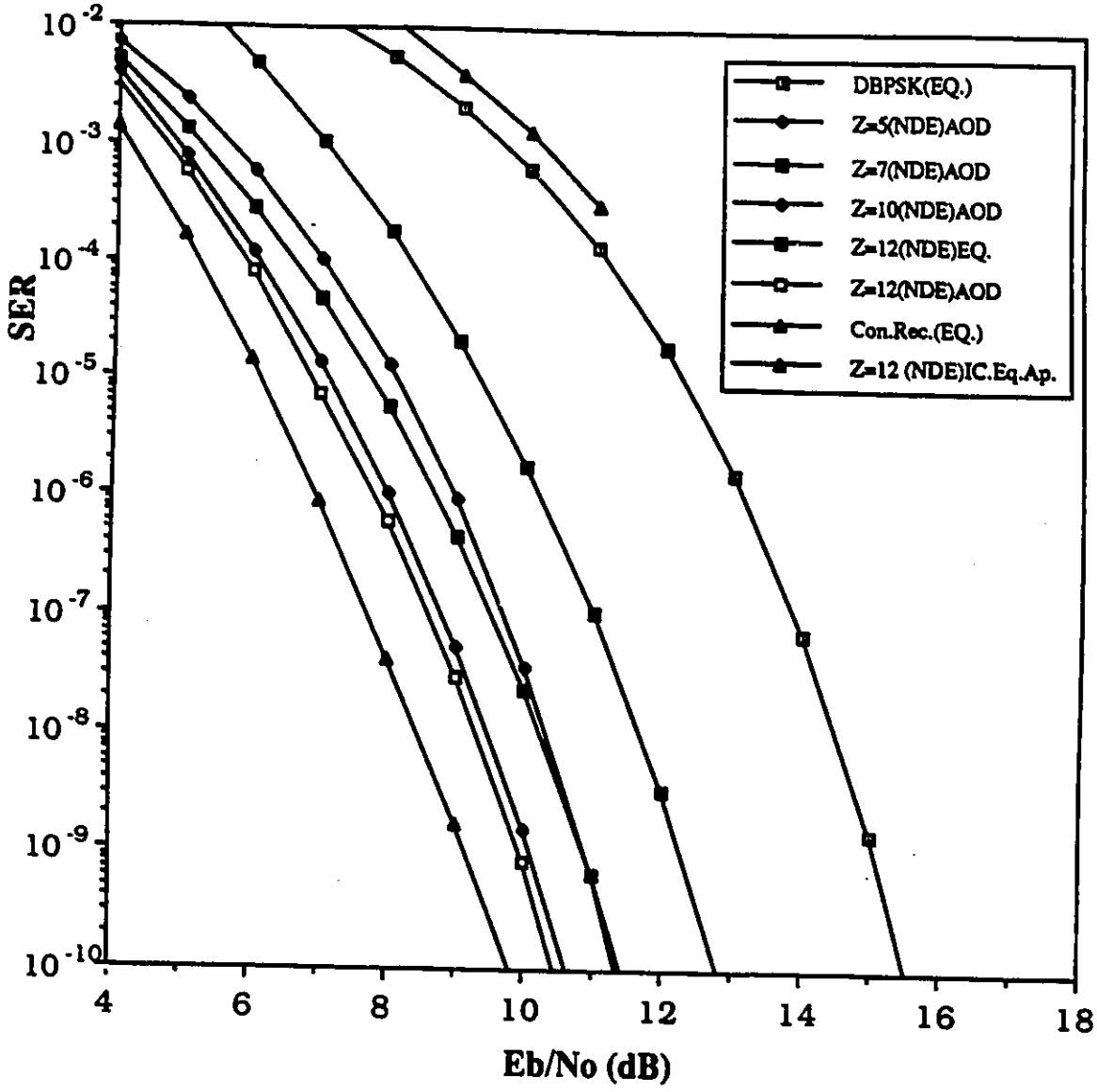

Figure 4.44: SER performance curves of code A (non differentially encoded) in the time dispersive channel. The results correspond to various non-coherent receiver configurations.

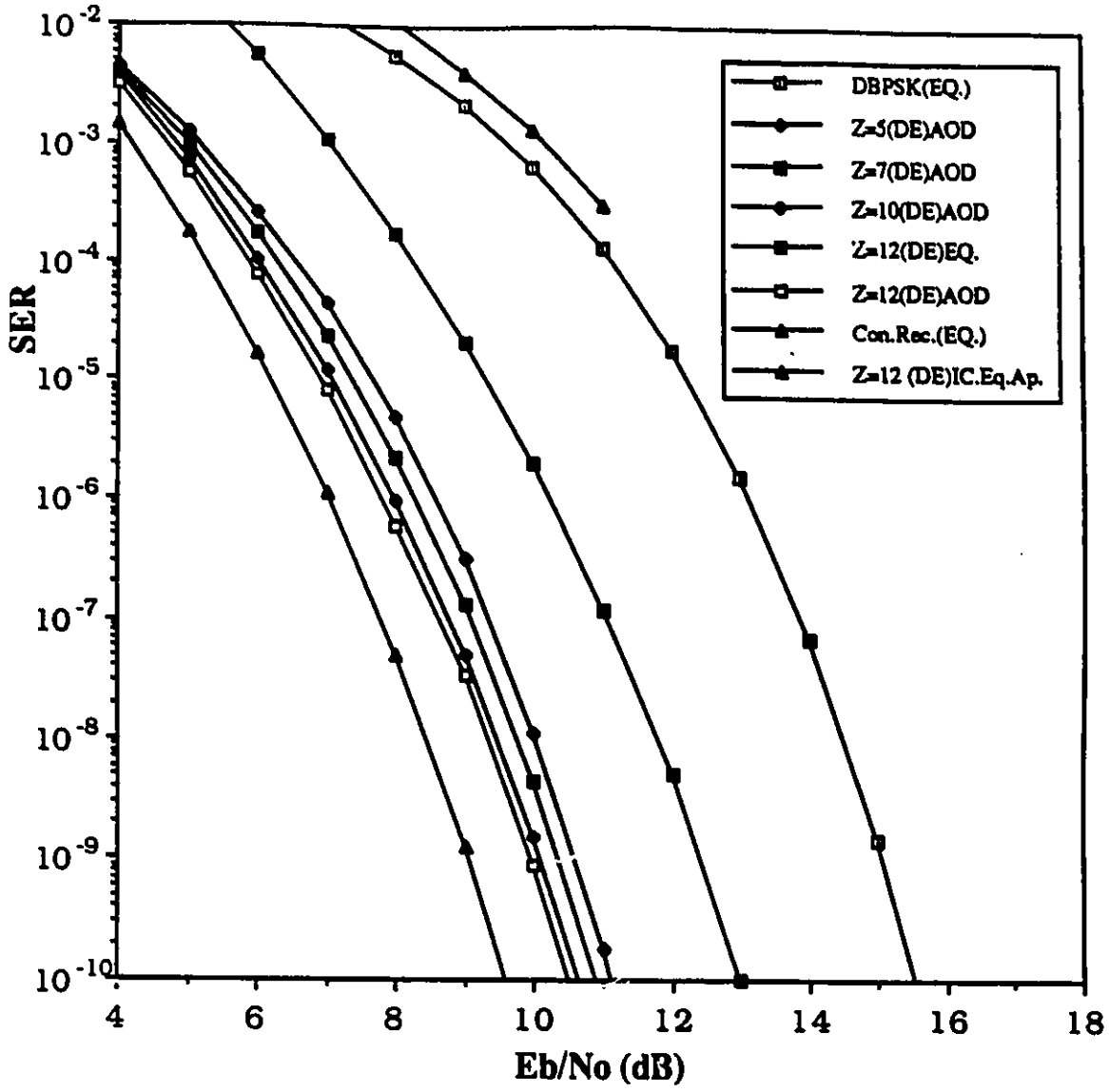

Figure 4.45: SER performance curves of code A (differentially encoded) in the time dispersive channel. The results correspond to various non-coherent receiver configurations.

4.7 PERFORMANCE ANALYSIS OF LINEAR MODULATIONS WITH MULTI-AMPLITUDE/PHASE SIGNAL CONSTELLATIONS

In the present section, we shall limit ourselves to the evaluation of uncoded systems, however, the analysis to be described applies to coded systems as well. An upper bound of the pairwise error event probability is needed. This is used with the union bound to upper bound the overall performance. In the following paragraphs, a brief description of the basic steps leading to the analytical evaluation of the non-coherently detected multi-amplitude/phase signals will be given.

4.7.1 Pairwise Error Bound for the Multi-Amplitude/Phase Signal

The error probability $P_e^{[MAD]HAO}$ of a multi-amplitude/phase signal can be upper bounded by $\mathcal{U}_{HAO}^{MAD}B^Z$ (i.e. $P_e^{[MAD]HAO} \leq \mathcal{U}_{HAO}^{MAD}B^Z$) where

$$\mathcal{U}_{HAO}^{MAD}B^Z = \frac{1}{2^{(Z-L_c-1)p}} \sum_{\{\bar{C}(\bar{A}^\nu)\in S_{CW}^Z\}} P_{HAO}^{MAD}B^{Z,\nu}, \tag{4.70}$$

with

$$P_{HAO}^{MAD}B^{Z,\nu} = \frac{1}{Z-L_c-1} \sum_{\{\bar{C}(\bar{A}^\zeta)\in S_{\bar{C}(\bar{A}^\nu)}\}} n_e(\{\bar{C}(\bar{A}^\zeta)\leftarrow\bar{C}(\bar{A}^\nu)\})\mathcal{MB}_{HAO[\nu,\zeta]}^Z. \tag{4.71}$$

$\mathcal{MB}_{HAO[\nu,\zeta]}^Z$ is the upper bound of the pairwise error probability corresponding to the error event $\{\bar{C}(\bar{A}^\zeta)\leftarrow\bar{C}(\bar{A}^\nu)\}$ and equal to

$$\mathcal{MB}_{HAO[\nu,\zeta]}^Z = \begin{cases} \mathcal{MB}_{PW[\nu,\zeta]}^Z & \text{for } \mathcal{MD}_Z^{\zeta,\nu}(h_0,\bar{h}) \geq 0 \\ \mathcal{MB}_{PW[\nu,\zeta]}^Z + Q(\frac{\overline{\mathcal{MED}}_{\nu,\zeta}^{\nu,*}(h_0,\bar{h})}{\sigma_{\nu,\nu}}) & \text{for } \mathcal{MD}_Z^{\zeta,\nu}(h_0,\bar{h}) < 0 \end{cases}$$

(4.72)

with

$$\mathcal{MD}_Z^{\zeta,\nu}(h_0,\bar{h}) = (MST(h_0,\bar{C}(\bar{A}^\zeta)) + IST(\bar{h},\bar{C}(\bar{A}^\zeta))) - (MST(h_0,\bar{C}(\bar{A}^\nu)) + IST(\bar{h},\bar{C}(\bar{A}^\nu))). \quad (4.73)$$

$$\sigma_{\nu,\eta}^2 = \sigma_n^2[\frac{\sum_{k=0}^{Z-1}(\mathcal{J}_k^\nu)^2}{2} + \sum_{l=1}^{Z-1}\rho_l^n\sum_{k=l}^{Z-1}\mathcal{J}_k^\nu\mathcal{J}_{k-l}^\nu\cos(\Delta\Phi_l^\eta(k))].$$

(4.74)

$\mathcal{J}_k^\eta = |c_k^\eta|$ and $\Delta\Phi_l^\eta(k) = \{Arg[c_k^\eta] \ominus Arg[c_{k-l}^\eta]\}$.

We remind the reader that $\rho_k^n = \frac{R_n(kT)}{R_n(0)}$. $R_n(\tau)$ is the noise autocorrelation function at the output of the post detection filter. $\sigma_n^2 = R_n(0)$.

Also,

$$\overline{\mathcal{MED}}_{\nu,\zeta}^{\nu,*}(h_0,\bar{h}) = \frac{h_0}{2}[|c_k^\nu|^2 + |c_k^\zeta|^2] + \sum_{l=1}^{Z-1}\sum_{k=l}^{Z-1}[Re\{h_l c_k^\zeta (c_{k-l}^\zeta)^*\} + Re\{h_l c_k^\nu (c_{k-l}^\nu)^*\}]$$

(4.75)

and

$$\mathcal{MB}_{PW[\nu,\zeta]}^Z = \frac{1}{2}[\mathcal{M}\Lambda_{PW}(\bar{C}(\bar{A}^\nu),\bar{C}(\bar{A}^\zeta))]\exp\{-\frac{1}{\sigma_n^2}\frac{|\alpha_{PW[\nu,\zeta]}^{MAD} - \beta_{PW[\nu,\zeta]}^{MAD}|^2}{2}\}.$$

(4.76)

with

$$\mathcal{M}\Lambda_{PW}(\bar{C}(\bar{A}^\nu),\bar{C}(\bar{A}^\zeta)) = \begin{cases} 1 & \text{for } \alpha_{PW[\nu,\zeta]}^{MAD} = 0 \\ [1 - \frac{v_{\nu\nu}^{MAD} - v_{\nu\zeta}^{MAD}}{[(v_{\nu\nu}^{MAD} + v_{\nu\zeta}^{MAD})^2 - 4|v_{[MAD]\nu\zeta}^{\zeta}|^2]^{\frac{1}{2}}}] & \\ \frac{1}{\sqrt{2\pi\frac{1}{\sigma_n^2}\alpha_{PW[\nu,\zeta]}^{MAD}\beta_{PW[\nu,\zeta]}^{MAD}}} & \text{for } \alpha_{PW[\nu,\zeta]}^{MAD} \neq 0. \end{cases}$$

(4.77)

$$\left\{ \begin{array}{c} \alpha_{PW[\nu,\zeta]}^{MAD} \\ \beta_{PW[\nu,\zeta]}^{MAD} \end{array} \right\} = [\frac{1}{v_{\nu\nu}^{MAD} + v_{\nu\zeta}^{MAD}}(\frac{|\overline{MED}_{\nu,\zeta}^{\nu,*}(h_0,\bar{h})|^2 + |\overline{ME}_{\zeta}^{\nu,*}|^2}{1-|\gamma_{\nu\zeta}|^2} - (\frac{2Re\{(\overline{ED}_{\nu,\zeta}^{\nu,*}(h_0,\bar{h}))^* \overline{ME}_{\zeta}^{\nu,*}\gamma_{\nu\zeta}^{MAD}\}}{1-|\gamma_{\nu\zeta}^{MAD}|^2} \mp \frac{|\overline{MED}_{\nu,\zeta}^{\nu,*}(h_0,\bar{h})|^2 - |\overline{ME}_{\zeta}^{\nu}|^2}{\sqrt{1-|\gamma_{\nu\zeta}^{MAD}|^2}})]^{\frac{1}{2}},$$

(4.78)

$$\overline{ME}_{\zeta}^{\nu,*} = \sum_{l=0}^{Z-1}\sum_{k=l}^{Z-1}[Re\{h_l c_k^{\zeta}(c_{k-l}^{\zeta})^*\} + Re\{h_l c_k^{\nu}(c_{k-l}^{\nu})^*\}] \quad .$$

(4.79)

Also,

$$v_{[\nu\eta]}^{MAD} = \sum_{k=0}^{Z-1}|c_k^{\eta}|^2 + \sum_{k=1}^{Z-1}\rho_k^n\sum_{l=k}^{Z-1}(|c_l^{\nu}c_{l-k}^{\eta}| + |c_l^{\eta}c_{l-k}^{\nu}|)\cos(\Delta\Phi_k^{\eta}(l)),$$

(4.80)

$(\eta \in \{\nu,\zeta\})$,

$$v_{MAD[\nu\zeta]}^{c} = [\sum_{k=0}^{Z-1}\rho_k^n\sum_{l=k}^{Z-1}[|c_l^{\zeta}c_{l-k}^{\nu}|e^{j(\Delta\Phi_l^{\zeta}(l)-\Delta\Phi_{l-k}^{\nu}(l-k))} + |c_l^{\nu}c_{l-k}^{\zeta}|e^{-j(\Delta\Phi_l^{\nu}(l)-\Delta\Phi_{l-k}^{\zeta}(l-k))}]]$$

(4.81)

and

$$\gamma_{\nu\zeta}^{MAD} = \frac{2v_{MAD[\nu\zeta]}^{c}}{(v_{[\nu\nu]}^{MAD} + v_{[\nu\zeta]}^{MAD})} . \tag{4.82}$$

$v_{\nu\eta}^{MAD}$, $v_{[MAD]\nu\zeta}^{c}$ represent the normalized variance and covariance respectively. When $E\{n_k n_{k-l}^{*}\} = 0 \quad \forall \quad l \neq 0$ (i.e. when the n_k noise terms happen to be uncorrelated with each other) then $v_{\nu\nu}^{MAD}$, $v_{\nu\zeta}^{MAD}$ and $v_{MAD[\nu\zeta]}^{c}$ become

$$v_{\nu\nu}^{MAD} = h_0 \sum_{k=0}^{Z-1} |c_k^{\nu}|^2, \tag{4.83}$$

$$v_{\nu\zeta}^{MAD} = h_0 \sum_{k=0}^{Z-1} |c_k^{\zeta}|^2 \tag{4.84}$$

and

$$v_{[MAD]\nu\zeta}^{c} = h_0 \sum_{k=0}^{Z-1} c_k^{\nu}(c_k^{\zeta})^{*}. \tag{4.85}$$

The distance metric for the multi-amplitude/phase signals is equal to

$$D_{[\nu,\zeta]}^{Z} = \frac{|\alpha_{PW[\nu,\zeta]}^{MAD} - \beta_{PW[\nu,\zeta]}^{MAD}|^2}{2} \tag{4.86}$$

The analysis leading to Eqs.(4.72) to (4.86) is identical to what is presented in Appendix F for PSK signals. The only difference is that the simplifications associated with ($|c_k|^2 = 1$) can not be applied due to the multi-amplitude nature of the signal. Following the steps described in Appendix F, the derivation of the material presented in this section is straight-forward.

4.7.2 Performance Evaluation Results

The asymptotically optimal decoder has been evaluated for a 16QAM signal and operation in an ideal channel perturbed by additive white Gaussian noise. The results are presented in Fig. 4.46 for various values of Z, together with

the curves of coherent 16PSK (C16PSK) with ideal carrier synchronization and differential 16PSK(D16PSK). In Table 4.17 the improvements achieved by the non-coherent 16QAM scheme (NC-16QAM) as compared to C16PSK 16DPSK are summarized. From the curves we realize that the non-coherent decoder outperforms the C16PSK by more than 3.5 dB. It also outperforms D16PSK by about 6 dB. These improvements demonstrate the potential of the proposed receiver.

Table 4.17: Gains offered by Non-Coherent 16QAM compared to coherent (C16PSK) and differential (D16PSK) 16PSK versus the sequence length Z.

		GAINS (dB)	
		D16PSK	C16PSK
Z	2	0.3	-2.6
	5	3.2	1.2
	10	4.8	2.6
	15	5.8	3.7

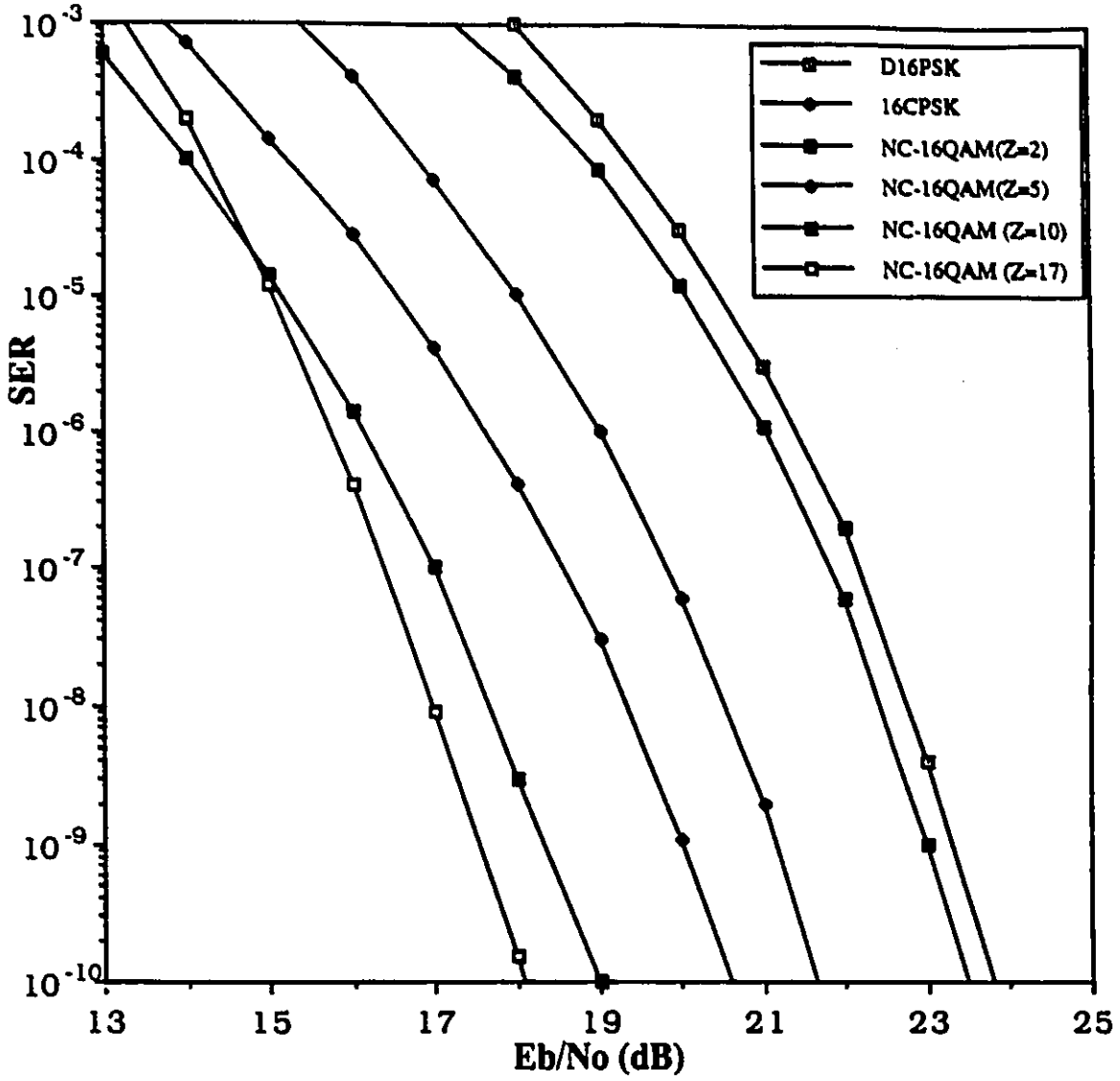

Figure 4.46: SER performance curves of D16PSK, C16PSK and Non-Coherent 16QAM (NC-16QAM).

4.8 PERFORMANCE IN FADING ENVIRONMENTS

This section will deal with the performance of the block decoder in a (Rician and Rayleigh) faded environment.

4.8.1 Performance Analysis

The detailed derivation of the pairwise error event probability $P_f(\{\bar{C}(\bar{A}^\zeta) \leftarrow \bar{C}(\bar{A}^\nu)\})$ for a PSK signal in a (Rayleigh or Rician) faded channel is presented in Appendix G. Here we shall give the final expression, it being the

$$\begin{aligned} P_f(\{\bar{C}(\bar{A}^\zeta) \leftarrow \bar{C}(\bar{A}^\nu)\}) &= Q_f(\frac{1}{\sigma_n}\alpha_{f[\nu,\zeta]}, \frac{1}{\sigma_n}\beta_{[f\nu,\zeta]}) \\ &- \frac{1}{2}[1 + \frac{v_{f[\nu\nu]} - v_{f[\nu\zeta]}}{[(v_{f[\nu\nu]} + v_{f[\nu\zeta]})^2 - 4|v^c_{f[\nu\zeta]}|^2]^{\frac{1}{2}}}] \\ &\quad I_o(\frac{1}{\sigma_n}\alpha_{f[\nu,\zeta]}\frac{1}{\sigma_n}\beta_{f[\nu,\zeta]}) \exp(-\frac{1}{\sigma_n^2}\frac{f\alpha^2_{[\nu,\zeta]} + \beta^2_{f[\nu,\zeta]}}{2}) \end{aligned} \tag{4.87}$$

(we remind the reader that $Q_f(\cdot,\cdot)$ is the Marcum's Q function [242, p. 585]) and

$$\begin{aligned} \left\{ \begin{array}{c} \alpha_{f[\nu,\zeta]} \\ \beta_{f[\nu,\zeta]} \end{array} \right\} &= [\frac{1}{v_{f[\nu\nu]} + v_{f[\nu\zeta]}}(\frac{|\bar{E}^f_{\nu,\nu}|^2 + |\bar{E}^f_{\nu,\zeta}|^2 - 2Re\{(\bar{E}^f_{\nu,\nu})^* \bar{E}^f_{\nu,\zeta}\gamma^f_{\nu\zeta}\}}{1 - |\gamma^f_{\nu\zeta}|^2} \\ &\mp \frac{|\bar{E}^f_{\nu,\nu}|^2 - |\bar{E}^f_{\nu,\zeta}|^2}{\sqrt{1 - |\gamma^f_{\nu\zeta}|^2}})]^{\frac{1}{2}}. \end{aligned} \tag{4.88}$$

$$\gamma^f_{\nu\zeta} = \frac{2v^c_{f[\nu\zeta]}}{(v_{f[\nu\nu]} + v_{f[\nu\zeta]})}. \tag{4.89}$$

The definitions of $\bar{E}^f_{\nu,\nu}$, $E^f_{\nu,\zeta}$, $v^c_{f[\nu\zeta]}$, $v_{f[\nu\nu]}$ and $v_{f[\nu\zeta]}$ can be found in Appendix G.

For a strong Rician fading channel (Rician fading factor $K_r = 10log\{K_F\} \geq 5dB$), the expression of Eq.(4.87) can be tightly upper bounded by the following expression:

$$P_f(\{\bar{C}(\bar{A}^\zeta) \leftarrow \bar{C}(\bar{A}^\nu)\}) \leq \mathcal{BF}^Z_{[\nu,\zeta]} = \frac{1}{2}\Lambda_F(\bar{C}(\bar{A}^\nu), \bar{C}(\bar{A}^\zeta)) \exp\{-\frac{1}{\sigma_n^2}\frac{(\alpha_{f[\nu,\zeta]} - \beta_{f[\nu,\zeta]})^2}{2}\} \quad (4.90)$$

with

$$\Lambda_F(\bar{C}(\bar{A}^\nu), \bar{C}(\bar{A}^\zeta)) = \begin{cases} 1 & \text{for } \alpha_{f[\nu,\zeta]} = 0 \\ [1 - \frac{v_{f[\nu\nu]} - v_{f[\nu\zeta]}}{[(v_{f[\nu\nu]} + v_{f[\nu\zeta]})^2 - 4|v^c_{f[\nu\zeta]}|^2]^{\frac{1}{2}}}] & \\ \frac{1}{\sqrt{2\pi\frac{1}{\sigma_n^2}\alpha_{f[\nu,\zeta]}\beta_{f[\nu,\zeta]}}} & \text{for } \alpha_{f[\nu,\zeta]} \neq 0. \end{cases} \quad (4.91)$$

For a Rayleigh fading channel ($K_R \rightarrow -\infty\, dB$) the pairwise error probability is reduced to

$$P_f(\{\bar{C}(\bar{A}^\zeta) \leftarrow \bar{C}(\bar{A}^\nu)\}) = \frac{1}{2}[1 - \frac{v_{f[\nu\nu]} - v_{f[\nu\zeta]}}{[(v_{f[\nu\nu]} + v_{f[\nu\zeta]})^2 - 4|v^c_{f[\nu\zeta]}|^2]^{\frac{1}{2}}}] \quad (4.92)$$

In previous sections where the results for an AWGN channel were reported, we used the union bound to effectively upper bound the overall performance. However, for the (slow) faded channel case, we have found that such an approach is not effective. The results provided by the union bound are quite loose and they do not effectively provide information for the performance of the system.

To understand the reason behind this, we should recall the *"Double Symbol Error"* behaviour of the differential detector [176], [199], [224], [235]. The differential detector has the tendency to produce errors in pairs (i.e. if a symbol g_k has been decided incorrectly by the differential detector, there is a high

probability that g_{k+1} will be decided incorrectly as well). The mechanism creating the appearance of errors in pairs comes from the differential detection process itself. The differential detector makes these decisions by comparing the phases of (or equivalently generating the difference of the phases by multiplying) two consecutive received signal samples (see Fig. 2.4 in Chapter 2). In the decision of g_k, the samples received at kT, $(k-1)T$ are involved. The decision of g_{k+1} is based on the samples received at $(k+1)T$, kT. As we see, the sample at kT is involved in both decisions. If this sample happens to be corrupted by strong noise, it is capable of forcing both decisions to the wrong side. In [199] [224] [235] this double symbol error mechanism of the signal has been verified (analytically as well as experimentally and by simulation means). In these works it has also been shown that as the operating E_b/N_o increases, the probability of double errors occurring is reduced.

In a faded channel, the signal envelope fluctuates randomly between zero and high values. As a result, even when the average E_b/N_o has high values, there is a finite probability that the instantaneous E_b/N_o will reside in low levels. This i) raises the double symbol error probability and ii) the reduction of the double symbol error probability with the increase in (average) E_b/N_o is lower as compared to the Gaussian noise case [168].

Similar behaviour with the one described above is experienced by the multiple differential detector. For an AWGN channel, the probability of multiple symbol error events decreases relatively quickly with the increase in E_b/N_o, leaving the single error events to dominate the performance. This makes the results given by the union bound tight enough and close to the actual performance of the system. However, for slow fading channels, the decrease in multiple symbol error probability is slower. By including all the possible error events in the union bound, its value becomes considerably higher from the actual performance of the system.

To overcome this problem, in our work, we have followed an alternative approach. In Appendix H we have reasoned that a more appropriate bounding approach is to include in the union bound only the error events which are defined as follows:

$$\{\bar{C}(\bar{A}^{\zeta}) \leftarrow \bar{C}(\bar{A}^{\nu})\} = \{[c_0^{\nu}, \ldots, c_k^{\nu}\, e^{j\pm\frac{2\pi}{M}}, \ldots, c_{Z-1}^{\nu}]\} \leftarrow \{[c_0^{\nu}, \ldots, c_k^{\nu}, \ldots, c_{Z-1}^{\nu}]\} \tag{4.93}$$

where $1 \leq k \leq (Z-1)$. These error events consist of sequences which differ only in one symbol. As well, the difference between the phases of these unequal symbols is $\pm\frac{2\pi}{M}$. In the following paragraphs, the performance of BPSK, QPSK, 8PSK with multiple differential detection in the fading channel is examined. The union bound, which includes only the (dominant) error events described by Eq.(4.93), will be called from now on *lower union bound* (LB) in order to be distinguished from cases where all the error events are used (see Eq.(4.46)). To make the distinction clear in the present and following sections, we shall be calling the latter *upper union bound* (UB).

4.8.2 Performance Results

4.8.2.1 Rayleigh Faded Channels

In the present section, performance evaluation results for BPSK, QPSK and 8PSK used with the block decoder will be provided. The results to be reported consider that the fading process follows the mobile radio fading model [174]. The spectrum of the considered fading process is described by the following expression:

$$S(f) = \begin{cases} (f^2 - B_F^2)^{-\frac{1}{2}} & \text{for } |f| \leq B_F \\ 0 & \text{elsewhere} \end{cases} \tag{4.94}$$

where B_F represents the fading bandwidth.

In Figs. 4.47, 4.48, 4.49 we provide the results for BPSK, QPSK and 8PSK in a static Rayleigh faded channel ($B_F T = 0$)[12]. We are addressing non-differentially encoded[13] and differentially encoded signals. In these figures, we display curves corresponding to the conventional differential detector

[12]The term *static fading channel* describes a multipath fading channel whose fading process is slow enough not to change over the period where the block of the received signal samples (processes by the decoder) are collected. This occurs when the fading bandwidth is very small, i.e. when $B_F T \approx 0$.

[13]For practical purposes, all the information symbols can be differentially encoded with reference to the first transmitted symbol in the processed block. Assume that the received signal samples $y_k, y_{k+1}, \cdots, y_{k+Z-1}$ are to be processed by the block decoder and the $g_{k+1}, g_{k+2}, \cdots, g_{k+Z-1}$ information symbols are to be decided. According to the differential encoding strategy described earlier in the third and fourth chapters, the g_{k+i} information

(DD) and the block decoder with $Z = 3, 4, 5, 10$ (Z= (NDE or DE)). For these results, the lower union bound has been used.

In Tables 4.18, 4.19 the relative performance between the block decoder and the differential detector is displayed, for various values of sequence length Z. Table 4.18 summarizes results for non-differentially encoded signals. Table 4.19 refers to differentially encoded signals.

Table 4.18: Gains offered by the block decoder versus the sequence length Z. The information sequence *is not differentially encoded.* The comparison is with the conventional differential detector.

		GAINS (dB)		
		BPSK (NDE)	QPSK (NDE)	8PSK (NDE)
Z	3	1.25	1.3	1.3
	4	1.7	1.8	1.8
	5	2.2	2.3	2.3
	10	3	3	3

We observe that when the transmitted information has not been differentially encoded, the block decoder is always superior as compared to the differential detector. The improvements range between 1.25 dB (Z=3(NDE)) to 3 dB (Z=10(NDE)). The Z=10(NDE) configuration achieves practically the same performance with the coherent detector (with perfect carrier reference) operating in the static Rayleigh channel [214, p. 718]. On the contrary, when differential encoding is used, the performance of the block decoder

symbol ($1 \leq i \leq Z-1$) is differentially encoded with reference to the c_{k+i-1} transmitted symbol and produces c_{k+i}. In the approach which we suggest here, all the information symbols g_{k+i} are encoded with reference to the c_k symbol (first symbol in the $[c_k, c_{k+1}, \ldots, c_{k+Z-1}]$ block of transmitted symbols). c_k can be the last transmitted symbol from the previous block of information processed by the block decoder. In the previous block, the samples $y_{k-Z+1}, y_{k-Z+2}, \ldots, y_{k-1}, y_k$ have been processed, and the $g_{k-Z+2}, g_{k-Z+3}, \ldots, g_{k-1}, g_k$ information symbols have been decided. This method does not require knowledge of the value of the first transmitted symbol in every processed block. Consequently, these symbols are part of the information carrying process rather than being used to only provide some initial symbol reference to the block decoder. As a result, useful resources are not wasted and the capacity of the system is not reduced.

Table 4.19: Gains offered by the block decoder versus the sequence length Z. The information sequence *is differentially encoded.* The comparison is with the conventional differential detector.

		GAINS (dB)		
		BPSK (DE)	QPSK (DE)	8PSK (DE)
Z	3	-0.65	-0.64	-0.64
	4	-0.3	-0.25	-0.25
	5	-0.1	-0.1	-0.1
	10	0	0	0

becomes inferior. The disadvantage of the block decoder ranges from 0.64 dB(Z=3(DE)) to 0 dB (Z=10(DE)).

To understand why there is such a change in behaviour between the non-differentially and differentially encoded cases, we have to look at the mechanism of the differential encoding itself and how it is reflected in the error patterns appearing at the output of the block decoder. In a differentially encoded sequence, one wrong decision regarding the transmitted symbol c_k generates two information symbol errors (g_k, g_{k+1}). Only in the case where the error appears at the end of the sequence, i.e. at c_{Z-1} the system suffers only one (instead of two) information symbol error (g_{Z-1}). On the contrary, the differential detector produces one error since it processes and decides only on one information symbol at a time.

When differential encoding is absent, a wrong decision regarding the transmitted symbol c_k always creates only one information symbol error (g_k). This reduces the number of occurring errors in half (compared to the errors occurring when differentially encoding is used) and provides a performance superior to the differential detector.

Such behaviour is not new in faded channels. For high E_b/N_o, the error probability $P_e^{Coh.(NDE)}$ of the coherent detector (for a BPSK signal, using perfect carrier reference for demodulation) operating in a static Rayleigh faded channel and processing a non-differentially encoded signal can be ap-

proximated as [214]

$$P_e^{Coh.(NDE)} \approx \frac{1}{4(E_b/N_o)}. \tag{4.95}$$

The error probability P_e^{DD} of the differential detector under the same conditions is approximated by

$$P_e^{DD} \approx \frac{1}{2(E_b/N_o)}. \tag{4.96}$$

The coherent detector produces half the errors of the differential detector for the same E_b/N_o. Equivalently, to achieve the same performance levels, the differential detector needs double the energy of the coherent detector (i.e. 3 dB additional E_b/N_o). However, when the coherent detector processes differentially encoded information, it produces double the errors generated by the non-differentially encoded case, since every error appearing at its output generates two information symbol errors after differential decoding. This reduces its error probability to

$$P_e^{Coh.(DE)} \approx \frac{1}{2(E_b/N_o)} \tag{4.97}$$

which is identical to the error probability of the differential detector. The doubling in errors costs 3 dB loss in E_b/N_o.

As mentioned previously, the performance of the $Z = 10$ block decoder (either non-differentially or differentially encoded), is practically equal to the performance of the coherent detector (non-differentially encoded or differentially encoded). When differential encoding is absent, the Z=10(NDE) decoder has a 3 dB superiority compared to the differential detector. However, when differential encoding is present, the decoder loses its 3 dB advantage (due to the doubling of errors, its performance is pushed back to the performance of the differential detector). The same effect appears in all the other configurations of the block decoder examined and results in inferior performance when differential encoding is present.

An alternative way to achieve superior performance in the slow fading channel, even with signals differentially encoded according to Eq.(3.27), is to apply a combination of sequence estimation and symbol-by-symbol detection.

This can be done as follows. Let us assume that the y_k, y_{k+1}, ..., y_{k+Z-1} samples are processed by the block decoder. The most possible sequence of information symbols g_{k+1}, g_{k+2}, ..., g_{k+Z-1} is chosen according to the sequence estimation strategy which has been described for the block decoder. However, instead of providing the decisions for all the g_{k+1}, g_{k+2}, ..., g_{k+Z-1} symbols, the decoder outputs the decision of first symbol (g_{k+1}) only. The following symbol (g_{k+2}) will be decided by following the same steps, but this time processing the y_{k+1}, y_{k+2}, ..., y_{k+Z} samples. By avoiding to decide on more than one symbol each time, we avoid the occurrence of double error patterns. The performance of a system following this detection approach is identical to the performance we achieve by not differentially encoding the transmitted information sequence (see Figs. 4.47 to 4.49). However, the processing of the receiver becomes $(Z-1)$ times heavier as compared to when the entire block of symbols is decided (rather than only one symbol each time).

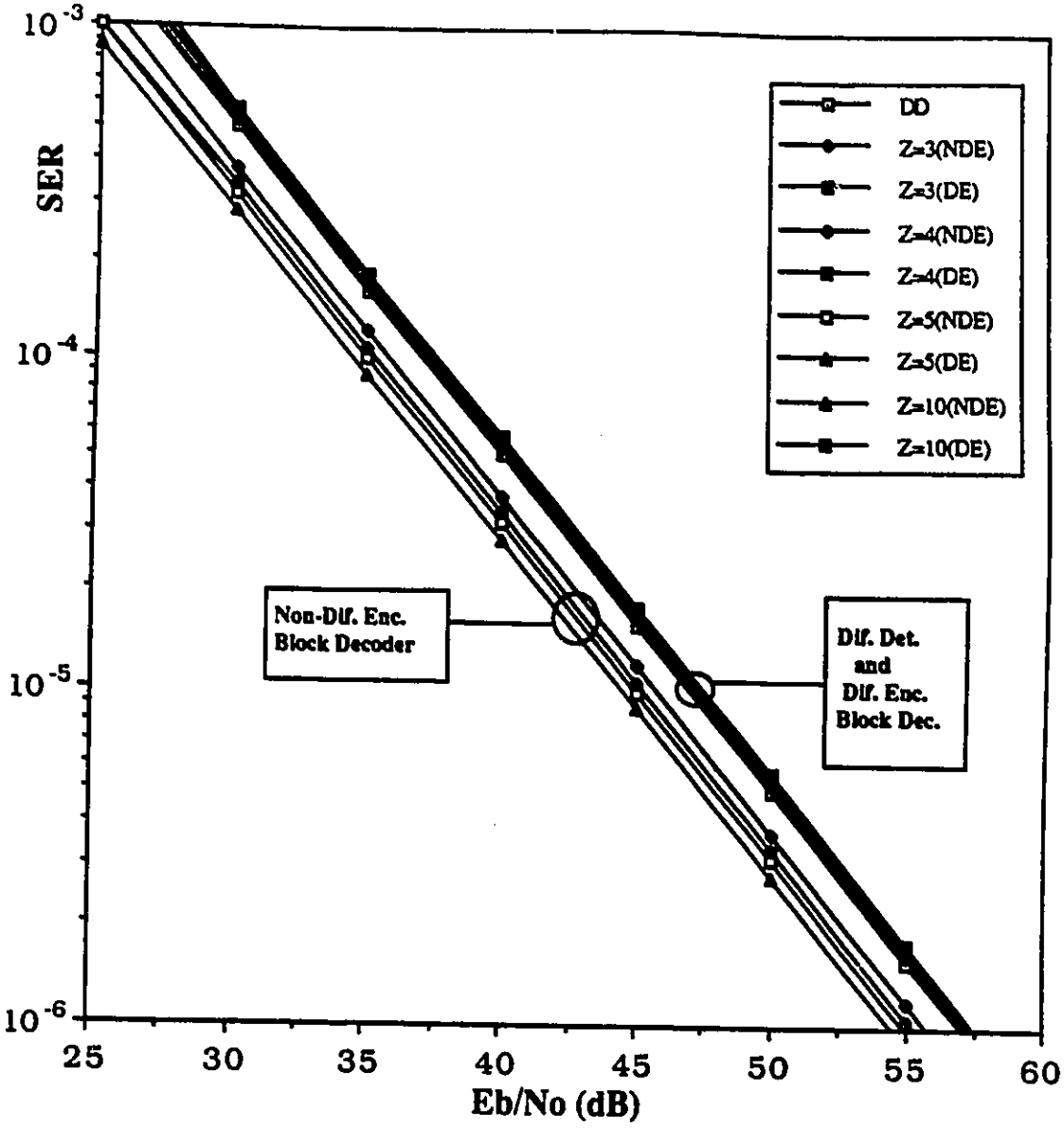

Figure 4.47: SER performance curves of non-coherently detected BPSK in a slow Rayleigh faded channel ($B_F T \approx 0$).

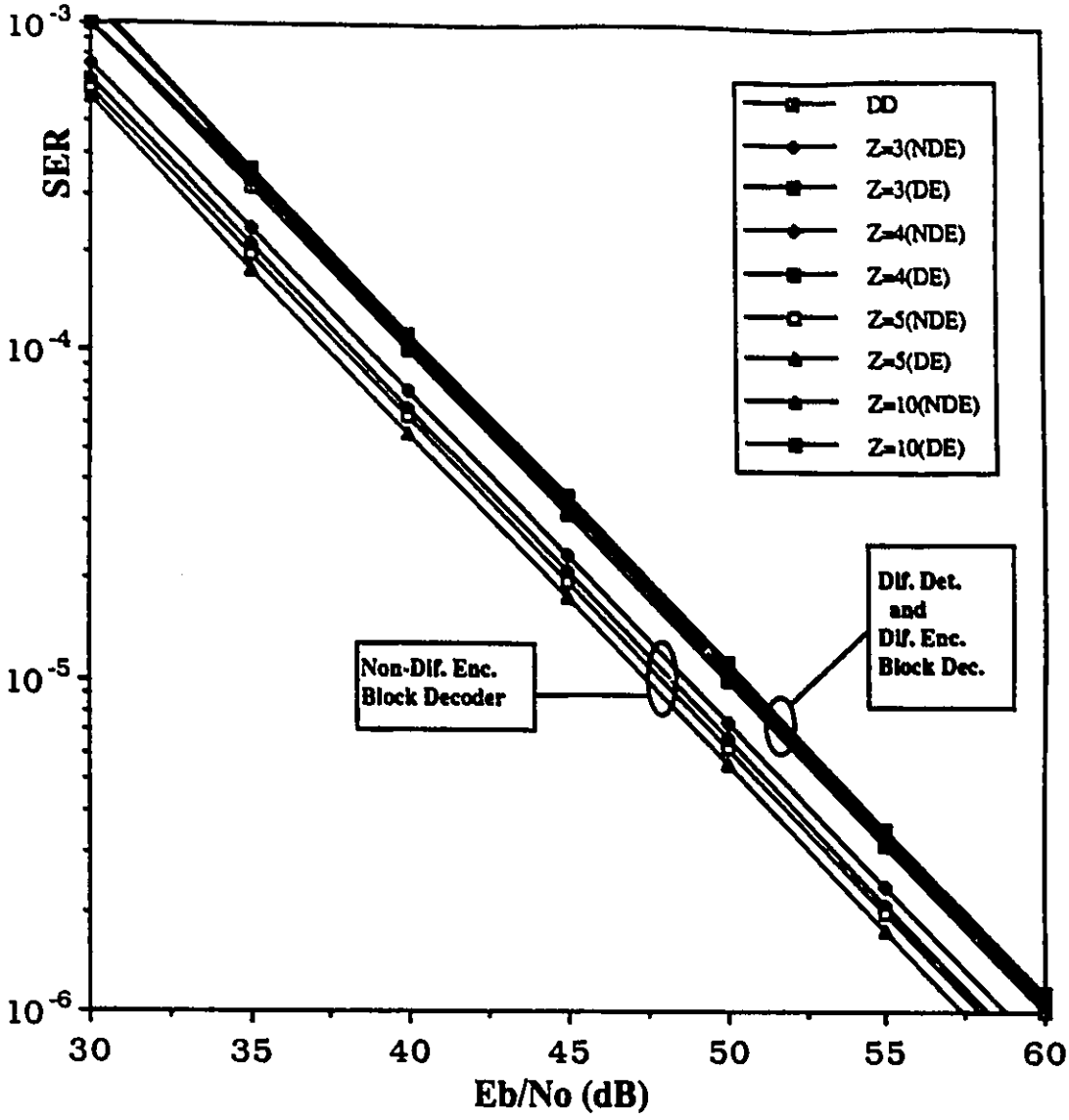

Figure 4.48: SER performance curves of non-coherently detected QPSK in a slow Rayleigh faded channel ($B_F T \approx 0$).

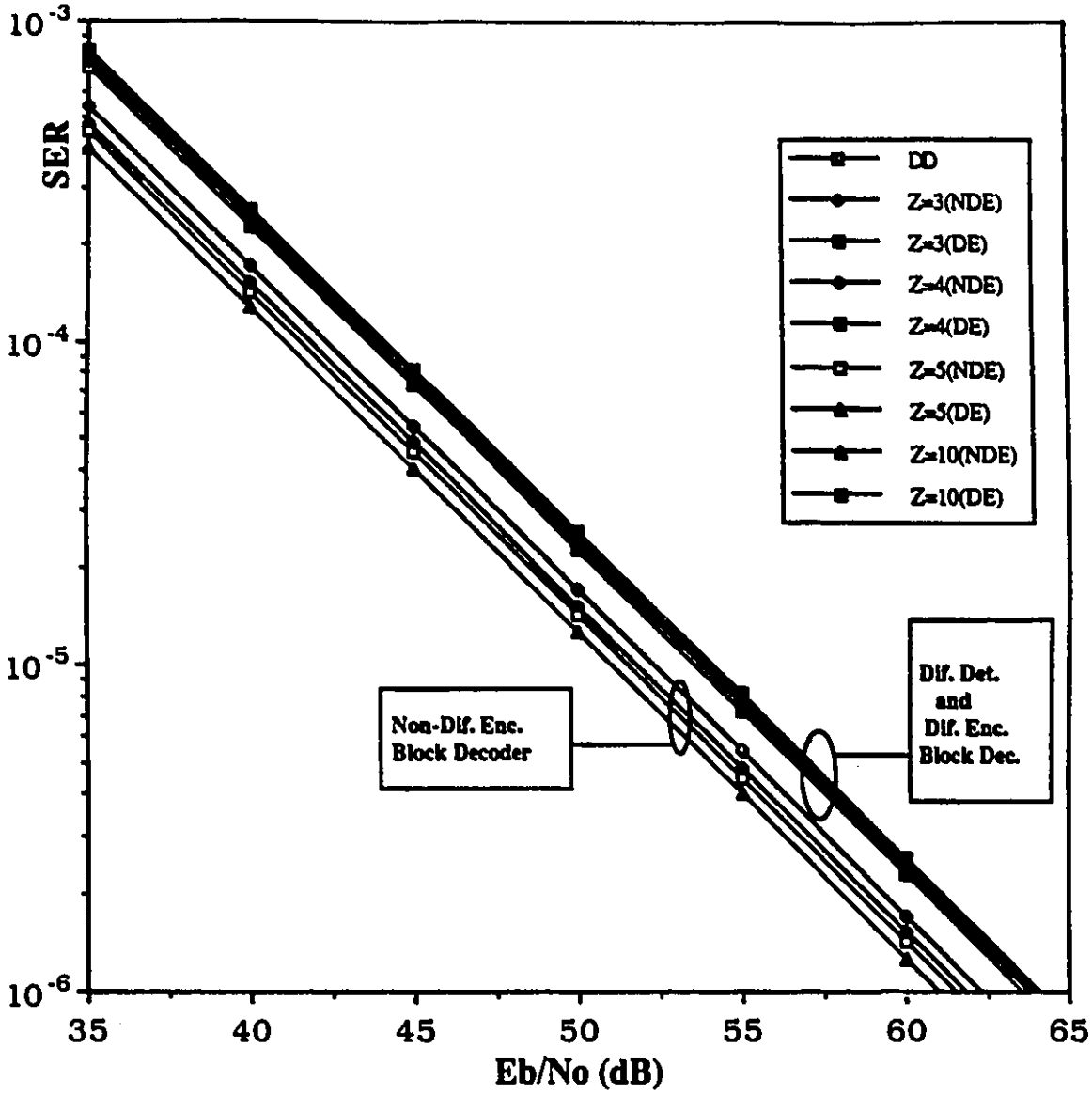

Figure 4.49: SER performance curves of non-coherently detected 8PSK in a slow Rayleigh faded channel ($B_F T \approx 0$).

4.8.2.2 Rician Faded Channels

In this section SER results for BPSK and QPSK (both of them differentially encoded) operating in a Rician faded channel will be provided. We have used the land mobile fading model described in Eq.(4.94). The evaluations have been carried out for Rician fading factor $Kr = 10dB, 15dB$ and fading bandwidth-symbol period products $B_FT = 0.1, 0.2, 0.4$.

The material to be covered in the following paragraphs, will be sectioned as follows. First we shall provide results based on the upper union bound and for different faded channel scenarios. The objective is to make a comparative study and show how the block decoder (used with various levels of complexity) behaves under different channel conditions. Afterwards, we shall present simulation results together with the curves provided by the upper and lower union bounds to provide a clear picture of its strengths and weaknesses.

Study Based on the Upper Union Bound

In Figs. 4.50 to 4.55 (BPSK) and Figs. 4.56 to 4.61 (QPSK) we provide SER curves for block decoders of different size (Z) ($Z = (K_r/B_FT)$)). For BPSK we have used $Z = 3, 4, 5, 6$ and for QPSK $Z = 3, 4, 5, 6, 8$. The curves in each figure correspond to the same value of K_r and B_FT and display results which are calculated by using the upper union bound. We include in the figures the curve of the differential detector operating under the same channel conditions ($DD(K_r/B_FT)$)).

The results presented in these figures lead to the realization that *in the fading channel, an increase in the length of the processed sequence does not always mean an improvement in performance.* On the contrary, the upper union bound results show that in some cases the differential detector has superior performance and that increase in the size of the sequence processed by the decoder, might result in loss of performance instead of improvement.

The curves displayed in Figs. 4.50 to 4.72 show error floors. The figures reporting results for the Rayleigh fading channel do not show the presence of error floors. The error floors appearing in the Rician fading channel results, occur due to the relative large values of fading bandwidth we have used ($B_FT = 0.1, 0.2, 0.4$). Both the amplitude and especially the phase fluctuations which impair the transmitted signal, change quite rapidly and as result, they generate the irreducible error rates we see in the figures. The results

reported for the Rayleigh fading channel are for very slow fading processes. The amplitude and phase distortions (introduced to the signal by the fading) remain unchanged during the transmission of the entire sequence of symbols ($B_FT \approx 0$).

In Tables 4.20 ($K_r = 10\ dB$, BPSK) , 4.21 ($K_r = 15\ dB$, BPSK), 4.22 ($K_r = 10\ dB$, QPSK), 4.23 ($K_r = 15\ dB$, QPSK), we have ordered the various configurations of the block decoder and the differential detector, according to their relative performance for $B_FT = 0.1, 0.2, 0.4$. In every column, the weakest receiver is first and the strongest is last; this order is based on the results provided by the upper union bound.

Table 4.20: Relative Performance of the Block Decoder and differential detector for various B_FT products. The channel is Rician with $K_r = 10\ dB$. The signal is BPSK.

B_FT		
0.1	**0.2**	**0.4**
DD	DD	DD
Z=3 (BD)	Z=3 (BD)	Z=3 (BD)
Z=4 (BD)	Z=4 (BD)	Z=4 (BD)
Z=5 (BD)	Z=5 (BD)	Z=5 (BD)
Z=6 (BD)	Z=6 (BD)	Z=6 (BD)

For BPSK, in most cases an increase in the length of the processed sequence (Z) results with an improvement in performance (exception is the [$K_r = 15dB$, $B_FT = 0.1$] case, where the $Z = 4$ block decoder outperforms all the other configurations). The same holds for QPSK when $B_FT = 0.4$. However, for $B_FT = 0.2$ there is dramatic change in the order of relative performance between the various configurations. The order of relative performance is different even for the two different K_r factors we have used. The differential detector is rated as the best. However, there is a complete mix up in the performance order of the various configurations of the block decoder. For $K_r = 10\ dB$ the $Z = 8$ block decoder is the second strongest, followed by the $Z = 3$. For $K_r = 15\ dB$ the $Z = 8$ still remains the strongest (after the DD); however, now the $Z = 6$ becomes the second strongest. One should

Table 4.21: Relative Performance of Block Decoder and differential detector for various B_FT products. The channel is Rician with $K_r = 15\ dB$. The signal is BPSK.

$\mathbf{B_FT}$		
0.1	**0.2**	**0.4**
DD	DD	DD
Z=3 (BD)	Z=3 (BD)	Z=3 (BD)
Z=5 (BD)	Z=4 (BD)	Z=4 (BD)
Z=6 (BD)	Z=5 (BD)	Z=5 (BD)
Z=4 (BD)	Z=6 (BD)	Z=6 (BD)

Table 4.22: Relative Performance of Block Decoder and differential detector for various B_FT products. The channel is Rician with $K_r = 10\ dB$. The signal is QPSK.

$\mathbf{B_FT}$		
0.1	**0.2**	**0.4**
Z=8 (BD)	Z=5 (BD)	DD
Z=6 (BD)	Z=4 (BD)	Z=3 (BD)
Z=5 (BD)	Z=6 (BD)	Z=4 (BD)
Z=4 (BD)	Z=3 (BD)	Z=5 (BD)
Z=3 (BD)	Z=8 (BD)	Z=6 (BD)
DD	DD	Z=8 (BD)

Table 4.23: Relative Performance of Block Decoder and differential detector for various B_FT products. The channel is Rician with $K_r = 15\ dB$. The signal is QPSK.

B_FT		
0.1	**0.2**	**0.4**
Z=8 (BD)	Z=4 (BD)	DD
Z=6 (BD)	Z=5 (BD)	Z=3 (BD)
Z=5 (BD)	Z=3 (BD)	Z=4 (BD)
Z=3 (BD)	Z=6 (BD)	Z=5 (BD)
DD	Z=8 (BD)	Z=6 (BD)
Z=4 (BD)	DD	Z=8 (BD)

observe that the $Z = 4$ and $Z = 5$ decoders exchange the order in which they appear, as we move from $K_r = 10\ dB$ to $K_r = 15\ dB$. For $B_FT = 0.1$ there is a pattern indicating deterioration in performance with increase in Z. The only exception is again the $Z = 4$ decoder where for K_r= 15 dB becomes the strongest (recall that exactly the same behaviour is observed in BPSK). Additional results for 8PSK, not presented in this document, indicate that this "anarchy" in order of performance becomes even stronger for 8PSK. This suggests that the task of drawing rules characterizing and predicting the performance of the block decoder in the fast Rician channel becomes more and more difficult as we move to denser PSK constellations. An explanation for the reason leading to this behaviour follows.

A PSK signal becomes more vulnerable to random phase fluctuations as its constellation becomes denser, simply because the (phase) distance between adjacent points becomes smaller. For a BPSK, the phase distance between adjacent points is 180°, for QPSK 90° and for 8PSK 45°. The large phase distance of BPSK (between its constellation points), gives it an invulnerability to phase fluctuations. For the BPSK signal and for a large range of the E_b/N_o scale, the main source of performance degradation is the signal envelope fluctuations introduced by the fading. The correctness of this statement can be verified by observing Fig. 4.68. As we see, the performance of the differential detector is practically independent from the value of the B_FT

product. For the same K_r, the curves corresponding to $B_FT = 0.1, 0.2, 0.4$ practically overlap[14]. In this case, the block decoder has an unquestionable advantage over the differential detector, since by processing a large number of signal samples it is capable of gathering more signal energy before it makes a decision. This gives a performance superiority and (almost) a constant trend in performance improvement as Z becomes higher.

On the contrary, QPSK, by having smaller distance between its constellation points, is more vulnerable to phase fluctuations. This makes the phase fluctuation factor capable of taking over the performance, becoming the dominant source of degradation at earlier values of E_b/N_o (compare Figs. 4.68 and 4.73), generating higher error floors for the system. As the distance between signal samples increases, the coherence between phase fluctuations corrupting these samples is reduced. The conventional differential detector processes the signal samples y_k, y_{k-1} which due to the short distance in time (one symbol period), they have quite a high degree of coherence between their randomly fluctuating phases when B_FT is relatively small. On the contrary, the block decoder processes a block of samples. If this block is quite large, the block decoder is bound to process signal samples having small correlation between their randomly fluctuating phases. This generates losses in the performance of the block decoder. When the fading bandwidth increases and even consecutive signal samples lose their phase coherence (between their random phase fluctuation values), the differential detector loses the mechanism which gave it some advantage over the block decoder. As a result, its performance deteriorates. At the same time, the block decoder, by accumulating higher energy levels though its block processing nature, makes it possible to provide more accurate decisions.

Based on the above results, it is quite difficult to predict the performance of the block decoder in the faded channel through accurate and reliable rules. We can say that for a fast faded process (large B_FT), decoders with large values of Z provide some improvement. However, as we move to lower B_FT products, the situation becomes unclear. For small B_FT products it seems that by increasing Z, the performance deteriorates. These comments are

[14]One more reason leading to this behaviour is the fact that the BPSK constellation has only two points, them being opposite to each other. Phase fluctuations generate only eye closure at the eye diagram but they do not introduce crosstalk between inphase and quadrature channels.

supported by Figs. 4.68 to 4.72 which correspond to QPSK. We see that while the $Z = 3$ block decoder performs better in slower fading channels (i.e. channels with smaller B_FT, see Fig. 4.68), the $Z = 8$ decoder performs better in fast faded ones (see Fig. 4.72). The rest of the decoders have a behaviour in the middle (for example the $Z = 5$ decoder performs better for $[K_r = 10\ dB,\ B_FT = 0.4]$ than $[K_r = 10\ dB,\ B_FT = 0.2]$ but performs the best for $[K_r = 10\ dB,\ B_FT = 0.1]$ (see Fig. 4.70). By observing these figures we can see a tendency of the block decoder to favour operation in faster faded channels as Z increases. However, these rules are very loose. There is a very strong (and non-linear) relation between Z and the parameters defining the fading channel (K_r, B_FT, fading model). Every case has to be looked independently if a decision for the choice of a system is to be made. The characteristics of the channel have a very strong effect on the performance especially for block decoders with large values of Z. For a different fading channel model we can see quite a change in the behaviour of the block decoder.

It was mentioned earlier that block decoders which process large blocks of received samples (Z large) seem to behave better in fast faded channels whereas their performance deteriorates as the bandwidth of the fading process is reduced (for example, compare the $Z = 6$ block decoder with BPSK in Figs. 4.51, 4.52 and the $Z = 8$ block decoder with QPSK in Figs. 4.57, 4.58). A heuristic explanation for this behaviour is the following. Reduction of the fading bandwidth makes the fading slower and increases the memory of the fading process. Since the block decoder is a sequence estimator, it is affected by the correlation properties of the channel impairments. Generally speaking, the more correlated the impairment is, the more degradation causes to the system. However, when the fading bandwidth increases, the fading becomes more and more uncorrelated and its memory is reduced (for large values of fading bandwidth, the diffused signal component appears as AWGN which corrupts the direct signal component). Without correlation in the fading process, the mechanism impairing the performance of the block decoder disappears and the performance of the block decoder bounces back to lower error rates.

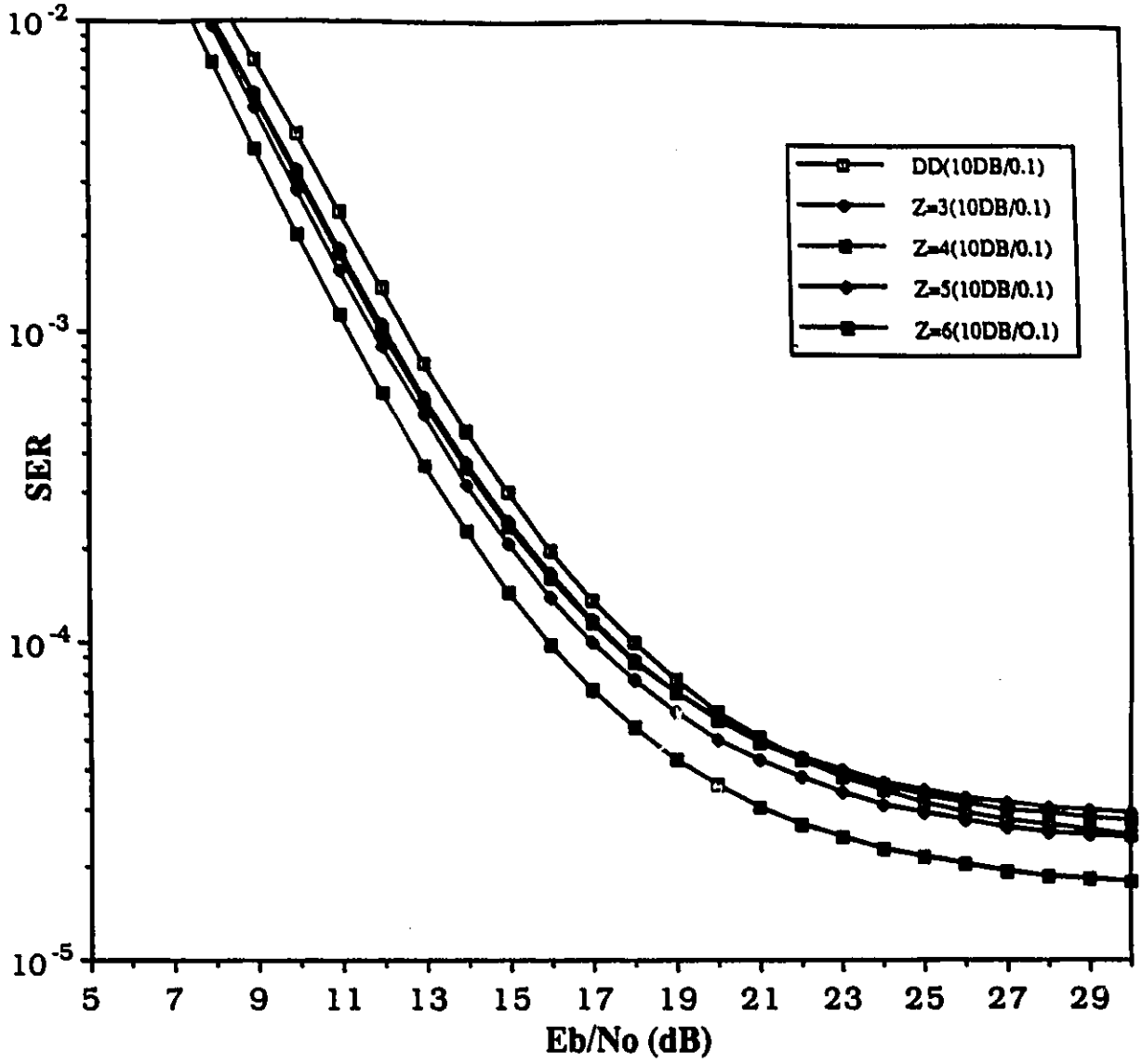

Figure 4.50: SER performance curves of non-coherently detected BPSK in a Rician faded channel with $K_r = 10\ dB$ and $B_F T = 0.1$. The displayed curves for the block decoder are based on the upper union bound.

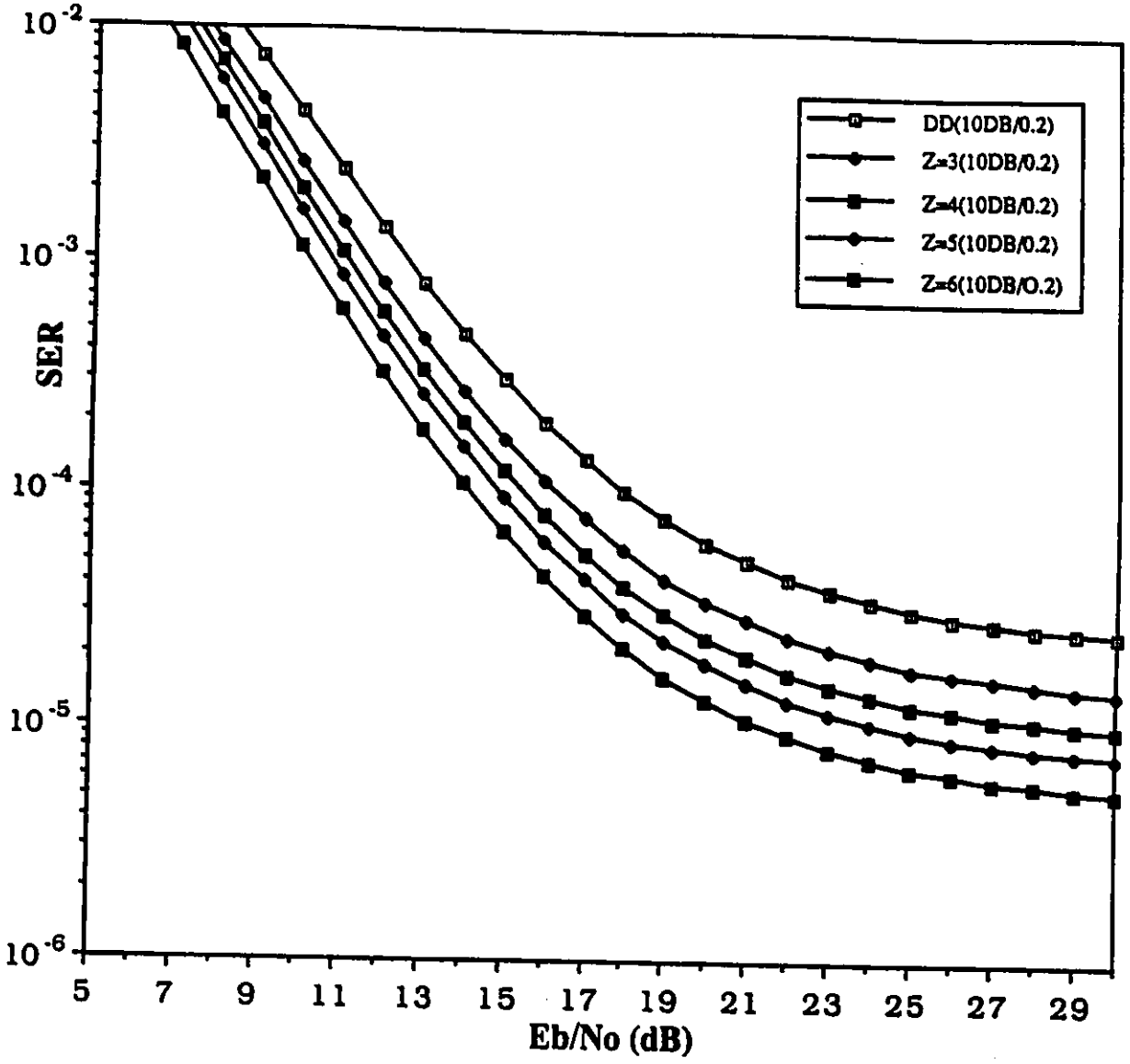

Figure 4.51: SER performance curves of non-coherently detected BPSK in a Rician faded channel with $K_r = 10\ dB$ and $B_F T = 0.2$. The displayed curves correspond to the upper union bound.

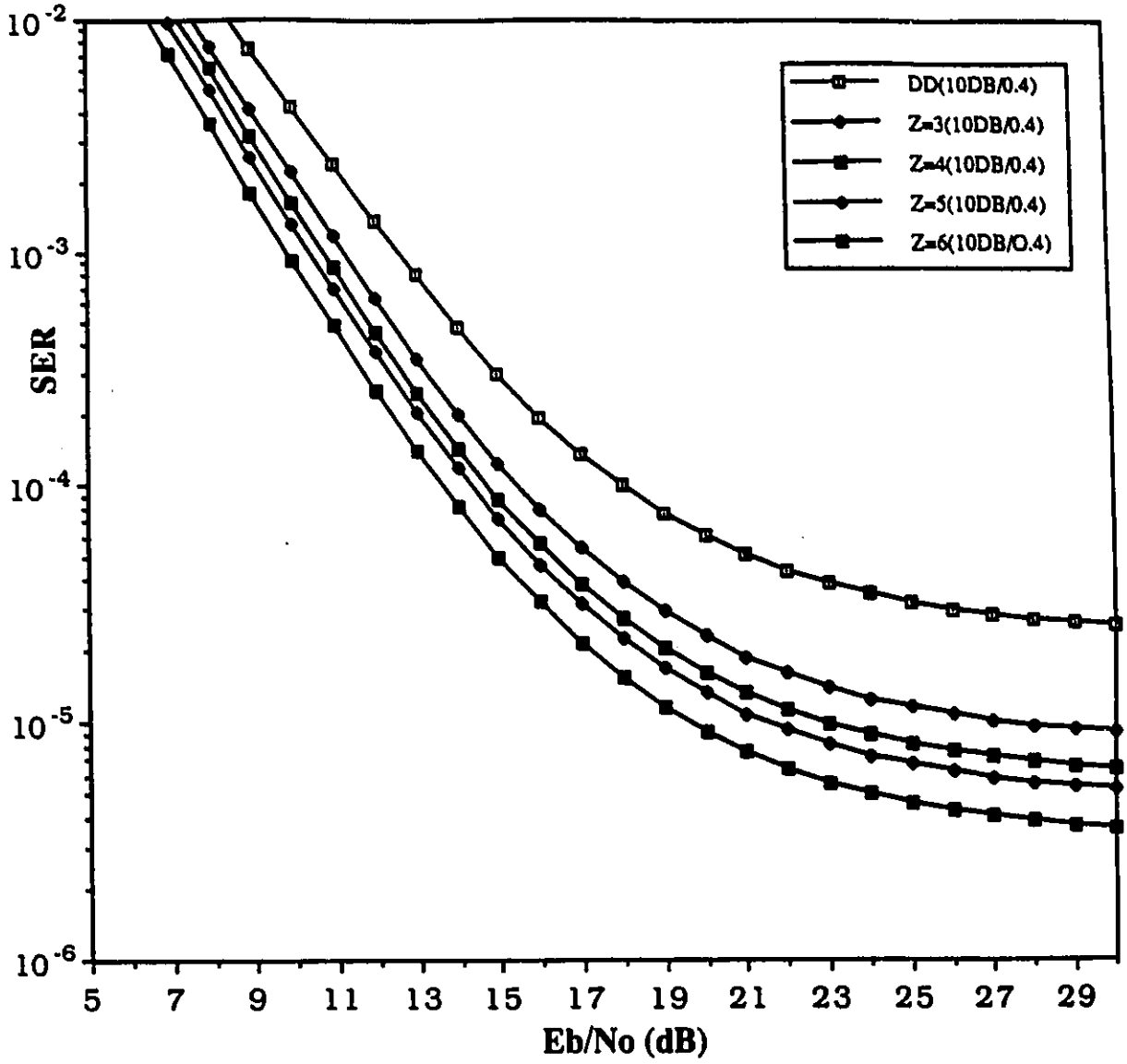

Figure 4.52: SER performance curves of non-coherently detected BPSK in a Rician faded channel with $K_r = 10\ dB$ and $B_F T = 0.4$. The displayed curves for the block decoder are based on the upper union bound.

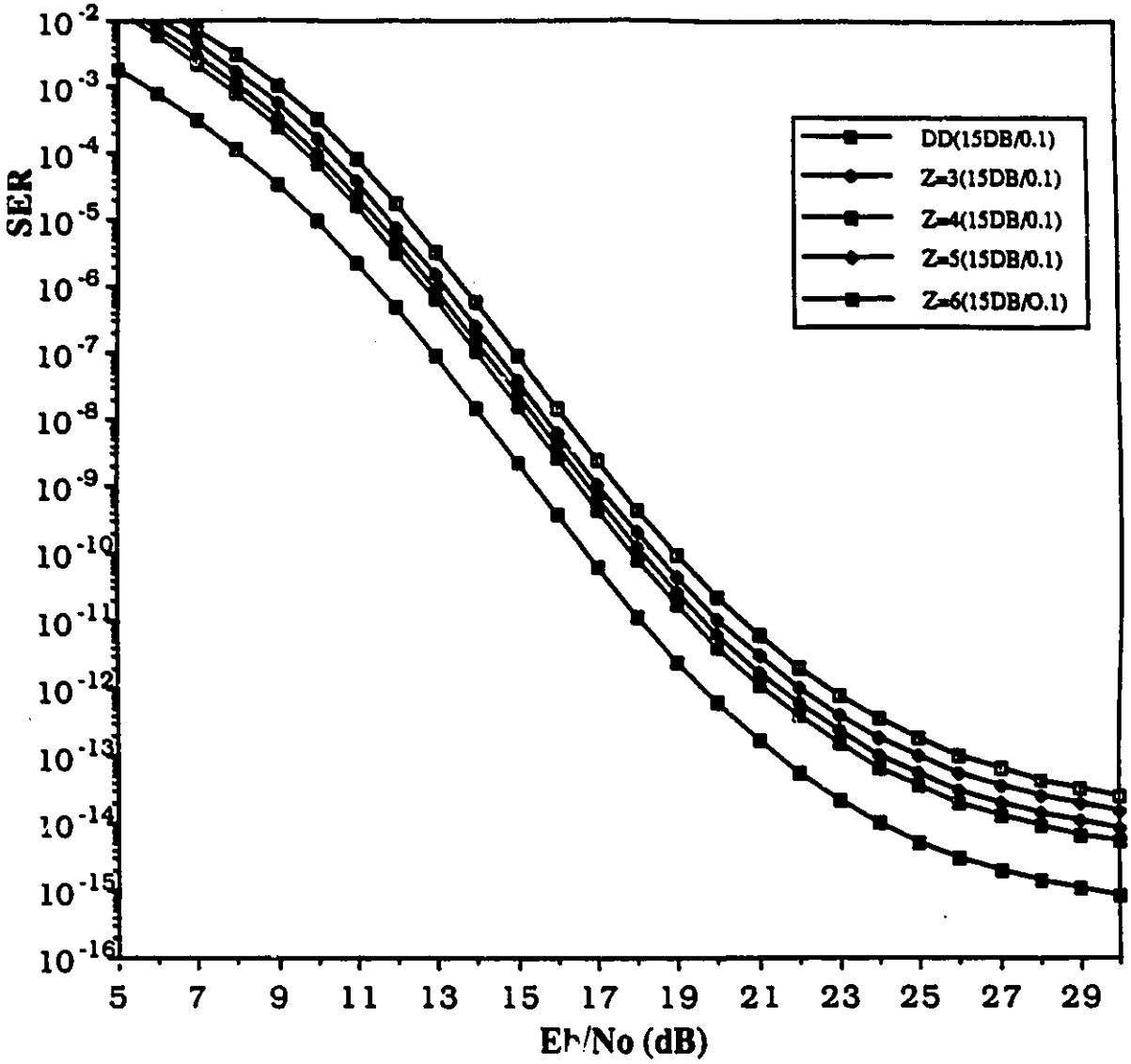

Figure 4.53: SER performance curves of non-coherently detected BPSK in a Rician faded channel with $K_r = 15\ dB$ and $B_F T = 0.1$. The displayed curves for the block decoder are based on the upper union bound.

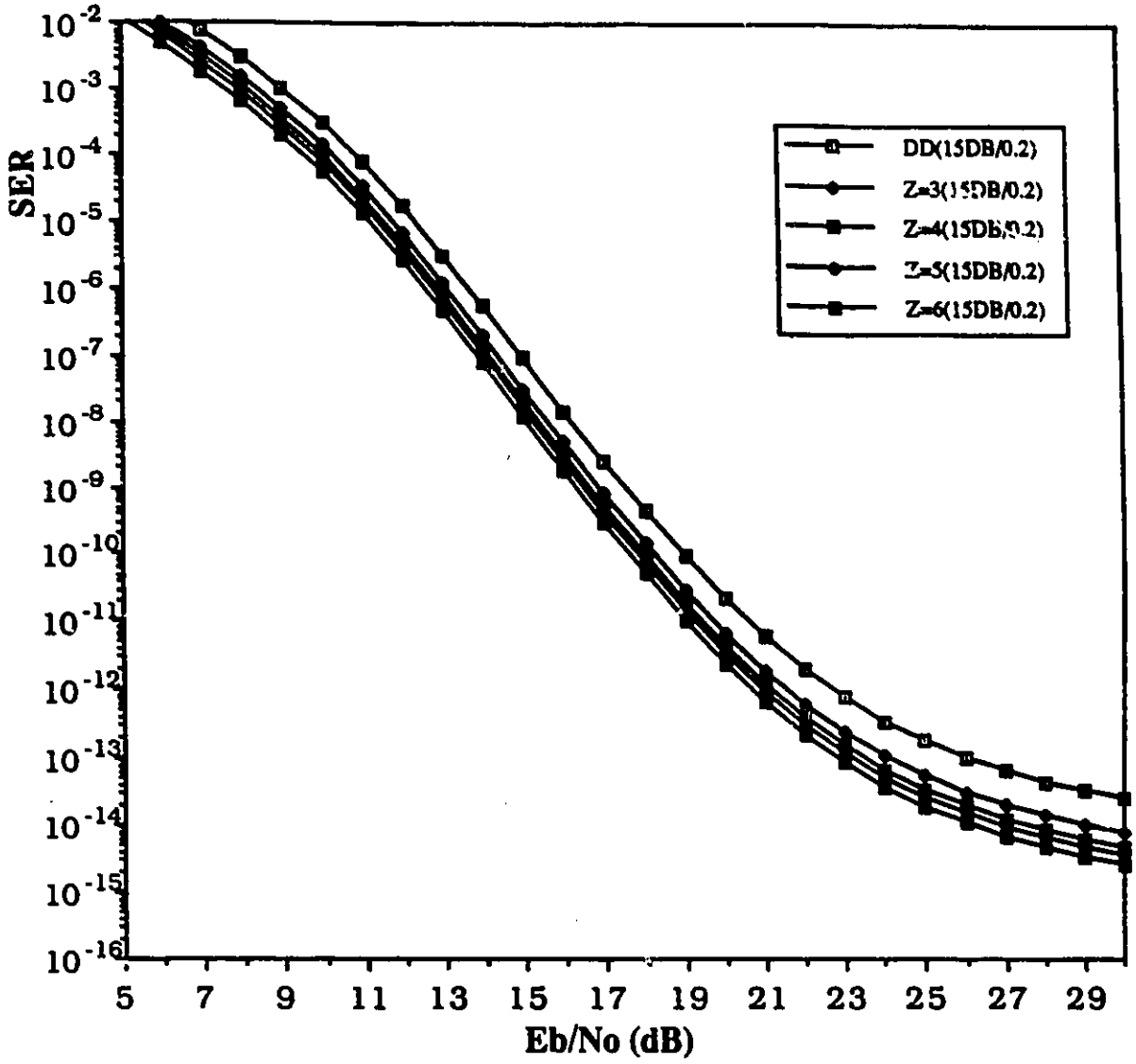

Figure 4.54: SER performance curves of non-coherently detected BPSK in a Rician faded channel with $K_r = 15\ dB$ and $B_F T = 0.2$. The displayed curves for the block decoder are based on the upper union bound.

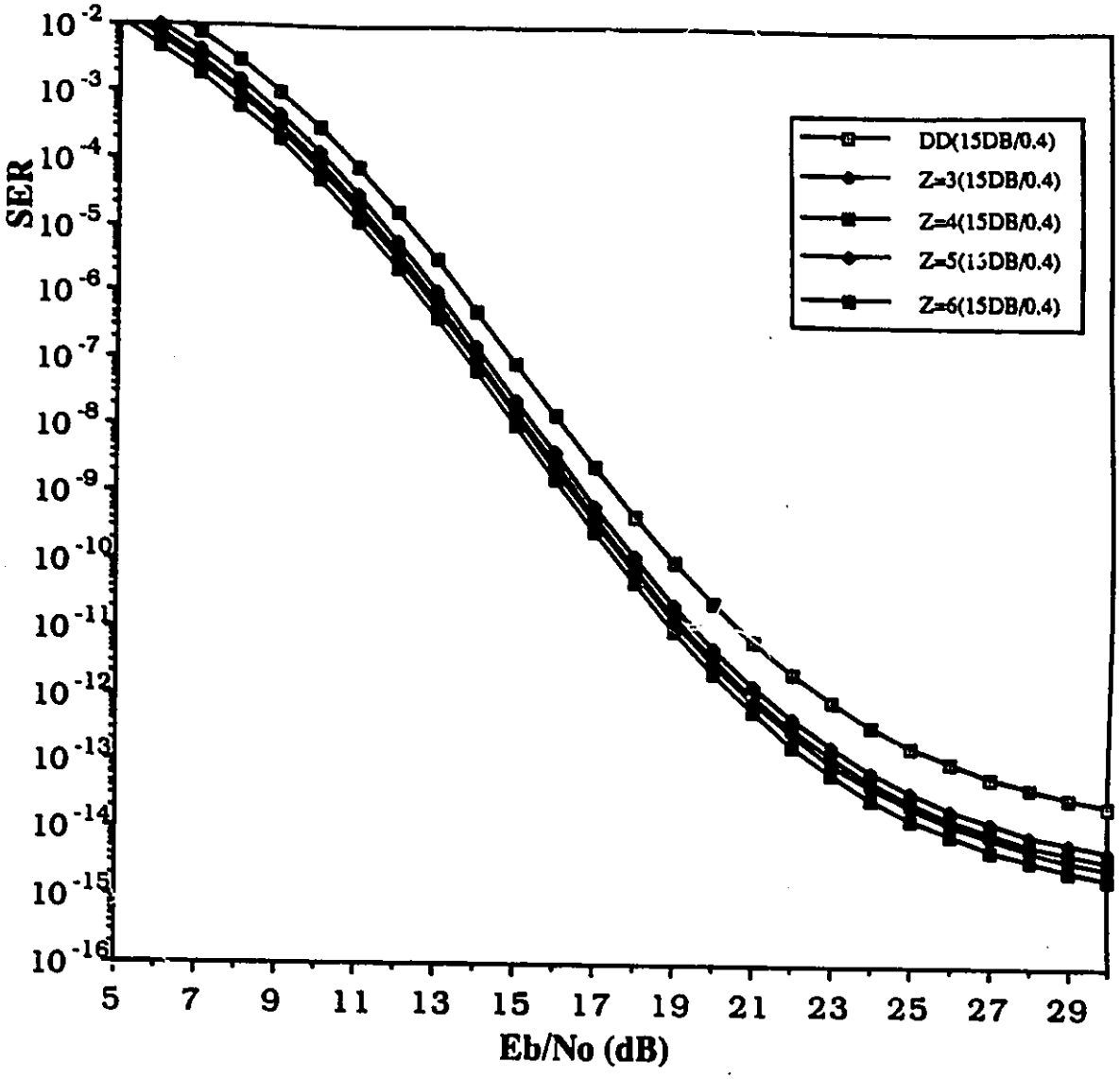

Figure 4.55: SER performance curves of non-coherently detected BPSK in a Rician faded channel with $K_r = 15\ dB$ and $B_F T = 0.4$. The displayed curves for the block decoder are based on the upper union bound.

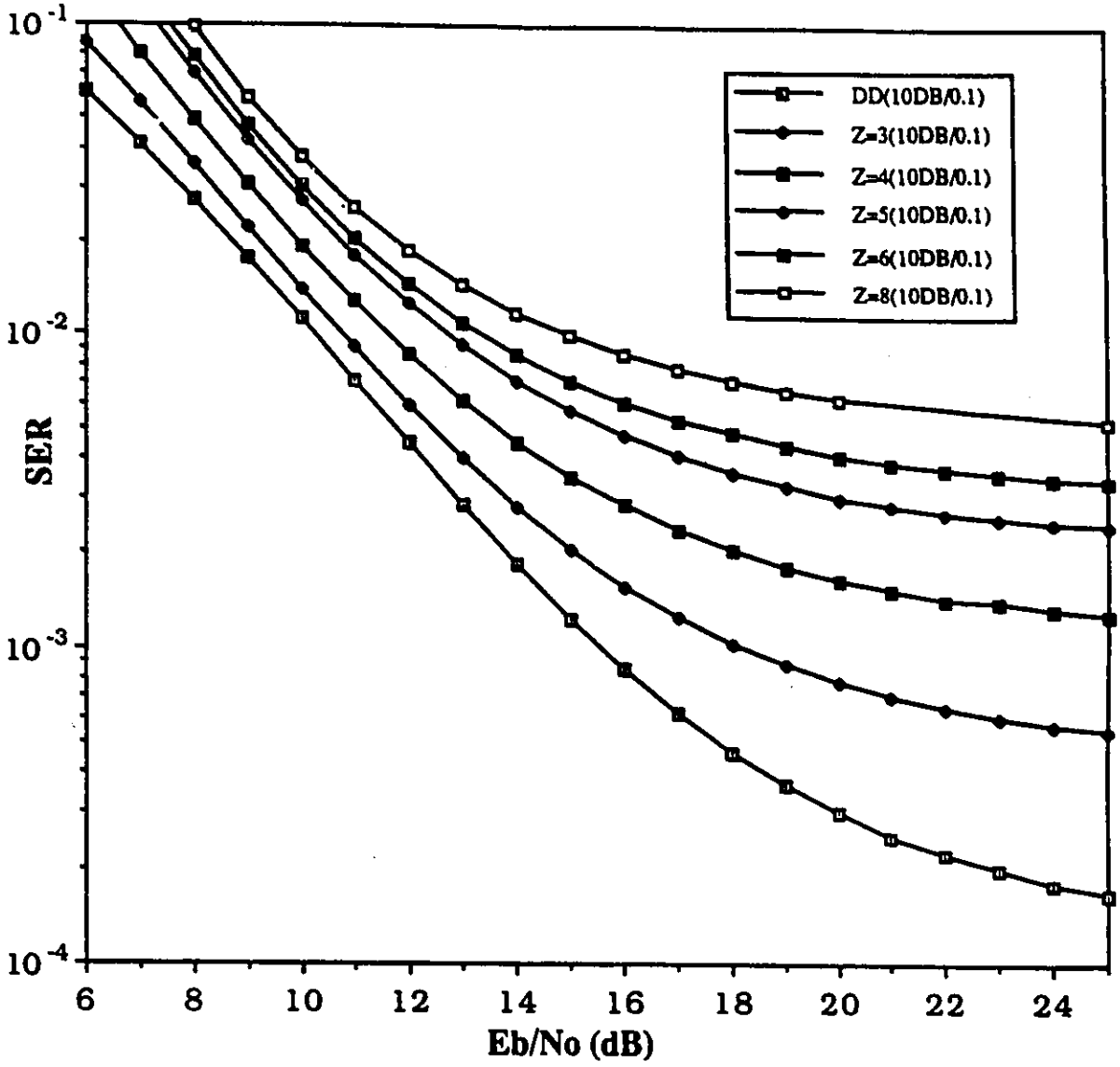

Figure 4.56: SER performance curves of non-coherently detected QPSK in a Rician faded channel with $K_r = 10\ dB$ and $B_F T = 0.1$. The displayed curves for the block decoder are based on the upper union bound.

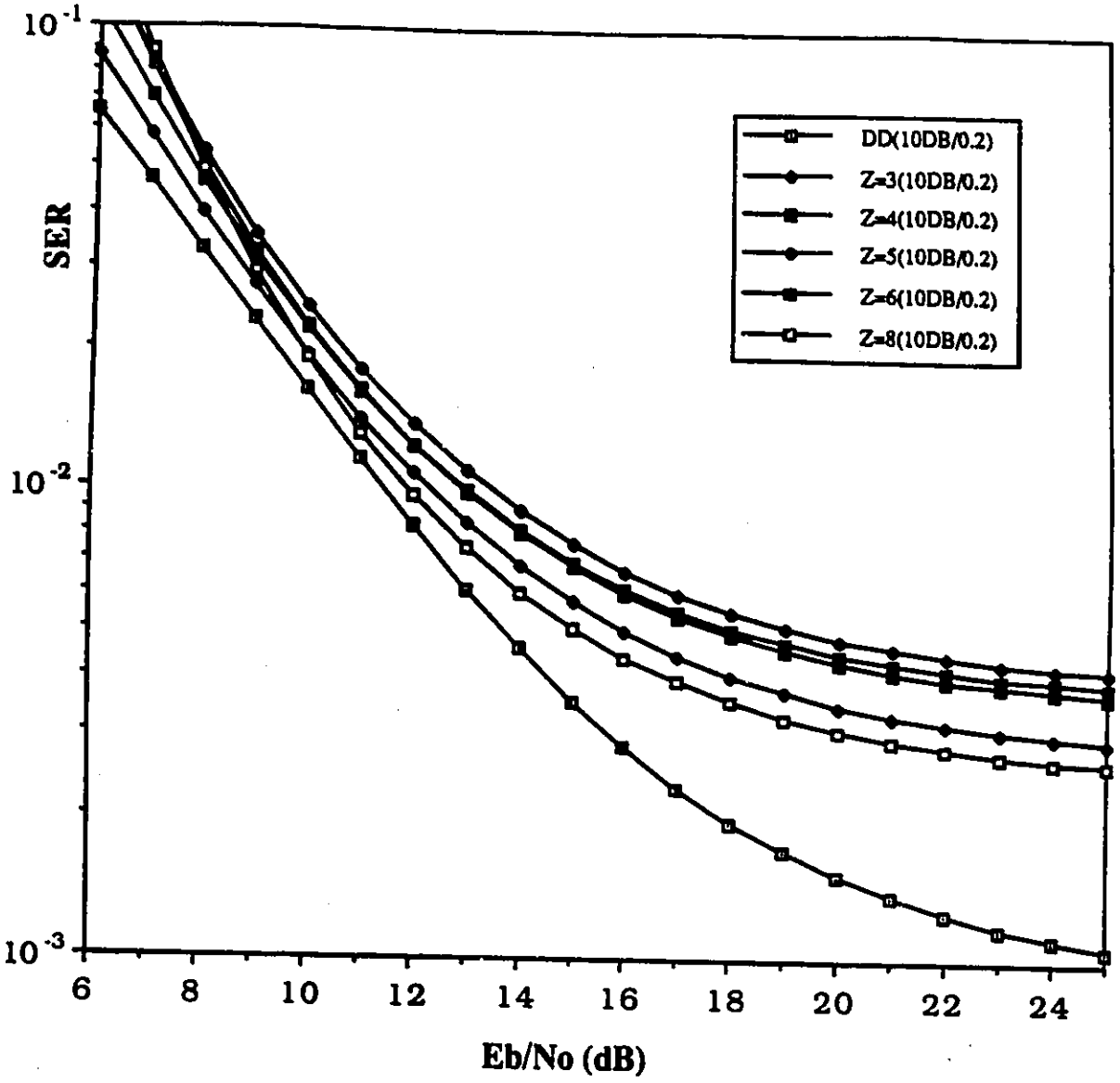

Figure 4.57: SER performance curves of non-coherently detected QPSK in a Rician faded channel with $K_r = 10\ dB$ and $B_F T = 0.2$. The displayed curves for the block decoder are based on the upper union bound.

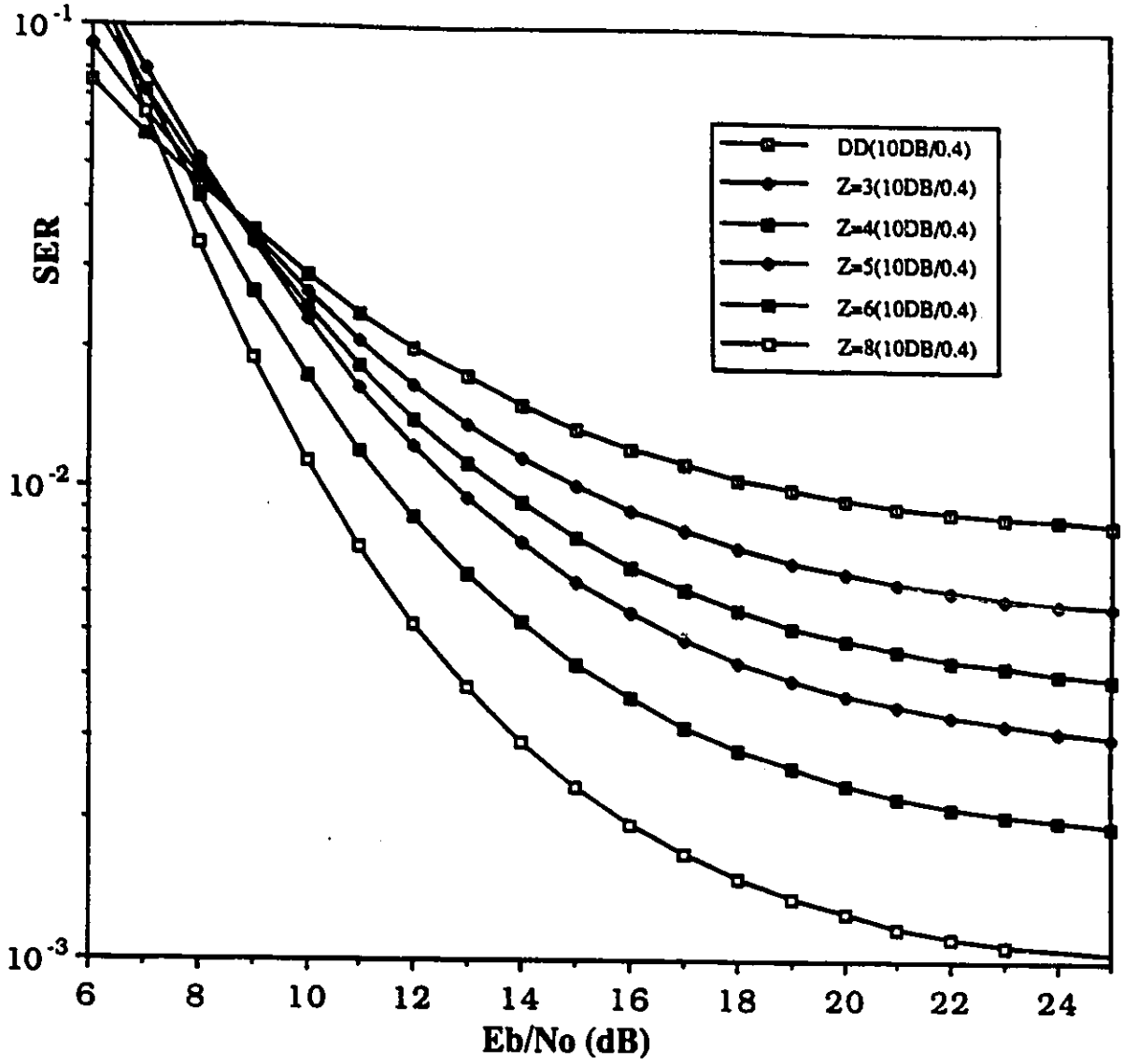

Figure 4.58: SER performance curves of non-coherently detected QPSK in a Rician faded channel with $K_r = 10\ dB$ and $B_F T = 0.4$. The displayed curves for the block decoder are based on the upper union bound.

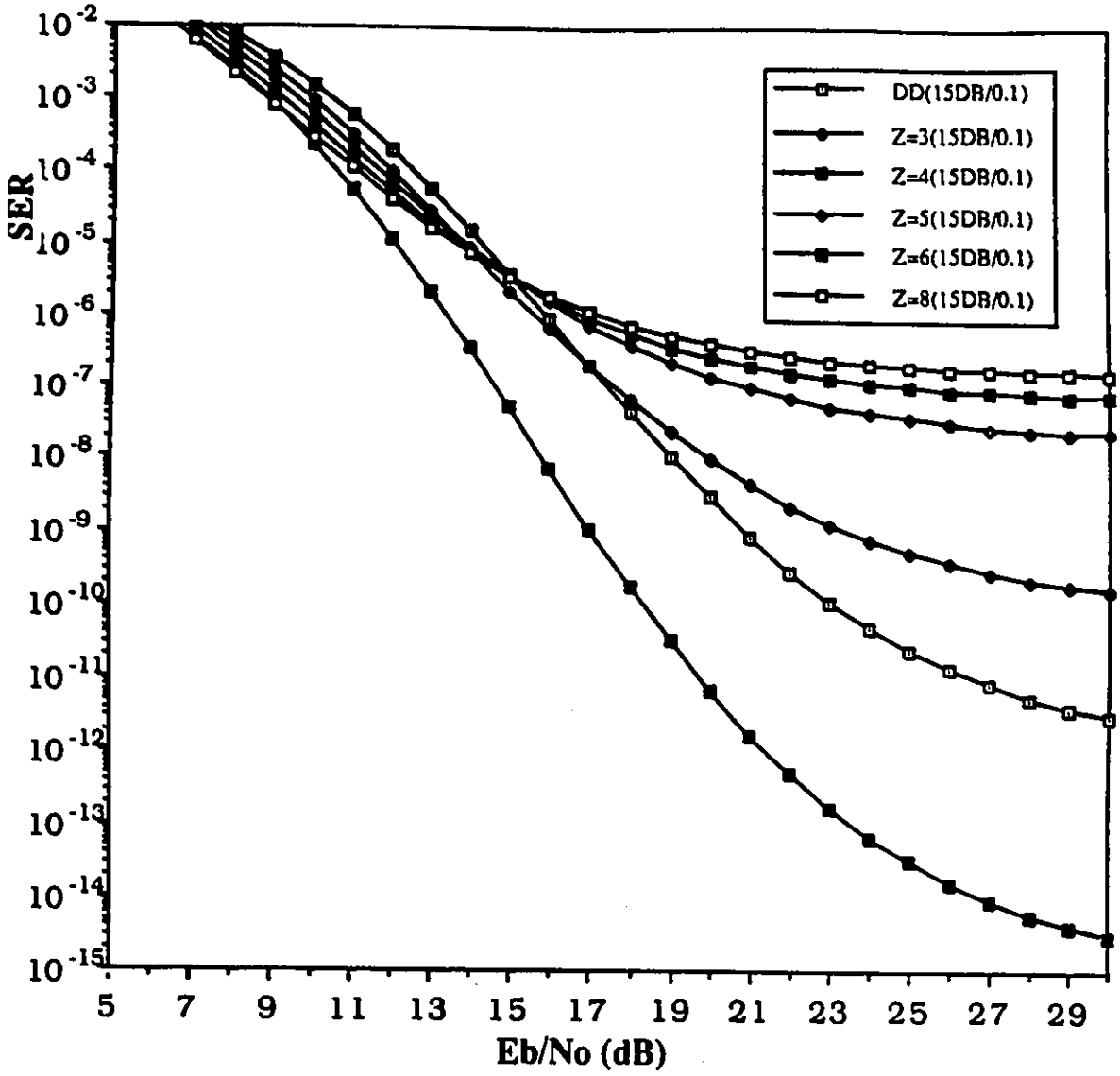

Figure 4.59: SER performance curves of non-coherently detected QPSK in a Rician faded channel with $K_r = 15\ dB$ and $B_F T = 0.1$. The displayed curves for the block decoder are based on the upper union bound.

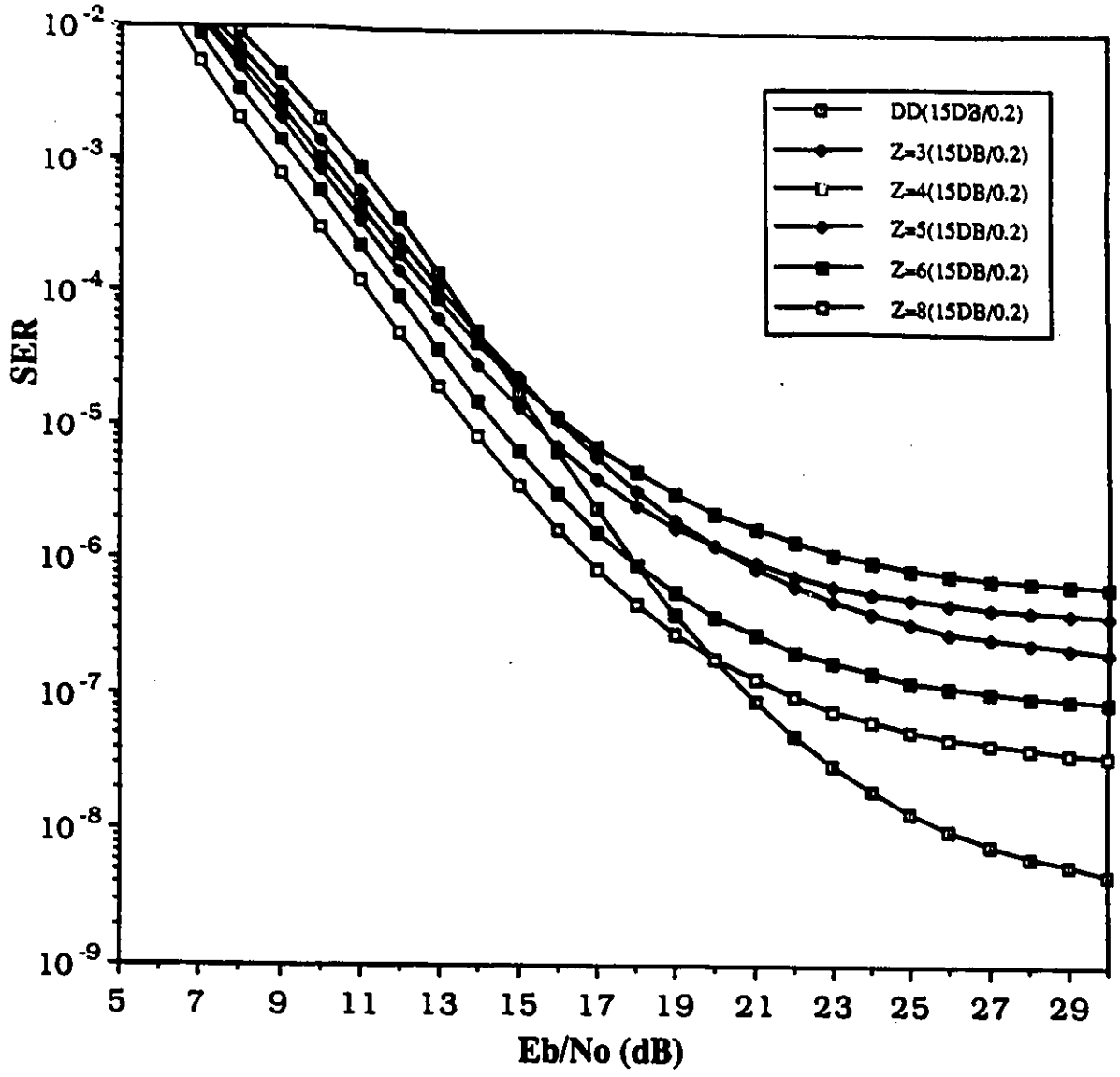

Figure 4.60: SER performance curves of non-coherently detected QPSK in a Rician faded channel with $K_r = 15\ dB$ and $B_F T = 0.2$. The displayed curves for the block decoder are based on the upper union bound.

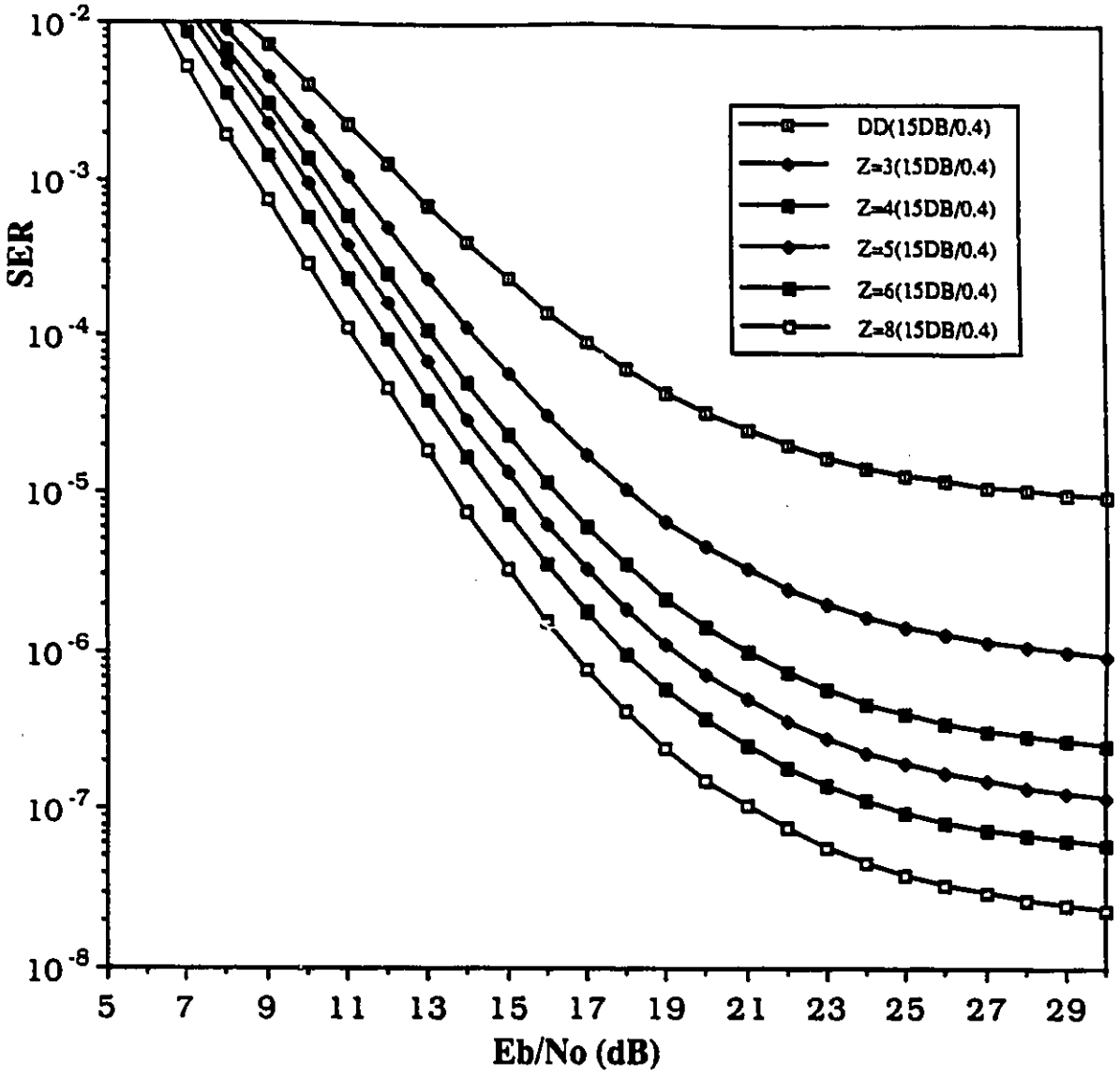

Figure 4.61: SER performance curves of non-coherently detected QPSK in a Rician faded channel with $K_r = 15\ dB$ and $B_F T = 0.4$. The displayed curves for the block decoder are based on the upper union bound.

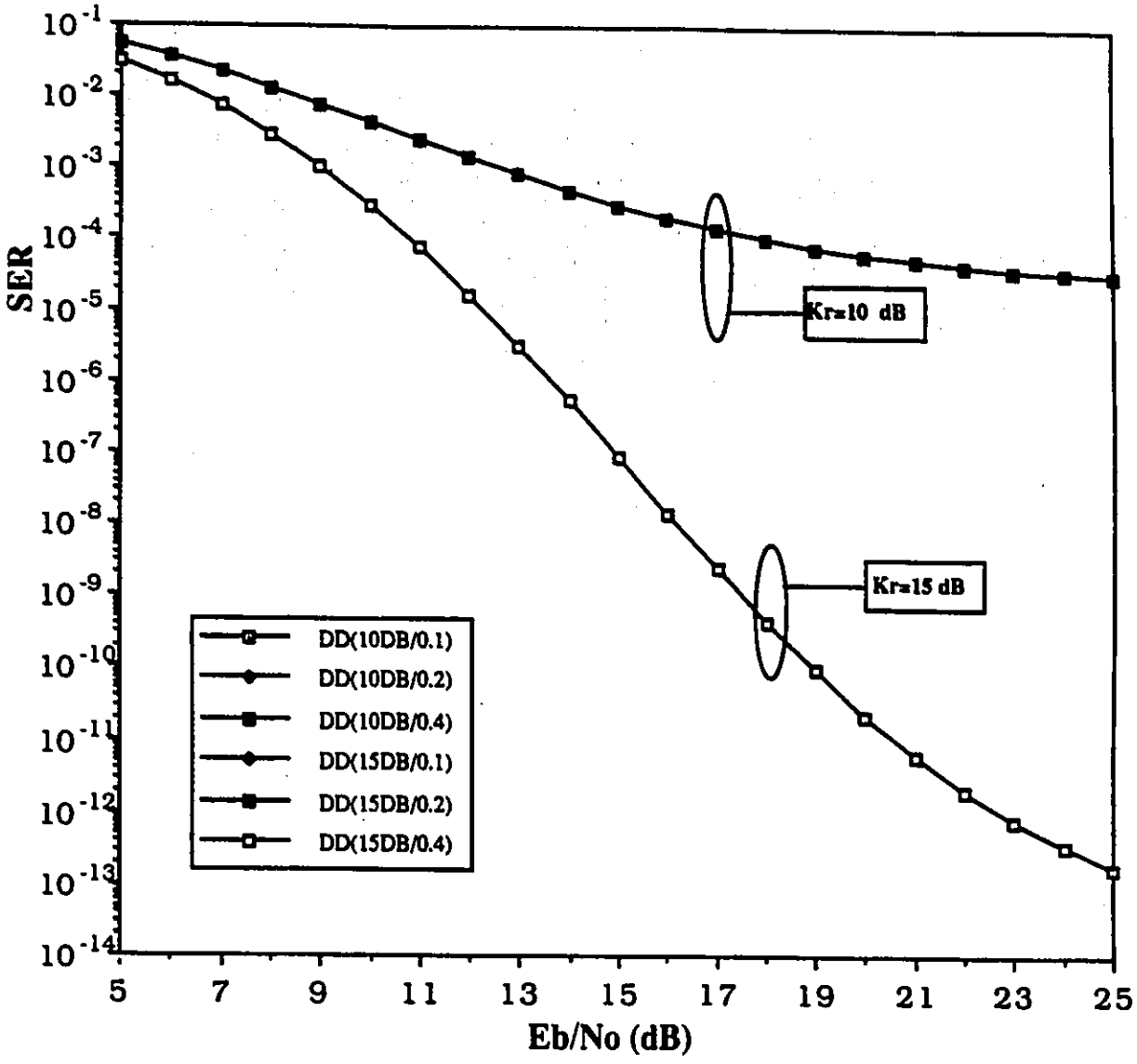

Figure 4.62: SER performance curves of the differential detector (DD) for a BPSK signal in Rician faded channels with $K_r = 10\ dB, 15\ dB$ and $B_F T = 0.1, 0.2, 0.4$.

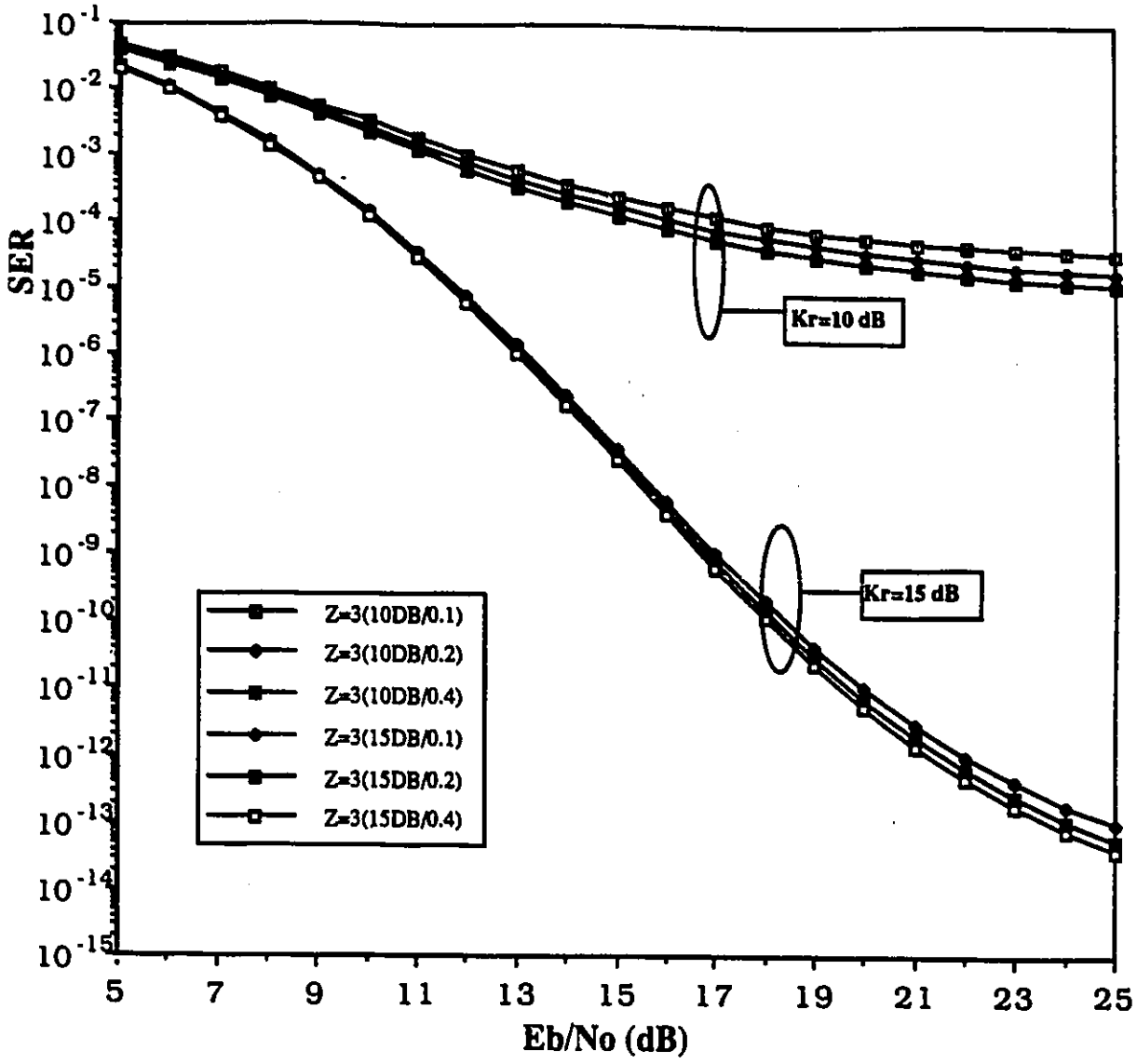

Figure 4.63: SER performance curves of the block decoder (BD) with Z=3 for a BPSK signal in Rician faded channels with $K_r = 10\ dB, 15\ dB$ and $B_F T = 0.1, 0.2, 0.4$. The displayed curves correspond to the upper union bound.

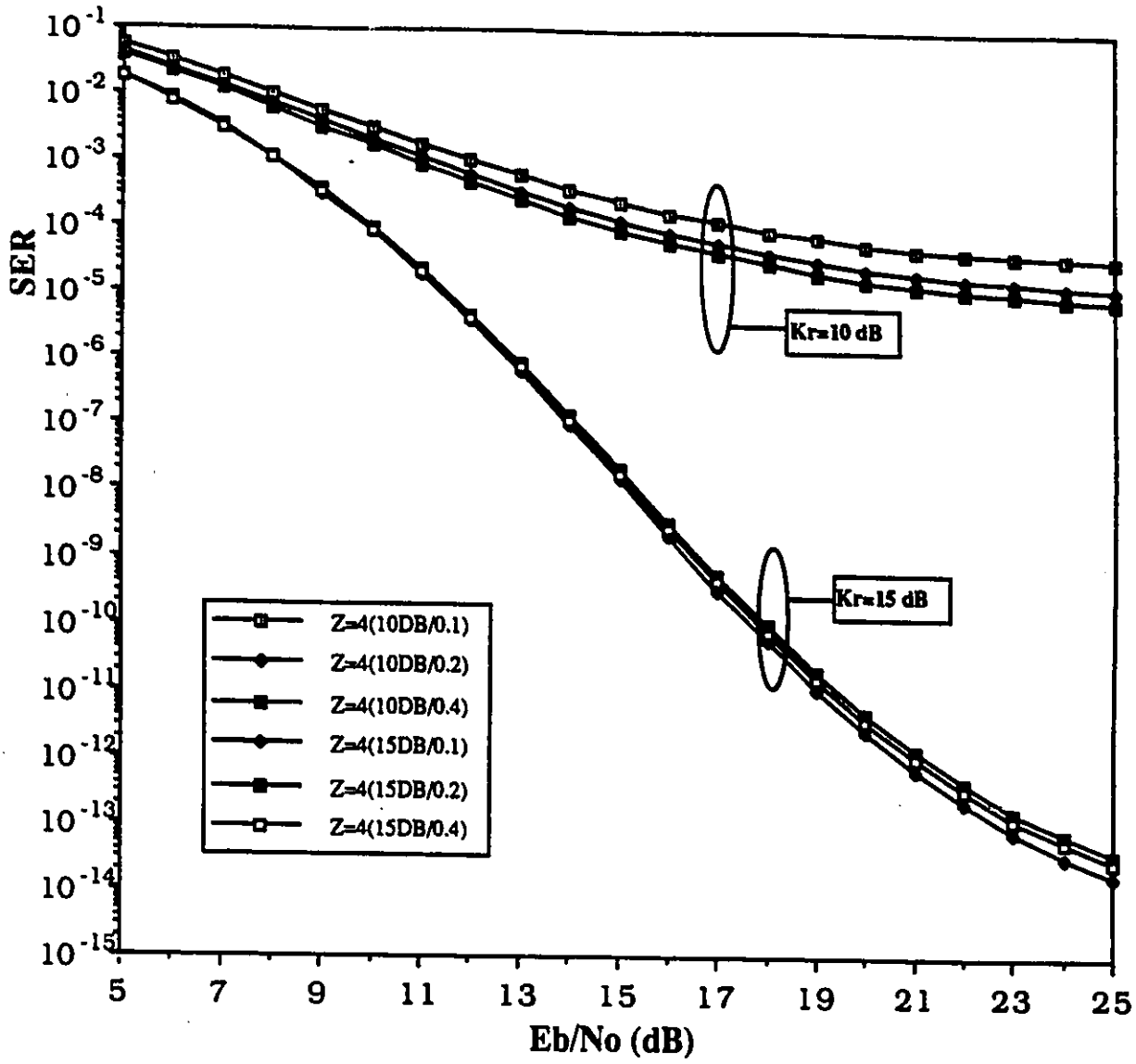

Figure 4.64: SER performance curves of the block decoder (BD) with Z=4 for a BPSK signal in Rician faded channels with $K_r = 10\ dB, 15\ dB$ and $B_F T = 0.1, 0.2, 0.4$. The displayed curves correspond to the upper union bound.

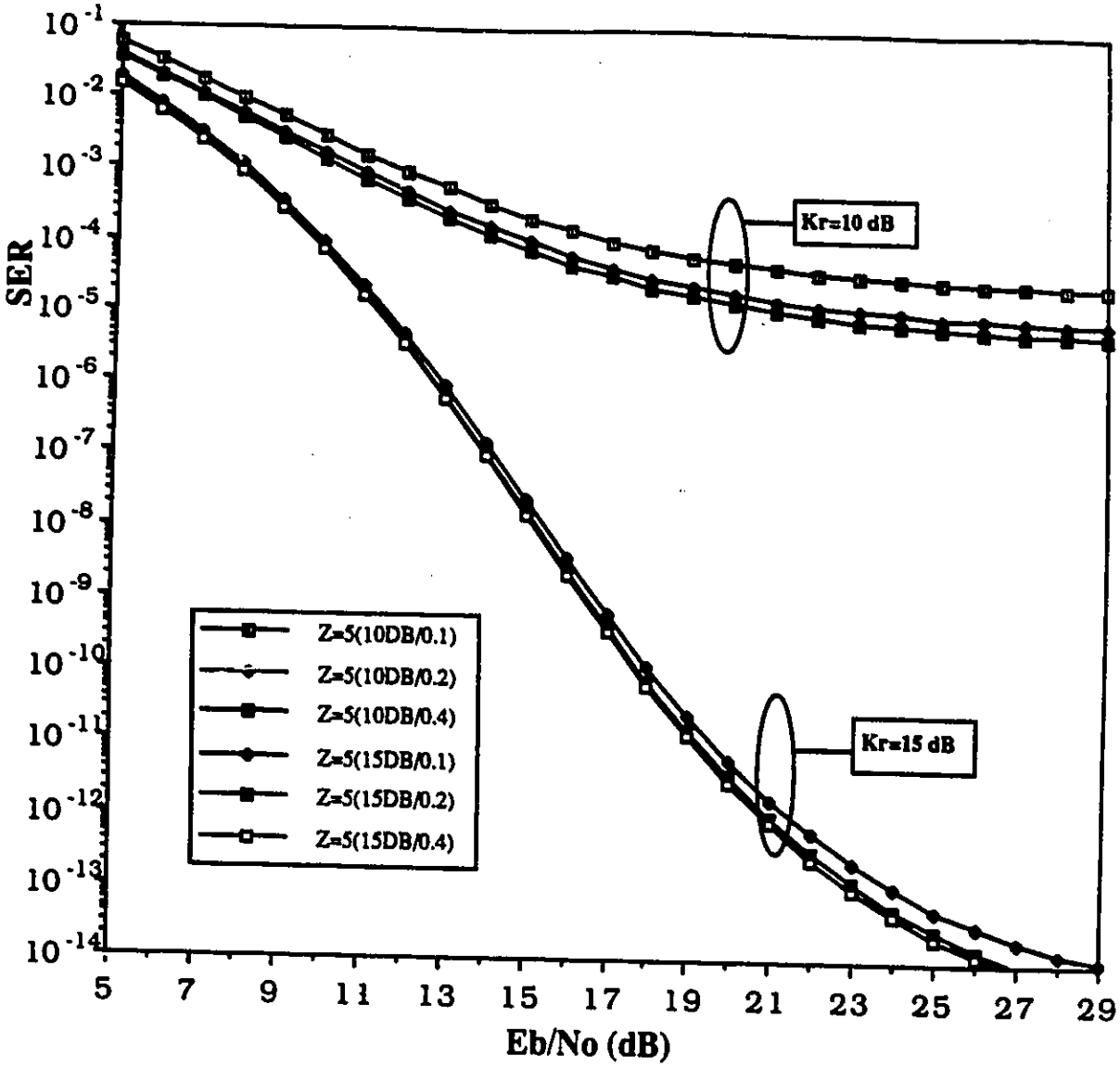

Figure 4.65: SER performance curves of the block decoder (BD) with Z=5 for a BPSK signal in Rician faded channels with $K_r = 10\ dB, 15\ dB$ and $B_F T = 0.1, 0.2, 0.4$. The displayed curves correspond to the upper union bound.

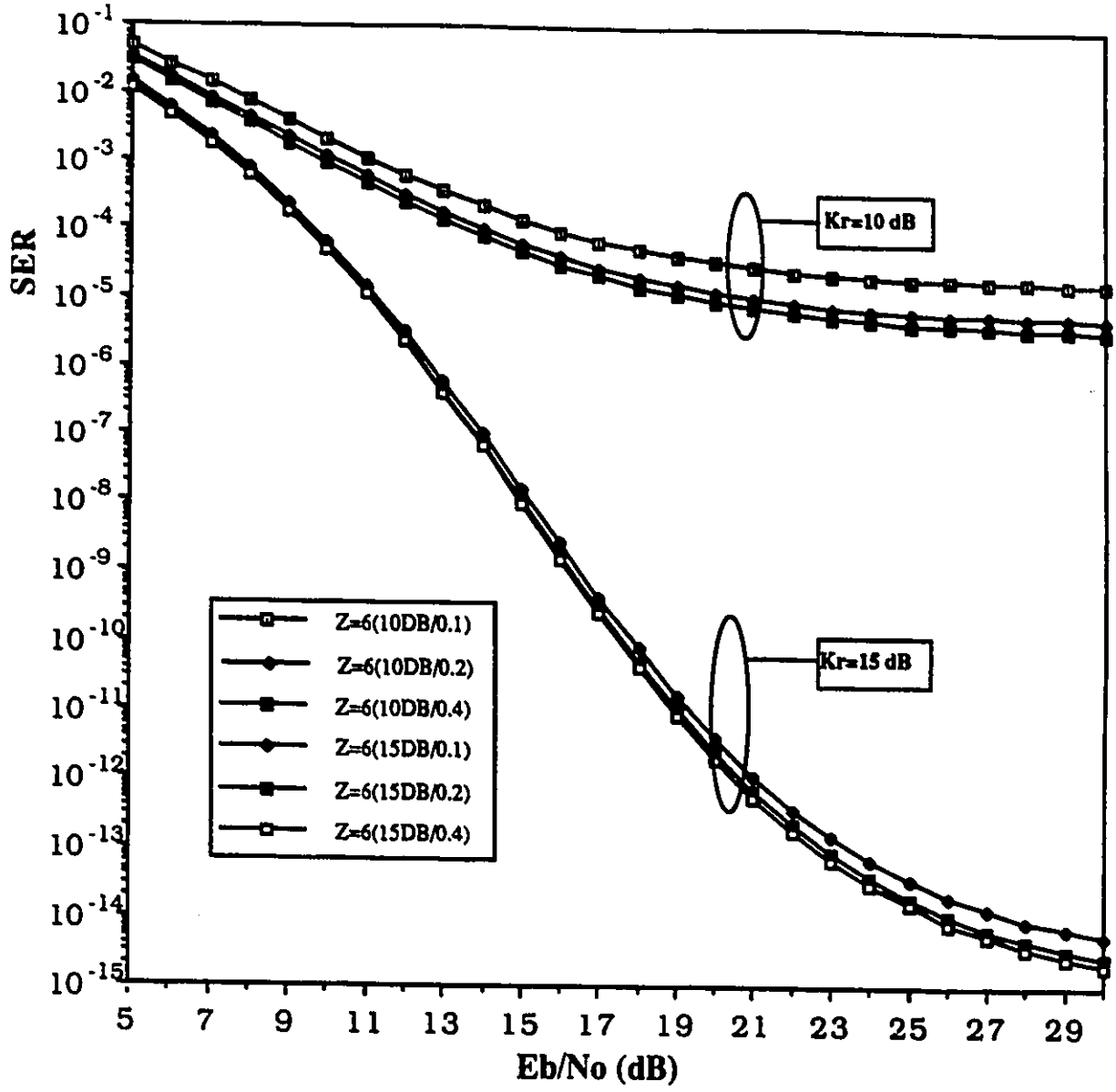

Figure 4.66: SER performance curves of the block decoder (BD) with Z=6 for a BPSK signal in Rician faded channels with $K_r = 10\ dB, 15\ dB$ and $B_F T = 0.1, 0.2, 0.4$. The displayed curves correspond to the upper union bound.

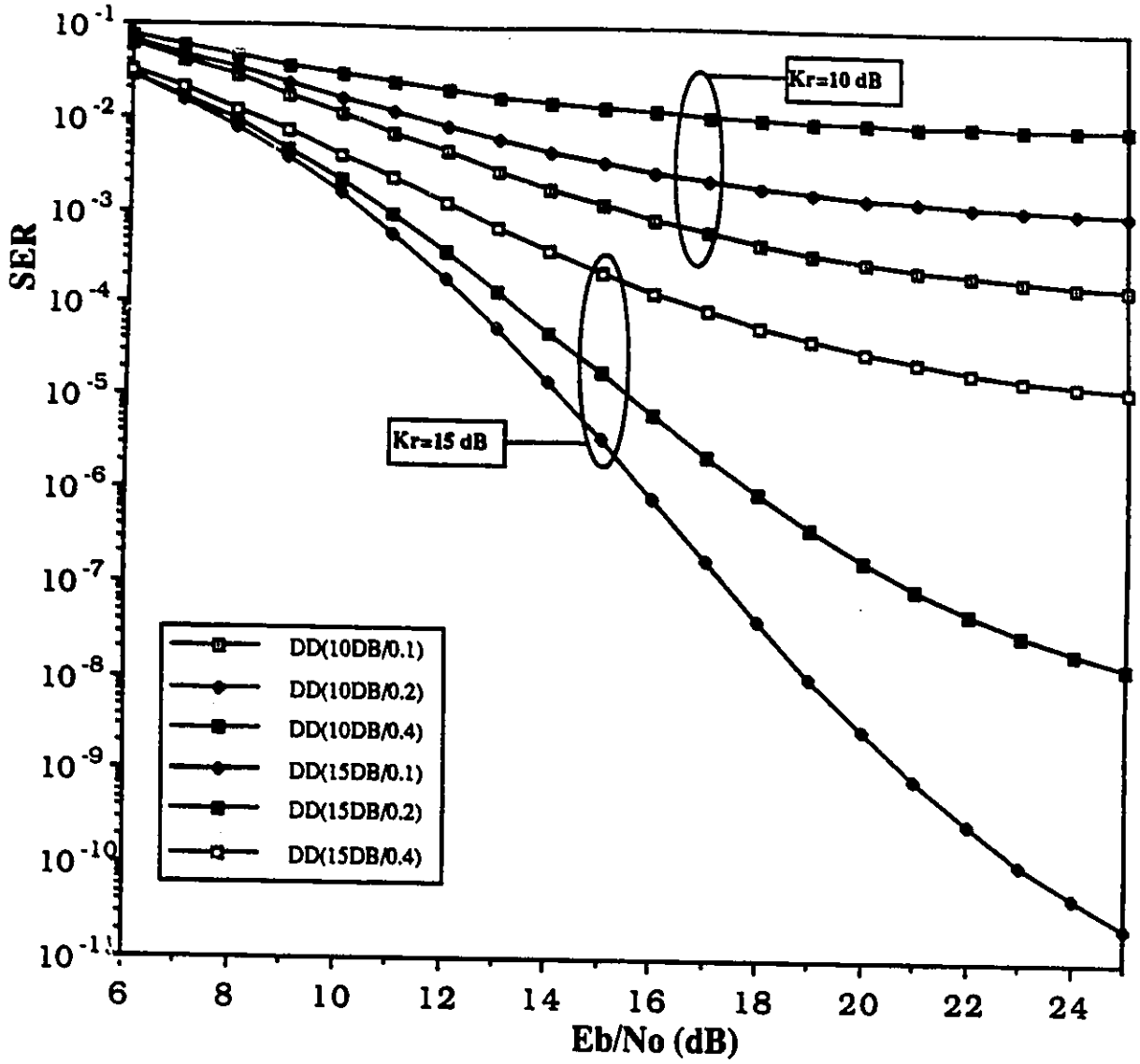

Figure 4.67: SER performance curves of the differential detector (DD) for a QPSK signal in Rician faded channels with $K_r = 10\ dB, 15\ dB$ and $B_F T = 0.1, 0.2, 0.4$.

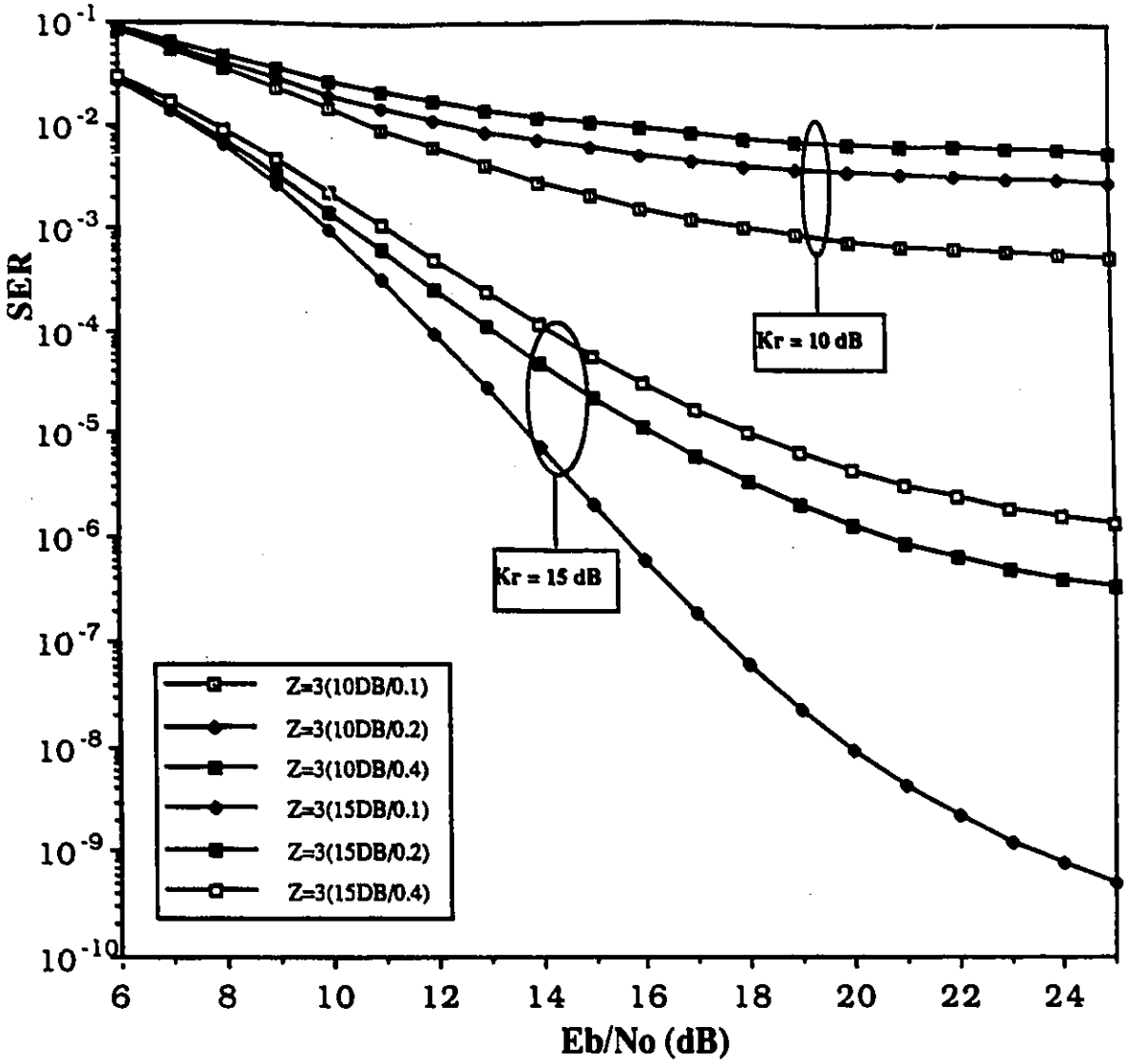

Figure 4.68: SER performance curves of the block decoder (BD) with Z=3 for a QPSK signal in Rician faded channels with $K_r = 10\ dB, 15\ dB$ and $B_F T = 0.1, 0.2, 0.4$. The displayed curves correspond to the upper union bound.

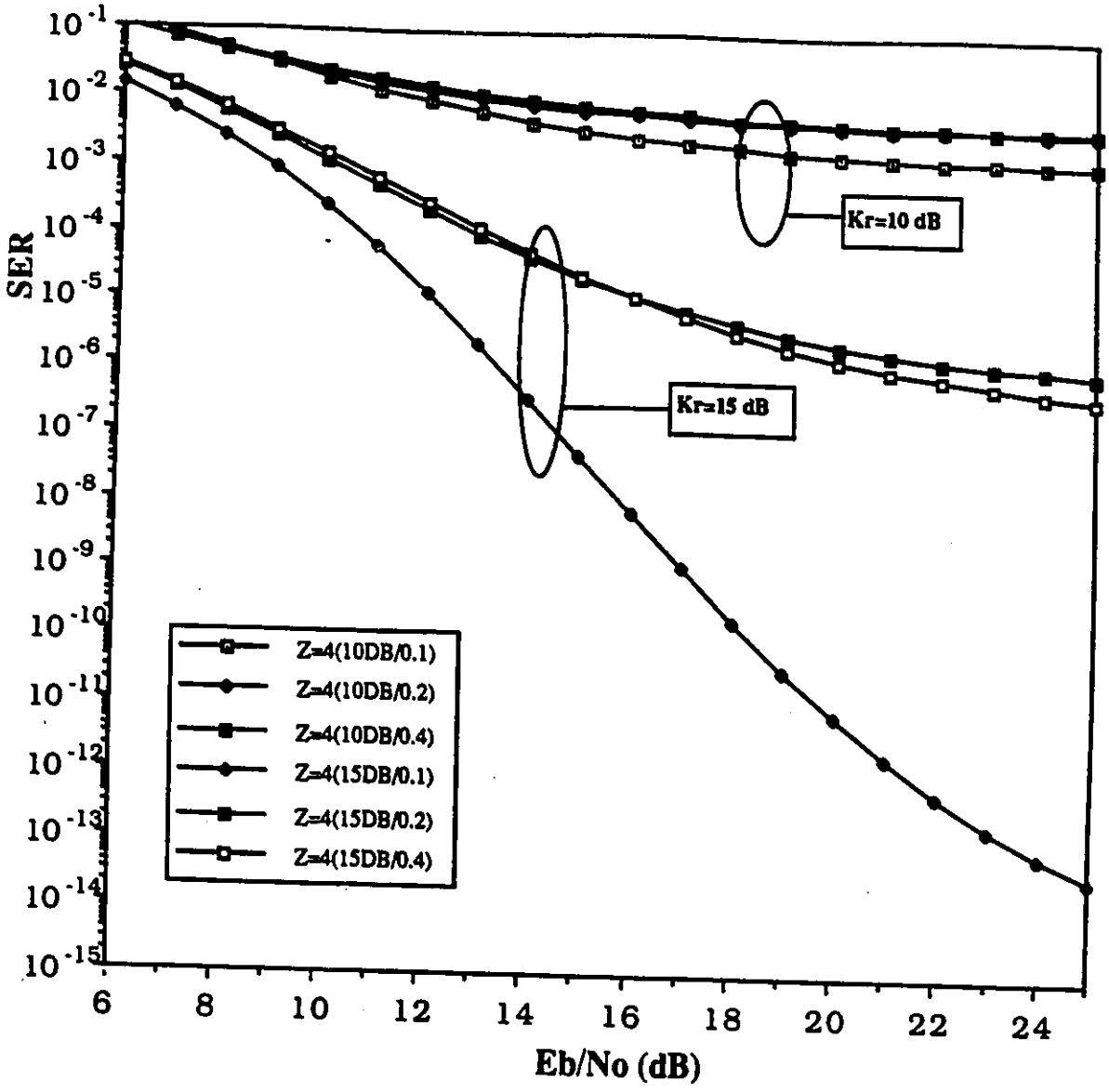

Figure 4.69: SER performance curves of the block decoder (BD) with Z=4 for a QPSK signal in Rician faded channels with $K_r = 10\ dB, 15\ dB$ and $B_F T = 0.1, 0.2, 0.4$. The displayed curves correspond to the upper union bound.

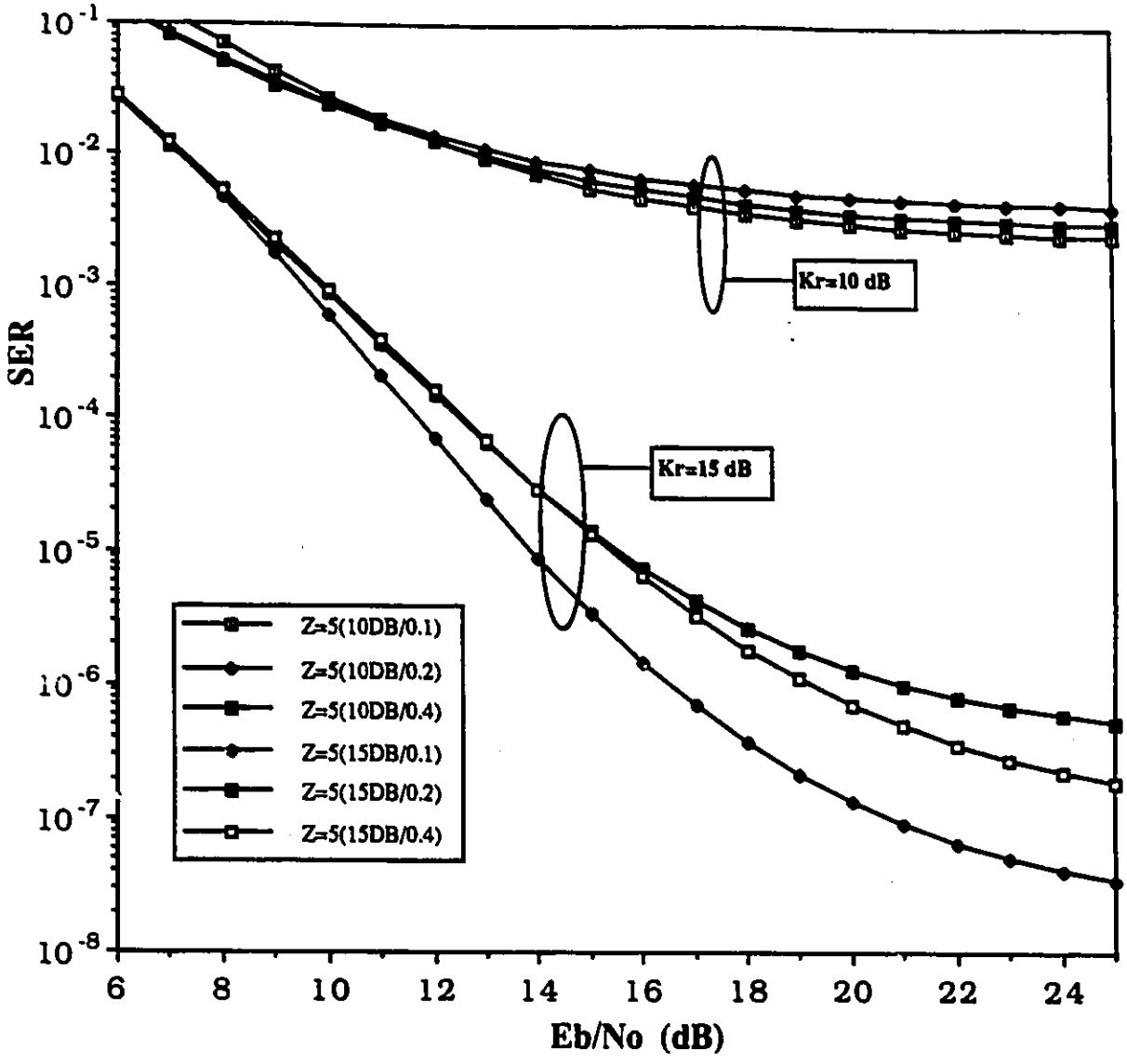

Figure 4.70: SER performance curves of the block decoder (BD) with Z=5 for a QPSK signal in Rician faded channels with $K_r = 10\ dB, 15\ dB$ and $B_F T = 0.1, 0.2, 0.4$. The displayed curves correspond to the upper union bound.

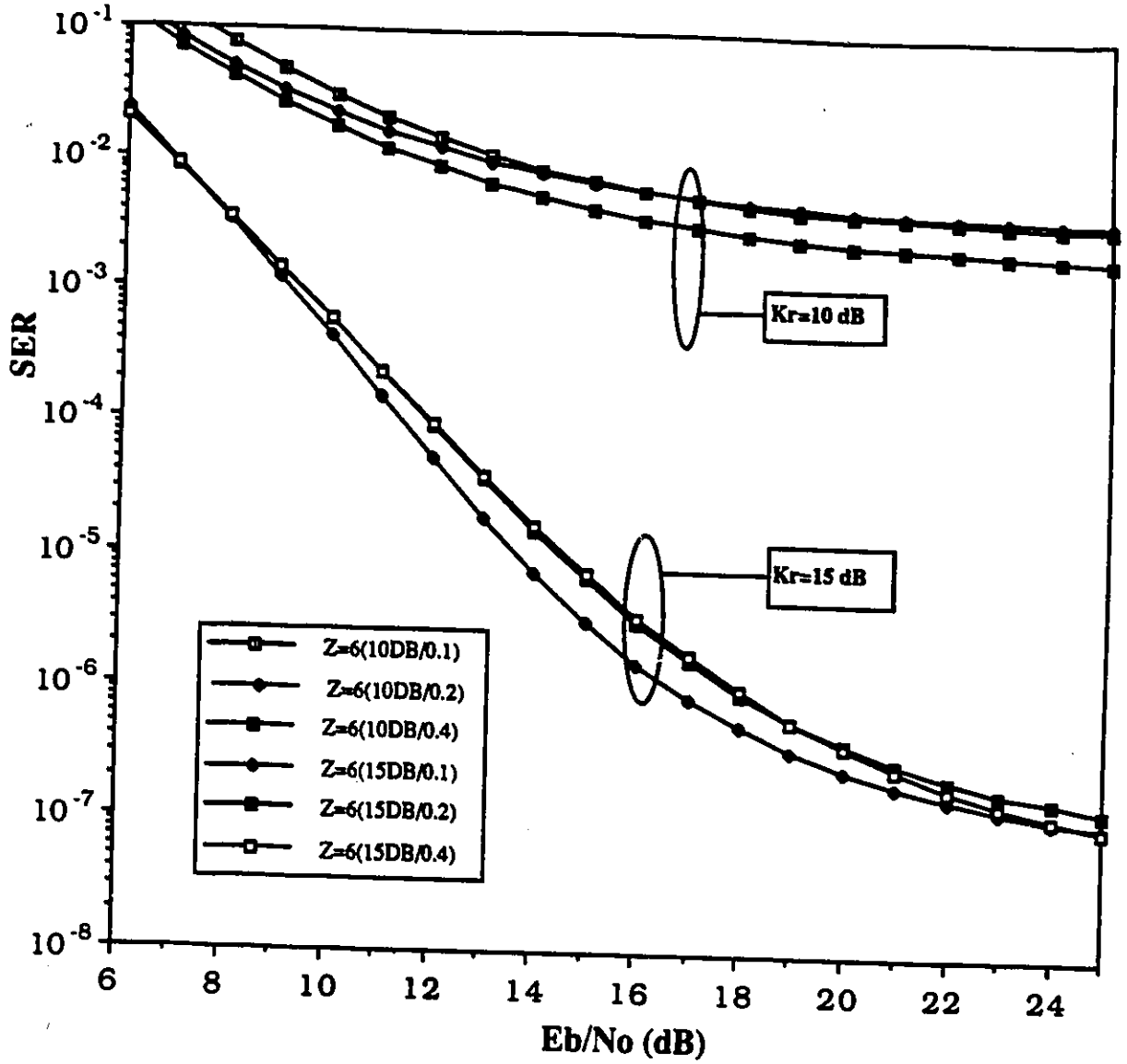

Figure 4.71: SER performance curves of the block decoder (BD) with Z=6 for a QPSK signal in Rician faded channels with $K_r = 10\ dB, 15\ dB$ and $B_F T = 0.1, 0.2, 0.4$. The displayed curves correspond to the upper union bound.

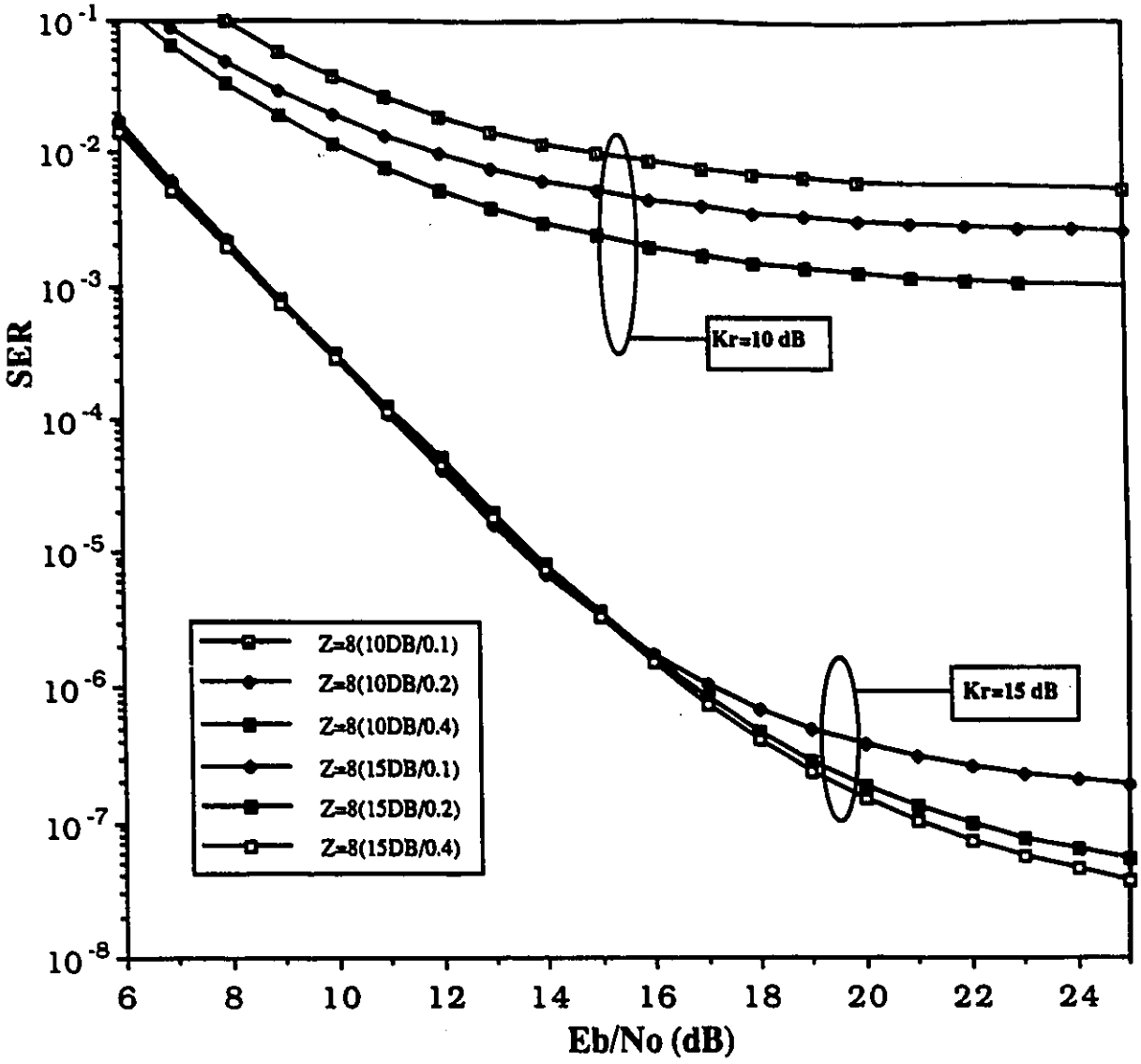

Figure 4.72: SER performance curves of the block decoder (BD) with Z=8 for a QPSK signal in Rician faded channels with $K_r = 10\ dB, 15\ dB$ and $B_F T = 0.1, 0.2, 0.4$. The displayed curves correspond to the upper union bound.

Study Based on the Upper/Lower Union Bounds and on Simulations

Up to this point, we have presented the analysis and studied the behaviour of the block decoder based on results of the upper union bound. However, in section 4.8.2, we have mentioned that for slowly faded channels, the upper union bound might be giving quite pessimistic results for the performance of the block decoder. Even though the Rician faded channels examined in this section are much faster compared to the static Rayleigh channel which we dealt in the previous subsection, they might still be slow enough that the lower union bound could provide results closer to the actual system's performance. For example, the $B_FT = 0.1$ channel has a correlation between the fading terms corrupting adjacent signal samples equal to 0.912; for $B_FT = 0.2, 0.4$ this correlation becomes 0.671 and -0.04 respectively. The objective of the material covered in the rest of this section is to make a comparative study between the accuracy of upper and lower union bounds by comparing them with Monte Carlo computer simulations[15]. This will also provide an accurate picture of the performance levels achieved by the block decoder, as compared to the differential detector.

In Figs. 4.73 to 4.84 we display the upper (Z= (K_r/B_FT)UB) and lower (Z= (K_r/B_FT)LB) bounds of the block decoder together with simulation results (Z= (K_r/B_FT)SIM.). We also include the curve of the differential detector to make the comparisons easier (DD(K_r/B_FT)). The curves correspond to all the channel scenarios with $K_r = 10\ dB$ examined previously and they are carried out for QPSK. The block decoders examined are the $Z = 3, 4, 5, 6$.

In Tables 4.24, 4.25 we list the improvements offered by the block decoder as compared to the differential detector for various combinations of Z and B_FT. The values summarized in Table 4.24 correspond to a SER=10^{-2} whereas Table 4.25 gives values for SER=10^{-3}. Wherever an *Error Floor* indication appears, it means that one of the two compared systems experiences

[15]For BER or SER in the range of 10^{-4} and higher, the Monte Carlo simulations reported in this thesis have been run until at least 100 errors were counted. This gives high confidence in the simulation results. For BER or SER below 10^{-4}, the simulations had to be terminated prior to the counting of 100 errors, due to the long time required to complete the simulation. The simulation curves displayed in the various figures present the average curves which pass through the simulation points.

error floor higher than the SER value.

Table 4.24: Gains achieved by the Block Decoder versus the sequence length Z and the B_FT product. The channel is Rician faded with $K_r = 10\ dB$. The signal is QPSK. The comparisons are made with the conventional differential detector and correspond to a SER=10^{-2}. For the comparisons, the Monte Carlo simulation results (we refer to the block decoder) are used.

		GAINS (dB)		
		$B_FT = 0.1$	$B_FT = 0.2$	$B_FT = 0.4$
Z	3	1.4	1.5	4
	4	0.8	1.5	6
	5	0.5	0.5	6.5
	6	1	1	7.5

Table 4.25: Gains achieved by the Block Decoder versus the sequence length Z and the B_FT product. The channel is Rician faded with $K_r = 10\ dB$. The signal is QPSK. The comparisons are made with the conventional differential detector and are referred to a SER=10^{-3}. For the comparisons, the Monte Carlo simulation results (we refer to the block decoder) are used.

		GAINS (dB)		
		$B_FT = 0.1$	$B_FT = 0.2$	$B_FT = 0.4$
Z	3	1	Error Floor	Error Floor
	4	0.5	Error Floor	Error Floor
	5	-2.5	Error Floor	Error Floor
	6	Error Floor	Error Floor	Error Floor

The results summarized through the two tables and displayed in the form of curves in Figs. 4.73 to 4.84, demonstrate that the performance projections provided by the upper union bound improve as the fading bandwidth increases. We see that for $B_FT = 0.4$, the simulation curves are very close to the upper bound results. For $B_FT = 0.1$ the simulation results seem to

be roughly in the middle between upper and lower bound (at least for the lower E_b/N_o area). We also see that the upper bound gives a more accurate picture regarding the level of the error floor and the range of E_b/N_o values where the error floor starts to appear.

Tables 4.24, 4.25 show that for high values of B_FT, the block decoder is superior compared to the conventional differential detector[16]. The gains improve as the block length (Z) increases. From Table 4.24 we see that for $B_FT = 0.4$ and at a SER=10^{-2}, *the block decoder with* $Z = 6$ *outperforms the differential detector 7.5 dB.* Also, Fig. 4.84 shows that *the* $Z = 6$ *block decoder has an error floor almost one order of magnitude lower from the error floor of the differential detector.* At lower values of B_FT (i.e. $B_FT = 0.1$), the block decoder seems to have a small advantage for SER in the range of 10^{-2} and higher. This advantage decreases at lower SER. In several cases, the error floor of the block decoder is higher from the error floor of the differential detector. Another observation is that for $B_FT = 0.1$, the block decoder seems to achieve the best performance when the block length $Z = 3$. Further increase in the size of the block length penalizes the performance and eventually, the block decoder becomes inferior to the conventional differential detector.

[16]Two applications where we meet channels corrupted by fast multipath fading are the aeronautical communications and EHF personal communications. Both communication services can be benefited from the proposed non-coherent technology.

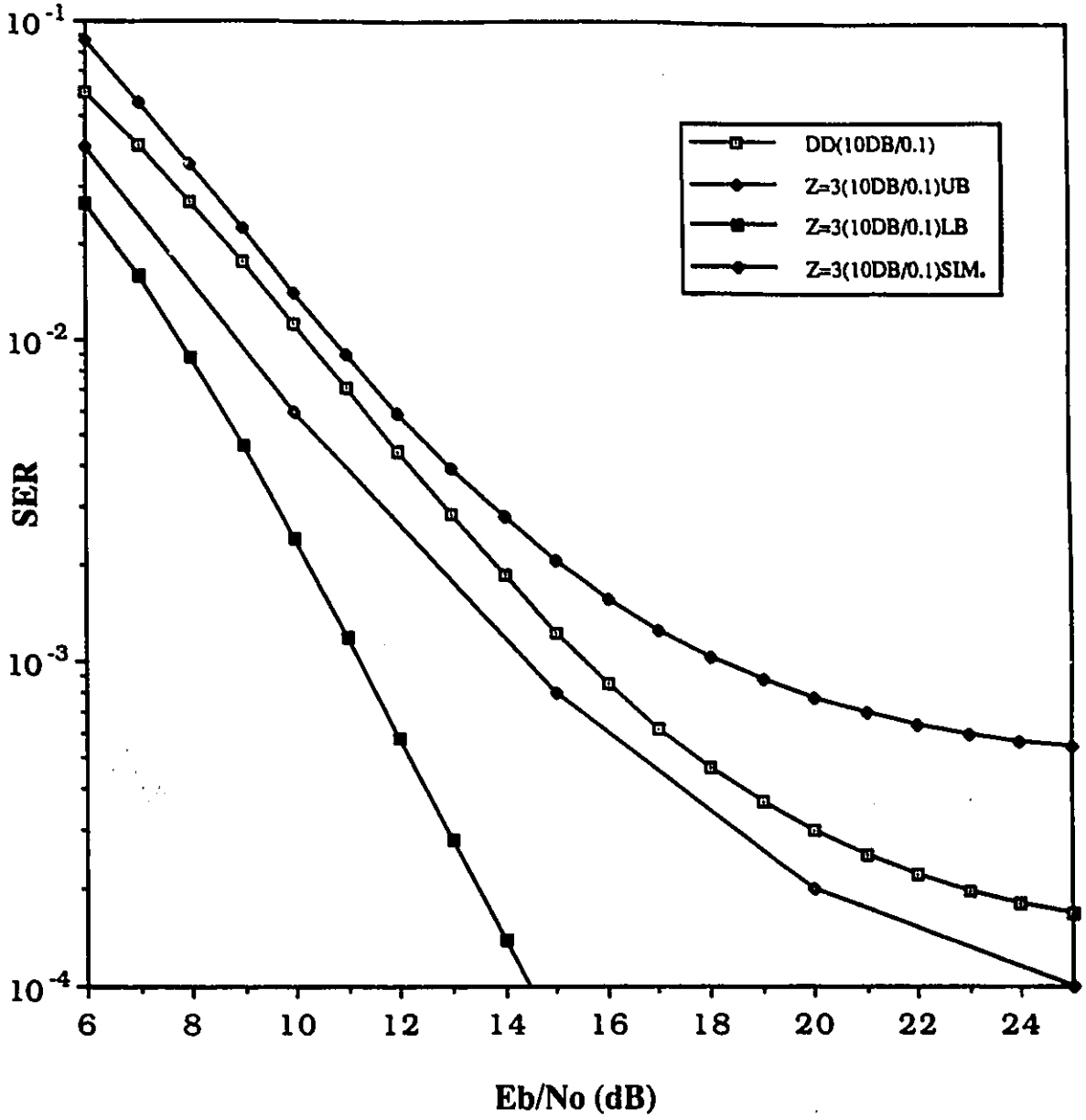

Figure 4.73: SER performance curves of the block decoder (BD) with Z=3 for a QPSK signal in a Rician faded channel with $K_r = 10\ dB$ and $B_F T = 0.1$. The displayed curves correspond to the upper (UB) and lower (LB) union bounds and to Monte Carlo simulations. We also display the curve of the differential detector under the same channel conditions.

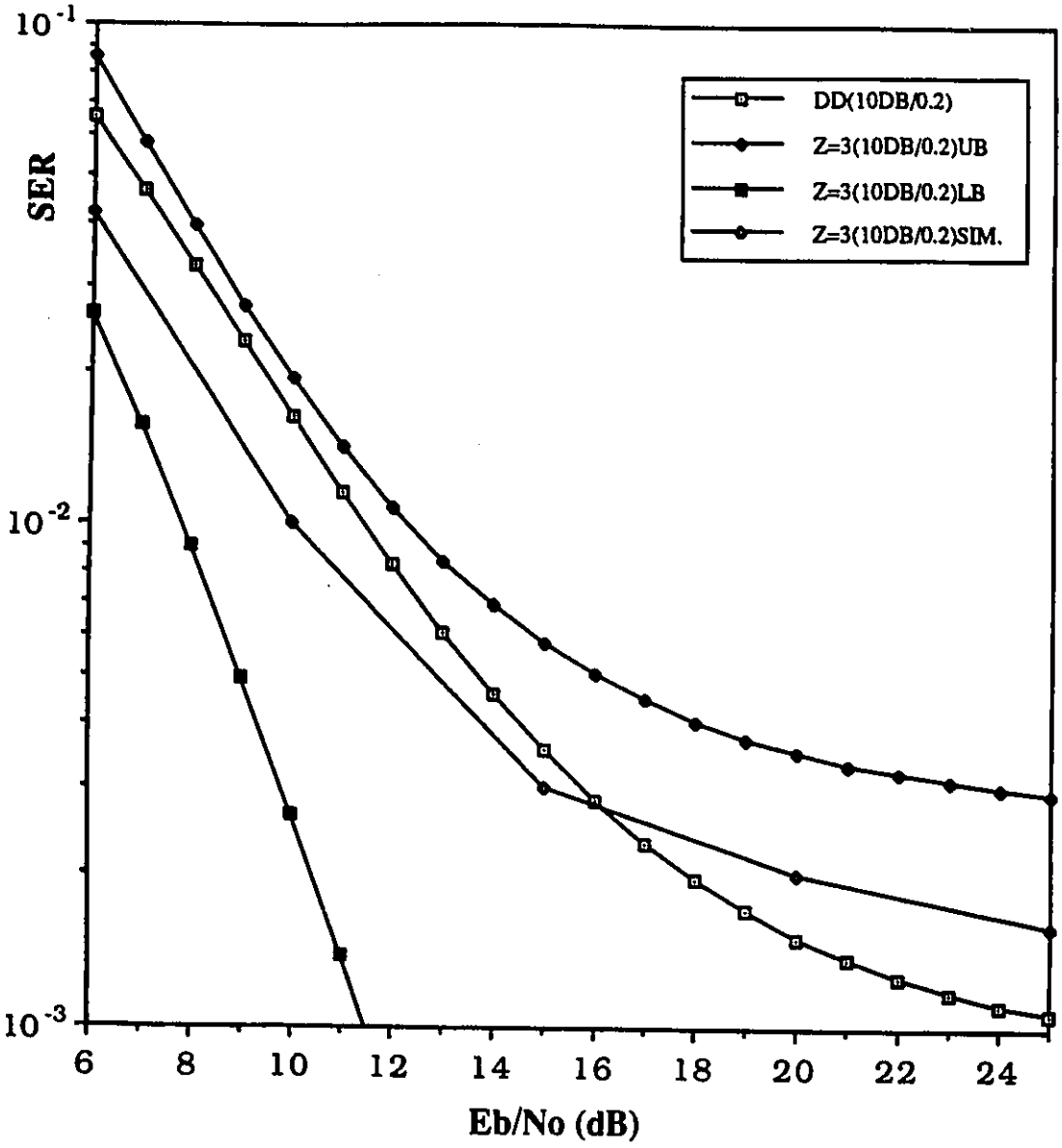

Figure 4.74: SER performance curves of the block decoder (BD) with Z=3 for a QPSK signal in a Rician faded channel with $K_r = 10\ dB$ and $B_F T = 0.2$. The displayed curves correspond to the upper (UB) and lower (LB) union bounds and to Monte Carlo simulations. We also display the curve of the differential detector under the same channel conditions.

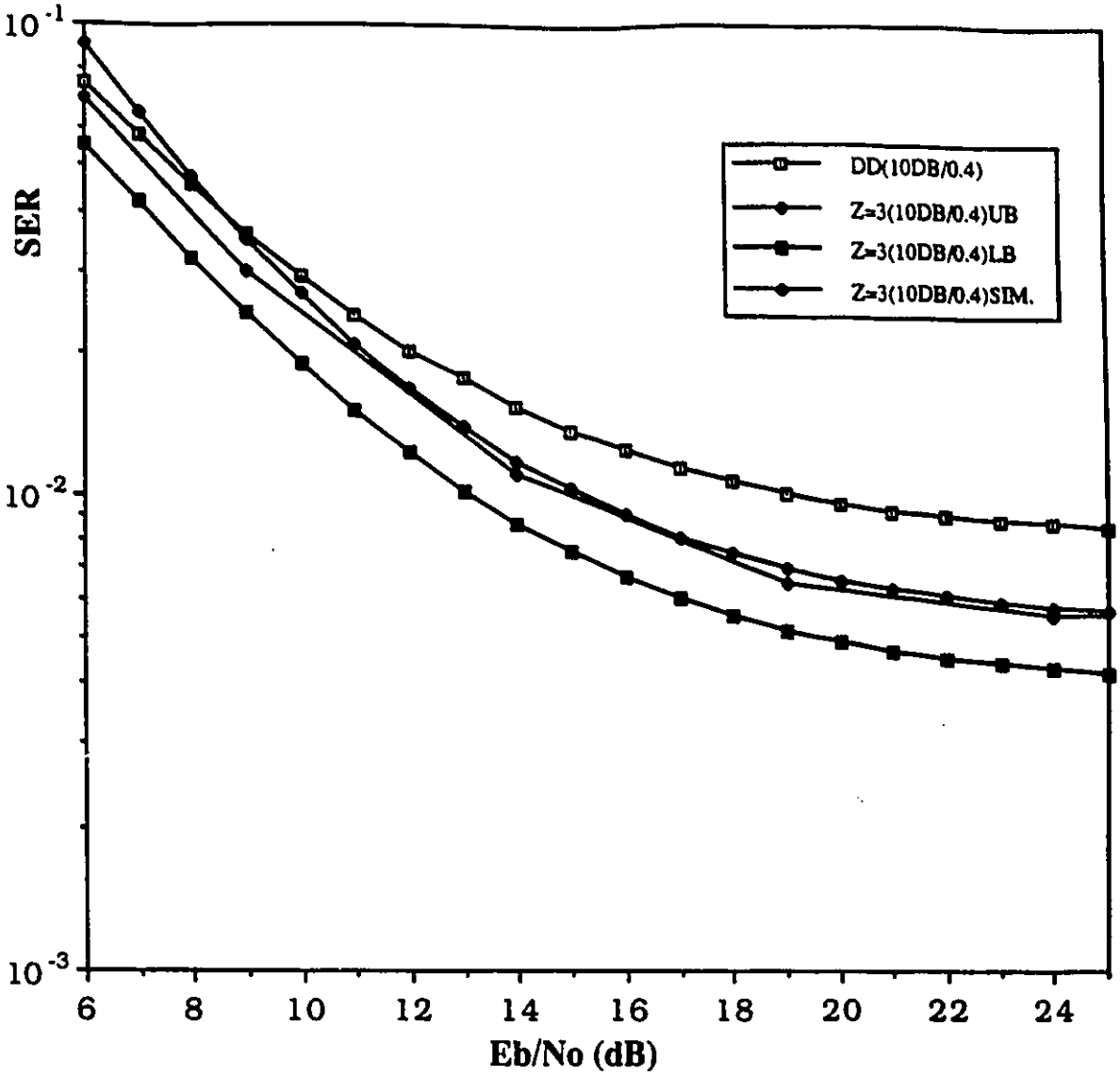

Figure 4.75: SER performance curves of the block decoder (BD) with Z=3 for a QPSK signal in a Rician faded channel with $K_r = 10\ dB$ and $B_F T = 0.4$. The displayed curves correspond to the upper (UB) and lower (LB) union bounds and to Monte Carlo simulations. We also display the curve of the differential detector under the same channel conditions.

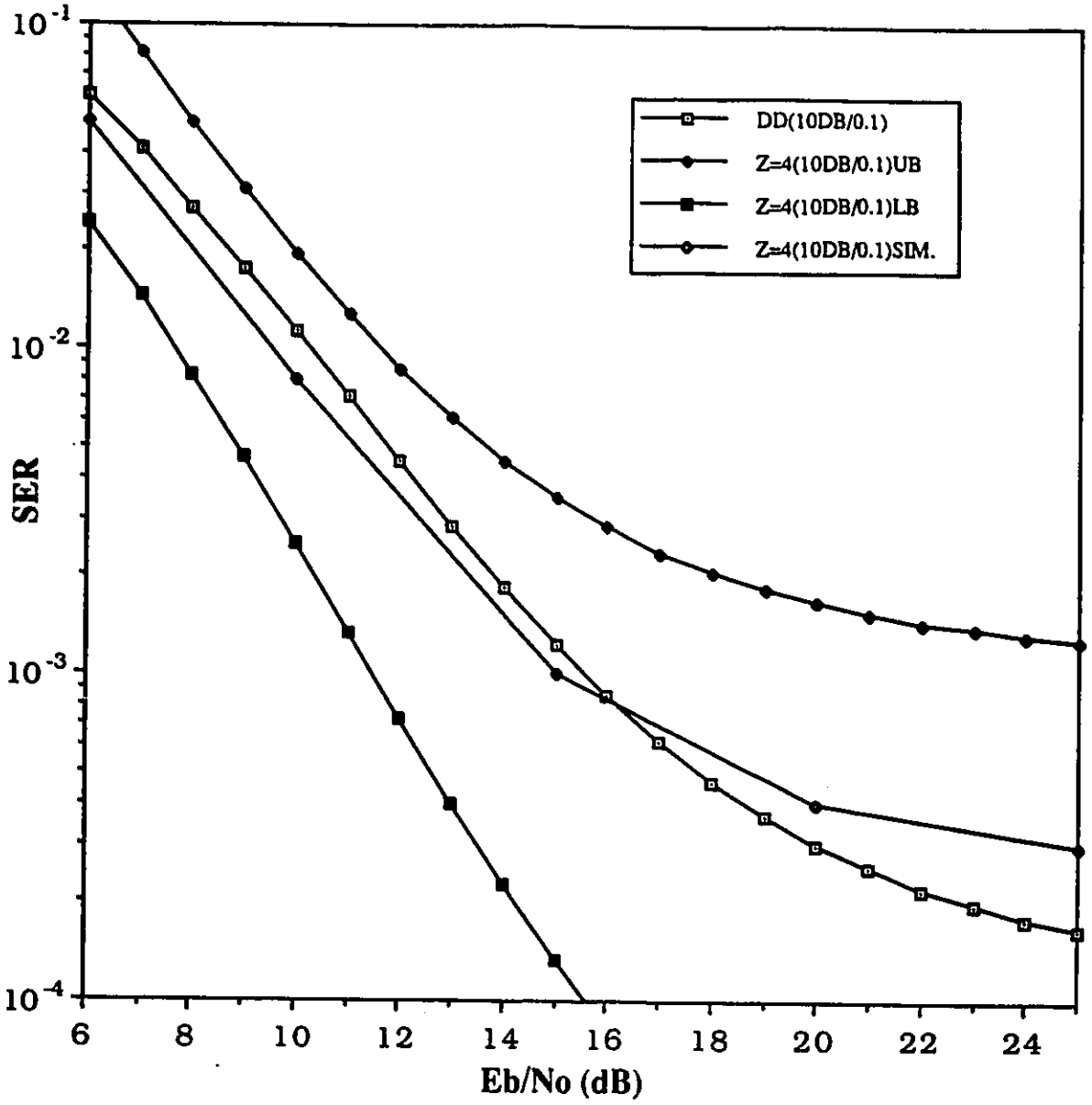

Figure 4.76: SER performance curves of the block decoder (BD) with Z=4 for a QPSK signal in a Rician faded channel with $K_r = 10\ dB$ and $B_F T = 0.1$. The displayed curves correspond to the upper (UB) and lower (LB) union bounds and to Monte Carlo simulations. We also display the curve of the differential detector under the same channel conditions.

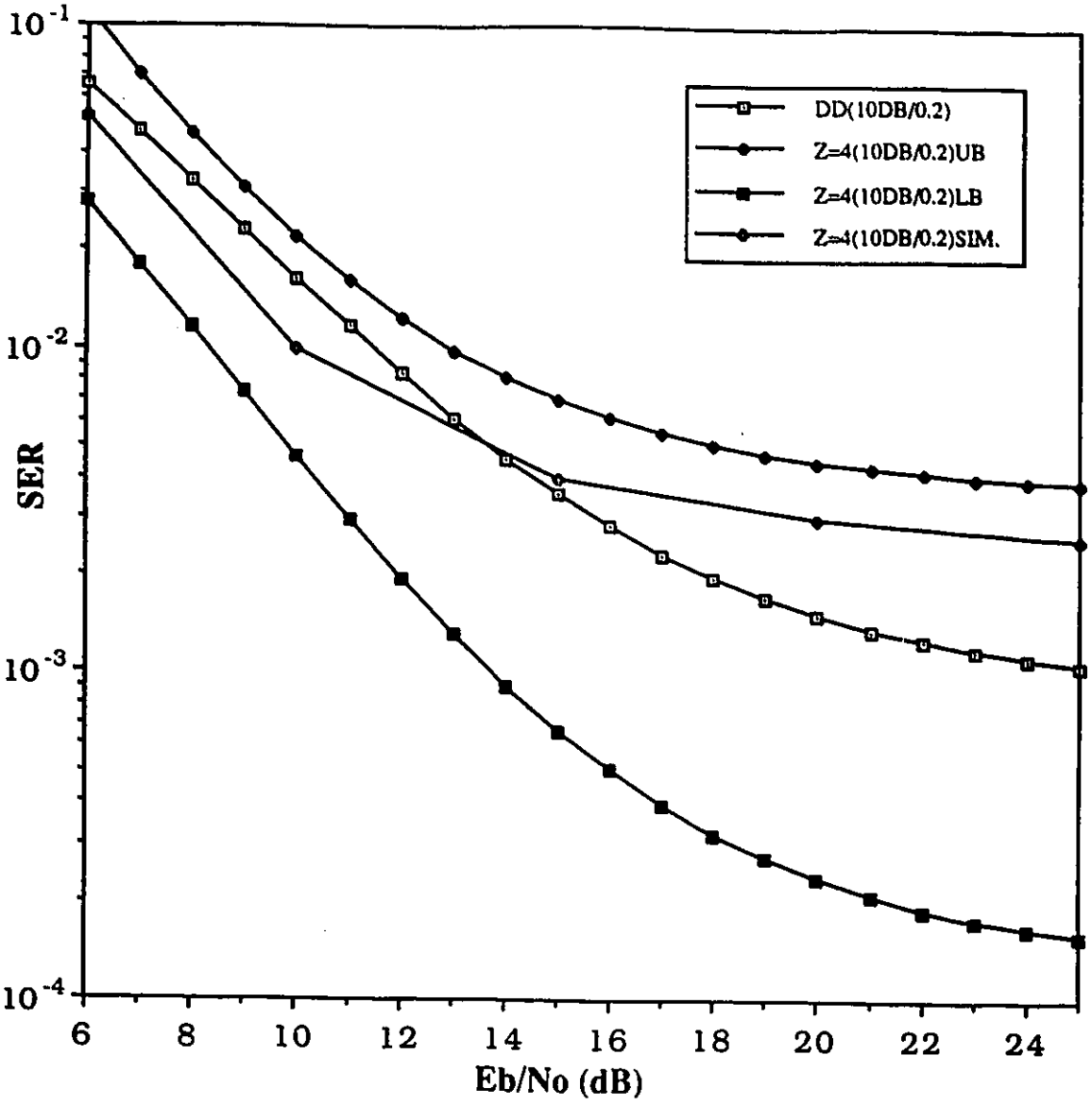

Figure 4.77: SER performance curves of the block decoder (BD) with Z=4 for a QPSK signal in a Rician faded channel with $K_r = 10\ dB$ and $B_F T = 0.2$. The displayed curves correspond to the upper (UB) and lower (LB) union bounds and to Monte Carlo simulations. We also display the curve of the differential detector under the same channel conditions.

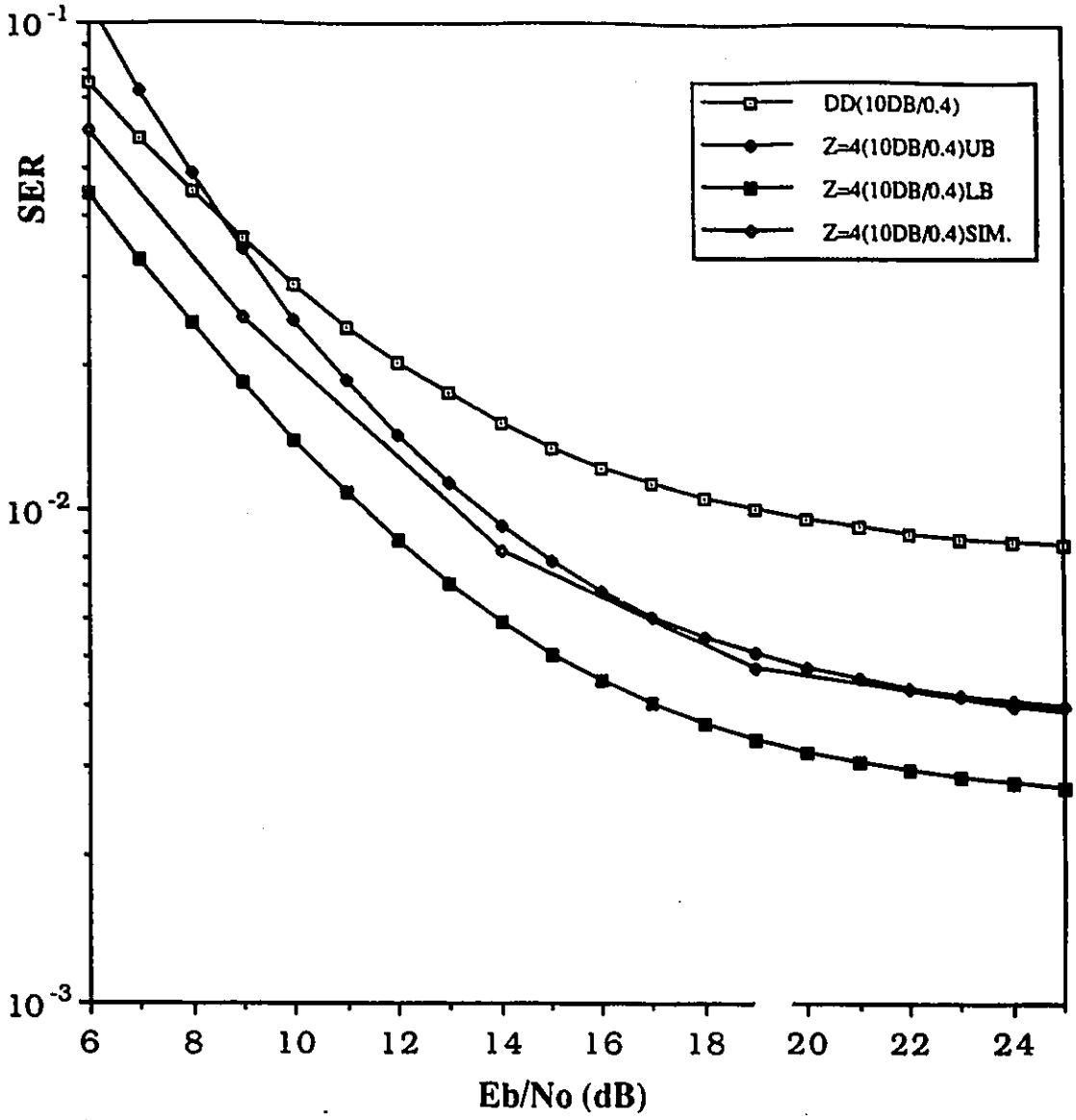

Figure 4.78: SER performance curves of the block decoder (BD) with Z=4 for a QPSK signal in a Rician faded channel with $K_r = 10\ dB$ and $B_F T = 0.4$. The displayed curves correspond to the upper (UB) and lower (LB) union bounds and to Monte Carlo simulations. We also display the curve of the differential detector under the same channel conditions.

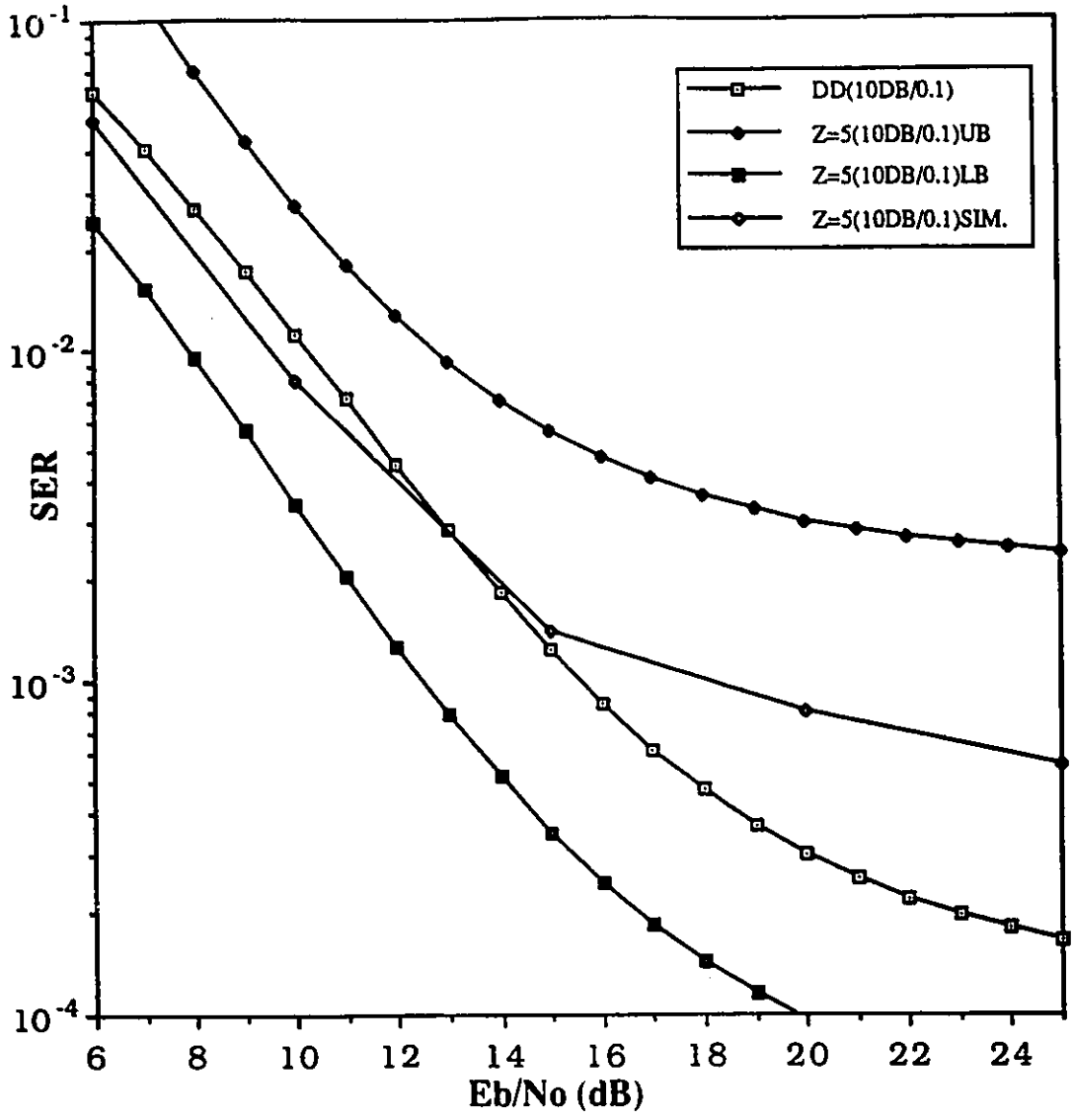

Figure 4.79: SER performance curves of the block decoder (BD) with Z=5 for a QPSK signal in a Rician faded channel with $K_r = 10\ dB$ and $B_F T = 0.1$. The displayed curves correspond to the upper (UB) and lower (LB) union bounds and to Monte Carlo simulations. We also display the curve of the differential detector under the same channel conditions.

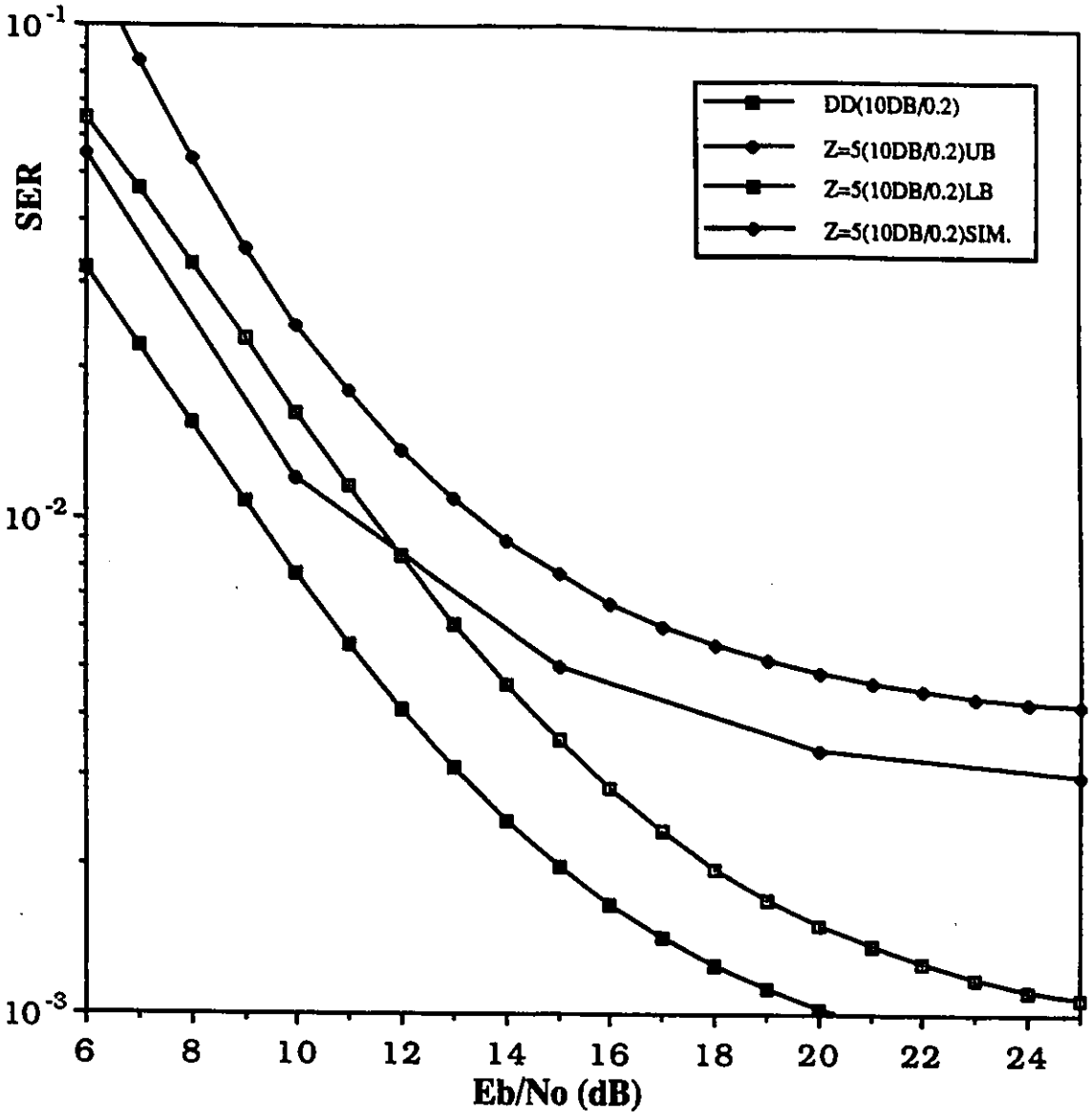

Figure 4.80: SER performance curves of the block decoder (BD) with Z=5 for a QPSK signal in a Rician faded channel with $K_r = 10\ dB$ and $B_F T = 0.2$. The displayed curves correspond to the upper (UB) and lower (LB) union bounds and to Monte Carlo simulations. We also display the curve of the differential detector under the same channel conditions.

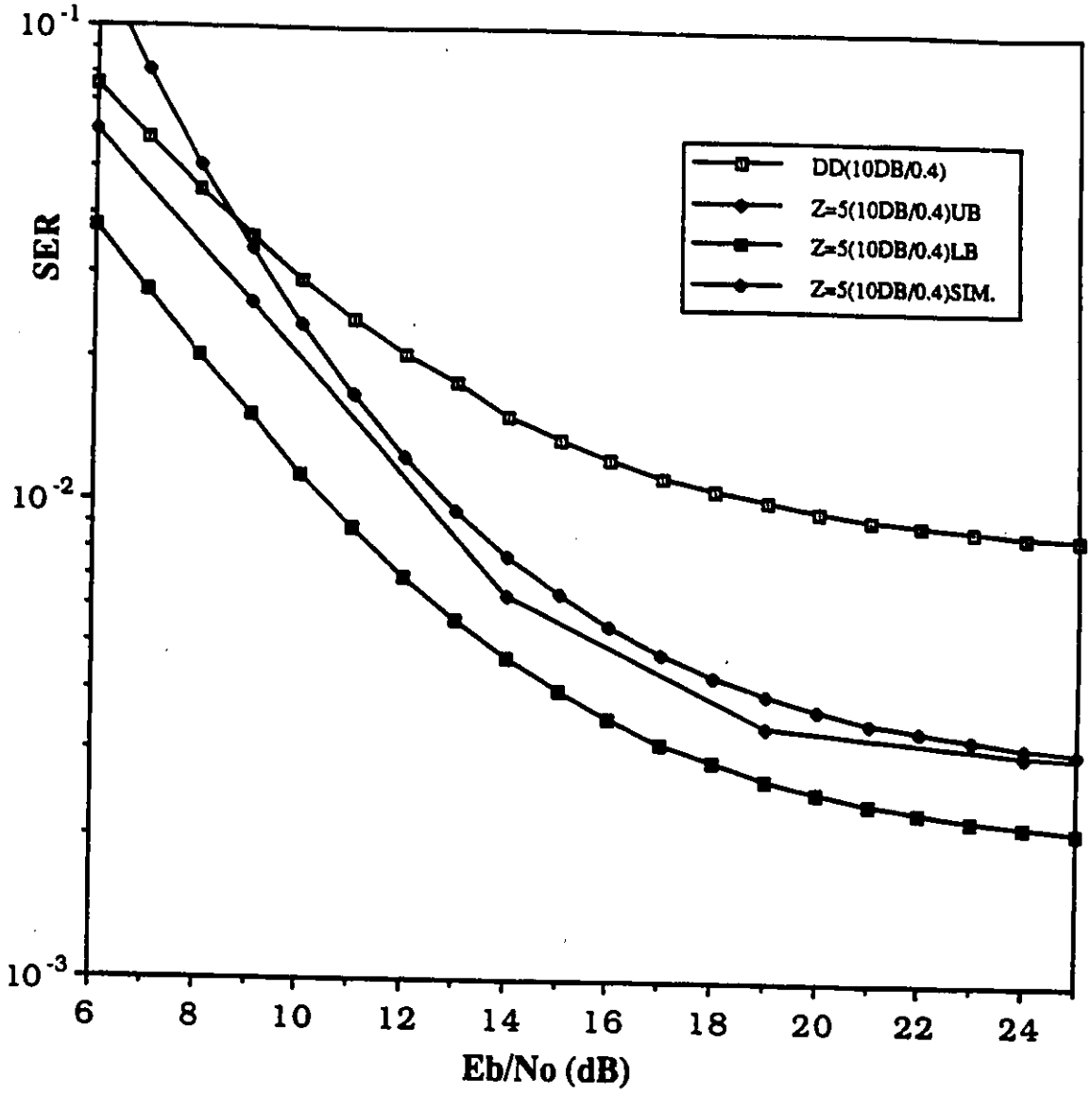

Figure 4.81: SER performance curves of the block decoder (BD) with Z=5 for a QPSK signal in a Rician faded channel with $K_r = 10\ dB$ and $B_F T = 0.4$. The displayed curves correspond to the upper (UB) and lower (LB) union bounds and to Monte Carlo simulations. We also display the curve of the differential detector under the same channel conditions.

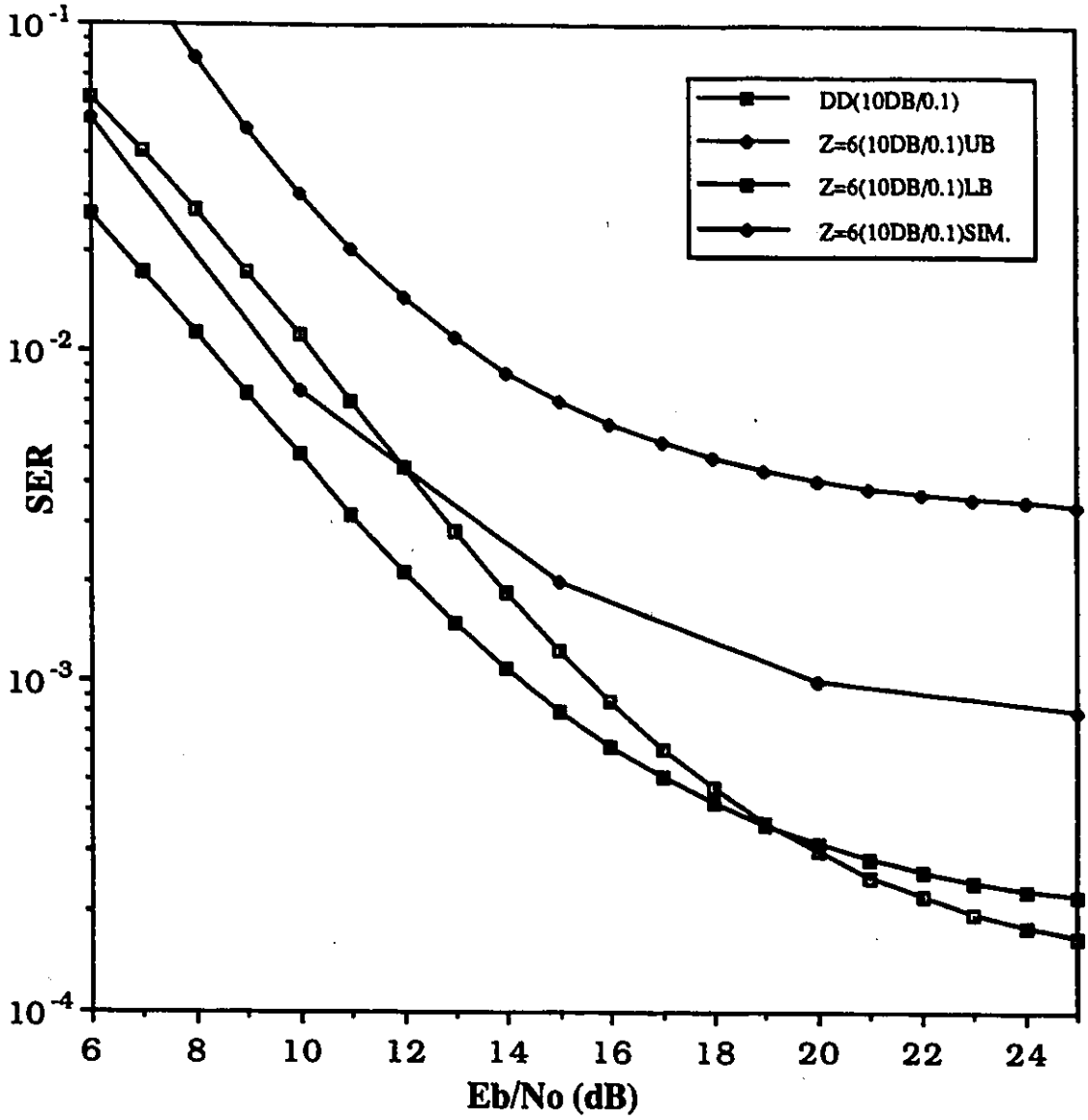

Figure 4.82: SER performance curves of the block decoder (BD) with Z=6 for a QPSK signal in a Rician faded channel with $K_r = 10\ dB$ and $B_F T = 0.1$. The displayed curves correspond to the upper (UB) and lower (LB) union bounds and to Monte Carlo simulations. We also display the curve of the differential detector under the same channel conditions.

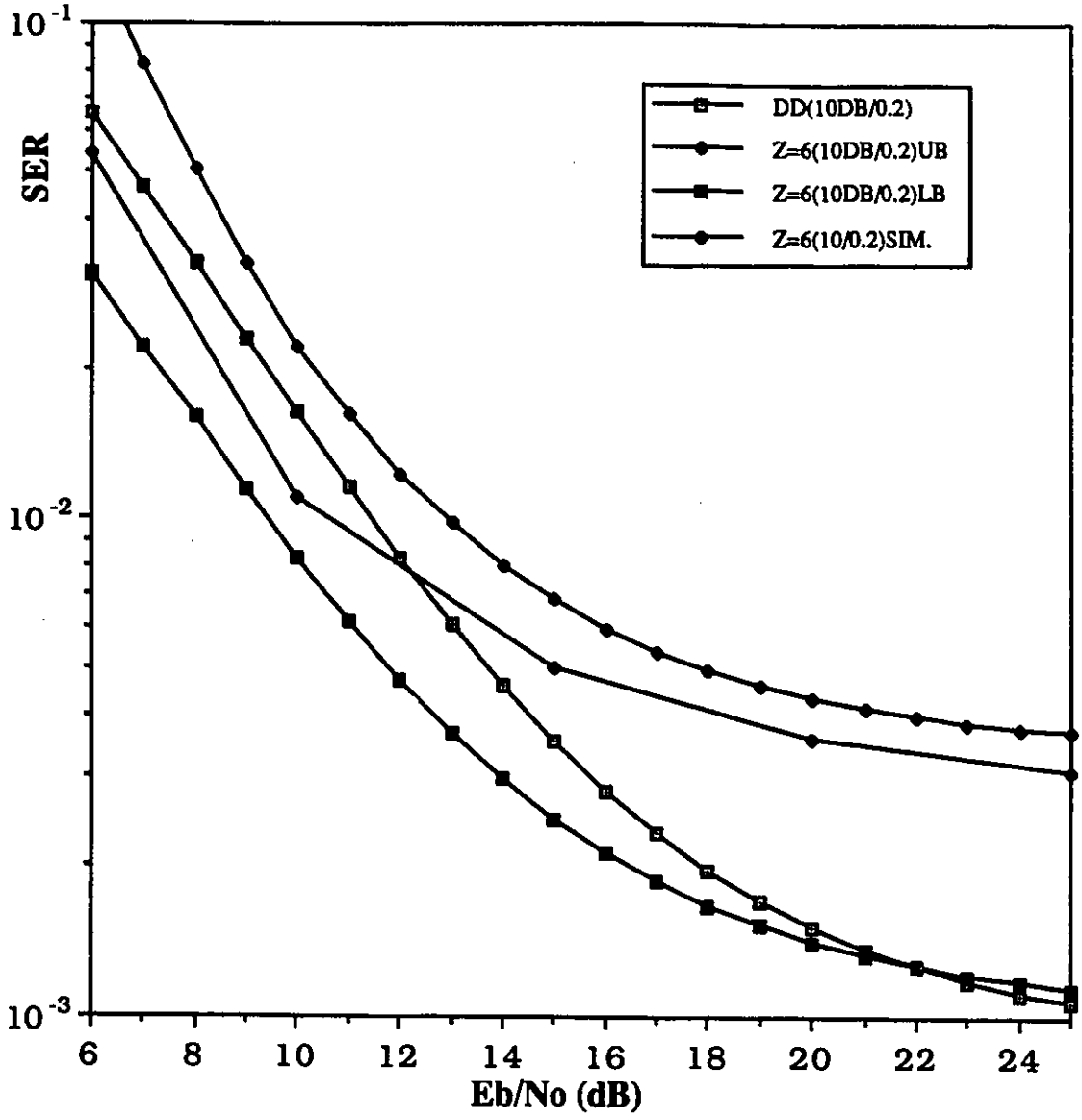

Figure 4.83: SER performance curves of the block decoder (BD) with Z=6 for a QPSK signal in a Rician faded channel with $K_r = 10\ dB$ and $B_F T = 0.2$. The displayed curves correspond to the upper (UB) and lower (LB) union bounds and to Monte Carlo simulations. We also display the curve of the differential detector under the same channel conditions.

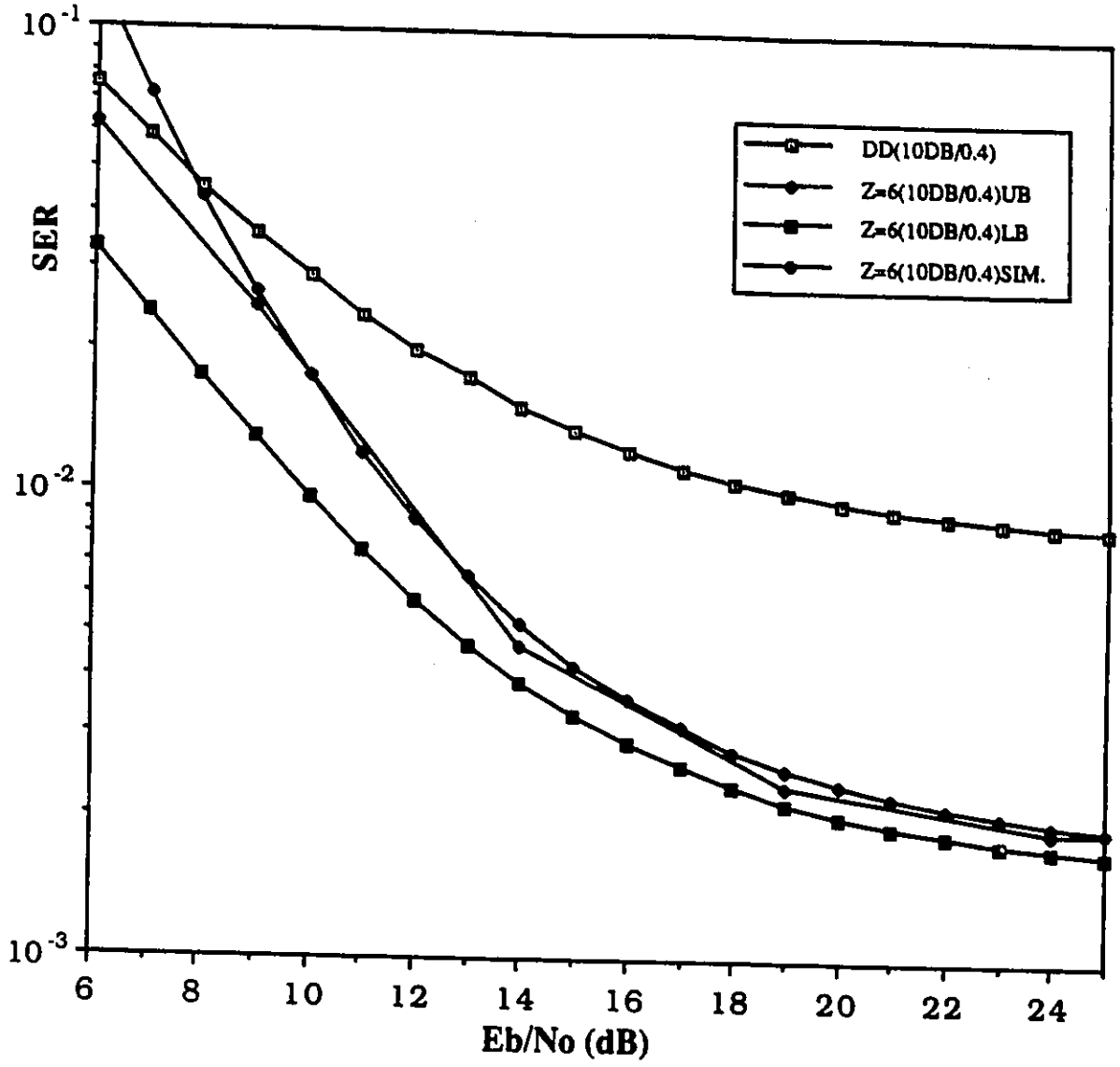

Figure 4.84: SER performance curves of the block decoder (BD) with Z=6 for a QPSK signal in a Rician faded channel with $K_r = 10\ dB$ and $B_F T = 0.4$. The displayed curves correspond to the upper (UB) and lower (LB) union bounds and to Monte Carlo simulations. We also display the curve of the differential detector under the same channel conditions.

4.9 REDUCED COMPLEXITY RECEIVERS FOR LONG DATA SEQUENCES

The receivers described up to this point, have one drawback. Their complexity increases exponentially with the size of the transmitted sequence Z. The objective of this section is to indicate simple ways to overcome this problem. Below, two different approaches are described: one is based on block decoding, the other on multiple differential detection. The use of differential encoding is mandatory for both receivers.

4.9.1 A Sliding Window Implementation of the Non-Coherent Receiver

Let us consider the trellis diagram of Fig. 4.85. In the diagram various diverging and re-emerging paths are indicated. Let us assume at this point that we wish to process in the decoder only the samples received between kT and $(k+L)T$ (a total of L y_i samples with $L < (Z-k-1)$, Z being the length of the transmitted sequence). Since the trellis diagram extends outside the area we are considering to use for detection, we realize that there are several possible error events which might have started before kT and others remaining in divergence after $(k+L)T$. Due to the truncation applied, the diverging paths of these error events are not allowed to grow to their full extent. As a result, the distances associated with these error events are reduced and the probabilities of erroneous decisions increase. The consequence is that symbols close to the beginning and end of the $(kT,(k+L)T)$ interval have greater chances of being decoded erroneously.

For high E_b/N_o, most of the errors are associated with divergences corresponding to the most dominant (i.e. having the smallest distance) error events. Consequently, if we ensure that all the possible error events influencing decision have at least the distance of the most dominant error event, we should not expect considerable losses in terms of performance by applying the truncation. In order to achieve this, we **do not** decide the first and last l_{bd} symbols (l_{bd} integer, $l_{bd} \leq \frac{L}{2}$) i.e. only decisions regarding the $g_{k+l_{bd}}, g_{k+l_{bd}+1}, \cdots, g_{k+L-l_{bd}+1}$ symbols are provided. The chosen value of l_{bd}

has to be large enough in order to ensure that no error events initialized before kT can re-emerge, having accumulated distance less than the (non-coherent) minimum distance of the code. For this reason, l_{bd} should be greater or at least equal to the length of the most dominant error events. In the next decoding round, the decoder should start processing the y_i in the time interval $((k+L-l_{bd}+1)T, (k+2L-2l_{bd})T)$ and the decisions which will be provided concern the symbols $g_{k+L+l_{bd}}$ up to $g_{k+2L-2l_{bd}+1}$.

In uncoded MPSK the lack of memory (due to the absence of coding) and the fact that the trellis diagram has transitions from every state towards every state (see Appendix C and Fig. C.1) creates dominant (i.e. minimum distance) error events with a length equal to 1. In this case, $l_{bd} = 1$. Consequently, when the symbols $g_k, g_{k+l+1}, \ldots, g_{k+L}$ are to be decided, we have to process the samples $y_{k-1}, y_k, \ldots, y_{k+L}$. At the next interaction, the $y_{k+L}, y_{k+L+1}, \ldots, y_{k+2L+1}$ are processed and the $g_{k+L+1}, g_{k+L+2}, \cdots, g_{k+2L+1}$ are decided.

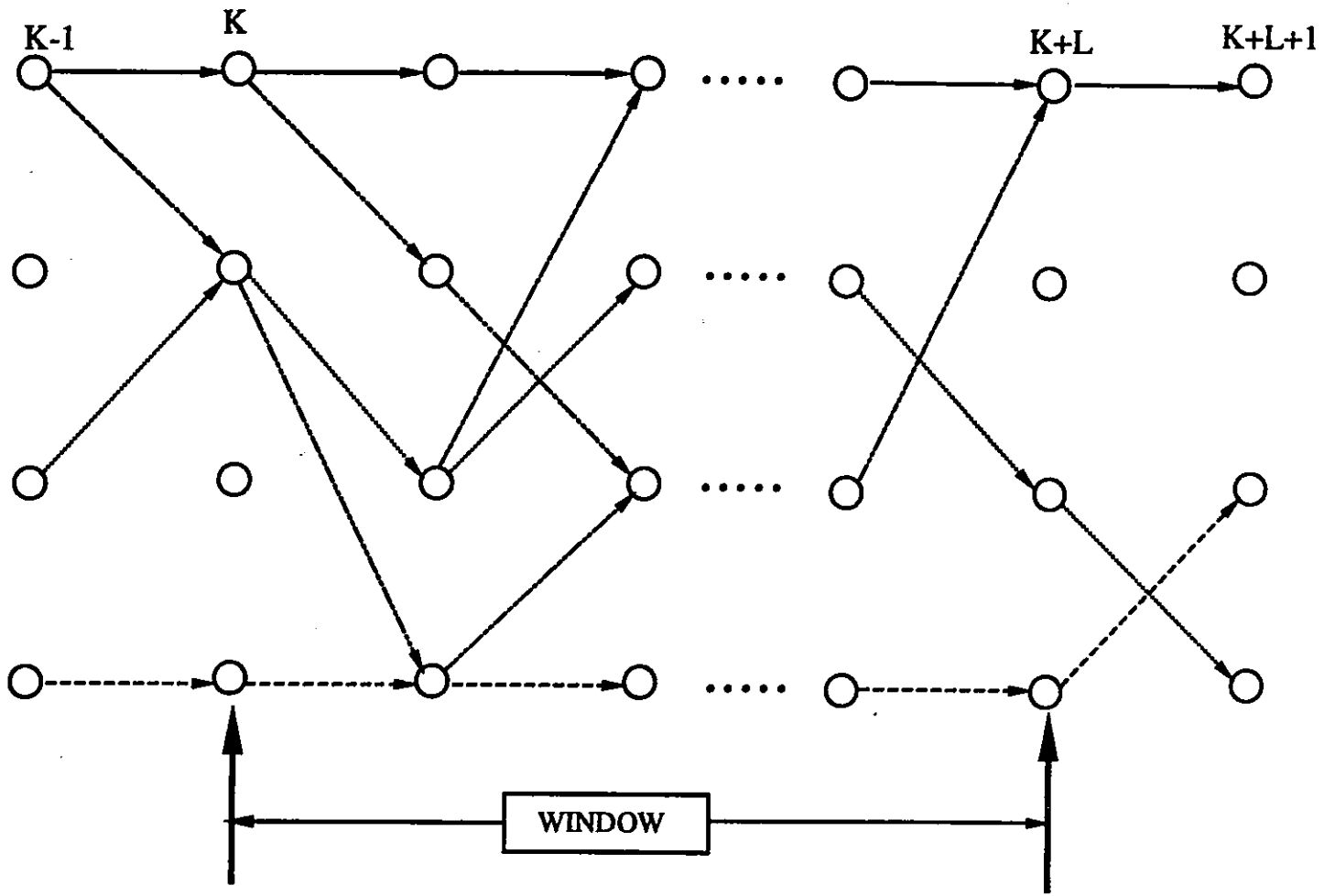

Figure 4.85: Various paths travelling through the trellis diagram.

4.9.2 A SEMDD Receiver Based on a Truncation Strategy

4.9.2.1 Structure of the Receiver

In section 4.4.2, where the SEMDD structure was presented, it was mentioned that a total of $(Z-1)$ differential detectors are needed to implement the receiver. Our approach towards providing reduced complexity receivers with SEMDD is to truncate the number of differential detectors used to a maximum of λ, where λ is an integer and $1 \leq \lambda \leq Z-1$. In this case, the metric $\Xi_1^D(\bar{y}, \bar{C}(\bar{A}))$ is approximated by

$$\wp_1^{MDD}(\lambda, \bar{y}, \bar{C}(\bar{A})) = \sum_{k=1}^{Z-1} \mathcal{J}_k \sum_{l=1}^{\varpi} \mathcal{J}_{k-l}[d_l^I(k)\cos(\Delta\Theta_l(k)) + d_l^Q(k)\sin(\Delta\Theta_l(k))] \tag{4.98}$$

where

$$\varpi = \begin{cases} k & \text{for } 1 \leq k \leq \lambda \\ \lambda & \text{for } k > \lambda\,. \end{cases} \tag{4.99}$$

For PSK signals, $(\mathcal{J}_k = 1)$. The value of λ regulates the complexity and performance of the receiver. An equivalent expression for the $\Xi_2^D(\bar{y}, \bar{C}(\bar{A}))$ presented in Eq.(4.34), is the following:

$$\wp_2^{MDD}(\lambda, \bar{y}, \bar{C}(\bar{A})) = \sum_{k=1}^{Z-1} \mathcal{J}_k Re\{y_k(\sum_{i=1}^{\varpi} y_{k-i}\mathcal{J}_{k-i}e^{j\Delta\Theta_l(k)})^*\}\,. \tag{4.100}$$

Replacing $\Xi_1^D(\bar{y}, \bar{C}(\bar{A}))$, $(\Xi_2^D(\bar{y}, \bar{C}(\bar{A})))$ with the approximate expressions $\wp_1^{MDD}(\lambda, \bar{y}, \bar{C}(\bar{A}))$ $(\wp_2^{MDD}(\lambda, \bar{y}, \bar{C}(\bar{A})))$ respectively in the formulas of the metrics presented in Eqs. (4.28) to (4.31) we get the following expressions:

$$\begin{aligned} \mathcal{Q}_1^{MAL}(h_0, \bar{h}, \bar{y}, \bar{C}(\bar{A})) \;=\; & \exp\{-\frac{1}{N_o}[\frac{h_0}{2}\sum_{k=0}^{Z-1}\mathcal{J}_k^2 + (\sum_{k=1}^{Z-1}\mathcal{J}_k\sum_{l=1}^{\varpi}\mathcal{J}_{k-l}Re\{h_l e^{j\Delta\Theta_l(k)}\})]\} \\ & I_o(\frac{[\Xi^E(\bar{y}) + 2\wp_1^{MDD}(\lambda, \bar{y}, \bar{C}(\bar{A}))]^{\frac{1}{2}}}{N_o}) \end{aligned}$$

(4.101)

$$Q_2^{MAL}(h_0,\bar{h},\bar{y},\bar{C}(\bar{A})) = -\frac{h_0}{2}\sum_{k=0}^{Z-1}\mathcal{J}_k^2 - \sum_{k=1}^{Z-1}\mathcal{J}_k\sum_{l=k}^{\varpi}\mathcal{J}_{k-l}Re\{h_l e^{j\Delta\Theta_l(k)}\} + [\Xi^E(\bar{y}) + 2\wp_i^{MDD}(\lambda,\bar{y},\bar{C}(\bar{A}))]^{\frac{1}{2}}.$$

(4.102)

For PSK signals, the metrics corresponding to Eqs.(4.30)-(4.32) are:

$$Q_1^{PSK}(\bar{h},\bar{y},\bar{C}(\bar{A})) = \exp\{-\frac{1}{N_o}[(\sum_{k=1}^{Z-1}\sum_{l=1}^{\varpi}Re\{h_l e^{j\Delta\Theta_l(k)}\})\} I_o(\frac{[\Xi^E(\bar{y}) + 2\wp_i^{MDD}(\lambda,\bar{y},\bar{C}(\bar{A}))]^{\frac{1}{2}}}{N_o})$$

(4.103)

$$Q_2^{PSK}(\bar{h},\bar{y},\bar{C}(\bar{A})) = -\sum_{k=1}^{Z-1}\sum_{l=k}^{\varpi}Re\{h_l e^{j\Delta\Theta_l(k)}\} + [\Xi^E(\bar{y}) + 2\wp_i^{MDD}(\lambda,\bar{y},\bar{C}(\bar{A}))]^{\frac{1}{2}},$$

(4.104)

$$Q_3(\lambda,\bar{y},\bar{C}(\bar{A})) = \wp_i^{MDD}(\lambda,\bar{y},\bar{C}(\bar{A})) \quad (4.105)$$

with i being either 1 or 2. It should be noticed that in Eqs.(4.101) to (4.104) the term associated with the presence of ISI, has been changed as well, in order to account for the truncation applied on the multiple differential detectors.

The maximization of $Q_1^{MAL}(h_0,\bar{h},\bar{y},\bar{C}(\bar{A}))$ ($Q_1^{PSK}(\bar{h},\bar{y},\bar{C}(\bar{A}))$) is quite inappropriate to be implemented in a recursive way, due to its structure (the problem being the presence of the Bessel function term). However, $Q_2^{MAL}(\bar{h},\bar{y},\bar{C}(\bar{A}))$, $Q_2^{PSK}(\bar{h},\bar{y},\bar{C}(\bar{A}))$ and $Q_3(\lambda,\bar{y},\bar{C}(\bar{A}))$ have expressions which permit carrying out the maximization process recursively. To give an idea of the structure and complexity level of the required algorithm, we present the recursive algorithm carrying out the maximization of the $Q_3(\lambda,\bar{y},\bar{C}(\bar{A}))$ in the following section. For $Q_2^{MAL}(\lambda,\bar{y},\bar{C}(\bar{A}))$, $Q_2^{PSK}(\lambda,\bar{y},\bar{C}(\bar{A}))$ the algorithms described in [149] can be used.

4.9.2.2 Description of the Recursive Algorithm

The implementation of the receiver, requires a decoder with a total number of

$$N_T = N_S.N_B 2^{(\lambda-1)} \tag{4.106}$$

states where N_S represents the number of states, in the trellis diagram of the original code and N_B the number of branches diverging from (or equivalently reemerging to) the states of the code. The states are represented as G_l with $1 \leq l \leq N_T$.

The choice between $\wp_1^{MDD}(\lambda, \bar{y}, \bar{C}(\bar{A}))$ and $\wp_2^{MDD}(\lambda, \bar{y}, \bar{C}(\bar{A}))$ to implement the MDD algorithm, influences the implementation of the receiver. In the following paragraphs, algorithms based on both metric expressions will be presented and the levels of their complexity will be examined.

Algorithm based on $\wp_1^{\mathbf{MDD}}(\lambda, \bar{\mathbf{y}}, \bar{\mathbf{C}}(\bar{\mathbf{A}}))$

The operation of the decoder, requires the execution of four different steps in each (recursive) interaction. The tasks executed by these functions are the recursive updating of the required metric quantity, the decision of the survivors and the decoding of the transmitted information by tracing back the strongest (i.e most possible) survivor path. A more detailed description of the four steps follows:

Step 1

The survivor metrics $M_{G_\mu}(k)$ are calculated for all the states G_μ ($1 \leq \mu \leq N_T$). The calculation starts by determining the value of the quantity

$$W^1_{G_\mu}(k) = max[\Psi^1_{G_\mu,G_i}(k) + M_{G_i}(k-1)] \tag{4.107}$$

where $G_i \in \{\underline{X}_{G_\mu}\}$. $\underline{X}_{G_\mu}$ is the set which includes as members all the states with transitions towards G_μ. Also,

$$\Psi^1_{G_\mu,G_i}(k) = d^I_\lambda(k)\cos(\Delta U^{G_\mu,G_i}_\lambda) + d^Q_\lambda(k)\sin(\Delta U^{G_\mu,G_i}_\lambda)\ . \tag{4.108}$$

$\Delta U^{G_\mu,G_i}_\lambda$ depends on the transition from G_i to G_μ. Its value is equal to the value $\Delta\Theta_\lambda(k)$ has when the transmitted information sequence $\bar{A}$ is such that the path of the transmitted sequence transits from G_i to G_μ at kT.

After $W^1_{G_\mu}(k)$ has been calculated, the path whose metric has been chosen as $W^1_{G_\mu}(k)$ becomes the survivor path going through G_μ.

Step 2

The path metrics $M_{G_\mu}(k)$ are updated as follows:

$$M_{G_\mu}(k) = \Omega^1_{G_\mu}(k) + W^1_{G_\mu}(k) \tag{4.109}$$

with

$$\Omega^1_{G_\mu}(k) = \sum_{l=1}^{\lambda-1} (d_l^I(k)\cos(\Delta V_l^{G_\mu}) + d_l^Q(k)\sin(\Delta V_l^{G_\mu})) \ . \tag{4.110}$$

The value of $\Delta V_l^{G_\mu}$ $(1 \leq l \leq (\lambda-1))$ depends only on the state G_μ. Its value is equal to the value $\Delta\Theta_l(k)$ has, if the path of the transmitted sequence passes through G_μ at kT.

Step 3

The quantity $\Upsilon(k)$ which corresponds to the metric of the most possible survivor, based on information accumulated up to time kT, is selected as follows:

$$\Upsilon(k) = max[M_{G_l}(k)] \text{ where } 1 \leq l \leq N_T \ . \tag{4.111}$$

Step 4

The path, whose metric has been selected as $\Upsilon(k)$, is traced back DL steps (DL being a positive integer) and the information symbol g_{k-DL} is decided. DL corresponds to the decoding depth. The process is repeated for the next time instant $kT+T$, and so on. It is to be noticed that when $\lambda = 1$ (i.e. only one differential detector with delay element equal to the symbol period is used), the decoder described above becomes identical to the conventional Viterbi decoder. In this case, step 2 is not performed.

When the $d_l^I(k)$, $d_l^Q(k)$ $(1 \leq l \leq \lambda)$ are provided by a bank of λ differential detectors, the processor has to execute in each recursive interaction $(2N_B+2\lambda)N_T$ multiplications, $(2N_B+\lambda)N_T$ additions/subtractions and $(N_B-1)N_T+1$ comparisons.

Algorithm based on $\wp_2^{\mathbf{MDD}}(\lambda, \bar{\mathbf{y}}, \bar{\mathbf{C}}(\bar{\mathbf{A}}))$:

The recursive operation of this decoder requires the execution of four steps as well. The two algorithms differ only in the first two steps, whereas the last two are identical for both cases. Hence, only the two first steps of this algorithm are described below.

Step 1

For each stage G_μ , calculate the path metrics

$$W^2_{G_\mu,G_i}(k) = \Psi^2_{G_\mu,G_i}(k) + M_{G_i}(k-1) \tag{4.112}$$

with

$$\Psi^2_{G_\mu,G_i}(k) = Re\{y_k \xi^*_{G_\mu,G_i}(k)\} \tag{4.113}$$

and

$$\xi_{G_\mu,G_i}(k) = y_{k-1} + [\widehat{\xi}_{G_i}(k-1) - y_{k-\lambda-1} e^{-j(\Delta U^{G_i}_{\lambda-1})}] e^{j(\Delta V^{G_i}_{\lambda})} \ . \tag{4.114}$$

Step 2

After $W^2_{G_\mu,G_i}(k)$ have been calculated, the $M_{G_\mu}(k)$ is chosen as follows:

$$M_{G_\mu}(k) = max[W^2_{G_\mu,G_i}(k)] \quad \text{for} \quad 1 \leq \mathrm{i} \leq \mathrm{N_T} \ . \tag{4.115}$$

The path whose metric has been decided as being the $M_{G_\mu}(k)$, is chosen as the survivor which passes through G_μ at kT. Afterwards, the value of $\xi_{G_\mu,G_i}(k)$ corresponding to the survivor path is decided as $\widehat{\xi}_{G_\mu}(k)$, and is used in the next step as indicated by Eqs.(4.114), (4.115). The interaction continues by executing the two last steps (3^{rd} and 4^{th}) described in the previous algorithm.

The implementation of the algorithm in its present form, requires the execution of $8N_BN_T$ of multiplications, $9N_BN_T$ additions/subtractions and $(N_B-1)(N_T+1)$ comparisons in each recursive step. Comparing the processing load required by the two approaches, we realize that the first one definitely has an advantage when the number of differential detectors, (i.e. λ) is less than $3N_B(\lambda < 3N_B)$. However, it requires higher load of IF processing. There is not a clear distinction as to which of the two approaches is more proper. The choice should be based on the special features of the particular application and the environment where the system will operate.

4.9.3 Performance Evaluation of the Truncated Multiple Differential Receiver

In Appendix I, the detailed analysis leading to the evaluation of the truncated multiple differential detection sequence estimator is given. Briefly described, the method works as follows. First, the error probabilities of the pairwise error events are upper and lower bounded. The upper and lower bounds of the pairwise error event probabilities are used with the union bound to provide upper and lower bounds for the performance of the receiver. To avoid unnecessary complication of the text, we shall limit the rest of this section to the presentation of the performance evaluation results. However, the interested reader can find a detailed description of the analysis in Appendix I. Below, we shall report results for Code A as well us the uncoded QPSK and 8PSK.

Fig. 4.86 provides SER curves for Code A[17]. The following curves are displayed. The upper and lower bounds of the truncated MDD sequence estimator for $\lambda = 4$ ((lamda=4,UB), (lamda=4,LB)). The curves of the truncated MDD receiver operating in an ideal channel for $\lambda = 2, 3, 4$ based on Monte Carlo simulations (lamda= ,Sim.AWGN). The curve of the truncated MDD receiver for $\lambda = 2$ operating in a Rician faded channel with $K_r = 10\ dB$ and $B_F T = 0.1$ (lamda=2,Sim.Fading) based also on Monte Carlo simulations. Again the land mobile fading model is used. For comparison, we also include the curves of the conventional receiver (Viterbi decoder processing the outputs of the one symbol differential detector) operating in the ideal (Con.Rec.(AWGN)) and faded (Con.Rec.(Fading)) channel. Both curves of the conventional receiver are based on Monte Carlo simulation results.

As we see from the curves, the simulation results fall within the area predicted by the upper and lower bounds. We also realize that the MDD receiver achieves improvements as high as 2 dB. In the fading channel, the improvement becomes even higher. While the $\lambda = 2$ MDD receivers give an improvement of 1.3 dB in ideal channel, in the Rician faded channel the improvement becomes 2.45 dB (all the above comparisons are made for a SER=10^{-4}). A major factor responsible for the improvements in the fading channels is an increase in the time diversity of a coded sequence, when it is

[17]Results for Codes B, C decoded by the multiple differential detection (recursive) algorithm can be found in [147].

decoded by the MDD sequence estimator. Use of the MDD receiver increases the length of divergence between paths traveling through the trellis diagram, which have been formed by different sequences. The larger the number of differential detectors used (λ) is, the larger the length of divergence becomes. This increases the time diversity of the decoded sequence, which is quite beneficial in faded channels [135]. We shall see similar behaviour when the MDD algorithm is applied with CPM signals in the following chapter.

To make a judgement regarding the tightness of the proposed upper and lower bounds of the MDD receiver, we present in Fig . 4.87 the ones corresponding to $\lambda = 4$ and $\lambda = 6$. For $\lambda = 4$ the distance between upper and lower bound is 0.8 dB and for $\lambda = 6$, 0.3 dB. For higher values of λ the distance becomes even smaller.

In Figs. 4.88 4.89 we display SER curves for uncoded QPSK and 8PSK respectively. We present the upper and lower bounds for $\lambda = 3$ (lamda =3, UB, lamda =3, LB) along with simulation curves for $\lambda = 2, 3$ (lamda= , Sim.AWGN). For comparison we include the curve of the differential detector (DD(AWGN)). In Fig. 4.88 (QPSK) we include simulation results of the MDD receiver with $\lambda = 3$ operating in Rician faded channel with $K_r = 10dB$ and $B_FT = 0.1, 0.2, 0.4$ (lamda=3,Sim.Fad.BfT=). To make a clear and easy comparison we include the curves of the differential detector under the same faded channel conditions (DD(Fad.BfT=)). The DD(Fad.BfT=0.4) curve can be barely seen at the upper left corner of Fig. 4.88; under such channel conditions the differential detector experiences an error floor at SER=10^{-2}.

From the displayed curves we see that the simulated results fall within the area predicted by the bounds. We also realize that use of the MDD receiver in the ideal channel provides improvements as high as 1.5 dB. For the faded channel case, and at SER=10^{-2}, the MDD receiver provides improvements of 1.6 dB ($B_FT = 0.1$) 2 dB ($B_FT = 0.2$) and 9.2 dB ($B_FT = 0.4$). However, for $B_FT = 0.1, 0.2$ the MDD receiver reaches the error floor before the differential detector. Comparing the uncoded with the coded case, the advantages offered by the MDD receiver in faded channels appear to be poorer. The reason for this is that the algorithm does not have the time diversity which appears when the signal is coded.

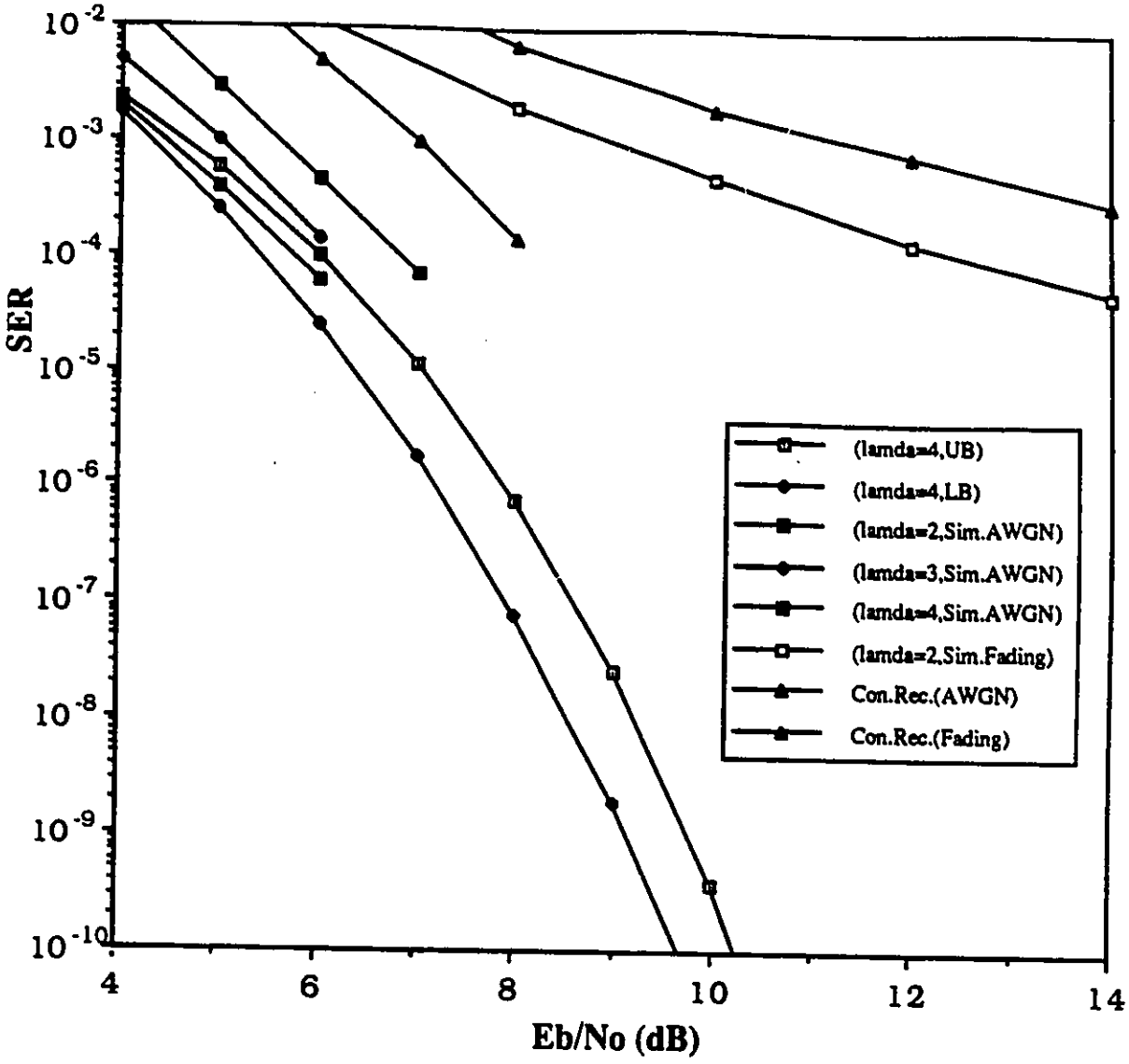

Figure 4.86: Upper/Lower bounds and simulation curves of the truncated MDD receiver for operation in ideal and Rician faded ($K_r = 10dB$, $B_F T = 0.1$) channels. Code A (differentially encoded) is used.

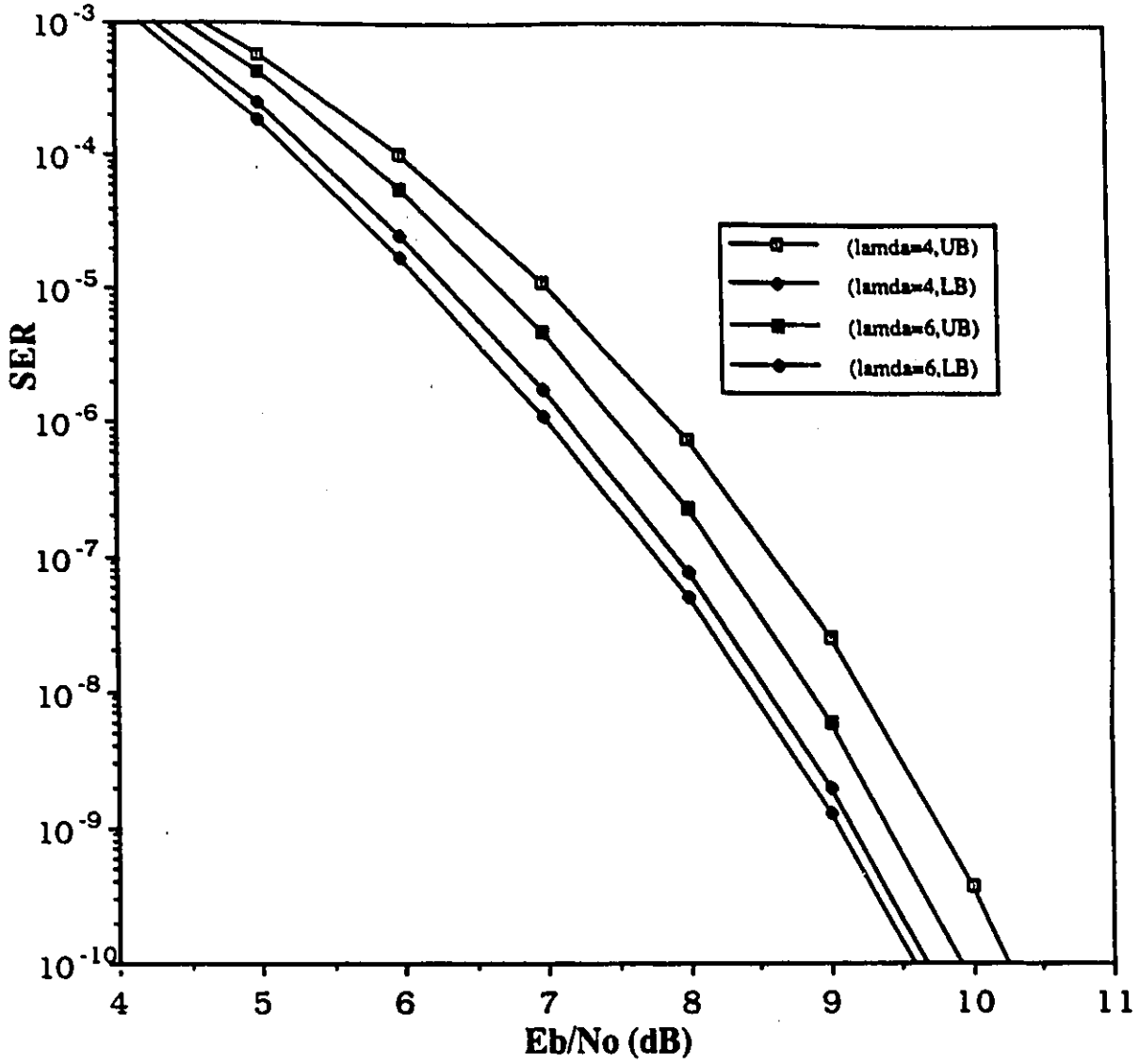

Figure 4.87: Upper/Lower bounds of the truncated MDD receiver for $\lambda = 4$ and $\lambda = 6$.

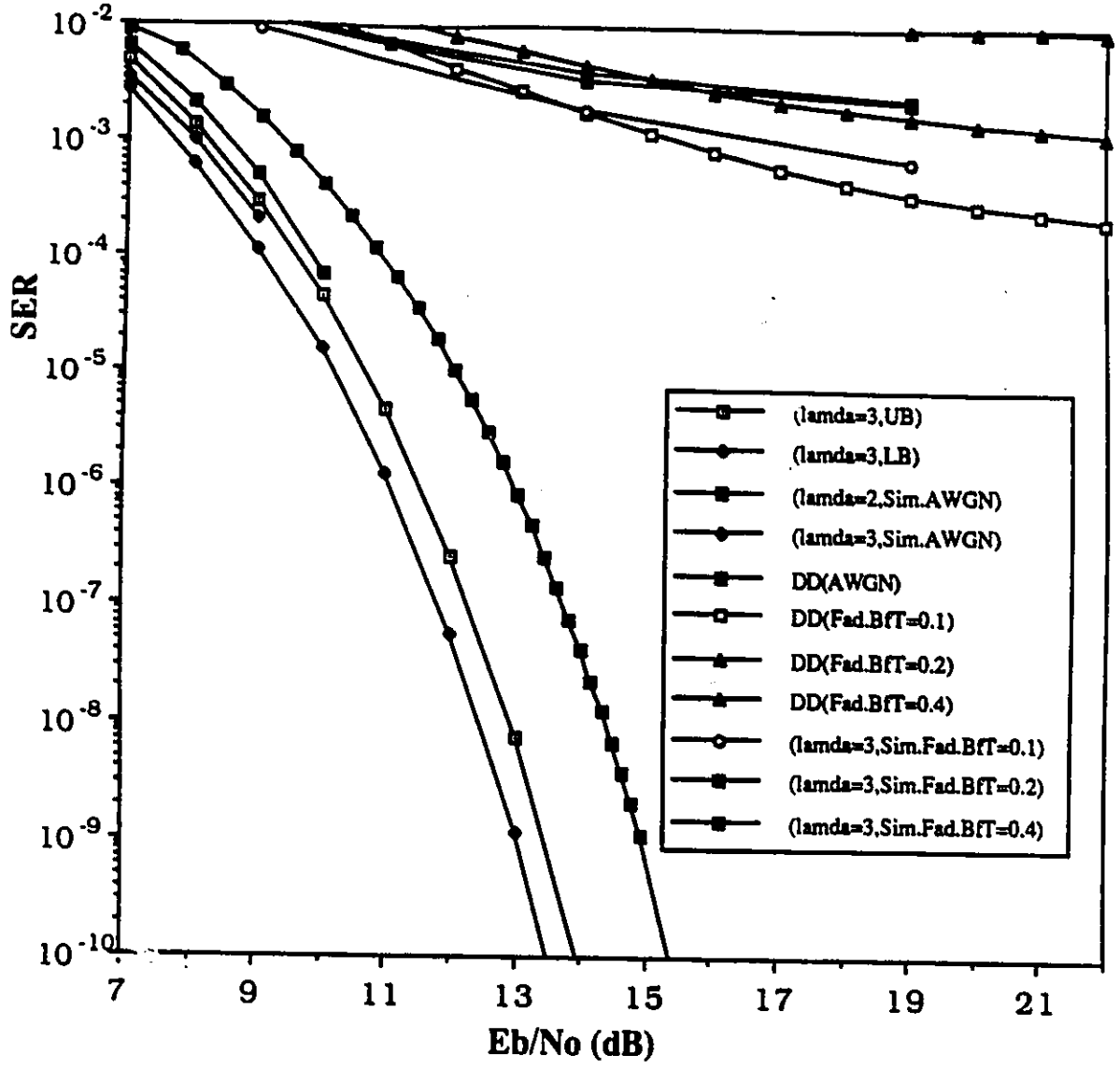

Figure 4.88: Upper/Lower bounds and simulation curves of the truncated MDD receiver for operation in ideal and Rician faded ($K_r = 10dB$, $B_FT = 0.1$) channels. QPSK (differentially encoded) is used.

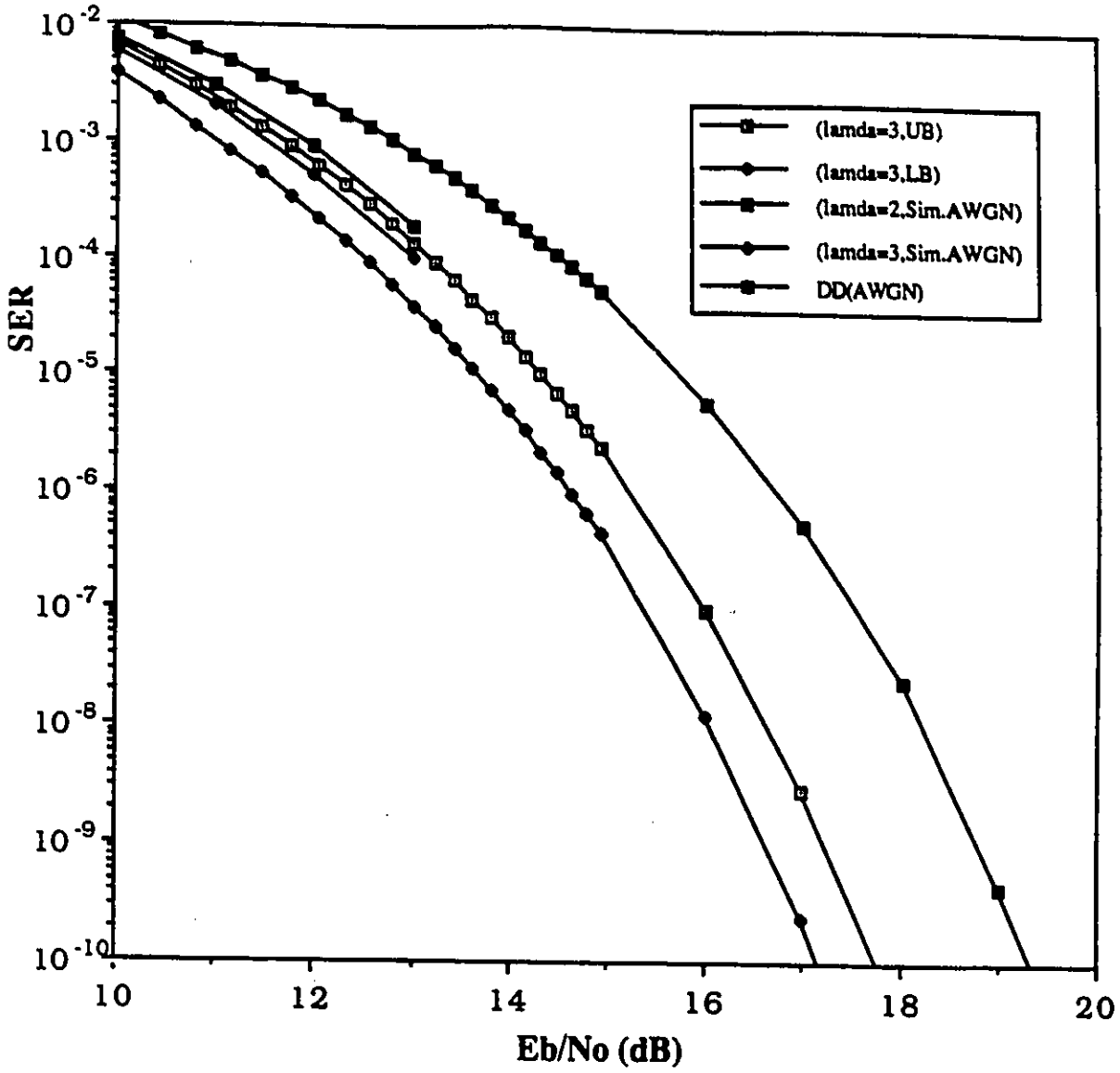

Figure 4.89: Upper/Lower bounds and simulation curves of the truncated MDD receiver for operation in ideal channel. 8PSK (differentially encoded) is used.

4.10 SYMBOL-BY-SYMBOL DETECTION

Up to this point, the present chapter has dealt with sequence estimation. In the rest of this chapter, the symbol-by-symbol detection concept will be examined.

The general structure of the optimal non-coherent symbol-by-symbol receiver has been presented in Eq.(3.58). The case of ideal channel/equal Nyquist filter apportioning is given in Eq.(3.59). The formulas are sums of modified zero order Bessel functions or sums of products between Bessel and exponential functions. In the form presented in Eq.(3.58), the decision laws are of small use for implementation. In the following section, through proper mathematical manipulations, simpler structures will be derived. The structures will be dealing with the two limiting cases. Operation under low E_b/N_o and high E_b/N_o conditions.

4.10.1 Asymptotically Optimal Symbol-By-Symbol Receivers

4.10.2 Low E_b/N_o

Using the Taylor series expansion of the exponential and modified Bessel functions (see Eqs.(4.1), (4.2)) in Eq.(3.58) and retaining only the terms where $\frac{1}{N_o}$ appears with power smaller or equal to 2, we end up with the following formula :

$$\widehat{\bar{a}_k^p} = \bar{S}_l \Longrightarrow \overset{1\le l\le M_p}{max} \quad \{ \sum_{\bar{C}(\bar{A}^\nu)\in\underline{C}_{\underline{S}}^{\bar{S}_l}(k)} [-[IST(\bar{h},\bar{C}(\bar{A}^\nu))] + \frac{[IST^2(\bar{h},\bar{C}(\bar{A}^\nu))]}{2N_o} + \frac{|\sum_{k=0}^{z-1} y_k(c_k^\nu)^*|^2}{4N_o}]\}. \tag{4.116}$$

Processing Eq.(4.116) furthermore, the decision law is reduced to

$$\widehat{\bar{a}_k^p} = \bar{S}_l \Longrightarrow \overset{1\le l\le M_p}{max} \quad \{-h_1 e^{j\Delta\Phi(\bar{S}_l)} + \frac{d_1^I(k)\cos(\Delta\Phi(\bar{S}_l)) + d_1^Q(k)\sin(\Delta\Phi(\bar{S}_l))}{2N_o}\}.$$

(4.117)

Eq. (4.117) is valid for symmetric[18] MPSK constellations. The decision metric for low E_b/N_o depends on two terms. The second term is the sum of products between the inphase and quadrature outputs of the conventional (one-symbol delay) differential detector with the cosine and sine functions of the phase $\Delta\Phi(\bar{S}_i)$. $\Delta\Phi(\bar{S}_i)$ represents the value the information phase ϕ_l has when the bit combination $\bar{S}_i$ is transmitted at (lT) (i.e. $\bar{a}_l^p = \bar{S}_i$). The term is scaled with respect to the inverse of the noise power density N_o. The first term is the product between the value of the impulse response h_1 and $e^{j\Delta\Phi(\bar{S}_i)}$. Notice that as N_o increases, the second term becomes weaker and weaker. For the limiting case where $N_o \to \infty$ (i.e. $\frac{E_b}{N_o} \to 0$), the second term disappears from the decision law, leaving only the first. Under these conditions, (i.e. for low E_b/N_o), the decision is dominated by the intersymbol interference controlled term. Again, this is a fundamental difference as compared to the coherent detection, where such domination of the ISI controlled component and virtual disappearance of the terms which depend on the received signal[19] does not exist. For non-time dispersive channels $h_1 = 0$. This leaves only the second term to base the decision, in which case, the decision law is equivalently expressed as

$$\widehat{\bar{a}_k^p} = \bar{S}_l \Longrightarrow \overset{1\le l\le M_p}{max} \quad \{d_1^I(k)\cos(\Delta\Phi(\bar{S}_l)) + d_1^Q(k)\sin(\Delta\Phi(\bar{S}_l))\} \ . \quad (4.118)$$

This is the conventional symbol-by-symbol detection based on the one-symbol differential detector. In order for h_1 to be equal to 0, the following condition has to be satisfied :

$$h_1 = \frac{1}{2\pi}\int_{-\infty}^{\infty} |H_E(\omega)|^2 e^{j\omega T} d\omega = \frac{1}{\pi}\int_0^{\infty} |H_E(\omega)|^2 \cos(\omega T) d\omega = 0. \quad (4.119)$$

Summarizing the present section, we conclude our findings as follows : For operation in low E_b/N_o:

[18]Let us assume a two-dimensional signal-space with axes x, y. The x and y axes intersect at the [x=0, y=0) point. We define as *symmetric constellations* the constellations where the symmetric of every constellation point in respect to the [x=0, y=0) is a constellation point as well.

[19]To the best of our knowledge, this behaviour of the non-coherent symbol-by-symbol receiver is reported for the first time in the open literature.

1. When Eq. (4.119) is satisfied, the optimal non-coherent symbol-by-symbol receiver is the simple differential detector with one-symbol delay element.

2. When Eq. (4.119) is not satisfied the decision is totally independent from the received signal. The receiver always chooses the symbol $\tilde{S}_l$ which (happens to) minimizes $Re\{h_1 e^{j\Delta\Phi(\tilde{S}_l)}\}$.

4.10.3 High E_b/N_o

For high $\frac{E_b}{N_o}$,

$$\sum_{\bar{C}(\bar{A}^\nu)\in\underline{\underline{C}}_{\underline{\underline{S}}}^{S_l}(k)} [\exp\{-\frac{1}{N_o} IST(\bar{h},\bar{C}(\bar{A}^\nu))\} I_0(\frac{|\sum_{k=0}^{Z-1} y_k(c_k^\nu)^*|}{N_0})]$$

$$\simeq \max_{\bar{C}(\bar{A}^\nu)\in\underline{\underline{C}}_{\underline{\underline{S}}}^{S_l}(k)} [\exp\{-\frac{1}{N_o} IST(\bar{h},\bar{C}(\bar{A}^\nu))\} I_0(\frac{|\sum_{k=0}^{Z-1} y_k(c_k^\nu)^*|}{N_0})]. \quad (4.120)$$

The meaning of Eq. (4.120) is that the value of the summation is very close to the largest value of all the terms present in the summation. Incorporating Eq. (4.120) in the decision law of Eq.(3.58), we get :

$$\widehat{\bar{a}_k^p} = \tilde{S}_l \Longrightarrow \max_{1\le l\le M_p} \{ \max_{\bar{C}(\bar{A}^\nu)\in\underline{\underline{C}}_{\underline{\underline{S}}}^{l}(k)} [\exp\{-IST(\bar{h},\bar{C}(\bar{A}^\nu))\} I_0(\frac{|\sum_{k=0}^{Z-1} y_k(c_k^\nu)^*|}{N_0})]\}]\}. \quad (4.121)$$

Incorporating the result of Appendix F in Eq.(4.121), we are given the following expression of the decision law:

$$\widehat{\bar{a}_k^p} = \tilde{S}_l \Longrightarrow \max_{1\le l\le M_p} \{ \max_{\bar{C}(\bar{A}^\nu)\in\underline{\underline{C}}_{\underline{\underline{S}}}^{S_l}(k)} \{ [-IST(\bar{h},\bar{C}(\bar{A}^\nu)) + |\sum_{k=0}^{Z-1} y_k(c_k^\nu)^*|]\}\}. \quad (4.122)$$

Under ideal channel/equal Nyquist filter apportioning conditions, $IST(\bar{h}, \bar{C}(\bar{A}^{\nu})) = 0$ and Eq.(4.121) becomes:

$$\widehat{\bar{a}_k^p} = \bar{S}_l \Longrightarrow \max_{1 \le l \le M_p} \{ \max_{\bar{C}(\bar{A}^{\nu}) \in \underline{\mathcal{C}}_S^{\bar{S}_l}(k)} \{ [| \sum_{k=0}^{Z-1} y_k (c_k^{\nu})^* |] \} \}. \qquad (4.123)$$

Replacing the $|\sum_{k=0}^{Z-1} y_k (c_k^{\nu})^*|$ term in Eqs.(4.122), (4.123) with the expression of $\aleph_{IC}^{SQ}(\bar{y}, \bar{C}(\bar{A}))$ of Eq.(4.33), we can express the decision laws of the symbol-by-symbol receivers in a multiple differential detection form.

4.10.4 Performance Evaluation of the Symbol-by-Symbol Receiver

The present section deals with the performance of the asymptotically optimal symbol-by-symbol receiver (for high E_b/N_o). The decoder will be evaluated for an ideal (equal/non-equal Nyquist filter apportioning) as well as a time dispersive channel. Results for a (non-differentially encoded) QPSK signal will be provided. However, before we continue with the presentation of the performance results, we shall describe first the analytical frame work we followed to acquire these results.

4.10.4.1 Performance Analysis

Let us assume that the sequence $\bar{C}(\bar{A}^{\nu}) \in \underline{\mathcal{C}}_S^{\bar{S}_l}(k)$ has been transmitted. The receiver will make a wrong decision only if it chooses a sequence $\bar{C}(\bar{A}^{\zeta})$ which does not belong to the $\underline{\mathcal{C}}_S^{\bar{S}_l}(k)$ set ($\bar{C}(\bar{A}^{\zeta}) \notin \underline{\mathcal{C}}_S^{\bar{S}_l}(k)$; $\notin$ represents *is not member of*). We can upper bound the probability of making a wrong decision when $\bar{C}(\bar{A}^{\nu})$ has been transmitted ($P_e^{SBS}(\bar{C}(\bar{A}^{\nu}))$), by the using the union, i.e.:

$$\begin{aligned} P_e^{SBS}(\bar{C}(\bar{A}^{\nu})) &\le \sum_{\bar{C}(\bar{A}^{\zeta}) \notin \underline{\mathcal{C}}_S^{\bar{S}_l}(k)} P^Z(\{\bar{C}(\bar{A}^{\zeta}) \leftarrow \bar{C}(\bar{A}^{\nu})\}) \\ &\le \sum_{\bar{C}(\bar{A}^{\zeta}) \notin \underline{\mathcal{C}}_S^{\bar{S}_l}(k)} B_{HAO[\nu,\zeta]}^Z \qquad (4.124) \end{aligned}$$

(for $B_{HAO[\nu,\zeta]}^Z$ see Eq.(4.56)).

The overall symbol error probability $\mathcal{P}e^Z_{SBS}$ can be upper bounded by averaging over all sequences $\bar{C}(\bar{A}^\nu) \in \underline{\mathcal{C}}^{S_l}_{\underline{S}}(k)$, ie.

$$\mathcal{P}e^Z_{SBS} \leq \mathcal{U}^{SBS}\mathcal{B} = \frac{1}{M^{Z-1}} \sum_{\bar{C}(\bar{A}^\nu)\in\underline{\mathcal{C}}^{S_l}_{\underline{S}}(k)} \sum_{\bar{C}(\bar{A}^\zeta)\notin\underline{\mathcal{C}}^{S_l}_{\underline{S}}(k)} B^Z_{HAO[\nu,\zeta]}. \quad (4.125)$$

When the channel is ideal, the following equality holds:

$$\sum_{\bar{C}(\bar{A}^\zeta)\notin\underline{\mathcal{C}}^{S_l}_{\underline{S}}(k)} B^Z_{[\nu,\zeta]} = \sum_{\bar{C}(\bar{A}^\eta)\notin\underline{\mathcal{C}}^{S_l}_{\underline{S}}(k)} B^Z_{[\xi,\eta]} \quad (4.126)$$

$\forall \ \bar{C}(\bar{A}^\nu), \bar{C}(\bar{A}^\xi) \in \underline{\mathcal{C}}^{S_l}_{\underline{S}}(k)$ (for $B^Z_{[\nu,\zeta]}$ see Eq.(4.44)). This leads to simplifications in the upper union bound expression which now becomes:

$$\mathcal{P}e^Z_{SBS} \leq \mathcal{U}^{SBS}\mathcal{B} = \sum_{\bar{C}(\bar{A}^\zeta)\notin\underline{\mathcal{C}}^{S_l}_{\underline{S}}(k)} B^Z_{[\nu,\zeta]}. \quad (4.127)$$

$\bar{C}(\bar{A}^\nu)$ can be any sequence, member of $\underline{\mathcal{C}}^{S_l}_{\underline{S}}(k)$.

4.10.5 Performance Results

In Fig. 4.90 we display the SER curves of the symbol-by-symbol receiver for operation in ideal channel. Values of Z used are $Z = 4, 7$. The curves are calculated by using the union bound approach described by Eq.(4.127). The curves are labelled as [(Z= (S-B-S)]. We also include the SER curve of the differential detector (DD). For $Z = 4$ the results indicate an improvement of 1.5 dB and for $Z = 7$ 2 dB.

In Fig. 4.91 the curves of the asymptotically optimal symbol-by-symbol receiver operating in a distorted channel are presented. We have used the channel model described by Eq.(4.55). $\rho_e = 0.5$ and $t_D = T$ and $mod_{2\pi}(\omega_c T) = \pm\pi$. The evaluated configurations use $Z = 4, 7, 18$ and they are labelled in the figure as [(Z= (AO.S-B-S)]. To make comparisons easier, we also include in the figure the SER curves of the equalized differential detector [(DD(Equal.)] (a zero forcing equalizer is used) and the Z=7 asymptotically optimal non-coherent symbol-by-symbol receiver operating in an ideal channel [(Z=7(S-B-S)IC)] (it has a performance which is practically identical to

the coherent detector with perfect carrier reference operating in ideal channel conditions). The displayed curves indicate the following improvements of the asymptotically optimal symbol-by-symbol receiver configurations: for $Z = 4$ 3 dB, for $Z = 7$ 4.4. dB and for $Z = 18$ 5 dB. The $Z = 18$ decoder has practically identical performance with the coherent receiver.

Table 4.26: Improvements offered by the asymptotically optimal symbol-by-symbol receiver as a function of the sequence length Z. The comparison is with the conventional differential detector.

		GAINS (dB)	
		Ideal Channel	Distorted Channel
Z	4	1.5	3
	7	2	4.4
	18	2	5

The results are summarized in Table 4.26. From the figures and the table, the superiority of the asymptotically optimal symbol-by-symbol receiver as compared to the differential detector is made clear.

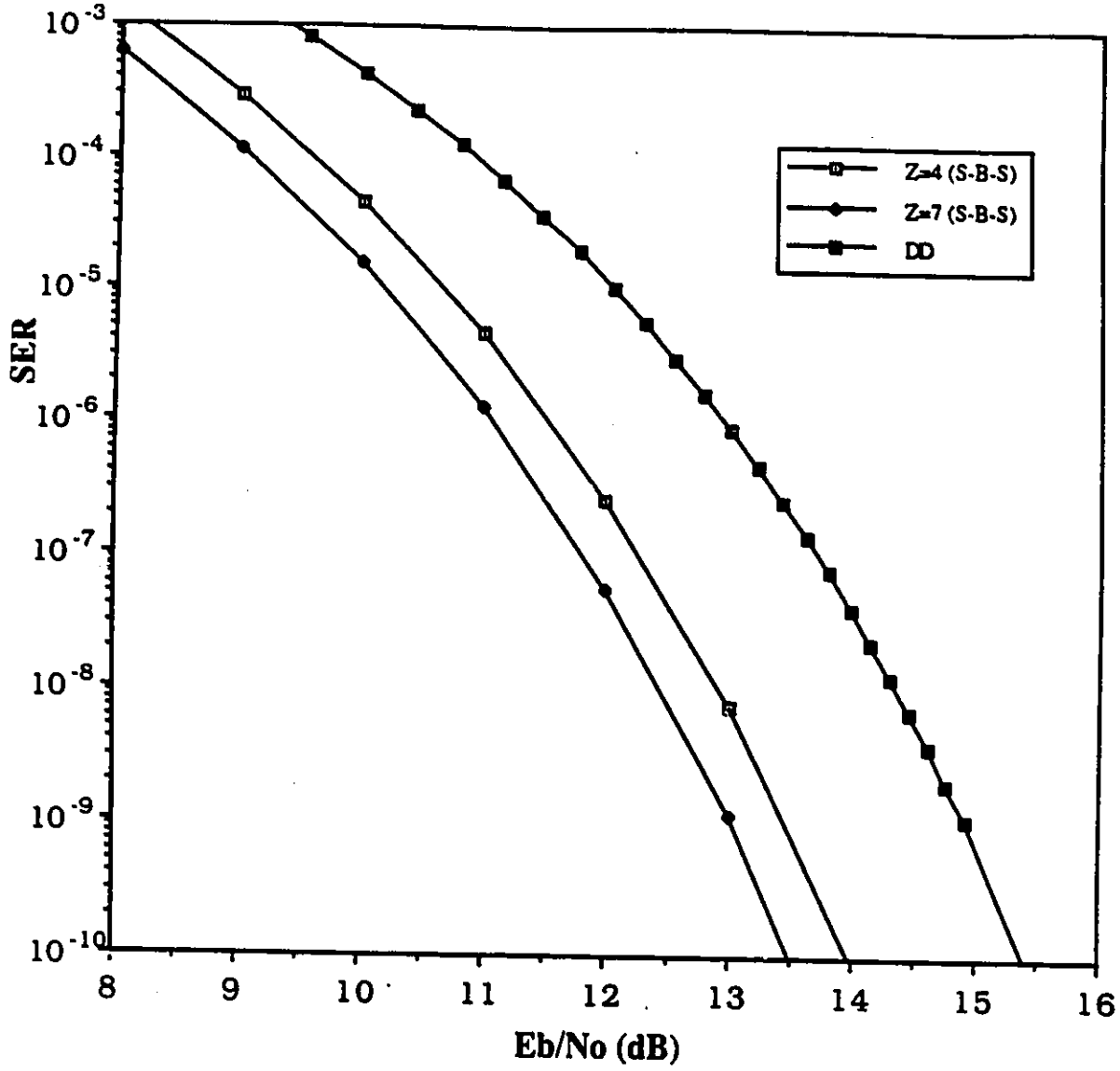

Figure 4.90: SER curves of the Asymptotically Optimal Symbol-By-Symbol receiver operating in ideal channel. QPSK is used.

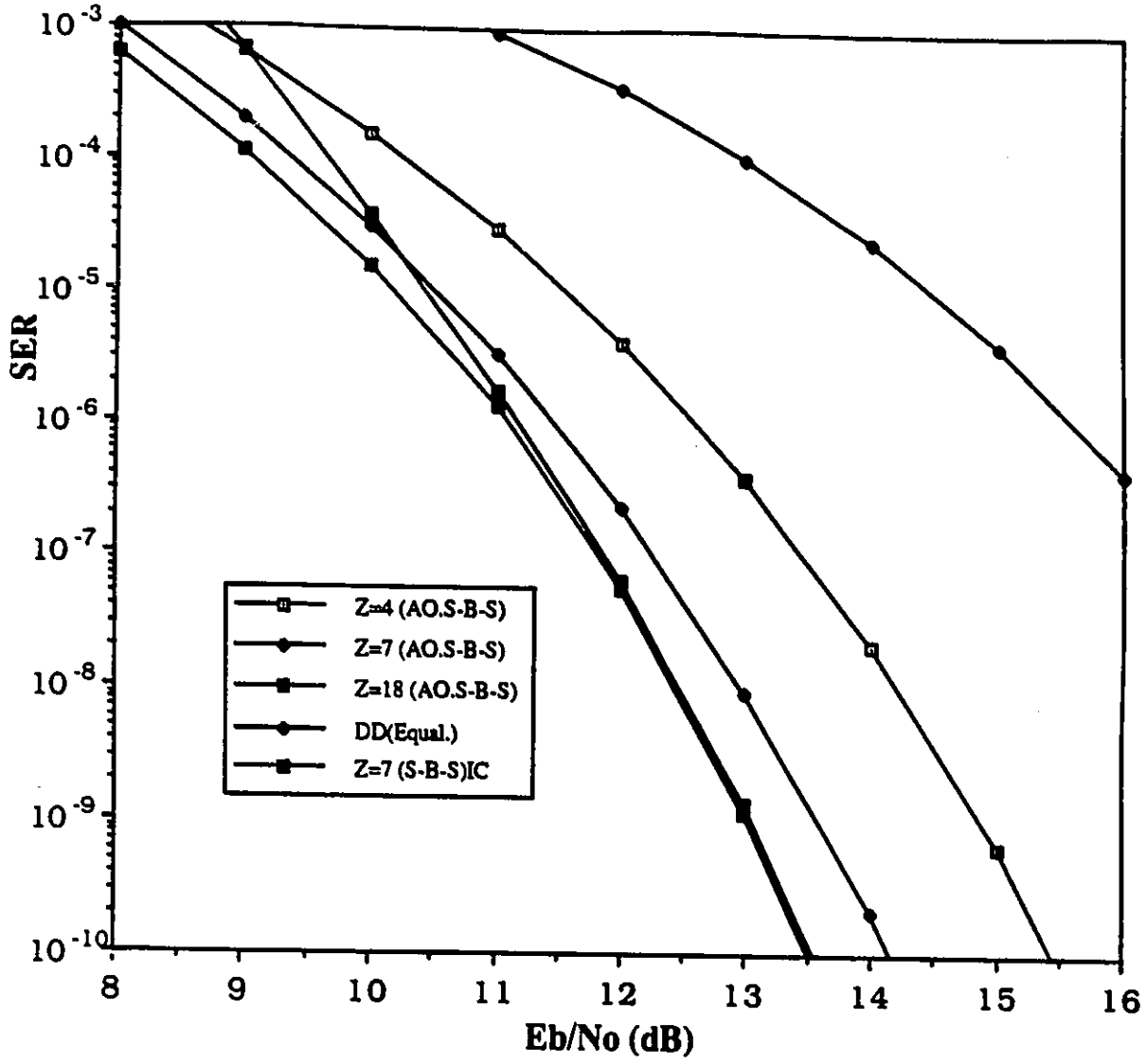

Figure 4.91: SER curves of the Asymptotically Optimal Symbol-By-Symbol receiver operating in a time dispersive channel. QPSK is used.

4.11 REDUCED COMPLEXITY SYMBOL-BY-SYMBOL RECEIVERS BASED ON SIGNAL COMBINING AND DECISION FEEDBACK

The asymptotically optimal symbol-by-symbol receivers examined in section 4.10 have the disadvantage that their complexity increases exponentially with the length of the processed sequence. In order to overcome complexity limitations, in this section we shall propose simpler receivers based on decision feedback and signal combining techniques.

In the following paragraphs, first a set of assumptions will be presented. Afterwards, based on these assumptions, the decision laws of the reduced complexity structures will be given.

Assumptions

Let us assume that the information word $\bar{a}_\xi^p$ has to be decided. Also, let us assume that for the decision of $\bar{a}_\xi^p$, the following information is available :

1. The signal samples $y_{\xi+i_F}, \ldots, y_{\xi+1}, y_\xi, y_{\xi-1}, \ldots, y_{\xi-i_P-1}$. ($i_F$, i_P are integers).

2. The decisions regarding the following symbols : $\bar{a}_{\xi+l_F}^p, \ldots, \bar{a}_{\xi+i_F+l_{ISI}-1}^p$, and $\bar{a}_{\xi-l_P}^p, \ldots, \bar{a}_{\xi-i_P-l_{ISI}}$

i_F, i_P are the number of signal samples which are processed by the receiver and which have been received after and before ξT (l_F, l_P are non-negative integers with $l_F \leq i_F$, $l_P \leq i_P$). l_{ISI} is the memory (in symbol periods) of the cascaded premodulation filter-channel-post detection filter impulse response.

The assumptions made above imply that for the decision of $\bar{a}_\xi^p$, a number of signal samples (some of them received before (ξT) and some after) are processed. These samples carry information and they are affected by other symbols transmitted before ($\bar{a}_{\xi-1}^p, \ldots, \bar{a}_{\xi-i_P-l_{ISI}}$) and some after $\bar{a}_\xi^p$

$(\bar{a}^p_{\xi+1}, \ldots, \bar{a}^p_{\xi+i_F+l_{ISI}})$. From these symbols, the ones listed at the second part of the assumption, are considered known. The rest remain to be used as variables in the detection process. We realize that for $i_F + l_{ISI} - 1 > l_F$, we are assuming knowledge of some information words transmitted after the under decision one (i.e. Fig. 4.92 (a)). In order to realize this receiver, two-stages of detection are needed.

The model of a two-stage receiver used in the past with various applications, is presented in Fig. 4.92 (a). The first stage of the receiver performs some decisions. Then, these decisions are communicated to the second stage where they are used together with decisions made by the second stage itself to provide more accurate estimates of the transmitted symbols. The single hat ($\hat{}$) indicates decisions made in the first detection stage, whereas triple hat ($\hat{\hat{\hat{}}}$), decisions provided by the second stage. A problem with the structure described above is the following. When the first stage makes an error, it transfers it to the second stage and initiates a process which can end up with an error propagation. These wrong decisions are re-used by the second stage itself at a later time and re-initiate another sequence of propagated errors. In one way, the error initiated in the first stage, responsible for initializing an error propagation in the second stage, is recycled and creates another set of errors for a second time. This (amplified) effect of error propagation penalizes the performance.

In order to avoid this double error propagation effect, we propose the following configuration. The first stage of detection is formed not by one but by two receivers (see Fig. 4.92 (b)). One receiver makes forward decisions (i.e. decides the symbols in the sequence that have been transmitted $\bar{a}^p_1, \bar{a}^p_2, \ldots, \bar{a}^p_{Z-1}$), whereas the second receiver decides them backwards ($\bar{a}^p_{Z-1}, \bar{a}^p_{Z-2}, \ldots, \bar{a}^p_1$). In Fig.4.92 (b), the decisions made by the forward receiver of the first stage are represented as ($\hat{}$). Decisions provided by the receiver performing backward decisions are marked with a ($\hat{}$). Both receivers communicate their decisions to the second stage where they are used to provide a better estimate. Notice that in this configuration, the second stage does not use its own decisions. The advantages of using the second configuration as compared to the first are the following. First, the fact that we use two independently deciding first stage receivers helps to avoid the initialization of errors in the second stage, or even if it does happen, a recovery back to correct decisions

is usually faster. The reason for this is simple. Chances are that the two receivers will not be making simultaneous errors most of the time. Even if one receiver makes an error, the correct decision of the other one is capable of protecting the second stage from making an erroneous decision. At the same time by not allowing the second stage to use its own decisions, it protects the system from recycling the errors appearing in the first stage and does not allow them to affect the performance of the second stage twice. For these two reasons, the second configuration of two-stage detection is expected to perform better than the first.

Coming back to the derivation of the decision law, based on the above assumptions , the optimal maximum likelihood symbol-by-symbol receiver is described by the following equation:

$$\hat{\hat{\bar{a}}}_{\xi}^{p} = \bar{S}_l \Longrightarrow \overset{1\le l\le M_p}{max} \{ \sum_{\bar{C}(\bar{A}^{\nu})\in \underline{C}_{\underline{S}}^{S_l}(k)} \{\exp\{-\frac{1}{N_o} IST(\bar{h},\bar{C}(\bar{A}))\}] \; I_o(\frac{|\sum_{k=i_P}^{i_F} y_k (c_k^{\nu})^*|}{N_o})\} \tag{4.128}$$

where

$$\bar{C}(\bar{A}^{\nu}) = [\widehat{DA}_{\xi}(-l_P, -i_P - l_{ISI}), \overline{DA}_{\xi}^{\nu}(-l_P+1, l_F-1), \hat{\hat{\bar{DA}}}_{\xi}(l_F, i_F + l_{ISI})] \tag{4.129}$$

and

$$\hat{\hat{\bar{DA}}}_{\xi}(k,\eta) = [\hat{\hat{\bar{a}}}_{\xi+k}^{p}, \hat{\hat{\bar{a}}}_{\xi+k+1}^{p}, ..., \hat{\hat{\bar{a}}}_{\xi+\eta}^{p}], \tag{4.130}$$

$$\widehat{\bar{DA}}_{\xi}(k,\eta) = [\widehat{\bar{a}}_{\xi+k}^{p}, \widehat{\bar{a}}_{\xi+k+1}^{p}, ..., \widehat{\bar{a}}_{\xi+\eta}^{p}], \tag{4.131}$$

$$\overline{DA}_{\xi}^{\nu}(k,\eta) = [\bar{a}_{\xi+k}^{\nu}, ...\bar{a}_{\xi+\eta}^{\nu}] \tag{4.132}$$

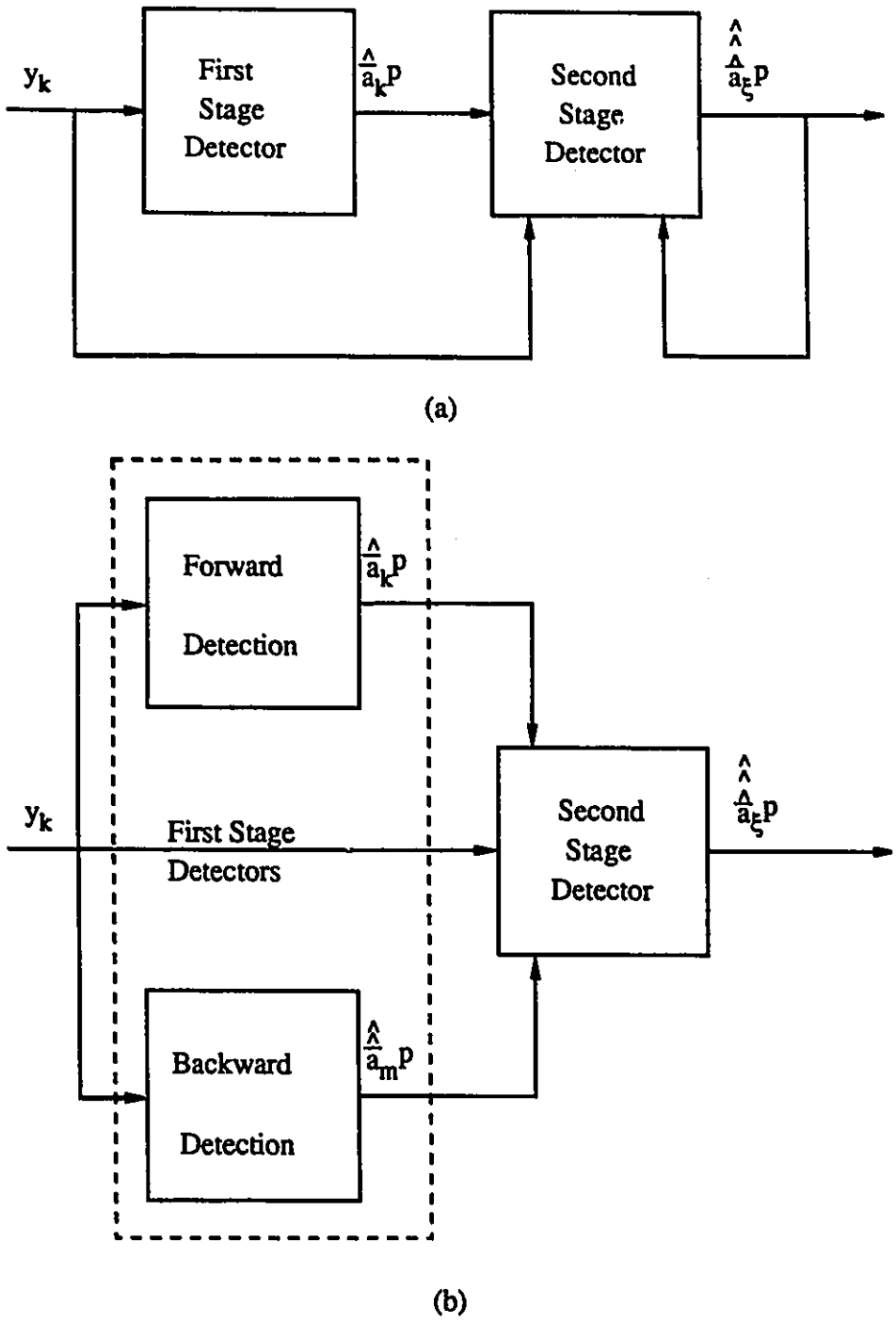

Figure 4.92: Two different scenarios for the implementation of the two-stage receiver: (a) the second stage uses its own decisions in the detection process; (b) the first stage consists of a forward and a backward deciding detector, also the second stage does not use its own decisions in the detection process.

$(k < \eta)$. ν represents the ν^{th} of the $2^{p(n-k)}$ combinations which can be constructed by the $\eta - k$ different information words $\bar{a}^p_{\xi+k}, ..., \bar{a}^p_{\xi+\eta}$. Following the approach described in subsection 4.10.4.1, we find the following expression as asymptotically optimal decision law for high E_b/N_o:

$$\widehat{\widehat{\widehat{\bar{a}^p_\xi}}} = \bar{S}_l \Longrightarrow \overset{1\le l\le M_p}{\bar{max}} \quad \{ \overset{\bar{C}(A^\nu)\in\underline{C}^{S_l}_S(k)}{\bar{max}} [-IST(\bar{h}, \bar{C}(A^\nu)) + | \sum_{k=-i_P}^{i_F} y_k (c^\nu_k)^* |] \} \tag{4.133}$$

In the following paragraphs, two specific structures of receivers (the first using one and the second using two stages of detection) will be examined. For simplicity, we shall assume that the channel is ideal and an equal apportioning filtering strategy is followed.

4.11.1 One Stage Receiver

For the decision of $\bar{a}^p_\xi$, the following information is available:

1. the samples $y_\xi, y_{\xi-1}, ..., y_{\xi-i_P}$ (where i_P can go as low as ξ).
2. $\widehat{\bar{a}^p_{\xi-1}}, \widehat{\bar{a}^p_{\xi-2}}, ..., \widehat{\bar{a}^p_{\xi-i_P}}$ (they are assumed correct).

The optimal decoding metric can be derived from Eq.(4.128), by setting $i_F = 0$, $l_F = 0$, $l_{ISI} = 0$, and $l_P = 1$. This gives the following expression:

$$\widehat{\bar{a}^p_\xi} = \bar{S}_l \Longrightarrow \overset{1\le l\le M_p}{\bar{max}} \quad \{ | y_\xi c^*_\xi + \sum_{i=1}^{i_P} y_{\xi-i} \hat{c}^*_{\xi-i} | \} \tag{4.134}$$

Using Eqs.(3.27) in Eq.(4.134) allows us to express the decision law in the following form:

$$\widehat{\bar{a}^p_\xi} = \bar{S}_l \Longrightarrow \overset{1\le l\le M_p}{\bar{max}} \quad \{ | y_\xi e^{-j\Delta\Phi(S_l)} (\Pi_{l=1}^{i_P-1} \hat{g}^*_{\xi-l}) + \sum_{i=1}^{i_P} y_{\xi-i} (\Pi_{l=i}^{i_P-1} \hat{g}^*_{\xi-l}) | \} \tag{4.135}$$

where $\hat{g}_l$ is the decision of the information symbol g_l (g_l is the information symbol which corresponds to the information word $\bar{a}^p_l$). Carrying out the

maximization of squares rather than absolute values and eliminating terms independent from the under decision information word we arrive at the following equivalent expression (to be maximized):

$$\widehat{\bar{a}_\xi^p} = \bar{S}_l \Longrightarrow \max_{1\le l\le M_p} \{\sum_{i=1}^{i_P}[d_i^I(\xi)Re\{c_\xi \hat{c}^*_{\xi-i}\} + d_i^Q(\xi)I_m\{c_\xi \hat{c}^*_{\xi-i}\}] =$$

$$\sum_{i=1}^{i_P}\{d_i^I(\xi)\cos(\Delta\Phi(\bar{S}_l) \oplus \Delta\Phi(\widehat{\bar{a}_{k-1}^p}) \oplus ... \oplus \Delta\Phi(\widehat{\bar{a}_{k-i}^p}))$$

$$+d_i^Q(\xi)\sin(\Delta\Phi(\bar{S}_l) \oplus \Delta\Phi(\widehat{\bar{a}_{k-1}^p}) \oplus ... \oplus \Delta\Phi(\widehat{\bar{a}_{k-i}^p}))\} \qquad (4.136)$$

In Eq.(4.134), Eqs.(4.24), (4.28) have been used. We remind the reader that $\Delta\Phi(\bar{S}_l)$ represents the value the information phase ϕ_ξ has when at ξT the transmitted information word $\bar{a}_\xi^p = \bar{S}_l$. The multiple differential detection nature of the decoder is obvious. The number (λ) of differential detectors used by the receiver is $\lambda = i_P$. We also realize that the outputs of the multiple differential detectors are combined in a way controlled by already available decisions. For this reason, we call this receiver **Multiple Differential Detection with Combining and Decision Feedback (MDD/CWF).**

For the implementation of the multiple differential receiver, we can choose either a baseband or an IF approach (depending on the application to be used with). Also, the logic described by Eq.(4.136) can be implemented quite easily and inexpensively. Let us consider for example the case of a QPSK signal and a MDD/CWF receiver with $i_F = 0$, $i_P = 1$. The decision logic for this case is the following (see [145], [146]):

i) if $\hat{a}_{\xi-1}^1 = 1$ and $\hat{a}_{\xi-1}^2 = 1$

$$\hat{a}_\xi^1 = hlm\{d_1^I(\xi) + d_2^I(\xi)\})$$

$$\hat{a}_\xi^2 = hlm\{d_1^Q(\xi) + d_2^Q(\xi)\}$$

ii) if $\hat{a}_{\xi-1}^1 = 0$ and $\hat{a}_{\xi-1}^2 = 1$

$$\hat{a}_\xi^1 = hlm\{d_1^I(\xi) - d_2^I(\xi)\}$$

$$\hat{a}_\xi^2 = hlm\{d_1^Q(\xi) + d_2^I(\xi)\}$$

iii) if $\hat{a}_{\xi-1}^1 = 0$ and $\hat{a}_{\xi-1}^2 = 0$

$$\hat{a}_\xi^1 = hlm\{d_1^I(\xi) - d_2^I(\xi)\}$$

$$\hat{a}_\xi^2 = hlm\{d_1^Q(\xi) - d_2^Q(\xi)\}$$

iv) if $\hat{a}_{\xi-1}^1 = 1$ and $\hat{a}_{\xi-1}^2 = 0$

$$\hat{a}_\xi^1 = hlm\{d_1^I(\xi) + d_2^Q(\xi)\}$$

$$\hat{a}_\xi^2 = hlm\{d_1^Q(\xi) - d_2^I(\xi)\} \tag{4.137}$$

where

$$hlm\{x\} = \begin{cases} 1 & \text{for } x > 0 \\ 0 & \text{elsewhere.} \end{cases} \tag{4.138}$$

In Fig. 4.93 we present a conceptual block diagram of the receiver.

The combining and the controlling logic which will provide the decisions described in Eq.(4.137) can be easily implemented using analog amplifiers and basic binary logic circuits (OR, AND, NOT, XOR).

Except for the form presented in Eq.(4.136), another formulation of the decision law (which might be more suitable for implementations based on digital signal processing) is possible. The alternative approach is administered through presentation of the metric of Eq.(4.134) in the following form:

$$\widehat{\bar{a}_\xi^p} = \bar{S}_l \Longrightarrow \overset{1\le l\le M_p}{\widetilde{max}} \quad \{|\hat{c}_{\xi-1}||y_\xi c_\xi^* + \sum_{i=1}^{i_P} y_{\xi-i}\hat{c}_{\xi-i}^*)^*|\} \tag{4.139}$$

Since $|\hat{c}_{\xi-1}| = 1$ Eq.(4.139) is equivalent to Eq.(4.134). Use of $|\epsilon_1||\epsilon_2| = |\epsilon_1\epsilon_2|$ (ϵ_1, ϵ_2 are complex numbers) with Eq.(4.139), gives the following expression:

$$\widehat{\bar{a}_\xi^p} = \bar{S}_l \Longrightarrow \overset{1\le l\le M_p}{\bar{m}\bar{a}x} \quad \{|y_\xi e^{-j(\Delta\Phi(\bar{S}_l))} + \mathcal{DH}_\xi^P(y_{\xi-1},\ldots,y_{\xi-i_P},\widehat{\bar{a}_{\xi-1}^p},\ldots,\widehat{\bar{a}_{\xi-i_P+1}^p})\}$$

(4.140)

where

$$\mathcal{DH}_\xi^P(y_{\xi-1},\ldots,y_{\xi-i_P},\widehat{\bar{a}_{\xi-1}^p},\ldots,\widehat{\bar{a}_{\xi-i_P+1}^p}) =$$

$$[y_{\xi-1} + \sum_{i=1}^{i_P-1} y_{\xi-i-1} e^{-j(\sum_{k=0}^{i-1}\Delta\Phi(\widehat{\bar{a}_{\xi-i-k}^p}))^*}]$$

(4.141)

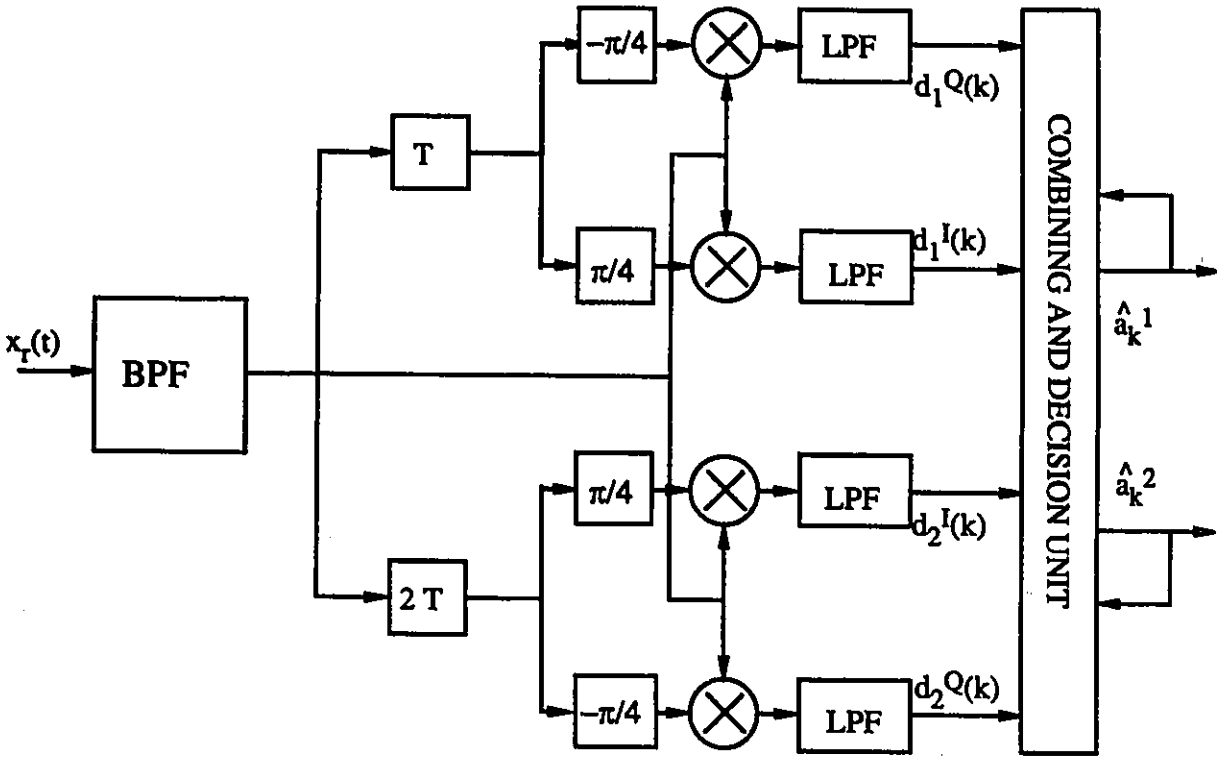

Figure 4.93: Block Diagram of the Multiple Differential Symbol-by-Symbol receiver using Combining with Feedback (MDD/CWF) for QPSK. The receiver uses the 1 and 2-symbol delay differential detectors.

4.11.2 Two-Stage Receiver

For the two-stage receiver, the assumptions stand as follows :

1. $y_{\xi+i_F}, y_{\xi+i_F-1}, \ldots, y_{i-i_P}$ are available for the decision.
2. The following decisions can be used: $\hat{\hat{\bar{a}}}^p_{\xi+i_F}, \ldots, \hat{\hat{\bar{a}}}^p_{\xi+1}, \hat{\bar{a}}^p_{\xi-1}, \ldots, \hat{\bar{a}}^p_{\xi-i_P}$.

Starting from Eq. (4.128) and following the approach presented for the one stage detector, we end up with the following decision law:

$$\begin{aligned}\hat{\hat{\bar{a}}}^p_\xi = \bar{S}_l \Longrightarrow \overset{1\le l\le M_p}{max} \{ \quad & \sum_{i=1}^{i_F}[d^I_i(\xi+i)\cos(\Delta\Phi(\widehat{\widehat{\bar{a}^p_{\xi+i}}}) \oplus \ldots\ldots \oplus (\Delta\Phi(\bar{S}_l)) \\ & + d^Q_i(\xi+i)\cos(\Delta\Phi(\widehat{\widehat{\bar{a}^p_{\xi+i}}}) \oplus \ldots\ldots \oplus (\Delta\Phi(\bar{S}_l))] \\ & + \sum_{i=1}^{i_P}[d^I_i(\xi)\cos(\Delta\Phi(\bar{S}_l) \oplus \Delta\Phi(\widehat{\bar{a}^p_{\xi-1}}) \oplus \ldots\ldots \oplus \Delta\Phi(\widehat{\bar{a}^p_{\xi-i}})) \\ & + d^Q_i(\xi)\cos(\Delta\Phi(\bar{S}_l) \oplus \Delta\Phi(\widehat{\bar{a}^p_{\xi-1}}) \oplus \ldots\ldots \oplus \Delta\Phi(\widehat{\bar{a}^p_{\xi-i}}))]\}\end{aligned} \tag{4.142}$$

A receiver implemented on the form expressed by Eq.(4.142) makes use of multiple differential detection.

An equivalent formulation of the decision law is the following :

$$\begin{aligned}\hat{\hat{\bar{a}}}^p_\xi \;=\; & \bar{S}_l \Longrightarrow \overset{1\le l\le M_p}{max} \{|y_\xi e^{j-\Delta\Phi(\bar{S}_l)} \\ & + \; y_{\xi-1} + (\sum_{i=1}^{i_P-1} y_{\xi-i-1} e^{-j(\sum_{k=0}^{Z-1}\Delta\Phi(\widehat{\bar{a}^p_{\xi-i-k}}))})] \\ & + \; [y_{\xi+1} + (\sum_{i=1}^{i_P-1} y_{\xi+i-1} e^{-j(\sum_{k=0}^{Z-1}\Delta\Phi(\widehat{\widehat{\bar{a}^p_{\xi+i-k}}}))})]|\}\end{aligned} \tag{4.143}$$

This formulation provides an implementation based on block processing.

4.11.3 Performance Evaluation of One-Stage Receivers

The receivers described in the present section are based on the use of decision feedback. Consequently, the probability of making a correct decision is directly related to the correctness of the previous decisions. This implies the presence of error propagation which affects all the decision feedback systems.

In order to provide performance results where the error propagation effect is include, we used Monte Carlo simulations. However, in Appendix J, we provide an analytical framework which gives the opportunity to calculate the performance of the receiver under the assumption that the previous decisions -used by the receiver to decide the present symbol- are correct[20].

In Fig. 4.94 we present the SER curves of the one-stage detector for a QPSK signal and for three receiver configurations. The first uses the 1 and 2 symbol detectors (S-B-S/CWF(lamda=2)), the second uses the 1, 2 and 3 symbol detectors (S-B-S/CWF(lamda=3)) and the third uses the one, two, three and four symbol detectors (S-B-S/CWF(lamda=4)). We also include the curve of the differential detector for reference.

The SER curves show that the (S-B-S/CWF(lamda=2)) receiver has an advantage of 0.8 dB as compared to the differential detector. The (S-B-S/CWF(lamda=3)) 1.1 dB and (S-B-S/CWF(lamda=4)) 1.3 dB. These results are summarized in Table 4.27

Table 4.27: Improvements achieved by the symbol-by-symbol receivers based on multiple differential detection and the use of combining with feedback. The signal is QPSK.

GAINS (dB)		
$\lambda = 2$	$\lambda = 3$	$\lambda = 4$
0.8	1.1	1.3

[20]The material of Appendix J can be used, together with Marcov chains theory [59] to provide a complete analytical performance evaluation of the receiver (with the effect of error propagation included).

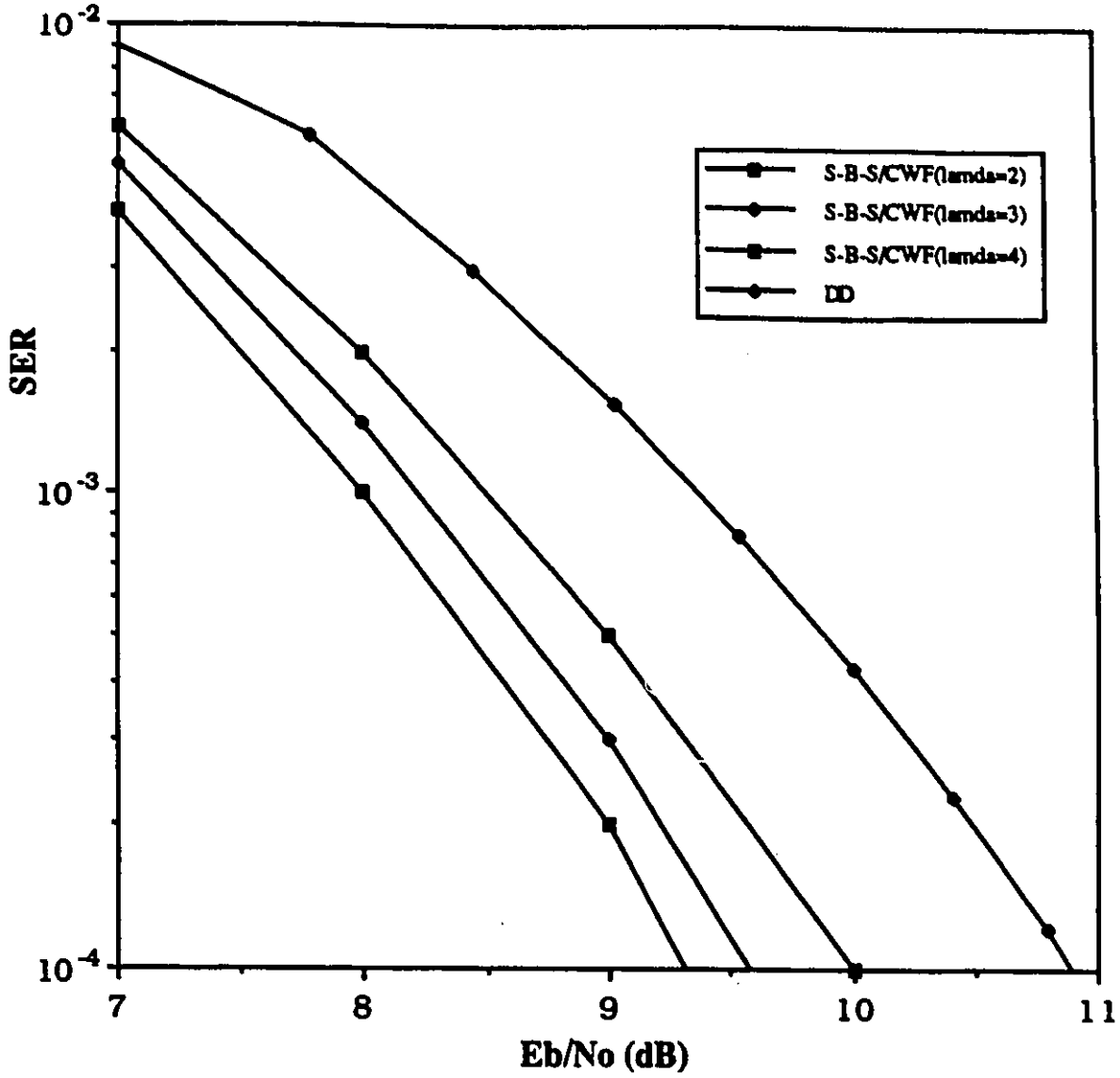

Figure 4.94: SER curves of the non-coherent receiver based on multiple differential detection and the use of signal combining controlled by decision feedback (MDD/CWF) . The results correspond to a QPSK signal.

4.12 CONCLUSIONS

The present chapter has introduced non-coherent receivers for linear modulation systems. The proposed structures have demonstrated good performances. At the same time, their complexity levels remain in reasonable levels, making their implementation with today's technology possible. These receivers are:

1. The block decoder.
2. The asymptotically optimal decoder for time dispersive channels and/or multi-amplitude/phase signals.
3. The multiple differential sequence estimator.
4. The multiple differential symbol-by-symbol receiver using signal combining controlled by decision feedback.

The analysis leading to the derivation of these structures has been presented. We have also provided the analytical framework for the evaluation of these schemes. New tight upper bounds have been derived and they have been presented in this chapter. The evaluation has covered Gaussian (ideal or time dispersive) and faded channels. Evaluations have been carried out for both uncoded as well as coded signals. The evaluation results have verified the superiority of the proposed receivers which in some cases achieve performance practically identical to the coherent receiver operating with perfect carrier synchronization (the best performance possible). Some of the proposed configurations actually reach these levels of performance levels with relatively low complexity. The receivers have demonstrated high robustness to channel imperfections and exceptional performance when used with coded signals (with coded signals the conventional differential receiver suffers considerable losses in performance). For the Gaussian channel we have reported improvements higher than 5 dB (for example see Tables 4.4, 4.12 and Figs. 4.14, 4.42). For the faded channel the gains exceeded 7 dB (see Table 4.24). Also, the proposed non-coherent receivers reduced the error floors by almost one order of magnitude (see Fig. 4.84).

Chapter 5

NON-COHERENT RECEIVERS FOR CPM SIGNALS

5.1 INTRODUCTION

The present chapter extends our work to Continuous Phase Modulation signals. Our aim remains the same, that is, to provide improved non-coherent receivers with reasonable complexity.

In the past few years, CPM signals have gained considerable popularity. This is mainly due to their good spectral behaviour and their constant envelope nature. By properly smoothing the modulating signal (usually through filtering with properly chosen premodulation filters), we are able to provide CPM signals with low power content in the sidelobes. This keeps the levels of adjacent channel interference low and allows for close packing of carriers. At the same time, their constant envelope nature, allows the use of cost efficient class-C power amplifiers -to be operated in saturation- without the signal suffering from non-linear distortions or sidelobe regrowth. Sidelobe regrowth increases the interference levels between adjacent channels, deteriorates the performance and reduces the capacity of the network. Today, CPM signals have already been applied to crucial applications of the WPDCS. Two ex-

amples are the European cellular radio (GSM) [81] [170] (it uses GMSK and a transmission rate of 270.833 Kbits/sec.), the Second Generation Cordless Telephone standard (CT2) [81] [243] (it uses binary FSK, with transmission rate 72 Kbits/sec. and applies time division doublex transmission -user and base station share the same frequency channel) and the improved Digital European Cordless Telephone (DECT) system [81] [201] (uses GMSK with 3 dB bandwidth of the premodulation filter $B_tT = 0.5$ and a transmission rate 1.152 Mbits/sec.).

Even though CPM signals have some very positive characteristics, they also have some weak aspects. Carrier recovery is quite a challenge with CPM signals. This is due to their continuous phase nature, which makes carrier recovery through non-linear processing on the received signal difficult. Such discrete tones are needed by the carrier recovery circuit to locally generate the carrier reference. This fact makes clear how important non-coherent detection techniques are to CPM signals.

When optimal non-coherent detection processing is applied to the CPM signal, good levels of performance are achieved [12], [13]. However, the required filtering is very complex and worsens as the bandwidth efficiency of the CPM signal increases. As a result, such a non-coherent receiver is of no practical use. On the other side, when conventional non-coherent detection techniques are used (i.e. differential or discriminator detection) the performance becomes quite poor. It deteriorates as we move from less to more bandwidth efficient systems and in some cases becomes unacceptable for any practical system [230], [160].

The potential of CPM signals to WPDCS, the weaknesses existing with their coherent detection and the inefficiency of low complexity non-coherent receivers to provide high performance levels when used with bandwidth efficient CPM systems led us to decide to extend our work towards the direction of CPM signals.

In section 3.4 of Chapter 3, we presented the structures of the optimal non-coherent CPM receiver. In our work, we addressed both ideal and distorted channels. Also, the derivations are general enough to address the cases of single or multi-amplitude CPM signals. The derived structures require a filter bank to process the received signal. The size of the filter bank and complexity of the individual filters forming it, increase as the spectral effi-

ciency of the CPM signal improves. In addition, the processing required for the calculation of the metrics needed to decide the transmitted information involves the use of exponential and Bessel functions and requires knowledge of the operating E_b/N_o. The consequence of the high complexity is that these structures are far from being able to be used in any practical application.

In order to reduce the high filtering complexity levels, in section 3.5 of Chapter 3 we have used the AMP signal decomposition approach [125]. The receivers derived through this approach had lower filtering complexity; however, the load and complexity of the processing required for the calculation of the metrics remained in high levels.

In Chapter 4, we came up with some new and relatively simple receivers for linear signals, by applying approximation on the metrics of the optimal receivers derived in Chapter 3. The results in terms of improvements offered by these receivers were quite impressive. Encouraged by the positive results of Chapter 4, we decided to pursue the same approach with CPM signals as well. The outcome of this work, which is reported in the present chapter, has proven our effort worth of being taken.

The remainder of this chapter is presented as follows. Sections 5.2 to 5.6 deal with sequence estimation. In section 5.2 we apply approximations on the optimal metrics of Chapter 3 and come up with asymptotically optimal sequence estimators for high and low E_b/N_o. In the previous parts of the present work, we included in our formulations time dispersion in our channel model and have considered the case of multi-amplitude signals. The same approach has been followed in the present chapter as well. We have formulated the derived receiver both, in the form of block decoders and multiple differential detectors. We also examine and highlight some fundamental differences existing between the receivers for the CPM signals and the structures of Chapter 4 for linear systems. The source of these differences is the phase continuity of the CPM signal. Through the results of this chapter, the presence of coding existing in the CPM signal and its use in the non-coherent detection processes become clear.

In order to achieve reduction in the filtering complexity, we have applied the same methodology discussed in the previous paragraph with the AMP decomposition approach. The outcome was to reach receivers having comparable levels of filtering and processing complexity with those we met in linear

systems. As a matter of fact, the AMP decomposition has led to receivers practically identical to those presented in Chapter 4 for the linear signals.

One drawback of the receivers designed through the AMP decomposition, is that they require the use of filters with time limited and sometimes complex impulse responses. Design of such filters is possible when the implementation and use of these filters is done in baseband form. However, if they have to be implemented as IF filters, there is quite a level of difficulty involved. In subsection 4.4.3 of the 4^{th} Chapter, we have commented on the advantages of the IF implementations for the proposed non-coherent receivers. In order to provide practical IF non-coherent receivers for CPM signals, we replace the complex filters indicated by the AMP decomposition with simple commercially available and low cost ones (i.e. Gaussian, Butterworth etc.). The design and evaluation of these reduced complexity systems is the topic covered in section 5.6. We have evaluated these simplified receivers for MSK, TFM and GMSK. The results are impressive. Simple multiple differential detection receivers (using either 2 or 3 differential detectors) are able to provide considerable improvements both in Gaussian as well as faded channels. They have also demonstrated the superiority of the proposed receivers when operating on signals suffering from ISI or severe fading. For MSK the evaluations have indicated improvements higher than **3 dB**. For TFM and Gaussian MSK operating in a Gaussian channel the results verified improvements **higher than 9 dB** and **7 dB** respectively. Impressive is the performance of the multiple differential receivers in a fast faded environment where they were able to provide a reduction in error floors **more than 3 orders of magnitude.**

Sections 5.7 to 5.10 deal with receivers deciding on a symbol-by-symbol basis. In section 5.7, the asymptotically optimal non-coherent detection concept -examined in section 5.2 in the sense of sequence estimation- is now applied to the symbol-by-symbol detection concept. In section 5.9 we use the AMP signal decomposition approach in the asymptotically optimal non-coherent symbol-by-symbol detection concept in order to derive receivers with reduced filtering requirements. In section 5.10, in order to further simplify the complexity of the symbol-by-symbol receivers and provide configurations feasible for implementation in the IF multiple differential detection form we proposed schemes based on the use of commercially available low cost filters. In order to reduce the complexity further, we introduce decision

feedback in the receiver structure. The design analysis carried out for the design of these simplified symbol-by-symbol receivers resulted in the invention of a new ISI cancellation technique for narrowband CPM signals which we have named *Data Aided Phase Correction* (see publications [160] to [169]). The technique opens the eye diagram at the output of the differential detector by using the previous decisions to cancel the ISI present in the phase of the narrowband (spectrally efficient) CPM signal. This way, a stronger and "cleaner" signal (i.e. less corrupted by the presence of ISI) is used to make the new decision. In section 5.10.1, a detailed analysis leading to this technique is given. The resulting receiver structure, apart from DAPC, it also uses the Combining with Feedback technique (CWF). We introduced this technique in section 4.11 of Chapter 4, where it was used with linear modulation. Now, we see its extension to CPM signals.

These symbol-by-symbol receiver concepts have been evaluated for MSK, TFM and GMSK, using low complexity configurations. The results demonstrated improvements higher than **1.3 dB**, **5.5 dB** and **4.5 dB** as compared to the conventional differential detectors.

Considering the poor performance, the conventional differential detection techniques experience when used with spectrally efficient CPM signals [230], [162], [161], we feel it is no exaggeration to say that *through the proposed receiver structures, the use of differential detection with narrowband CPM signals has been made possible.*

5.2 ASYMPTOTICALLY OPTIMAL CPM SEQUENCE ESTIMATORS IN A TIME DISPERSIVE CHANNEL

The approximations described in Eqs.(4.1), (4.2), (low E_b/N_o), (4.5) (high E_b/N_o) in section 4.2 of Chapter 4 can be used with the expression of $\aleph_{OP}^{CPMD}(\bar{C}(\bar{A}), h_{c,B}(t), t))$ (see Eq.(3.90) in Chapter 3) in order to derive asymptotically optimal sequence estimators for the CPM signals. The steps to be followed are identical to those described in section 4.2. To avoid unnecessary duplications, here we shall limit ourselves to the presentation of the final metric expressions.

5.2.1 Low E_b/N_o

For low E_b/N_o, the metric expression is the following:

$$\aleph_{LAO}^{CPMD}(\bar{C}(\bar{A}), \mathcal{F}_{[Z-1,0]}^{CPM}, h_{c,B}(t), t)) =$$

$$-[MST_{CPM}(\bar{C}(\bar{A}), h_{c,B}(t), t) + IST_{CPM}(\bar{C}(\bar{A}), h_{c,B}(t), t)]$$

$$+\frac{(MST_{CPM}(\bar{C}(\bar{A}), h_{c,B}(t), t) + IST_{CPM}(\bar{C}(\bar{A}), h_{c,B}(t), t))^2}{2N_o}$$

$$+\frac{|\sum_{k=0}^{Z-1} F_k(x_r(t), \tilde{\varphi}_{k-L+1}^k(\bar{C}(\bar{A})))e^{-j\beta_1(\tilde{\varphi}_0^{k-1}(\bar{C}(\bar{A}))}|^2}{4N_o}. \qquad (5.1)$$

The $MST_{CPM}(\bar{C}(\bar{A}), h_{c,B}(t), t)$, $IST_{CPM}(\bar{C}(\bar{A}), h_{c,B}(t), t)$ have been defined in Eqs.(3.91) and (3.92) respectively. From Eq.(5.1) it can be seen that as $\frac{E_b}{N_o} \rightarrow 0$, the strength of the two terms appearing in the expression with power of 2 vanishes to zero, leaving only the $(MST_{CPM}(\bar{C}(\bar{A}), h_{c,B}(t), t) + IST_{CPM}(\bar{C}(\bar{A}), h_{c,B}(t), t))$ component to dominate the decision. This term is independent from the received signal $x_r(t)$. Exactly the same behaviour has been observed for the linear systems as well (see subsection 4.2.1 in Chapter 4).

5.2.2 High E_b/N_o

For high E_b/N_o, the asymptotically optimal metric expression (to be maximized) is the:

$$\aleph_{HAO}^{CPMD}(\bar{C}(\bar{A}), \mathcal{F}_{[Z-1,0]}^{CPM}, h_{c,B}(t), t)) = -\{\sum_{k=0}^{Z-1} \frac{1}{2}|J_{k,0}|^2 + \frac{1}{2}\sum_{k=1}^{Z-1}\sum_{l=1}^{k}$$

$$[e^{-j\Delta_l\beta_1(k,\bar{\varphi}_{k-l}^{k}(\bar{C}(\bar{A})))}J_{k,l} + e^{j\Delta_l\beta_1(k,\bar{\varphi}_{k-l}^{k}(\bar{C}(\bar{A})))}J_{k,l}^{*}]\}$$

$$+|\sum_{k=0}^{Z-1} F_k(x_r(t), \bar{\varphi}_{k-L+1}^{k}(\bar{C}(\bar{A})))e^{-j\beta_1(\bar{\varphi}_0^{k-1}(\bar{C}(\bar{A})))}|,$$

(5.2)

or equivalently

$$\aleph_{HAO}^{CPMD}(\bar{C}(\bar{A}), \mathcal{F}_{[Z-1,0]}^{CPM}, h_{c,B}(t), t)) = -\{MST_{CPM}(\bar{C}(\bar{A}), h_{c,B}(t), t)$$

$$+IST_{CPM}(\bar{C}(\bar{A}), h_{c,B}(t), t)\} + |\sum_{k=0}^{Z-1} F_k(x_r(t), \bar{\varphi}_{k-L+1}^{k}(\bar{C}(\bar{A})))e^{-j\beta_1(\bar{\varphi}_0^{k-1}(\bar{C}(\bar{A})))}|$$

(5.3)

5.3 CPM SEQUENCE ESTIMATORS IN IDEAL CHANNEL

The metric of the maximum likelihood sequence estimator for an ideal channel has been described in Eq.(3.93) (see subsection 3.4.1). Applying to it the approximations of Eq.(4.1) , (4.2), (low E_b/N_o), (4.5) (high E_b/N_o) we end up with the following asymptotically optimal metric expressions:

For low E_b/N_o:

$$\aleph_{LAO}^{CPMI}(\bar{C}(\bar{A}), \mathcal{F}_{[Z-1,0]}^{CPM}, h_{c,B}(t), t)) = -(MST_{CPM}(\bar{C}(\bar{A}), h_{c,B}(t), t) +$$

$$+\frac{(MST_{CPM}(\bar{C}(\bar{A}), h_{c,B}(t), t))^2}{2N_o}$$

$$+\frac{|\sum_{k=0}^{Z-1} F_k(x_r(t), \bar{\varphi}_{k-L+1}^{k}(\bar{C}(\bar{A})))e^{-j\beta_1(\bar{\varphi}_0^{k-1}(\bar{C}(\bar{A}))}|^2}{4N_o}. \tag{5.4}$$

(*CPMI* stands for Continuous Phase (modulation), Multi-amplitude (signal), Ideal (channel)).

For high E_b/N_o:

$$\aleph_{HAO}^{CPMI}(\bar{C}(\bar{A}), \mathcal{F}_{[Z-1,0]}^{CPM}, h_{c,B}(t), t)) = -\{\frac{1}{2}[\sum_{k=0}^{Z-1} \mathcal{A}_k^2]\}$$

$$+|\sum_{k=0}^{Z-1} \mathcal{A}_k F_k(x_r(t), \bar{\varphi}_{k-L+1}^{k}(\bar{C}(\bar{A})))e^{-j\beta_1(\bar{\varphi}_0^{k-1}(\bar{C}(\bar{A}))}|.$$

(5.5)

When the CPM signal is single amplitude ($\mathcal{A}_k = 1$), the exponential term in Eq.(3.93) does not carry any information regarding $\bar{C}(\bar{A})$, consequently it

can be removed from the metric expression.This leaves only the maximization of the Bessel function term, or equivalently the maximization of its argument

$$\aleph_{CPIC}(\bar{C}(\bar{A}), \mathcal{F}^{CPM}_{[Z-1,0]}, t)) = |\sum_{k=0}^{Z-1} F_k(x_\tau(t), \bar{\varphi}^k_{k-L+1}(\bar{C}(\bar{A})))e^{-j\beta_1(\bar{\varphi}^{k-1}_0(\bar{C}(\bar{A})))}|.$$

(5.6)

In section 4.4 of Chapter 4, we have shown how the various improved non-coherent receivers could be implemented in the form of processors using the outputs of squared envelope and multiple differential detectors (SEMDD) to provide the decision. In the following section, we shall propose and study similar structures for the non-coherent CPM receivers.

5.4 CPM SEQUENCE ESTIMATORS BASED ON SQUARED ENVELOPE AND MULTIPLE DIFFERENTIAL DETECTION

The development of multiple differential detection receivers for the CPM signals, starts with the formulation of the square of $\aleph_{CPIC}(\bar{C}(\bar{A}), \mathcal{F}^{CPM}_{[Z-1,0]}, t))$ $(\aleph^{SQ}_{CPIC}(\bar{C}(\bar{A}), \mathcal{F}^{CPM}_{[Z-1,0]}, t)$ i.e.

$$[\aleph^{SQ}_{CPIC}(\bar{C}(\bar{A}), \mathcal{F}^{CPM}_{[Z-1,0]}, t))]^2 = \sum_{k=0}^{Z-1} |F_k(x_r(t), \bar{\varphi}^k_{k-L+1}(\bar{C}(\bar{A})))|^2$$

$$+2\sum_{l=1}^{Z-1}\sum_{k=l}^{Z-1}(Re\{F_k(x_r(t), \bar{\varphi}^k_{k-L+1}(\bar{C}(\bar{A})))F^*_{k-l}(x_r(t), \bar{\varphi}^{k-l}_{k-L-l+1}(\bar{C}(\bar{A}))\}$$

$$\cos\{\Delta_l\beta_1(k, \varphi^{k-1}_{k-l}(\bar{C}(\bar{A})))\}$$

$$+Im\{F_k(x_r(t), \bar{\varphi}^k_{k-L+1}(\bar{C}(\bar{A})))F^*_{k-l}(x_r(t), \bar{\varphi}^{k-l}_{k-L-l+1}(\bar{C}(\bar{A}))\}$$

$$\sin\{\Delta_l\beta_1(k, \varphi^{k-1}_{k-l}(\bar{C}(\bar{A})))\}). \tag{5.7}$$

The term at the right side of the equation resembles multiple differential and squared envelope detection. Entering these terms in Eq.(5.2), provides the following metric expression:

$$\aleph^{CPMD}_{HAO}(\bar{C}(\bar{A}), \mathcal{F}^{CPM}_{[Z-1,0]}, h_{c,B}(t), t)) = -\frac{1}{2}(\sum_{k=0}^{Z-1} |J_{k,0}(\bar{C}(\bar{A})|^2+$$

$$+2\sum_{l=1}^{Z-1}\sum_{k=l}^{Z-1} Re\{(e^{-j\Delta_l\beta_1(k,\bar{\varphi}^k_{k-l}(\bar{C}(\bar{A})))}J_{k,l}\}$$

$$+(\{\sum_{k=0}^{Z-1} |F_k(x_r(t), \bar{\varphi}^k_{k-L+1}(\bar{C}(\bar{A})))|^2 + 2\sum_{l=1}^{Z-1}\sum_{k=l}^{Z-1}$$

$$(Re\{F_k(x_r(t),\bar{\varphi}^k_{k-L+1}(\bar{C}(\bar{A})))F^*_{k-l}(x_r(t),\bar{\varphi}^{k-l}_{k-L-l+1}(\bar{C}(\bar{A}))\}$$

$$\cos\{\Delta_l\beta_1(k,\varphi^{k-1}_{k-l}(\bar{C}(\bar{A})))\}+$$

$$Im\{F_k(x_r(t),\bar{\varphi}^k_{k-L+1}(\bar{C}(\bar{A})))F^*_{k-l}(x_r(t),\bar{\varphi}^{k-l}_{k-L-l+1}(\bar{C}(\bar{A})))\}$$

$$\sin\{\Delta_l\beta_1(k,\varphi^{k-1}_{k-l}(\bar{C}(\bar{A})))\}])^{\frac{1}{2}}. \tag{5.8}$$

If the signal is single-amplitude and the channel does not experience any time dispersion, the metric to be maximized is the one presented in Eq.(5.7).

Recalling the case of PSK signals examined in Chapter 4, we found that the squared envelope terms are not needed in the detection process when the channel is ideal. However, examining Eq.(5.7), we see the presence of terms resembling squared envelope detection ($|F_k(x_r(t),\bar{\varphi}^k_{k-L+1}(\bar{C}(\bar{A})))|^2$). The explanation for this difference between PSK and CPM signals follows.

In PSK (and generally linear) signals, the information regarding a symbol (c_k) is put at a specific instant in the time domain (kT). At the receiver (considering that the channel does not experience time dispersion), the information regarding the symbol (c_k) appears on a single sample of the received signal (y_k). Since PSK uses single amplitude symbols, the $|y_k|^2$ does not convey any special information about c_k and can be eliminated. On the contrary, the phase continuity of continuous phase modulation introduces memory to the CPM signal. This memory spreads the information about the symbol (c_k) in the entire time interval, starting from the moment c_k appears for transmission (at kT) up to the end of the signal transmission. As a result, the $|F_k(x_r(t),\bar{\varphi}^k_{k-L+1}(\bar{C}(\bar{A})))|^2$ terms contain information not only about c_k, but also all the symbols transmitted prior to c_k. This is useful information for the detection and keeps the squared envelope terms in the detection process. What we described *is a fundamental difference between linear and CPM systems. It brings out the presence of memory and coding which are created from the phase continuity of the continuous phase modulation and shows the different nature of linear continuous phase modulation.*

5.4.1 Truncated Squared Envelope and Multiple Differential Detection for CPM Signals

Similarly to the linear systems (examined in section 4.9), by limiting the number of differential detectors used, we can provide reduced complexity structures. The two (truncated) metrics corresponding to Eqs.(5.7), (5.13) are the following:

$$Q_2^{CPM}(\bar{C}(\bar{A}), \mathcal{F}_{[Z-1,0]}^{CPM}, h_{c,B}(t), t) =$$

$$-\frac{1}{2}(\sum_{k=0}^{Z-1}|J_{k,0}|^2 + [\sum_{k=1}^{Z-1}\sum_{l=1}^{\varpi} Re\{e^{-j\Delta_l\beta_1(k,\bar{\varphi}_{k-l}^{k}(\bar{C}(\bar{A})))}J_{k,l}\}]$$

$$+[(\{\sum_{k=0}^{Z-1}|F_k(x_r(t), \bar{\varphi}_{k-L+1}^{k}(\bar{C}(\bar{A})))|^2$$

$$+2\sum_{k=0}^{Z-1}\sum_{l=1}^{\varpi}(Re\{F_k(x_r(t), \bar{\varphi}_{k-L+1}^{k}(\bar{C}(\bar{A})))F_{k-l}^{*}(x_r(t), \bar{\varphi}_{k-L-l+1}^{k-l}(\bar{C}(\bar{A}))\}$$

$$\cos\{\Delta_l\beta_1(k, \varphi_{k-l}^{k-1}(\bar{C}(\bar{A})))\}+$$

$$Im\{F_k(x_r(t), \bar{\varphi}_{k-L+1}^{k}(\bar{C}(\bar{A})))F_{k-l}^{*}(x_r(t), \bar{\varphi}_{k-L-l+1}^{k-l}(\bar{C}(\bar{A})))\}$$

$$\sin\{\Delta_l\beta_1(k, \varphi_{k-l}^{k-1}(\bar{C}(\bar{A})))\}]^{\frac{1}{2}} \tag{5.9}$$

and

$$Q_3^{CPM}(\bar{C}(\bar{A}), \mathcal{F}_{[Z-1,0]}^{CPM}, t) = \sum_{k=0}^{Z-1}|F_k(x_r(t), \bar{\varphi}_{k-L+1}^{k}(\bar{C}(\bar{A})))|^2 +$$

$$2\sum_{k=0}^{Z-1}\sum_{l=1}^{\varpi}(Re\{F_k(x_r(t), \bar{\varphi}_{k-L+1}^{k}(\bar{C}(\bar{A})))F_{k-l}^{*}(x_r(t), \bar{\varphi}_{k-L-l+1}^{k-l}(\bar{C}(\bar{A}))\}$$

$$\cos\{\Delta_l\beta_1(k, \bar{\varphi}_{k-l}^{k-1}(\bar{C}(\bar{A})))\} +$$

$$+Im\{F_k(x_r(t), \bar{\varphi}_{k-L+1}^{k}(\bar{C}(\bar{A})))F_{k-l}^{*}(x_r(t), \bar{\varphi}_{k-L-l+1}^{k-l}(\bar{C}(\bar{A}))\}$$

$$\sin\{\Delta_l\beta_1(k, \varphi_{k-l}^{k-1}(\bar{C}(\bar{A})))\}) \tag{5.10}$$

with

$$\varpi = \begin{cases} k & \text{for } 1 \leq k \leq \lambda \\ \lambda & \text{for } k > \lambda \,. \end{cases} \tag{5.11}$$

λ is the number of differential detectors used.

In section 4.9, a reduced complexity block decoder using a "processing by a window approach" has been proposed. The method is applicable to CPM signals as well, however we shall not elaborate furthermore on this matter.

The metrics of the asymptotically optimal sequence estimators examined in sections 5.2 to 5.4 definitely require simpler processing to decide the information sequence, as compared to the optimal structures presented in Chapter 3. There is no need to include in the processing use of exponential, Bessel functions or scaling according to the operating E_b/N_o point. However, the filter complexity of these asymptotically optimal structures is as high as their optimal counterparts. In Chapter 3 it was explained that the CPM receiver, requires the use of a complex filter-bank in order to supply the processing units with the needed information for the calculation of the metric quantities. It was also mentioned that the complexity of the filtering process needed increases with the increase in spectral efficiency of the CPM signal. Both, the number of the filters required to be used becomes high and their shaping is complex, difficult and costly for implementation. Implementation of these receivers in IF multiple differential detection form is a very challenging task in this case, due to the complex shaping the IF filter should have.

The above discussion makes clear that the only way to achieve our target (i.e. provide practical non-coherent, spectrally/power efficient CPM systems appropriate for use in WPDCS) is by reducing the filtering requirements of these non-coherent receivers.

In Chapter 3 we have shown that by using the AMP signal decomposition, it is possible to design optimal non-coherent receivers for CPM signals, having lower filtering complexity from the structures described in the previous and present section of this chapter. In the following sections we shall extend the AMP decomposition approach and use it in the asymptotically optimal non-coherent detection concept.

5.5 SEQUENCE ESTIMATORS BASED ON THE AMP SIGNAL DECOMPOSITION

The advantage of the AMP decomposition is that it can very closely approximate the CPM signal by using a small number of AMP pulses. The profit for the non-coherent receiver is that it can acquire the information needed by the processing units (which calculate the values of the metric expression corresponding to the various possible sequences and provide a decision through comparison of these values) by filtering the received signal with only a small number of filters matched to these AMP pulses. For some popular CPM schemes only one pulse is enough to approximate the signal, in which case only one filter is required at the receiver.

The metric expression of the optimal non-coherent receiver for the general case (more than one AMP filters are used to represent the signal) has been given in Eq.(3.114) of Chapter 3. When only one AMP pulse is used, the metric is provided in Eq.(3.117). Following identical steps to those presented in the previous section, we can derive asymptotically optimal decoders for low and high E_b/N_o. The metrics of these decoders are presented below.

5.5.1 Low E_b/N_o

$$\aleph_{LAO_{app.}}^{CPMD}(\bar{\Re}_{E,[0,0]}^{AMP},\ldots,\bar{\Re}_{E,[0,\mathcal{N}]}^{AMP},\bar{\Re}_{E,[1,0]}^{AMP},\ldots,\bar{\Re}_{E,[\mathcal{N},\mathcal{N}]}^{AMP},\bar{\mathcal{Y}}_0^{AMP},\ldots,\bar{\mathcal{Y}}_{\mathcal{N}}^{AMP},\bar{C}(\bar{A}))=$$

$$\{-\frac{1}{2}[\sum_{k=0}^{Z-1}(\mathcal{A}_k)^2\sum_{n_1=0}^{\mathcal{N}}\sum_{n_2=0}^{\mathcal{N}}\alpha_{n_1,k}^{AMP}(\alpha_{n_2,k}^{AMP})^*\Re_{E,[n_1,n_2]}^{AMP}(0)$$

$$+\sum_{l=1}^{Z-1}\sum_{k=l}^{Z-1}\mathcal{A}_k\mathcal{A}_{k-l}\sum_{n_1=0}^{\mathcal{N}}\sum_{n_2=0}^{\mathcal{N}}[\alpha_{n_1,k}^{AMP}(\alpha_{n_2,k-l}^{AMP})^*$$

$$\Re_{E,[n_1,n_2]}^{AMP}(l)+\alpha_{n_2,k-l}^{AMP}(\alpha_{n_1,k}^{AMP})^*(\Re_{E,[n_1,n_2]}^{AMP}(l))^*]]\}$$

$$+\frac{1}{2N_o}\{-[\sum_{k=0}^{Z-1}(\mathcal{A}_k)^2\sum_{n_1=0}^{\mathcal{N}}\sum_{n_2=0}^{\mathcal{N}}\alpha_{n_1,k}^{AMP}(\alpha_{n_2,k}^{AMP})^*\Re_{E,[n_1,n_2]}^{AMP}(0)$$

$$+\sum_{l=1}^{Z-1}\sum_{k=l}^{Z-1}\mathcal{A}_k\mathcal{A}_{k-l}\sum_{n_1=0}^{\mathcal{N}}\sum_{n_2=0}^{\mathcal{N}}[\alpha_{n_1,k}^{AMP}(\alpha_{n_2,k-l}^{AMP})^*$$

$$\Re_{E,[n_1,n_2]}^{AMP}(l)+\alpha_{n_2,k-l}^{AMP}(\alpha_{n_1,k}^{AMP})^*(\Re_{E,[n_1,n_2]}^{AMP}(l))^*]]\}^2$$

$$+\frac{|\sum_{k=0}^{Z-1}\mathcal{A}_k\sum_{n=0}^{\mathcal{N}}\mathcal{Y}_{n,k}^{AMP}(\alpha_{n,k}^{AMP})^*|^2}{4N_o}. \tag{5.12}$$

When the CPM signal is approximated by only one AMP pulse (i.e. $\mathcal{N}=0$) the metric becomes:

$$\aleph_{LAO_{appr}}^{CPMD}(\bar{\Re}_{E,[0,0]}^{AMP},\bar{\mathcal{Y}}_0,\bar{C}(\bar{A}))=-\{[\sum_{k=0}^{Z-1}(\mathcal{A}_k)^2\Re_{E,[0,0]}^{AMP}(0)$$

$$+\sum_{l=1}^{Z-1}\sum_{k=l}^{Z-1}\mathcal{A}_k\mathcal{A}_{k-l}[\alpha_{0,k}^{AMP}(\alpha_{0,k-l}^{AMP})^*\Re_{E,[0,0]}^{AMP}(l)+\alpha_{0,k-l}^{AMP}(\alpha_{0,k}^{AMP})^*(\Re_{E,[0,0]}^{AMP}(l))^*]]\}$$

$$+\frac{1}{2N_o}[\sum_{k=0}^{Z-1}(\mathcal{A}_k)^2\Re_{E,[0,0]}^{AMP}(0)$$

$$+\sum_{l=1}^{Z-1}\sum_{k=l}^{Z-1}\mathcal{A}_k\mathcal{A}_{k-l}[\alpha_{0,k}^{AMP}(\alpha_{0,k-l}^{AMP})^*\Re_{E,[0,0]}^{AMP}(l)+\alpha_{0,k-l}^{AMP}(\alpha_{0,k}^{AMP})^*$$

$$(\Re_{E,[0,0]}^{AMP}(l))^*]]^2+\frac{|\sum_{k=0}^{Z-1}\mathcal{A}_k\mathcal{Y}_{0,k}^{AMP}(\alpha_{0,k}^{AMP})^*|}{4N_o}. \tag{5.13}$$

In the above equations, the $|\alpha_{n,k}^{AMP}|^2=1$ has been used.

5.5.2 High E_b/N_o

For high E_b/N_o, the metric of the asymptotically optimal sequence estimator based on the AMP decomposition is the following:

$$\aleph^{CPMD}_{HAO_{appr}}(\bar{\Re}^{AMP}_{E,[0,0]},\ldots,\bar{\Re}^{AMP}_{E,[0,\mathcal{N}]},\bar{\Re}^{AMP}_{E,[1,0]},\ldots,\bar{\Re}^{AMP}_{E,[\mathcal{N},\mathcal{N}]},\bar{\mathcal{Y}}_0,\ldots,\bar{\mathcal{Y}}_{\mathcal{N}},\bar{C}(\bar{A})) =$$

$$-\frac{1}{2}[\sum_{k=0}^{Z-1}(\mathcal{A}_k)^2\sum_{n_1=0}^{\mathcal{N}}\sum_{n_2=0}^{\mathcal{N}}\alpha^{AMP}_{n_1,k}(\alpha^{AMP}_{n_2,k})^*\Re^{AMP}_{E,[n_1,n_2]}(0)-2\sum_{l=1}^{Z-1}\sum_{k=l}^{Z-1}\mathcal{A}_k\mathcal{A}_{k-l}$$

$$\sum_{n_1=0}^{\mathcal{N}}\sum_{n_2=0}^{\mathcal{N}}[Re\{\alpha^{AMP}_{n_1,k}(\alpha^{AMP}_{n_2,k-l})^*\Re^{AMP}_{E,[n_1,n_2]}(l)\}]]+|\sum_{k=0}^{Z-1}\mathcal{A}_k\mathcal{Y}^{AMP}_{0,k}(\alpha^{AMP}_{0,k})^*|. \tag{5.14}$$

For $\mathcal{N}=0$

$$\aleph^{CPMD}_{HAO_{appr}}(\bar{\Re}^{AMP}_{E,[0,0]},\bar{\mathcal{Y}}_0,\bar{C}(\bar{A}))=|\sum_{k=0}^{Z-1}\mathcal{A}_k\mathcal{Y}^{AMP}_{0,k}(\alpha^{AMP}_{0,k})^*|-\frac{1}{2}[\sum_{k=0}^{Z-1}(\mathcal{A}_k)^2\Re^{AMP}_{E,[0,0]}(0)]$$

$$-[\sum_{l=1}^{Z-1}\sum_{k=l}^{Z-1}\mathcal{A}_k\mathcal{A}_{k-l}[Re\{(\alpha^{AMP}_{0,k})^*\alpha^{AMP}_{0,k-l}\Re^{AMP}_{E,[0,0]}(l)\}]. \tag{5.15}$$

There is a strong similarity between the expression of Eq.(5.15) and the metric expression of the asymptotically optimal sequence estimator for linear signals (see Eq.(4.6) in Chapter 4). As a matter of fact, if we perform the following replacements in Eq.(4.6)

$$\mathcal{J}_k \rightarrow \mathcal{A}_k$$

$$y_k \rightarrow \mathcal{Y}^{AMP}_{0,k}$$

$$h_l \rightarrow \Re^{AMP}_{E,[0,0]}(l)$$

$$c_k \rightarrow \mathcal{A}_k \alpha^{AMP}_{0,k} \tag{5.16}$$

Eq.(5.15) results.

The block diagram of the sequence estimator implementing the non-coherent receiver described by Eq.(5.15) can be generated from the the block diagram of the asymptotically optimal decoder for linear systems (see Fig. 4.1 in Chapter 4), by performing the replacement of parameters described in Eq.(5.16). Also, in this case, the post detection filter $H_R(\omega)$ should have an impulse response equal to

$$h_R(t) = h^{AMP}_0(t) \otimes h_{c,B}(t). \tag{5.17}$$

We remind the reader that $h^{AMP}_0(t)$ is the first AMP pulse, $h_{c,B}(t)$ is the baseband equivalent of the channel impulse response and $\otimes$ represents the convolution operation. Similarly, the block diagram of the processing unit carrying on the calculation of the metric $\aleph^{CPMD}_{HAO_{appr}}(\bar{\Re}^{AMP}_{E,[0,0]}, \bar{\mathcal{Y}}_0, \bar{C}(\bar{A}))$ can be generated by Fig. 4.2 of Chapter 4 (block diagram of the processing unit for the asymptotically optimal decoder of linear signals) by performing the same replacements.

For single amplitude signals ($\mathcal{A}_k = 1$) the metric becomes:

$$\aleph^{CPSD}_{HAO_{appr}}(\bar{\Re}^{AMP}_{E,[0,0]}, \bar{\mathcal{Y}}_0, \bar{C}(\bar{A})) = |\sum_{k=0}^{Z-1} \mathcal{Y}^{AMP}_{0,k} (\alpha^{AMP}_{0,k})^*|$$

$$-[\sum_{l=1}^{Z-1} \sum_{k=l}^{Z-1} [Re\{(\alpha^{AMP}_{0,k})^* \alpha^{AMP}_{0,k-l} \Re^{AMP}_{E,[0,0]}(l)\}]] \tag{5.18}$$

Finally, if $\Re^{AMP}_{E,[0,0]}(l) = 0 \quad \forall \quad l \neq 0$ (this is the case for ideal channels), the metric is furthermore reduced to the maximization of

$$\aleph_{CPIC_{appr}}(\bar{\Re}^{AMP}_{E,[0,0]}, \bar{\mathcal{Y}}_0, \bar{C}(\bar{A})) = |\sum_{k=0}^{Z-1} \mathcal{Y}^{AMP}_{0,k} (\alpha^{AMP}_{0,k})^*|. \tag{5.19}$$

$\aleph^{CPSD}_{HAO_{appr}}(\bar{\Re}^{AMP}_{E,[0,0]}, \bar{\mathcal{Y}}_0, \bar{C}(\bar{A}))$ and $\aleph_{CPIC_{appr}}(\bar{\Re}^{AMP}_{E,[0,0]}, \bar{\mathcal{Y}}_0, \bar{C}(\bar{A}))$ can be also generated from the metric expressions $\aleph^{PSK}_{HAO}(\bar{h}, \bar{y}, \bar{C}(\bar{A}))$ (asymptotically optimal decoder for a PSK signal in a time dispersive channel, see Eq.(4.11))

and $\aleph_{IC}(\bar{y}, \bar{C}(\bar{A}))$ (block decoder for a PSK signal see Eq.(4.10)) by going through the replacement of parameters. Also, the receivers can be described by the block diagrams of Figs. 4.1, 4.2 and 4.3, 4.4 applying the same replacements.

The above discussion leads to the conclusion that for CPM signals accurately approximated by a single AMP pulse, the design of relatively simple improved non-coherent receivers is possible. The non-coherent receivers for this case have comparable levels of complexity with the structures examined in Chapter 4 for linear signals.

In subsection 4.4 we presented a non-coherent sequence estimator for linear systems, based on squared envelope and multiple differential detection. These receiver structures can also be extended to the examined case of CPM signal, by applying the replacement of parameters as described by Eq. (5.16). Also in this case, an additional replacement has to be done, it being the following:

$$\Delta\Theta_l(k) \rightarrow Arg\{\alpha_{0,k}^{AMP}(\alpha_{0,k-l}^{AMP})^*\}$$

$$\cos(\Delta\Theta_l(k)) \rightarrow Re\{\alpha_{0,k}^{AMP}(\alpha_{0,k-l}^{AMP})^*\}$$

$$\sin(\Delta\Theta_l(k)) \rightarrow Im\{\alpha_{0,k}^{AMP}(\alpha_{0,k-l}^{AMP})^*\} \tag{5.20}$$

These expressions are:

$$\aleph_{HAO_{appr}}^{CPMD}(\tilde{\Re}_{E,[0,0]}^{AMP}, \bar{\mathcal{Y}}_0, \bar{C}(\bar{A})) =$$

$$-((\frac{1}{2}(\sum_{k=0}^{Z-1}\mathcal{A}_k^2) + \sum_{l=1}^{Z-1}\sum_{k=l}^{Z-1} Re\{\Re_{E,[0,0]}^{AMP}(l)\alpha_{0,k}^{AMP}(\alpha_{0,k-l}^{AMP})^*\} + [\sum_{k=0}^{Z-1}|\mathcal{Y}_{0,k}|^2\mathcal{A}_k^2$$

$$+2\sum_{k=1}^{Z-1}\mathcal{A}_k\sum_{l=1}^{k}\mathcal{A}_{k-l}[d_l^I(k)Re\{\alpha_{0,k}^{AMP}(\alpha_{0,k-l}^{AMP})^*\} + d_l^Q(k)Im\{\alpha_{0,k}^{AMP}(\alpha_{0,k-l}^{AMP})^*\}]^{\frac{1}{2}}\ , \tag{5.21}$$

$$\aleph^{CPSD}_{HAO_{appr}}(\tilde{\Re}^{AMP}_{E,[0,0]}, \tilde{\mathcal{Y}}_0, \tilde{C}(\tilde{A})) =$$

$$-(\sum_{l=1}^{Z-1}\sum_{k=l}^{Z-1} Re\{\Re^{AMP}_{E,[0,0]}(l)\alpha^{AMP}_{0,k}(\alpha^{AMP}_{0,k-l})^*\} + [\sum_{k=0}^{Z-1}|\mathcal{Y}_{0,k}|^2 +$$

$$2\sum_{k=1}^{Z-1}\sum_{l=1}^{k}[d^I_l(k)Re\{\alpha^{AMP}_{0,k}(\alpha^{AMP}_{0,k-l})^*\}) + d^Q_l(k)Im\{\alpha^{AMP}_{0,k}(\alpha^{AMP}_{0,k-l})^*\}]^{\frac{1}{2}} . \tag{5.22}$$

$$\begin{aligned}\aleph^{SQ}_{CPIC}(\tilde{\mathcal{Y}}_0, \tilde{C}(\tilde{A})) \;=\; & \sum_{k=1}^{Z-1}\sum_{l=1}^{k}[d^I_l(k)Re\{\alpha^{AMP}_{0,k}(\alpha^{AMP}_{0,k-l})^*\} \\ & + d^Q_l(k)Im\{\alpha^{AMP}_{0,k}(\alpha^{AMP}_{0,k-l})^*\}] .\end{aligned} \tag{5.23}$$

We bring to the reader's attention that in this case,

$$d_l(k) = \mathcal{Y}_{0,k}\mathcal{Y}^*_{0,k-l}, \quad d^I_l(k) = Re\{(\mathcal{Y}_{0,k}\mathcal{Y}^*_{0,k-l})\}, \quad d^Q_l(k) = I_m\{(\mathcal{Y}_{0,k}\mathcal{Y}^*_{0,k-l})\}, \tag{5.24}$$

In subsection 4.9.2 of Chapter 4 we have shown how a truncation can be applied on the number of differential detectors used, in order to reduce the complexity of the receiver for long sequences. The same strategy can be applied in the presented CPM receivers and the equivalent metrics can be derived by those metrics presented in the above mentioned section (for linear systems) going again through the replacements described previously. To avoid unnecessary repetition, we shall not give these expressions here.

5.5.3 Performance Evaluation of MSK

In the present section, a popular CPM signal, the MSK, will be evaluated with the proposed sequence estimators. The premodulation filter of the MSK signal has the following impulse response:

$$h_T(t) = \begin{cases} 1 & \text{for } 0 \le t \le T \\ 0 & \text{elsewhere.} \end{cases} \tag{5.25}$$

The MSK signal can be constructed by using only one AMP pulse, it being equal to [125]:

$$h_0^{AMP}(t) = \begin{cases} sin(\frac{\pi t}{T}) & \text{for } 0 \leq t \leq 2T \\ 0 & elsewhere. \end{cases} \tag{5.26}$$

Also

$$\alpha_{0,k}^{AMP} = j\alpha_{0,k-1}^{AMP} c_k \tag{5.27}$$

where $c_k = \pm 1$.

We shall evaluate the MSK under ideal channel conditions. For the detection of the transmitted information, either, the $\aleph_{CPIC_{appr}}(\bar{\Re}_{E,[0,0]}^{AMP}, \bar{\mathcal{Y}}_0, \bar{C}(\bar{A}))$ (see Eq.(5.19)) or $\aleph_{CPIC}(\bar{C}(\bar{A}), t))$(see Eq.(5.6)) can be used.

To find an upper bound of the SER probability, an upper bound for the pairwise probability of an error event formed between two sequences $\bar{C}(\bar{A}^{\nu})$ $\bar{C}(\bar{A}^{\varsigma})$ ($\{\bar{C}(\bar{A}^{\varsigma}) \leftarrow \bar{C}(\bar{A}^{\nu})\}$) is needed. The derivation of the pairwise error event bounds can be performed by following exactly the same methodology and steps as those described in sections 4.5, 4.6 and in more detail in Appendixes B to F. The bounds of the pairwise error events are used in the union bound to provide the upper bound of the overall performance (see sections 4.5, (Eq.(4.46)), 4.6 (Eq.(4.65)) in Chapter 4). To avoid unnecessary repetition, we shall not elaborate any further and limit ourselves to the presentation of the results.

In Fig. 5.1 the curves of the differential detector, as well as the proposed sequence estimator with length $Z = 4, 7$ are displayed. We realize that there is some improvement; however, this is quite minimal (practically zero for $Z = 4$ and 0.2 dB for $Z = 7$). This behaviour is similar to BPSK examined in subsection 4.5.6 of Chapter 4.

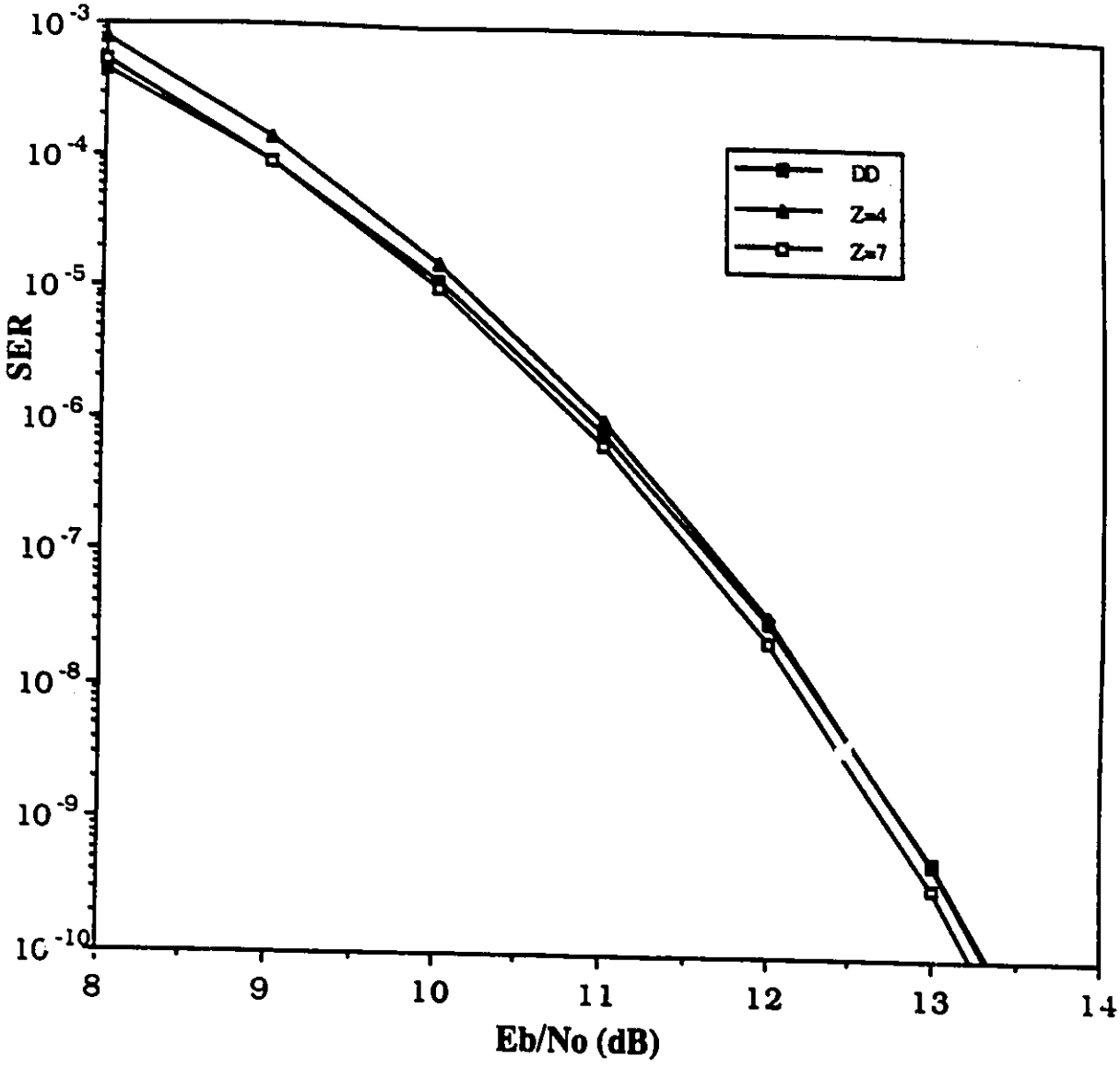

Figure 5.1: SER curves of non-coherent receivers for MSK. The channel is assumed ideal.

5.6 PRACTICAL NON-COHERENT CPM SEQUENCE ESTIMATORS FOR SPECTRALLY EFFICIENT CPM SIGNALS

According to the analysis presented in section 5.5.3, the AMP decomposition has helped considerably in reducing the complexity of the improved non-coherent receivers for CPM signals. The simplification extends both in the filtering requirements and the processing needed to calculate the metrics for the estimator. For CPM signals which can be accurately represented by a single AMP pulse, the complexity (in numbers of filters needed and processing load to carry out the calculations), is identical to the complexity of the receivers proposed for linear systems. However there remains one question yet unanswered. How simple and cost efficient is the implementation of a filter matching the pulse $h_0^{AMP}(t)$?

In section 3.5 of Chapter 3 it was mentioned that all the AMP pulses $h_i^{AMP}(t)$ are of limited time duration. This creates a problem since the implementation of filters with time limited impulse response is quite difficult and costly. As the spectral efficiency of the CPM signal increases, the shaping of $h_0^{AMP}(t)$ becomes more and more complex.

In subsection 4.4.3 of Chapter 4, we have commented on the advantages the communication system would have, if the proposed non-coherent receivers are implemented in IF multiple differential detection form. Such advantages are low cost, fast synchronization, simplicity, better performance in impaired (i.e. faded e.t.c.) channels, even higher capacity for the network. However, implementation of filters in IF is more difficult compared to baseband and definitely, a challenge for filters like those indicated by the AMP decomposition. Consequently, in order to be able to provide improved CPM receivers having the advantages mentioned above, it is necessary to further simplify the filter further. A simple way to resolve the problem is to make use of cost efficient, simple and commercially available filters (i.e. Gaussian, Butterworth, Raised Cosine) instead of those indicated by the AMP decomposition. Today, there are already WPDCS systems making use of the CPM technology [55], [81], [82], [170], [201] and receivers using simple commercially available filters.

Research conducted in the past has shown that even though low complexity non-coherent receivers -using commercially available filters and classical non-coherent detection techniques- perform quite well with CPM signals of low spectral efficiency, they lose a great deal of performance when applied to spectrally efficient signals (i.e. TFM, GMSK with narrow Gaussian premodulation filters etc.) [33], [34], [230], [162], [161]. As we shall see later on, the degradations are so severe, that they make use of simple differential receivers with these signals impossible. One question that arises, is how the proposed structures will perform when used with some simple commercially available filters. This question will be answered in the present section. As a matter of fact, it will be shown that the proposed algorithms behave exceptionally well even when they are applied with bandwidth efficient CPM signals and receivers which use simple practical filters instead of the complex optimal ones. With the same filters, the conventional differential schemes demonstrate poor performance.

5.6.1 Receiver Structure

To start the analysis, in Fig. 5.2 we provide a conceptual block diagram of the simplified CPM receiver. In the figure, we have adopted a baseband implementation of the receiver (i.e. the received signal is first demodulated before further processing is applied to it). However, this approach does not have to be followed in practice. As we shall see, the simplified receiver will be able to be implemented with IF multiple differential detection which was examined in previous sections and chapters. The block in the figure indicated as "Decision Unit" is the part of the receiver processing the samples of the received signal in order to provide a decision. Its structure will be defined later on, through the analysis that follows.

The incoming signal is first down converted (lock in frequency of the incoming carrier is only assumed) and afterwards filtered by the post detection filter $H_R^{CPM}(\omega)$. $H_R^{CPM}(\omega)$ is assumed to be wide enough in order to allow the information carrying signal to pass through it without any significant distortion. The signal $y^{CPM}(t)$ present at the output of $H_R^{CPM}(\omega)$, is sampled at kT. The samples y_k^{CPM} are equal to

$$y_k^{CPM} = x_{tr,B}(\bar{C}(\bar{A}), kT)e^{j\psi} + n_k^{CPM} = e^{j\beta_1(\tilde{\sigma}_0^{k-1}(\bar{C}(\bar{A})))} + n_k^{CPM} \qquad (5.28)$$

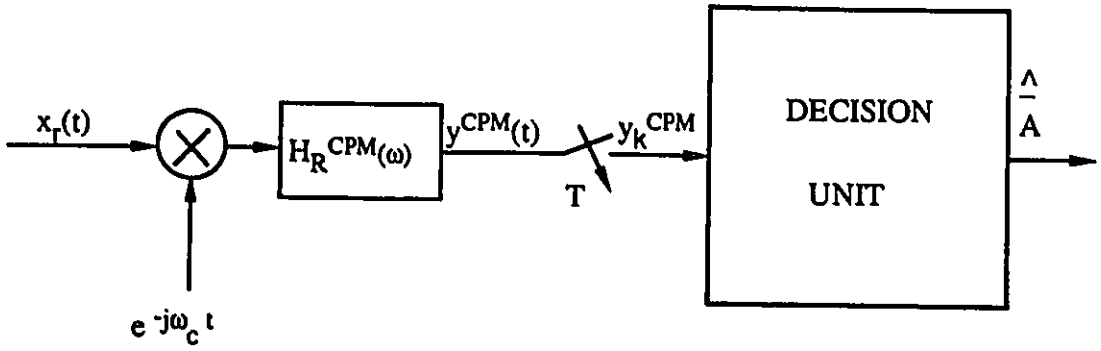

Figure 5.2: Conceptual block diagram of the receiver.

with $n_k^{CPM} = n^{CPM}(kT)$. $n^{CPM}(t)$ is the Gaussian noise corrupting $y^{CPM}(t)$. The correlation properties between the n_k^{CPM} terms are determined by the shaping of $H_R^{CPM}(\omega)$, however, when $H_R^{CPM}(\omega)$ is relatively wide $E\{n_k^{CPM} n_{k-l}^{CPM}\} \approx 0 \ \forall \ l \neq 0$. This condition will be assumed from now on in our analysis.

Let as assume that the impulse response of the premodulation filter $h_T(t)$ satisfies the following equation:

$$\int_{kT-T}^{kT} h_T(t)dt \begin{cases} \neq 0 & \text{for } 1 \leq k \leq \mathcal{L}_e \\ = 0 & \text{elsewhere.} \end{cases} \tag{5.29}$$

where $\mathcal{L}_e$ is a positive integer. We are assuming that transmission takes place in the time period $[0, (Z + \mathcal{L}_e)T)$.

The most possible sequence $\bar{C}(\bar{A})$ (to be the transmitted one) is the sequence which maximizes the probability density function (pdf) $f(\bar{y}_{[Z+\mathcal{L}_e,0]}^{CPM}/\bar{C}(\bar{A}))$, where $\bar{y}_{[Z+\mathcal{L}_e,0]}^{CPM} = [y_0^{CPM}, y_1^{CPM}, \ldots, y_{Z+\mathcal{L}_e}^{CPM}]$. Following steps similar to those described in Chapter 3 and in section 4.3 of Chapter 4 (but this time applying them on a discrete rather than a continuous signal) we find that the maximization of this pdf is equivalent to the maximization of

$$I_0\left(\frac{\left|\sum_{k=0}^{Z+\mathcal{L}_e} y_k^{CPM} e^{-j\beta_1(\bar{e}_0^{k-1}(\bar{C}(\bar{A})))}\right|}{N_o}\right) \tag{5.30}$$

which is reduced to the maximization of

$$\aleph_{RC}^{CPM}(\bar{y}_{[Z+\mathcal{L}_e,0]}^{CPM},\bar{C}(\bar{A}))=|\sum_{k=0}^{Z+\mathcal{L}_e}y_k^{CPM}e^{-j\beta_1(\bar{\varphi}_0^{k-1}(\bar{C}(\bar{A})))}|. \tag{5.31}$$

Eq.(5.31) has the form of the block decoder, introduced first with PSK signals in Chapter 4. We met the block decoder again, this time applied on CPM signals in subsection 5.5.3 of the present chapter[1].

Squaring $\aleph_{RC}^{CPM}(\bar{y}_{[Z+\mathcal{L}_e,0]}^{CPM},\bar{C}(\bar{A}))$ and eliminating terms independent from $\bar{C}(\bar{A}))$, we end up with the following (equivalent) metric expression (to be maximized):

$$\begin{aligned}\aleph_{MDD}^{CPM}(\bar{y}_{[Z+\mathcal{L}_e,0]}^{CPM},\bar{C}(\bar{A})) &= \sum_{k=1}^{Z+\mathcal{L}_e}\sum_{l=1}^{k}[d_l^I(k)\cos(\Delta_l\beta_1(k,\bar{\varphi}_{k-l-\mathcal{L}_e+1}^{k}(\bar{C}(\bar{A}))))\\ &\quad +d_l^Q(k)\sin(\Delta_l\beta_1(k,\bar{\varphi}_{k-l}^{k}(\bar{C}(\bar{A}))))]\ .\end{aligned} \tag{5.32}$$

where

$$\begin{aligned}\Delta_l\beta_1(k,\varphi_{k-l-\mathcal{L}_e+1}^{k-1}(\bar{C}(\bar{A})) &= \beta_1(\bar{\varphi}_0^{k-\mathcal{L}_e-1}(\bar{C}(\bar{A})))-\beta_1(\bar{\varphi}_0^{k-l-\mathcal{L}_e-1}(\bar{C}(\bar{A})))\\ &= \sum_{\nu=1}^{l}c_{k-\nu}\vartheta_0^k+\sum_{\nu=l+1}^{\mathcal{L}_e+l}c_{k-\nu}\vartheta_{\nu-l}^{\nu}\end{aligned} \tag{5.33}$$

(see also Eq.(3.80) in Chapter 3). In the rest of the present chapter,

$$d_l(k)=y_k^{CPM}(y_{k-l}^{CPM})^*,$$

$$d_l^I(k)=Re\{y_k^{CPM}(y_{k-l}^{CPM})^*\},$$

$$d_l^Q(k)=I_m\{y_k^{CPM}(y_{k-l}^{CPM})^*\}. \tag{5.34}$$

[1] As a matter of fact, $\aleph_{RC}^{CPM}(\bar{y}_{[Z+\mathcal{L}_e,0]}^{CPM},\bar{C}(\bar{A}))$ can be derived from $\aleph_{CPIC_{e,p,r}}(\bar{\Re}_{E,[0,0]}^{AMP},\bar{\mathcal{Y}}_0,\bar{C}(\bar{A}))$, simply by replacing $\bar{\mathcal{Y}}_0$ with $\bar{y}_{[Z+\mathcal{L}_e,0]}^{CPM}$, $\mathcal{Y}_{0,k}$ with y_k^{CPM} and $\alpha_{0,k-1}^{AMP}$ with $e^{-j\beta_1(\bar{\varphi}_0^{k-1}(\bar{C}(\bar{A})))}$.

It is easy to identify the multiple differential detection nature of the receiver described by Eq.(5.34). As a matter of fact, comparing $\aleph_{MDD}^{CPM}(\bar{y}_{[Z+\mathcal{L}_e,0]}^{CPM}, \bar{C}(\bar{A}))$ with the multiple differential detection metric for PSK signals ($\aleph_{IC}^{SQ}(\bar{y}, \bar{C}(\bar{A}))$, (see Eq.(4.33)) makes us realize that the two metric expressions are identical.

As it was discussed in section 4.4.3, the multiple differential receiver can be implemented either in baseband or IF form. In the same section, we have provided block diagrams of the two different implementations (see Figs. 4.5, 4.6) and have commented on the advantages and disadvantages of each approach.

Truncating the number of differential detectors used to a maximum of λ, the metric expression becomes:

$$\begin{aligned} Q_{MDD}^{CPM}(\bar{y}_{[Z+\mathcal{L}_e,0]}^{CPM}, \bar{C}(\bar{A})) &= \sum_{k=1}^{Z+\mathcal{L}_e} \sum_{l=1}^{\varpi} [d_l^I(k) \cos(\Delta_l \beta_1(k, \bar{\varphi}_{k-l}^k(\bar{C}(\bar{A})))) \\ &\quad + d_l^Q(k) \sin(\Delta_l \beta_1(k, \bar{\varphi}_{k-l}^k(\bar{C}(\bar{A}))))] \end{aligned} \tag{5.35}$$

where

$$\varpi = \begin{cases} k & \text{for } 1 \leq k \leq \lambda \\ \lambda & \text{for } k > \lambda \,. \end{cases} \tag{5.36}$$

Equivalently, Eq.(5.35) can be expressed as

$$Q_{MDD}^{CPM}(\bar{y}_{[Z+\mathcal{L}_e,0]}^{CPM}, \bar{C}(\bar{A})) = \sum_{k=1}^{Z+\mathcal{L}_e} \mho_k^{\varpi}(\overline{\mathcal{DO}}_k^{\varpi}, [c_k, c_{k-1}, \ldots, c_{k-l-\mathcal{L}_e}]) \tag{5.37}$$

where

$$\begin{aligned} \mho_k^{\varpi}(\overline{\mathcal{DO}}_k^{\varpi}, [c_k, c_{k-1}, \ldots, c_{k-l-\mathcal{L}_e}]) &= \sum_{l=1}^{\varpi} [d_l^I(k) \cos(\Delta_l \beta_1(k, \bar{\varphi}_{k-l}^k(\bar{C}(\bar{A})))) \\ &\quad + d_l^Q(k) \sin(\Delta_l \beta_1(k, \bar{\varphi}_{k-l}^k(\bar{C}(\bar{A}))))] \end{aligned} \tag{5.38}$$

and

$$\overline{\mathcal{DO}}_k^{\varpi} = [d_1^I(k), d_l^Q(k), d_2^I(k), d_2^Q(k), \ldots, d_{\varpi}^I(k), d_{\varpi}^Q(k)]. \tag{5.39}$$

$\mathcal{U}_k^{\varpi}(\overline{\mathcal{DO}}_k^{\varpi}, [c_k, c_{k-1}, \ldots, c_{k-l-\mathcal{L}_c}])$ is the increment in the value of the metric as the decoder moves to process the information received at the next sampling instant.

The maximization of $\mathcal{Q}_{MDD}^{CPM}(\bar{y}^{CPM}, \bar{C}(\bar{A}))$ can be carried out recursively, by using either one of the two recursive algorithms described in subsection 4.9.2.2.

Below, we provide performance evaluation results of the truncated MDD sequence estimator for MSK as well as TFM [103] and GMSK [191]. The results to be reported are based on Monte Carlo simulations; however, analytical evaluation is possible by following exactly the same steps with those described in section 4.9.3. We have chosen the simulation approach in order to access the effects of the post modulation and post detection filtering on the performance. The reason for applying post modulation filtering to the transmitted signal is to reduce the levels of adjacent channel interference and allow close packing of carriers in a Frequency Division Multiple Access (FDMA) environment. At the receiver, a simple filter is used, whose main purpose is to reduce the noise levels. The bandwidth of this filter should not be chosen too wide because a large amount of noise will enter and deteriorate the performance. At the same time if chosen too narrow, it will distort the information signal through its filtering effect which also deteriorates the performance. The optimal value of the bandwidth the filter should have depends on the transmitted CPM signal and the type of filter used (Gaussian, Butterworth etc.).

The performance of the non-coherent receiver (implemented either in the block decoding or multiple differential detection form) will be affected both by the signal distortion created by the pre-modulation filter and pre- or post-detection filtering (it appears as ISI) as well as the power levels and the autocorrelation properties (i.e. the autocorrelation function) of the noise at the output of the receiver filter. We remind the reader that the combined effect of ISI and noise correlation has been considered in the case of linear signals through analytical evaluations (see section 4.5.7 in Chapter 4, also Appendix B). In principle, the analysis applied for the linear systems on this matter can be extended and used in the present case. However, the complex nature of the CPM signal and the filters used create somewhat complicated expressions and require a relatively high amount of computational processing.

Instead, we decided to resort to Monte Carlo simulations.

5.6.2 Performance Evaluation of the MDD Receiver with CPM Signals

5.6.2.1 Minimum Shift Keying

For the MSK signal, $\mathcal{L}_e = 1$. Also,

$$\Delta_l \beta_1(k, \bar{\varphi}_{k-l}^k(\bar{C}(\bar{A}))) = (\sum_{i=0}^{l} c_{k-i} \frac{\pi}{2})_{(mod 2\pi)}. \tag{5.40}$$

In Figs. 5.3, 5.4, SER curves of the MSK signal (corresponding to different non-coherent receivers) are presented. We consider an IF implementation of the differential detection. The results presented in Fig. 5.3 correspond to an unfiltered MSK signal (no post modulation filtering is applied). Fig. 5.4 provides results for a post modulation filtered MSK signal. As a post modulation filter we have used a 4^{th} order Butterworth with $BT = 1.0$. In both cases, at the receiver a 4^{th} order Butterworth with $B_rT = 1.1$ has been used. The value of B_rT has been chosen because it gives the best performance when applied with the post modulation filtered signal [40]. The optimization in performance refers to the performance of the conventional 1-bit differential detector.

The curves displayed correspond to the conventional differential detector (DD), a receiver based on the non-redundant error correction (NEC) [172] with single error correction capability (the 1 and 2-bit differential detectors are used) and a 4-state multiple differential detection decoder (see Eq.(5.32)) with $\lambda = 2$ (i.e. the 1 and 2-bit differential detectors are used) (MDD).

In Tables 5.1, 5.3 we summarize the improvements offered by the non-redundant error correction and multiple differential detection receiver as compared to the conventional differential detector. We realize that the MDD decoder always outperforms the other two schemes (DD and NEC). We also realize that the MDD receiver is less sensitive to filtering effects. As a matter of fact, its gains (as compared to DD and NEC) are increased when the transmitted signal becomes distorted due to filtering. In the non-filtered

case, the MDD receiver has a superiority of 1.7 and 0.5 dB as compared to DD and NEC (SER=10^{-4}). However for the filtered case and for SER=10^{-3}, the improvements become 2.7 dB and 1.1 dB. For SER=10^{-4} they increase even more, becoming 3.1 dB and 1.4 dB.

Table 5.1: Improvements offered by non-redundant error correction (NEC) and multiple differential detection (MDD) (both use the 1 and 2-bit differential detectors) as compared to the conventional (1-bit) differential detector (DD) . The transmitted MSK signal is unfiltered. The reported gains correspond to a SER=10^{-4}.

GAINS (dB)	
NEC	MDD
1.1	1.7

Table 5.2: Improvements offered by the non-redundant error correction (NEC) and multiple differential detection (MDD) (both use the 1 and 2-bit differential detectors) as compared to the conventional (1-bit) differential detector (DD). Post modulation filtering has been applied to the transmitted MSK signal. As a post-modulation filter, a 4^{th} order Butterworth with $BT = 1.0$ has been used.

		GAINS (dB)	
		NEC	MDD
SER	10^{-3}	1.6	2.7
	10^{-4}	1.7	3.1

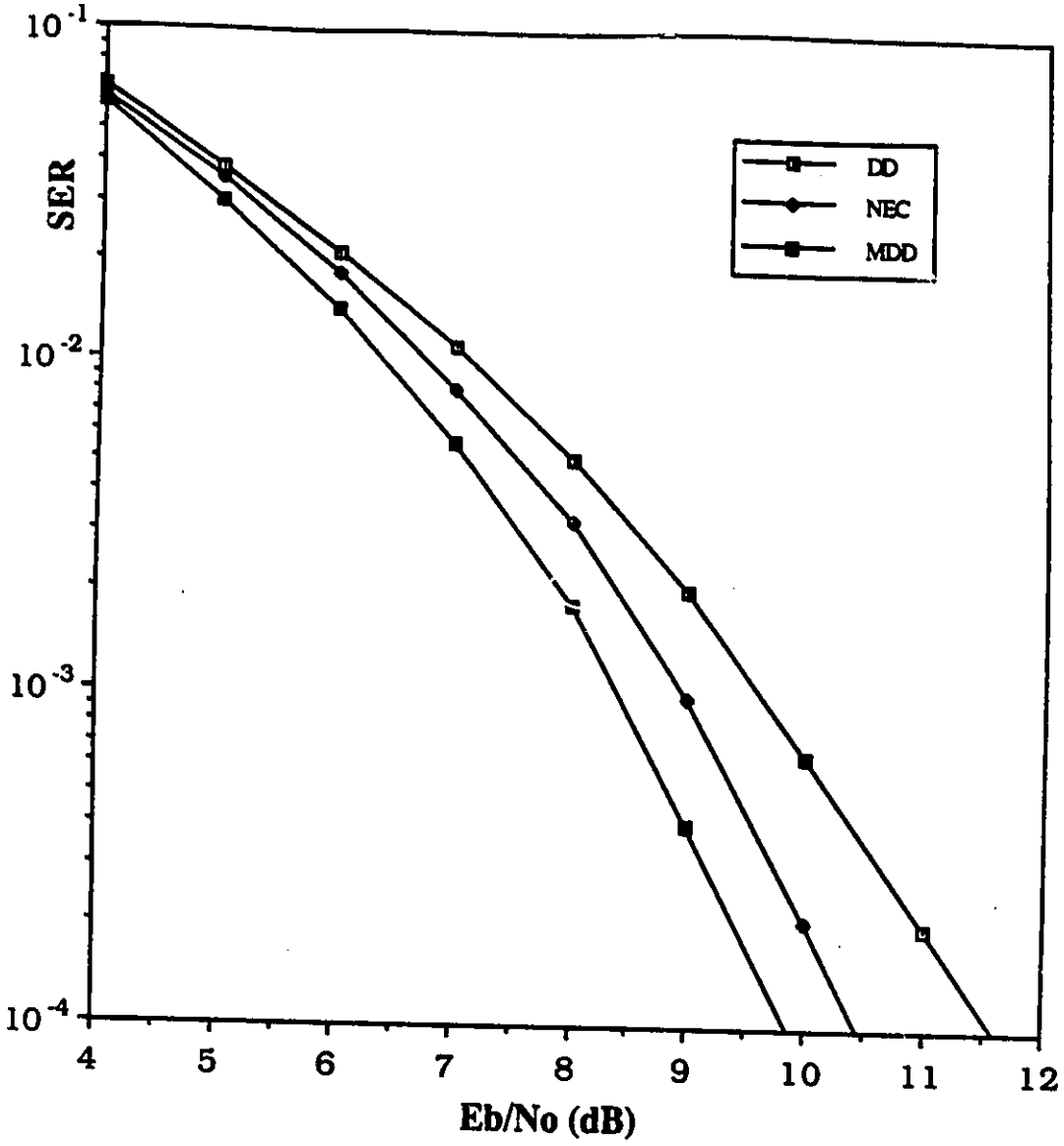

Figure 5.3: SER performance curves of MSK corresponding to various non-coherent receivers. The transmitted signal is unfiltered. At the receiver, a predetection 4^{th} order Butterworth filter with $B_rT = 1.1$ is used.

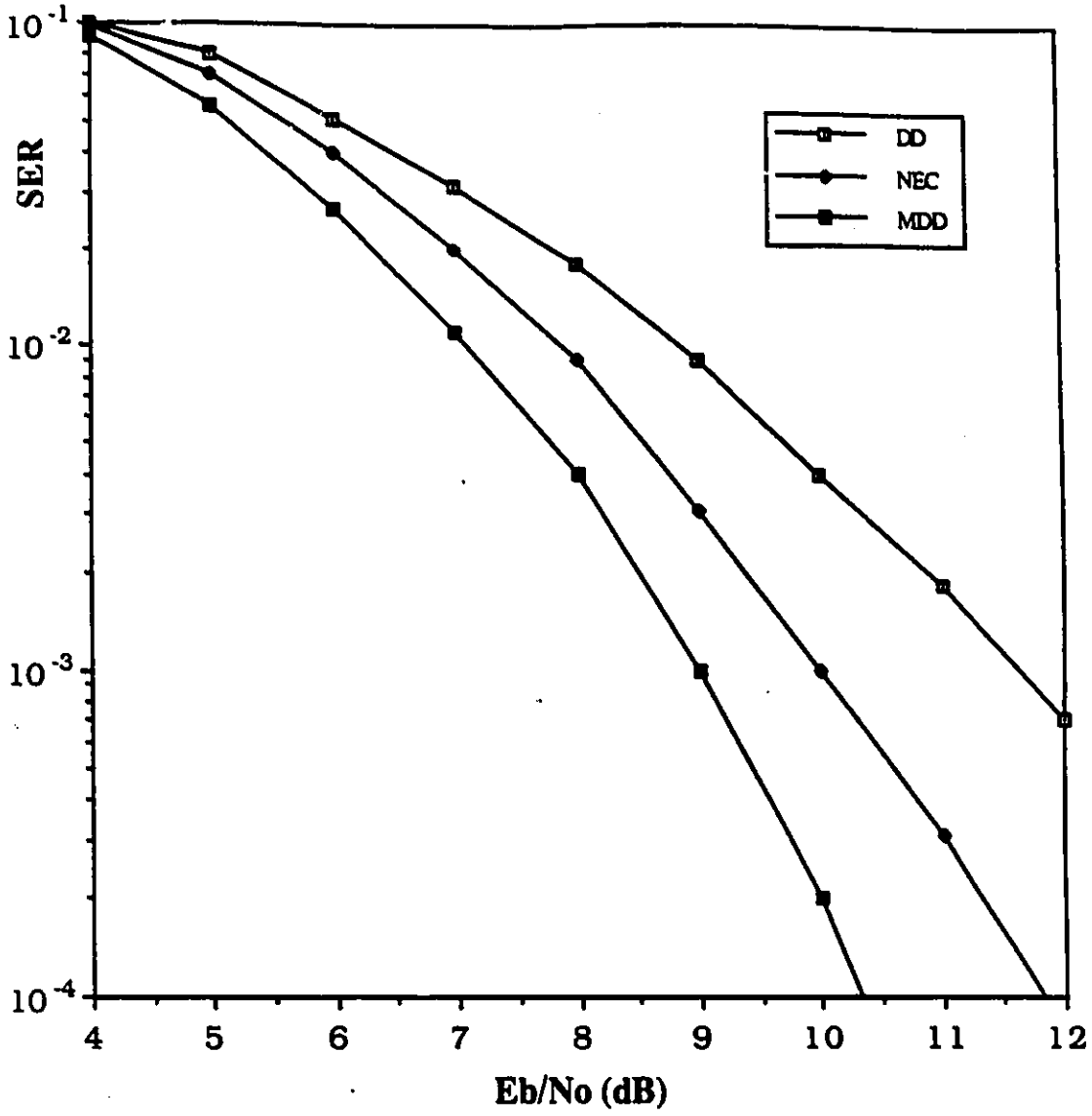

Figure 5.4: SER performance curves of MSK with various non-coherent receivers. The transmitted signal has been filtered with a (post-modulation) 4^{th} order Butterworth filter having $BT = 1.0$. At the receiver, a predetection 4^{th} order Butterworth filter with $B_rT = 1.1$ is used.

5.6.2.2 Tamed Frequency Modulation

TFM belongs to the family of Correlative Encoded CPM signals (CECPM) [12], [240]. The premodulation filter $h_T(t)$ for a TFM signal can be described as follows:

$$h_T(t) = \frac{1}{8}h_{N3}(t) + \frac{1}{4}h_{N3}(t-T) + \frac{1}{8}h_{N3}(t-2T) \tag{5.41}$$

where $h_{N3}(t)$ represents the impulse response of a filter satisfying the 3^{rd} Nyquist criterion [206], i.e.:

$$\int_{kT-T}^{kT} h_{N3}(t)dt = \begin{cases} 1 & \text{for } k = 1 \\ 0 & \text{elsewhere.} \end{cases} \tag{5.42}$$

For the TFM, $\Delta_l\beta_1(k, \wp_{k-l}^{k-1}(\bar{C}(\bar{A})))$ is equal to:

$$\Delta_l\beta_1(k, \wp_{k-l}^{k-1}(\bar{C}(\bar{A}))) = \begin{cases} \frac{\pi}{8}c_k + \frac{\pi}{4}c_{k-1} + \frac{\pi}{8}c_{k-2} & \text{for } l = 1 \\ \frac{\pi}{8}c_k + \frac{3\pi}{8}c_{k-1} + \frac{3\pi}{8}c_{k-2} + \frac{\pi}{8}c_{k-3} & \text{for } l = 2 \\ \frac{\pi}{8}c_k + \frac{3\pi}{8}c_{k-1} + \sum_{i=1}^{l-2}\frac{\pi}{2}c_{k-i-1} & \\ +\frac{3\pi}{8}c_{k-l} + \frac{\pi}{8}c_{k-l-1} & \text{for } l > 2. \end{cases} \tag{5.43}$$

In Figs. 5.5, 5.6, the SER performance curves of the TFM in an AWGN (Fig. 5.5) and a Rician faded channel (Fig. 5.6) are presented. The received signal is filtered with a 4^{th} order Butterworth filter, having $B_rT = 0.8$. For the Rician fading channel, we are assuming a Rician fading factor K_r=10 dB and $B_FT = 0.2$. The fading process simulated uses the land mobile model (its power spectral density has been described in Eq.(4.94)). The evaluated receiver configurations are the: i) 2-bit differential detector[2] (2-bit DD), ii) a 4-state decoder using the multiple differential detection algorithm

[2][160] shows that for the TFM signal, all the differential detectors using delay elements m-bit are completely closed when m is odd. They have an open and symmetric eye when m is even; however, they require the use of differential encoding in order to allow binary decisions according to the signal polarity. Since the $m = 2$ case requires the simplest differential encoding process, it is the most appropriate to be used for detection.

with $\lambda = 1$ (i.e. only the 1-bit detector is used, (1)-bit MDD), iii) an 8-state decoder using the multiple differential detection algorithm with $\lambda = 2$ (the 1 and 2-bit detectors are used, (1+2)-bit MDD)), iv) a 16-state decoder using the multiple differential detection algorithm with $\lambda = 3$ (the 1, 2 and 3-bit detectors are used, (1+2+3)-bit MDD)) and v) the coherent detector (CD) (the SER curve of the CD has been taken from [103], [34]). From the presented figures the superiority of the multiple differential detection receivers is obvious, since **they provide improvements higher than 9 dB**, being less than 1 dB away from the coherent receiver. In Table 5.3 the improvements offered by the MDD receivers are summarized.

Table 5.3: Improvements offered by the multiple differential receivers (as compared to the conventional 2-bit differential detector) for a TFM signal in an AWGN channel. The reported gains correspond to a SER=10^{-4}.

GAINS (dB)		
(1)-bit MDD	(1+2)-bit MDD	(1+2+3)-bit MDD
6.5	8.6	9.3

Interesting and impressive is the performance of the multiple differential detection receivers in the fading channel, where **they reduce the error floors more than three orders of magnitude.** This demonstrates a strong resistance of the MDD receivers to fading. The reasons for this resistance and robustness in performance when operating in faded channels follow.

First of all, the MDD receivers use for detection both, the inphase and quadrature channels, whereas the 2-bit DD makes use of only one (the inphase channel). The use of both channels act as as a diversity mechanism against fading. The fading distortion corrupting the signal at a particular time does not usually appear with the same strength in both channels. Most of the time, one of them suffers less. Use of both of them provides a protection and keeps the performance in high levels. The second reason is associated with the nature of the multiple differential detection. The MDD receivers, introduce *time diversity* in the detection process. The conventional 2-bit DD bases its decision only on one signal sample. However, for the (1)-bit MDD,

the shortest possible error events have the length of a 3-bit interval. One such error event is displayed in Fig. 5.7 (where the trellis diagram of the 1-bit MDD decoder is shown) and corresponds to the pair formed between the paths passing from the states $[G_1, G_1, G_1, G_1]$ and $[G_1, G_2, G_3, G_1]$. In order for the decoder to choose one between the two of them, it has to use three signal samples. This provides the chance that even if one or two of them are hit by severe fading, the third signal sample might not and its effect might keep the decision on the correct side. As the number of differential detectors (used by the algorithm) increases, the length of the shortest error events increases as well and with it the time diversity and resistivity to fading. For the (1+2)-bit MDD receiver, the minimum length increases from 3 to 4 (see paths $[G_1, G_1, G_1, G_1, G_1]$ and $[G_1, G_2, G_3, G_5, G_1]$ in Fig. 5.8) whereas for the (1+2+3)-bit MDD receiver it becomes 5 bit intervals. The beneficial nature of time diversity in fading environments has also been highlighted in [135].

One conclusion arising out of our evaluations is that the value of the decoding depth, required to obtain almost all of the improvement, is smaller in the fading case compared to the Gaussian channel. Similar conclusions have been reached in [180] for the trellis coded and differentially detected MPSK signal.

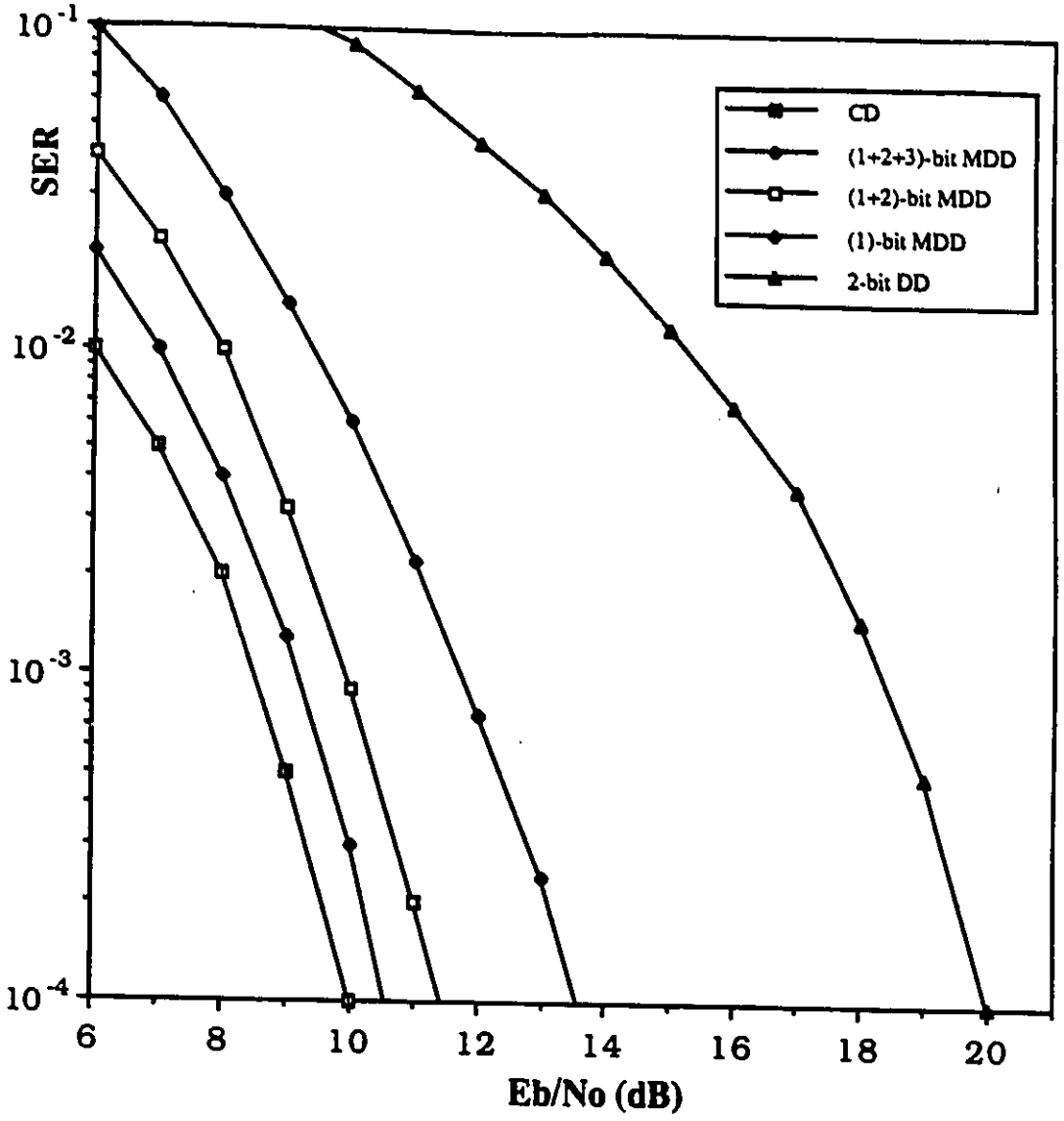

Figure 5.5: SER performance curves of multiple differential detection decoders used with TFM in an AWGN channel. The curve of the 2-bit differential detector is displayed as well.

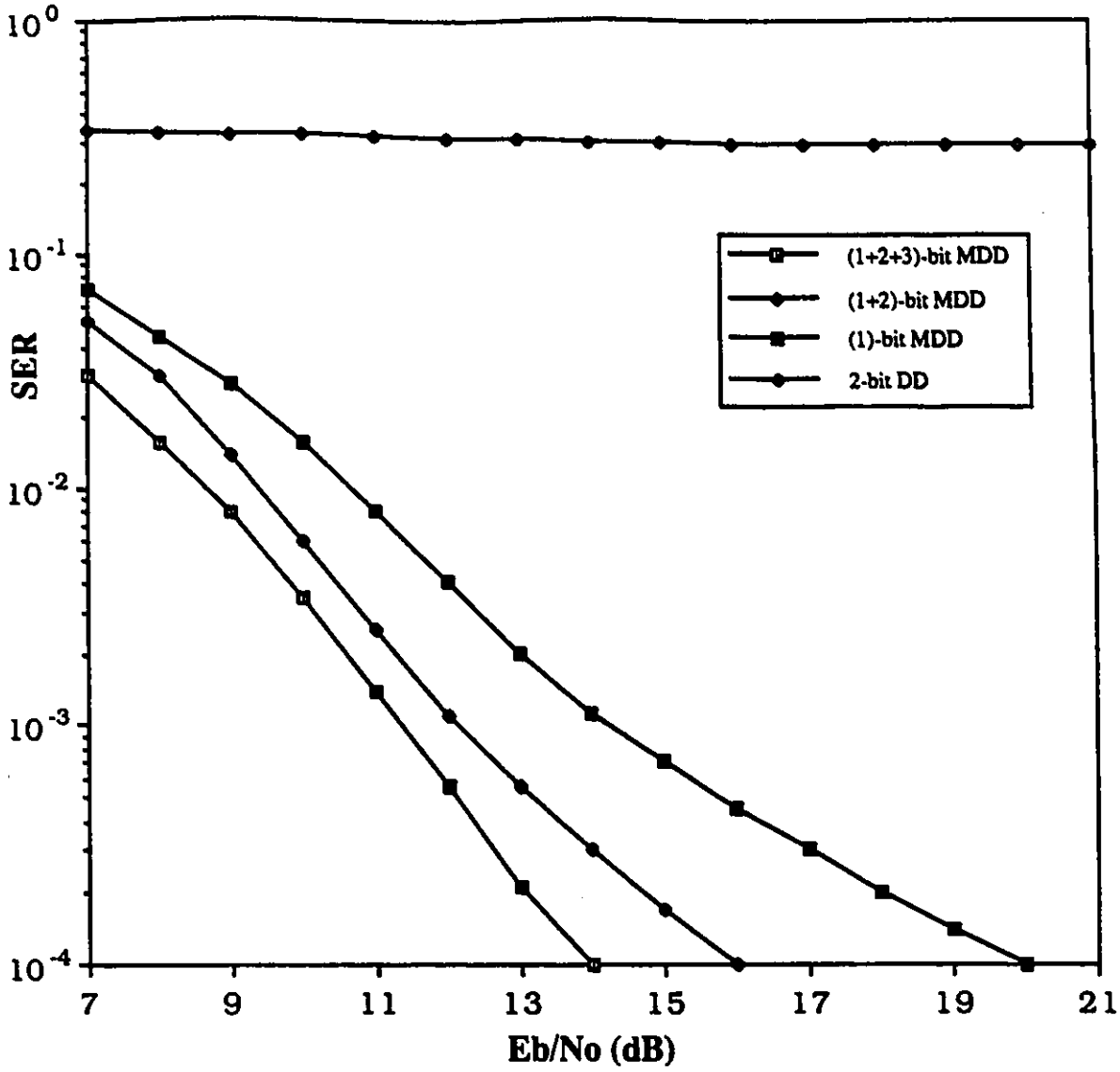

Figure 5.6: SER performance curves of multiple differential detection decoders used with TFM in a Rician faded channel ($K_r = 10dB$, $B_FT = 0.2$). The curve of the 2-bit differential detector is displayed as well.

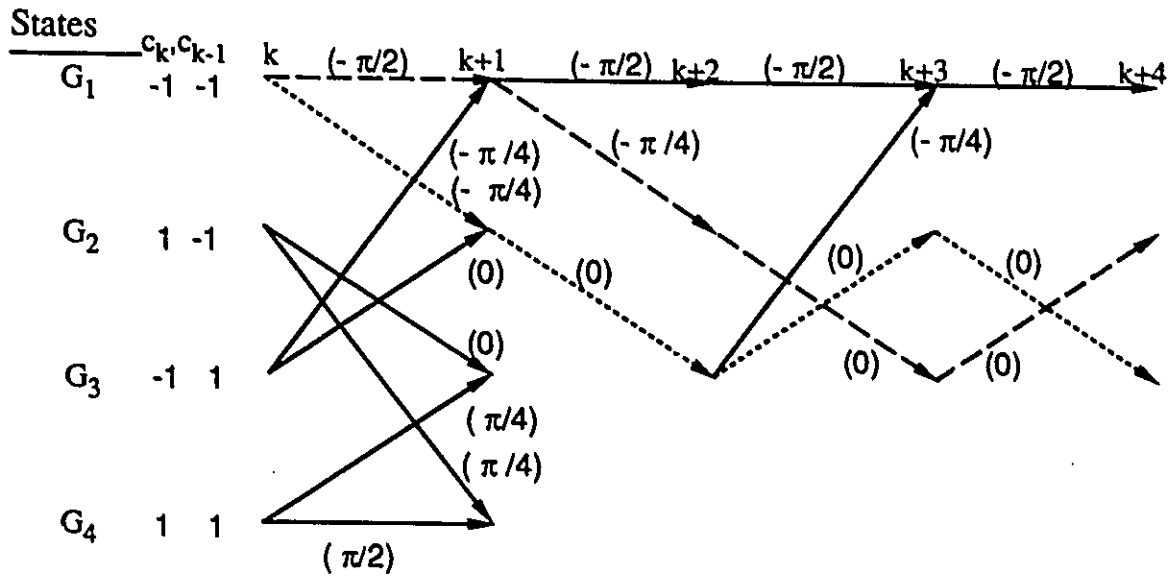

Figure 5.7: Trellis diagram of the multiple differential detection decoder (using the 1-bit differential detector) for a TFM signal. The values indicated on the transition branches correspond to the values of $\Delta_1\beta_1(k, [c_k, c_{k-1}, c_{k-2}])$

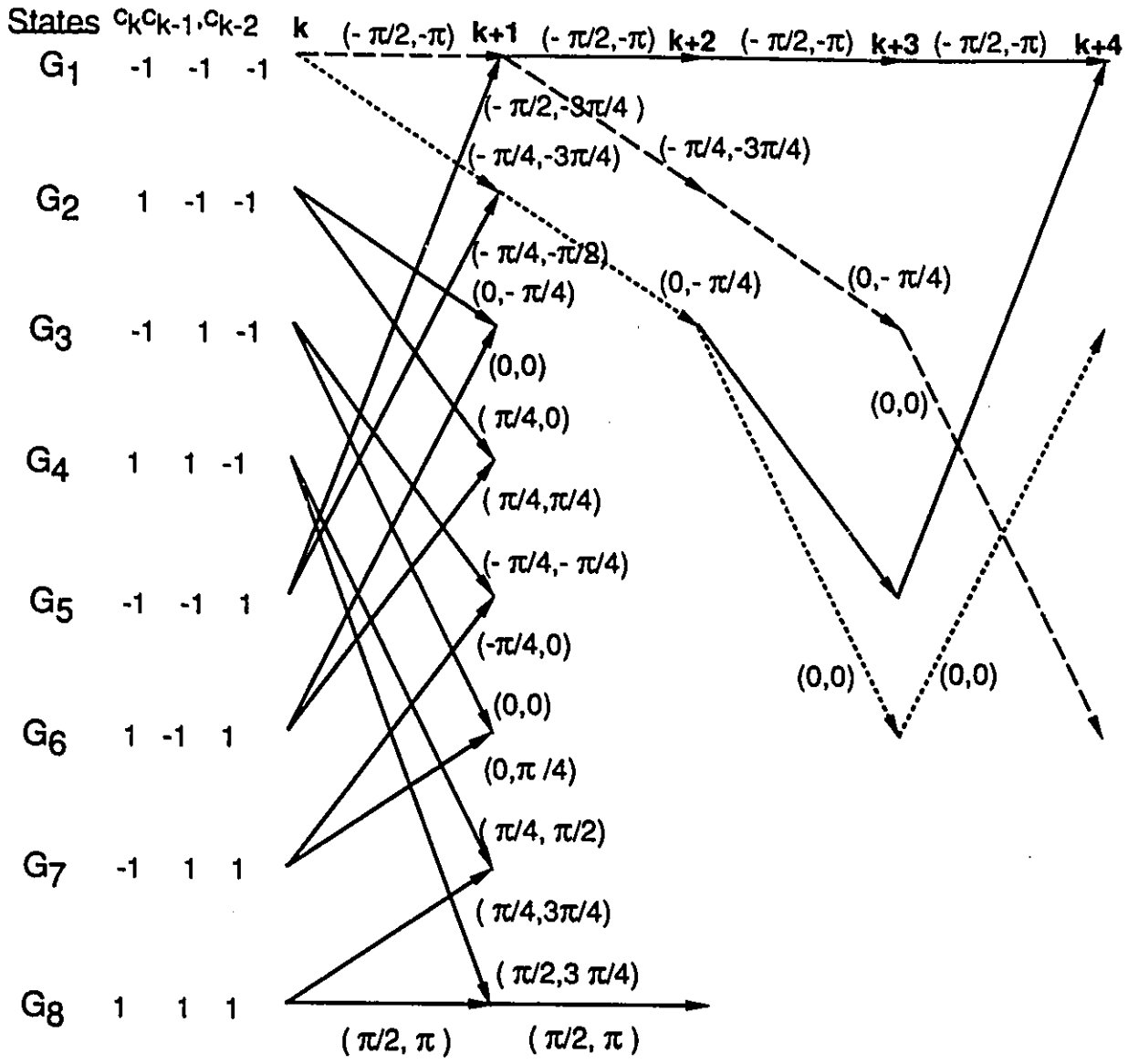

Figure 5.8: Trellis diagram of the multiple differential detection decoder (using the 1 and 2-bit differential detectors) for a TFM signal. The values indicated on the transition branches correspond to the values of $\Delta_2\beta_1(k, [c_k, c_{k-1}, c_{k-2}, c_{k-3}])$.

Catastrophic Behaviour of the TFM Receivers

When multiple differential detection sequence estimation is used, it is important to make sure that the decoder does not experience catastrophic behaviour.

Let us assume that two sequences $\bar{C}(\bar{A}^{\nu})$, $\bar{C}(\bar{A}^{\varsigma})$ diverge for the first time at $(\eta_1 T)$ and after that they remain in divergence until the end of transmission $((Z-1)T)$. The decoder chooses between the two sequences by comparing the values of of the metrics $\mathcal{Q}_{MDD}^{CPM}(\bar{y}_{[Z+\mathcal{L}_e,0]}^{CPM}, \bar{C}(\bar{A}^{\nu}))$, $\mathcal{Q}_{MDD}^{CPM}(\bar{y}_{[Z+\mathcal{L}_e,0]}^{CPM}, \bar{C}(\bar{A}^{\varsigma}))$ (see Eq.(5.37)). If after $(\eta_2 T)$ $(0 < \eta_1 \leq (\eta_2 < (Z-1))$ $\mathcal{U}_k^{\varpi}(\overline{\mathcal{DO}}, [c_k^{\nu}, c_{k-1}^{\nu}, \ldots, c_{k-l-\mathcal{L}_e}^{\nu}])$ and $\mathcal{U}_k^{\varpi}(\overline{\mathcal{DO}}_k^{\varpi}, [c_k^{\varsigma}, c_{k-1}^{\varsigma}, \ldots, c_{k-l-\mathcal{L}_e}^{\varsigma}])$ (see Eq.(5.38)) are always equal, there is no way that the value of difference between $\mathcal{Q}_{MDD}^{CPM}(\bar{y}_{[Z+\mathcal{L}_e,0]}^{CPM}, \bar{C}(\bar{A}^{\nu}))$ and $\mathcal{Q}_{MDD}^{CPM}(\bar{y}_{[Z+\mathcal{L}_e,0]}^{CPM}, \bar{C}(\bar{A}^{\varsigma}))$ can change after $(\eta_2 T)$. If one of the two sequences has been transmitted and the decoder up to $(\eta_2 T)$ has erroneously chosen the other, there is no way to reverse its decision at a later time. The result is that endless number of errors will occur (up to the end of the transmission). Pairs of sequences having this behaviour form a *catastrophic error event*. The presence of catastrophic behaviour is a serious threat to the communication system, since, due to their large number the presence of these errors can not be detected even if error control coding is added. Consequently there is a chance for the destination receiver to provide its user with a large amount of incorrect information.

The MDD receivers for TFM experience such behaviour. For example let us consider the 4-state (1)-bit MDD receiver. Its trellis diagram is presented in Fig. 5.7. On the various branches, we indicate the values of the differential phases $\Delta_1\beta_1(k, [c_k, c_{k-1}, c_{k-2}])$, corresponding to these transitions. In the figure, a pair of paths diverging from the same stage (G_1, corresponding to $c_k = -1, c_{k-1} = -1$) at $t = kT$ has been highlighted. These paths correspond to the following data sequences:

$$c_k = -1, c_{k+1} = -1, c_{k+2} = -1, c_{k+3} = 1, c_{k+4} = -1, c_{k+5} = 1, c_{k+6} = -1, \ldots$$

and

$$c_k = -1, c_{k+1} = -1, c_{k+2} = 1, c_{k+3} = -1, c_{k+4} = 1, c_{k+5} = -1, c_{k+6} = 1, \ldots$$

The two paths, after $t = (k+2)T$, have identical differential phases $(\Delta_1\beta_1(k, [c_k, c_{k-1}, c_{k-2}]) = \Delta_1\beta_1(k, [c_k, c_{k-1}, c_{k-2}]) = 0$ for $i > k+2)$. Examining their metrics (see Eq.(5.32)),we see that after $t = (k+2)T$, these metrics

change identically. The result is that if one of the two sequences presented above is transmitted, and the algorithm of up to $(k+2)T$ favours the other one, there is no way to reverse its decision. We mention that in addition to these paths highlighted here, there are other pairs of paths having similar behaviour.

For the algorithm based on the 1 and 2-bit detectors, the 8-state trellis diagram is presented in Fig. 5.8. In the figure, we indicate the values of the differential phases $[\Delta_1\beta_1(k,[c_k,c_{k-1},c_{k-2}]),\ \Delta_2\beta_1(k,[c_k,c_{k-1},c_{k-2},c_{k-3}])$]corresponding to the various branches. Again, a pair of paths with catastrophic behaviour has been highlighted. After $t=(k+3)T$, the paths have identical values of $\Delta_1\beta_1(k,[c_k,c_{k-1},c_{k-2}])$ and $\Delta_2\beta_1(k,[c_k,c_{k-1},c_{k-2},c_{k-3}])$ (in the $mod(2\pi)$ sense). The highlighted paths correspond to the sequences

$$c_k=-1,c_{k+1}=-1,c_{k+2}=-1,c_{k+3}=-1,c_{k+4}=\ 1,c_{k+5}=-1,c_{k+6}=\ 1,...$$

and

$$c_k=-1,c_{k+1}=-1,c_{k+2}=-1,c_{k+3}=\ 1,c_{k+4}=-1,c_{k+5}=\ 1,c_{k+6}=-1,...$$

The same behaviour exists for the receiver based on the 1-,2- and 3-bit differential detectors. It can be shown that for the TFM, any combination of differential detectors used in the multiple differential detection algorithm will result with a receiver suffering from catastrophic behaviour.

Solution to the problem

This catastrophic behaviour problem can be resolved by using differential encoding at the transmitter and differential decoding at the receiver. At the transmitter, the information symbols a_k ($a_k=1$or 0) are encoded as follows:

$$c_k=glm\{a_k\}c_{k-1} \tag{5.44}$$

where

$$glm\{a_k\}=\begin{cases}1 & \text{for } a_k=1\\ -1 & \text{for } a_k=0\end{cases} \tag{5.45}$$

The decoding needed at the receiver is

$$\hat{a}_k=hlm\{\hat{c}_k\hat{c}_{k-1}\}. \tag{5.46}$$

A reminder,

$$hlm\{x\} = \begin{cases} 1 & \text{for } x > 0 \\ 0 & \text{elsewhere.} \end{cases} \tag{5.47}$$

$\hat{a}_k$, $\hat{c}_k$ represent decisions made for a_k , c_k respectively. This technique has been extensively used in the past to resolve similar problems in Partial Response Signals [62] or to eliminate the phase ambiguity problems associated with the carrier recovery [60].

For the TFM, differential encoding is always necessary (regardless the choice of differential detectors used by the MDD algorithm).

5.6.2.3 Gaussian Minimum Shift Keying

The impulse response of the Gaussian premodulation filter $h_T(t)$ is equal to:

$$h_T(t) = \frac{1}{2T}[Q(Co_g B_t T(\frac{-t}{T})) - Q(Co_g B_t T(1 - \frac{-t}{T}))] \tag{5.48}$$

where $Co_g = 7.546$ and

$$Q(x) = \frac{1}{\sqrt{2\pi}} \int_x^\infty \exp(-\frac{y^2}{2}) dy. \tag{5.49}$$

For the GMSK with $B_t T = 0.25$,

$$\Delta_1\beta_1(k, [c_k, c_{k-1}, c_{k-2}]) \approx \frac{\pi}{9.89} c_k + \frac{\pi}{3.36} c_{k-1} + \frac{\pi}{9.89} c_{k-2}. \tag{5.50}$$

$\Delta_l\beta_1(k, [c_k, c_{k-1}, \ldots, c_{k-l-1}])$ can be calculated from $\Delta_1\beta_1(k, [c_k, c_{k-1}, c_{k-2}])$ as follows:

$$\Delta_l\beta_1(k, \varphi_{k-l}^{k-1}(\bar{C}(\bar{A}))) = (\sum_{i=0}^{l-1} \Delta_1\beta_1(k-i, [c_k, c_{k-1}, c_{k-2}])_{mod(2\pi)}. \tag{5.51}$$

GMSK has been evaluated under the same channel conditions used with TFM (AWGN and Rician faded channel; the K_r, $B_F T$ and fading model are identical to those used for TFM). For the premodulation filter we have used

$B_tT = 0.25$. The results are similar to those of TFM and they are presented in Figs. 5.11 (AWGN) and 5.12 (Rician fading). In Fig. 5.11 we also present the SER curve of the coherent receiver, taken from [191]. The gains achieved over the 2-bit differential detector (2-bit DD) [230] have been summarized in Table 5.4. Under pure AWGN conditions, the (1+2+3)-bit MDD, (1+2)-bit MDD and (1)-bit MDD outperform the conventional 2-bit DD [230] **7.4 dB, 6.2 dB and 5.5 dB** respectively. Comparing their performance to the performance of the coherent detector [191], we realize that they are only 0.5 dB, 1.2 dB and 2 dB inferior.

Table 5.4: Improvements offered by the truncated multiple differential receivers (as compared to the 2-bit differential detector) for a GMSK signal ($B_tT = 0.25$) in an AWGN channel. The reported gains correspond to a SER=10^{-4}.

GAINS (dB)		
(1)-bit MDD	(1+2)-bit MDD	(1+2+3)-bit MDD
7.4	6.2	5.5

For the Rician fading channel, the (1+2+3)-bit MDD and (1+2)-bit MDD suffer degradations of 2.8 dB and 4.3 dB respectively, compared to the pure Gaussian noise channel. The (1)-bit MDD loses 5.1 dB of its performance, while the 2-bit DD is tailing off, suffering from high error floors. The results have shown again that **the multiple differential detectors are capable of reducing the error floors of the non-coherent narrowband CPM signals. For this particular case of GMSK the error floors are reduced by more than three orders of magnitude.** A comparison between the curves presented for TFM and GMSK makes us realize that all comments made for the TFM apply to the GMSK as well.

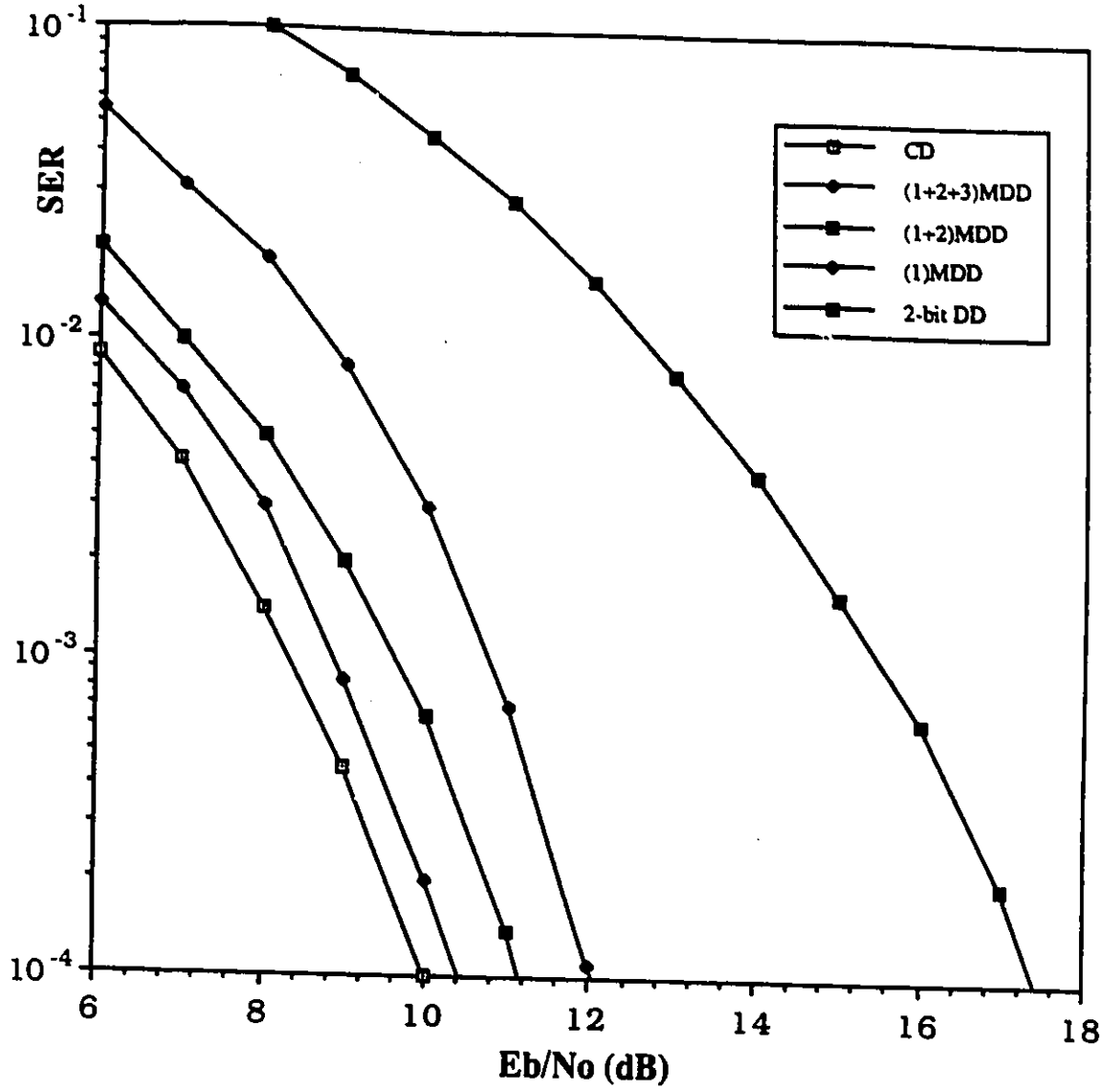

Figure 5.9: SER performance curves of multiple differential receivers used with GMSK ($B_tT = 0.25$) in an AWGN channel. The curve of the 2-bit differential detector is displayed as well.

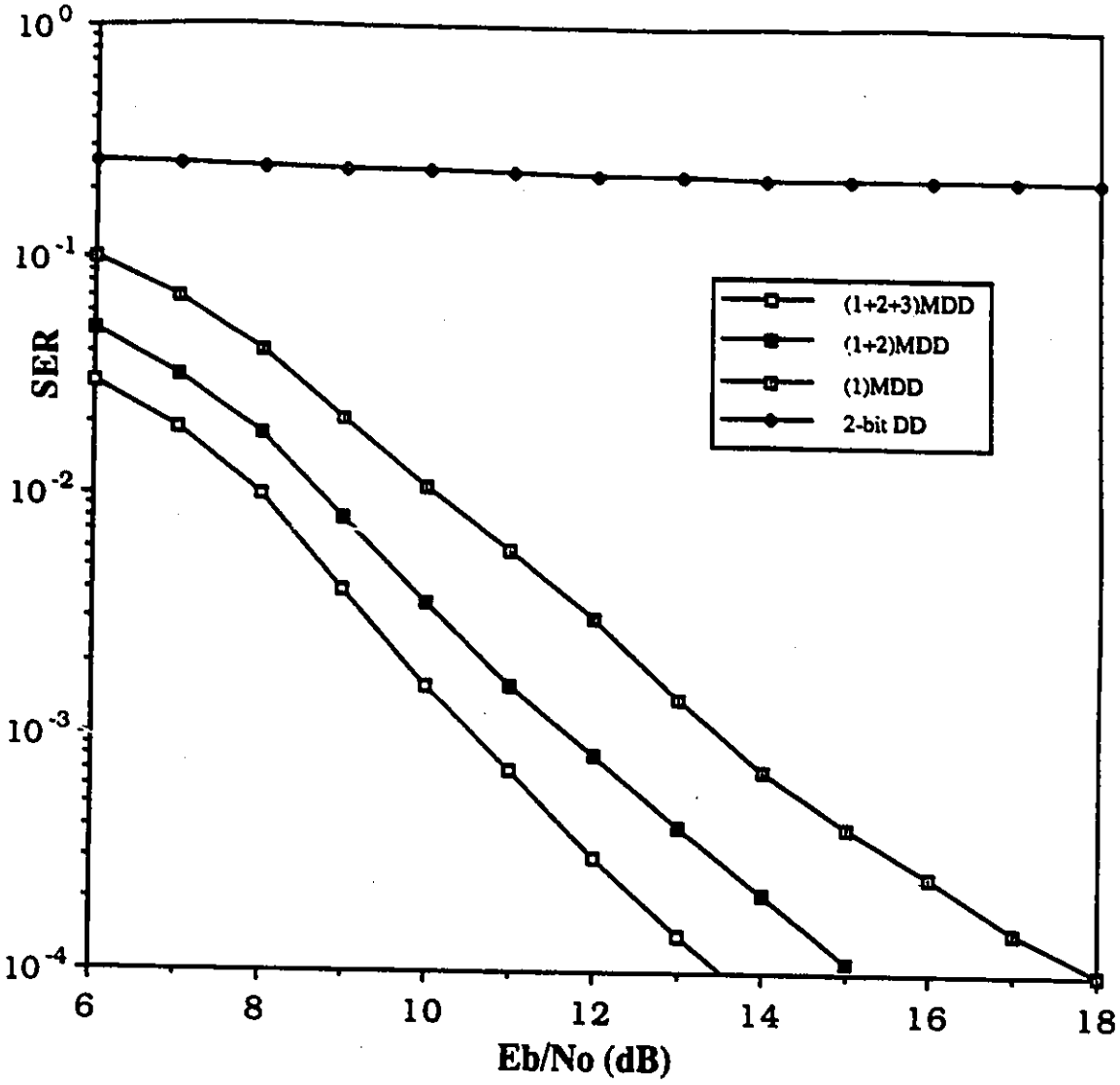

Figure 5.10: SER performance curves of truncated multiple differential receivers used, with GMSK in a Rician faded channel ($K_r = 10dB$, $B_FT = 0.2$). The curve of the 2-bit differential detector is displayed as well.

5.7 ASYMPTOTICALLY OPTIMAL SYMBOL-BY-SYMBOL CPM RECEIVERS

5.7.1 Asymptotically Optimal Structures of Non-Coherent Symbol-by-Symbol CPM Receivers in Time Dispersive Channels

Using Eq.(3.95) and following the same methodology and approximations with those described in sections 4.2, we come up with expressions describing asymptotically optimal symbol-by-symbol receivers for CPM signals. These expressions are:

5.7.2 Low E_b/N_0

$$\widehat{c_m} = S_l^{CPM} \Longrightarrow \overset{1\le l\le M_p}{max} \{ \sum_{\bar{C}(\bar{A})\in \underline{\mathcal{C}}_{\underline{S}^{CPM}}^{S_l^{CPM}}(m)} - [MST_{CPM}(\bar{C}(\bar{A}), h_{c,B}(t), t)$$

$$+IST_{CPM}(\bar{C}(\bar{A}), h_{c,B}(t), t)]$$

$$+\frac{[(MST_{CPM}(\bar{C}(\bar{A}), h_{c,B}(t), t) + IST_{CPM}(\bar{C}(\bar{A}), h_{c,B}(t), t))]^2}{2N_o}$$

$$+\frac{|\sum_{k=0}^{Z-1} F_k(x_r(t), \bar{\varphi}_{k-L+1}^k(\bar{C}(\bar{A})))e^{-j\beta_1(\bar{\varphi}_0^{k-1}(\bar{C}(\bar{A})))}|^2}{4N_o}\} \qquad (5.52)$$

where S_l^{CPM} represents the l^{th} -from a total of M_p- possible values a symbol c_m can take. Also, $\underline{\mathcal{C}}_{\underline{S}^{CPM}}^{S_l^{CPM}}(m)$ is the set, containing as elements all the possible sequences $\bar{C}(\bar{A})$ having $c_m = S_l^{CPM}$.

For ideal channels, Eq.(5.52) is reduced to:

$$\widehat{c_m} = \bar{S}_l^{CPM} \Longrightarrow \max_{1\le l\le M_p} \{ \sum_{\bar{C}(\bar{A})\in \underline{\underline{C}}_{S^{CPM}}^{S_l^{CPM}}(m)} -[MST_{CPM}(\bar{C}(\bar{A}), \dot{h}_{c,B}(t), t)]$$

$$+\frac{[MST_{CPM}(\bar{C}(\bar{A}), h_{c,B}(t), t)]^2}{2N_o}.$$

$$+\frac{|\sum_{k=0}^{Z-1} F_k(x_r(t), \bar{\varphi}_{k-L+1}^k(\bar{C}(\bar{A})))e^{-j\beta_1(\bar{\varphi}_0^{k-1}(\bar{C}(\bar{A})))}|^2}{4N_o}\}. \qquad (5.53)$$

When single amplitude signals are used, the metric becomes:

$$\widehat{c_m} = S_l^{CPM} \Longrightarrow \max_{1\le l\le M_p} \{ \sum_{\bar{C}(\bar{A})\in \underline{\underline{C}}_{\underline{S}}^{S_l}(m)}$$

$$\frac{|\sum_{k=0}^{Z-1} F_k(x_r(t), \bar{\varphi}_{k-L+1}^k(\bar{C}(\bar{A})))e^{-j\beta_1(\bar{\varphi}_0^{k-1}(\bar{C}(\bar{A})))}|^2}{4N_o}\}.$$

(5.54)

In section 4.10.4, we had mentioned that for PSK signals in ideal channels and for low E_b/N_o, the asymptotically optimal symbol-by-symbol detector is the conventional one bit differential detector. This is not the case for CPM signals.

5.7.3 High E_b/N_o

For high E_b/N_o, the decision law of the optimal decoder becomes:

$$\widehat{c_m} = S_l^{CPM} \Longrightarrow \max_{1\le l\le M_p} \{ \max_{\bar{C}(\bar{A}^\nu)\in \underline{\underline{C}}_{S^{CPM}}^{S_l^{CPM}}(m)} \{-[ISM_{CPM}(\bar{C}(\bar{A}), h_{c,B}(t), t)$$

$$+IST_{CPM}(\bar{C}(\bar{A}),h_{c,B}(t),t)]+|\sum_{k=0}^{Z-1}F_k(x_r(t),\bar{\varphi}_{k-L+1}^{k}(\bar{C}(\bar{A})))e^{-j\beta_1(\bar{\varphi}_0^{k-1}(\bar{C}(\bar{A})))}|\}\}$$

(5.55)

For ideal channels, the metric is reduced to

$$\widehat{c_m}=S_l^{CPM}\implies\overset{1\le l\le M_p}{\bar{m}\bar{a}x}\{\overset{\bar{C}(\bar{A}^\nu)\in\underline{\underline{C}}_{S^{CPM}}^{S_l^{CPM}}(m)}{\bar{m}\bar{a}x}\{-[ISM_{CPM}(\bar{C}(\bar{A}),h_{c,B}(t),t)]$$

$$+|\sum_{k=0}^{Z-1}F_k(x_r(t),\bar{\varphi}_{k-L+1}^{k}(\bar{C}(\bar{A})))e^{-j\beta_1(\bar{\varphi}_0^{k-1}(\bar{C}(\bar{A})))}|\}\}$$

(5.56)

Finally, for single amplitude signals the decision law becomes:

$$\widehat{c_m}=S_l^{CPM}\implies\overset{1\le l\le M_p}{\bar{m}\bar{a}x}\{\overset{\bar{C}(\bar{A}^\nu)\in\underline{\underline{C}}_{S^{CPM}}^{S_l^{CPM}}(m)}{\bar{m}\bar{a}x}$$

$$\{|\sum_{k=0}^{Z-1}F_k(x_r(t),\bar{\varphi}_{k-L+1}^{k}(\bar{C}(\bar{A})))e^{-j\beta_1(\bar{\varphi}_0^{k-1}(\bar{C}(\bar{A})))}|\}\} \tag{5.57}$$

5.8 ASYMPTOTICALLY OPTIMAL SYMBOL-BY-SYMBOL CPM RECEIVERS BASED ON AMP DECOMPOSITION

When the AMP signal decomposition is used, the decision laws are:

5.8.1 Low E_b/N_0

$$\widehat{c_m} = S_l^{CPM} \Longrightarrow \max_{1\le l\le M_p} \{ \sum_{\bar{C}(\bar{A})\in \underline{\underline{C}}_{\underline{\underline{S}}^{CPM}}^{S_l^{CPM}}(m)} \{-[\sum_{k=0}^{Z-1}(\mathcal{A}_k)^2$$

$$\sum_{n_1=0}^{\mathcal{N}}\sum_{n_2=0}^{\mathcal{N}} \alpha_{n_1,k}^{AMP}(\alpha_{n_2,k}^{AMP})^* \Re_{E,[n_1,n_2]}^{AMP}(0) + \sum_{l=1}^{Z-1}\sum_{k=l}^{Z-1} \mathcal{A}_k\mathcal{A}_{k-l} \sum_{n_1=0}^{\mathcal{N}}\sum_{n_2=0}^{\mathcal{N}}$$

$$[\alpha_{n_1,k}^{AMP}(\alpha_{n_2,k-l}^{AMP})^* \Re_{E,[n_1,n_2]}^{AMP}(l) + \alpha_{n_2,k-l}^{AMP}(\alpha_{n_1,k}^{AMP})^* (\Re_{E,[n_1,n_2]}^{AMP}(l))^*]]\}\}$$

$$+\frac{1}{2N_o}\{-[\sum_{l=1}^{Z-1}(\mathcal{A}_k)^2 \sum_{n_1=0}^{\mathcal{N}}\sum_{n_2=0}^{\mathcal{N}} \alpha_{n_1,k}^{AMP}(\alpha_{n_2,k}^{AMP})^* \Re_{E,[n_1,n_2]}^{AMP}(0)$$

$$+\sum_{l=1}^{Z-1}\sum_{k=l}^{Z-1} \mathcal{A}_k\mathcal{A}_{k-l} \sum_{n_1=0}^{\mathcal{N}}\sum_{n_2=0}^{\mathcal{N}} [\alpha_{n_1,k}^{AMP}(\alpha_{n_2,k-l}^{AMP})^*$$

$$\Re_{E,[n_1,n_2]}^{AMP}(l) + \alpha_{n_2,k-l}^{AMP}(\alpha_{n_1,k}^{AMP})^* (\Re_{E,[n_1,n_2]}^{AMP}(l))^*]]\}^2$$

$$+\frac{|\sum_{k=0}^{Z-1}\mathcal{A}_k \sum_{n=0}^{\mathcal{N}} \mathcal{Y}_{n,k}^{AMP}(\alpha_{n,k}^{AMP})^*|^2}{4N_o}\}. \qquad (5.58)$$

When only one AMP pulse is adequate to approximate the CPM signal, the decision law is:

$$\widehat{c_m} = S_l^{CPM} \Longrightarrow \max_{1\le l\le M_p} \{ \sum_{\tilde{C}(\tilde{A})\in\underline{\underline{C}}_{\underline{\underline{S}}}^{S_l}(k)} [\sum_{k=0}^{Z-1} (\mathcal{A}_k)^2 \Re_{E,[0,0]}^{AMP}(0)$$

$$+ \sum_{l=1}^{Z-1}\sum_{k=i}^{Z-1} \mathcal{A}_k\mathcal{A}_{k-l}[\alpha_{0,k}^{AMP}(\alpha_{0,k-l}^{AMP})^*\Re_{E,[0,0]}^{AMP}(l) + \alpha_{0,k-l}^{AMP}(\alpha_{0,k}^{AMP})^*(\Re_{E,[0,0]}^{AMP}(l))^*]]$$

$$+\frac{1}{2N_o}[\sum_{k=0}^{Z-1}(\mathcal{A}_k)^2\Re_{E,[0,0]}^{AMP}(0)$$
$$+ \sum_{l=1}^{Z-1}\sum_{k=l}^{Z-1} \mathcal{A}_k\mathcal{A}_{k-l}[\alpha_{0,k}^{AMP}(\alpha_{0,k-l}^{AMP})^*\Re_{E,[0,0]}^{AMP}(l) + \alpha_{0,k-l}^{AMP}(\alpha_{0,k}^{AMP})^*$$

$$(\Re_{E,[0,0]}^{AMP}(l))^*]]^2 + \frac{|\sum_{k=0}^{Z-1}\mathcal{A}_k\mathcal{Y}_{0,k}^{AMP}(\alpha_{0,k}^{AMP})^*|}{4N_o}\}. \qquad (5.59)$$

5.8.1.1 High E_b/N_o

For high E_b/N_o, the decision law based on the AMP decomposition is:

$$\widehat{c_m} = S_l^{CPM} \Longrightarrow \max_{1\le l\le M_p} \{ \max_{\tilde{C}(\tilde{A}^\nu)\in\underline{\underline{C}}_{\underline{\underline{S}}}^{S_l^{CPM}}(m)}$$

$$-\{[[\sum_{k=0}^{Z-1}(\mathcal{A}_k)^2 \sum_{n_1=0}^{\mathcal{N}}\sum_{n_2=0}^{\mathcal{N}} \alpha_{n_1,k}^{AMP}(\alpha_{n_2,k}^{AMP})^*\Re_{E,[n_1,n_2]}^{AMP}(0)] + [\sum_{l=1}^{Z-1}\sum_{k=l}^{Z-1}\mathcal{A}_k\mathcal{A}_{k-l}$$

$$\sum_{n_1=0}^{\mathcal{N}}\sum_{n_2=0}^{\mathcal{N}}[\alpha_{n_1,k}^{AMP}(\alpha_{n_2,k-l}^{AMP})^*\Re_{E,[n_1,n_2]}^{AMP}(l) + \alpha_{n_2,k-l}^{AMP}(\alpha_{n_1,k}^{AMP})^*(\Re_{E,[n_1,n_2]}^{AMP}(l))^*]]$$

$$+|\sum_{k=0}^{Z-1}\mathcal{A}_k\mathcal{Y}_{0,k}^{AMP}(\alpha_{0,k}^{AMP})^*|\}\} \tag{5.60}$$

and for $\mathcal{N}=0$

$$\widehat{c_m}=S_l^{CPM} \implies \overset{1\le l\le M_p}{max}\{\overset{\tilde{C}(\tilde{A}^\nu)\in\underline{\underline{C}}_{\underline{\underline{S}}^{CPM}(m)}^{S_l^{CPM}}}{max}\{|\sum_{k=0}^{Z-1}\mathcal{A}_k\mathcal{Y}_{0,k}^{AMP}(\alpha_{0,k}^{AMP})^*|$$

$$-[\sum_{k=0}^{Z-1}(\mathcal{A}_k)^2\Re_{E,[0,0]}^{AMP}(0)]$$

$$+2\sum_{l=1}^{Z-1}\sum_{k=l}^{Z-1}\mathcal{A}_k\mathcal{A}_{k-l}[Re\{\alpha_{0,k}^{AMP}(\alpha_{0,k-l}^{AMP})^*\Re_{E,[0,0]}^{AMP}(l)\}]]\} \tag{5.61}$$

For single amplitude signals ($\mathcal{A}_k=1$):

$$\widehat{c_m}=S_l^{CPM} \implies \overset{1\le l\le M_p}{max}\{\overset{\tilde{C}(\tilde{A}^\nu)\in\underline{\underline{C}}_{\underline{\underline{S}}^{CPM}(m)}^{S_l^{CPM}}}{max}\{|\sum_{k=0}^{Z-1}\mathcal{Y}_{0,k}^{AMP}(\alpha_{0,k}^{AMP})^*|$$

$$-[\sum_{k=0}^{Z-1}\Re_{E,[0,0]}^{AMP}(k)$$

$$+2\sum_{l=1}^{Z-1}\sum_{k=l}^{Z-1}[Re\{\alpha_{0,k}^{AMP}(\alpha_{0,k-l}^{AMP})^*\Re_{E,[0,0]}^{AMP}(l)\}]]\}\ . \tag{5.62}$$

Finally, if $\Re_{E,[0,0]}^{AMP}(k)=0\ \ \forall\ \ k\neq 0$ (this is the case for ideal channel), the metric is furthermore reduced to the maximization of

$$\widehat{c_m}=S_l^{CPM} \implies \overset{1\le l\le M_p}{max}\{\overset{\tilde{C}(\tilde{A}^\nu)\in\underline{\underline{C}}_{\underline{\underline{S}}^{CPM}(m)}^{S_l^{CPM}}}{max}\{|\sum_{k=0}^{Z-1}\mathcal{Y}_{0,k}^{AMP}(\alpha_{0,k}^{AMP})^*|\}. \tag{5.63}$$

Similarly with the sequence estimators examined in sections 5.2 to 5.5, the AMP decomposition has helped to reduce the complexity of the non-coherent CPM receiver in terms of filtering. However, as it was discussed at the beginning of section 5.6, the filters indicated by the AMP decomposition are quite complex especially for CPM systems of high spectral efficiency. The difficulty in implementation becomes even higher if the filter has to be implemented as an IF filter, in order to be used in an IF implementation of the multiple differential detection receiver.

In section 5.6 which dealt with sequence estimation we resolved this problem by replacing the complex IF filter with commercially available ones. The evaluations indicated that relatively simple receivers were able to provide considerable gains as compared to the classical differential detector. In the present and following sections we shall use the same approach with symbol-by-symbol receivers. To further simplify the structure of the symbol-by-symbol receiver, we shall also add one additional characteristic to the proposed and evaluated structures -the use of decision feedback. We remind the reader that we have already applied decision feedback in multiple differential receivers for PSK signals in Chapter 4.

5.9 DESIGN OF REDUCED COMPLEXITY SYMBOL-BY-SYMBOL RECEIVERS FOR CPM SIGNALS BASED ON DECISION FEEDBACK AND SIGNAL COMBINING

To start the analysis, we shall use again the conceptual block diagram of the receiver presented in Fig. 5.2. The received signal $x_r(t)$ is first demodulated and afterwards passed through a post detection filter $H_R^{CPM}(\omega)$. Its output $y^{CPM}(t)$ is sampled at kT.

Let us assume that we want to decide the symbol c_ξ. The information available to make the decision is:

1. The set of signal samples $\bar{y}^{CPM}_{[\xi+i_F,\xi-i_P]} = [y^{CPM}_{\xi+i_F}, \ldots, y^{CPM}_{\xi}, \ldots, y^{CPM}_{\xi-i_P}]$.
2. The decisions regarding the following symbols: $\{c_{\xi-1}, \ldots c_{\xi-i_P-\mathcal{L}_c}\}$,

where i_P, i_F are positive integers. The optimal law to decide c_ξ based on the information described above is shown in the following expression:

$$\hat{c}_\xi = S_l^{CPM} \Longrightarrow \overset{1\le l\le M_p}{max} \{ \sum_{\bar{p}_{\xi+1}^{\xi+i_F+\mathcal{L}_c}(\bar{C}(\bar{A}))\in \underline{\mathcal{DC}}^{CPM}_{[\xi+i_F+\mathcal{L}_c,\xi+1]}} f(y^{CPM}_{[\xi+i_F,\xi-i_P]}/\bar{C}(\bar{A}) = [\bar{\varphi}_{\xi+1}^{\xi+i_F+\mathcal{L}_c}(\bar{C}(\bar{A})), \bar{S}_l^{CPM}, \hat{\bar{\varphi}}_{\xi-i_P-\mathcal{L}_c}^{\xi 1})]\} \qquad (5.64)$$

where $\underline{\mathcal{DC}}^{CPM}_{[\xi+i_F+\mathcal{L}_c,\xi+1]}$ is the set containing as elements the sequences formed by all possible combinations of $[c_{\xi+i_F+\mathcal{L}_c}, \ldots, c_{\xi+1}]$.

Considering single amplitude CPM signals and applying further processing, the decision law described by Eq.(5.64) is reduced to

$$\hat{c}_\xi = S_l^{CPM} \Longrightarrow \overset{1\le l\le M_p}{max} \{ \sum_{\bar{p}_{\xi+1}^{\xi+i_F+\mathcal{L}_c}(\bar{C}(\bar{A}))\in \underline{\mathcal{DC}}^{CPM}_{[\xi+i_F+\mathcal{L}_c,\xi+1]}}$$

$$I_0(\frac{|\sum_{k=\xi-i_P}^{\xi+i_F} y_k^{CPM} c^{j\Delta_{k-i_P}\beta_1(\bar{\varphi}_{i_P-\mathcal{L}_e}^{k-1}(\bar{C}(\bar{A})))}|}{N_o})\}. \tag{5.65}$$

5.9.1 Low E_b/N_o

Applying the approximations described by Eqs.(4.1), (4.2) (in Chapter 4) the expression of Eq.(5.65) is reduced to

$$\hat{c}_\xi = S_l^{CPM} \Longrightarrow \overset{1\le l\le M_P}{max} \{ \sum_{\bar{\varphi}_{\xi+1}^{\xi+i_F+\mathcal{L}_e}(\bar{C}(\bar{A}))\in \underline{\mathcal{DC}}_{[\xi+i_F+\mathcal{L}_e,\xi+1]}^{CPM}}$$

$$|\sum_{k=\xi-i_P}^{\xi+i_F} y_k^{CPM} e^{j\Delta_{k-i_P}\beta_1(\bar{\varphi}_{i_P-\mathcal{L}_e}^{k-1}(\bar{C}(\bar{A})))}|^2\}. \tag{5.66}$$

The asymptotically optimal symbol-by-symbol receiver consists of the summation of squared envelope terms. Carrying out the squaring process and eliminating common terms, we come up with the following expression as the decision law:

$$\hat{c}_\xi = S_l^{CPM} \Longrightarrow \overset{1\le l\le M_P}{max} \{ \sum_{\bar{\varphi}_{\xi+1}^{\xi+i_F+\mathcal{L}_e}(\bar{C}(\bar{A}))\in \underline{\mathcal{DC}}_{[\xi+i_F+\mathcal{L}_e,\xi+1]}^{CPM}}$$

$$\sum_{k=\xi+1}^{\xi+i_F} \sum_{l=1}^{k+i_P+1} Re\{y_k^{CPM}(y_{k-l}^{CPM})^* e^{j\Delta_l\beta_1(k,\bar{\varphi}_{k-l-\mathcal{L}_e}^{k-1}(\bar{C}(\bar{A})))}\}\} \tag{5.67}$$

Using Eq.(3.80), we find that $\Delta_l\beta_1(k,\bar{\varphi}_{k-l-\mathcal{L}_e}^{k-1}(\bar{C}(\bar{A})))$ can be expressed as follows:

$$\begin{aligned}\Delta_l\beta_1(k,\bar{\varphi}_{k-l-\mathcal{L}_e}^{k-1}(\bar{C}(\bar{A}))) &= \Delta_l^F\beta_1(k,\bar{\varphi}_{\xi+1}^{k-1}(\bar{C}(\bar{A}))) + \Delta_l^D\beta_1(k,[c_\xi]) \\ &\quad +\Delta_l^P\beta_1(k,\bar{\varphi}_{\xi-i_P-\mathcal{L}_e}^{\xi-1}(\bar{C}(\bar{A})))\end{aligned} \tag{5.68}$$

where

$$\Delta_l^F \beta_1(k, \bar{\varphi}_{\xi+1}^{k-1}(\bar{C}(\bar{A}))) = \begin{cases} \sum_{\nu=1}^{l} c_{k-\nu}\vartheta_0^\nu + & \\ \sum_{\nu=l+1}^{\mathcal{L}_e+l-1} c_{k-\nu}\vartheta_{\nu-l}^\nu & \text{for } l < k-\xi-\mathcal{L}_e+1 \\ \sum_{\nu=1}^{l} c_{k-\nu}\vartheta_0^\nu + & \\ \sum_{\nu=l+1}^{\mathcal{L}_e+l-2} c_{k-\nu}\vartheta_{\nu-l}^\nu & \text{for } l = k-\xi-\mathcal{L}_e+1 \\ \sum_{\nu=1}^{l} c_{k-\nu}\vartheta_0^\nu + & \\ \sum_{\nu=l+1}^{\xi+1} c_{k-\nu}\vartheta_{\nu-l}^\nu & \text{for } l < k-\xi \le l+\mathcal{L}_e-1 \\ \sum_{\nu=1}^{l} c_{k-\nu}\vartheta_0^\nu & \text{for } l = k-\xi \\ \sum_{\nu=1}^{l-\xi-1} c_{k-\nu}\vartheta_0^\nu & \text{for } l > k-\xi, \end{cases} \tag{5.69}$$

$$\Delta_l^D \beta_1(k, [c_\xi]) = \begin{cases} 0 & \text{for } l < k-\xi-\mathcal{L}_e+1 \\ c_\xi \vartheta_{\mathcal{L}_e-1}^{\mathcal{L}_e} & \text{for } l = k-\xi-\mathcal{L}_e+1 \\ c_{k-\nu}\vartheta_0^\nu + & \\ c_\xi \vartheta_{k-\xi-l}^{k-\xi} & \text{for } l < k-\xi \le l+\mathcal{L}_e-1 \\ c_\xi \vartheta_0^{k-\xi} & \text{for } l =\geq k-\xi\ , \end{cases} \tag{5.70}$$

$$\Delta_l^P \beta_1(k, \widehat{\bar{\varphi}}_{\xi-l-\mathcal{L}_e}^{\xi-1}(\bar{C}(\bar{A}))) = \begin{cases} 0 & \text{for } l < k-\xi-\mathcal{L}_e+1 \\ 0 & \text{for } l = k-\xi-\mathcal{L}_e+1 \\ \sum_{\nu=\xi+2}^{k+\mathcal{L}_1-1} \hat{c}_{k-\nu}\vartheta_{\nu-l}^{\nu} & \text{for } l < k-\xi \leq l+\mathcal{L}_e-1 \\ \sum_{\nu=k-\xi}^{k-l-\xi-1} \hat{c}_{k-\nu}\vartheta_{\nu-k+\xi}^{\nu} & \text{for } l = k-\xi \\ \sum_{\nu=k-\xi+1}^{l} c_{k-\nu}\vartheta_0^{\nu} + & \\ \sum_{\nu=l+1}^{\mathcal{L}_e+l-1} \hat{c}_{k-\nu}\vartheta_{\nu-l}^{\nu} & \text{for } l > k-\xi, \end{cases}$$

(5.71)

(for the definition of $\vartheta_{l_1}^{l_2}$ see Eq.(3.70) in Chapter 3). Use of Eq.(5.68) in Eq.(5.67), gives:

$$\widehat{c_\xi} = S_i^{CPM} \implies \overset{1\leq i\leq M_P}{max} \{ \sum_{k=1}^{i_F} \sum_{l=1}^{k+i_P+1}$$

$$Re\{d_l(\xi+k)e^{-j\Delta_l^P\beta_1(\xi+k,\widehat{\bar{\varphi}}_{\xi-l-\mathcal{L}_e}^{\xi-1}(\bar{C}(\bar{A})))}\}\hbar_l^R(k,\xi,c_\xi = S_i^{CPM}, \bar{\varphi}_{\xi+1}^{\xi+k-1}(\bar{C}(\bar{A})))$$

$$Im\{d_l^{CPM}(\xi+k)e^{-j\Delta_l^P\beta_1(\xi+k,\widehat{\bar{\varphi}}_{\xi-l-\mathcal{L}_e}^{\xi-1}(\bar{C}(\bar{A})))}\}\hbar_l^I(k,\xi,c_\xi = S_i^{CPM}, \bar{\varphi}_{\xi+1}^{\xi+k-1}(\bar{C}(\bar{A})))$$

(5.72)

where

$$\hbar_l^R(k,\xi,c_\xi,\ \bar{\varphi}_{\xi+1}^{\xi+k-1}(\bar{C}(\bar{A}))) =$$

$$\sum_{\bar{\varphi}_{\xi+1}^{\xi+i_F+\mathcal{L}_e}(\bar{C}(\bar{A}))\in\underline{DC}_{\{\xi+i_F+\mathcal{L}_e,\xi+1\}}^{CPM}} \cos(\Delta_l^F\beta_1(\xi+k,\bar{\varphi}_{\xi+1}^{\xi+k+1}(\bar{C}(\bar{A}))) + \Delta_l^D\beta_1(\xi+k,[c_\xi]))$$

(5.73)

$$\hbar_l^I(k,\xi,c_\xi,\bar{\varphi}_{\xi+1}^{\xi+k-1}(\bar{C}(\bar{A}))) =$$

$$\sum_{\bar{\varphi}_{\xi+1}^{\xi+i_F+\mathcal{L}_e}(\bar{C}(\bar{A}))\in\underline{\mathcal{DC}}_{[\xi+i_F+\mathcal{L}_e,\xi+1]}^{CPM}} \sin(\Delta_l^F\beta_1(\xi+k,\bar{\varphi}_{\xi+1}^{\xi+k+1}(\bar{C}(\bar{A}))) + \Delta_l^D\beta_1(\xi+k,[c_\xi]))$$

(5.74)

Without any loss of generality let us assume that the values S_i^{CPM} $(1 \leq i \leq M_p)$ which a symbol c_m can take, have the following order:

$$S_{i-1}^{CPM} < S_i^{CPM} < S_{i+1}^{CPM} \quad \text{with} \quad 1 < i < M_p\,. \tag{5.75}$$

If the following identity holds

$$2\pi m_h \int_0^{\mathcal{L}_e T} h_T(t)dt \quad \times \quad min\{|S_1^{CPM}|,\ldots,|S_{M_p}^{CPM}|\} = 2\pi\mathcal{I} \tag{5.76}$$

where $\mathcal{I}$ is an integer number, it can be shown that Eq.(5.72) can be reduced to

$$\hat{c}_\xi = S_i^{CPM} \implies \max_{1\leq i\leq M_p}\{\sum_{k=1}^{\min\{i_F,\mathcal{L}_e\}}\sum_{l=1}^{k+i_P+1}$$

$$Re\{d_l(\xi+k)e^{j\Delta_l^P\beta_1(\xi+k,\widehat{\bar{\varphi}}_{\xi-1}^{\xi-l-\mathcal{L}_e}(\bar{C}(\bar{A})))}\}\hbar_l^R(k,\xi,c_\xi=S_i^{CPM},\bar{\varphi}_{\xi+1}^{\xi+k-1}(\bar{C}(\bar{A})))$$

$$Im\{d_l^{CPM}(\xi+k)e^{j\Delta_l^P\beta_1(\xi+k,\widehat{\bar{\varphi}}_{\xi-1}^{\xi-l-\mathcal{L}_e}(\bar{C}(\bar{A})))}\}\hbar_l^I(k,\xi,c_\xi=S_i^{CPM},\bar{\varphi}_{\xi+1}^{\xi+k-1}(\bar{C}(\bar{A}))).$$

(5.77)

In this case,

$$\hbar_l^R(k,\xi,c_\xi,\bar{\varphi}_{\xi+1}^{\xi+k-1}(\bar{C}(\bar{A}))) =$$

$$\sum_{\bar{\rho}_{\xi+1}^{\xi+i_F+\mathcal{L}_e}(\bar{C}(\bar{A}))\in \underline{\mathcal{DC}}^{CPM}_{[\xi+\min\{i_F+\mathcal{L}_e,2\mathcal{L}_e\},\xi+1]}}$$

$$\cos(\Delta_l^F\beta_1(\xi+k,\bar{\varphi}_{\xi+1}^{\xi+k+1}(\bar{C}(\bar{A}))) \div \Delta_l^D\beta_1(\xi+k,[c_\xi]))$$

(5.78)

$$h_l^I(k,\xi,c_\xi,\bar{\varphi}_{\xi+1}^{\xi+k-1}(\bar{C}(\bar{A}))) =$$

$$\sum_{\bar{\rho}_{\xi+1}^{\xi+i_F+\mathcal{L}_e}(\bar{C}(\bar{A}))\in \underline{\mathcal{DC}}^{CPM}_{[\xi+\min\{i_F+\mathcal{L}_e,2\mathcal{L}_e\},\xi+1]}}$$

$$\sin(\Delta_l^F\beta_1(\xi+k,\bar{\varphi}_{\xi+1}^{\xi+k+1}(\bar{C}(\bar{A}))) + \Delta_l^D\beta_1(\xi+k,[c_\xi])).$$

(5.79)

We remind the reader that m_h is the modulation index used. Also,

$$d_l(m) = \{y_m^{CPM}(y_{m-l}^{CPM})^*\} \tag{5.80}$$

is the output of the l-symbol differential detector (i.e. the detector using a delay element lT). The phase of its output is shifted by minus $(\Delta_l^P\beta_1(\xi+k,\hat{\bar{\varphi}}_{\xi-l-\mathcal{L}_e}^{\xi-1}(\bar{C}(\bar{A}))))$. $(\Delta_l^P\beta_1(\xi+k,\hat{\bar{\varphi}}_{\xi-l-\mathcal{L}_e}^{\xi-1}(\bar{C}(\bar{A}))))$ is the contribution of the decided symbols on the phase of the differential signal. Thus the shifting removes all the contributions of the past symbols from the differential signal phase (assuming that the decisions are correct) and with it their effect on the performance. These symbols (transmitted prior to the c_ξ) are appearing as ISI introduced in the signal phase. In spectrally efficient CPM schemes, these ISI terms become quite strong, resulting in eye closure. This is the reason why a large number of spectrally efficient CPM signals perform very poorly, when differentially detected (see curves in Figs. 5.5, 5.11, also [33], [34], [230], [160], [162]). The elimination of these symbols from the signal phase through the phase subtraction acts as an ISI cancellation mechanism,

and results in eye opening which improves the performance. We have named this phase correction technique **Data Aided Phase Correction (DAPC).**

Defining as

$$d_{[l]cor}(k,\xi) = d_l(k,\xi)e^{-j\Delta_l^P \beta_1(k,\widehat{\bar{\rho}}_{k-l-\mathcal{L}_e-1}^{\xi-1}(\bar{C}(\bar{A})))}, \tag{5.81}$$

$$d^I_{[l]cor}(k,\xi) = Re\{d_l(k)e^{-j\Delta_l^P \beta_1(k,\widehat{\bar{\rho}}_{k-l-\mathcal{L}_e-1}^{\xi-1}(\bar{C}(\bar{A})))}\}, \tag{5.82}$$

$$d^Q_{[l]cor}(k,\xi) = Im\{d_l(k)e^{-j\Delta_l^P \beta_1(k,\widehat{\bar{\rho}}_{k-l-\mathcal{L}_e-1}^{\xi-1}(\bar{C}(\bar{A})))}\}, \tag{5.83}$$

and using them with Eq.(5.72), the decision law becomes:

$$\begin{aligned}
\widehat{c}_\xi = S_i^{CPM} \implies & \overset{1\le i\le M_p}{max}\{\sum_{k=1}^{i_F}\sum_{l=1}^{k+i_P+1} \\
& d^I_{[l]cor}(\xi+k,\xi)\hbar_l^R(k,\xi,c_\xi = S_i^{CPM},\bar{\varphi}_{\xi+1}^{\xi+k-1}(\bar{C}(\bar{A}))) \\
& d^I_{[Q]cor}(\xi+k,\xi)\hbar_l^I(k,\xi,c_\xi = S_i^{CPM},\bar{\varphi}_{\xi+1}^{\xi+k-1}(\bar{C}(\bar{A}))).
\end{aligned} \tag{5.84}$$

The maximum number of differential detectors used by the receiver described in Eq.(5.85) is equal to $\lambda = i_F + i_P + 1$. If Eq.(5.76) holds, the decision law is deduced from Eq. (5.77). The expression for this case is:

$$\begin{aligned}
\widehat{c}_\xi = S_i^{CPM} \implies & \overset{1\le i\le M_p}{max}\{\sum_{k=1}^{\min\{i_F,\mathcal{L}_e\}}\sum_{l=1}^{k+i_P+1} \\
& d^I_{[l]cor}(\xi+k,\xi)\hbar_l^R(k,\xi,c_\xi = S_i^{CPM},\bar{\varphi}_{\xi+1}^{\xi+k-1}(\bar{C}(\bar{A})))
\end{aligned}$$

$$d^{Q}_{[l]cor}(\xi+k,xi)\hbar^{I}_{l}(k,\xi,c_{\xi}=S^{CPM}_{i},\ \bar{\varphi}^{\xi+k-1}_{\xi+1}(\bar{C}(\bar{A}))).$$

(5.85)

The maximum number of differential detectors required now is $\lambda = min\{i_F, \mathcal{L}_e\}+ i_P + 1$.

In Fig. 5.11, we present the conceptual implementation of such a differential detector (IF implementation of the differential detectors has been used).

When c_k are binary symbols, ($c_k = \pm 1$), and Eq.(5.76) holds, further simplifications in the expression of the decision law (see Eq.(5.85)) are possible. Performing them, we end up with the following expression:

$$\hat{c}_{\xi} = sgn\{ \sum_{k=1}^{\min\{i_F,\mathcal{L}_e\}} \sum_{l=1}^{k+i_P+1} + d^{Q}_{[l]cor}(\xi+k,\xi)$$

$$[\hbar^{I}_{l}(k,\xi,1,\bar{\varphi}^{\xi+k-1}_{\xi+1}(\bar{C}(\bar{A}))) - [\hbar^{I}_{l}(k,\xi,-1,\bar{\varphi}^{\xi+k-1}_{\xi+1}(\bar{C}(\bar{A})))] \ .$$

(5.86)

In this case, only the quadrature channels of the multiple differential detectors are needed in the decision process. We also see that the decision is based on the polarity of a function.

The expressions presented in this subsection are general in order to include and be able to describe any CPM signal. Later on, these generalized forms will be applied to specific CPM signals and the reader will have the chance to see the simplicity of receivers produced by the above analysis.

5.9.2 High E_b/N_o

For high E_b/N_o, the asymptotically optimal decision law is given by the following expression:

$$\hat{c}_{\xi} = S^{CPM}_{i} \implies \overset{1\le i\le M_p}{max} \{ \overset{\bar{\varphi}^{\xi+i_F+\mathcal{L}_e}_{\xi+1}(\bar{C}(\bar{A}))\in \underline{\mathcal{DC}}^{CPM}_{[\xi+i_F+\mathcal{L}_e,\xi+1]}}{max} \{$$

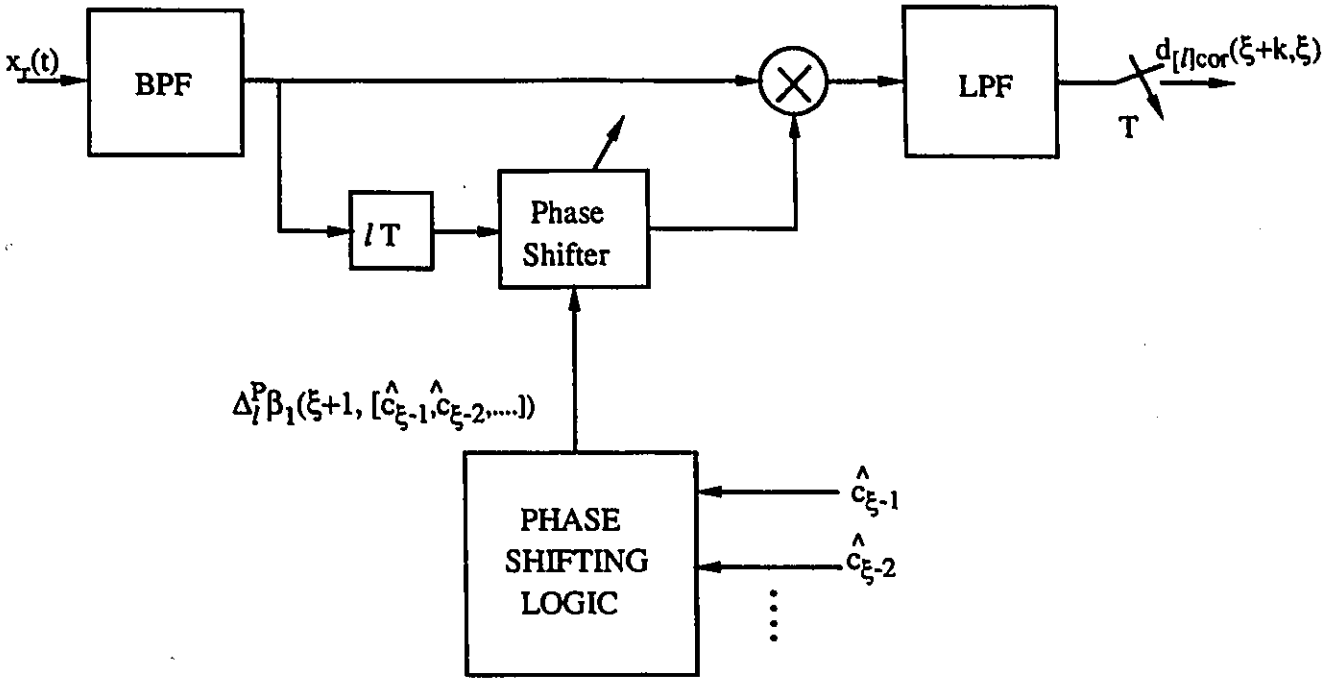

Figure 5.11: Block diagram of the l-symbol differential detector using Data Aided Phase Correction (DAPC).

$$\left| \sum_{k=\xi-i_P}^{\xi+i_F} y_k^{CPM} e^{-j\Delta_{k-i_P}\beta_1(\bar{\varphi}_{i_P-\mathcal{L}_e}^{k-1}(\bar{C}(\bar{A}))=[\bar{\varphi}_{\xi+1}^{\xi+i_F+\mathcal{L}_e}(\bar{C}(\bar{A})),S_i^{CPM},\widehat{\bar{\varphi}}_{\xi+i_P-\mathcal{L}_e}^{\xi-1}])} \right| \} \}.$$

(5.87)

Using the fact that maximization of $\{|\cdot|\}$ is equivalent to the maximization of $\{|\cdot|^2\}$ and applying elimination of terms independent from the transmitted information, the decision is reduced to:

$$\widehat{c}_\xi = S_i^{CPM} \implies \underset{1\le i\le M_p}{max} \left\{ \underset{\bar{\varphi}_{\xi+1}^{\xi+i_F+\mathcal{L}_e}(\bar{C}(\bar{A}))\in \mathcal{DC}_{[\xi+i_F+\mathcal{L}_e,\xi+1]}^{CPM}}{max} \sum_{k=1}^{i_F} \sum_{l=1}^{k+i_P+1} \right.$$

$$Re\{d_l(\xi+k,\xi)e^{-j\Delta_l^P\beta_1(\xi+k,\widehat{\bar{\varphi}}_{\xi-l-\mathcal{L}_e}^{\xi-1}(\bar{C}(\bar{A})))}\}$$

$$\cos(\Delta_l^F\beta_1(\xi+k,\bar{\varphi}_{\xi+k-1}^{\xi+1}(\bar{C}(\bar{A}))) + \Delta_l^D\beta_1(\xi+k,[S_i]))$$

$$+Im\{d_l^{CPM}(\xi+k,\xi)e^{-j\Delta_l^P\beta_1(\xi+k,\widehat{\bar{\varphi}}_{\xi-l-\mathcal{L}_e}^{\xi-1}(\bar{C}(\bar{A})))}\}$$

$$\left. \sin(\Delta_l^F\beta_1(\xi+k,\bar{\varphi}_{\xi+k-1}^{\xi+1}(\bar{C}(\bar{A}))) + \Delta_l^D\beta_1(\xi+k,[S_i])) \right\}.$$

(5.88)

Using the definitions of Eq.(5.83) with Eq.(5.88) the decision law becomes:

$$\widehat{c}_\xi = S_i^{CPM} \implies \underset{1\le i\le M_p}{max} \left\{ \underset{\bar{\varphi}_{\xi+1}^{\xi+i_F+\mathcal{L}_e}(\bar{C}(\bar{A}))\in \mathcal{DC}_{[\xi+i_F+\mathcal{L}_e,\xi+1]}^{CPM}}{max} \sum_{k=1}^{i_F} \sum_{l=1}^{k+i_P+1} \right.$$

$$d_{[l]cor}^I(\xi+k,\xi)\cos(\Delta_l^F\beta_1(\xi+k,\bar{\varphi}_{\xi+1}^{\xi+k-1}(\bar{C}(\bar{A}))) + \Delta_l^D\beta_1(\xi+k,[S_i]))$$

$$\left. +d_{[l]cor}^Q(\xi+k,\xi)\sin(\Delta_l^F\beta_1(\xi+k,\bar{\varphi}_{\xi+1}^{\xi+k-1}(\bar{C}(\bar{A}))) + \Delta_l^D\beta_1(\xi L,[S_i])) \right\}.$$

(5.89)

With the condition of Eq.(5.76), Eq.(5.89) is reduced to:

$$\widehat{c}_\xi = \bar{S}_i^{CPM} \implies \max_{1\le i\le M_p} \Big\{ \max_{\bar{\varphi}_{\xi+1}^{\xi+i_F+\mathcal{L}_e}(\bar{C}(\bar{A}))\in \underline{\mathcal{DC}}^{CPM}_{[\xi+\min\{i_F+\mathcal{L}_e,2\mathcal{L}_e\},\xi+1]}} \sum_{k=1}^{\min\{i_F+\mathcal{L}_e,2\mathcal{L}_e\}} \sum_{l=1}^{k+i_p+1}$$

$$d^I_{[l]cor}(\xi+k,\xi)\cos(\Delta_l^F\beta_1(\xi+k,\bar{\varphi}_{\xi+1}^{\xi+k-1}(\bar{C}(\bar{A}))) + \Delta_l^D\beta_1(\xi+k,[S_i]))$$

$$+d^Q_{[l]cor}(\xi+k,\xi)\sin(\Delta_l^F\beta_1(\xi+1,\bar{\varphi}_{\xi+1}^{\xi+k-1}(\bar{C}(\bar{A}))) + \Delta_l^D\beta_1(\xi+1,[S_i]))\ .$$

(5.90)

Further simplification in the decision law described by Eq.(5.90) is not possible. In the decision, both the inphase and quadrature channels are needed. Also, the receiver, even for binary symbols ($c_m = \pm 1$) has to calculate 2^{i_F+1} different parameters and compare them with each other. On the contrary, the receiver derived for the low E_b/N_o case has some very positive futures. It uses only the quadrature channel of the differential detectors. At the end, the quadrature outputs are combined appropriately and the final decision is made according to the polarity of a single function. Obviously, these receivers require less complexity to implement both their IF and baseband processing functions. The simplicity of these receivers led us to decide to study them more carefully. Our results showed that even though they have been optimized for low E_b/N_0 values, they still are capable of offering considerable gains as compared to the conventional differential detectors. This will be shown in the sections which follow.

Since these receivers use both DAPC and CWF, they will be represented in short form as DAPC/CWF.

5.10 APPLYING DAPC AND SIGNAL COMBINING TECHNIQUES WITH SOME POPULAR CPM SIGNALS

5.10.1 Minimum Shift Keying

The premodulation filter $h_T(t)$ for an MSK signal has been described in Eq.(5.26). Also, the expression of $\Delta_l\beta_1(k, \bar{\varphi}^k_{k-l}(\bar{C}(\bar{A})))$ has been provided in Eq.(5.40). ($c_k = \pm 1$). Applying Eq.(5.34) in the decision law of Eq.(5.86) we come up with the following expression as decision law:

$$\begin{aligned}
\hat{c}_\xi &= sgn\{d^Q_{[1]cor}(\xi+1,\xi) - d^Q_{[2]cor}(\xi+1,\xi)e^{-j\frac{\pi}{2}(\hat{c}_{\xi-1})} \\
&\quad + d^Q_{[3]cor}(\xi+1,\xi)e^{-j\frac{\pi}{2}(\hat{c}_{\xi-1}+\hat{c}_{\xi-2})} + \ldots\} \\
&= sgn\{d^Q_{[1]cor}(\xi+1,\xi) + \sum_{l=2}^{\lambda} d^Q_{[l]cor}(\xi+1,\xi)e^{-j\frac{\pi}{2}(\sum_{i=1}^{l-1}\hat{c}_{\xi-i})}\} \\
&= sgn\{d^Q_{[1]cor}(\xi+1,\xi) + [\Pi_{i=1}^{\lambda-1}(-\hat{c}_{k-i})]\sum_{l=2}^{\lambda} d^{CPM}_{[l]\mathcal{D}}(\xi+1,\xi)\} \quad (5.91)
\end{aligned}$$

λ is the number of differential detectors used. In Eq.(5.91) $\mathcal{D}$ defines Inphase (I) or Quadrature (Q) channel and

$$\mathcal{D} = \begin{cases} Q & \text{when } l \text{ is odd} \\ I & \text{when } l \text{ is even.} \end{cases} \quad (5.92)$$

(In Eq.(5.91), the $\sin(\theta - \frac{\pi}{2}) = \cos(\theta)$ has been used). When the differential detector uses a delay element which is an odd multiple of the time duration, the quadrature (Q) channel is used; when the delay is an even multiple of the symbol period, the inphase (I) channel is used. One notices that for the MSK case, phase correction is not needed. This happens because the impulse response of the premodulation filter $h_T(t)$ is zero outside the symbol period (see Eq.(5.40)) and consequently, the MSK signal phase does not suffer from ISI. Only the signal combining controlled by decision feedback is used (CWF). In Fig. 5.12 we provide the block diagram of the receiver which uses the 1 and 2-bit differential detectors.

We have evaluated the proposed multiple differential receiver using signal combining with feedback for $\lambda = 2$ (MDD(CWF)). Similarly to the sequence estimators examined in subsection 5.6.2.1, the evaluation has been carried out for two different scenarios concerning the characteristics of the transmitted signal. In the first case, the transmitted signal is unfiltered, whereas in the second case post modulation filtering is applied. The post modulation filter is a 4^{th} order Butterworth with $B_tT = 1.0$. The filter used at the receiver is also a Butterworth filter with $B_tT = 1.1$. The results for the unfiltered case are displayed in Fig. 5.13. For the filtered one, they are displayed in Fig. 5.14. In every figure we include the curves of the 1-bit differential detector (DD), the non-redundant error correction scheme (NEC) and the multiple differential sequence estimator examined in subsection 5.6.2.1 (MDD(Seq.Est.)). The last two also use the outputs of the 1 and 2-bit differential detectors in their detection process. The results demonstrate the superiority of the MDD(CWF) receiver as compared to the DD. In both cases, it achieves superior performance (for the non-filtered case, it has a difference of 1.2 dB at SER=10^{-4}; when the signal is filtered, the improvement becomes 1.4 dB at SER=10^{-3} and 2.6 dB at SER=10^{-4}). When compared to the NEC, it has a very marginal improvement for the non-filtered case; however, it provides a gain of 0.56 dB when filtering is applied on the transmitted signal. This demonstrates the robustness of the multiple differential detection in distorted channels. Compared to the MDD(Seq.Est.), it has inferior performance (at SER=10^{-4}, it lacks 0.5 dB when the signal is unfiltered and 0.9 dB when filtering is applied). This was expected since the sequence estimator is more powerful but at the same time more complex. In Tables 5.5 (post detection filtering is not applied), 5.6 (post detection filtering is applied) we have summarized the improvements offered by the three more advanced schemes (NEC, MDD(CWF), MDD(Seq.Est.)) as compared to DD.

Table 5.5: Improvements offered by the NEC, MDD(CWF) and MDD(Seq.Est.) (all of them use the 1 and 2-bit differential detectors) as compared to the conventional (1-bit) differential detector. The transmitted MSK signal is unfiltered. The reported gains correspond to a SER=10^{-4}.

GAINS (dB)		
NEC	MDD(CWF)	MDD(Seq.Est.)
1.1	1.2	1.7

Table 5.6: Improvements offered by the NEC, MDD(CWF) and MDD(Seq.Est.) (all of them use the 1 and 2-bit differential detectors) as compared to the conventional (1-bit) differential detector. Post modulation filtering has been used on the transmitted MSK signal. As post modulation filter, a 4^{th} order Butterworth with $B_tT = 1.0$ has been used.

		GAINS (dB)		
		NEC	MDD(CWF)	MDD(Seq.Est.)
SER	10^{-3}	1.6	2	2.7
	10^{-4}	1.7	2.4	3.1

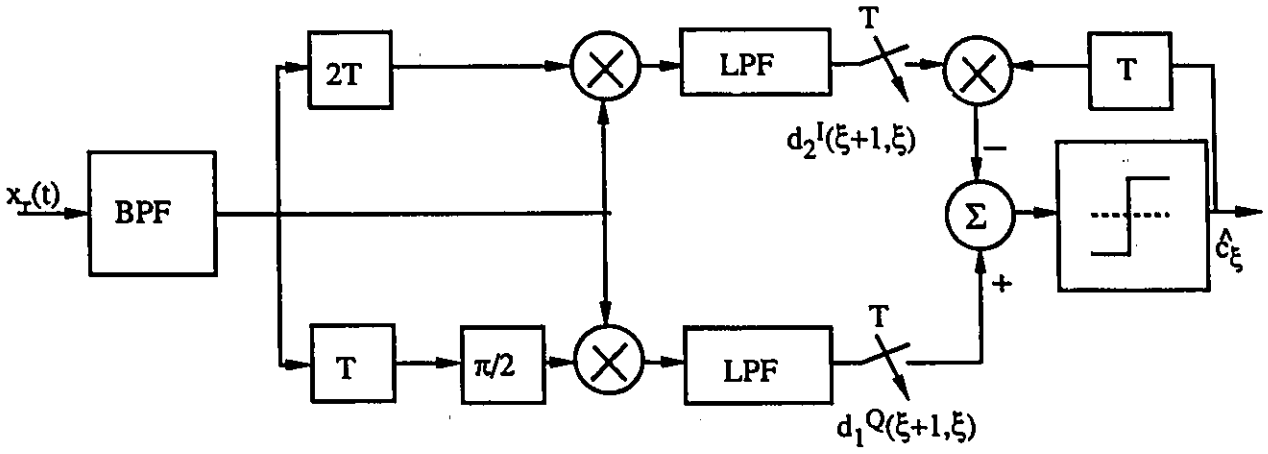

Figure 5.12: Block diagram of the multiple differential detection receiver of MSK, using decision directed signal combining (CWF). The one and 2-bit differential detectors are used.

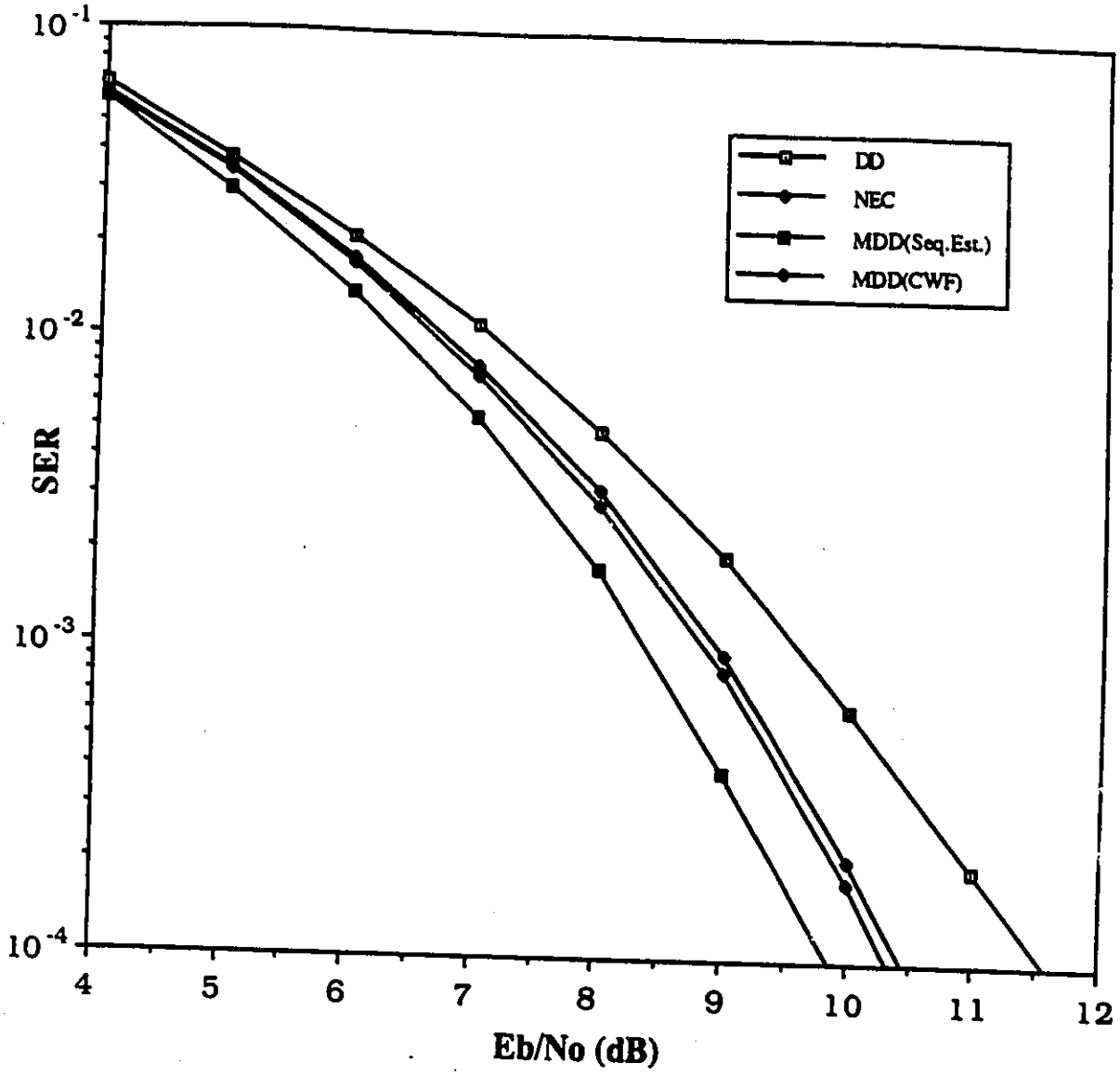

Figure 5.13: SER performance curves of MSK with various non-coherent receivers (DD, NEC, MDD(CWF), MDD(Seq.Est.)). The transmitted signal is unfiltered. At the receiver, a 4^{th} order Butterworth with $B_rT = 1.1$ is used.

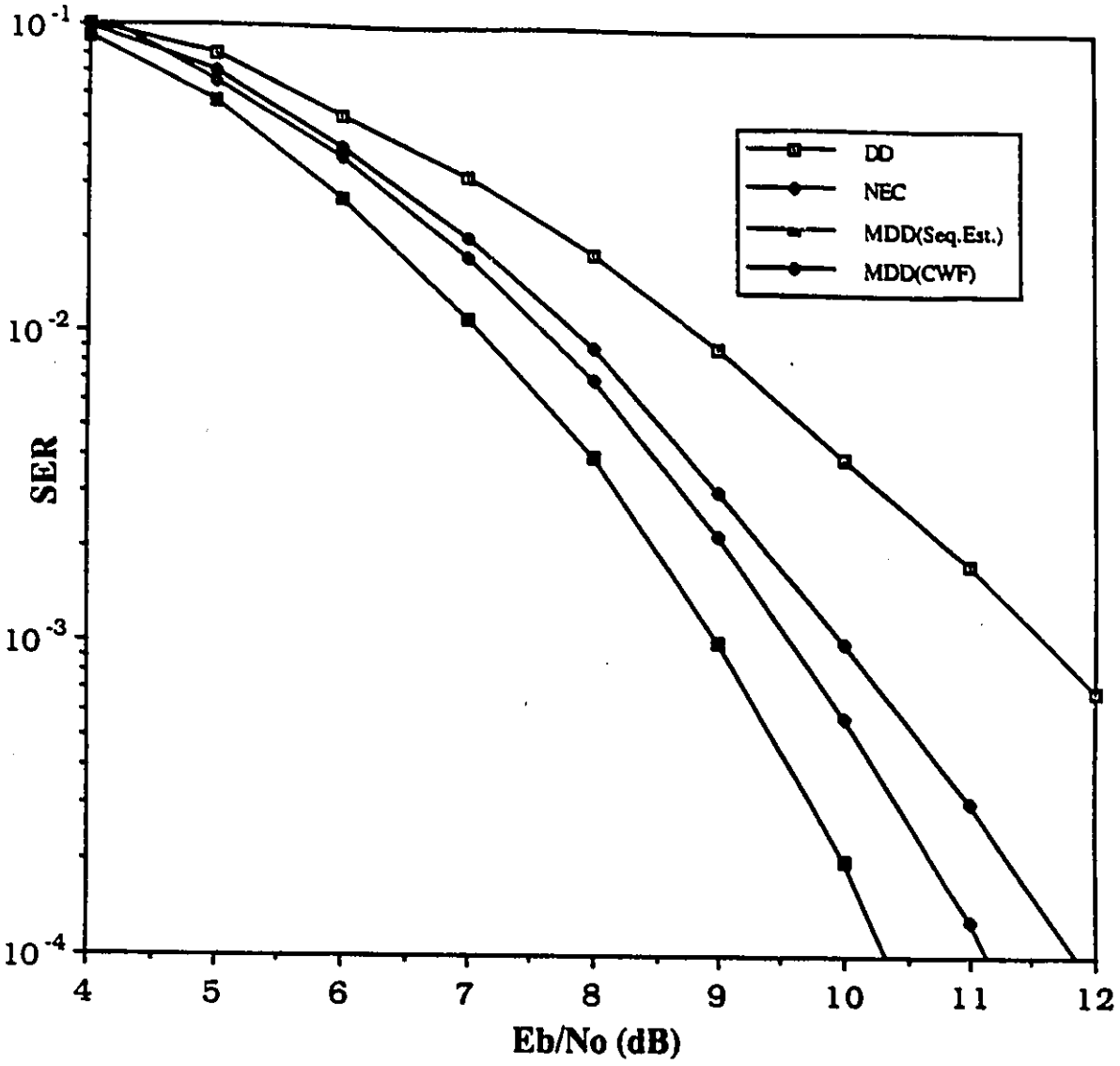

Figure 5.14: SER performance curves of MSK with various non-coherent receivers (DD, NEC, MDD(CWF), MDD(Seq.Est.)). The transmitted signal has been filtered with a 4^{th} order Butterworth, having $BT = 1.0$. At the receiver, a 4^{th} order Butterworth with $B_rT = 1.1$ is used.

5.10.2 Tamed Frequency Modulation

The premodulation filter $h_T(t)$ corresponding to TFM has been described in Eq.(5.34). For the TFM, $\mathcal{L}_c = 3$. The values of $\theta^{\nu}_{\nu-1}$ are the following:

$$\vartheta^{\nu}_{\nu-1} = \begin{cases} \frac{\pi}{8} & \text{for } \nu = 1 \\ \frac{\pi}{4} & \text{for } \nu = 2 \\ \frac{\pi}{8} & \text{for } \nu = 3. \\ 0 & \text{for } \nu \neq 1,2,3. \end{cases} \tag{5.93}$$

$\vartheta^{\eta}_{\mu} = (\sum_{i=\mu+1}^{\eta} \vartheta^{i-1}_{i})$ $(\mu, \eta \text{integers}, \mu < \eta)$.

We have developed and evaluated the following configurations of DAPC/CWF receivers: i) $i_F = 2$, $i_P = -1$ $(\lambda = 1)$, ii) $i_F = 2$, $i_P = 0$ $(\lambda = 2)$ and $i_F = 2$, $i_P = 1$ $(\lambda = 3)$. (the design is based on Eq.(5.86)). For the TFM

$$\Delta^P_1 \beta_1(\xi + 2, [\hat{c}_{\xi-1}]) = (\hat{c}_{\xi-1}\frac{\pi}{8})$$

$$\Delta^P_2 \beta_1(\xi + 2, [\hat{c}_{\xi-1}, \hat{c}_{\xi-2}]) = (\hat{c}_{\xi-1}\frac{3\pi}{8} + \hat{c}_{\xi-2}\frac{\pi}{8})$$

$$\Delta^P_3 \beta_1(\xi + 2, [\hat{c}_{\xi-1}, \hat{c}_{\xi-2}, \hat{c}_{\xi-3}]) = (\hat{c}_{\xi-1}\frac{\pi}{2} + \hat{c}_{\xi-2}\frac{3\pi}{8} + \hat{c}_{\xi-3}\frac{\pi}{8}) \,. \tag{5.94}$$

Before proceeding to the presentation of the specific decision laws of these three receivers and the examination of the performance, it is useful to demonstrate how DAPC applies on the specific case.

In Figs. 5.15, 5.16 we display the phase-state diagram of the 1-bit differential detector of TFM before (Fig. 5.15) and after (Fig. 5.16) DAPC has been applied. In the figures we indicate what symbol combinations ($[c_{\xi+1}, c_{\xi}, c_{\xi-1}]$ for the conventional detector, $[c_{\xi+1}, c_{\xi}]$ and for the detector with DAPC) generate these states. With circles we indicate states where c_{ξ} appears with the value 1 $(c_{\xi} = 1)$ and with squares states where it appears with -1 $(c_{\xi} = -1)$.

From Fig. 5.15 we see that in the conventional differential detector, states generated by bit combinations where c_ξ appears with opposite polarity are overlapping (see the states lying right on the Inphase axes, generated by the bit combinations $[c_{\xi+1} = -1, c_\xi = 1, c_{\xi-1} = -1]$ and $[c_{\xi+1} = 1, c_\xi = -1, c_{\xi-1} = 1]$). This results in a completely closed eye at the sampling instant and makes the detection using the 1-bit differential detector impossible. On the contrary, when data aided phase correction is applied, there is no overlapping between phase states. Also, the smallest phase distances between states having c_ξ with opposite polarities is 45° degrees (see states generated by $[c_{\xi+1} = -1, c_\xi = 1]$ and $[c_{\xi+1} = 1, c_\xi = -1]$). Due to DAPC, the eye diagram of the 1-bit detector is now open and can be used for detection.

In Figs. 5.17, 5.18 we present the phase state diagrams of the 2-bit differential detector before and after DAPC has been applied. Again, with circles we mark states where c_ξ appears with the value 1 and with squares states where it appears with -1. When the conventional 2-bit differential detector is used, the information symbols have to be differentially encoded prior to their transmission [161]).

Fig. 5.17 shows (for the conventional 2-bit differential detector) that overlapping between states having c_ξ with different combinations does not occur. Now, the closest states having c_ξ with opposite polarity have a (phase) distance of 45°. This keeps the eye diagram at the sampling instant open and makes detection of the transmitted information possible. We also realize that the states for $c_\xi = 1$ and $c_\xi = -1$ are not symmetrically distributed around the quadrature axis. This generates an asymmetry in the eye diagram. In order to make possible detection and take full advantage of the eye opening, the decision threshold should be shifted to the right side of the quadrature axis (the value of shifting giving the best performance is actually a function of the operational E_b/N_o).

When DAPC is applied, the 2-bit differential detector has a full symmetry in respect to the inphase axis. This makes the eye diagram symmetric as well. The phase distance between the closest states having c_ξ with opposite polarity is now 90° degrees, which is quite an improvement as compared to the conventional 2-bit differential detector. When DAPC is not used, the width of the eye opening is only 0.707; when DAPC is used, the width of the eye opening becomes twice this value.

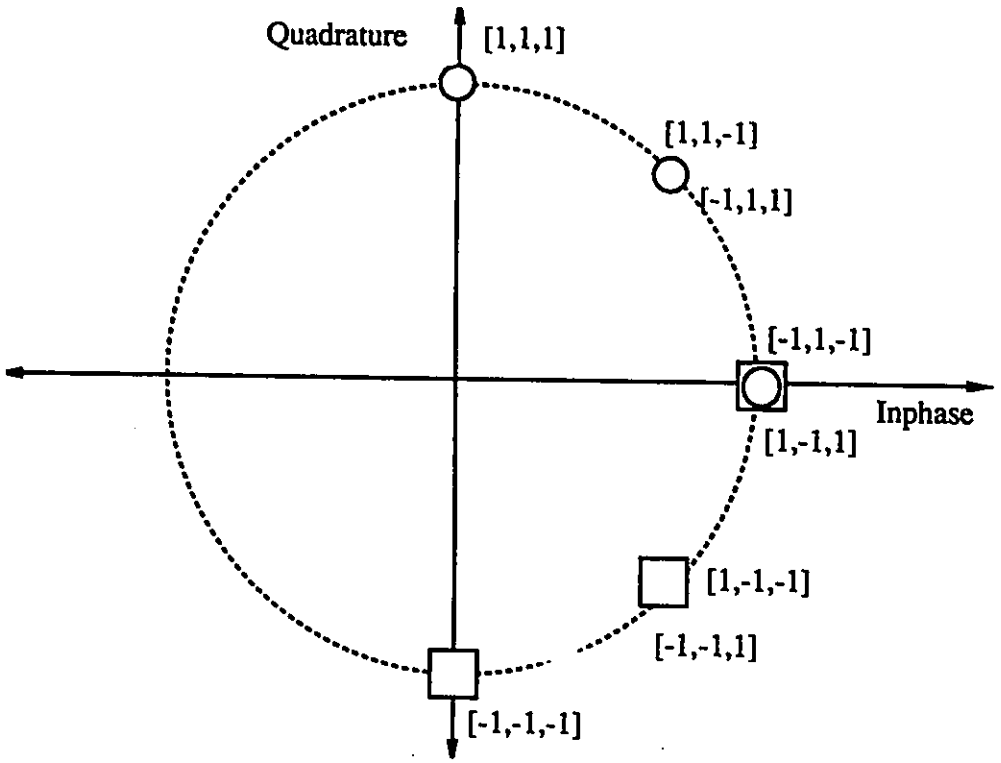

Figure 5.15: Phase state diagram of the conventional 1-bit differential detector for TFM. The values of the bit combinations $[c_{\xi+1}, c_\xi, c_{\xi-1}]$ generating every state are indicated in the figure. With a circle we mark states where c_ξ appears with the value 1 ($c_\xi = 1$) and with a square, states where c_ξ appears with -1 ($c_\xi = -1$).

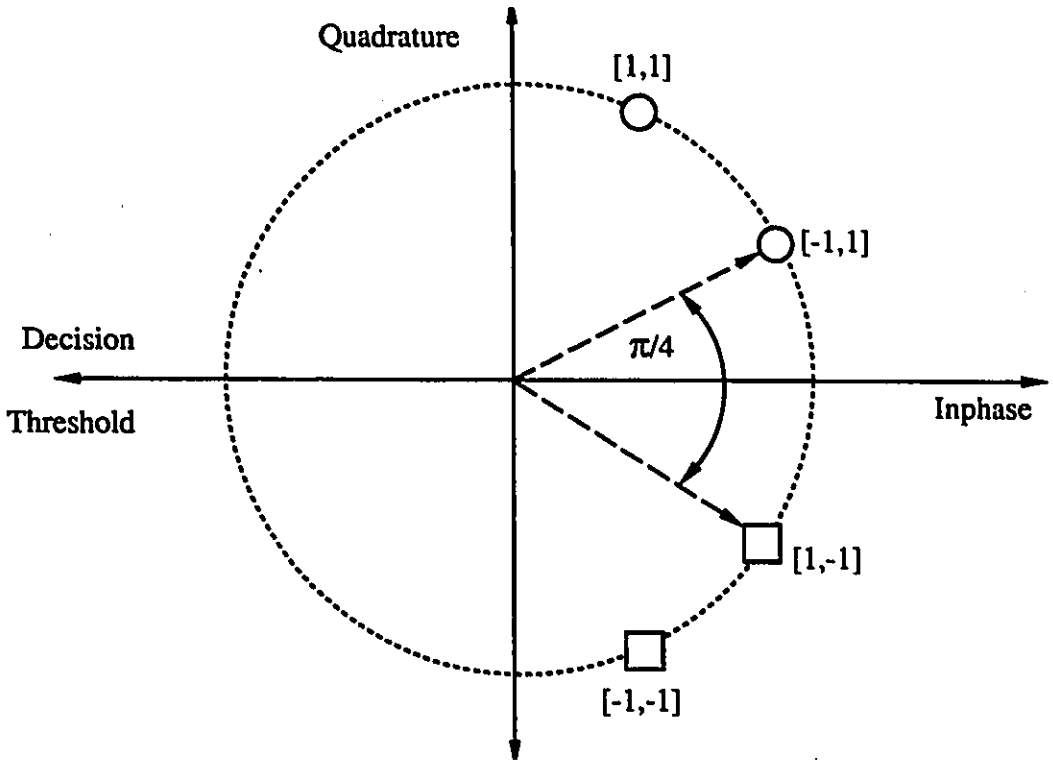

Figure 5.16: Phase state diagram of the 1-bit differential detector for TFM after the data aided phase correction (DAPC) has been applied. The values of the bit combinations $[c_{\xi+1}, c_\xi]$ generating every state are indicated in the figure. With a circle we mark states where c_ξ appears with the value 1 ($c_\xi = 1$) and with a square, states where c_ξ appears with -1 ($c_\xi = -1$).

The above discussion has shown how the DAPC is capable of opening the CPM signal at the sampling instant. It is only reasonable to expect that such a considerable increase in the eye opening could only result in performance improvements.

The decision laws corresponding to the three λ values are:

$\lambda = 1$

$$\hat{c}_k = sgn\{Im\{d_1(\xi+2)e^{-j(\hat{c}_{\xi-1}\frac{\pi}{8})}\}\} \tag{5.95}$$

$\lambda = 2$

$$\begin{aligned}\hat{c}_k &= sgn\{C_{TFM}Re\{d_1(\xi+2)e^{-j(\hat{c}_{\xi-1}\frac{\pi}{8})}\} \\ &\quad +Im\{d_2^{CPM}(\xi+2)e^{-j(\hat{c}_{\xi-2}\frac{\pi}{8}+\hat{c}_{\xi-1}\frac{3\pi}{8})}\hat{C}^{k-1}\}\}\end{aligned} \tag{5.96}$$

$\lambda = 3$

$$\begin{aligned}\hat{c}_k &= sgn\{C_{TFM}Im\{d_1^{CPM}(\xi+2)e^{-j(\hat{c}_{\xi-1}\frac{\pi}{8})}\} \\ &\quad +Im\{d_2^{CPM}(\xi+2)e^{-j(\hat{c}_{\xi-2}\frac{\pi}{8}+\hat{c}_{\xi-1}\frac{3\pi}{8})}\hat{C}^{k-1}\} \\ &\quad +Im\{d_3^{CPM}(\xi+2)e^{-j(\hat{c}_{\xi-3}\frac{\pi}{8}+\hat{c}_{\xi-2}\frac{3\pi}{8})+\hat{c}_{\xi-1}\frac{\pi}{2})}\}\}\,.\end{aligned} \tag{5.97}$$

C_{TFM} is a coefficient determining the strength which the one-bit differential detector should have in the decision process. The value of C_{TFM} as calculated from Eq.(5.86) is equal to:

$$\begin{aligned}C_{TFM} &= \frac{[\hbar_1^Q(\xi+2,\xi,1,\wp_{\xi+1}^{\xi+1}(\bar{C}(\bar{A}))=[c_{\xi+1}=+1])}{[\hbar_2^Q(\xi+2,\xi,1,\wp_{\xi+1}^{\xi+1}(\bar{C}(\bar{A}))=[c_{\xi+1}=+1])} \\ &= \frac{[\hbar_1^Q(\xi+2,\xi,1,\bar{\wp}_{\xi+1}^{\xi+1}(\bar{C}(\bar{A}))=[c_{\xi+1}=+1])}{[\hbar_3^I(\xi+2,\xi,1,\bar{\wp}_{\xi+1}^{\xi+1}(\bar{C}(\bar{A}))=[c_{\xi+1}=+1])} \\ &= \frac{(\sin(\frac{\pi}{8})+\sin(\frac{3\pi}{8})}{(\sin(\frac{\pi}{4})+\sin(\frac{\pi}{2})} = 0.7653\end{aligned} \tag{5.98}$$

(in the calculation of C_{TFM} Eqs.(5.78), (5.94) have been used). This value of C_{TFM} gives the best performance for low E_b/N_o values. With the increase in E_b/N_o, the value of C_{TFM} that gives the best performance changes gradually,

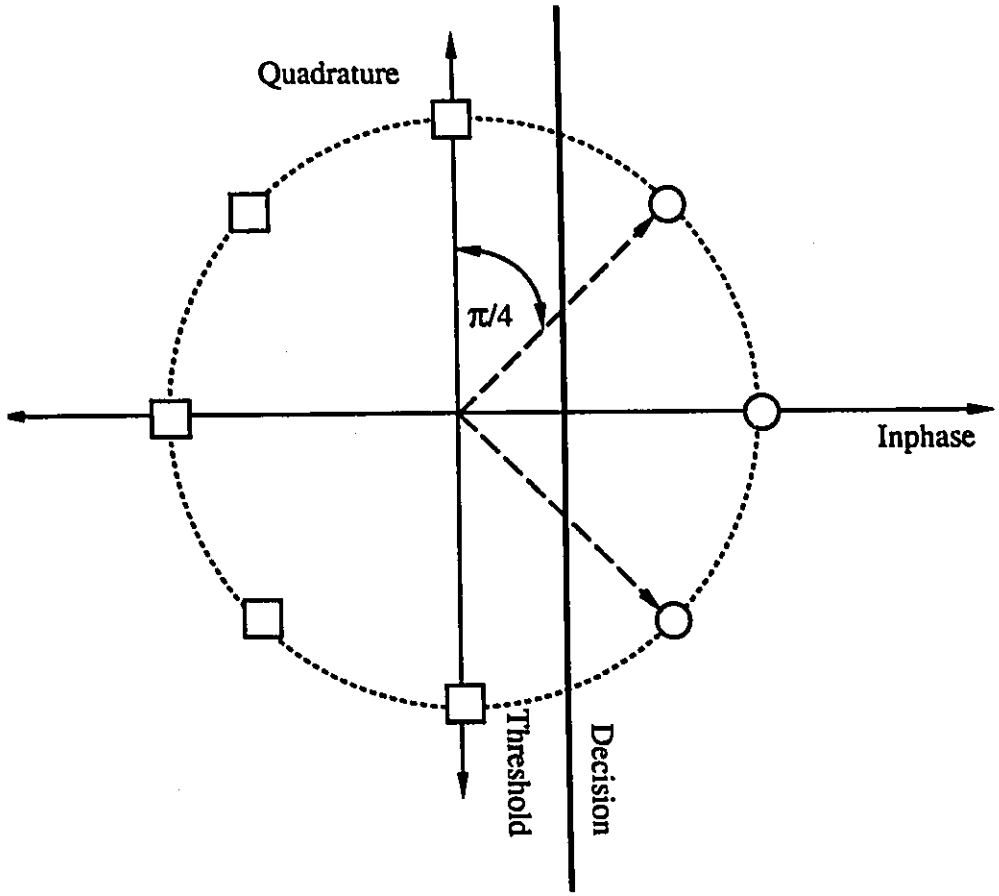

Figure 5.17: Phase state diagram of the conventional 2-bit differential detector for TFM. With a circle we mark states where c_ξ appears with the value 1 ($c_\xi = 1$) and with a square, states where it appears with -1 ($c_\xi = -1$).

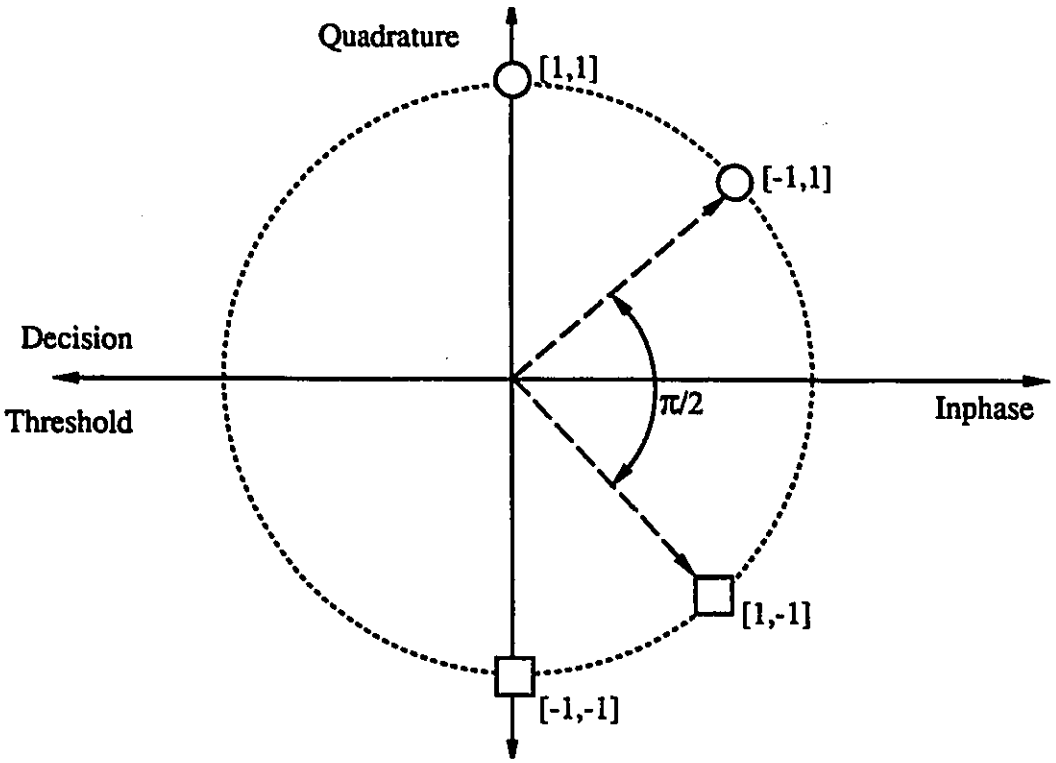

Figure 5.18: Phase state diagram of the 2-bit differential detector for TFM after the data aided phase correction (DAPC) has been applied. The values of the bit combinations $[c_{\xi+1}, c_\xi]$ generating every state are indicated in the figure. With a circle we mark states where c_ξ appears with the value 1 ($c_\xi = 1$) and with a square, states where c_ξ appears with -1 ($c_\xi = -1$).

approaching (for high E_b/N_o) the

$$\begin{aligned} C_{TFM} &= \frac{\sin(\Delta_1^F\beta_1(\xi+1,[c_{\xi+1}=-1])+\Delta_1^D\beta_1(\xi+1,[c_\xi=1])}{\sin(\Delta_2^F\beta_1(\xi+1,[c_{\xi+1}=-1])++\Delta_1^D\beta_1(\xi+1,[c_\xi=1])} \\ &= \frac{\sin(\Delta_1^F\beta_1(\xi+1,[c_{\xi+1}=-1])+\Delta_1^D\beta_1(\xi+1,[c_\xi=1])}{\sin(\Delta_3^F\beta_1(\xi+1,[c_{\xi+1}=-1])++\Delta_1^D\beta_1(\xi+1,[c_\xi=1])} \\ &= \frac{\sin(\frac{\pi}{8})}{\sin(\frac{\pi}{4})}=0.541 \end{aligned} \tag{5.99}$$

This value corresponds to the case where the decision law of Eq.(5.86) considers only the presence of two symbol combinations: the $[c_{\xi+1}=-1,c_\xi=1]$ and $[c_{\xi+1}=1,c_\xi=-1]$. These combinations give the closest sates having c_ξ with opposite polarity. (see Figs. 5.16, 5.18). For high E_b/N_o, these two combinations are the ones involved in most of the errors appearing (the receiver chooses one over the other). The best thing the receiver can do in order to minimize its error probability, is to optimize its decision so that the probability of errors occurring due to these two combinations becomes minimal. This is exactly what a value of $C_{TFM}=0.541$ does.

Using simple trigonometric identities, the decision laws described in Eqs.(5.96), (5.97) can be further simplified for the $\lambda=2$, $\lambda=3$ configurations. The new equivalent expressions are:

$\lambda=2$

$$\begin{aligned} \hat{c}_k &= sgn\{C_{TFM}Im\{d_1(\xi+2)e^{-j(\hat{c}_{\xi-1}\frac{\pi}{8})}\} \\ &\quad -\hat{c}_{\xi-1}Re\{d_2^{CPM}(\xi+2)e^{-j((\hat{c}_{\xi-2}-\hat{c}_{\xi-1})\frac{\pi}{8}}\}\} \end{aligned} \tag{5.100}$$

$\lambda=3$

$$\begin{aligned} \hat{c}_k &= sgn\{C_{TFM}Im\{d_1^{CPM}(\xi+1)e^{-j(\hat{c}_{\xi-1}\frac{\pi}{8})}\} \\ &\quad -\hat{c}_{\xi-1}Re\{d_2^{CPM}(\xi)e^{-j((\hat{c}_{\xi-2}-\hat{c}_{\xi-1})\frac{\pi}{8}}\} \\ &\quad +\hat{c}_{\xi-1}\hat{c}_{\xi-2}Re\{d_3^{CPM}(\xi+1)e^{-j((\hat{c}_{\xi-3}-\hat{c}_{\xi-2})\frac{\pi}{8}}\}\}\ . \end{aligned} \tag{5.101}$$

In Fig. 5.19 we present a block diagram of the $\lambda=2$ receiver. The $\chi_1(\hat{c}_{\xi-1})$, $\chi_2(\hat{c}_{\xi-1},\hat{c}_{\xi-2})$ appearing in the figure represent the following functions:

$$\chi_1(\hat{c}_{\xi-1})=(\hat{c}_{\xi-1}\frac{\pi}{8})+\frac{\pi}{2} \tag{5.102}$$

$$\chi_2(\hat{c}_{\xi-1}, \hat{c}_{\xi-2}) = (\hat{c}_{\xi-2} - \hat{c}_{\xi-1})\frac{\pi}{8} \tag{5.103}$$

For the 3-bit detector with DAPC, an equivalent (and simpler to implement) phase shifting strategy is the

$$\chi_3(\hat{c}_{\xi-2}, \hat{c}_{\xi-3}) = (\hat{c}_{\xi-3} - \hat{c}_{\xi-2})\frac{\pi}{8} \,. \tag{5.104}$$

In the above described receivers we see the presence of both the data aided phase correction (to reduce the ISI present in the phase of the signal) and the signal combining which again depends on the decisions made regarding the previous symbols.

In Fig. 5.20, we present the phase state diagram of the 2-bit differential detector when the DAPC uses the phase shifting as indicated by Eq.(5.96). The signal in this case is observed on the inphase channel. The phase state diagram is symmetric (in respect to both inphase and quadrature axis) and the minimum phase distance (between states with opposite polarities of c_ξ) remains 90° degrees. Also, the eye opening remains $2 \times 0.707 = 1.41$ (notice that in this case the receiver has to observe the output of the inphase channel instead of the quadrature).

In Fig. 5.21 we provide the SER curves of the conventional 2-bit differential detector (2-bit DD), the 1-bit detector using data aided phase correction ((1)-bit DAPC) the 1 and 2-bit phase corrected detectors, combined according to decisions provided by feedback ((1+2)-bit DAPC/CWF) and the 1, 2 and 3-bit phase corrected detectors, again combined according to decisions made ((1+2+3)-bit DAPC/CWF). The results are based on Monte Carlo simulations. For the 2-bit differential detector, we have optimized the level of the decision threshold for the E_b/N_o where we run the simulations. We did the same with the C_{TFM} coefficient for the receiver which uses signal combining. As a predetection filter at the receiver we have used a 4^{th} order Butterworth with $B_rT = 0.8$. From the curves we see that all the proposed structures outperform the 2-bit DD. We also see that there is a crossing between the (1)-bit DAPC and the 2-bit DD. Such behaviour is common in decision feedback systems, due to the error propagation effect. *The other two structures have shown resistance to error propagation* (this gives quite an improvement in performance which can be verified by comparing the curves of the (1)-bit DAPC receiver with the curves of the (1+2)-bit DAPC/CWF,

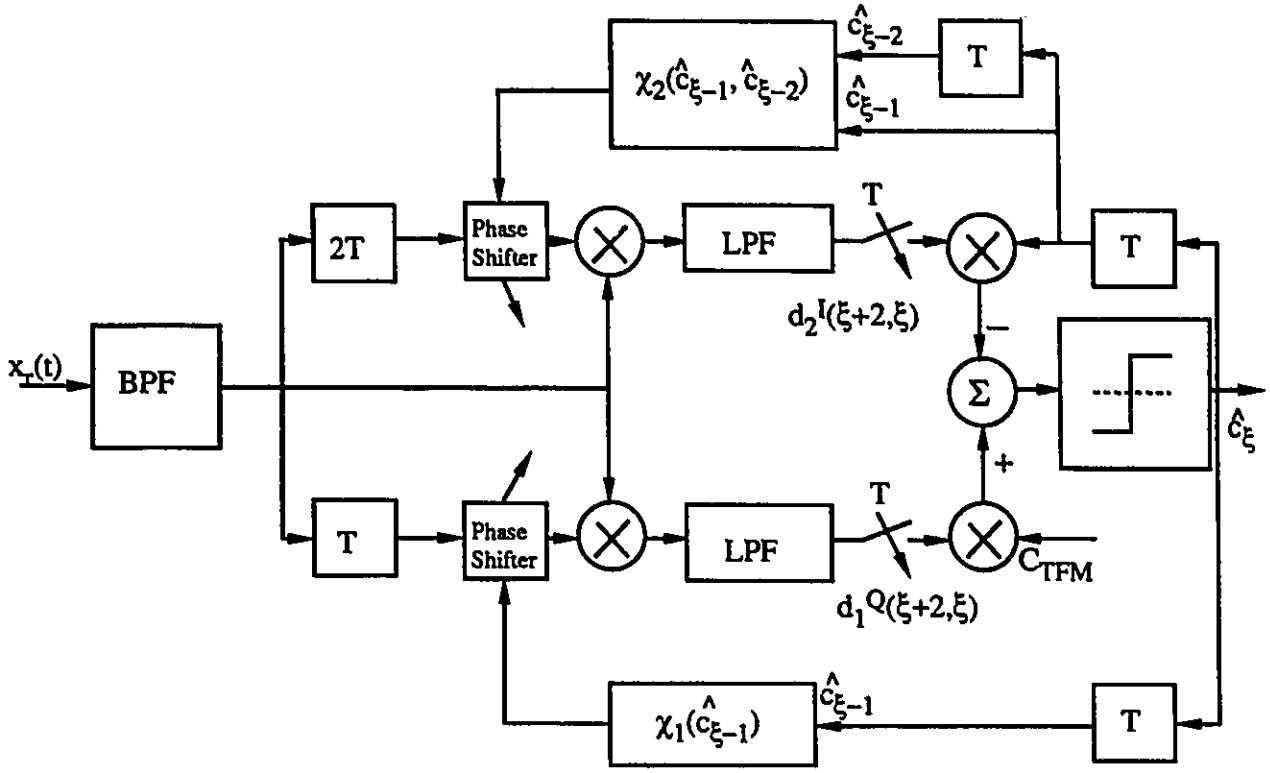

Figure 5.19: Block Diagram of the TFM symbol-by-symbol receiver using data aided phase correction and combining with feedback. The 1 and 2-bit differential detectors are used.

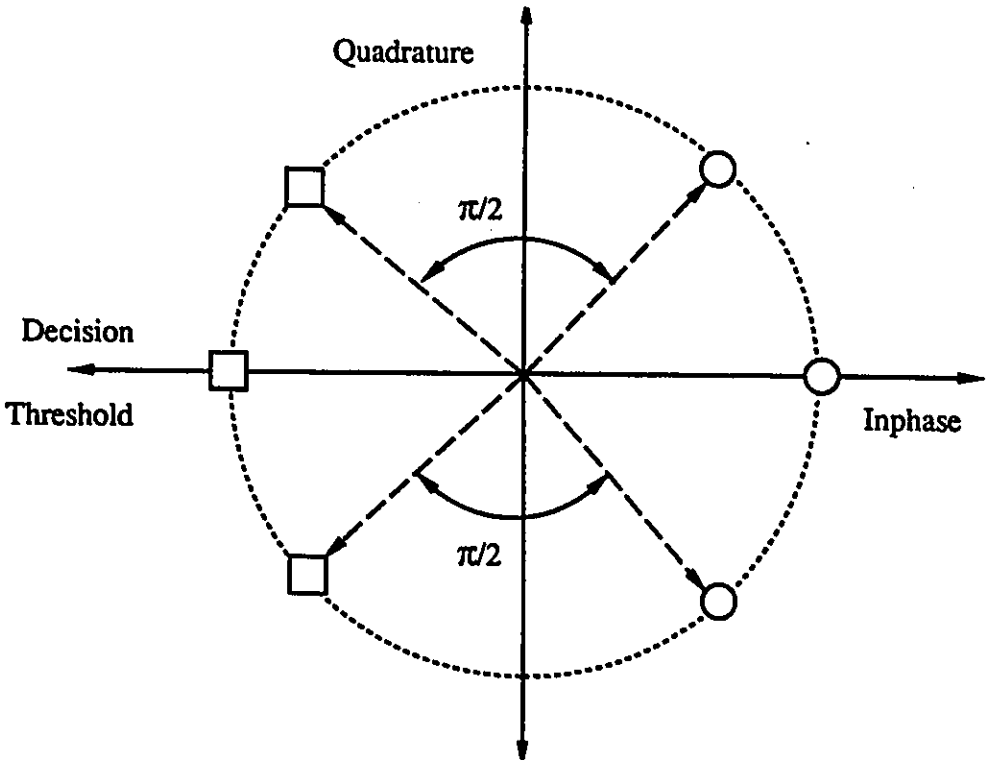

Figure 5.20: Phase state diagram of the 2-bit differential detector for TFM after the data aided phase correction (DAPC) has been applied. The values of the bit combinations $[c_{\xi+1}, c_\xi]$ generating every state are indicated in the figure. The phase shifting rule of Eq.(5.103) is used. With a circle we mark states where c_ξ appears with the value 1 ($c_\xi = 1$) and with a square, the states where c_ξ appears with -1 ($c_\xi = -1$).

(1+2+3)-bit DAPC/CWF). *The reason for this resistivity is the presence of a self recovering mechanism the 2-bit detector develops when DAPC is used with it.* In [169] this self recovery mechanism is presented in more detail. It has been shown that only two consecutive symbol errors are enough to rotate the phase correction by one full circle (i.e. 2π) back to the correct value.

From the SER curves we see the superiority of the proposed receivers. The (1)-bit DAPC outperforms the 2-bit DD 2 dB. The (1+2)-bit DAPC/CWF 5.5 dB and the (1+2+3)-bit DAPC/CWF 7.5 dB. The comparison refers to a SER=10^{-4}. In Table 5.7 we summarize the improvements offered by these receivers. Considering that these improvements are offered by relatively simple structures, we realize the potential of the described receivers.

Table 5.7: Improvements offered by the multiple differential symbol-by-symbol receivers using data aided phase correction and combining with decision feedback (DAPC/CWF) for a TFM signal. The comparison is made with the conventional 2-bit differential detector.

SER	GAINS (dB)		
	(1)-bit DAPC	(1+2)-bit DAPC/CWF	(1+2+3)-bit DAPC/CWF
10^{-2}	0.8	4.2	5.1
10^{-4}	2	5.5	7.5

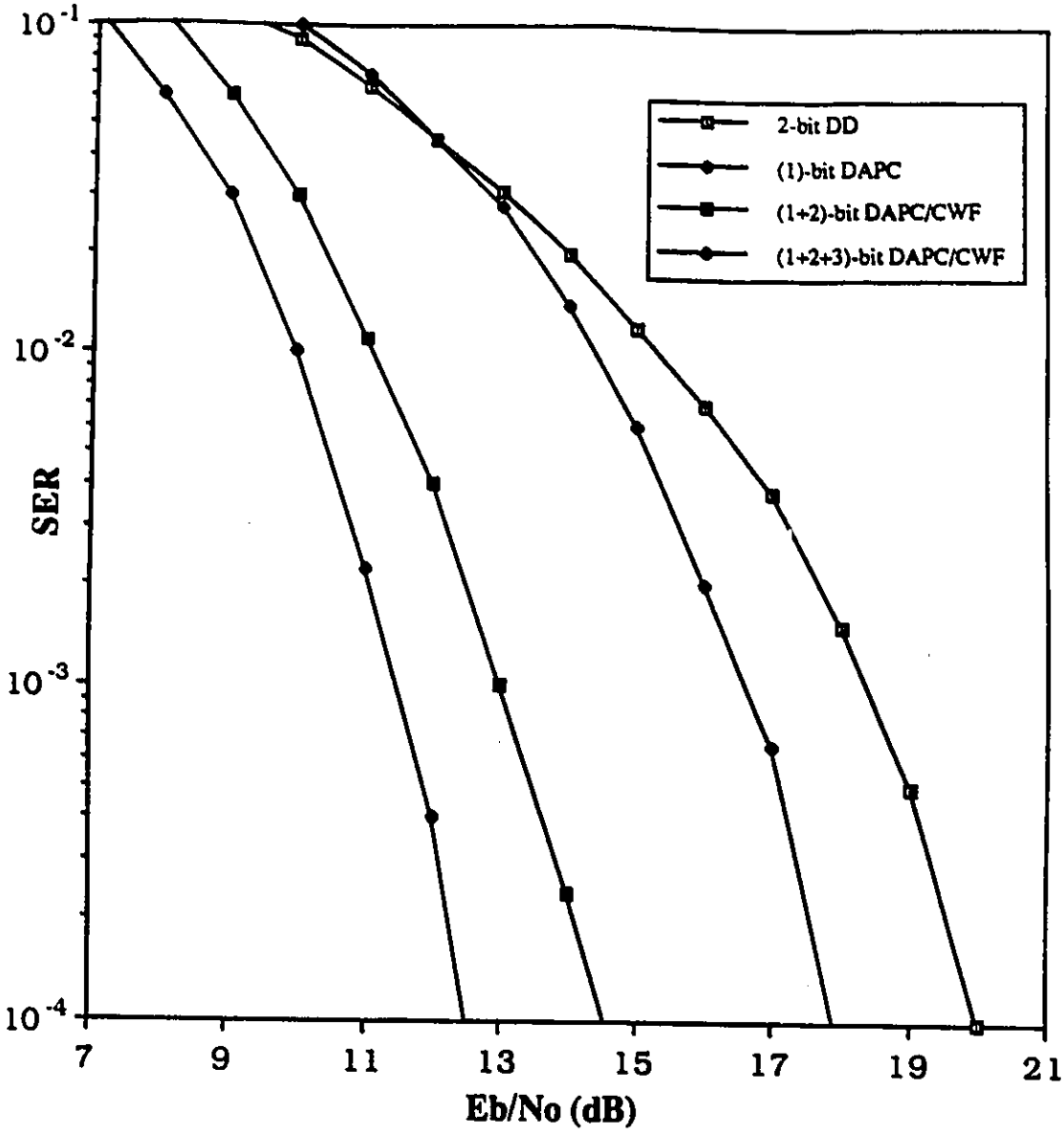

Figure 5.21: SER performance curves of TFM with various non-coherent receivers using data aided phase correction and signal combining with feedback ((1)-bit DAPC, (1+2)-bit DAPC/CWF, (1+2+3)-bit DAPC/CWF). The curve of the conventional 2-bit differential detector is also displayed (2-bit DD).

5.10.3 Gaussian Minimum Shift Keying

Here we shall consider the case where the B_tT product of the Gaussian premodulation filter (see Eq.(5.48)) equals $B_tT = 0.25$. For this product,

$$\vartheta_{\nu-1}^{\nu} \approx \begin{cases} \frac{\pi}{9.89} & \text{for } \nu = 1 \\ \frac{\pi}{3.36} & \text{for } \nu = 2 \\ \frac{\pi}{9.89} & \text{for } \nu = 3 \\ 0 & \text{for } \nu \neq 1,2,3. \end{cases} \tag{5.105}$$

We have developed and evaluated with GMSK, the same receivers used for TFM. For GMSK with $B_tT = 0.25$,

$$\Delta_1^P \beta_1(\xi+2, [\hat{c}_{\xi-1}]) \approx (\hat{c}_{\xi-1}\frac{\pi}{9.89})$$

$$\Delta_2^P \beta_1(\xi+2, [\hat{c}_{\xi-1}, \hat{c}_{\xi-2}]) \approx (\hat{c}_{\xi-1}\frac{\pi}{2.51} + \hat{c}_{\xi-2}\frac{\pi}{9.89})$$

$$\Delta_3^P \beta_1(\xi+2, [\hat{c}_{\xi-1}, \hat{c}_{\xi-2}, \hat{c}_{\xi-3}]) \approx (\hat{c}_{\xi-1}\frac{\pi}{2} + \hat{c}_{\xi-2}\frac{\pi}{2.51} + \hat{c}_{\xi-3}\frac{\pi}{9.89}) \tag{5.106}$$

The decision laws corresponding to the three cases are the following:

$\lambda = 1$

$$\hat{c}_k = sgn\{Im\{d_1^{CPM}(\xi+2)e^{-j(\hat{c}_{\xi-1}\frac{\pi}{9.89})}\}\} \tag{5.107}$$

$\lambda = 2$

$$\begin{aligned} \hat{c}_k \;=\; & sgn\{C_{GMSK} Im\{d_1^{CPM}(\xi+2)e^{-j(\hat{c}_{\xi-1}\frac{\pi}{9.89})}\} \\ & -\hat{c}^{k-1} Re\{d_2^{CPM}(\xi+2)e^{-j((\hat{c}_{\xi-2}-\hat{c}_{\xi-1})\frac{\pi}{9.89})}\}\} \end{aligned} \tag{5.108}$$

$\lambda = 3$

$$\begin{aligned} \hat{c}_k \;=\; & sgn\{C_{GMSK} Im\{d_1^{CPM}(\xi+2)e^{-j(\hat{c}_{\xi-1}\frac{\pi}{9.89})}\} \\ & -\hat{c}_{\xi-1} Re\{d_2^{CPM}(\xi+2)e^{-j(\hat{c}_{\xi-2}\frac{\pi}{9.89})}\} \\ & +[\hat{c}_{\xi-1}\hat{c}_{\xi-2}] Re\{d_3^{CPM}(\xi+2)e^{-j((\hat{c}_{\xi-3}-\hat{c}_{\xi-3})\frac{\pi}{9.89})}\}\} \end{aligned} \tag{5.109}$$

The expressions described above use the simplified phase shifting rules given in Eqs.(5.101) to (5.103) for TFM, only now they have been modified according to the phase characteristics of the GMSK signal. The block diagram of the receiver implementing the DAPC and CWF functions is identical to the one presented in Fig. 5.19 for the TFM.

For low E_b/N_o, the optimal value of C_{GMSK} (i.e. providing the best performance) is $C_{GMSK} = 0.846$. However, again, as E_b/N_o increases, the optimal value of C_{GMSK} is reduced. For high E_b/N_o it becomes $C_{GMSK} = 0.71$.

To demonstrate the effect of DAPC on the GMSK signal, we have plotted in Figs. 5.22 to 5.25 the phase-state diagrams of the conventional 1 and 2-bit differential detectors of GMSK (Figs. 5.22 and 5.24 respectively) and the 1 and 2-bit differential detectors with DAPC (Figs. 5.23 and 5.25). From Fig. 5.22 we see that in this case, for the 1-bit detector there is no overlapping between states created by combinations having c_ξ with opposite polarity. In this case, the closest phases, where c_ξ appears with opposite polarity, have a phase distance of 32°. This allows detection using the one bit differential detector; however, its performance is poor. For GMSK, the 2-bit differential detector has a phase difference of 64°. However, when DAPC is used, the minimum phase distance between states having c_ξ with opposite polarity becomes: i) for the 1-bit detector 68° and ii) for the 2-bit detector 103°. DAPC has again helped to increase the phase distance between states having c_ξ with opposite polarity and with it, DAPC has increased the width of the eye diagram at the sampling instant as well.

In Fig. 5.26 we provide the SER curves for the same systems evaluated in TFM (the conventional 2-bit differential detector (2-bit DD), and the three receivers described above. In this case, we include the curve of the conventional 1-bit differential detector as well. The results again correspond to Monte Carlo simulations. At the receiver, a 4^{th} order Butterworth with $B_rT = 1.0$ has been used. In Table 5.8 we have summarized the improvements offered by the proposed receivers, using DAPC and CWF, as compared to the conventional 1-bit differential detector (1-bit DD). In Table 5.9 the same receivers are compared with the conventional 2-bit differential detector (2-bit DD). The comparisons are performed for SER equal to 10^{-2} and 10^{-4}. From the results we see that all the DAPC/CWF receivers outperform the

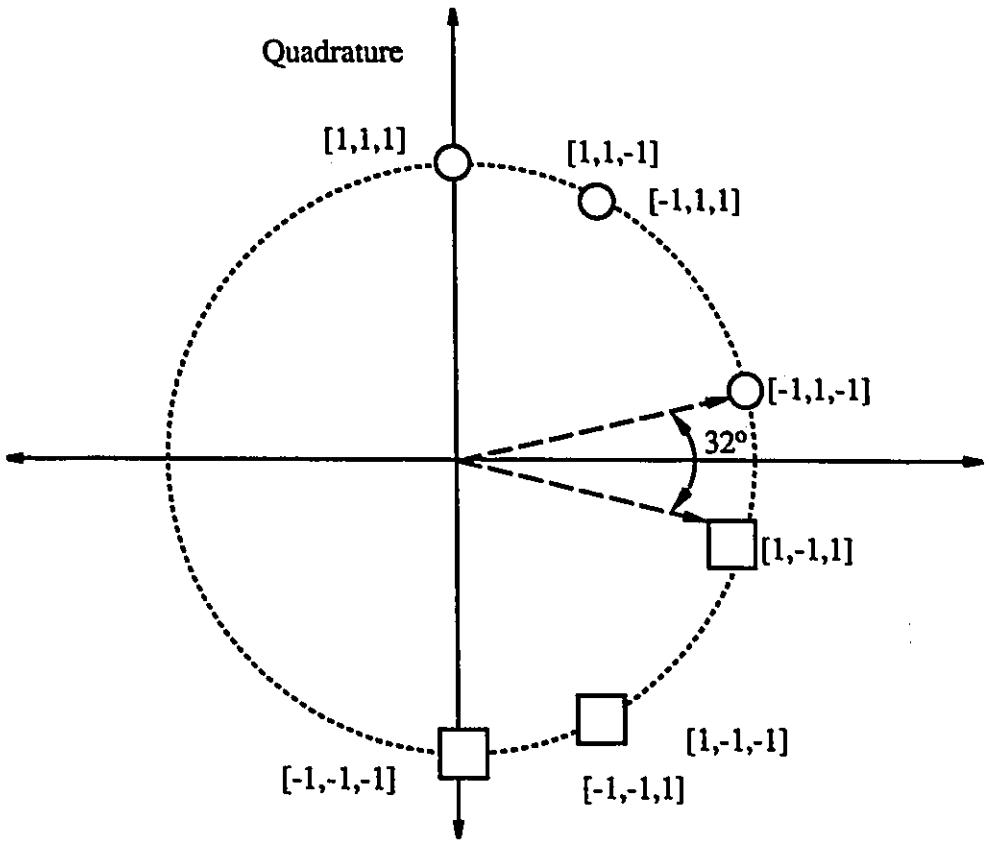

Figure 5.22: Phase state diagram of the conventional 1-bit differential detector for GMSK with $B_tT = 0.25$. The values of the bit combinations $[c_{\xi+1}, c_\xi, c_{\xi-1}]$ generating every state are indicated in the figure. With a circle we have marked states where c_ξ appears with the value 1 ($c_\xi = 1$) and with a square, states where c_ξ appears with -1 ($c_\xi = -1$).

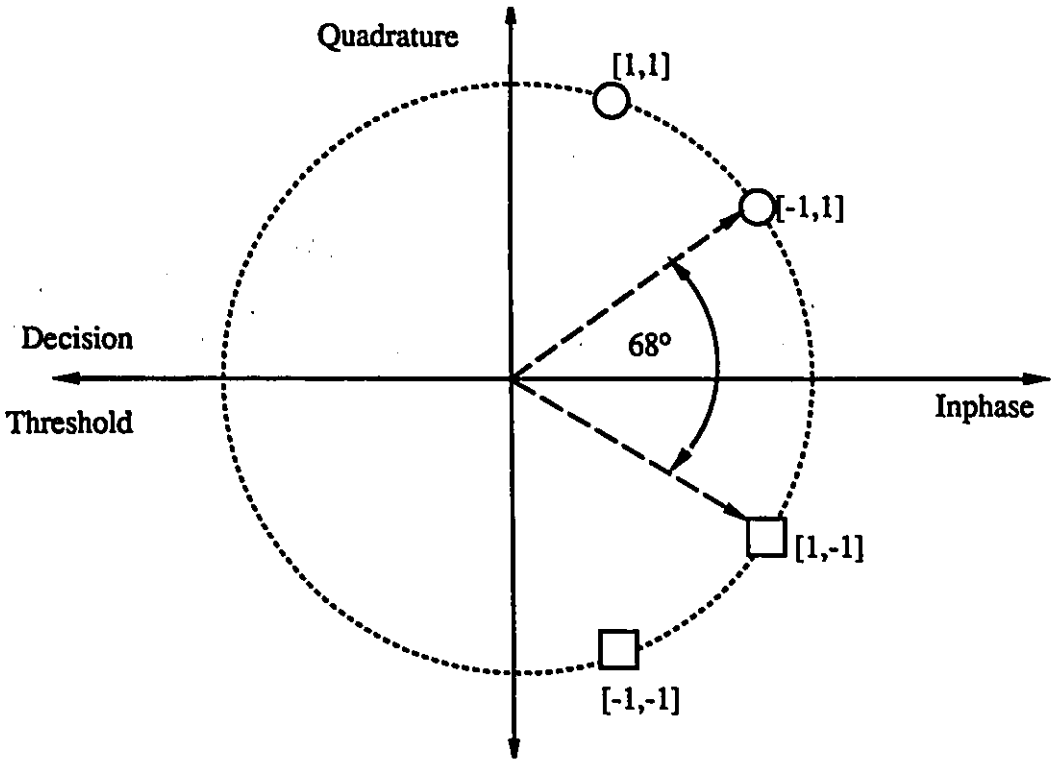

Figure 5.23: Phase state diagram of the 1-bit differential detector for GMSK (with $B_tT = 0.25$ after the data aided phase correction (DAPC) has been applied. The values of the bit combinations $[c_{\xi+1}, c_\xi]$ generating every state are indicated in the figure. With a circle we have marked states where c_ξ appears with the value 1 ($c_\xi = 1$) and with a square states where c_ξ appears with -1 ($c_\xi = -1$).

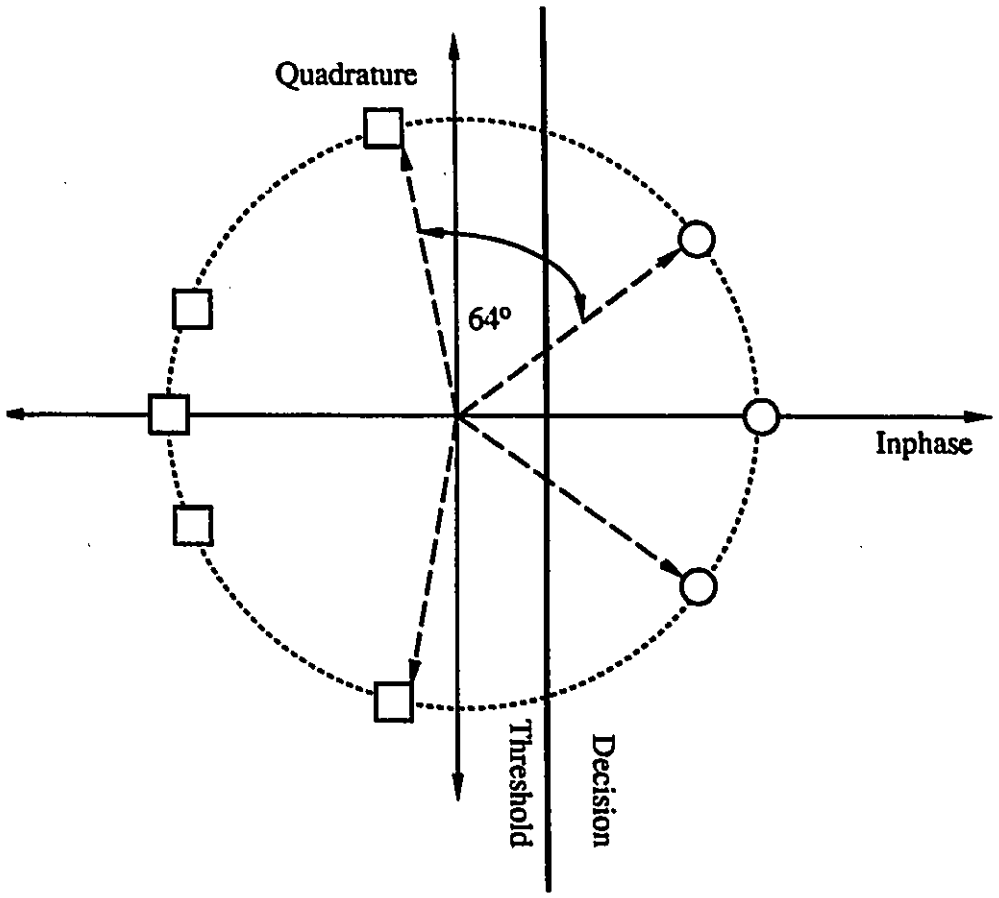

Figure 5.24: Phase state diagram of the conventional 2-bit differential detector for GMSK with $B_tT = 0.25$. The values of the bit combinations $[c_{\xi+1}, c_\xi, c_{\xi-1}]$ generating every state are indicated in the figure. With a circle we have marked states where c_ξ appears with the value 1 ($c_\xi = 1$) and with a square, states where c_ξ appears with -1 ($c_\xi = -1$).

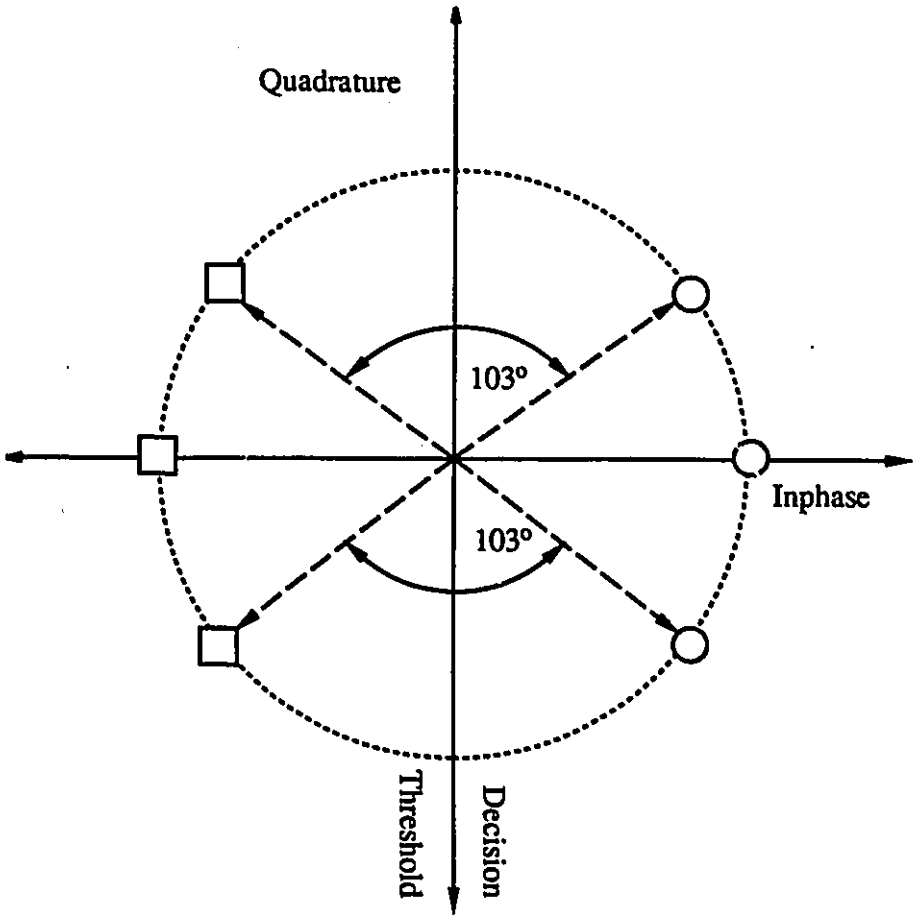

Figure 5.25: Phase state diagram of the 2-bit differential detector for GMSK (with $B_tT = 0.25$ after the data aided phase correction (DAPC) has been applied. The values of the bit combinations $[c_{\xi+1}, c_\xi]$ generating every state are indicated in the figure. With a circle we have marked states where c_ξ appears with the value 1 ($c_\xi = 1$) and with a square states where c_ξ appears with -1 ($c_\xi = -1$).

1-bit DD and achieve improvements of as high as 11.8 dB. Compared to 2-bit DD, the (1+2)-bit DAPC/CWF, (1+2+3)-bit DAPC/CWF perform better. The improvements the DAPC/CWF receivers offer are higher than 4 dB. However, the (1)-bit DAPC lacks 1 dB in performance as compared to 2-bit DD.

As the B_tT of the premodulation filter becomes smaller (the signal becomes more spectrally efficient) the improvements become higher.

Table 5.8: Improvements offered by the multiple differential symbol-by-symbol receivers using data aided phase correction and combining with feedback (DAPC/CWF) for a GMSK signal ($B_tT = 0.25$). The comparison is made with the conventional 1-bit differential detector.

SER	GAINS (dB)		
	(1)-bit DAPC	(1+2)-bit DAPC/CWF	(1+2+3)-bit DAPC/CWF
10^{-2}	6.5	8.7	10.5
10^{-4}	7	9.8	11.8

Table 5.9: Improvements offered by the multiple differential symbol-by-symbol receivers using data aided phase correction and combining with feedback (DAPC/CWF) for a GMSK signal ($B_tT = 0.25$). The comparison is made with the conventional 2-bit differential detector.

SER	GAINS (dB)		
	(1)-bit DAPC	(1+2)-bit DAPC/CWF	(1+2+3)-bit DAPC/CWF
10^{-2}	-1.2	1.5	3
10^{-4}	-1	2	4

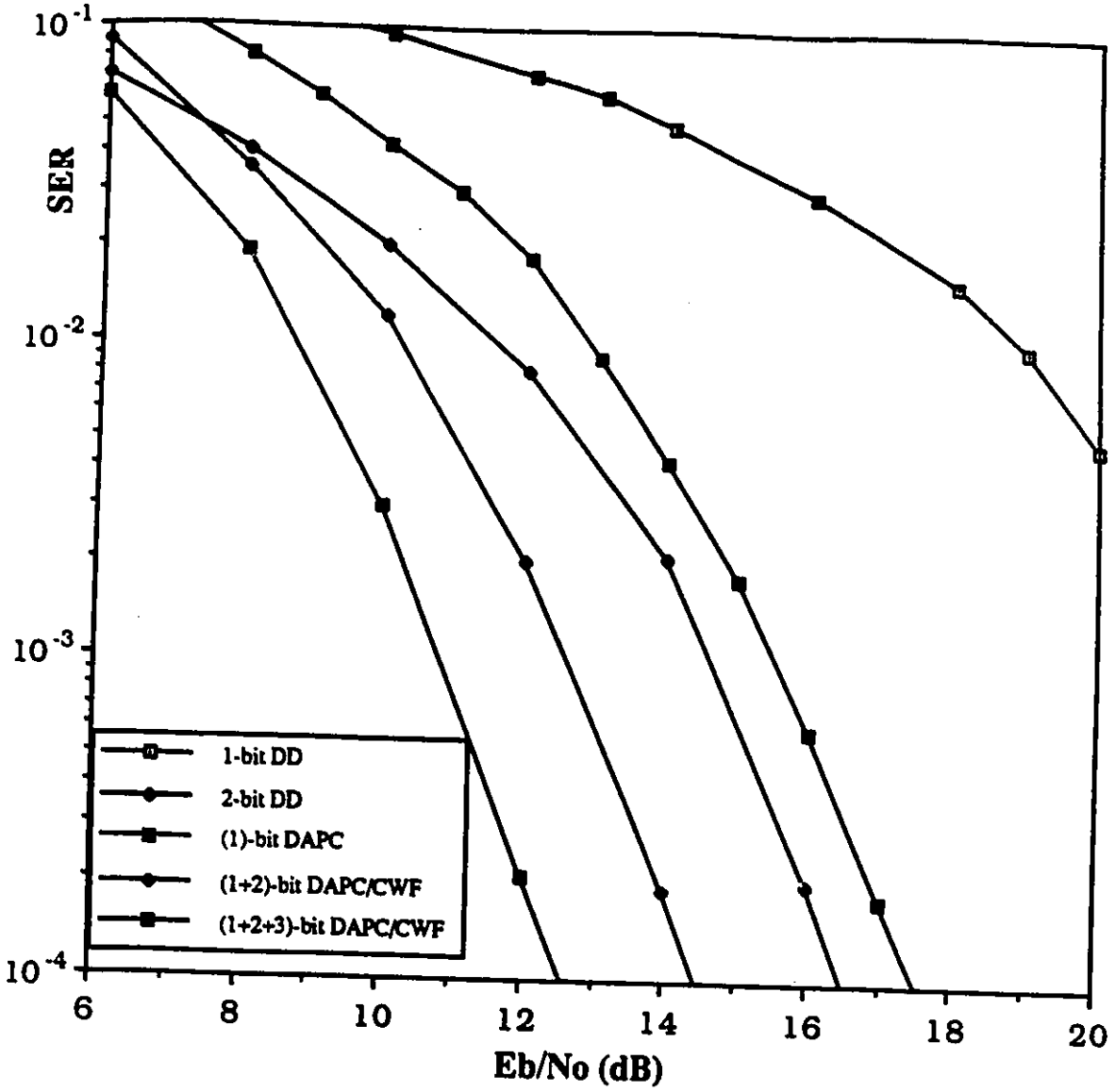

Figure 5.26: SER performance curves of GMSK ($B_tT = 0.25$) with various non-coherent receivers using data aided phase correction and signal combining with feedback ((1)-bit DAPC, (1+2)-bit DAPC/CWF, (1+2+3)-bit DAPC/CWF). The curves of the conventional 1-bit (1-bit DD) and 2-bit (2-bit DD) differential detectors are also included.

5.11 CONCLUSIONS

The present Chapter has extended the development of improved (yet practical) non-coherent receivers to CPM signals. It has addressed both sequence estimation and symbol-by-symbol detection. The derived receivers can be implemented in a block decoding or multiple differential detection form.

The design of the non-coherent CPM receivers has started with the derivation of metrics for asymptotically optimal non-coherent detection. Afterwards, the AMP signal decomposition is used, in order to obtain reduction in the filtering requirements of the receivers.

In order to make possible a cost efficient implementation of the non-coherent receivers in the IF multiple differential detection form, the relatively complex (and difficult to be implemented as IF) filters provided by the AMP signal decomposition analysis have been replaced with simple commercially available filters. All the evaluated sequence estimators and symbol-by-symbol receivers have been implemented in the multiple differential detection form. The evaluated configurations use up to three differential detectors and they have relatively low complexity.

The reduced complexity symbol-by-symbol receivers use decision feedback. The use of decision feedback in these structures introduces a new technique, the *Data Aided Phase Correction* (DAPC) whose primary function is to cancel (using the already made decisions) the ISI present at the phase of the (m-bit) differentially detected signal. This ISI has been generated by symbols transmitted before the symbol under decision. The use of DAPC increases the width of the eye diagram at the output of the (m-bit) differential detector, prior to its use in the decision process. The DAPC is used together with signal combining directed by decision feedback (CWF). Function of the CWF technique is to combine the outputs of the multiple differential detectors prior to the decision, in a way controlled by the previous decisions. Use of CWF increases the signal to noise ratio at the input of the decision unit (for binary transmission it is a threshold detector).

We have evaluated the multiple differential symbol-by-symbol receivers and sequence estimators with three popular CPM signals, the MSK, TFM and GMSK. The results were excellent. For sequence estimation and operation in a Gaussian channel, they demonstrated improvements higher than

9 dB as compared to the conventional differential detector. In a Rician faded channel they achieved reduction of error floors by more than three orders of magnitude. The evaluated multiple differential symbol-by-symbol receivers (using DAPC/CWF) achieved improvements higher than 5 dB compared to the conventional differential detectors. Considering the weakness and poor performance of the conventional differential detectors when used with highly spectrally efficient CPM signals, we feel it is justifiable to say that the introduced improved non-coherent receivers have made possible the use of practical differential detection receivers with spectrally efficient CPM systems.

In the following chapter, we shall summarize the main contribution of this work and suggest some potential extensions of the covered research material.

Chapter 6

CONCLUSIONS

6.1 SUMMARY OF THE CONTRIBUTIONS

This thesis has introduced new non-coherent receiver structures for the linear and CPM signals. The contributions of this thesis can be summarized as follows:

1) *A Generalized Non-Coherent Detection Theory for Linear and CPM signals has been introduced.*

It has provided the structures of optimal symbol-by-symbol receivers and sequence estimators both for the ideal as well as the time dispersive channel. It has extended the non-coherent detection concept to multi-amplitude/phase signal formats. It has also provided the linking between various non-coherent detection techniques and how they relate to the concept of optimal non-coherent detection.

2) *It has provided a number of novel, improved non-coherent receivers.*

Whenever the optimal receiver structures became complicated and impractical, we applied proper approximations and simplifications in order to derive reduced complexity (improved performance) receivers. Such structures are:

1. *Asymptotically Optimal Decoders for the time dispersive channel.* These structures applied on trellis coded as well as uncoded signals provided improvements **higher than 5 dB** as compared to the conventional

differential receiver (for example see Tables 4.4, 4.12 and Figs. 4.14, 4.42). Used with multi-amplitude/phase signals they outperformed the differential and coherent PSK systems of equal spectral efficiency by **6 and 3.5 dB** respectively (see Fig. 4.46). These receivers have made the application of non-coherent technology to the power/bandwidth efficient multi-amplitude/phase systems possible.

2. *Block Decoders.* Evaluated in ideal as well as time dispersive channels (both for uncoded and trellis coded signals) they were capable of achieving improvements by **more than 3.4 dB** as compared to the conventional differential systems (see Table 4.9 and Figs. 4.37, 4.38). Also evaluation in Rician faded channels demonstrated their capability to reduce the error floors experienced by the differential systems. Our evaluation results demonstrated **improvements higher than 7 dB and a reduction of error floors by almost one order of magnitude** (see Table 4.24 and Fig. 4.84).

3. *Recursive Sequence Estimators based on Combined Squared Amplitude and Multiple Differential Detection.* These structures have been proven very powerful both in AWGN as well as faded channels. Evaluations demonstrated improvements **higher than 8 dB** compared to the conventional differential receiver, when operating in an AWGN channel (see Table 5.3 and Fig. 5.5). Operating in a Rician faded channel they were capable of reducing the error floors experienced by the conventional differential receiver **by more than three orders of magnitude** (see Figs. 5.6, 5.10). These improvements are provided while the structure of the receiver remains in very logical levels of complexity.

4. *A class of simple symbol-by-symbol receivers based on phase ISI cancellation and decision feedback directed signal combining.* They achieve the improvements by: i) opening the eye diagram of the signal (this is made possible by reducing the ISI present in the signal phase) and ii) combining the outputs of more than one (multiple) differential detector in a way determined by the values of the already decided symbols. Evaluations indicated their capability to achieve considerable improvements as compared to the conventional differential receiver. Improvements **in excess of 5 dB** have been verified (see Table 5.7 and Fig. 5.21). At the same time the complexity of these structures remains in low levels.

3) *It has provided the framework for the analytical evaluation of the proposed symbol by symbol receivers and sequence estimators.* It covers evaluation of the proposed schemes in AWGN (ideal or time dispersive) channels as well as in faded channels. As a result of the performance analysis we identified the distance expressions which characterize the performance of these receivers (equivalent to the Euclidean distance which characterizes the performance of coherent schemes). Through the performance analysis carried out we identified that the existing codes (developed for the coherent systems) are not optimal when they are used with non-coherent techniques. The identified distance metric expressions can be used to develop new optimal codes which are appropriate for these non-coherent schemes.

6.2 FURTHER RESEARCH AREAS

In the present work, we have provided a generalized non-coherent detection framework. We developed and analyzed different optimal and near optimal non-coherent receivers. We applied them to PSK, QAM and CPM signals. Our study has been exhaustive. However, even though this thesis has answered a number of questions related to non-coherent detection and provided non-coherent receiver structures capable to achieve considerable gains, at the same time it has generated a new set of questions and directions. Below we list some of them.

1. *Extension of the proposed (multiple differential) receivers for optimal/ asymptotically optimal detection of digital signals operating in fast faded environments.* Even though fading has been considered in the evaluation of the proposed schemes, the design of the proposed receivers is based on the assumption that the signal travels through the channel (ideal or time dispersive) is corrupted only by Gaussian noise. No consideration of the fading and its statistical behaviour has been taken. Consideration of the statistical behaviour of the faded channel in the design, results in modified forms of multiple differential detection structures, exhibiting superb performance. The error floors are virtually eliminated or very significantly reduced (depending on the complexity levels used by the application). Some work on this subject can be found

in [166], [167], [22]. Such a system can be very valuable to applications encountering fast faded channels such as aeronautical communications, personal satellite communications operating in the EHF band etc.

2. *Design of new coding techniques to "match" the characteristics of the proposed receivers.* One of the findings of this thesis was the non-optimality of existing coding schemes (developed and optimized under the maximization of Euclidean distance criterion; Euclidean distance characterizes the performance of coherent systems) when used with the proposed receivers, especially for the case where the operation takes place in a distorted channel. Instead new codes are required -their design based on the distance metrics (described in this thesis) which apply and characterize the performance of the proposed receivers.

3. *Apply the introduced non-coherent detection techniques to block encoded signals.* Even though in the present work we considered only convolutional codes, the receivers can be used with block coded systems as well. In the text we have indicated ways to reduce the complexity of the non-coherent receivers, when they process long sequences. However, the same approaches do not necessarily apply to block encoded signals. For block codes using long codewords (Reed-Solomon codes, BCH codes e.t.c.) other approaches might be needed in order to provide reduced complexity near optimal non-coherent receivers.

4. *Extend the Generalized Non-Coherent Detection concept to the partially coherent detection.* Some initial work on this subject can be found in [249], [250]. Further extensions on this topic are possible.

5. *Extend the analysis and the proposed structures to systems with both, carrier frequency and phase uncertainties.* One assumption which has been used in the design of the proposed schemes is that while the carrier phase is unknown, the carrier frequency is estimated quite accurately at the receiver and it is used for signal demodulation. An alternative implementation method, which avoids the signal demodulation, is to use Multiple Differential Detection. In this second case, the carrier frequency has to be kept close to a value which is a multiple of the symbol transmission rate. This is needed to ensure that phase offsets do not appear at the outputs of the differential detectors. However, in certain

cases (especially in channels experiencing deep fades), it is difficult to always achieve accurate estimate of the frequency, as for example when the signal enters in or comes out from a deep fade and of course, during the fading period. Similarly, Doppler shifts, Phase Noise or other types of impairments make any effort to keep the carrier frequency always at a certain value practically impossible. By considering frequency uncertainties in the model of the communication channel and using this model in the mathematical formulation leading to the design of the receiver, new improved schemes can be generated.

Appendix A

Metric of the Non-Coherent Asymptotically Optimal Sequence Estimator for High E_b/N_o

The objective of this appendix is to prove that the metric expression $\aleph_{HAO}^{LMD}(\bar{h}, \bar{y}, \bar{C}(\bar{A}))$ of Eq. (4.7) is asymptotically optimal for high E_b/N_o.

Proof

Let us consider two transmitted information sequences $\bar{A}^\nu$, $\bar{A}^\varsigma$. We want to decide as to which of the two is the most probable one. According to the analysis presented in Chapter 3,

$$\aleph_{OP}^{LMD}(\bar{h}, \bar{y}, \bar{C}(\bar{A}^\nu)) \underset{\bar{A}^\varsigma}{\overset{\bar{A}^\nu}{\gtrless}} \aleph_{OP}^{LMD}(\bar{h}, \bar{y}, \bar{C}(\bar{A}^\varsigma)). \tag{A.1}$$

Case 1: $|\sum_{k=0}^{Z-1} y_k(c_k^\nu)^*| > 0$, $|\sum_{k=0}^{Z-1} y_k(c_k^\varsigma)^*| > 0$

Using the approximation

$$I_o(|z|) \simeq \frac{1}{\sqrt{2\pi|z|}} e^{|z|} \quad \text{for} \quad |z| > 6.8 \tag{A.2}$$

Eq.(A.1) can be expressed as

$$\frac{1}{\sqrt{2\pi}\sqrt{\frac{|\sum_{k=0}^{Z-1} y_k(c_k^\nu)^*|}{N_o}}}$$

$$\exp\{\frac{1}{N_o}[-(MST(h_0, \bar{C}(\bar{A}^\nu)) + IST(\bar{h}, \bar{C}(\bar{A}^\nu))) + |\sum_{k=0}^{Z-1} y_k(c_k^\nu)^*|)]\} \underset{\bar{A}^\zeta}{\overset{\bar{A}^\nu}{\gtrless}}$$

$$\frac{1}{\sqrt{2\pi}\sqrt{\frac{|\sum_{k=0}^{Z-1} y_k(c_k^\zeta)^*|}{N_o}}}$$

$$\exp\{\frac{1}{N_o}[-(MST(h_0, \bar{C}(\bar{A}^\zeta)) + IST(\bar{h}, \bar{C}(\bar{A}^\zeta))) + |\sum_{k=0}^{Z-1} y_k(c_k^\zeta)^*|)]\}$$

(A.3)

or equivalently

$$[\frac{|\sum_{k=0}^{Z-1} y_k(c_k^\zeta)^*|}{|\sum_{k=0}^{Z-1} y_k(c_k^\nu)^*|}]^{\frac{1}{2}}$$

$$\exp\{\frac{1}{N_o} \quad (\quad |\sum_{k=0}^{Z-1} y_k(c_k^\nu)^*| - (MST(h_0, \bar{C}(\bar{A}^\nu)) + IST(\bar{h}, \bar{C}(\bar{A}^\nu))))-$$

$$(|\sum_{k=0}^{Z-1} y_k(c_k^\zeta)^*| - (MST(h_0, \bar{C}(\bar{A}^\zeta)) + IST(\bar{h}, \bar{C}(\bar{A}^\zeta))))\} \underset{\bar{A}^\zeta}{\overset{\bar{A}^\nu}{\gtrless}} 1 . \tag{A.4}$$

Defining the terms

$$\Re_1(\bar{y}, \bar{C}(\bar{A}^\nu), \bar{C}(\bar{A}^\varsigma)) = ln([\frac{|\sum_{k=0}^{Z-1} y_k(c_k^\varsigma)^*|}{|\sum_{k=0}^{Z-1} y_k(c_k^\nu)^*|}]^{\frac{1}{2}}) \ , \tag{A.5}$$

$$\Re_2(h_0, \bar{h}, \bar{y}, \bar{C}(\bar{A}^\nu), \bar{C}(\bar{A}^\varsigma)) =$$

$$(|\sum_{k=0}^{Z-1} y_k(c_k^\nu)^*| - (MST(h_0, \bar{C}(\bar{A}^\nu)) + IST(\bar{h}, \bar{C}(\bar{A}^\nu)))$$

$$-(|\sum_{k=0}^{Z-1} y_k(c_k^\varsigma)^*| - (MST(h_0, \bar{C}(\bar{A}^\varsigma)) + IST(\bar{h}, \bar{C}(\bar{A}^\varsigma))) \tag{A.6}$$

and using them in Eq.(A.4) we get

$$\exp\{[\frac{1}{N_o}(N_o\Re_1(\bar{y}, \bar{C}(\bar{A}^\nu), \bar{C}(\bar{A}^\varsigma))) + \Re_2(h_0, \bar{h}, \bar{y}, \bar{C}(\bar{A}^\nu), \bar{C}(\bar{A}^\varsigma))]\} \underset{\bar{A}^\varsigma}{\overset{\bar{A}^\nu}{\gtrless}} \quad 1$$

(A.7)

or equivalently

$$N_o\Re_1(\bar{y}, \bar{C}(\bar{A}^\nu), \bar{C}(\bar{A}^\varsigma)) + \Re_2(h_0, \bar{y}, \bar{C}(\bar{A}^\nu), \bar{C}(\bar{A}^\varsigma)) \underset{\bar{A}^\varsigma}{\overset{\bar{A}^\nu}{\gtrless}} \quad 0. \tag{A.8}$$

For $N_o \rightarrow 0$ (i.e. $\frac{E_b}{N_o} \rightarrow \infty$) the first term in Eq.(A.8) vanishes to zero and Eq.(A.8) becomes:

$$\Re_2(h_0, \bar{h}, \bar{y}, \bar{C}(\bar{A}^\nu), \bar{C}(\bar{A}^\varsigma)) \underset{\bar{A}^\varsigma}{\overset{\bar{A}^\nu}{\gtrless}} \quad 0$$

or equivalently

$$|\sum_{k=0}^{Z-1} y_k(c_k^\nu)^*| - (MST(h_0, \bar{C}(\bar{A}^\nu)) + IST(\bar{h}, \bar{C}(\bar{A}^\nu)))$$

$$\begin{matrix}\bar{A}^{\nu} \\ > \\ < \\ \bar{A}^{\zeta}\end{matrix}$$

$$(|\sum_{k=0}^{Z-1} y_k(c_k^{\zeta})^*| - (MST(h_0, \bar{C}(\bar{A}^{\zeta})) + IST(\bar{h}, \bar{C}(\bar{A}^{\zeta}))) \tag{A.9}$$

Case 2: $|\sum_{k=0}^{Z-1} y_k(c_k^{\nu})^*| = 0$, $|\sum_{k=0}^{Z-1} y_k(c_k^{\zeta})^*| > 0$

Using the $I_0(0) = 1$, we can express Eq.(A.1) as

$$\exp\{\frac{1}{N_o}[-(MST(h_0, \bar{C}(\bar{A}^{\nu})) + IST(\bar{h}, \bar{C}(\bar{A}^{\nu})))) + |\sum_{k=0}^{Z-1} y_k(c_k^{\nu})^*|)]\} \quad \begin{matrix}\bar{A}^{\nu} \\ > \\ < \\ \bar{A}^{\zeta}\end{matrix}$$

$$\frac{1}{\sqrt{2\pi}\sqrt{\frac{|\sum_{k=0}^{Z-1} y_k(c_k^{\zeta})^*|}{N_o}}}$$

$$\exp\{\frac{1}{N_o}[-(MST(h_0, \bar{C}(\bar{A}^{\zeta})) + IST(\bar{h}, \bar{C}(\bar{A}^{\zeta})))) + |\sum_{k=0}^{Z-1} y_k(c_k^{\zeta})^*|)]\}.$$

(A.10)

Defining as

$$\Re_3(\bar{y}, \bar{C}(\bar{A}^{\zeta})) = ln([2\pi|\sum_{k=0}^{Z-1} y_k(c_k^{\zeta})^*\|^{\frac{1}{2}}) - \frac{1}{2} ln(N_o) \tag{A.11}$$

and repeating the steps described in Case 1, we end up with the following expression:

$$N_o \Re_3(\bar{y}, \bar{C}(\bar{A}^{\zeta})) + \Re_2((\bar{y}, \bar{C}(\bar{A}^{\nu}), \bar{C}(\bar{A}^{\zeta})) - \frac{N_o}{2} ln(N_o) \begin{matrix}\bar{A}^{\nu} \\ \geq \\ < \\ \bar{A}^{\zeta}\end{matrix} 0. \tag{A.12}$$

which for $N_o \rightarrow 0$ (i.e. $\frac{E_b}{N_o} \rightarrow \infty$) becomes:

$$\Re_2(h_0, \bar{h}, \bar{y}, \bar{C}(\bar{A}^\nu), \bar{C}(\bar{A}^\varsigma)) \underset{\bar{A}^\varsigma}{\overset{\bar{A}^\nu}{\gtrless}} 0$$

(the $\frac{x}{2} ln(x) \underbrace{\longrightarrow}_{x \rightarrow 0} 0$ has been used) or equivalently

$$|\sum_{k=0}^{Z-1} y_k (c_k^\nu)^*| - (MST(h_0, \bar{C}(\bar{A}^\nu)) + IST(\bar{h}, \bar{C}(\bar{A}^\nu)))$$

$$\underset{\bar{A}^\varsigma}{\overset{\bar{A}^\nu}{\gtrless}}$$

$$(|\sum_{k=0}^{Z-1} y_k (c_k^\varsigma)^*| - (MST(h_0, \bar{C}(\bar{A}^\varsigma)) + IST(\bar{h}, \bar{C}(\bar{A}^\varsigma))) \qquad \text{(A.13)}$$

Eq.(A.13) is identical to Eq.(A.9).

Case 3: $|\sum_{k=0}^{Z-1} y_k (c_k^\nu)^*| = 0$, $|\sum_{k=0}^{Z-1} y_k (c_k^\varsigma)^*| = 0$

Eq.(A.1) can be expressed as

$$\exp\{\frac{1}{N_o}[-(MST(h_0, \bar{C}(\bar{A}^\nu)) + IST(\bar{h}, \bar{C}(\bar{A}^\nu))) + |\sum_{k=0}^{Z-1} y_k (c_k^\nu)^*|]\} \underset{\bar{A}^\varsigma}{\overset{\bar{A}^\nu}{\gtrless}}$$

$$\exp\{\frac{1}{N_o}[-(MST(h_0, \bar{C}(\bar{A}^\varsigma)) + IST(\bar{h}, \bar{C}(\bar{A}^\varsigma))) + |\sum_{k=0}^{Z-1} y_k (c_k^\varsigma)^*|]\}$$

(A.14)

and equivalently,

$$|\sum_{k=0}^{Z-1} y_k(c_k^{\nu})^*| - (MST(h_0, \bar{C}(\bar{A}^{\nu})) + IST(\bar{h}, \bar{C}(\bar{A}^{\nu})))$$

$$\begin{matrix} \bar{A}^{\nu} \\ > \\ < \\ \bar{A}^{\varsigma} \end{matrix}$$

$$(|\sum_{k=0}^{Z-1} y_k(c_k^{\varsigma})^*| - (MST(h_0, \bar{C}(\bar{A}^{\varsigma})) + IST(\bar{h}, \bar{C}(\bar{A}^{\varsigma}))) \; . \qquad \text{(A.15)}$$

Eq.(A.15) is identical to Eq.(A.9).

For $\frac{E_b}{N_o} \rightarrow \infty$ the decision law of Eq.(A.9) is equivalent to the optimal decision law described by Eq.(A.1) . Consequently it is asymptotically optimal for high $\frac{E_b}{N_o}$. Notice, that the equivalence is in a deterministic sense (i.e., as the $\frac{E_b}{N_o} \rightarrow \infty$ the two decoders are bound to give the same decisions).

Q.E.D.

Appendix B

Pairwise Error Event Bound of the Block Decoder

Assume that $\bar{A}^{\nu}$ is the transmitted information sequence. Assume that now $\bar{C}(\bar{A}^{\nu})$ is compared with $\bar{C}(\bar{A}^{\varsigma})$, the decision being based on the maximization of the metric $\aleph_{IC}(\bar{y}, \bar{C}(\bar{A}))$, presented in Eq.(4.12). The criterion which will choose one over the other codeword is the following:

$$|F_Z^{\nu}(\bar{y}, \bar{C}(\bar{A}^{\nu}))| \underset{\bar{A}^{\varsigma}}{\overset{\bar{A}^{\nu}}{\gtrless}} |F_Z^{\nu}(\bar{y}, \bar{C}(\bar{A}^{\varsigma}))| \tag{B.1}$$

where

$$F_Z^{\nu}(\bar{y}, \bar{C}(\bar{A}^{i})) = \sum_{k=0}^{Z-1} y_k (c_k^i)^*. \tag{B.2}$$

c_k^i represents the value the symbol c_k would have, if the sequence $\bar{A}^i$ is the transmitted one.

Using Eq.(B.2) $F_Z^{\nu}(\bar{y}, \bar{C}(\bar{A}^{\nu}))$, $F_Z^{\nu}(\bar{y}, \bar{C}(\bar{A}^{\varsigma}))$ can be expressed as:

$$F_Z^{\nu}(\bar{y}, \bar{C}(\bar{A}^{\eta})) = e^{j\psi}[\sum_{i=0}^{Z-1} \sum_{l=0}^{Z-1} c_l^{\nu} (c_i^{\eta})^* h_{i-l}] + \sum_{i=0}^{Z-1} n_i (c_i^{\eta})^* \tag{B.3}$$

where η can be either ν or ζ ($\eta \epsilon \{\nu, \zeta\}$). Because of the Gaussian nature of

n_k, $F_Z^\nu(\bar{y}, \bar{C}(\bar{A}^\eta))$ is a complex Gaussian random variable with an average of

$$\bar{E}_\eta^\nu = e^{j\psi}(\sum_{i=0}^{Z-1}\sum_{l=0}^{Z-1} c_l^\nu (c_i^\eta)^* h_{i-l}). \tag{B.4}$$

For the case where there is no ISI, $\bar{E}_\eta^\nu$, becomes:

$$\bar{E}_\eta^\nu = e^{j\psi}(\sum_{l=0}^{Z-1} c_l^\nu (c_l^\eta)^*). \tag{B.5}$$

The variance of $F_Z^\nu(\bar{y}, \bar{C}(\bar{A}^\eta))$ is equal to:

$$\mu_{\nu\eta} = E\{|\sum_{k=0}^{Z-1} n_k (c_k^\eta)^*|^2\} = (ZR_o^n + 2\sum_{k=1}^{Z-1} R_k^n \sum_{l=k}^{Z-1} \cos(\Delta\Phi_k^\eta(i))) \tag{B.6}$$

where $\Delta\Phi_k^\eta(i)$ represents the value $\Delta\Phi_k(i)$ would have, if $\bar{A}^\eta$ was the transmitted information sequence.

The cross-covariance $\mu_{\nu\zeta}^c$ between $F_Z^\nu(\bar{y}, \bar{C}(\bar{A}^\nu))$ and $F_Z^\nu(\bar{y}, \bar{C}(\bar{A}^\zeta))$ is equal to:

$$\mu_{\nu\zeta}^c = \sum_{k=0}^{Z-1} R_k^n \sum_{l=k}^{Z-1} [e^{j(\Delta\Phi_l^\zeta(l) \ominus \Delta\Phi_{l-k}^\nu(l-k))} + e^{-j(\Delta\Phi_l^\nu(l) \ominus \Delta\Phi_{l-k}^\zeta(l-k))}] \,. \tag{B.7}$$

At this point, it is convenient to define the parameters,

$$\upsilon_{\nu\eta} = \frac{\mu_{\nu\eta}}{\sigma_n^2} = Z + 2\sum_{k=1}^{Z-1} \rho_k^n \sum_{l=k}^{Z-1} \cos(\Delta\Phi_k^\eta(l)), \tag{B.8}$$

$$\upsilon_{\nu\zeta}^c = \frac{\mu_{\nu\zeta}^c}{\sigma_n^2} = [\sum_{k=0}^{Z-1} \rho_k^n \sum_{l=k}^{Z-1} [e^{j(\Delta\Phi_l^\zeta(l) - \Delta\Phi_{l-k}^\nu(l-k))} + e^{-j(\Delta\Phi_l^\nu(l) - \Delta\Phi_{l-k}^\zeta(l-k))}]] \tag{B.9}$$

where $\rho_k^n = \frac{R_k^n}{R_0^n} = \frac{R_k^n}{\sigma_n^2}$. We remind the reader that σ_n^2 is the noise power, coming through the $H_R(\omega)$ filter ($\sigma_n^2 = E\{|n_k|^2\} = R_o^n$). $\upsilon_{\nu\eta}$, $\upsilon_{\nu\zeta}^c$ represent the normalized variance and covariance respectively. When $E\{n_k n_{k-l}^*\} = 0$

$\forall \quad l \neq 0$ (i.e. when the n_k noise terms happen to be uncorrelated with each other) then $v_{\nu\nu}$, $v_{\nu\zeta}$ and $v^c_{\nu\zeta}$ become: $v_{\nu\nu} = v_{\nu\zeta} = Z$ and $v^c_{\nu\zeta} = \sum_{k=0}^{Z-1} c^\nu_k (c^\zeta_k)^*$.

One interesting observation coming from Eqs.(B.8) to (B.9) is that for the case where the noise terms happen to be correlated, the $v_{\nu\nu}$, $v_{\nu\zeta}$ and $v^c_{\nu\zeta}$ are dependent on the entire sequences $\bar{C}(\bar{A}^\nu)$, $\bar{C}(\bar{A}^\zeta)$. On the contrary, when n_k are independent, $v_{\nu\nu}$, $v_{\nu\zeta}$ become independent from the data sequences. Also, $v^c_{\nu\zeta}$ depends only on the symbols c^ν_i, c^ζ_i that belong to the segment(s) of divergence between $\bar{C}(\bar{A}^\nu)$ and $\bar{C}(\bar{A}^\zeta)$, i.e. only from those symbols that happen to be $c^\nu_i \neq c^\zeta_i$ (in the other case, $c^\nu_i (c^\zeta_i)^* = |c^\nu_i|^2 = 1$). The case of equal apportioning of the Nyquist filter between transmitter and receiver (i.e. $\varepsilon = 0.5$) falls into the second category.

Using the material of [214, pp.223-228] we find the following expression for the $P(\{\bar{C}(\bar{A}^\zeta) \leftarrow \bar{C}(\bar{A}^\nu)\})$.

$$\begin{aligned} P(\{\bar{C}(\bar{A}^\zeta) \leftarrow \bar{C}(\bar{A}^\nu)\}) \;=\; & Q_f\left(\frac{1}{\sigma_n}\alpha_{[\nu,\zeta]}, \frac{1}{\sigma_n}\beta_{[\nu,\zeta]}\right) \\ & -\frac{1}{2}\left[1 + \frac{v_{\nu\nu} - v_{\nu\zeta}}{[(v_{\nu\nu} + v_{\nu\zeta})^2 - 4|v^c_{\nu\zeta}|^2]^{\frac{1}{2}}}\right] \\ & I_o\left(\frac{1}{\sigma_n}\alpha_{[\nu,\zeta]}\frac{1}{\sigma_n}\beta_{[\nu,\zeta]}\right) \exp\left(-\frac{1}{\sigma_n^2}\frac{\alpha^2_{[\nu,\zeta]} + \beta^2_{[\nu,\zeta]}}{2}\right) \end{aligned} \tag{B.10}$$

with $Q_f(x,y)$ being the Marcum's Q function [242, p. 585] and

$$\left\{ \begin{array}{c} \alpha_{[\nu,\zeta]} \\ \beta_{[\nu,\zeta]} \end{array} \right\} = \left[\frac{1}{v_{\nu\nu} + v_{\nu\zeta}}\left(\frac{|\bar{E}^\nu_\nu|^2 + |\bar{E}^\nu_\zeta|^2 - 2Re\{(\bar{E}^\nu_\nu)^* \bar{E}^\nu_\zeta \gamma_{\nu\zeta}\}}{1 - |\gamma_{\nu\zeta}|^2} \mp \frac{|\bar{E}^\nu_\nu|^2 - |\bar{E}^\nu_\zeta|^2}{\sqrt{1 - |\gamma_{\nu\zeta}|^2}}\right)\right]^{\frac{1}{2}} \tag{B.11}$$

with

$$\gamma_{\nu\zeta} = \frac{2v^c_{\nu\zeta}}{(v_{\nu\nu} + v_{\nu\zeta})} \,. \tag{B.12}$$

For high $\frac{E_b}{N_o}$ $Q_f(x,y)$, $I_0(x)$ can be approximated as follows:

$$Q_f(x,y) \approx \begin{cases} e^{(-\frac{y^2}{2})} & \text{for } x = 0 \\ \frac{1}{\sqrt{2\pi xy}} e^{(-\frac{[y-x]^2}{2})} & \text{for } x > 0, \end{cases} \tag{B.13}$$

$$I_0(z) = \frac{e^{|z|}}{\sqrt{2\pi|z|}} \tag{B.14}$$

The expression at the right side of Eq.(B.13) is actually an upper bound for $Q_f(x,y)$. When $x >> 1, y >> 1$, and $(y-x)^2 >> 0$ this bound becomes tight (see [242]). Application of these approximations on Eq.(B.10) provides the following upper bound expression for $P(\{\bar{C}(\bar{A}^\varsigma) \leftarrow \bar{C}(\bar{A}^\nu)\})$:

$$P(\{\bar{C}(\bar{A}^\varsigma) \leftarrow \bar{C}(\bar{A}^\nu)\}) \leq B^Z_{[\nu,\varsigma]} = \frac{1}{2}\Lambda(\bar{C}(\bar{A}^\nu), \bar{C}(\bar{A}^\varsigma)) \exp\{-\frac{1}{\sigma_n^2}\frac{(\alpha_{[\nu,\varsigma]} - \beta_{[\nu,\varsigma]})^2}{2}\} \tag{B.15}$$

with

$$\Lambda(\bar{C}(\bar{A}^\nu), \bar{C}(\bar{A}^\varsigma)) = \begin{cases} 1 & \text{for } \alpha_{[\nu,\varsigma]} = 0 \\ [1 - \frac{v_{\nu\nu} - v_{\nu\varsigma}}{[(v_{\nu\nu}+v_{\nu\varsigma})^2 - 4|v^c_{\nu\varsigma}|^2]^{\frac{1}{2}}}] \frac{1}{\sqrt{2\pi\frac{1}{\sigma_n^2}\alpha_{[\nu,\varsigma]}\beta_{[\nu,\varsigma]}}} & \text{for } \alpha_{[\nu,\varsigma]} \neq 0. \end{cases} \tag{B.16}$$

When n_k are uncorrelated ($v_{\nu\nu} - v_{\nu\varsigma} = 0$) and the y_k samples are free from ISI, the following equations are valid:

$$(\alpha_{[\nu,\varsigma]} - \beta_{[\nu,\varsigma]})^2 = Z - |\sum_{k=0}^{Z-1} c_k^\nu (c_k^\varsigma)^*|, \quad \alpha_{[\nu,\varsigma]}\beta_{[\nu,\varsigma]} = \frac{|\sum_{k=0}^{N-1} c_k^\nu (c_k^\varsigma)^*|}{2} \tag{B.17}$$

and $B^Z_{[\nu,\varsigma]}$ becomes equal to:

$$B^Z_{[\nu,\varsigma]} = \frac{1}{2}\Lambda_{IC}(\bar{C}(\bar{A}^\nu), \bar{C}(\bar{A}^\varsigma)) \exp\{-\frac{1}{\sigma_n^2}(Z - |\sum_{k=0}^{Z-1} c_k^\nu (c_k^\varsigma)^*|)\} \tag{B.18}$$

with $\Lambda_{IC}(\bar{C}(\bar{A}^{\nu}), \bar{C}(\bar{A}^{\zeta}))$ being equal to :

$$\Lambda_{IC}(\bar{C}(\bar{A}^{\nu}), \bar{C}(\bar{A}^{\zeta})) = \begin{cases} 1 & \text{for } \sum_{k=0}^{Z-1} c_k^{\nu}(c_k^{\zeta})^* = 0 \\ \frac{1}{\sqrt{2\pi}} \frac{1}{\sqrt{\frac{1}{\sigma_n^2}}} \frac{\sqrt{2}}{\sqrt{|\sum_{k=0}^{Z-1} c_k^{\nu}(c_k^{\zeta})^*|}} & \text{elsewhere.} \end{cases} \tag{B.19}$$

In Eq.(B.15), the $\exp\{-\frac{1}{\sigma_n^2}\frac{(\alpha_{[\nu,\zeta]}-\beta_{[\nu,\zeta]})^2}{2}\}$ is the dominant term which determines the value of the pairwise error probability. Its value becomes smaller as $(\alpha_{[\nu,\zeta]} - \beta_{[\nu,\zeta]})^2$ becomes larger. We define the

$$D^Z_{[\nu,\zeta]} = \frac{|\alpha_{[\nu,\zeta]} - \beta_{[\nu,\zeta]}|^2}{2} \tag{B.20}$$

to provide a distance quantity for the non-coherent receiver, equivalent to the Euclidean distance used for the coherently detected schemes. As the minimum of the Euclidean distances characterizes the performance of the coherently detected system for high E_b/N_o, the minimum of the distance metrics $D^Z_{[\nu,\zeta]}$ characterizes the performance of the non-coherent systems. From Eq.(B.18) we realize that when $R_l^n = 0 \ \forall \ l \neq 0$ (i.e. the n_k terms are uncorrelated) and no ISI is present, $D^Z_{[\nu,\zeta]}$ is equal to

$$D^Z_{IC[\nu,\zeta]} = \frac{Z - |\sum_{k=0}^{Z-1} c_k^{\nu}(c_k^{\zeta})^*|}{2}. \tag{B.21}$$

Appendix C

Exact Upper Bound of the Uncoded MPSK with Non-Coherent Block Decoding

Exact Upper Bound for the ISI and Noise Correlation Free Systems

In Fig. C.1, the trellis diagram of the M-ary PSK signal is illustrated. There are M different states G_i ($0 \leq i \leq M-1$), each one being associated with a phase value φ_i. φ_i is equal to the value ϕ_k^ν would have if the path of $\bar{C}(\bar{A}^\nu)$ goes through G_i at kT (i.e. $\varphi_i = \phi_k^\nu$, where ϕ_k^ν represents the value ϕ_k has, when $\bar{C}(\bar{A}^\nu)$ is the transmitted sequence). The value of φ_i is defined as follows :

$$\varphi_i = \frac{2\pi i}{M} \quad (0 \leq i \leq M-1). \tag{C.1}$$

Notice that the value of φ_i depends only on the state G_i. As a result, the value of ϕ_k^ν depends only on the state which happens to be the destination of the transition (from $(k-1)T$ to kT). Notice should also be made that there is a full connectivity between the states (i.e., from every state, transitions occur towards any other state, including itself).

Let us assume that $\bar{C}(\bar{A}^\lambda)$ has been transmitted, with

$$\bar{C}(\bar{A}^\lambda) = [1, e^{j(i_1^\lambda \frac{2\pi}{M})}, e^{j(i_2^\lambda \frac{2\pi}{M})}, \ldots, e^{j(i_{2-1}^\lambda \frac{2\pi}{M})}] \tag{C.2}$$

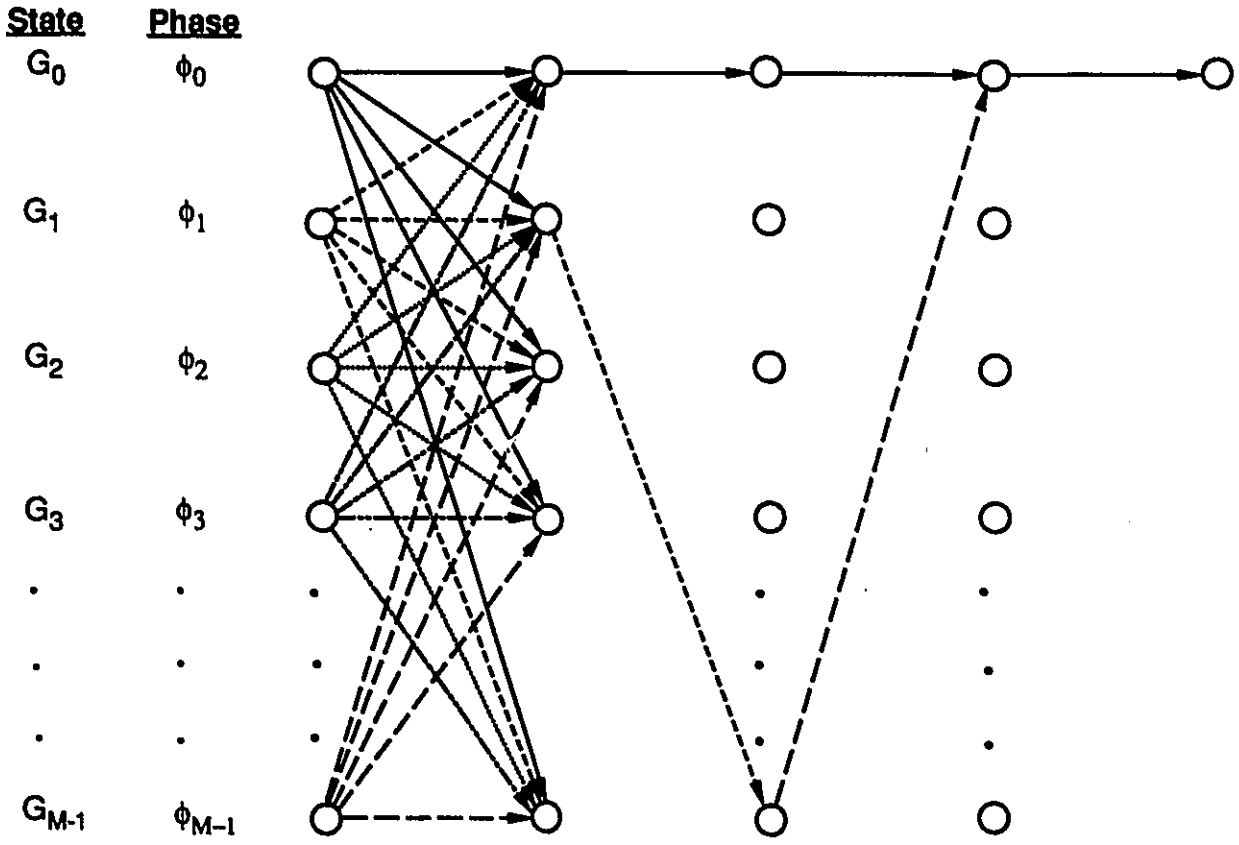

Figure C.1: Trellis Diagram of the Uncoded MPSK Signal.

(i_k^λ is integer with $0 \leq i_k^\lambda \leq M-1$ and $1 \leq k \leq Z-1$). The first step is to find the upper bound of the pairwise error probability for the error event $\{\bar{C}(\bar{A}^\eta)) \leftarrow \bar{C}(\bar{A}^\lambda)\}$.

$$\bar{C}(\bar{A}^\eta) = [1, e^{j(i_1^\eta \frac{2\pi}{M})}, e^{j(i_2^\eta \frac{2\pi}{M})}, \ldots, e^{j(i_{M-1}^\eta \frac{2\pi}{M})}] \tag{C.3}$$

(i_k^η is integer with $0 \leq i_k^\eta \leq M-1$ and $1 \leq k \leq Z-1$). Following the results of Appendix B (see Eqs.(B.15), (B.16)) the reader can easily verify that:

$$B_{[\nu,\zeta]}^Z = \frac{1}{2}\Upsilon(0, i_1^{\lambda,\eta}, i_2^{\lambda,\eta}, \ldots, i_{Z-1}^{\lambda,\eta}) \exp\{-\frac{1}{2\sigma_n^2}[Z - |1 + \sum_{k=1}^{Z-1} \exp[-j\frac{2\pi}{M}(i_1^{\lambda,\eta} \oplus i_2^{\lambda,\eta} \oplus \cdots \oplus i_k^{\lambda,\eta})_{mod(M)}]|]\} \tag{C.4}$$

with $\Upsilon(0, i_1^{\lambda,\eta}, i_2^{\lambda,\eta}, \ldots, i_{Z-1}^{\lambda,\eta}) = \Lambda_{IC}(\bar{C}(\bar{A}^\lambda), \bar{C}(\bar{A}^\eta))$ and $i_k^{\lambda,\eta} = (i_k^\lambda \ominus i_k^\eta)_{mod(M)}$ $(1 \leq k \leq Z-1)$. Using Eq. (B.19), $\Upsilon(i_0^{\lambda,\eta}, i_1^{\lambda,\eta}, \ldots, i_{Z-1}^{\lambda,\eta})$ can be expressed as :

$$\Upsilon(i_0^{\lambda,\eta}, i_1^{\lambda,\eta}, \ldots, i_{Z-1}^{\lambda,\eta}) =$$

$$\begin{cases} 1 & \text{for } [\sum_{k=0}^{Z-1} \exp\{-j\frac{2\pi}{M}(i_0^{\lambda,\eta} \oplus \ldots \oplus i_k^{\lambda,\eta})_{mod(M)}\}] = 0 \\ \dfrac{\sqrt{\frac{\sigma_n^2}{2\pi}}\sqrt{2}}{\sqrt{\sum_{k=0}^{Z-1} \exp\{-j\frac{2\pi}{M}(i_1^{\lambda,\eta} \oplus \cdots \oplus i_k^{\lambda,\eta})_{mod(M)}\}|}} & \text{for } [\sum_{k=1}^{Z-1} \exp\{-j\frac{2\pi}{M}(i_0^{\lambda,\eta} \oplus \ldots \oplus i_k^{\lambda,\eta})_{mod(M)}\}] \neq 0 \end{cases} \tag{C.5}$$

with $i_0^{\lambda,\eta} = Arg[c_0^\lambda (c_o^\eta)^*] = \phi_o^\lambda \ominus \phi_o^\eta = 0$.

For an uncoded MPSK signal, the union bound $\mathcal{UB}^Z$ has the following expression:

$$\mathcal{UB}^Z = \frac{1}{2^{(Z-1)p}} \sum_{\{\bar{C}(\bar{A}^\nu) \in S^Z_{\bar{C}W}\}} PB^{Z,\nu} \tag{C.6}$$

where

$$PB^{Z,\nu} = \frac{1}{Z-1} \sum_{\{\bar{C}(\bar{A}^\zeta) \in S_{\bar{C}(\bar{A}^\nu)}\}} n_e(\{\bar{C}(\bar{A}^\zeta) \leftarrow \bar{C}(\bar{A}^\nu)\}) B^Z_{[\nu,\zeta]}. \tag{C.7}$$

As can be seen from Eq.(C.7), for the calculation $PB^{Z,\nu}$, a summation of $B^Z_{[\lambda,\eta]}$ over all elements $\bar{C}(\bar{A}^\eta)$ of $S_{\bar{C}(\bar{A}^\lambda)}$ has to be carried out. Due to the full connectivity of the trellis diagram, $S_{\bar{C}(\bar{A}^\lambda)}$ contains as members all sequences $\bar{C}(\bar{A}^\eta) = [1, e^{(j\frac{2\pi}{M}(i_1^\eta)_{mod(M)})}, e^{(j\frac{2\pi}{M}(i_1^\eta \oplus i_2^\eta)_{mod(M)})}, \ldots, e^{(j\frac{2\pi}{M}(i_1^\eta \oplus i_2^\eta \cdots \oplus i_{Z-1}^\eta)_{mod(M)})}]$, defined by any possible combination $\{i_1^\eta, i_2^\eta, \cdots, i_{Z-1}^\eta\}$, except the $\{i_1^\eta = i_1^\lambda, i_2^\eta = i_2^\lambda, \cdots, i_{Z-1}^\eta = i_{Z-1}^\lambda\}$. This allows us to express Eq.(C.7) as:

$$PB^{Z,\lambda} = \frac{1}{Z-1}\frac{1}{2}\frac{1}{\sqrt{\sigma_n^2}} \underbrace{\sum_{i_1^{\lambda,\eta}=0}^{M-1} \sum_{i_2^{\lambda,\eta}=0}^{M-1} \cdots \sum_{i_{Z-1}^{\lambda,\eta}=0}^{M-1}}_{i_1^{\lambda,\eta}+i_2^{\lambda,\eta}+\ldots+i_{Z-1}^{\lambda,\eta} \neq 0} [\sum_{l=1}^{Z-1} \delta_f(i_l^{\lambda,\eta})] \Upsilon(0, i_1^{\lambda,\eta}, \ldots, i_{Z-1}^{\lambda,\eta})$$
$$\exp\{-\frac{1}{2\sigma_n^2}[Z - |1 + \sum_{k=1}^{Z-1} \exp[-j\frac{2\pi}{M}(i_1^{\lambda,\eta} \oplus i_2^{\lambda,\eta} \oplus \cdots \oplus i_k^{\lambda,\eta})_{mod(M)}]|]\} \tag{C.8}$$

with

$$\delta_f(x) = \begin{cases} 0 & \text{for } x = 0 \\ 1 & \text{for } x \neq 0. \end{cases} \tag{C.9}$$

The $i_1^{\lambda,\eta} + i_2^{\lambda,\eta} + \ldots + i_{Z-1}^{\lambda,\eta} \neq 0$ condition is needed so that the $\{i_1^\eta = i_1^\lambda, i_2^\eta = i_2^\lambda, \cdots, i_{Z-1}^\eta = i_{Z-1}^\lambda\}$ combination is excluded from the summation of Eq.(C.8). Since in Eq.(C.8), $\{i_1^{\lambda,\eta}, i_2^{\lambda,\eta}, \cdots, i_{Z-1}^{\lambda,\eta}\}$ takes all possible combinations but the $\{0, 0, \cdots, 0\}$, $PB^{Z,\lambda}$ is independent from the sequence $\bar{C}(\bar{A}^\lambda)$ i.e.

$$PB^{Z,\lambda} = PB^{Z,\zeta} \quad \forall \quad \lambda, \zeta. \tag{C.10}$$

Using in Eq.(C.6) Eqs.(C.7), (C.10) we get:

$$\mathcal{UB}^Z = PB^{Z,\lambda} \tag{C.11}$$

with $\bar{C}(\bar{A}^\lambda)$ being any sequence, member of the S^Z_{CW}. Consequently,

$$\mathcal{UB}^Z = \frac{1}{Z-1}\frac{1}{2}\frac{1}{\sqrt{\sigma_n^2}} \underbrace{\sum_{i_1^{\lambda,\eta}=0}^{M-1}\sum_{i_2^{\lambda,\eta}=0}^{M-1}\cdots\sum_{i_{Z-1}^{\lambda,\eta}=0}^{M-1}}_{i_1^{\lambda,\eta}+i_2^{\lambda,\eta}+\ldots+i_{Z-1}^{\lambda,\eta}\neq 0} [\sum_{l=1}^{Z-1}\delta_f(i_l^{\lambda,\eta})]\Upsilon(0,i_1^{\lambda,\eta},\ldots,i_{Z-1}^{\lambda,\eta})$$
$$\exp\{-\frac{1}{2\sigma_n^2}[Z-|1+\sum_{k=1}^{Z-1}\exp[-j\frac{2\pi}{M}(i_1^{\lambda,\eta}\oplus i_2^{\lambda,\eta}\oplus\cdots\oplus i_k^{\lambda,\eta})_{mod(M)}]|]\} \tag{C.12}$$

Appendix D

Approximate Upper Bound of the Uncoded MPSK with Non-Coherent Block Decoding

The objective of the present Appendix is to provide an alternative bound expression, capable of characterizing the performance of the proposed receivers with lower processing load. However, before we continue with the derivation of the approximate bound, two lemmas will be given. Their content will be used later on in the derivation which will follow.

Lemma 1

Let us assume that for the sequences $\bar{C}(\bar{A}^{\varsigma})$, $\bar{C}(\bar{A}^{\nu})$, $\theta_k^{\varsigma} \neq \theta_k^{\nu}$ (θ_k^{ς} represents the value θ_k has when $\bar{C}(\bar{A}^{\varsigma})$ is the transmitted sequence). We shall prove the following two statements:

For $\theta_k^{\varsigma} \neq \theta_k^{\nu} (\Rightarrow c_k^{\varsigma} \neq c_k^{\nu})$,

Statement 1
if $\theta_{k+1}^{\varsigma} = \theta_{k+1}^{\nu} \Longrightarrow \phi_{k+1}^{\varsigma} \neq \phi_{k+1}^{\nu}$
Statement 2
if $\theta_{k-1}^{\varsigma} = \theta_{k-1}^{\nu}$ and $\phi_{k-1}^{\varsigma} \neq \phi_{k-1}^{\nu} \Longrightarrow \theta_{k-2}^{\varsigma} \neq \theta_{k-2}^{\nu}$

Proof

Statement 1

When differential encoding is applied,

$$\theta_k = \theta_{k-1} \oplus \phi_k \ . \tag{D.1}$$

From Eq. (D.1), we have $\theta^{\zeta}_{k+1} = \theta^{\zeta}_k \oplus \phi^{\zeta}_{k+1}$ and $\theta^{\nu}_{k+1} = \theta^{\nu}_k \oplus \phi^{\nu}_{k+1}$. Since $\theta^{\zeta}_{k+1} = \theta^{\nu}_{k+1}$ has been assumed,

$$\theta^{\zeta}_k \oplus \phi^{\zeta}_{k+1} = \theta^{\nu}_k \oplus \phi^{\nu}_{k+1} \Longrightarrow \phi^{\zeta}_{k+1} = \theta^{\nu}_k \ominus \theta^{\zeta}_k \oplus \phi^{\nu}_{k+1}. \tag{D.2}$$

Because $\theta^{\nu}_k \neq \theta^{\zeta}_k \Longrightarrow \theta^{\nu}_k \ominus \theta^{\zeta}_k \neq 0$. Using it in Eq. (D.2), we get $\phi^{\zeta}_{k+1} \neq \phi^{\nu}_{k+1}$, which proves the first statement.

Statement 2
$\theta^{\zeta}_{k-1} = \theta^{\zeta}_{k-2} \oplus \phi^{\zeta}_{k-1}$ and $\theta^{\nu}_{k-1} = \theta^{\nu}_{k-2} \oplus \phi^{\nu}_{k-1}$. Since $\theta^{\zeta}_{k-1} = \theta^{\nu}_{k-1}$,

$$\theta^{\zeta}_{k-2} \oplus \phi^{\zeta}_{k-1} = \theta^{\nu}_{k-2} \oplus \phi^{\nu}_{k-1} \Longrightarrow \theta^{\zeta}_{k-2} = \theta^{\nu}_{k-2} \oplus \phi^{\nu}_{k-1} \ominus \phi^{\zeta}_{k-1} \ . \tag{D.3}$$

$\phi^{\nu}_{k-1} \neq \phi^{\zeta}_{k-1} \Longrightarrow \phi^{\nu}_{k-1} \ominus \phi^{\zeta}_{k-1} \neq 0$. Use of it in Eq. (D.3), leads to $\theta^{\zeta}_{k-1} \neq \theta^{\nu}_{k-1}$, which proves the second statement.

From the first statement, the following can be concluded. If the two sequences $\bar{C}(\bar{A}^{\nu})$, $\bar{C}(\bar{A}^{\zeta})$ have $c^{\zeta}_k \neq c^{\nu}_k$, there is the possibility at $(k+1)T$ to have an information symbol error ($\phi^{\nu}_{k+1} \neq \phi^{\zeta}_{k+1} \Rightarrow g^{\nu}_{k+1} \neq g^{\zeta}_{k+1}$, with g^{ζ}_{k+1} representing the value the information symbol g_{k+1} has, when $\bar{C}(\bar{A}^{\zeta})$ is the transmitted sequence) even if c^{ν}_{k+1}, c^{ζ}_{k+1} happen to be equal ($\theta^{\nu}_{k+1} = \theta^{\zeta}_{k+1} \Longrightarrow c^{\nu}_{k+1} = c^{\zeta}_{k+1}$). Consequently, a $\{c^{\nu}_k \neq c^{\zeta}_k\}$ event might be associated with both $\{\phi^{\nu}_k \neq \phi^{\zeta}_k\}$ and $\{\phi^{\nu}_{k+1} \neq \phi^{\zeta}_{k+1}\}$ events. When a decision in favor of $\bar{C}(\bar{A}^{\zeta})$ is made, while $\bar{C}(\bar{A}^{\nu})$ has been transmitted, this would give two information symbol errors, resulting from only one "disagreement" between the symbols c^{ν}_k, c^{ζ}_k (i.e., $c^{\nu}_k \neq c^{\zeta}_k$) of the sequences $\bar{C}(\bar{A}^{\nu})$ and $\bar{C}(\bar{A}^{\zeta})$ [1].

The question "Is it possible to associate the event $\{c^{\nu}_k \neq c^{\zeta}_k\}$ with more than two information symbol errors?" is answered by the second statement, where it has been shown that in order to have a symbol error at $(k-1)T$ ($\{g^{\nu}_{k-1} \neq g^{\zeta}_{k-1}\}$) while $c^{\nu}_{k-1} = c^{\zeta}_{k-1}$, we have to have unequal symbols c^{ν}_{k-2},

[1] This behaviour is familiar to systems which differentially encode the information sequence [60].

c_{k-2}^{ζ} at $(k-2)T$ (i.e., $\{c_{k-2}^{\nu} \neq c_{k-2}^{\zeta}\}$), consequently, the $\{g_{k-1}^{\nu} \neq g_{k-1}^{\zeta}\}$ is associated with the $\{c_{k-2}^{\nu} \neq c_{k-2}^{\zeta}\}$ rather than the $\{c_k^{\nu} \neq c_k^{\zeta}\}$. Every $\{c_k^{\nu} \neq c_k^{\zeta}\}$ can be associated at most with two information symbol errors.

Lemma 2

Consider the function:

$$\Lambda_{IC}(\bar{C}(\bar{A}^{\nu}), \bar{C}(\bar{A}^{\zeta})) = \begin{cases} 1 & \text{for } \sum_{k=0}^{Z-1} c_k^{\nu}(c_k^{\zeta})^* = 0 \\ \frac{1}{\sqrt{2\pi}} \frac{1}{\sqrt{\frac{1}{\sigma_n^2}}} \frac{\sqrt{2}}{\sqrt{\left|\sum_{k=0}^{Z-1} c_k^{\nu}(c_k^{\zeta})^*\right|}} & \text{for } \sum_{k=0}^{Z-1} c_k^{\nu}(c_k^{\zeta})^* \neq 0 \end{cases} \tag{D.4}$$

Let us assume that from the Z $\{c_k^{\nu}(c_k^{\zeta})^*\}$ product terms, m of them are equal to $e^{j(\frac{2\pi}{M})}$ (i.e., $c_k^{\nu}(c_k^{\zeta})^* = e^{j(\frac{2\pi}{M})}$) [2] whereas the rest (a total of $Z-m$) are equal to 1. We shall prove that under these conditions, $\Lambda_{IC}(\bar{C}(\bar{A}^{\nu}), \bar{C}(\bar{A}^{\zeta})) = \wp(M,m)$ with

$$\wp(M,m) = \begin{cases} 1 & \text{for } M = 2 \text{ and } m = \frac{Z}{2} \\ \frac{1}{\sqrt{2\pi}} \frac{1}{\sqrt{\frac{1}{\sigma_n^2}}} \frac{\sqrt{2}}{\sqrt{Z^2+2m^2(1-\cos(\frac{2\pi}{M}))-2mZ(1-\cos(\frac{2\pi}{M}))}} & \text{elsewhere} \end{cases} \tag{D.5}$$

Proof

Let us define the function $\gamma(\{\bar{C}(\bar{A}^{\zeta}) \leftarrow \bar{C}(\bar{A}^{\nu})\}) = \sum_{k=0}^{Z-1} c_k^{\nu}(c_k^{\zeta})^*$. With the assumption made above being valid, we have:

$$\gamma(\{\bar{C}(\bar{A}^{\zeta}) \leftarrow \bar{C}(\bar{A}^{\nu})\}) = Z - m + me^{j(\frac{2\pi}{M})}. \tag{D.6}$$

At this point, it is convenient to define the function $G_Z^M(x) = 2x^2(1-\cos(\frac{2\pi}{M})) - 2x\cos(\frac{2\pi}{M}) + Z^2$. The determinant of $G_Z^M(x)$, $\Delta_G^Z(M)$ equals:

$$\Delta_G(Z,M) = -4Z^2(1-\cos(\frac{2\pi}{M}))(1+\cos(\frac{2\pi}{M})) = -4Z^2\sin^2(\frac{2\pi}{M}). \tag{D.7}$$

[2] The same results will be reached if the m c_k^{ζ} symbols instead of being equal to $e^{j\frac{2\pi}{M}}$, are equal to $e^{j((M-1)\frac{2\pi}{M})}$.

Using Eq.(D.6) it is easy to prove that:

$$\gamma_{sq}(\{\bar{C}(\bar{A}^{\varsigma}) \leftarrow \bar{C}(\bar{A}^{\nu})\}) = |\gamma(\{\bar{C}(\bar{A}^{\varsigma}) \leftarrow \bar{C}(\bar{A}^{\nu})\})|^2 = G_Z^M(m). \quad \text{(D.8)}$$

When $\gamma(\{\bar{C}(\bar{A}^{\varsigma}) \leftarrow \bar{C}(\bar{A}^{\nu})\}) = 0$, $\gamma_{sq}(\{\bar{C}(\bar{A}^{\varsigma}) \leftarrow \bar{C}(\bar{A}^{\nu})\}) = G_Z^M(m) = 0$ as well. Since $Z^2 > 0$ and $\sin^2(\frac{2\pi}{M}) > 0 \; \forall \; M > 2$, $\sin^2(\frac{2\pi}{M}) = 0$ for $M = 2$,

$$\Delta_G(Z, M) \begin{cases} < 0 & \text{for } M > 2 \\ = 0 & \text{for } M = 2. \end{cases} \quad \text{(D.9)}$$

From the theory of quadratic functions, we conclude that for $M > 2$, $G_Z^M(x)$ has two complex roots whereas for $M = 2$, there is one real root, equal to:

$$\varpi = \frac{2Z(1 - \cos(\frac{2\pi}{M}))}{4(1 - \cos(\frac{2\pi}{M}))} = \frac{Z}{2}. \quad \text{(D.10)}$$

For the first case ($\Delta_G(Z, M > 2) < 0$), $G_Z^M(x) > 0 \; \forall \; x$, with x being an arbitrary real number. For the second one ($\Delta_G(Z, M = 2) = 0$):

$$G_Z^M(x) \begin{cases} = 0 & \text{for } x = \frac{Z}{2} \\ > 0 & \text{for } x \neq \frac{Z}{2}. \end{cases} \quad \text{(D.11)}$$

Summarizing, we have :

$$G_Z^M(x) \begin{cases} = 0 & \text{for } M = 2 \text{ and } x = \frac{Z}{2} \\ > 0 & \text{elsewhere.} \end{cases} \quad \text{(D.12)}$$

Eq. (D.12) together with Eqs. (D.4), (D.6), (D.8) gives :

$$\Lambda_{IC}(\bar{C}(\bar{A}^{\nu}), \bar{C}(\bar{A}^{\varsigma})) = \begin{cases} 1 & \text{for } M = 2 \\ & \text{and } m = \frac{Z}{2} \\ \frac{1}{\sqrt{2\pi}} \frac{1}{\sqrt{\frac{1}{\sigma_n^2}}} \frac{\sqrt{2}}{\sqrt{Z^2 - 2mZ(1-\cos(\frac{2\pi}{M})) + 2m^2(1+\cos(\frac{2\pi}{M}))}} & \text{elsewhere} \end{cases} \quad \text{(D.13)}$$

which is identical with Eq. (D.5).

Derivation of the Approximate Upper Bound

Upper Bounding the number of errors associated with an error event.

Let us assume that $\bar{C}(\bar{A}^{\nu})$ has been transmitted. As first step, the elements of $\underline{S}_{\bar{C}(\bar{A}^{\nu})}$ are split into $Z-1$ different groups, $\underline{GR}_1^{Z,\nu}, \underline{GR}_2^{Z,\nu}, ..., \underline{GR}_{Z-1}^{Z,\nu}$. $\bar{C}(\bar{A}^{\zeta})$ belongs to $\underline{GR}_m^{Z,\nu}$ $(1 \leq m \leq Z-1)$, if and only if the following condition is satisfied:

$$\sum_{i=1}^{Z-1} \Im_i^{\nu,\zeta} = m \tag{D.14}$$

with

$$\Im_i^{\nu,\zeta} = \begin{cases} 1 & \text{for } c_i^{\nu}(c_i^{\zeta})^* \neq 1 \ (\Longrightarrow c_i^{\zeta} \neq c_i^{\nu} \Longrightarrow \theta_i^{\zeta} \neq \theta_i^{\nu}) \\ 0 & \text{for } c_i^{\nu}(c_i^{\zeta})^* = 1 \ (\Longrightarrow c_i^{\zeta} = c_i^{\nu} \Longrightarrow \theta_i^{\zeta} = \theta_i^{\nu}). \end{cases} \tag{D.15}$$

The meaning of Eq.(D.14) is that $\bar{C}(\bar{A}^{\zeta})$ belongs to $\underline{GR}_m^{Z,\nu}$ if and only if between $\bar{C}(\bar{A}^{\nu})$ and $\bar{C}(\bar{A}^{\zeta})$, there are m symbols $c_k^{\zeta} \neq c_k^{\nu}$ $(0 \leq k \leq Z-1)$.

We separate $\underline{GR}_m^{Z,\nu}$ in two subgroups, $\underline{G^1R}_m^{Z,\nu}$ and $\underline{G^2R}_m^{Z,\nu}$. $\underline{G^2R}_m^{Z,\nu}$ includes all members of $\underline{GR}_m^{Z,\nu}$ which happen to have their $(Z-1)^{th}$ symbol identical with that of $\bar{C}(\bar{A}^{\nu})$ (i.e., $\bar{C}(\bar{A}^{\zeta}) \in \underline{G^2R}_m^{Z,\nu}$ if and only if $\bar{C}(\bar{A}^{\zeta}) \in \underline{GR}_m^{Z,\nu}$ and $c_{Z-1}^{\zeta} = c_{Z-1}^{\nu}$). $\underline{G^1R}_m^{Z,\nu}$ includes as members, all elements of $\underline{GR}_m^{Z,\nu}$ which have their $Z-1^{th}$ symbol, different than that of $\bar{C}(\bar{A}^{\nu})$ (i.e., $\bar{C}(\bar{A}^{\zeta}) \in \underline{G^1R}_m^{Z,\nu}$ if and only if $\bar{C}(\bar{A}^{\zeta}) \in \underline{GR}_m^{Z,\nu}$ and $c_{Z-1}^{\zeta} \neq c_{Z-1}^{\nu}$). In *Lemma 1*, it was shown that every inequality between symbols of $\bar{C}(\bar{A}^{\nu})$, $\bar{C}(\bar{A}^{\zeta})$ (i.e., $c_k^{\nu} \neq c_k^{\zeta}$) can be associated with two information symbol errors ($\{g_k^{\zeta} \neq g_k^{\nu}\}$ and $\{g_{k+1}^{\zeta} \neq g_{k+1}^{\nu}\}$ or equivalently, $\{\phi_k^{\zeta} \neq \phi_k^{\nu}\}$ and $\{\phi_{k+1}^{\zeta} \neq \phi_{k+1}^{\nu}\}$). Following the conclusion of *Lemma 1*, we realize that the maximum number of information symbols $g_k^{\nu} \neq g_k^{\zeta}$ which can be found between elements of $\underline{G^2R}_m^{Z,\nu}$ and $\bar{C}(\bar{A}^{\nu})$ is $2m$, whereas for the members of $\underline{G^1R}_m^{Z,\nu}$ it is $(2m-1)$ (since there is no symbol transmitted after $(Z-1)T$, the $\{c_{Z-1}^{\zeta} \neq c_{Z-1}^{\nu}\}$ event will be associated with at most one information symbol error, i.e $\{g_{Z-1}^{\zeta} \neq g_{Z-1}^{\nu}\}$). However, since there is a total of $Z-1$ symbols transmitted, the number of unequal symbols between two sequences is at most equal to $Z-1$. Summarizing the above discussion, we come up with the following upper bounding expression for $\eta_e(\{\bar{C}(\bar{A}^{\zeta}) \longleftarrow \bar{C}(\bar{A}^{\nu})\})$.

With $\bar{C}(\bar{A}^{\zeta}) \in \underline{GR}_m^{Z,\nu}$,

$$\eta_e(\{\bar{C}(\bar{A}^{\zeta}) \longleftarrow \bar{C}(\bar{A}^{\nu})\}) \leq n_e^b(m) = \begin{cases} 2m & \text{for } m \leq \lceil \frac{Z-1}{2} \rceil \\ & \quad \text{and } c_{Z-1}^{\zeta} = c_{Z-1}^{\nu} \\ & \quad (i.e., \bar{C}(\bar{A}^{\zeta}) \in \underline{G^2 R}_m^{Z,\nu}) \\ 2m-1 & \text{for } m \leq \lceil \frac{Z-1}{2} \rceil \\ \vdots & \quad \text{and } c_{Z-1}^{\zeta} \neq c_{Z-1}^{\nu} \\ & \quad (i.e., \bar{C}(\bar{A}^{\zeta}) \in \underline{G^1 R}_m^{Z,\nu}) \\ Z-1 & \text{for } m > \lceil \frac{Z-1}{2} \rceil. \end{cases} \tag{D.16}$$

Minimum Distance between members of $\underline{\mathbf{GR}}_{\mathbf{m}}^{\mathbf{Z},\nu}$ and $\bar{\mathbf{C}}(\bar{\mathbf{A}}^{\nu})$.

Since a sequence $\bar{C}(\bar{A}^{\zeta}) \in \underline{GR}_m^{Z,\nu}$, has m symbols of $c_k^{\zeta} \neq c_k^{\nu}$, it will have the following distance expression with $\bar{C}(\bar{A}^{\nu})$:

$$D_{[\nu,\zeta]}^{Z} = [Z - |Z - m + \sum_{i=1}^{Z-1} \delta_f(\theta_i^{\zeta} \ominus \theta_i^{\nu}) e^{j(\theta_i^{\nu} \ominus \theta_i^{\zeta})}|]^{\frac{1}{2}}. \tag{D.17}$$

$D_{[\nu,\zeta]}^{Z}$ becomes minimum when one of the following two conditions is satisfied:

$$\forall \quad \theta_i^{\zeta} \neq \theta_i^{\nu}, \quad \theta_i^{\zeta} = \theta_i^{\nu} \oplus \frac{2\pi}{M} \quad (1 \leq i \leq Z-1) \tag{D.18}$$

or

$$\forall \quad \theta_i^{\zeta} \neq \theta_i^{\nu}, \quad \theta_i^{\zeta} = \theta_i^{\nu} \oplus (M-1)\frac{2\pi}{M} \quad (1 \leq i \leq Z-1) \tag{D.19}$$

These values, used with Eq.(D.17) give:

$$D_{min_{\underline{GR}_m^{Z,\nu}}}^{Z} = \sqrt{Z^2 + 2m^2 - 2Zm + 2(Z-m)m\cos(\frac{2\pi}{M})} \tag{D.20}$$

where $D^Z_{min_{\underline{GR}^{Z,\nu}_m}}$ is the smallest distance which we can find between elements of $\underline{GR}^{Z,\nu}_m$ and $\bar{C}(\bar{A}^\nu)$.

For high E_b/N_o, the elements of $\underline{GR}^{Z,\nu}_m$ having distance equal to $D^Z_{min_{\underline{GR}^{Z,\nu}_m}}$ are the ones which give the highest contribution to the value of the error bound. The rest of them, having values of $B^Z_{[\nu,\zeta]}$ orders of magnitude smaller, can be ignored. At this point, it is convenient to define the $\underline{G^1_{min}R}^{Z,\nu}_m$, $\underline{G^2_{min}R}^{Z,\nu}_m$, $\underline{G^\cup_{min}R}^{Z,\nu}_m$. $\underline{G^1_{min}R}^{Z,\nu}_m$ ($\underline{G^2_{min}R}^{Z,\nu}_m$) is the set consisting of all sequences $\bar{C}(\bar{A}^\zeta) \in \underline{G^1R}^{Z,\nu}_m(\underline{G^2R}^{Z,\nu}_m)$, which happen to have minimum distance with $\bar{C}(\bar{A}^\nu)$ ($D^Z_{min_{\underline{GR}^{Z,\nu}_m}}$). The set $\underline{G^\cup_{min}R}^{Z,\nu}_m$ includes as members all elements of $\underline{G^1_{min}R}^{Z,\nu}_m$ and $\underline{G^2_{min}R}^{Z,\nu}_m$ together (i.e $\underline{G^\cup_{min}R}^{Z,\nu}_m = \underline{G^1_{min}R}^{Z,\nu}_m \bigcup \underline{G^2_{min}R}^{Z,\nu}_m$, where $\bigcup$ represents the union operation between sets). $\underline{N^1_{min}S}^{Z,\nu}_m$, $\underline{N^2_{min}S}^{Z,\nu}_m$ is the number of elements $\underline{G^1_{min}R}^{Z,\nu}_m$, $\underline{G^2_{min}R}^{Z,\nu}_m$ have respectively. Using only the sequences, members of $\underline{G^1_{min}R}^{Z,\nu}_m$, $\underline{G^2_{min}R}^{Z,\nu}_m$ in $PB^{Z,\nu}$ (see Eq.(C.7) of Appendix C) and replacing $n_e(\{\bar{C}(\bar{A}^\zeta) \leftarrow \bar{C}(\bar{A}^\nu)\})$ with $n^b_e(m)$, we end up with the following approximation of $PB^{Z,\nu}$:

$$
\begin{aligned}
PB^{Z,\nu}_{app.} \;=\; & \frac{1}{Z-1}\Big(\sum_{m=1}^{\lceil\frac{Z-1}{2}\rceil} 2m\Big[\sum_{\{\bar{C}(\bar{A}^\zeta) \in \underline{G^2_{min}R}^{Z,\nu}_m\}} B^Z_{[\nu,\zeta]}\Big] + (2m-1) \\
& \Big[\sum_{\{\bar{C}(\bar{A}^\zeta) \in \underline{G^1_{min}R}^{Z,\nu}_m\}} B^Z_{[\nu,\zeta]}\Big] \\
& +(Z-1)\Big(\sum_{m=\lceil\frac{Z-1}{2}\rceil+1}^{Z-1}\Big[\sum_{\{\bar{C}(\bar{A}^\zeta) \in \underline{G^\cup_{min}R}^{Z,\nu}_m\}} B^Z_{[\nu,\zeta]}\Big]\Big).
\end{aligned}
\tag{D.21}
$$

Replacing $PB^{Z,\nu}$ with $PB^{Z,\nu}_{app.}$ in Eq.(C.6) of Appendix C, we get the following approximate expression of $\mathcal{UB}^Z$.

$$
\mathcal{UB}^Z_{app.} = \frac{1}{2^{(Z-1)p}} \sum_{\{\bar{C}(\bar{A}^\nu) \in S^Z_{CW}\}} PB^{Z,\nu}_{app.} \tag{D.22}
$$

When ISI and noise correlation are not present, it can be shown that $PB^{Z,\nu}_{app.} = PB^{Z,\xi}_{app.}\ \forall\ \nu,\xi\ \in\ S^Z_{\bar{C}W}$. This reduces the expression of $\mathcal{U}B^Z_{app.}$ to $\mathcal{U}B^Z_{app.} = PB^{Z,\nu}_{app.}$ ($\bar{C}(\bar{A}^\nu)$ can be any member of $S^Z_{\bar{C}W}$) which, together with Eqs.(B.18), (B.19) and *Lemma 2* (Eq.(D.5)), leads to:

$$\mathcal{U}B^Z_{app.} = \frac{1}{Z-1}\frac{1}{2}\sum_{m=1}^{Z-1} N_e^B(M,m)\wp(M,m) \exp\{-\frac{1}{2\sigma_n^2}(Z-\sqrt{Z^2+2m^2-2Zm+2(Z-m)m\cos(\frac{2\pi}{M})}\} \tag{D.23}$$

with

$$N_e^B(M,m) = \begin{cases} 2m\underline{N^2_{min}S^{Z,\nu}_m} + (2m-1)\underline{N^1_{min}S^{Z,\nu}_m} & \text{for } m \le \lceil\frac{Z-1}{2}\rceil \\ Z-1 & \text{for } m > \lceil\frac{Z-1}{2}\rceil\ . \end{cases} \tag{D.24}$$

The last step of this Appendix is to calculate $N_e^B(M,m)$ as a function of only M, m. At first, let us assume that the values of θ_k^ζ follow Eq.(D.18) (i.e. if $\theta_i^\zeta \neq \theta_i^\nu$, $\theta_i^\zeta = \theta_i^\nu \oplus \frac{2\pi}{m}$). There are $\binom{Z-2}{m} = \frac{(Z-2)!}{m!(Z-m-2)!}$ different ways to distribute the m $c_i^\zeta \neq c_i^\nu$ symbols (or equivalently, the $\theta_i^\zeta \neq \theta_i^\nu$ phases) between T and $(Z-2)T$. Each one gives a sequence element of $\underline{G^2_{min}R^{Z,\nu}_m}$ ($k!$ means k factorial). For the $\underline{G^1R^{Z,\nu}_m}$ subset, there are $\binom{Z-2}{m-1} = \frac{(Z-2)!}{(m-1)!(Z-m-1)!}$ ways to distribute the $m-1$ phases in the $(T,(Z-2)T)$ interval (the last phase $\theta_i^\zeta \neq \theta_i^\nu$ has to be at $Z-1$ since $c^\zeta_{Z-1} \neq c^\nu_{Z-1}$).

For $M > 2$ (QPSK,8PSK,16PSK, etc.), the case described by Eq.(D.19) (i.e. if $\theta_i^\zeta \neq \theta_i^\nu$, $\theta_i^\zeta = \theta_i^\nu \oplus \frac{2\pi}{M}(M-1)$ $(1 \le i \le Z-1)$) will give additional $\binom{Z-2}{m}$ and $\binom{Z-2}{m-1}$ sequences, members of $\underline{G^2_{min}R^{Z,\nu}_m}$, $\underline{G^1_{min}R^{Z,\nu}_m}$ respectively, making the total number of $\underline{N^2_{min}S^{Z,\nu}_m} = 2\binom{Z-2}{m}$ (for $\underline{G^2R^{Z,\nu}_m}$)

and $\underline{N^1_{min}S^{Z,\nu}_m} = 2\begin{pmatrix} Z-2 \\ m-1 \end{pmatrix}$ (for $\underline{G^1R^{Z,\nu}_m}$). For BPSK ($M = 2$), $\frac{2\pi}{M} = \frac{2\pi}{M}(M-1)$ and the two cases described by Eqs. (D.18), (D.19) are identical. Consequently for BPSK, the number of the minimum distance sequences will be: i) $\underline{N^2_{min}S^{Z,\nu}_m} = \begin{pmatrix} Z-2 \\ m \end{pmatrix}$ (for $\underline{G^2R^{Z,\nu}_m}$) and ii) $\underline{N^1_{min}S^{Z,\nu}_m} = \begin{pmatrix} Z-2 \\ m-1 \end{pmatrix}$ (for $\underline{G^1R^{Z,\nu}_m}$). Eq. (D.24) used with the comments presented above, provides the following upper bound expression regarding the number of errors contributed by the members of $\underline{G^1_{min}R^{Z,\nu}_m}$, $\underline{G^2_{min}R^{Z,\nu}_m}$:

$$N^B_e(M,m) = \begin{cases} [1+\delta_f(log_2(M)-1)] & \\ [2m\begin{pmatrix} Z-2 \\ m \end{pmatrix} + (2m-1)\begin{pmatrix} Z-2 \\ m-1 \end{pmatrix}] & \text{for } m \leq \lceil\frac{Z-1}{2}\rceil \\ & \\ [1+\delta_f(log_2(M)-1)] & \\ [(Z-1)[\begin{pmatrix} Z-2 \\ m \end{pmatrix} + \begin{pmatrix} Z-2 \\ m-1 \end{pmatrix}] & \text{for } m > \lceil\frac{Z-1}{2}\rceil \end{cases}$$

(D.25)

Appendix E

Supplementary to Appendix F

Let us consider the complex Gaussian random variable F and the real positive number $\mathcal{J}$. We assume that F has an average $\bar{F}$ with $\bar{F}$ being a positive number. F can be expressed as :

$$F = \bar{F} + N_I + jN_Q. \tag{E.1}$$

N_I, N_Q are zero mean Gaussian random variables having the following properties :

$$E\{N_I\} = E\{N_Q\} = 0,$$

$$E\{(N_I)^2\} = \sigma^2_{N,I},$$

$$E\{(N_Q)^2\} = \sigma^2_{N,Q},$$

$$E\{N_I N_Q\} = 0 \tag{E.2}$$

their pdf being equal to $f_{N_W}(u) = \frac{1}{\sqrt{2\pi}\sigma_{N_W}} \exp\{-\frac{u^2}{2\sigma^2_{N_W}}\}$, with $W \in \{I, Q\}$.

Let us define the functions:

$$g_1(F, \mathcal{J}) = |F - \mathcal{J}|, \qquad g_2(F, \mathcal{J}) = |F| - \mathcal{J}\ . \tag{E.3}$$

We shall prove that as $\sigma^2_{N_Q} \to 0$ the following equation holds with probability 1.

$$g_1(F,\mathcal{J}) - g_2(F,\mathcal{J}) \simeq \begin{cases} 0 & \text{for } N_I > \mathcal{J} - \bar{F} \\ 2(\mathcal{J} - \bar{F} - N_I) & \text{for } \mathcal{J} - \bar{F} > N_I > -\bar{F} \\ 2\mathcal{J} & \text{for } N_I < -\bar{F} \end{cases} \quad \text{(E.4)}$$

Proof :

For convenience we define the function:

$$g_3(F,\mathcal{J}) = g_1(F,\mathcal{J}) - g_2(F,\mathcal{J}) = |F - \mathcal{J}| - (|F| - \mathcal{J}) \quad \text{(E.5)}$$

The theory of complex numbers gives that $|\zeta_1 - \zeta_2| \geq |\zeta_1| - |\zeta_2|$ (with ζ_1, ζ_2 being two arbitrary complex numbers). Using it, we can easily verify that :

$$g_3(F,\mathcal{J}) \geq 0 \quad \text{(E.6)}$$

The average of $g_3(F,\mathcal{J})$ with respect to N_Q equals :

$$\overline{g_3(F,\mathcal{J})_{N_Q}} = \int_{-\infty}^{\infty} (|\bar{F} - \mathcal{J} + N_I + jN_Q| - (|\bar{F} + N_I + jN_Q| - \mathcal{J}))f_{N_Q}(u)du \quad \text{(E.7)}$$

For $\sigma^2_{N_Q} \to 0$ $f_{N_Q}(u) \to \delta(u)$ ($\delta(u)$ is the delta function), leading to the following value for $\overline{g_3(F,\mathcal{J})_{N_Q}}$:

$$\overline{g_3(F,\mathcal{J})_{N_Q}} \underbrace{\Longrightarrow}_{\sigma^2_{N_Q} \to 0} |\bar{F} - \mathcal{J} + N_I| - (|\bar{F} + N_I| - \mathcal{J}). \quad \text{(E.8)}$$

Use of

$$|x| = \begin{cases} x & \text{for } x \geq 0 \\ -x & \text{for } x < 0 \end{cases} \quad \text{(E.9)}$$

(x represents a real number) with Eq.(E.8) gives:

$$\overline{g_3(F,\mathcal{J})_{N_Q}} = \begin{cases} 0 & \text{for } N_I > \mathcal{J} - \bar{F} \\ 2(\mathcal{J} - \bar{F} - N_I) & \text{for } \mathcal{J} - \bar{F} > N_I > -\bar{F} \\ 2\mathcal{J} & \text{for } N_I < -\bar{F} \end{cases} . \tag{E.10}$$

From Chebychev's inequality [203, Eq.(5.50 (a))], we have :

$$P\{|g_3(F,\mathcal{J}) - \overline{g_3(F,\mathcal{J})_{N_Q}}|\} \geq 1 - \frac{\sigma_{f_I}^2}{\epsilon^2} \tag{E.11}$$

with ϵ being a positive number and $\sigma_{f_I}^2$ the variance of $g_3(F,\mathcal{J})$ given N_I.

$$\begin{aligned} \sigma_{f_I}^2 &= \int_{-\infty}^{\infty} [g_3(\bar{F} + N_I + ju, \mathcal{J}) - \overline{g_3(F,\mathcal{J})_{N_Q}}]^2 f_{N_Q}(u) du \\ &\underbrace{\longrightarrow}_{\sigma_{N_Q}^2 \to 0} [(|F - \mathcal{J} + N_I| - |F + N_I| - \mathcal{J}) \\ &- (|F - \mathcal{J} + N_I| - |F + N_I| + \mathcal{J})]^2 = 0 \end{aligned} \tag{E.12}$$

In Eq. (E.12) the $f_{N_Q}(u) \underbrace{\longrightarrow}_{\sigma_{N_Q}^2 \to 0} \delta(u)$ has been used. Since $1 - \frac{\sigma_{f_I}^2}{\epsilon^2} \underbrace{\longrightarrow}_{\sigma_{N_Q}^2 \to 0} 1$, we have (from Eq. (E.11)) :

$$P(|g_3(F,\mathcal{J}) - \overline{g_3(F,\mathcal{J})_{N_Q}}| \leq \epsilon) \underbrace{\longrightarrow}_{\sigma_{N_Q}^2 \to 0} 1 . \tag{E.13}$$

Assuming that ϵ becomes infinitesimally small and using Eq.(E.13), we arrive at

$$P(g_3(F,\mathcal{J}) \simeq \overline{g_3(F,\mathcal{J})_{N_Q}}) \underbrace{\longrightarrow}_{\sigma_{N_Q}^2 \to 0} 1 . \tag{E.14}$$

Eq.(E.10) together with (E.14) leads to the conclusion that for $\sigma_{N_Q}^2 \to 0$:

$$g_3(F,\mathcal{J}) = \begin{cases} 0 & \text{for } N_I > \mathcal{J} - \bar{F} \\ 2(\mathcal{J} - \bar{F} - N_I) & \text{for } \mathcal{J} - \bar{F} \geq N_I \geq -\bar{F} \\ 2\mathcal{J} & \text{for } N_I < -\bar{F} \end{cases} \tag{E.15}$$

with probability 1.

Appendix F

Upper Bound of the Pairwise Error Event Probability for the Asymptotically Optimal Non-Coherent Sequence Estimator

Let us assume that the sequence $\bar{C}(\bar{A}^{\nu})$ is the transmitted information sequence. Assume that $\bar{C}(\bar{A}^{\nu})$ is compared to $\bar{C}(\bar{A}^{\varsigma})$, the decision being based on the maximization of the metric $\aleph_{HAO}^{PSK}(\bar{h}, \bar{y}, \bar{C}(\bar{A}))$ presented in Eq.(4.9) of Chapter 4. The criterion which will choose one over the other sequence is the following :

$$|F_Z^{\nu}(\bar{y}, \bar{C}(\bar{A}^{\nu}))| - IST(\bar{h}, \bar{C}(A^{\nu})) \underset{\bar{A}^{\varsigma}}{\overset{\bar{A}^{\nu}}{\gtrless}} |F_Z^{\nu}(\bar{y}, \bar{C}(\bar{A}^{\varsigma}))| - IST(\bar{h}, \bar{C}(\bar{A}^{\varsigma})) \tag{F.1}$$

(for the definition of the $F_Z^{\nu}(\bar{y}, \bar{C}(\bar{A}^{i}))$ see Eq.(B.2) of Appendix B). The decision rule of Eq. (F.1) can be equivalently expressed as :

Decision Law 1 (DL1)

$$|F_Z^{\nu}(\bar{y},\bar{C}(\bar{A}^{\nu}))| + \mathcal{D}_Z^{\zeta,\nu}(\bar{h}) \underset{\bar{A}^{\zeta}}{\overset{\bar{A}^{\nu}}{\gtrless}} |F_Z^{\nu}(\bar{y},\bar{C}(\bar{A}^{\zeta}))| \tag{F.2}$$

with

$$\begin{aligned}\mathcal{D}_Z^{i,\eta}(\bar{h}) &= IST(\bar{h},\bar{C}(\bar{A}^{i})) - IST(\bar{h},\bar{C}(\bar{A}^{\eta})) \\ &= \sum_{l=1}^{Z-1}\sum_{k=l}^{Z-1} Re\{h_l[c_k^i(c_{k-l}^i)^* - c_k^{\eta}(c_{k-l}^{\eta})^*]\}\end{aligned} \tag{F.3}$$

In Appendix B, it has been shown that $F_Z^{\nu}(\bar{y},\bar{C}(\bar{A}^{\nu}))$, $F_Z^{\nu}(\bar{y},\bar{C}(\bar{A}^{\zeta}))$ are complex Gaussian random variables, their averages $\bar{E}_{\nu}^{\nu}$, $\bar{E}_{\zeta}^{\nu}$ being described by Eq.(B.4) of Appendix B. Since $F_Z^{\nu}(\bar{y},\bar{C}(\bar{A}^{\nu}))$, $F_Z^{\nu}(\bar{y},\bar{C}(\bar{A}^{\zeta}))$ appear as absolute values in Eq.(F.2), the decision law would not change by replacing them with

$$F_Z^{\nu,*}(\bar{y},\bar{C}(\bar{A}^{\eta})) = e^{-j\psi}F_Z^{\nu}(\bar{y},\bar{C}(\bar{A}^{\eta})) \tag{F.4}$$

where $\eta \in \{\nu,\zeta\}$. $F_Z^{\nu,*}(\bar{y},\bar{C}(\bar{A}^{\eta}))$, can be expressed as

$$F_Z^{\nu,*}(\bar{y},\bar{C}(\bar{A}^{\eta})) = \bar{E}_{\eta}^{\nu,*} + N_{\eta,I}^{\nu,*} + jN_{\eta,Q}^{\nu,*} \tag{F.5}$$

with

$$\bar{E}_{\eta}^{\nu,*} = e^{-j\psi}\bar{E}_{\eta}^{\nu} = h_0\sum_{k=0}^{Z-1} c_k^{\nu}(c_k^{\eta})^* + 2\sum_{l=1}^{Z-1}\sum_{k=l}^{Z-1} h_l[c_k^{\nu}(c_{k-l}^{\eta})^* + (c_k^{\eta})^* c_{k-l}^{\nu}]\ , \tag{F.6}$$

$$N_{\eta,I}^{\nu,*} = Re\{e^{-j\psi}\sum_{k=0}^{Z-1} n_k(c_k^{\eta})^*\}, \qquad N_{\eta,Q}^{\nu,*} = Im\{e^{-j\psi}\sum_{k=0}^{Z-1} n_k(c_k^{\eta})^*\}\ . \tag{F.7}$$

$F_Z^{\nu,*}(\bar{y},\bar{C}(\bar{A}^{\nu}))$, $F_Z^{\nu,*}(\bar{y},\bar{C}(\bar{A}^{\zeta}))$ have the same autocorrelation and cross correlation properties with $F_Z^{\nu}(\bar{y},\bar{C}(\bar{A}^{\nu}))$, $F_Z^{\nu}(\bar{y},\bar{C}(\bar{A}^{\zeta}))$ (they are given in Eqs.(B.6), (B.7) of Appendix B). Also,

$$E\{N_{\nu,I}^{\nu,*}\} = E\{N_{\nu,Q}^{\nu,*}\} = E\{N_{\zeta,I}^{\nu,*}\} = E\{N_{\zeta,Q}^{\nu,*}\} = 0, \tag{F.8}$$

$$\sigma^2_{\nu,\eta} = E\{(N^{\nu,*}_{\eta,I})^2\} = E\{(N^{\nu,*}_{\eta,Q})^2\} = \sigma^2_n[\frac{Z}{2} + \sum_{l=1}^{Z-1} \rho^n_l \sum_{k=l}^{Z-1} \cos(\Delta\Phi^\eta_l(k))] \quad \text{(F.9)}$$

(for the definition of $\Delta\Phi^\eta_l(k)$ see Appendix B),

$$E\{N^{\nu,*}_{\nu,I} N^{\nu,*}_{\nu,Q}\} = E\{N^{\nu,*}_{\zeta,I} N^{\nu,*}_{\zeta,Q}\} = 0 \quad \text{(F.10)}$$

(a reminder, $R^n_i = E\{n_k n^*_{k-i}\}$ and $\rho^n_l = \frac{R^n_l}{R^n_0} = \frac{R^n_l}{\sigma^2_n}$).

At this point, consider that instead of choosing between $\bar{A}^\nu$, $\bar{A}^\zeta$ following the rule described by Eq.(F.1), we decide according to the following decision law:

*Decision Law 2 (*DL2)

$$|F^{\nu,*}_Z(\bar{y}, \bar{C}(\bar{A}^\nu)) + \mathcal{D}^{\zeta,\nu}_Z(\bar{h})| \underset{\bar{A}^\zeta}{\overset{\bar{A}^\nu}{\gtrless}} |F^{\nu,*}_Z(\bar{y}, \bar{C}(\bar{A}^\zeta))|. \quad \text{(F.11)}$$

It can be easily shown that $F^{\nu,*}_Z(\bar{y}, \bar{C}(\bar{A}^\nu)) + \mathcal{D}^{\zeta,\nu}_Z(\bar{h})$ has an average $\overline{E\mathcal{D}}^{\nu,*}_{\nu,\zeta}(h_0, \bar{h})$ equal to:

$$\begin{aligned} \overline{E\mathcal{D}}^{\nu,*}_{\nu,\zeta}(h_0, \bar{h}) &= \bar{E}^{\nu,*}_\nu + \mathcal{D}^{\zeta,\nu}_Z(\bar{h}) \\ &= Zh_0 + \sum_{l=1}^{Z-1} \sum_{k=l}^{Z-1} [Re\{h_l c^\zeta_k (c^\zeta_{k-l})^*\} + Re\{h_l c^\nu_k (c^\nu_{k-l})^*\}] \end{aligned} \quad \text{(F.12)}$$

Case 1 : $\mathcal{D}^{\zeta,\nu}_Z(\bar{h}) \geq 0$

In this case, $|\mathcal{D}^{\zeta,\nu}_Z(\bar{h})| = \mathcal{D}^{\zeta,\nu}_Z(\bar{h})$. From the algebra of complex numbers we have that: for ϵ_1, ϵ_2 being two arbitrary complex numbers, $|\epsilon_1| + |\epsilon_2| \geq |\epsilon_1 + \epsilon_2|$ always. Using the above identity, with $F^{\nu,*}_Z(\bar{y}, \bar{C}(\bar{A}^\nu))$, $\mathcal{D}^{\zeta,\nu}_Z(\bar{h})$ we have:

$$|F^{\nu,*}_Z(\bar{y}, \bar{C}(\bar{A}^\nu))| + \mathcal{D}^{\zeta,\nu}_Z(\bar{h}) \geq |F^{\nu,*}_Z(\bar{y}, \bar{C}(\bar{A}^\nu)) + \mathcal{D}^{\zeta,\nu}_Z(\bar{h})|. \quad \text{(F.13)}$$

With Eq.(F.13) being valid, when the inequality of Eq.(F.11) holds with the $\{\geq\}$ direction (giving correct decision), the inequality of Eq.(F.1) (or equivalently Eq.(F.2)) will certainly hold as well. This guarantees that when $\mathcal{D}^{\zeta,\nu}_Z(\bar{h}) \geq 0$, the pairwise error probability $P_{DL1}(\{\bar{C}(\bar{A}^\zeta) \longleftarrow \bar{C}(\bar{A}^\nu)\})$ (i.e. the probability of the error event $\{\bar{C}(\bar{A}^\zeta) \longleftarrow \bar{C}(\bar{A}^\nu)\}$ happening when the

decision law $DL1$ described by Eq.(F.2) is used) will be smaller or equal to $P_{DL2}(\{\bar{C}(\bar{A}^{\varsigma}) \longleftarrow \bar{C}(\bar{A}^{\nu})\})$ (the probability of the $\{\bar{C}(\bar{A}^{\varsigma}) \longleftarrow \bar{C}(\bar{A}^{\nu})\}$ happening when the decision law $DL2$ described by Eq.(F.11) is used). Consequently, for $\mathcal{D}_Z^{\varsigma,\nu}(\bar{h}) \geq 0$,

$$P_{DL1}(\{\bar{C}(\bar{A}^{\varsigma}) \longleftarrow \bar{C}(\bar{A}^{\nu})\}) \leq P_{DL2}(\{\bar{C}(\bar{A}^{\varsigma}) \longleftarrow \bar{C}(\bar{A}^{\nu})\}). \qquad (F.14)$$

Comparing the decision law $DL2$ of Eq.(F.11) with the one presented in Appendix B (refer to Eq.(B.1)), we realize that they have the same form ($DL2$ can be described by the decision law presented in Eq.(B.1) of Appendix B, by simply substituting $F_Z^{\nu}(\bar{y}, \bar{C}(\bar{A}^{\nu}))$ with $\{F_Z^{\nu,*}(\bar{y}, \bar{C}(\bar{A}^{\nu})) + \mathcal{D}_Z^{\varsigma,\nu}(\bar{h})\}$). Consequently, similar to $P(\{\bar{C}(\bar{A}^{\varsigma}) \longleftarrow \bar{C}(\bar{A}^{\nu})\})$ (which was upper bounded from $B_{[\nu,\varsigma]}^Z$), an upper bound $B_{PW[\nu,\varsigma]}^Z$ for $P_{DL2}(\{\bar{C}(\bar{A}^{\varsigma}) \longleftarrow \bar{C}(\bar{A}^{\nu})\})$ can be given as well (i.e. $P_{DL2}(\{\bar{C}(\bar{A}^{\varsigma}) \longleftarrow \bar{C}(\bar{A}^{\nu})\}) \leq B_{PW[\nu,\varsigma]}^Z$). $B_{PW[\nu,\varsigma]}^Z$ can be derived by following exactly the same steps described in Appendix B, the only difference in this case being that $\bar{E}_{\nu}^{\nu}$ should be substituted by $\overline{E\mathcal{D}}_{\nu,\varsigma}^{\nu,*}(h_0, \bar{h})$. The result is:

$$B_{PW[\nu,\varsigma]}^Z = \frac{1}{2}\Lambda_{PW}(\bar{C}(\bar{A}^{\nu}), \bar{C}(\bar{A}^{\varsigma}))\exp\{-\frac{1}{\sigma_n^2}\frac{(\alpha_{PW[\nu,\varsigma]} - \beta_{PW[\nu,\varsigma]})^2}{2}\} \quad (F.15)$$

with

$$\Lambda_{PW}(\bar{C}(\bar{A}^{\nu}), \bar{C}(\bar{A}^{\varsigma})) = \begin{cases} 1 & \text{for } \alpha_{PW[\nu,\varsigma]} = 0 \\ [1 - \frac{v_{\nu\nu} - v_{\nu\varsigma}}{[(v_{\nu\nu}+v_{\nu\varsigma})^2 - 4|v_{\nu\varsigma}^c|^2]^{\frac{1}{2}}}] & \\ \frac{1}{\sqrt{2\pi\frac{1}{\sigma_n^2}\alpha_{PW[\nu,\varsigma]}\beta_{PW[\nu,\varsigma]}}} & \text{for } \alpha_{PW[\nu,\varsigma]} \neq 0 \end{cases} \qquad (F.16)$$

and

$$\begin{Bmatrix} \alpha_{PW[\nu,\varsigma]} \\ \beta_{PW[\nu,\varsigma]} \end{Bmatrix} = [\frac{1}{v_{\nu\nu} + v_{\nu\varsigma}}(\frac{|\overline{E\mathcal{D}}_{\nu,\varsigma}^{\nu,*}(h_0, \bar{h})|^2 + |\bar{E}_{\varsigma}^{\nu}|^2 - 2Re\{(\overline{E\mathcal{D}}_{\nu,\varsigma}^{\nu,*}(h_0, \bar{h}))^* \bar{E}_{\varsigma}^{\nu}\gamma_{\nu\varsigma}\}}{1 - |\gamma_{\nu\varsigma}|^2}$$
$$\mp \frac{|\overline{E\mathcal{D}}_{\nu,\varsigma}^{\nu,*}(h_0, \bar{h})|^2 - |\bar{E}_{\varsigma}^{\nu}|^2}{\sqrt{1 - |\gamma_{\nu\varsigma}|^2}})]^{\frac{1}{2}} \qquad (F.17)$$

(for the definition of $v_{\nu\nu}$, $v_{\nu\zeta}$, $v^{\zeta}_{\nu\zeta}$, $\gamma_{\nu\zeta}$, see Eqs.(B.8) and (B.9) of Appendix B). Since Eq.(F.14), is valid, the following inequality is valid as well:

$$P_{DL1}(\{\bar{C}(\bar{A}^{\zeta}) \longleftarrow \bar{C}(\bar{A}^{\nu})\}) \leq P_{DL2}(\{\bar{C}(\bar{A}^{\zeta}) \longleftarrow \bar{C}(\bar{A}^{\nu})\}) \leq B^{Z}_{PW[\nu,\zeta]} \tag{F.18}$$

Case 2 : $\mathcal{D}^{\zeta,\nu}_{Z}(\bar{h}) < 0$

In this case, $|\mathcal{D}^{\zeta,\nu}_{Z}(\bar{h})| = -\mathcal{D}^{\zeta,\nu}_{Z}(\bar{h})$. For ϵ_1, ϵ_2 complex numbers, $|\epsilon_1 + \epsilon_2| \geq |\epsilon_1| - |\epsilon_2|$, which gives us

$$|F^{\nu,*}_{Z}(\bar{y}, \bar{C}(\bar{A}^{\nu})) + \mathcal{D}^{\zeta,\nu}_{Z}(\bar{h})| \geq |F^{\nu,*}_{Z}(\bar{y}, \bar{C}(\bar{A}^{\nu}))| + \mathcal{D}^{\zeta,\nu}_{Z}(\bar{h}) \tag{F.19}$$

In the second case, when the inequality of Eq.(F.11) holds with the $\{>\}$ direction, it does not guarantee that the same will be happening with Eq.(F.2) as well. Consequently, for $\mathcal{D}^{\zeta,\nu}_{Z}(\bar{h}) < 0$, the upper bound of $P_{DL2}(\{\bar{C}(\bar{A}^{\nu}) \longleftarrow \bar{C}(\bar{A}^{\zeta})\})$ does not upper bound $P_{DL1}(\{\bar{C}(\bar{A}^{\nu}) \longleftarrow \bar{C}(\bar{A}^{\zeta})\})$ necessarily. In the paragraphs to follow, we shall provide an upper bound of $P_{DL1}(\{\bar{C}(\bar{A}^{\nu}) \longleftarrow \bar{C}(\bar{A}^{\zeta})\})$ which covers this second case.

The outcome of Appendix E shows us that for $\frac{E_b}{N_o} \rightarrow \infty$ $(\Rightarrow \sigma_n^2 \rightarrow 0)$

$$|F^{\nu,*}_{Z}(\bar{y}, \bar{C}(\bar{A}^{\nu}))| + \mathcal{D}^{\zeta,\nu}_{Z}(\bar{h}) \simeq$$

$$\begin{cases} |F^{\nu,*}_{Z}(\bar{y}, \bar{C}(\bar{A}^{\nu})) + \mathcal{D}^{\zeta,\nu}_{Z}(\bar{h})| & \text{for } N^{\nu,*}_{Z,\zeta} \geq -\overline{ED}^{\nu,*}_{\nu,\zeta}(h_0, \bar{h}) \\ |F^{\nu,*}_{Z}(\bar{y}, \bar{C}(\bar{A}^{\nu})) + \mathcal{D}^{\zeta,\nu}_{Z}(\bar{h})| & \\ +2(\overline{ED}^{\nu,*}_{\nu,\zeta}(h_0, \bar{h}) + N^{\nu,*}_{\nu,I}) & \text{for } -\overline{ED}^{\nu,*}_{\nu,\zeta}(h_0, \bar{h}) \geq N^{\nu,*}_{\nu,I} \geq -\bar{E}^{\nu,*}_{\nu} \\ |F^{\nu,*}_{Z}(\bar{y}, \bar{C}(\bar{A}^{\nu})) + \mathcal{D}^{\zeta,\nu}_{Z}(\bar{h})| + 2\mathcal{D}^{\zeta,\nu}_{Z}(\bar{h}) & \text{for } N^{\nu,*}_{\nu,I} < -\bar{E}^{\nu,*}_{\nu} \end{cases} \tag{F.20}$$

with a probability of 1.

For the second and third cases presented in Eq. (F.20), $(|F_Z^{\nu,*}(\bar{y},\bar{C}(\bar{A}^\nu))|+ \mathcal{D}_Z^{\zeta,\nu}(\bar{h}) \leq (|F_Z^{\nu,*}(\bar{y},\bar{C}(\bar{A}^\nu))+\mathcal{D}_Z^{\zeta,\nu}(\bar{h})|)$. For both of them, $N_{\nu,I}^{\nu,*} < -\overline{ED}_{\nu,\zeta}^{\nu,*}(h_0,\bar{h})$. Due to the Gaussian nature of the $N_{\nu,I}^{\nu,*}$, the probability of $N_{\nu,I}^{\nu,*} < -\overline{ED}_{\nu}^{\nu,*}(h_0,\bar{h})$ is equal to :

$$P(N_{\nu,I}^{\nu,*} < -\overline{ED}_{\nu,\zeta}^{\nu,*}(h_0,\bar{h})) = Q(\frac{\overline{ED}_{\nu,\zeta}^{\nu,*}(h_0,\bar{h})}{\sigma_{\nu,\nu}}). \tag{F.21}$$

$$Q(x) = \frac{1}{\sqrt{2\pi}}\int_x^\infty \exp\{-\frac{u^2}{2}\}du\ . \tag{F.22}$$

The probability of the pairwise error event $\{\bar{C}(\bar{A}^\zeta) \longleftarrow \bar{C}(\bar{A}^\nu)\}$ when the decision is made according to $DL1$ (described by Eq. (F.2)), can be expressed as:

$$\begin{aligned} & P_{DL1}(\{\bar{C}(\bar{A}^\zeta) \longleftarrow \bar{C}(\bar{A}^\nu)\}) = \\ & \int_{-\infty}^{-\overline{ED}_{\nu,\zeta}^{\nu,*}(h_0,\bar{h})} P_{DL1}(\{\bar{C}(\bar{A}^\zeta) \longleftarrow \bar{C}(\bar{A}^\nu)\}|N_{\nu,I}^{\nu,*}=u) f_{N_{N,I}^{\nu,*}}(u)du \\ + & \int_{-\overline{ED}_{\nu,\zeta}^{\nu,*}(h_0,\bar{h})}^{\infty} P_{DL1}(\{\bar{C}(\bar{A}^\zeta) \longleftarrow \bar{C}(\bar{A}^\nu)\}|N_{\nu,I}^{\nu,*}=u) f_{N_{N,I}^{\nu,*}}(u)du \end{aligned} \tag{F.23}$$

where $f_{N_{N,I}^{\nu,*}}(u)$ is the pdf of $N_{N,I}^{\nu,*}$.

Considering that :

i) $P_{DL1}(\{\bar{C}(\bar{A}^\zeta) \longleftarrow \bar{C}(\bar{A}^\nu)\}|N_{\nu,I}^{\nu,*}) \leq 1$ and
ii) $P_{DL1}(\ \{\bar{C}(\bar{A}^\zeta) \longleftarrow \bar{C}(\bar{A}^\nu)\}|N_{\nu,I}^{\nu,*}=u\ ) = P_{DL2}(\ \{\bar{C}(\bar{A}^\zeta) \longleftarrow \bar{C}(\bar{A}^\nu)\}|N_{\nu,I}^{\nu,*} = u\ )$ for $u \geq -\overline{ED}_{\nu,\zeta}^{\nu,*}(h_0,\bar{h})$ (due to the first case of Eq. (F.20)), we have:

$$P_{DL1}(\{\bar{C}(\bar{A}^\nu) \longleftarrow \bar{C}(\bar{A}^\zeta)\}) \leq \int_{-\infty}^{-\overline{ED}_{\nu,\zeta}^{\nu,*}(h_0,\bar{h})} f_{N_{N,I}^{\nu,*}}(u)du +$$

$$\int_{-\overline{ED}_{\nu,\zeta}^{\nu,*}(h_0,\bar{h})}^{\infty} P_{DL2}(\{\bar{C}(\bar{A}^\zeta) \longleftarrow \overline{C}(\bar{A}^\nu)\}|N_{\nu,I}^{\nu,*}=u) f_{N_{\nu,I}^{\nu,*}}(u)du.$$

(F.24)

Also,

$$\int_{-\overline{ED}^{\nu,*}_{\nu,\zeta}(h_0,\bar{h})}^{\infty} P_{DL2}(\{\bar{C}(\bar{A}^{\zeta}) \longleftarrow \bar{C}(\bar{A}^{\nu})\}|N^{\nu,*}_{\nu,I} = u) f_{N^{\nu,*}_{\nu,I}}(u)du \leq$$

$$\int_{-\infty}^{\infty} P_{DL2}(\{\bar{C}(\bar{A}^{\zeta}) \longleftarrow \bar{C}(\bar{A}^{\nu})\}|N^{\nu,*}_{\nu,I} = u) f_{N^{\nu,*}_{\nu,I}}(u)du =$$

$$P_{DL2}(\{\bar{C}(\bar{A}^{\zeta}) \longleftarrow \bar{C}(\bar{A}^{\nu})\}). \tag{F.25}$$

Using Eq.(F.22) and Eq.(F.25) with Eq.(F.24), we get:

$$P_{DL1}(\{\bar{C}(\bar{A}^{\zeta}) \longleftarrow \bar{C}(\bar{A}^{\nu})\}) \leq Q(\frac{\overline{ED}^{\nu,*}_{\nu,\zeta}(h_0,\bar{h})}{\sigma_{\nu,\nu}}) + P_{DL2}(\{\bar{C}(\bar{A}^{\zeta}) \longleftarrow \bar{C}(\bar{A}^{\nu})\}) .$$

(F.26)

Replacing $P_{DL2}(\{\bar{C}(\bar{A}^{\zeta}) \longleftarrow \bar{C}(\bar{A}^{\nu})\})$ in Eq.(F.26) with its upper bound $B^{Z}_{PW[\nu,\zeta]}$ (see Eq.(F.15)), we get:

$$P_{DL1}(\{\bar{C}(\bar{A}^{\zeta}) \longleftarrow \bar{C}(\bar{A}^{\nu})\}) \leq Q(\frac{\overline{ED}^{\nu,*}_{\nu,\zeta}(h_0,\bar{h})}{\sigma_{\nu,\nu}}) + B^{Z}_{PW[\nu,\zeta]}. \tag{F.27}$$

Summarizing the outcomes of Eqs.(F.18), (F.27), we end up with the following inequality:

$$P_{DL1}(\{\bar{C}(\bar{A}^{\zeta}) \longleftarrow \bar{C}(\bar{A}^{\nu})\}) \leq B^{Z}_{HAO[\nu,\zeta]} \tag{F.28}$$

where

$$B^{Z}_{HAO[\nu,\zeta]} = \begin{cases} B^{Z}_{PW[\nu,\zeta]} & \text{for } \mathcal{D}^{\zeta,\nu}_{Z}(\bar{h}) \geq 0 \\ B^{Z}_{PW[\nu,\zeta]} + Q(\frac{\overline{ED}^{\nu,*}_{\nu,\zeta}(h_0,\bar{h})}{\sigma_{\nu,\nu}}) & \text{for } \mathcal{D}^{\zeta,\nu}_{Z}(\bar{h}) < 0. \end{cases} \tag{F.29}$$

Appendix G

Pairwise Error Event Bound of the Block Decoder Operating in a Fading Environment

G.1 Model of the Channel and the Received Signal

The expression for the transmitted signal $x_{tr}(\bar{C}(\bar{A}),t)$ has been given in Chapter 3. For the reader's convenience, we present it again here.

$$\begin{aligned} x_{tr}(\bar{C}(\bar{A}),t) &= x_B(\bar{C}(\bar{A}),t)e^{j(\omega_c t+\psi)} \\ &= (\sum_{k=0}^{Z-1} c_k h_T(t-kT))e^{j(\omega_c t+\psi)} \end{aligned} \tag{G.1}$$

where $x_B(\bar{C}(\bar{A}),t)$ is the signal at the output of the premodulation filter $H_T(\omega)$ (baseband signal). It is assumed, that $x_{tr}(\bar{C}(\bar{A}),t)$ is corrupted by a mixture of multiplicative nonselective fading noise $f_F(t)$, and AWGN $n_w(t)$. The AWGN has one sided power spectral density N_0. As shown in Fig. G.1, $f_F(t)$ is modelled as a complex summation of two white and independent Gaussian noise processes, $n_I^F(t)$ and $n_Q^F(t)$, filtered by two identical filters,

$H_F(\omega)$, of bandwidth B_F, i.e., $f_F(t) = f_F^I(t) + jf_F^Q(t)$. The shaping and the (B_FT) product of these filters determines the fading model [174] and the dynamics of the fading process. It should be mentioned that $f_F(t)$ can have Rayleigh as well as Rician characteristics. $f_F^I(t)$ and $f^Q(t)$ have the same autocorrelation function given by

$$\begin{aligned} R_F(\tau) &= E\{[f_F^I(t) - \overline{f_F^I}][f_F^I(t-\tau) - \overline{f_F^I}]\} \\ &= E\{[f_F^Q(t) - \overline{f_F^Q}][f^Q(t-\tau) - \overline{f_F^Q}]\} \\ &= N_F \int_{-\infty}^{\infty} \mid H_F(f) \mid^2 e^{j2\pi f\tau} d\tau \end{aligned}$$

and cross-correlation function of zero value. In the above equation, $E\{\cdot\}$ denotes expected value, $\overline{f_F^I} = E\{f_F^I(t)\}$, $\overline{f_F^Q} = E\{f_F^Q(t)\}$ and N_F is the power spectral density of $n_I^F(t)$ or $n_Q^F(t)$. Without any loss of generality, it will be assumed that $\overline{f_F^Q}$=0.

The received signal $x_r(t)$ can then be expressed as

$$x_r(t) = f_F(t)x_{tr}(\bar{C}(\bar{A}), t) + n_w(t). \tag{G.2}$$

In subsection 4.3.2 of Chapter 4, the receiver performing non-coherent block decoding has been introduced. Its block diagram has been presented in Figs. 4.3, 4.4.

The signal $y(t)$ at the output of the post detection filter $H_R(\omega)$ is equal to:

$$y(t) = f_F(t) \sum_{k=0}^{Z-1} c_k h(t - kT) + n(t)\ . \tag{G.3}$$

$n(t)$ is the element of the Gaussian noise, passing through the post detection filter. In Eq.(G.3) we have made the assumption

$$\{f_F(t)x_B(\bar{C}(\bar{A}), t)\} \otimes h_R(t) = f_F(t)\{x_B(\bar{C}(\bar{A}), t) \otimes h_R(t)\} \tag{G.4}$$

This is a reasonable assumption, since $f_F(t)$ has a bandwidth of about 200 Hz, whereas the post detection filter $H_R(\omega)$ and the baseband information carrying signal $x_B(\bar{C}(\bar{A}), t)$ have a bandwidth of several thousands of Hz [1].

[1]The same assumption has been used in [117] as well.

By sampling $y(t)$ at kT we get:

$$y_k = y(kT) = f_k^F c_k + n_k \tag{G.5}$$

with $y_k = y(kT)$, $f_k^F = f_F(kT)$ and $n_k = n(kT)$. The metric of the block decoder presented in subsection 4.3.2 of Chapter 4 has been found to be equal to:

$$\aleph_{IC}(\bar{y}, \bar{C}(\bar{A})) = |\sum_{k=0}^{Z-1} y_k c_k^*| \,. \tag{G.6}$$

with $\bar{y} = [y_0, y_1, \ldots, y_{Z-1}]$.

In Fig. 4.4, the block diagram of the Processing Unit (PU) performing the calculation of $\aleph_{IC}(\bar{y}, \bar{C}(\bar{A}))$ has been presented.

G.2 Derivation of the Pairwise Error Bound

Assume that $\bar{A}^\nu$ is the transmitted information sequence. Assume that now $\bar{C}(\bar{A}^\nu)$ is compared with $\bar{C}(\bar{A}^\zeta)$, the decision being based on the maximization of the metric $\aleph_{IC}(\bar{y}, (\bar{C}(\bar{A}))$, presented in Eq.(G.6). The criterion which will choose one or the other sequence is the following:

$$|F_Z^\nu(\bar{y}, \bar{C}(\bar{A}^\nu))| \underset{\bar{A}^\zeta}{\overset{\bar{A}^\nu}{\gtrless}} |F_Z^\nu(\bar{y}, \bar{C}(\bar{A}^\zeta))| \tag{G.7}$$

where

$$F_Z^{f[\nu]}(\bar{y}, \bar{C}(\bar{A}^i)) = \sum_{k=0}^{Z-1} y_k (c_k^i)^* . \tag{G.8}$$

Using Eq.(G.6) $F_Z^{f[\nu]}(\bar{y}, \bar{C}(\bar{A}^\nu))$, $F_Z^{f[\nu]}(\bar{y}, \bar{C}(\bar{A}^\zeta))$ can be expressed as:

$$F_Z^{f[\nu]}(\bar{y}, \bar{C}(\bar{A}^\eta)) = \bar{E}_{\nu,\eta}^f + \mathcal{N}_{[\nu,\eta]}^F + \mathcal{N}_{[\nu,\eta]}^G \tag{G.9}$$

where η can be either ν or ζ ($\eta \epsilon \{\nu, \zeta\}$) and

$$\bar{E}_{\nu,\eta}^f = e^{j\psi} \sqrt{\frac{K_F}{K_F + 1}} [\sum_{k=0}^{Z-1} c_k^\nu (c_k^\eta)^*], \tag{G.10}$$

$$\mathcal{N}^F_{[\nu,\eta]} = e^{j\psi} \sum_{k=0}^{Z-1} n f^F_k c^\nu_k (c^\eta_k)^* \tag{G.11}$$

$$\mathcal{N}^G_{[\nu,\eta]} = e^{j\psi} \sum_{i=0}^{Z-1} n_i (c^\eta_i)^*. \tag{G.12}$$

where $K_F = \frac{\overline{f^I_F}^2}{R^F_0}$ and $R^F_k = R_F(kT)$. In Eq.(G.10), the $\overline{f^I_F} = \sqrt{\frac{K_F}{K_F+1}}$ has been used). The first term is the contribution of the direct signal component, while the second and third terms are due to the diffused (multipath) signal component and the Gaussian noise. Because of the zero mean complex Gaussian nature of f^F_k, n_k, $F^{f[\nu]}_Z(\bar{y}, \bar{C}(\bar{A}^\eta))$ is a complex Gaussian random variable with average $\bar{E}^f_{\nu,\eta}$ and variance

$$\begin{aligned} \mu_{f[\nu\eta]} &= E\{|F^{f[\nu]}_Z(\bar{y}, \bar{C}(\bar{A}^\eta)) - \bar{E}^f_{\nu,\eta}|^2\} = E\{|\mathcal{N}^F_{[\nu,\eta]} + \mathcal{N}^G_{[\nu,\eta]}|^2\} \\ &= R^F_0 [Z + \sum_{k=1}^{Z-1} 2\rho^F_k \{\sum_{l=k}^{Z-1} \cos(\Delta\Phi^\nu_k - \Delta\Phi^\eta_k)\}] + R^n_0 Z \end{aligned} \tag{G.13}$$

where

$$\rho^F_k = \frac{R^F_k}{R^F_0}. \tag{G.14}$$

The cross-covariance between $F^{f[\nu]}_Z(\bar{y}, \bar{C}(\bar{A}^\nu))$ and $F^{f[\nu]}_Z(\bar{y}, \bar{C}(\bar{A}^\varsigma))$ equals:

$$\mu^c_{f[\nu\varsigma]} = \frac{R^F_0}{2} [\sum_{k=0}^{Z-1} (2 - \delta_K(k)) \rho^F_k \sum_{l=k}^{Z-1} \{(c^\nu_l)^* c^\varsigma_l + (c^\nu_{l-k})^* c^\varsigma_{l-k}\}] + \frac{1}{SNR} [\sum_{k=0}^{Z-1} c^\nu_k (c^\varsigma_k)^*] \tag{G.15}$$

where $\delta_K(i)$ is the *Kroneker delta* function:

$$\delta_K(i) = \begin{cases} 1 & \text{for } i = 0 \\ 0 & \text{elsewhere.} \end{cases} \tag{G.16}$$

SNR stands for Signal to Noise Ratio.

At this point, it is convenient to define the parameters,

$$\upsilon_{f[\nu\eta]} = \frac{\mu_{f[\nu\eta]}}{\sigma_n^2} = \frac{SNR}{K_F+1}[\sum_{k=0}^{Z-1} c_k^{\nu}(c_k^{\eta})^* + \sum_{k=1}^{Z-1} 2\rho_k^F\{\sum_{l=k}^{Z-1}\cos(\Delta\Phi_k^{\nu} - \Delta\Phi_k^{\eta})\}] + Z, \tag{G.17}$$

$$\begin{aligned}\upsilon^c_{f[\nu\zeta]} &= \frac{\mu^c_{f[\nu\zeta]}}{\sigma_n^2} \\ &= \frac{SNR}{2(K_F+1)}[\sum_{k=0}^{Z-1}(2-\delta_K(k))\rho_k^F\sum_{l=k}^{Z-1}\{(c_l^{\nu})^* c_l^{\zeta} + (c_{l-k}^{\nu})^* c_{l-k}^{\zeta}\}] + [\sum_{k=0}^{Z-1} c_k^{\nu}(c_k^{\zeta})^*].\end{aligned} \tag{G.18}$$

In Eqs.(G.17), (G.18), the $\frac{R_0^F}{R_0^n} = \frac{R_0^F}{\sigma_n^2} = \frac{SNR}{K_F+1}$ has been used.

Using the material of [214, pp.223-228] we find the following expression for the $P_f(\{\bar{C}(\bar{A}^{\zeta}) \leftarrow \bar{C}(\bar{A}^{\nu})\})$.

$$\begin{aligned}P_f(\{\bar{C}(\bar{A}^{\zeta}) \leftarrow \bar{C}(\bar{A}^{\nu})\}) &= Q_f(\frac{1}{\sigma_n}\alpha_{f[\nu,\zeta]}, \frac{1}{\sigma_n}\beta_{f[\nu,\zeta]}) \\ &- \frac{1}{2}[1 + \frac{\upsilon_{f[\nu\nu]} - \upsilon_{f[\nu\zeta]}}{[(\upsilon_{f[\nu\nu]} + \upsilon_{f[\nu\zeta]})^2 - 4|\upsilon^c_{f[\nu\zeta]}|^2]^{\frac{1}{2}}}] \\ &\quad I_o(\frac{1}{\sigma_n}\alpha_{f[\nu,\zeta]}\frac{1}{\sigma_n}\beta_{f[\nu,\zeta]})\exp(-\frac{1}{\sigma_n^2}\frac{\alpha^2_{f[\nu,\zeta]} + \beta^2_{f[\nu,\zeta]}}{2})\end{aligned} \tag{G.19}$$

with $Q_f(x,y)$ being the Marcum's Q function [242, p. 585] and

$$\begin{aligned}\left\{\begin{array}{c}\alpha_{f[\nu,\zeta]} \\ \beta_{f[\nu,\zeta]}\end{array}\right\} &= [\frac{1}{\upsilon_{f[\nu\nu]} + \upsilon_{f[\nu\zeta]}}(\frac{|\bar{E}^f_{\nu,\nu}|^2 + |\bar{E}^f_{\nu,\zeta}|^2 - 2Re\{(\bar{E}^f_{\nu,\nu})^*\bar{E}^f_{\nu,\zeta}\gamma^c_{f[\nu\zeta]}\}}{1-|\gamma^c_{f[\nu\zeta]}|^2} \\ &\quad \mp\frac{|\bar{E}^f_{\nu,\nu}|^2 - |\bar{E}^f_{\nu,\zeta}|^2}{\sqrt{1-|\gamma^f_{f[\nu\zeta]}|^2}})]^{\frac{1}{2}}\end{aligned} \tag{G.20}$$

with

$$\gamma^c_{f[\nu\zeta]} = \frac{2\upsilon^c_{f[\nu\zeta]}}{(\upsilon_{f[\nu\nu]} + \upsilon_{f[\nu\zeta]})} \cdot \tag{G.21}$$

The expression provided by Eq.(G.19) is general, providing the capability of evaluating the non-coherent schemes considered, under any value of signal to noise ratio (SNR) and Rician fading factor (K_F). However, for some specific cases the expression provided by Eq.(G.19) can be replaced by simpler expressions, which require smaller processing. Below we shall examine two specific cases which are frequently met in channels where PWDCS operate.

G.2.1 Rician Fading Channel with a Strong Line of Sight (Direct) Component and High SNR

Under these conditions, the $\frac{K_F}{1+\frac{K_F+1}{SNR}}$ has large values. When this is the case $Q_f(x,y)$, $I_0(x)$ can be approximated as follows:

$$Q_f(x,y) \approx \begin{cases} e^{(-\frac{y^2}{2})} & \text{for } x = 0 \\ \frac{1}{\sqrt{2\pi xy}} e^{(-\frac{|y-x|^2}{2})} & \text{for } x > 0, \end{cases} \tag{G.22}$$

$$I_0(z) = \frac{e^{|z|}}{\sqrt{2\pi|z|}} \tag{G.23}$$

The expression at the right side of Eq.(G.22) is actually an upper bound for $Q_f(x,y)$. When $x >> 1, y >> 1$, and $(y-x)^2 >> 0$ this bound becomes tight (see [242]). Application of these approximations on Eq.(G.19) provides the following upper bound expression for $P_f(\{\bar{C}(\bar{A}^\zeta) \leftarrow \bar{C}(\bar{A}^\nu)\})$:

$$P_f(\{\bar{C}(\bar{A}^\zeta) \leftarrow \bar{C}(\bar{A}^\nu)\}) \leq B\mathcal{F}^Z_{[\nu,\zeta]} = \frac{1}{2}\Lambda_F(\bar{C}(\bar{A}^\nu), \bar{C}(\bar{A}^\zeta)) \exp\{-\frac{1}{\sigma_n^2}\frac{(\alpha_{[\nu,\zeta]} - \beta_{[\nu,\zeta]})^2}{2}\} \tag{G.24}$$

with

$$\Lambda_F(\bar{C}(\bar{A}^\nu),\bar{C}(\bar{A}^\varsigma)) = \begin{cases} 1 & \text{for } \alpha_{f[\nu,\zeta]} = 0 \\ [1 - \frac{\upsilon_{f[\nu\nu]} - \upsilon_{f[\nu\zeta]}}{[(\upsilon_{f[\nu\nu]} + \upsilon_{f[\nu\zeta]})^2 - 4|\upsilon^c_{f[\nu\zeta]}|^2]^{\frac{1}{2}}}] & \\ \frac{1}{\sqrt{2\pi \frac{1}{\sigma_n^2} \alpha_{f[\nu,\zeta]} \beta_{f[\nu,\zeta]}}} & \text{for } \alpha_{f[\nu,\zeta]} \neq 0. \end{cases}$$

(G.25)

G.2.2 Rayleigh Faded Channels

In this case, $K_F = 0$, which leads to $\frac{K_F}{1+\frac{K_F+1}{SNR}} = 0$. Under these conditions, it can be shown that $\alpha_{f[\nu,\zeta]} = \beta_{f[\nu,\zeta]} = 0$. Using the $Q_f(0,0) = 1$ and $I_0(0) = 1$ with Eq.(G.19) we get:

$$P_f(\{\bar{C}(\bar{A}^\varsigma) \leftarrow \bar{C}(\bar{A}^\nu)\}) = \frac{1}{2}[1 - \frac{\upsilon_{f[\nu\nu]} - \upsilon_{f[\nu\zeta]}}{[(\upsilon_{f[\nu\nu]} + \upsilon_{f[\nu\zeta]})^2 - 4|\upsilon^c_{f[\nu\zeta]}|^2]^{\frac{1}{2}}}]$$

(G.26)

For very slow Rayleigh fading, a BPSK signal and for $Z = 2$ (which corresponds to the conventional differential detector), Eq.(G.26) becomes equal to:

$$P(\{\bar{C}(\bar{A}^\varsigma) \leftarrow \bar{C}(\bar{A}^\nu)\}) = \frac{1}{2}\frac{1}{1 + \frac{E_b}{N_o}}. \qquad \text{(G.27)}$$

This is identical to the result presented in [242, p. 407].

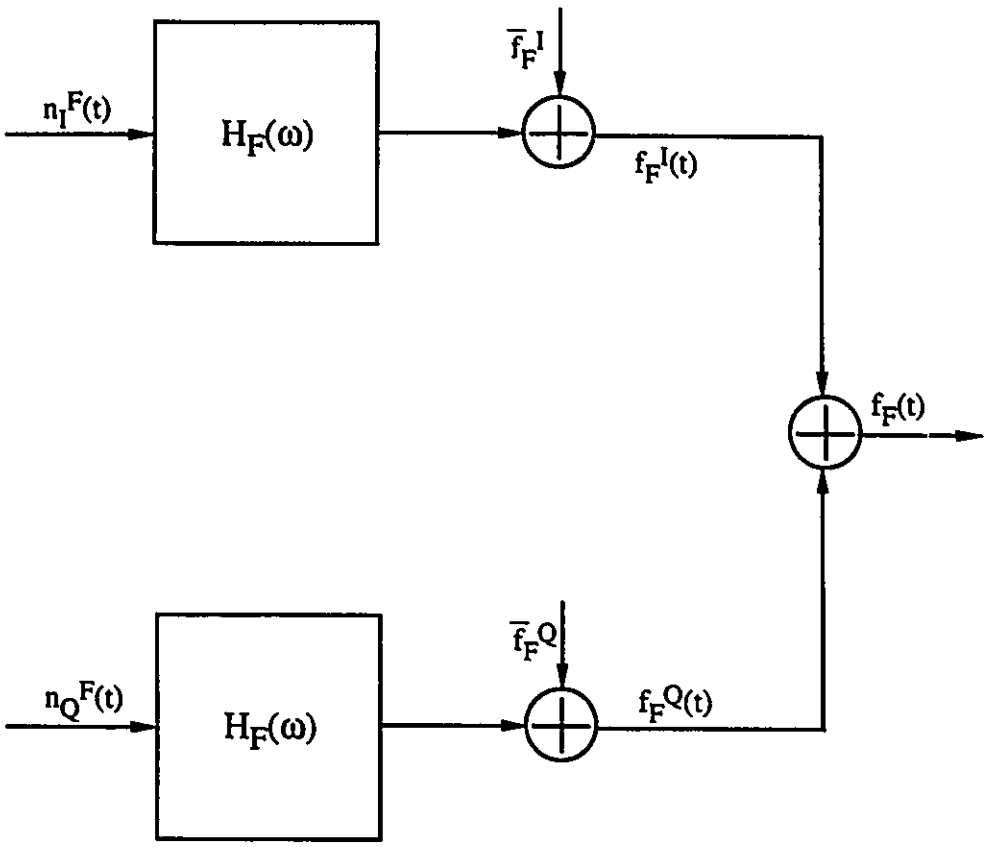

Figure G.1: Model of the fading process.

Appendix H

Performance Bound of the Non-Coherent Block Decoder In Slow Faded Channels

The objective of this appendix is to provide a tighter bounding expression for the performance of the block decoder, when operating in a slow faded channel.

When the block decoder is used, the choice between two sequences $\bar{C}(\bar{A}^{\nu})$, $\bar{C}(\bar{A}^{\zeta})$ is based on the direction of the following inequality:

$$|\sum_{k=0}^{Z-1} y_k(c_k^{\nu})^*| \underset{\bar{A}^{\zeta}}{\overset{\bar{A}^{\nu}}{\gtrless}} |\sum_{k=0}^{Z-1} y_k(c_k^{\zeta})^*| \tag{H.1}$$

where Z is the number of signal samples processed in order to make a decision (see Eqs.(B 1), (B.2) in Appendix B).

Without loss of generality, let us assume that the transmitted sequence is the

$$\bar{C}(\bar{A}^0) = [c_0^0 = 1, c_1^0 = 1 \ldots, c_{Z-1}^0 = 1]. \tag{H.2}$$

At this point let us consider the sequences

$$\bar{C}(\bar{A}^{\lambda}) = [c_0^{\lambda} = 1, c_1^{\lambda} = 1 \ldots, c_{k-1}^{\lambda} = 1, c_k^{\lambda} = e^{ji_k\frac{2\pi}{M}}, c_{k+1}^{\lambda} = 1 \ldots, c_{Z-1}^{\lambda} = 1],$$

$$\bar{C}(\bar{A}^{\xi}) = [c_0^{\xi} = 1, c_1^{\xi} = 1 \ldots, c_{l-1}^{\xi} = 1, c_l^{\xi} = e^{ji_l\frac{2\pi}{M}}, c_{l+1}^{\xi} = 1 \ldots, c_{Z-1}^{\xi} = 1],$$

$$\begin{aligned}\bar{C}(\bar{A}^{\mu}) = [\quad c_0^{\mu} &= 1, c_1^{\mu} = 1 \ldots, \ldots, c_{k-1}^{\mu} = 1, c_k^{\mu} = e^{ji_k\frac{2\pi}{M}}, c_{k+1}^{\mu} = 1 \ldots, \\ c_{l-1}^{\mu} &= 1, c_l^{\mu} = e^{ji_l\frac{2\pi}{M}}, c_{l+1}^{\mu} = 1 \ldots, c_{Z-1}^{\mu} = 1]\end{aligned}$$

(H.3)

where the i_k, i_l are integers with $1 \leq i_k, i_l \leq M-1$. While $\bar{C}(\bar{A}^{\lambda})$, $\bar{C}(\bar{A}^{\xi})$ differs only in one symbol with $\bar{C}(\bar{A}^0)$ (c_k, c_l respectively), $\bar{C}(\bar{A}^{\mu})$ differs in two symbols with $\bar{C}(\bar{A}^0)$ (c_k and c_l). Also, $c_k^{\mu} = c_k^{\lambda}$, $c_l^{\mu} = c_l^{\xi}$.

Let us represent with $EV_{0\leftarrow\epsilon}$ the event that $\{\bar{C}(\bar{A}^{\epsilon}) \leftarrow \bar{C}(\bar{A}^0)\}$ occurs and with $\overline{EV}_{0\leftarrow\epsilon}$ the event that $\{\bar{C}(\bar{A}^{\epsilon}) \leftarrow \bar{C}(\bar{A}^0)\}$ does not occur ($\epsilon \in \{\lambda, \xi, \mu\}$).

The probability that the block decoder will choose one of the three sequences $\bar{C}(\bar{A}^{\lambda})$, $\bar{C}(\bar{A}^{\xi})$, $\bar{C}(\bar{A}^{\mu})$ as the transmitted one instead of $\bar{C}(\bar{A}^0)$, when in reality $\bar{C}(\bar{A}^0)$ has been transmitted, is equal to

$$\begin{aligned}PE_{NB} &= P(EV_{0\leftarrow\lambda} \bigcup EV_{0\leftarrow\xi}) + P(\overline{EV}_{0\leftarrow\lambda}, \overline{EV}_{0\leftarrow\xi}, EV_{0\leftarrow\mu}) \\ &= P(EV_{0\leftarrow\lambda}) + P(EV_{0\leftarrow\xi}) \\ &- P(EV_{0\leftarrow\lambda}, EV_{0\leftarrow\xi}) + P(\overline{EV}_{0\leftarrow\lambda}, \overline{EV}_{0\leftarrow\xi}, EV_{0\leftarrow\mu}) \qquad \text{(H.4)}\end{aligned}$$

where $P(\cdot)$ represents the probability of the event $\{\cdot\}$ happening. $\bigcup$ is the *union operator* between sets. $P(EV_{0\leftarrow\lambda} \bigcup EV_{0\leftarrow\xi})$ is the probability that with $\bar{C}(\bar{A}^0)$ being transmitted $\bar{C}(\bar{A}^{\lambda})$ or $\bar{C}(\bar{A}^{\xi})$ or both of them are chosen by the decoder, when they are compared to $\bar{C}(\bar{A}^0)$. $P(EV_{0\leftarrow\lambda}, EV_{0\leftarrow\xi})$ is the probability that both $\bar{C}(\bar{A}^{\lambda})$ and $\bar{C}(\bar{A}^{\xi})$ are chosen over $\bar{C}(\bar{A}^0)$. Finally, $P(\overline{EV}_{0\leftarrow\lambda}, \overline{EV}_{0\leftarrow\xi}, EV_{0\leftarrow\mu})$ is the probability that the decoder decides in favour of $\bar{C}(\bar{A}^0)$ when it compares $\bar{C}(\bar{A}^0)$ to $\bar{C}(\bar{A}^{\lambda})$ or $\bar{C}(\bar{A}^{\xi})$, but at the same time it rejects $\bar{C}(\bar{A}^0)$ when it compares it to $\bar{C}(\bar{A}^{\mu})$.

The contribution of the error events (formed between $\bar{C}(\bar{A}^0)$ and each one of three sequences presented in Eq.(H.3)) in the value of the union bound is the following:

$$EP_{UB} = P(EV_{0\leftarrow\lambda}) + P(EV_{0\leftarrow\xi}) + P(EV_{0\leftarrow\mu}). \qquad \text{(H.5)}$$

Since $P(EV_{0\leftarrow\mu}) \geq P(\overline{EV}_{0\leftarrow\lambda}, \overline{EV}_{0\leftarrow\xi}, EV_{0\leftarrow\mu})$, it is obvious that $EP_{UB} \geq EP_{NB}$. When $\frac{P(\overline{EV}_{0\leftarrow\lambda}, \overline{EV}_{0\leftarrow\xi}, EV_{0\leftarrow\mu})}{P(EV_{0\leftarrow\mu})} \rightarrow 0$ and $P(EV_{0\leftarrow\mu})$ has value comparable to the values of $P(EV_{0\leftarrow\lambda})$, $P(EV_{0\leftarrow\xi})$, the union bound becomes loose.

When the instantaneous signal to noise ratio of the faded signal is moderate to high, single error events dominate the performance of the block decoder. Under these conditions, $P(EV_{0\leftarrow\mu})$ (which is the probability of a double error event) is considerably smaller when compared to $P(EV_{0\leftarrow\xi})$, $P(EV_{0\leftarrow\lambda})$ ($P(EV_{0\leftarrow\mu}) << P(EV_{0\leftarrow\xi})$, $P(EV_{0\leftarrow\mu}) << P(EV_{0\leftarrow\lambda})$). Since $P(EV_{0\leftarrow\mu}) \geq P(\overline{EV}_{0\leftarrow\lambda}, \overline{EV}_{0\leftarrow\xi}, EV_{0\leftarrow\mu})$ we can eliminate $P(\overline{EV}_{0\leftarrow\lambda}, \overline{EV}_{0\leftarrow\xi}, EV_{0\leftarrow\mu})$ from the right side of Eq.(H.4) without practically affecting the value of PE_{NB}.

When the instantaneous signal to noise ratio of the processed signal is low, $P(EV_{0\leftarrow\mu})$ has a value comparable to the values of $P(EV_{0\leftarrow\xi})$, $P(EV_{0\leftarrow\lambda})$. However, in (most) of the cases where the $EV_{0\leftarrow\mu}$ occurs, it occurs due to strong noise values that corrupt either or both of the received signal samples y_k, y_l. In this case, $EV_{0\leftarrow\xi}$ or $EV_{0\leftarrow\lambda}$ or both of them will occur simultaneously with $EV_{0\leftarrow\mu}$. Consequently, $P(\overline{EV}_{0\leftarrow\lambda}, \overline{EV}_{0\leftarrow\xi}, EV_{0\leftarrow\mu})$ (which requires that both the $\overline{EV}_{0\leftarrow\xi}$ and $\overline{EV}_{0\leftarrow\lambda}$ occur simultaneously) will again be very small and can be omitted from Eq.(H.4) without significant error. This allows us to express Eq.(H.4) as follows:

$$\begin{aligned} PE_{NB} &\approx P(EV_{0\leftarrow\lambda}) + P(EV_{0\leftarrow\xi}) - P(EV_{0\leftarrow\lambda}, EV_{0\leftarrow\xi}) \\ &\leq P(EV_{0\leftarrow\lambda}) + P(EV_{0\leftarrow\xi}) \end{aligned} \tag{H.6}$$

The outcome of the previous discussion, is that the effect of these three error events on the performance is more accurately determined if we include in the bound only the contributions of the single error events. To demonstrate the case, we considered only three events, however, the case holds for any number of error events chosen. In the discussion to follow we shall show that even from all these single error events there is only a small portion that has to be used. In the Lemma which follows, we shall identify these error events and prove the statement made above.

Lemma 1

Let us assume again that $\bar{C}(\bar{A}^0)$ is the transmitted sequence. Let us

consider the sequences:

$$\bar{C}(\bar{A}^{\eta}) = [c_0^{\eta} = 1, c_1^{\eta} = 1 \ldots, c_{k-1}^{\eta} = 1, c_k^{\eta} = e^{j\frac{2\pi}{M}}, c_{k+1}^{\eta} = 1 \ldots, c_{Z-1}^{\lambda} = 1]$$

$$\bar{C}(\bar{A}^{\varsigma}) = [c_0^{\varsigma} = 1, c_1^{\varsigma} = 1 \ldots, c_{k-1}^{\varsigma} = 1, c_l^{\varsigma} = e^{j(M-1)\frac{2\pi}{M}}, c_{k+1}^{\xi} = 1 \ldots, c_{Z-1}^{\varsigma} = 1]$$

$$\bar{C}(\bar{A}^{\nu}) = [c_0^{\nu} = 1, c_1^{\nu} = 1 \ldots, c_{k-1}^{\nu} = 1, c_l^{\nu} = e^{jm\frac{2\pi}{M}}, c_{k+1}^{\nu} = 1 \ldots, c_{Z-1}^{\nu} = 1]$$

(H.7)

where $1 < m < M-1$. We shall prove that whenever the error event $\{\bar{C}(\bar{A}^{\nu}) \leftarrow \bar{C}(\bar{A}^{0})\}$ happens, at least one or both of the $\{\bar{C}(\bar{A}^{\eta}) \leftarrow \bar{C}(\bar{A}^{0})\}$, $\{\bar{C}(\bar{A}^{\varsigma}) \leftarrow \bar{C}(\bar{A}^{0})\}$will happen with certainty. This event is represented as $\{\{\bar{C}(\bar{A}^{\eta}) \leftarrow \bar{C}(\bar{A}^{0})\} \cup \{\bar{C}(\bar{A}^{\varsigma}) \leftarrow \bar{C}(\bar{A}^{0})\}\}$.

Following the decision law described by Eq.(H.1), a decision in favour of $\bar{C}(\bar{A}^{\nu})$ takes place, when

$$|\sum_{i=0}^{Z-1} y_i| < |\sum_{i=0, i\neq l}^{Z-1} y_i + y_l e^{-j\frac{2m\pi}{M}}|. \tag{H.8}$$

Similarly, to decide in favour of $\bar{C}(\bar{A}^{\eta})$, $\bar{C}(\bar{A}^{\varsigma})$, the following inequalities should hold:

$$|\sum_{i=0}^{Z-1} y_i| < |\sum_{i=0, i\neq l}^{Z-1} y_i + y_l e^{-j\frac{2\pi}{M}}| \tag{H.9}$$

$$|\sum_{i=0}^{Z-1} y_i| < |\sum_{i=0, i\neq k}^{Z-1} y_i + y_k e^{j\frac{2\pi}{M}}|. \tag{H.10}$$

Let us define as $\Psi_k(\bar{y}) = Arg\{\sum_{i=0, i\neq k}^{Z-1} y_i\}$ and $\theta_k^r = Arg\{y_k\}$. We also define as $\Delta\Psi_k(\bar{y}) = [\theta_k^r \ominus \Psi_k(\bar{y})]$. It can be shown that the inequalities of Eqs.(H.8)-(H.10) are equivalent to the following inequalities respectively:

$$\cos(\Delta\Psi_k(\bar{y})) < \cos(\Delta\Psi_k(\bar{y}) - \frac{2m\pi}{M}), \tag{H.11}$$

$$\cos(\Delta\Psi_k(\bar{y})) < \cos(\Delta\Psi_k(\bar{y}) - \frac{2\pi}{M}), \tag{H.12}$$

$$\cos(\Delta\Psi_k(\bar{y})) < \cos(\Delta\Psi_k(\bar{y}) + \frac{2\pi}{M}). \tag{H.13}$$

The first inequality is satisfied when $\Delta\Psi_k(\bar{y})$ falls within the $\mathcal{QC}_1 = [\frac{m\pi}{M}, \pi + \frac{m\pi}{M})$ area of the circle, whereas the second and third in the following areas: $\mathcal{QC}_2 = [\frac{\pi}{M}, \pi + \frac{\pi}{M})$, $\mathcal{QC}_3 = [\pi - \frac{\pi}{M}, 2\pi - \frac{m\pi}{M})$ (see Fig. H). It can be easily verified that if $\Delta\Psi_k(\bar{y})$ falls within the $\mathcal{QC}_1$ area, it will certainly fall at least in one (or may be both) of $\mathcal{QC}_2$, $\mathcal{QC}_3$. This guarantees that whenever the $\{\bar{C}(\bar{A}^\nu) \leftarrow \bar{C}(\bar{A}^0)\}$ event takes place, one or both of the $\{\bar{C}(\bar{A}^\eta) \leftarrow \bar{C}(\bar{A}^0)\}$, $\{\bar{C}(\bar{A}^\zeta) \leftarrow \bar{C}(\bar{A}^0)\}$ error events will be occurring simultaneously.

The contribution of the three different error events on the performance is as follows:

$$\begin{aligned} EP_{NB} &= P(EV_{\eta\leftarrow 0} \bigcup EV_{\zeta\leftarrow 0}) + P(\overline{EV}_{\eta\leftarrow 0}, \overline{EV}_{\zeta\leftarrow 0}, EV_{\nu\leftarrow 0}) \\ &= P(EV_{\eta\leftarrow 0}) + P(EV_{\zeta\leftarrow 0}) - P(EV_{\eta\leftarrow 0}, EV_{\zeta\leftarrow 0}) \\ &\quad + P(\overline{EV}_{\eta\leftarrow 0}, \overline{EV}_{\zeta\leftarrow 0}, EV_{\nu\leftarrow 0}) \end{aligned} \tag{H.14}$$

However, according to Lemma 1, $P(\overline{EV}_{\eta\leftarrow 0}, \overline{EV}_{\zeta\leftarrow 0}, EV_{\nu\leftarrow 0}) = 0$. Consequently,

$$\begin{aligned} EP_{NB} &= P(EV_{\eta\leftarrow 0} \bigcup EV_{\zeta\leftarrow 0}) + P(\overline{EV}_{\eta\leftarrow 0}, \overline{EV}_{\zeta\leftarrow 0}, EV_{\nu\leftarrow 0}) \\ &= P(EV_{\eta\leftarrow 0}) + P(EV_{\zeta\leftarrow 0}) - P(EV_{\eta\leftarrow 0}, EV_{\zeta\leftarrow 0}) \\ &\leq P(EV_{\eta\leftarrow 0}) + P(EV_{\zeta\leftarrow 0}) \end{aligned} \tag{H.15}$$

The conclusion of the above discussion is that when operating in slow faded channels, the performance of the block decoder is more accurately estimated if the union bound is formed by the single error events having differential phase between the unequal symbols equal to $\pm\frac{2\pi}{M}$.

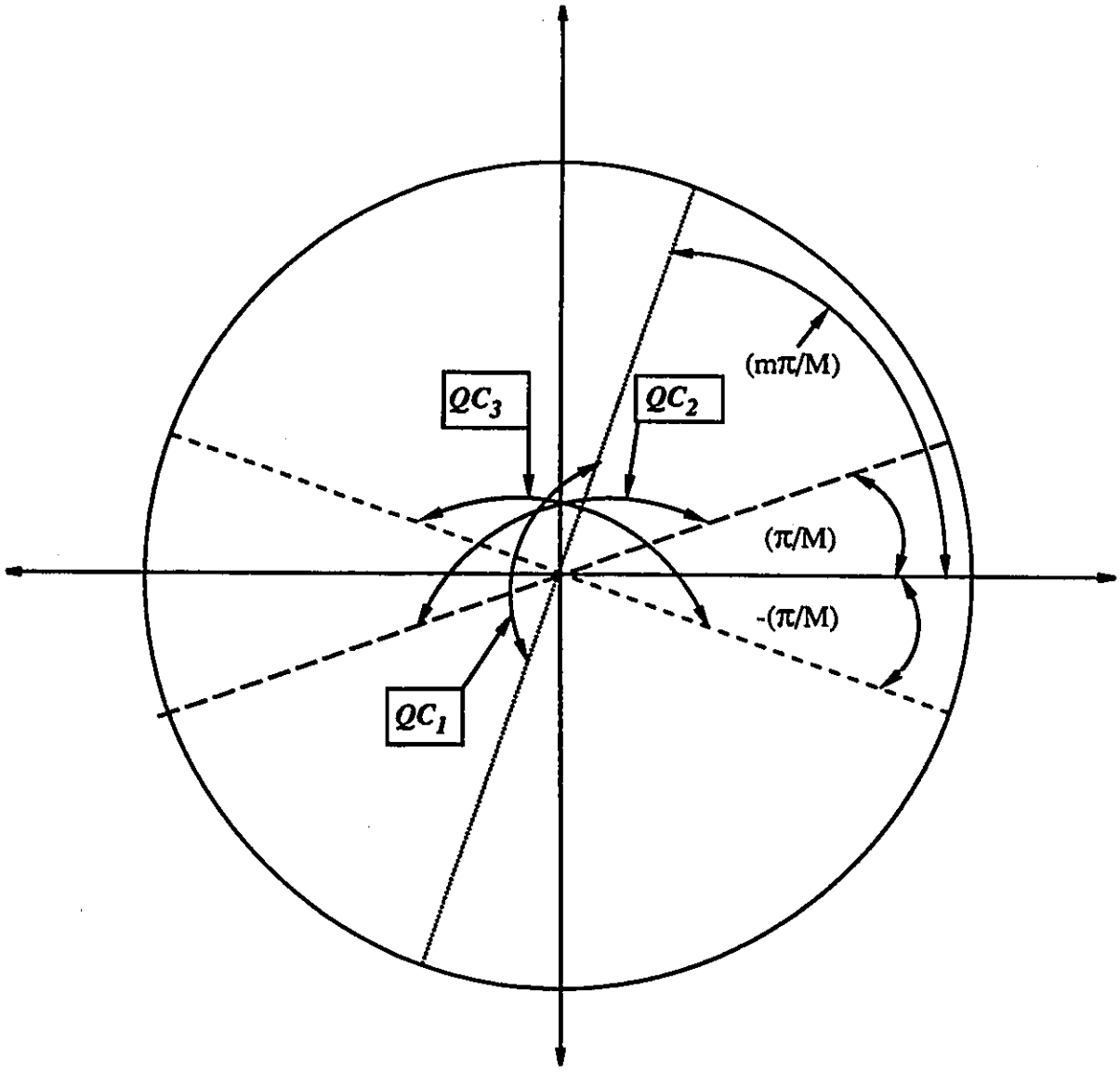
QC_3
QC_2
QC_1
(mπ/M)
(π/M)
-(π/M)

Appendix I

Performance Analysis of the Truncated Multiple Differential Detection Sequence Estimator

The analysis to follow considers an MPSK signal. The present Appendix will be sectioned in two parts. In the first, an upper and lower bound of the pairwise error event probability of the multiple differential detection (MDD) sequence estimator (decoder) will be provided. Afterwards, these upper and lower bounds will be used in the union bound to provide upper and lower bounds for the overall performance.

I.1 Pairwise Error Probability

Let us consider again the coded sequences, $\bar{C}(\bar{A}^{\nu})$, $\bar{C}(\bar{A}^{\varsigma})$ and assume that $\bar{C}(\bar{A}^{\nu})$ has been transmitted. Now let us assume that the path of $\bar{C}(\bar{A}^{\varsigma})$ diverges for the first time from the path of $\bar{C}(\bar{A}^{\nu})$ at $\ell_1^{\nu\varsigma}T$ (with $\ell_1^{\nu\varsigma}$ integer), and re-emerges back to the path of $\bar{C}(\bar{A}^{\nu})$ at $\ell_2^{\nu\varsigma}T$ (see Fig. I.1).

$$\ell_2^{\nu\varsigma} = \ell_1^{\nu\varsigma} + \ell_{Id}^{\nu\varsigma} - 1 \tag{I.1}$$

where $\ell_{1d}^{\nu\zeta}$ represents the number of symbol periods, during which the two paths move through the trellis diagram separately (i.e. length of divergence). The following identity holds:

$$c_i^{\nu} = c_i^{\zeta} \quad \forall \quad i < \ell_1^{\nu\zeta} \quad \text{and} \quad i \geq \ell_2^{\nu\zeta} = \ell_1^{\nu\zeta} + \ell_{1d}^{\nu\zeta} \tag{I.2}$$

The criterion towards choosing either $\bar{A}^{\nu}$ or $\bar{A}^{\zeta}$ can be expressed through the following two sided inequality:

$$\wp_1^{MDD}(\lambda, \bar{y}, \bar{C}(\bar{A}^{\nu})) \underset{\bar{A}^{\zeta}}{\overset{\bar{A}^{\nu}}{\gtrless}} \wp_1^{MDD}(\lambda, \bar{y}, \bar{C}(\bar{A}^{\zeta})) \tag{I.3}$$

where $\wp_1^{MDD}(\bar{y}, \bar{C}(\bar{A}^{i}))$ has been defined in Eq.(4.98) of Chapter 4. Eliminating all the common terms present on both sides of the inequality, we arrive at the following formula:

$$\Im(\lambda, \ell_1^{\nu\zeta} - 1, \ell_1^{\nu\zeta} + \ell_{1d}^{\nu\zeta} - 1, \bar{y}, \bar{C}(\bar{A}^{\nu}))$$

$$\overset{\bar{A}^{\nu}}{\underset{\bar{A}^{\zeta}}{\gtrless}}$$

$$\Im(\lambda, \ell_1^{\nu\zeta} - 1, \ell_1^{\nu\zeta} + \ell_{1d}^{\nu\zeta} - 1, \bar{y}, \bar{C}(\bar{A}^{\zeta})) \tag{I.4}$$

with

$$\Im(\lambda, l_1, l_2, \bar{y}, \bar{C}(\bar{A}^{\eta})) = \Lambda_1(\lambda, l_1 + \lceil \frac{l_2 - l_1}{2} \rceil - \lceil \frac{\lambda}{2} \rceil, \bar{y}, \bar{C}(\bar{A}^{\eta}))$$

$$+\Lambda_2(\lambda, l_1 + \lceil \frac{l_2 - l_1}{2} \rceil - \lceil \frac{\lambda}{2} \rceil, l_1 + \lceil \frac{l_2 - l_1}{2} \rceil + \lceil \frac{\lambda + 1}{2} \rceil, \bar{y}, \bar{C}(\bar{A}^{\eta}))$$

$$+\Lambda_3(\lambda, l_1 + \lceil \frac{l_2 - l_1}{2} \rceil - \lceil \frac{\lambda}{2} \rceil, l_1 + \lceil \frac{l_2 - l_1}{2} \rceil + \lceil \frac{\lambda + 1}{2} \rceil, \bar{y}, \bar{C}(\bar{A}^{\eta})), \tag{I.5}$$

$$\Lambda_1(\lambda, k_1, \bar{y}, \bar{C}(\bar{A}^{\eta})) = \sum_{l=1}^{\lambda} \sum_{k=k_1+1}^{k_1+i} [d_i^I(k) Re\{c_k^{\eta}(c_{k-l}^{\eta})^*\} + d_i^Q(k) Im\{c_k^{\eta}(c_{k-l}^{\eta})^*\}]$$

(I.6)

$$\Lambda_2(\lambda,k_1,k_2,\bar{y},\bar{C}(\bar{A}^\eta)) = \sum_{l=1}^{k_2}\sum_{k=1}^{i}[d_k^I(k_1+i)Re\{c_{k_1+i}^\eta(c_{k_1+i-k}^\eta)^*\} + d_k^Q(k_2+i)Im\{c_{k_1+i}^\eta(c_{k_1+i-k}^\eta)^*\}] \quad (I.7)$$

and

$$\Lambda_3(\lambda,k_1,k_2,\bar{y},\bar{C}(\bar{A}^\eta)) = \sum_{k=1}^{\lambda-1}\sum_{k=1}^{k_2}[d_i^I(k_1+k_2+k)Re\{c_{k_1+k_2+k}^\eta(c_{k_1+k_2}^\eta)^*\} + d_i^Q(k_1+k_2+k)Im\{c_{k_1+k_2+k}^\eta(c_{k_1+k_2}^\eta)^*\}] \quad (I.8)$$

where $\lceil\cdot\rceil$ represents the largest integer smaller than or equal to $\{\cdot\}$.

In subsection 4.3.2 of Chapter 4, the non-coherent block decoder has been introduced. In Appendix B an upper bound of its pairwise error event probability has been derived. Its performance for various MPSK signals in a Gaussian noise channel has been studied in section 4.5.

Let us consider the block decoder which is attempting to make a decision between the $\bar{A}^\nu$ and $\bar{A}^\varsigma$ sequences by processing the samples y_k received in the interval $[(\ell_1^{\nu\varsigma}-\lambda)T,(\ell_1^{\nu\varsigma}+\ell_{ld}^{\nu\varsigma}+\lambda-1)T]$ (i.e. $\ell_1^{\nu\varsigma}-\lambda \le k \le \ell_1^{\nu\varsigma}+\ell_{ld}^{\nu\varsigma}+\lambda-1$). The decoder is processing a total of $(\ell_{ld}^{\nu\varsigma}+2\lambda-1)$ y_k samples. In Eq.(4.12) the detection metric $\aleph_{IC}(\bar{y},\bar{C}(\bar{A}))$ of the block decoder is given. Applying this metric expression in the present case, we find that the choice between the two sequences depends on the direction of the following inequality:

$$\left|\sum_{k=\ell_1^{\nu\varsigma}-\lambda}^{\ell_1^{\nu\varsigma}+\ell_{ld}^{\nu\varsigma}+\lambda-1} y_k(c_k^\nu)^*\right|^2 \underset{\bar{A}^\varsigma}{\overset{\bar{A}^\nu}{\gtrless}} \left|\sum_{k=\ell_1^{\nu\varsigma}-\lambda}^{\ell_1^{\nu\varsigma}+\ell_{ld}^{\nu\varsigma}+\lambda-1} y_k(c_k^\varsigma)^*\right|^2 . \quad (I.9)$$

Working with squares rather than absolute values, the inequality of Eq.(I.9) can be expressed equivalently in the following form:

$$\left|\sum_{k=\ell_1^{\nu\varsigma}-\lambda}^{\ell_1^{\nu\varsigma}+\ell_{ld}^{\nu\varsigma}+\lambda-1} y_k(c_k^\nu)^*\right| \underset{\bar{A}^\varsigma}{\overset{\bar{A}^\nu}{\gtrless}} \left|\sum_{k=\ell_1^{\nu\varsigma}-\lambda}^{\ell_1^{\nu\varsigma}+\ell_{ld}^{\nu\varsigma}+\lambda-1} y_k(c_k^\varsigma)^*\right| . \quad (I.10)$$

Carrying on the squaring process, eliminating the common terms on both sides of the inequality and using the definitions given in Eq. (I.8), we arrive at the following form:

$$\Im(\lambda, \ell_1^{\nu\zeta} - 1, \ell_1^{\nu\zeta} + \ell_{ld}^{\nu\zeta} - 1, \bar{y}, \bar{C}(\bar{A}^{\nu})) + \Lambda_4(\lambda, \ell_1^{\nu\zeta} - 1, \ell_1^{\nu\zeta} + \ell_{ld}^{\nu\zeta} - 1, \bar{y}, \bar{C}(\bar{A}^{\nu}))$$

$$\begin{matrix} \bar{A}^{\nu} \\ > \\ < \\ \bar{A}^{\zeta} \end{matrix}$$

$$\Im(\lambda, \ell_1^{\nu\zeta} - 1, \ell_1^{\nu\zeta} + \ell_{ld}^{\nu\zeta} - 1, \bar{y}, \bar{C}(\bar{A}^{\zeta})) + \Lambda_4(\lambda, \ell_1^{\nu\zeta} - 1, \ell_1^{\nu\zeta} + \ell_{ld}^{\nu\zeta} - 1, \bar{y}, \bar{C}(\bar{A}^{\zeta}))$$

(I.11)

with

$$\begin{aligned} \Lambda_4(\lambda, k_1, k_2, \bar{y}, \bar{C}(\bar{A}^{\eta})) \;=\; & \sum_{k=-\lambda}^{k_2} \sum_{l=\lambda+1}^{k_2+\lambda-1-k} [d_i^I(k_1+k+i) Re\{c_{k_1+k+i}^{\eta}(c_{k_1+k}^{\eta})^*\} \\ & + d_i^Q(k_1+k+i) Im\{c_{k_1+k+i}^{\eta}(c_{k_1+k}^{\eta})^*\}] \,. \end{aligned} \qquad \text{(I.12)}$$

Comparing Eqs.(I.4) and (I.11), we realize that in the second case there is an extra function, the $\Lambda_4(\lambda, \ell_1^{\nu\zeta} - 1, \ell_1^{\nu\zeta} + \ell_{ld}^{\nu\zeta} - 1, \bar{y}, \bar{C}(\bar{A}^{\eta}))$ with $\eta \in \{\nu, \zeta\}$. Careful examination of this function will make the reader realize that it consists of the outputs of differential detectors with delay elements iT, the i being between $\lambda+1$ and $\ell_{ld}^{\nu\zeta} + \lambda - 1$ ($\lambda+1 \leq i \leq \ell_{ld}^{\nu\zeta} + \lambda - 1$). The truncated MDD receiver does not have this information available to it, due to the restriction of using only λ differential detectors to carry on the sequence estimators. Such information is useful for the detection. Since the block decoder uses this additional information -on top of the information being available and processed by the truncated MDD sequence estimator- it should be able to make more reliable estimates compared to the truncated MDD receiver. In Appendix B, a tight upper bound $B_{[\nu,\zeta]}^{Z}$ of the pairwise error event probability for the block decoder has been provided (see Eqs.(B.15) and (B.18) in Appendix B). Z is the number of received signal samples processed by the block decoder. In this case, $Z = (\ell_{ld}^{\nu\zeta} + 2\lambda - 1)$. According to the above discussion, the following relation exists between $B_{[\nu,\zeta]}^{\ell_{ld}^{\nu\zeta}+2\lambda-1}$ and

the pairwise error event probability of $P_{MDD}(\lambda, \{\bar{C}(\bar{A}^{\zeta}) \leftarrow \bar{C}(\bar{A}^{\nu})\})$ of the truncated MDD receiver.

$$B_{[\nu,\zeta]}^{\ell_{Id}^{\nu\zeta}+2\lambda-1} \leq P_{MDD}(\lambda, \{\bar{C}(\bar{A}^{\zeta}) \leftarrow \bar{C}(\bar{A}^{\nu})\}) \ . \tag{I.13}$$

Let us consider now the block decoder which processes the y_k samples received in the $[(\ell_1^{\nu\zeta} + [\frac{\ell_{Id}^{\nu\zeta}}{2}] - [\frac{\lambda}{2}] - 1)T, (\ell_1^{\nu\zeta} + [\frac{\ell_{Id}^{\nu\zeta}}{2}] + [\frac{\lambda+1}{2}])T$ time interval. Following the same logic and methodology with the one described above, we arrive at the following inequality whose direction determines the choice between the two sequences:

$$\Lambda_2(\lambda, \ell_1^{\nu\zeta} - 1, \ell_1^{\nu\zeta} + \ell_{Id}^{\nu\zeta} - 1, \bar{y}, \bar{C}(\bar{A}^{\nu}))$$

$$\begin{matrix} \bar{A}^{\nu} \\ > \\ < \\ \bar{A}^{\zeta} \end{matrix}$$

$$\Lambda_2(\lambda, \ell_1^{\nu\zeta} - 1, \ell_1^{\nu\zeta} + \ell_{Id}^{\nu\zeta} - 1, \bar{y}, \bar{C}(\bar{A}^{\zeta})) \ . \tag{I.14}$$

Comparing Eqs.(I.4), (I.5) and (I.14) we realize that Eq.(I.14) can be derived from Eqs.(I.4),(I.5), by truncating the $\Lambda_1(\lambda, \ell_1^{\nu\zeta} - 1, \bar{y}, \bar{C}(\bar{A}^{\eta}))$, $\Lambda_3(\lambda, \ell_1^{\nu\zeta} - 1, \ell_1^{\nu\zeta} + \ell_{Id}^{\nu\zeta} - 1, \bar{y}, \bar{C}(\bar{A}^{\eta}))$ terms ($\eta \in \{\nu, \zeta\}$). Since such truncation takes away useful information from the decoding process, (it is the information about the received signal present in the terms $\Lambda_1(\lambda, \ell_1^{\nu\zeta} - 1, \bar{y}, \bar{C}(\bar{A}^{\eta}))$ and $\Lambda_3(\lambda, \ell_1^{\nu\zeta} - 1, \ell_1^{\nu\zeta} + \ell_{Id}^{\nu\zeta} - 1, \bar{y}, \bar{C}(\bar{A}^{\eta}))$, it is natural to expect that the considered block decoder will provide less accurate decisions compared to the truncated MDD receiver (which is making use of the extra information available in $\Lambda_1(\lambda, \ell_1^{\nu\zeta} - 1, \bar{y}, \bar{C}(\bar{A}^{\eta}))$ and $\Lambda_3(\lambda, \ell_1^{\nu\zeta} - 1, \ell_1^{\nu\zeta} + \ell_{Id}^{\nu\zeta} - 1, \bar{y}, \bar{C}(\bar{A}^{\eta}))$). Consequently, the upper bound of the pairwise error probability of this block decoder can act as an upper bound for $P_{MDD}(\lambda, \{\bar{C}(\bar{A}^{\zeta}) \leftarrow \bar{C}(\bar{A}^{\nu})\})$. The number of y_k samples $(\ell_1^{\nu\zeta} + \lceil\frac{\ell_{Id}^{\nu\zeta}}{2}\rceil - \lceil\frac{\lambda}{2}\rceil - 1 \leq k \leq \ell_1^{\nu\zeta} + \lceil\frac{\ell_{Id}^{\nu\zeta}}{2}\lceil + \lceil\frac{\lambda+1}{2}\rceil)$ processed by the block decoder is equal to $\lambda + 1$. Following the above discussion,

$$P_{MDD}(\lambda, \{\bar{C}(\bar{A}^{\zeta}) \leftarrow \bar{C}(\bar{A}^{\nu})\}) \leq B_{[\nu,\zeta]}^{\lambda+1} \ . \tag{I.15}$$

Summarizing the discussion presented so far, we have the following relation regarding the pairwise error probability $P_{MDD}(\lambda, \{\bar{C}(\bar{A}^{\zeta}) \leftarrow \bar{C}(\bar{A}^{\nu})\})$.

$$B_{[\nu,\zeta]}^{\ell_{Id}^{\nu\zeta}+2\lambda-1} \leq P_{MDD}(\lambda, \{\bar{C}(\bar{A}^{\zeta}) \leftarrow \bar{C}(\bar{A}^{\nu})\}) \leq B_{[\nu,\zeta]}^{\lambda+1} \ . \tag{I.16}$$

I.2 Upper and Lower Bounding the overall Symbol Error Probability of the Truncated MDD Sequence Estimator

Following the union bound approach discussed in section 4.5 of Chapter 4, we can write the following expression:

$$\begin{aligned} P_e^{MDD}(\lambda) &\leq \frac{1}{(Z-L_c-1)2^{(Z-L_c-1)p}} \sum_{\bar{C}(\bar{A}^\nu)\in S_{\bar{C}W}^Z} \sum_{\bar{C}(\bar{A}^\zeta)\in S_{\bar{C}(\bar{A}^\nu)}} \\ &\quad n_e(\{\bar{C}(\bar{A}^\zeta)\leftarrow\bar{C}(\bar{A}^\nu)\})P^{RS}(\{\bar{C}(\bar{A}^\zeta)\leftarrow\bar{C}(\bar{A}^\nu)\} \\ &= B_e^{MDD}(\lambda) \end{aligned} \tag{I.17}$$

where $P_e^{MDD}(\lambda)$ is the overall error probability of the truncated multiple differential sequence estimator using a total of λ differential detectors for detection. $B_e^{MDD}(\lambda)$ is the upper bound of $P_e^{MDD}(\lambda)$. We remind the reader that $n_e(\{\bar{C}(\bar{A}^\zeta)\leftarrow\bar{C}(\bar{A}^\nu)\})$ represents the number of symbol errors associated with the error event $\{\bar{C}(\bar{A}^\zeta)\leftarrow\bar{C}(\bar{A}^\nu)\}$. Also, L_c is the constraint length of the code. For uncoded signals, $L_c = 0$. Using Eqs.(I.16), (I.17) we can write the following inequality:

$$\mathcal{LB}_\lambda^{MDD} \leq B_e^{MDD}(\lambda) \leq \mathcal{UB}_\lambda^{MDD} \tag{I.18}$$

where

$$\begin{aligned} \mathcal{LB}_\lambda^{MDD} &= \frac{1}{(Z-L_c-1)2^{(Z-L_c-1)p}} \sum_{\bar{C}(\bar{A}^\nu)\in S_{\bar{C}W}^Z} \sum_{\bar{C}(\bar{A}^\zeta)\in S_{\bar{C}(\bar{A}^\nu)}} \\ &\quad n_e(\{\bar{C}(\bar{A}^\zeta)\leftarrow\bar{C}(\bar{A}^\nu)\})B_{[\nu,\zeta]}^{\ell_{id}^{\nu\zeta}+2\lambda-1} \end{aligned} \tag{I.19}$$

and

$$\begin{aligned} \mathcal{UB}_\lambda^{MDD} &= \frac{1}{(Z-L_c-1)2^{(Z-L_c-1)p}} \sum_{\bar{C}(\bar{A}^\nu)\in S_{\bar{C}W}^Z} \sum_{\bar{C}(\bar{A}^\zeta)\in S_{\bar{C}(\bar{A}^\nu)}} \\ &\quad n_e(\{\bar{C}(\bar{A}^\zeta)\leftarrow\bar{C}(\bar{A}^\nu)\})B_{[\nu,\zeta]}^{\lambda+1} \end{aligned}$$

(I.20)

Through Eqs.(I.18), (I.19), (I.20), the SER performance of the truncated multiple differential detection sequence estimator has been upper and lower bounded.

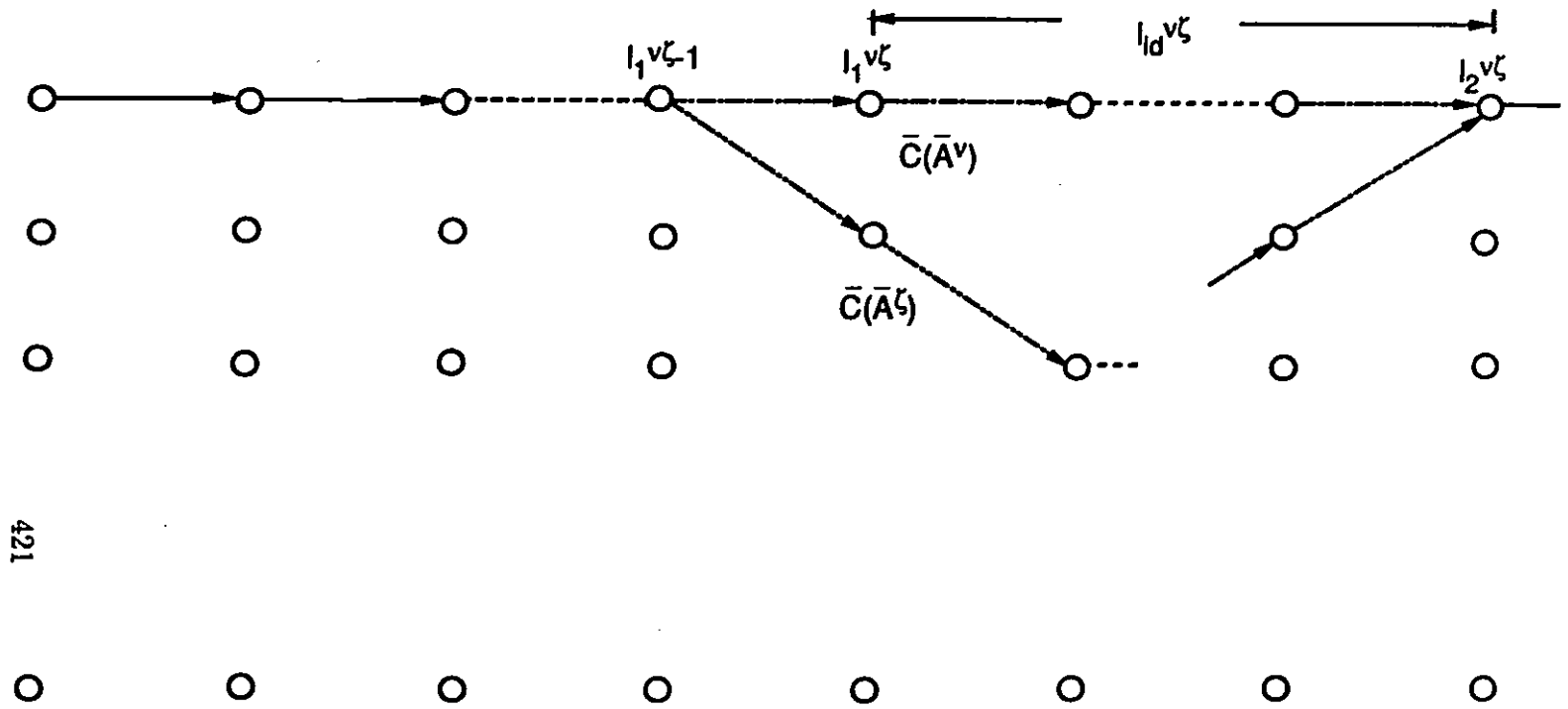

Figure I.1: Trellis diagram displaying the diverging paths of the error event which is formed between the sequences $\bar{C}(\bar{A}^{\nu})$, $\bar{C}(\bar{A}^{\zeta})$.

Appendix J

Performance Analysis of the Symbol-by-Symbol Multiple Differential Receiver using Combining with Feedback

This appendix provides the analytical framework for the evaluation of the multiple differential detection symbol-by-symbol receiver which uses combining with feedback.

Let us assume that the receiver uses λ differential detectors ($\lambda = i_P$). The receiver makes a decision on the value of the symbol g_ξ, using the decisions of the $(\lambda - 1)$ previous symbols ($\hat{g}_{\xi-1}, \hat{g}_{\xi-2}, \ldots, \hat{g}_{\xi-\lambda+1}$). The symbols g_l can have one out of M different values, i.e.

$$g_l = e^{j\varphi_i} = e^{ji\frac{2\pi}{M}} \quad \text{where} \quad 0 \leq i \leq M-1. \tag{J.1}$$

The decision law of the receiver can be seen in Eq.(4.135) of Chapter 4. For the reader's convenience we write it here again:

$$\widehat{g_\xi} = \widehat{e^{j\varphi_i}} = e^{ji\frac{2\pi}{M}} \Longrightarrow \max_{1\leq i\leq M} \{|y_\xi e^{-ji\frac{2\pi}{M}}(\Pi_{l=1}^{\lambda-1}\hat{g}^*_{\xi-l}) + \sum_{i=1}^{\lambda-1} y_{\xi-i}(\Pi_{l=i}^{\lambda-1}\hat{g}^*_{\xi-i}) + y_{\xi-\lambda}|\} \tag{J.2}$$

One notices that in Eq.(J.2) we have replaced $\bar{a}_\xi^p$ with g_ξ. $\bar{a}_\xi^p$ represents the information word, whereas g_ξ is the information symbol produced by the information word $\bar{a}_\xi^p$. Also, since we deal with uncoded signals, we have replaced M_p with M (for uncoded signals $M_p = M$).

Without any loss of generality, we assume that the actual information symbol g_ξ transmitted is the $g_\xi = 1$. For the analysis which follows it has also been assumed that the decisions used by the receiver in the decision feedback are correct ($\hat{g}_{\xi-1} = g_{\xi-1}$, $\hat{g}_{\xi-2} = g_{\xi-2}$, $\ldots$, $\hat{g}_{\xi-\lambda+1} = g_{\xi-\lambda+1}$). Using these assumptions in Eq.(J.2), it becomes:

$$\widehat{g_\xi^p} = \bar{e}^{j\varphi_i} = e^{ji\frac{2\pi}{M}} \Longrightarrow \overset{1\le i\le M}{\max} \{|y_\xi e^{-ji\frac{2\pi}{M}}(\Pi_{l=1}^{\lambda-1} g_{\xi-l}{}^*) + \sum_{i=1}^{\lambda-1} y_{\xi-i}(\Pi_{l=i}^{\lambda-1} g_{\xi-i}^*) + y_{\xi-\lambda}|\}. \tag{J.3}$$

An error in detection will occur, if the maximization process described by Eq.(J.3) chooses a value $e^{j\varphi_i} \neq 1$ ($\varphi_i \neq 0$) as the most possible value for g_ξ. In this case,

$$|y_\xi e^{-ji\frac{2\pi}{M}}(\Pi_{l=1}^{\lambda-1} g_{\xi-l}{}^*) + \sum_{i=1}^{\lambda-1} y_{\xi-i}(\Pi_{l=i}^{\lambda-1} g_{\xi-i}^*) + y_{\xi-\lambda}|$$

$$>$$

$$|y_\xi(\Pi_{l=1}^{\lambda-1} g_{\xi-l}{}^*) + \sum_{i=1}^{\lambda-1} y_{\xi-i}(\Pi_{l=i}^{\lambda-1} g_{\xi-i}^*) + y_{\xi-\lambda}| \,. \tag{J.4}$$

Following the same steps with those described in the Lemma of Appendix H, we find out that when the inequality of Eq.(J.4) holds with $1 < i < M-1$, it is certain that one or both of the following inequalities will be happening as well:

$$|y_\xi e^{-j\frac{2\pi}{M}}(\Pi_{l=1}^{\lambda-1} g_{\xi-l}{}^*) + \sum_{i=1}^{\lambda-1} y_{\xi-i}(\Pi_{l=i}^{\lambda-1} g_{\xi-i}^*) + y_{\xi-\lambda}|$$

$$>$$

$$|y_\xi(\Pi_{l=1}^{\lambda-1} g_{\xi-l}{}^*) + \sum_{i=1}^{\lambda-1} y_{\xi-i}(\Pi_{l=i}^{\lambda-1} g_{\xi-i}^*) + y_{\xi-\lambda}|, \tag{J.5}$$

$$|y_\xi e^{-j(M-1)\frac{2\pi}{M}}(\Pi_{l=1}^{\lambda-1} g_{\xi-l}{}^*) + \sum_{i=1}^{\lambda-1} y_{\xi-i}(\Pi_{l=i}^{\lambda-1} g_{\xi-i}^*) + y_{\xi-\lambda}|$$

$$>$$

$$|y_\xi(\Pi_{l=1}^{\lambda-1} g_{\xi-l}{}^*) + \sum_{i=1}^{\lambda-1} y_{\xi-i}(\Pi_{l=i}^{\lambda-1} g_{\xi-i}^*) + y_{\xi-\lambda}| \,. \tag{J.6}$$

This means that whenever a value $e^{j\varphi_i} = e^{ji\frac{2\pi}{M}}$ is chosen as the most possible value for g_ξ (instead of $e^{j\varphi_0} = 1$) it is certain that the maximization process described by Eq.(J.3) will also indicate that one or both of the $e^{j\varphi_1} = e^{j\frac{2\pi}{M}}$, $e^{j\varphi_{M-1}} = e^{j(M-1)\frac{2\pi}{M}}$ are more possible than $e^{j\varphi_0} = 1$. The above discussion leads to the conclusion that in order to find the error probability of the receiver, it is enough to find out what the probability is, that $e^{j\varphi_1} = e^{j\frac{2\pi}{M}}$ and/or $e^{j\varphi_{M-1}} = e^{j(M-1)\frac{2\pi}{M}}$ are chosen over $e^{j\varphi_0} = 1$. The probability that $e^{j\varphi_1} = e^{j\frac{2\pi}{M}}$ is chosen over $e^{j\varphi_0} = 1$ is represented as $P(\{e^{j\varphi_1} \leftarrow e^{j\varphi_0}\})$. The probability that $e^{j\varphi_{M-1}} = e^{j(M-1)\frac{2\pi}{M}}$ is chosen over $e^{j\varphi_0} = 1$ is represented as $P(\{e^{j\varphi_{M-1}} \leftarrow e^{j\varphi_0}\})$. Finally, the probability that both error events happen simultaneously, is represented as $P(\{e^{j\varphi_1} \leftarrow e^{j\varphi_0}\} \bigcup \{e^{j\varphi_{M-1}} \leftarrow e^{j\varphi_0}\})$. According to what has been discussed,

$$P_e^{CWF} = P(\{e^{j\varphi_1} \leftarrow e^{j\varphi_0}\} \bigcup \{e^{j\varphi_{M-1}} \leftarrow e^{j\varphi_0}\}) \tag{J.7}$$

where P_e^{CWF} is the error probability of the receiver.

Using the material of Appendixes B, C, we find that $P(\{e^{j\varphi_1} \leftarrow e^{j\varphi_0}\})$ can be upper bounded by the following expression:

$$P(\{e^{j\varphi_1} \leftarrow e^{j\varphi_0}\}) \leq B_{CWF}^{(\lambda+1)} = \frac{1}{2}\wp(M,1)$$

$$\exp\{-\frac{1}{2\sigma_n^2}((\lambda+1) - \sqrt{(\lambda+1)^2 + 2 - 2(\lambda+1) + 2\lambda\cos(\frac{2\pi}{M})}\} \tag{J.8}$$

where

$$\wp(M,1)=\begin{cases}1 & \text{for } M=2 \\ & \text{and } \lambda=1 \\ \frac{1}{\sqrt{2\pi}}\frac{1}{\sqrt{\frac{1}{\sigma_n^2}}}\frac{\sqrt{2}}{\sqrt{(\lambda+1)^2+2(1-\cos(\frac{2\pi}{M}))-2(\lambda+1)(1-\cos(\frac{2\pi}{M}))}} & \text{elsewhere.}\end{cases}$$

(J.9)

The same expression is also an upper bound for $P(\{e^{j\varphi_{M-1}} \leftarrow e^{j\varphi_0}\})$.

$$\begin{aligned}P(\{e^{j\varphi_1} \leftarrow e^{j\varphi_0}\} \quad \cup \quad \{e^{j\varphi_{M-1}} \leftarrow e^{j\varphi_0}\}) &= P(\{e^{j\varphi_1} \leftarrow e^{j\varphi_0}\}) \\ &+P(\{e^{j\varphi_{M-1}} \leftarrow e^{j\varphi_0}\}) \\ &-P(\{e^{j\varphi_1} \leftarrow e^{j\varphi_0}\},\{e^{j\varphi_{M-1}} \leftarrow e^{j\varphi_0}\}) \\ &\leq P(\{e^{j\varphi_1} \leftarrow e^{j\varphi_0}\})+P(\{e^{j\varphi_{M-1}} \leftarrow e^{j\varphi_0}\}).\end{aligned}$$

(J.10)

From Eqs.(J.7) to (J.10), the following inequality holds:

$$\begin{aligned}P_e^{CWF} \leq\ & P(\{e^{j\varphi_1} \leftarrow e^{j\varphi_0}\})+P(\{e^{j\varphi_{M-1}} \leftarrow e^{j\varphi_0}\}) \leq 2B_{CWF}^{(\lambda+1)}=\wp(M,1) \\ & \exp\{-\frac{1}{2\sigma_n^2}((\lambda+1)-\sqrt{(\lambda+1)^2+2-2(\lambda+1)+2\lambda\cos(\frac{2\pi}{M})}\}\end{aligned}$$

(J.11)

Eq.(J.11) provides an upper performance bound for the CWF receiver.

Bibliography

[1] M. Abramovitz and I.A. Stegun, "*Handbook of Mathematical Functions*", Dover Publications Incorporation, New York, 1972.

[2] F. Adachi, "Postdetection Selection Diversity Effects on Digital Land Mobile Radio", IEEE Trans. on Vehicular Tech., Vol. VT-31, pp. 166-172, Nov.1982.

[3] F. Adachi and K. Ohno, "Performance Analysis of GMSK frequency detection with decision feedback in digital land mobile radio, IEE Proc. Part F, Vol.135, pp. 199-207, June 1988.

[4] Y. Akaiwa, et. al., "Highly Efficient Digital Mobile Communications with a Linear Modulation Method", IEEE Jour. on Selected Areas in Comm.,Vol. SAC-5, No. 5, pp. 890-895, June 1987.

[5] Y. Akaiwa, et. al., "Performance of baseband bandlimited multilevel FM with discriminator detection for digital mobile telephony", Trans. of IECE Japan, Vol. E64, pp. 463-469, 1981.

[6] F. Amoroso and J.A. Kivet, "Simplified MSK signalling technique", IEEE Trans. on Comm., Vol. COM-25,pp.433-441, Apr. 1977.

[7] J. B. Anderson, T. Aulin and C.-E. Sundberg, "*Digital Phase Modulation*", Plenum Press, New York, U.S.A., 1986.

[8] S. Ariyavistakul te. al., "Fractional Bit differential detection of MSK – A scheme to avoid outages due to frequency selective fading", IEEE Trans. on Vehicular Tech., Vol. VT-30, pp. 36-42, Feb. 1987.

[9] N. Arne, B. Swensson and C. W. Sundberg,"Performance evaluation of differential and discriminator detection of continuous phase modulation", IEEE Trans. on Vehicular Tech., Vol. VT-35, pp 106-117, Aug. 1986.

[10] R. Arredondo, "AMPS - Advanced mobile phone system", Bell Systems Technical Journal, Jan. 1979.

[11] C. J. Ashton, "Archimides: land mobile communications for highly inclined satellite orbits", IEE 4^{th} International Conference on Satellite Systems for Mobile Communications and Navigation, Oct. 1988.

[12] T. Aulin, N. Rydbeck and C.W.Sundberg,"Continuous Phase Modulation - Part II: Partial Response Signaling", IEEE Trans. on Comm., Vol. COM-29, pp. 210-225, March 1981.

[13] T. Aulin and C. W. Sundberg, "Partially Coherent Detection of Digital Full Response Continuous Phase Modulated Signals", IEEE Trans. on Comm., Vol. COM-30, pp. 1096-1116, May 1982.

[14] T. Aulin and C. W. Sundberg, "On Partially Coherent Detection of Digital Continuous Phase Modulated Signals", Proc. of International Conference on Communications (ICC'80), pp. 26.2.1-26.2.6., June 1980.

[15] T. Aulin and C.W.Sundberg, "Synchronization Properties of Continuous Phase Modulation", Proc. of Global Communications Conference (GLOBECOM'82), pp. 877-883, Dec. 1982.

[16] A. J. Bateman et al., "Speech and Data Communications Over 942 MHz TAB and TTIB Single Sideband Mobile Radio Systems Incorporating Feed-Forward Signal Regeneration", IEEE Trans. on Vehicular Tech., Vol. VT-34, pp. 13-21, Feb. 1985.

[17] W. R. Bennett and J. R. Davey, "*Data Transmission*", McGraw-Hill, New York, 1965.

[18] W. R. Bennett and J. Saltz, "Binary Data Transmission by FM over a Real Channel", Bell System Technical Journal, pp. 2387-2426, Sept. 1963.

[19] E. Braun and S. Schon, "A Cordless Infrared Telephone", Telecommunications Report, Vol. 2, No. 2, pp. 83-86, Feb. 1985.

[20] C. W. Broderick, "A digital transmission system for TD–2 Radio", Bell System Technical Journal, Feb. 1971.

[21] D. Bouras, P. T. Mathiopoulos and D. Makrakis, "Near Optimal Non-Coherent Detection of Multi-Amplitude $\pi/4$-QPSK Schemes", Proc. of 4^{th} Nordic Seminar on Digital Mobile Radio Communications (DMR IV), pp.1.1.1-6, June 1990.

[22] D. Bouras, *Optimal Decoding of PSK and QAM Signals in Frequency Nonselective Fading Channels*", M.A.Sc Dissertation Thesis, Department of Electrical Engineering, University of British Columbia, Sept. 1991.

[23] J. J. Bussgang and M. Leither, "Error Performance of Differential Phase Shift Transmission Over a Telephone Line", IEEE Trans. on Comm., Vol. COM-16, pp. 411-418, May 1978.

[24] G. Calhoun, "*Digital Cellular radio*", Boston, Artech House, 1989.

[25] M. Callendar, "International Standards for personal communications", Canadian Conference on Electrical and Computer Engineering, pp. 239-245, Sept. 1989.

[26] S. N. Carney, "Co-Channel Interference Comparison for Conventional Land Mobile Frequency Modulation and 2400 LPC/FSK Systems", Proc. of IEEE Vehicular Technology Conference (VTC'84), pp. 131-135, May 1984.

[27] P. C. Carpender, "FM Video Spectra modeling for satellite signal interference prediction", IEEE Trans. on Broadcasting, Vol.34, No. 2, pp. 70-74, March 1988.

[28] CCITT Study Group XVIII, Part C of the Report of the Seoul Meeting, Report R55(C), Feb. 1988.

[29] M. F. Choquet and H. J. Nussbaumer, "Microcoded Modem Transmitters", IBM Journal on Research and Development, pp. 338-351, July 1974.

[30] P. E. K. Chow and D. H. S. Ho, "Improving DCPSK Transmission by Means of Error Control", IEEE Trans. on Comm., Vol. COM-19, Oct. 1971, pp. 715-719.

[31] J. C.-I. Chuang, "The effects of time delay spread on portable radio communication channels with digital modulation", IEEE Jour. on Selected Areas in Comm.,Vol. SAC-5, pp. 879-889, June 1987.

[32] J. C.-I. Chuang, "Comparison of Coherent and Differential Detection of BPSK and QPSK in a Quasi-static Fading Channel", IEEE Trans. on Vehicular Tech., Vol. VT-38, No. 2, pp. 565-567, May 1990.

[33] K. S. Chung, "A Noncoherent Receiver for GTFM Signals", Proc. of Global Communications Conference (GLOBECOM'82), pp. B3.5.1-5, Dec. 1982.

[34] K. S. Chung, "Generalized Tamed Frequency Modulation and its Application for Mobile Radio Communications", IEEE Jour. on Selected Areas in Comm.,Vol. SAC-2, pp. 487-497, July 1984.

[35] K. S. Gilhosen et. al., "On the Capacity of Cellular CDMA System, IEEE Trans. on Vehicular Tech., Vol. VT-40, No. 2, pp. 303-312, May 1991.

[36] G. C. Clark and J.B. Cain, "*Error Correction Coding for Digital Communications*, Plennum Press, New York, 1981.

[37] D. C. Cox, "Universal digital portable radio communications", Proceedings of IEEE, pp. 436-477, April 1987.

[38] D. C. Cox, "Portable Digital Radio Communications - our approach to the tetherless access", IEEE Communications Magazine, Vol. 27, pp. 30-40, July 1989.

[39] D. C. Cox, "Personal Communications – A viewpoint", IEEE Communications Magazine, Vol. 28, pp. 8-20, Nov. 1990.

[40] S. Crozier et. al., "Performance evaluation of differential detection of MSK", Proc. of Global Communications Conference (GLOBECOM'82), pp. A.5.1.1.-5.

[41] Y. Daido et al., "256 QAM Modem for High Capacity Digital Radio Systems", Proc. of Global Communications Conference (GLOBECOM'84), pp. 16.8.1-5, Dec. 1984.

[42] F. Davarian, "Fade margin calculation for channels impaired by Rician fading", IEEE Trans. on Vehicular Tech., Vol. VT-34, pp. 41-44, Feb. 1985.

[43] F. Davarian, "Comments on *'BPSK System with Sounder to Combat Rayleigh Fading Mobile in Mobile Radio Communications'* ", IEEE Trans. on Vehicular Tech., Vol. VT-34, pp. 154-156, Nov.1985.

[44] F. Davarian,"Channel Simulation to facilitate Mobile-Satellite Communications Research", IEEE Trans. on Comm., Vol. COM-35, pp. 47-56, Jan. 1987.

[45] D. Divsalar and M. K. Simon, "Trellis Coded Modulation for 4800-9600 bits/sec. Transmission Over a Fading Mobile Satellite Channel", IEEE Jour. on Selected Areas in Comm.,Vol. SAC-5, pp. 162-175, Feb. 1987.

[46] D. Divsalar, M. K. Simon and J.Y. Yuen, "Trellis Coding with Asymmetric Modulations", IEEE Trans. on Comm., Vol. COM-35, pp. 130-140, Feb. 1987.

[47] D. Divsalar and M. K. Simon, "The Design of Trellis Coded MPSK for Fading Channels: Performance Criteria", IEEE Trans. on Comm., Vol. COM-36, pp. 1004-1012, Sep. 1988.

[48] D. Divsalar and M. K. Simon, "The Design of Trellis Coded MPSK for Fading Channels: Set Partitioning for Optimum Code Design", IEEE Trans. on Comm., Vol. COM-36, pp. 1013-1021, Sep. 1988.

[49] D. Divsalar and M. K. Simon, "Multiple Trellis Coded Modulation (MTCM)", IEEE Trans. on Comm., Vol. COM-36, pp. 410-419, April 1988.

[50] D. Divsalar and M. K. Simon, "Multiple Trellis Coded Modulation (MTCM)", Proc. of Global Communications Conference (GLOBECOM'86), pp. 30.8.1-7, Dec. 1986.

[51] D. Divsalar and M. K. Simon, "Multiple Trellis Coded Modulation (MTCM) performance on a Fading Satellite Channel", Proc. of Global Communications Conference (GLOBECOM'87), pp. 43.8.1-6, Nov. 1987.

[52] D. Divsalar and M. K. Simon, "Multiple-Symbol Differential Detection of MPSK", IEEE Trans. on Comm., Vol. COM-38, No.3, pp. 300-308, March 1991.

[53] D. Divsalar, M . K. Simon and M. Hhahshahani, "The Performance of Trellis-Coded MDPSK with Multiple Symbol Detection", IEEE Trans. on Comm., Vol. COM-38, No. 9, pp. 1391-1403, Sept. 1991.

[54] P. Dondl, "Loopus opens a new dimension in satellite communications', International Journal of Satellite Communications, Vol. 2, 1984, pp. 241-251.

[55] Electronic Industries Association Specification IS-54, "Dual-mode subscriber equipment compatibility specification", EIA project No. 2215, Dec. 1989.

[56] S. M. Elnoubi and S. C. Gupta, "Error rate performance of non-coherent detection of duobinary coded MSK and TFM in mobile radio communication systems", IEEE Trans. on Vehicular Tech., Vol. VT-30, pp. 62-76, May 1981.

[57] S. M. Elnoubi, "Analysis of GMSK with differential detection in land mobile channels", IEEE Trans. on Vehicular Tech., Vol. VT-35, pp. 71-76, May 1986.

[58] S. M. Elnoubi, "Probability of error analysis of digital partial response continuous phase modulation with differential detection in mobile radio channels", Proc. of IEEE Vehicular Technology Conference (VTC'87), pp. 51-58, June 1987.

[59] W. Feller, "*An Introduction to Probability Theory and Its Applications*", Volume I, 3rd Edition, J. Wiley & Sons, New York, 1970.

[60] K. Feher, "*Digital Communications Satellite-Earth Station Engineering*", Prentice-Hall Inc., Englewood Cliffs, N.J., Jan. 1983.

[61] K. Feher, "*Digital Modulation Techniques in an Interference Environment*", EMC Encyclopedia, Vol. 9, Don White Consultants, Germantown, Maryland, 1971.

[62] K. Feher, "*Digital Communications: Microwave Applications*", Prentice-Hall Inc., Englewood Cliffs, N.J., Jan. 1981.

[63] K. Feher, "*Advanced Digital Communications: Systems and Signal Processing Techniques*", Prentice-Hall Inc., Englewood Cliffs, N.J., Jan. 1986.

[64] K. Feher, "*Telecommunications Measurements, Analysis and Instrumentation*", Prentice-Hall Inc., Englewood Cliffs, N.J., Jan. 1986.

[65] K. Feher, "MODEMS for Emerging Digital Cellular-Mobile Radio Systems", IEEE Trans. on Vehicular Tech., Vol. VT-40, No. 2, pp. 355-365, May 1991.

[66] K. Feher, R. Goulet and S. Morissette, "1544 Mb/Sec. Data Above FDM Voice (DAV) and Data Under FDM Voice (DUV) Microwave Transmission", IEEE Transactions on Communications, Nov. 1975.

[67] K. Feher and M. Morris, "Developments in Canadian and International Data Above Voice – Video Telecommunications", Proc. of IEEE Canadian Communications Conference, Oct. 1978.

[68] K. Feher and M. Morris, "Simultaneous Transmission of Digital Phase Shift Keying and of Analog Television Signals", IEEE Transactions on Communications, Dec. 1975.

[69] K. Feher, R. Goulet and S. Morissette, "Baseband Diversity for Hybrid Microwave Systems", IEEE Transactions on Communications, May 1984.

[70] T. A. Fitch, "The Effects of Rayleigh Distributed Multipath Fading on Carrier Recovery Performance", Proc. of IEEE Vehicular Technology Conference (VTC'86), pp. 252-255, May 1986.

[71] G. D. Forney Jr., "The Viterbi Algorithm", Proceeding of IEEE, Vol. 61, pp. 268-278, March 1973.

[72] G. D. Forney Jr., "Maximim-Likelihood Sequence Estimation of Digital Sequences in the Presence of Intersymbol Interference", IEEE Trans. on Information Theory, Vol. IT-18, pp. 363-378, May 1972.

[73] G. D. Forney Jr. et al., "Efficient Modulation for Band Limited Channels", IEEE Jour. on Selected Areas in Comm.,Vol. SAC-2, pp. 659-672, Sept. 1984.

[74] F. M. Gardner, "*Phaselock Techniques*", John Wiley & Sons Inc., New York, 1979.

[75] A. Gersho and V.B. Laurence, "Multidimensional Signal Constellations for Voiceband Data Transmission", IEEE Jour. on Selected Areas in Comm.,Vol. SAC-2, pp. 687-703, Sept. 1984.

[76] E. R. Gfeller et. al., "Infrared Communications for In-house application", Proc of IEEE CAMPCON'78, pp. 132-138, Sept. 1979.

[77] E. R. Gfeller et. al., "Wireless In-house Data Communication via Defuse Infrared Radiation", Proceedings of IEEE, Vol. 67, No. 11, pp. 1474-1486, Nov. 1979.

[78] E. R. Gfeller, "Infrared microbroadcasting network for In-house Data Communication", Proc. ECOC 81, pp. 27.1-4, Sept. 1981.

[79] K. S. Gilhousen et al., "On the Capacity of Cellular CDMA Systems", IEEE Trans. on Vehicular Tech., Vol. VT-40, No. 2, pp. 303-312, May 1991.

[80] F. Glave and L. B. Dunn, "Data route Transmission; System Growth and Extension", Proc. of International Conference on Communications (ICC'74), June 1974.

[81] D. J. Goodman, "Second generation Wireless Information Networks", IEEE Trans. on Vehicular Tech., Vol. VT-40, No. 2, pp. 366-374, May 1991.

[82] D. J. Goodman, "Trends in cellular and cordless communications", IEEE Communications Magazine, Vol. 29, pp. 31-40, June 1991.

[83] L. S. Golding et al., "VSATs: Expert Views On Future Trends", IEEE Communications Magazine, pp. 58-64, May 1989.

[84] S. Ginn, "Personal Communication Services: Expanding the freedom to communicate", IEEE Communications Magazine, Vol. 29, pp. 30-39, Feb. 1991.

[85] S. Goode, "A Comparison of Gaussian Minimum Shift Keying to Frequency Shift Keying for Land Mobile Radio", Proc. of IEEE Vehicular Technology Conference (VTC'84), pp. 136-141, May 1984.

[86] S. Goode et. al., "A comparison of limiter-discriminator, delay and coherent detection for $\pi/4$-QPSK", Proc. of IEEE Vehicular Technology Conference (VTC'90), pp. 687-694, May 1990.

[87] S. A. Gronemeyer and A.L. McBridge, "MSK and offset QPSK modulation", IEEE Trans. on Comm., Vol. COM-24, pp. 809-820, Aug. 1976.

[88] G.S.M., "Physical layer on the radio-path", GSM 05.04, ETSI, July 1988.

[89] W. C. Hagmann, "Carrier Synchronizer for Overlapped Raised Cosine Pulse Amplitude Modulation", Comsat Technical Review, Vol. 14, No. 1, pp. 25-52, Spring 1984.

[90] A. R. Hambley and O. Tanaka, "Generalized serial MSK modulation", IEEE Trans. on Comm., Vol. COM-32, pp. 305-308, March 1984.

[91] W. H. Harrold and N. Kingsbury, "A Partially Coherent Detector for Continuous Phase Modulation", IEEE Jour. on Selected Areas in Comm.,Vol. SAC-7, pp.1415-1426, Sept.1989.

[92] E.J. Hayes, "Beyond MSAT to Personal Communications Via Satellite", Proc. of WIRELESS 90, Calgary Alberta, July 1990.

[93] E.J. Hayes and P. I. Garland, "An Advanced Payload Concept for Personal, Mobile and Private Business Communications", 13^{th} Annual Pacific Telecommunications Conference, Honolulu, Hawai, Jan. 1991.

[94] K. Hirade, M. Ishizuka and F. Adachi, "Error-Rate Performance of Digital FM with Differential Detection in Land Mobile Radio Channels", IEEE Trans. on Vehicular Tech., Vol. VT-28, pp. 204-212, Aug. 1979.

[95] K. Hirade, M. Ishizuka and F. Adachi, "Error-Rate Performance of Digital FM with Discriminator Detection in the presence of co-channel interference under fast Rayleigh fading environment", Trans. of IECE Japan, Vol. E61, pp. 704-709, 1978.

[96] M. Hirono, T. Miki and K. Murota, "Multilevel decision method for band limited digital FM with limiter discriminator detection", IEEE Jour. on Selected Areas in Comm.,Vol. SAC-2, pp.498-506, July 1981.

[97] IEEE Communications Magazine, Issue on Personal Communications Regulations, Vol. 29, Feb. 1991.

[98] IEEE Communications Magazine, Issue on Satellite and Terrestrial Systems and Services for Travelers, Vol. 29, Nov. 1991.

[99] IEEE Journal on Selected Areas in Communications, Issue on Portable and Mobile Communications, Vol. 9, Jan. 1989.

[100] IEEE Transactions on Vehicular Technology, Special issue on Digital Cellular Technologies, May 1991.

[101] Y. Iwadate, "Analysis of distortion in a PAM-FM television transmission and application to MUSE signal", IEEE Trans. on Broadcasting, Vol.37, No. 3, pp. 89-96, Sept. 1991.

[102] W. C. Jakes (Editor), "*Microwave Mobile Communications*", Wiley and Sons, New York, 1974.

[103] F. deJager and C. Dekker, "Tamed Frequency Modulation: A novel approach to achieve spectral economy in digital transmission", IEEE Trans. on Comm., Vol. COM-26, pp. 534-542, May 1978.

[104] T. G. Jedrey, N.E Lay and W. Raferty, "An All Digital 8-DPSK TCM Modem for Land Mobile Satellite Communications", Proc. of IEEE International Conference on Acoustics Speech ans Signal Processing (ICASSP'88), pp. 1722-1725, May 1988.

[105] N. L. Johnson, "Satcom in the Soviet Union", Satellite Communications, June 1988, pp. 21-24.

[106] V. Joshi and D. D. Falconer, "Reduced State Sequence Estimation Techniques for Digital Subscriber Loop Application", Proc. of Global Communications Conference (GLOBECOM'88), pp. 799-803, Dec. 1988.

[107] V. Joshi and D. D. Falconer, "Sequence Estimation Techniques for digital subscriber loop transmission with crosstalk interference", IEEE Trans. on Comm., Vol. COM-38, No. 9, pp. 1367-1374, Sept. 1990.

[108] Y. Juo and K. Feher, "Performance Evaluation of differential $\pi/4$-shift QPSK systems in a Rayleigh fading /delay/spread/CCI/AWGN environment", Proc. of IEEE Vehicular Technology Conference (VTC'90), pp. 420-424, May 1990.

[109] I. P. Kaminov, "FSK with Direct Detection in Optical Multiple-Access FDM Networks", IEEE Jour. on Selected Areas in Comm.,Vol. SAC-8, No. 8, pp. 1005-1014, Aug. 1991.

[110] M. Kavehrad and P. J. McLane, "Performance of low-complexity Channel Coding and Diversity for Spread Spectrum in Indoor Wireless Communications", AT& T Technical Journal, Vol. 64, pp. 1927-1965, Oct. 1985.

[111] M. Kavehrad and B. Ramamurthi, "Direct Sequence Spread Spectrum with DPSK Modulation diversity for Indoor Wireless Communications", IEEE Trans. on Comm., Vol. COM-235, pp. 224-236, Feb. 1987.

[112] M. H. Khan, T. Le-Ngoc and V. K. Bargava, "Efficient Adaptive Error Control Schemes for Ka-Band Satellite Systems", IEEE Jour. on Selected Areas in Comm.,Vol. SAC-4, pp. 361-367, May 1986.

[113] M. H. Khan, T. Le-Ngoc and V. K. Bargava, "Efficient Adaptive Error Control Schemes for Ka-Band Satellite Systems", Proc. of International Conference on Digital Satellite Communications (ICDSC-6), pp. 369-376, May 1986.

[114] H. Kobayashi, "Correlative Level Coding and Maximum Likelihood Decoding", IEEE Trans. on Information Theory, Vol. IT-17, No. 5, pp. 586-594, Sept. 1971.

[115] Y. Konishi and Y. Fukuoka, "Satellite Receiver Technologies", IEEE Trans. on Broadcasting, Vol.34, No. 4, pp. 449-456, Dec. 1988.

[116] I. Korn, "Error probability of offset differential phase shift keying with intersymbol and adjacent channel interference", IEE Proc. Part F, Vol.135, pp. 155-182, April 1988.

[117] I. Korn, "Offset DPSK with Differential Phase Detector in Satellite mobile Channel with Narrow-Band Receiver Filter", IEEE Trans. on Vehicular Tech., Vol. VT-38, pp. 193-203, Nov. 1989.

[118] I. Korn, "M-ary Frequency Shift Keying with Limiter–Discriminator-Integrator Detector in Satellite Mobile Channel with Narrow-Band Receiver Filter", IEEE Trans. on Comm., Vol. COM-38, No. 10, pp. 1771-1778, Oct. 1990.

[119] I. Korn, "GMSK with Differential Phase Detection in Satellite Mobile Channel", IEEE Trans. on Comm., Vol. COM-38, pp. 1980-1986, Nov. 1990.

[120] I. Korn, "Error Probability of M-ary FSK with a Limiter-Discriminator Detector in Satellite Mobile Channels", International Journal of Satellite Communications, Vol. 9, pp. 227-238, Nov. 1991.

[121] A. D. Kucar, "Mobile radio: an overview", IEEE Communications Magazine, Vol. 29, pp. 72-85, Nov. 1991.

[122] H. P. Kuchenbecker and M. Aldinger, "Digital Speech Transmission on Mobile Radio Channels", *Signal Processing II: Theories and Applications*, Elsevier Science Publishers B.V. (North-Holland), pp. 535-538, EURASIP, 1983.

[123] D. L. Landis, "Subcarrier audio for wide-area data broadcast via satellite", IEEE Trans. on Broadcasting, Vol.34, No.2, pp. 50-57, March 1988.

[124] P. B. Lathy, "*Modern Digital and Analog Communications Systems*", Holt, Rinehart and Winston, The Dryden Press, New York, 1983.

[125] P. A. Laurrent, "Exact and Approximate Construction of Digital Phase Modulation by Superposition of Amplitude Modulated Pulses", IEEE Trans. on Comm., Vol. COM-34, pp. 150-160, Feb. 1986.

[126] W. C. Y. Lee, "*Mobile Communications Engineering*", McGraw-Hill, New York, 1982.

[127] W. C. Y. Lee, "Overview of Cellular CDMA", IEEE Trans. on Vehicular Tech., Vol. VT-40, No. 2, pp. 291-302, May 1991.

[128] W. C. Y. Lee, "*Mobile Cellular Telecommunication Systems*", New York: McGraw Hill Book Co., 1989.

[129] A. Lender, "Correlative level coding for binary-data transmission", IEEE Spectrum, Vol. 3, Feb. 1966, pp. 104-115.

[130] S. Lin and D. J. Costello, "*Error Control Coding: Fundamentals and Applications*", Prentice-Hall Inc., 1983.

[131] C-L. Liu and K. Feher, "Non-Coherent $\pi/4$-QPSK in an AWGN-CCI combined interference environment", Proc. of IEEE Vehicular Technology Conference (VTC'89), pp. 83-87, May 1989.

[132] C-L. Liu and K. Feher, "$\pi/4$-QPSK Modems for Satellite Sound/Data Broadcast Systems", IEEE Trans. on Broadcasting, Vol.37, No. 1, pp. 1-8, March 1991.

[133] C-L. Liu and K. Feher, "Bit Error Rate Performance of $\pi/4$-QPSK in a Frequency-Selective Fast Rayleigh Fading Channel", IEEE Trans. on Vehicular Tech., Vol. VT-40, No. 3, pp. 558-568, Aug. 1991.

[134] J. H. Lodge, "Mobile satellite communication systems – Towards global personal communications", IEEE Communications Magazine, Vol. 29, pp. 24-30, Nov. 1991.

[135] H. Lodge and M. L. Moher, "Time Diversity for Mobile-Satellite Channels Using Trellis Coding Modulations", Proc. of Global Communications Conference (GLOBECOM '87), Tokyo, Japan, pp. 303-307, Nov. 1987.

[136] C. Loo, "A Statistical Model for a Land Mobile Satellite Link", Proc. of International Conference on Communications (ICC '84).

[137] C. Loo, "Measurements and Models of a Mobile-Satellite Link with Applications", Proc. of Global Communications Conference (GLOBECOM '85), Dec. 1985.

[138] C. Loo, "A statistical model for a land mobile satellite link", IEEE Trans. on Vehicular Tech., Vol. VT-34, pp. 122-127, Aug. 1985.

[139] C. Loo, "Measurements and models of a land mobile satellite channel and their applications to MSK signals", IEEE Trans. on Vehicular Tech., Vol. VT-36, pp. 114-121, Aug. 1987.

[140] C. Loo, "Digital Transmission Through a Land Mobile Satellite Channel", IEEE Trans. on Comm., Vol. COM-38, No. 5, pp. 693-698, May 1990.

[141] C. Loo, E. E. Matt, J. S. Butterworth and M. Dufour, "Measurements and Modeling of Land Mobile Satellite Signal Statistics", Proc. of IEEE Vehicular Technology Conference (VTC '86), May 1986.

[142] G. Lourens, "On the Sibilance Problem of FM Sound Transmission", IEEE Trans. on Broadcasting, Vol.37, No. 3, pp. 115-120, Sept. 1991.

[143] R. W. Lucky, J. Salz and E. J. Weldon, "*Principles of Data Communications*", McGraw-Hill, New York, 1968.

[144] B. B. Lusignan, "Single-Sideband Transmissions for Land Mobile Radio", IEEE Spectrum, pp. 33-37, July 1978.

[145] D. Makrakis, A. Yongacoglu and K. Feher, "Novel Receiver Structures for Systems Using Differential Detection", IEEE Trans. on Vehicular Tech., Vol. VT-36, pp. 71-77, May 1987.

[146] D. Makrakis, A. Yongacoglu and K. Feher, "Novel Receiver Structures for Systems Using Differential Detection" Proc. of International Conference on Digital Satellite Communications (ICDSC-7), pp. 681-688, May 1986.

[147] D. Makrakis, A. Yongacoglu and K. Feher, "A sequential decoder for the Differential Detection of Trellis Coded PSK Signals", Proc. of International Conference on Communications (ICC'88), pp. 1433-1438, June 1988.

[148] D. Makrakis and K. Feher, "Optimal Non-Coherent Detection of PSK Signals", Electronics Letters, Vol. 26, pp. 398-401, March 15 1990.

[149] D. Makrakis and P. T. Mathiopoulos, "Trellis Coded Non-Coherent QAM: A New Bandwidth and Power Efficient Scheme", Proc. of IEEE Vehicular Technology Conference (VTC'89), pp. 95-100, April 1989.

[150] D. Makrakis and P. T. Mathiopoulos, "Non-Coherent Multilevel Trellis Coded Continuous Phase Modulation", Proc. of International Conference on Communications (ICC'89), pp. 275-280, June 1989.

[151] D. Makrakis, K. Sreenath and K. Feher, "Optimum and Near Optimum Non-Coherent Sequential Detection of Trellis Coded PSK Signals. Part I: Block Decoding Approach", Technical Report TR-COM-90-1, University of Ottawa, May 1990.

[152] D. Makrakis, K. Sreenath and K. Feher, "Optimum and Near Optimum Non-Coherent Sequential Detection of Trellis Coded PSK Signals. Part II: Squared Envelope and Multiple Differential Detection", Technical Report TR-COM-90-2, University of Ottawa, May 1990.

[153] D. Makrakis, K. Sreenath and K. Feher, "Optimal Non-Coherent Sequential Detection of Trellis Coded Signals in Non-Ideal Channels", Proc. of Global Communications Conference (GLOBECOM '90), Dec. 1990, pp. 371-375.

[154] D. Makrakis, "Improved Non-Coherent Receivers. Part I: Evaluation Under Non-Ideal Conditions", CRC/NSERC/Communications Final Report No.1, May 1991.

[155] D. Makrakis, "Improved Non-Coherent Receivers . Part II: Optimal and Asymptotically Optimal Decoders in a Time Dispersive Environment", CRC/NSERC/Communications Final Report No. 2, May 1991.

[156] D. Makrakis and K. Feher, "Multiple Sequential Detection of Continuous Phase Modulation Signals", to appear in the IEEE Transactions on Vehicular Technology.

[157] D. Makrakis and K. Feher, "An Improved Viterbi Decoder for the Differential Detection of Continuous Phase Modulation Schemes", IEEE WESCANEX'88, May 1988, Saskatoon Sask., pp. 78-87.

[158] D. Makrakis, A. Yongacoglu and K. Feher, "A new Soft Decision Sequential Decoder for the Differential detection of TFM", Proc. of Global Communications Conference (GLOBECOM '87), Nov. 1987, Tokyo Japan, pp. 8.8. 1-4.

[159] D. Makrakis, A. Yongacoglu and K. Feher, "Interleaving for Differential Detection using Multiple Detectors", Proc. of IEEE Vehicular Technology Conference (VTC'88), pp. 267-272, June 1988.

[160] D. Makrakis and P. T. Mathiopoulos, "Differential Detection of Correlative Encoded Continuous Phase Modulation Schemes using Decision Feedback", IEE Proc. Part I, Vol.198, Oct. 1991, pp. 473-480.

[161] D. Makrakis and P.T. Mathiopoulos, "Differential Detection of Correlative Encoded Continuous Phase Modulation Schemes using Decision Feedback", Proc. of International Conference on Communications (ICC'90), June 1990, Atlanta Georgia, pp. 619-625.

[162] A. Yongacoglu, D. Makrakis and K. Feher, "Differential Detection of GMSK Using Decision Feedback", IEEE Trans. on Comm., Vol. COM-36, June 1988, pp. 637-649.

[163] D. Makrakis, A. Yongacoglu and K. Feher, "Two-Bit Differential Detection of GMSK with and without Precoding and Using Decision Feedback", Proc. of International Conference on Communications (ICC '87), June 1987, Seattle Washington., pp. 25.4.1-25.4.6.

[164] A. Yongacoglu, D. Makrakis, H.Ohnishi and K. Feher, "A New Receiver for the Differential Detection of GMSK", Proc. of Global Communications Conference (GLOBECOM '86), Dec. 1986, Houston Texas, pp. 29.5.1-6.

[165] A. Yongacoglu D. Makrakis and K. Feher, "One-bit Differential Detection of GMSK with Data-Aided Phase Control", Proc. of International Conference on Communications (ICC '86), June 1986, Toronto, Ont., pp. 57.8.1-5.

[166] D. Makrakis, P. T. Mathiopoulos and D. Bouras, "Optimal Decoding in Fading Channels: A Combined Envelope, Multiple Differential and Coherent Detection Approach'", to appear in the IEEE Transactions on Communications.

[167] D. Makrakis and P. T. Mathiopoulos, "Optimal Decoding in Fading Channels: A Combined Envelope, Multiple Differential and Coherent Detection Approach", Proc. of Global Communications Conference (GLOBECOM '89), Nov. 1989, Dallas Texas, pp. 1551-1557.

[168] D. Makrakis, "Double Symbol Error Rates of Differential Receivers operating in Faded and Interference Controlled Environments", under preparation.

[169] D. Makrakis, A. Yongacoglu and K. Feher, "A New Receiver for the Differential Detection of Duobinary MSK", IEEE TECHNICOM'87, Oct. 1987, Miami, Fla., pp. 87-89.

[170] A. Maloberti, "Radio transmission interface of the digital pan-European mobile system", Proc. of IEEE Vehicular Technology Conference (VTC '89), May 1989, San Francisco, CA, pp. 712-717.

[171] G. Maral, J-J. de Ridder, B.G. Evans and M. Richharia, "Low Earth Orbit Satellite Systems for Communications", International Journal of Satellite Communications, Vol. 9, No. 4, July-Aug. 1991, pp. 209-221.

[172] T. Masamura, S. Samejima, Y. Morihiro and H. Fuketa, "Differential Detection of MSK with Non-redundant Error Correction", IEEE Trans. on Comm., Vol. COM-27, June 1979, pp. 912-919.

[173] T. Masamura, "Intersymbol Interference reduction for DMSK with non-redundant error correction", IEE Proc. Part I, Vol.137, Dec. 1990.

[174] L. J. Mason, "Error Probability Evaluation for systems employing differential detection in a Rician fast fading environment and Gaussian noise", IEEE Trans. on Comm., Vol. COM-35, pp. 39-46, Jan. 1987.

[175] L. J. Mason, "An Error Probability formula for M-ary DPSK in fast Rician fading and Gaussian noise", IEEE Trans. on Comm., Vol. COM-35, pp. 976-978, Sept. 1987.

[176] M. Masonson, "UNICOM Progress Report for 7^{th} and 8^{th} Quarters", Vol. II, App. 58, Jan. 1991.

[177] M. Matsushita and S. Yokoyama, "Experience of Operating a DBS system (BS–2) In Japan", IEEE Trans. on Broadcasting, Vol.34, No. 4, pp. 430-434, Dec. 1988.

[178] J. P. McGeehan and A. J. Bateman, "Phaselocked Transparent Tone in Band (TTIB): A New Spectrum Configuration Particularly Suited to the Transmission of Data Over SSB Mobile Radio Networks", IEEE Trans. on Comm., Vol. COM-32, pp. 81-87, Jan. 1984.

[179] P. J. McLane, P. H. Wittke, P.K.M. Ho and C. Loo, "Performance of binary multi-h modulation for fast fading shadowed mobile satellite communication channels", Proc. of IEEE Vehicular Technology Conference (VTC'87), pp. 194-199, June 1987.

[180] P. J. McLane, P. H. Wittke, P. K-M. Ho and C. Loo, "PSK and DPSK Trellis Codes for Fast Fading, Shadowed Mobile Satellite Communication Channels", IEEE Trans. on Comm., Vol. COM-36, pp. 1242-1245, Nov. 1988.

[181] P. J. McLane, P. H. Wittke, P. K-M. Ho and C. Loo, "PSK and DPSK Trellis Codes for Fast Fading, Shadowed Mobile Satellite Communication Channels", Proc. of International Conference on Communications (ICC'87), pp. 726-731, June 1987.

[182] D. Middleton, "*An Introduction to Statistical Communication Theory*", McGraw -Hill, New York, 1960.

[183] B. Miric, "Simulation Methods for ARI/RDS secondary services with VHF-FM transmission system", IEEE Trans. on Broadcasting, Vol.35, No. 4, pp. 277-387, Dec. 1989.

[184] T. Miyagaki, N. Morinara and T. Namekawa, "Error rate performance of M-ary DPSK systems in satellite/aircraft communications", Proc. of International Conference on Communications (ICC'79), pp.34.6.1-6, May 1979.

[185] J. W. Modestino and S. Y. Wui, "Convolutional code performance in the Rician fading channel", IEEE Trans. on Comm., Vol. COM-24, pp. 592-606, June 1976.

[186] P. Monharaj et. al., "Reduced complexity trellis coding/decoding for high bit rate digital subscriber loop transmission", Proc. of International Conference on Communications (ICC'89), June 1989.

[187] P. Monharaj et. al., "Baseband Trellis–Coded Modulation with Combined Equalization/Decoding for High Bit Rate Digital Subscriber Loops", IEEE Jour. on Selected Areas in Comm.,Vol. SAC-9, No. 6, pp. 871-875, Aug. 1991.

[188] "*MSAT System Concept Document*", Communications Research Centre, Canada, March 22, 1983.

[189] "*Definition Study to Determine the Technical Requirements and Develop Cost Estimates for MSAT Data Services*", for the Department of Communications, by Miller Communications Systems, July 1984.

[190] D. Muilwijk, "Correlative phase shift keying-A class of constant envelope modulation techniques", IEEE Trans. on Comm., Vol. COM-29, pp. 226-236, March 1981.

[191] K. Murota and K. Hirade,"GMSK Modulation for Digital Mobile Radio Telephony", IEEE Trans. on Comm., Vol. COM-29, pp. 1044-1050, July 1981.

[192] K. M. S. Murthy and K.G. Gordon, "VSAT Networking Concepts and New Applications Development", IEEE Communications Magazine, pp. 43-49, May 1989.

[193] K. M. S. Murthy et. al., "VSAT User Network Example", IEEE Communications Magazine, pp. 50-57, May 1989.

[194] K .M. S. Murthy, "Hybrid Networks for Personal Communications: Proposed Architectures and Planned Experiments", Workshop on Advanced Network and Technology Concepts for Mobile, Micro and Personal Communications, May 1991, Pasadena, CA.

[195] K. M. S. Murthy, "Internetworking ISDN & PCN in a Satellite Environment: Alternative Rate Structures", AIAA Conference, March 1992.

[196] K. M. S. Murthy, F. H. Smart, N. Salem and D. Makrakis, "Personal Communication Trials Using Ku & Ka-band Satellite Systems", Proceedings of the International Conference on Selected Topics in Wireless Communications, Vancouver B.C., pp. 250-253, June 1992.

[197] N. Nakajima and K. Kinoshita, "A system design for TDMA mobile radios", Proc. of IEEE Vehicular Technology Conference (VTC '90), May 1990.

[198] Y. Ninomiya et. al., "An HDTV Broadcasting System Utilizing a Bandwidth Compression Technique–MUSE", IEEE Trans. on Broadcasting, Vol.33, No. 4, pp. 130-140, Dec. 1987.

[199] J. F. Oberst and D. L. Scilling, "Double Error Probability in Differential PSK", Proceedings of IEEE, pp. 1099-1100, June 1968.

[200] J. Obuchowski, "Wireless communications and Spectrum Conservation: Sending a signal to Conserve", IEEE Communications Magazine, Vol. 29, pp. 26-29, Feb. 1991.

[201] H. Ochner, " DECT-Digital European cordless telecommunications", Proc. of IEEE Vehicular Technology Conference (VTC'89), San Francisco, CA, pp. 718-721, May 1989.

[202] W. P. Osborne and M. B. Lunz, "Coherent and Noncoherent Detection of CPFSK", IEEE Trans. on Comm., Vol. COM-22, pp. 1023-1036, Aug. 1974.

[203] A. Papoulis, "*Probability, Random Variables and Stochastic Processes*", McGraw-Hill Book Inc., 1965.

[204] A. Papoulis, "*Probability, Random Variables and Stochastic Processes*", McGraw-Hill Book Inc., second edition, 1984.

[205] S. Pasupathy, "Minimum Shift Keying: A spectrally efficient modulation", IEEE Communications Magazine., Vol. 17, pp. 14-22, July 1979.

[206] S. Pasupathy, "Nyquist's third criterion", Proceedings of IEEE, Vol. 62, pp. 860-861, June 1974.

[207] C. K. Pauw and D. L. Schilling, "Probability of error for M-ary PSK and DPSK on Rayleigh fading channel", IEEE Trans. on Comm., Vol. COM-36, pp. 755-756, June 1988.

[208] R. F. Pawula, "On the theory of error rates for narrow band digital FM", IEEE Trans. on Comm., Vol. COM-30, pp. 1228-1241, Aug. 1982.

[209] R.F. Pawula, S.O. Rice and J.H. Roberts, "Distribution of the Phase Angle Between Two Vectors Perturbed by Gaussian Noise", IEEE Trans. on Comm., Vol. COM-29, pp. 1634-1643, Nov. 1981.

[210] R. F. Pawula, "Offset DPSK and a comparison of conventional and symmetric DPSK with noise correlation and power imbalance", IEEE Trans. on Comm., Vol. COM-32, pp. 233-240, March 1984.

[211] R. F. Pawula, "On M-ary DPSK transmission over terrestrial and satellite channels", IEEE Trans. on Comm., Vol. COM-32, pp. 752-761, July 1984.

[212] R. L. Picholtz et al., "Spread Spectrum for Mobile Communications", IEEE Trans. on Vehicular Tech., Vol. VT-40, No. 2, pp. 313-322, May 1991.

[213] T. Pratt and C. W. Bostian, "*Satellite Communications*", J. Wiley and Sons, 1986.

[214] J. G. Proakis, "*Digital Communications*", McGraw-Hill Book Inc., 1983.

[215] T. S. Rappaport, "The wireless revolution", IEEE Communications Magazine, Vol. 29, pp. 52-71, Nov. 1991.

[216] T. S. Rappaport, S.Y. Seidel and R. Singh, "900-MHz multipath propagation measurements for U.S. digital cellular radio telephone", IEEE Trans. on Vehicular Tech., Vol. VT-39, pp. 132-139, May 1990.

[217] S. A. Rhodes et. al., "Signal Design for Inmarsat Standard C Ship Earth Station", Proc. of Global Communications Conference (GLOBECOM'82), pp. E5.5.1-10, 1982.

[218] S. A. Rhodes, "FSOQ, a new modulation method that yields a constant envelope", Proceedings of IEEE National Telecommunications Conference, pp. 51.1.1-7, June 1980.

[219] M. Richaria, P. Hansel, P. W. Bousquet and M. O'Donnel, "A feasibility study of a mobile communications network using a constellation of low earth orbit satellites, Proc. of Global Communications Conference (GLOBECOM'89), Nov. 1989, Dallas, Texas.

[220] I. M. Ross, "Wireless Network Directions", IEEE Communications Magazine, Vol. 29, pp. 40-42, Feb. 1991.

[221] D. Rouffet, J. F. Dulck, R. Larregola and G. Mariet, "Sycomores: a new concept for land mobile satellite communications", IEE 4^{th} International Conference on Satellite Systems for Mobile Communications and Navigation, Oct. 1988.

[222] H. Salwen, "DPSK Performance under time dispersive Multipath Fading", IEEE Trans. on Comm., Vol. COM-23, pp. 383-385, March 1985.

[223] J. Salz, "Coherent Lightwave Communications", AT& T Techical Journal, Vol. 64, pp. 2153-2209, Dec. 1985.

[224] J. Salz and B. R. Sattzberg, "Double Error Rate in Differentially Coherent Phase Systems", IEEE Trans. on Comm., Vol. COM-12, pp. 202-205, June 1964.

[225] S. Samejima et.al., "Differential PSK System with Non-redundant Error Correction", IEEE Jour. on Selected Areas in Comm.,Vol. SAC-1, No. 1, Jan. 1983, pp. 74-81.

[226] G. J. Sauliner and W. Raferty, "DSP-Based Noncoherent Dual Detector Demodulator for Land Mobile Radio Channels", Proc. of International Conference on Communications (ICC'86), pp. 32.2.1-5, June 1986.

[227] Shu Lin and D. J. Costello Jr., "*Error Control Coding: Fundamentals and Applications*", Prentice-Hall, Inc.

[228] M. K. Simon, J. M. Omura, R. A. Scholtz and B. A. Levitt, *Spread Spectrum Communications, Vols. I, II & III*, Computer Science Press, Maryland, 1985.

[229] M. K. Simon, "Dual-Pilot Tone Calibration Technique", IEEE Trans. on Vehicular Tech., Vol. VT-35, pp. 63-70, May 1986.

[230] M. K. Simon and C. C. Wang, "Differential Detection of Gaussian MSK in a Mobile Radio Environment", IEEE Trans. on Vehicular Tech., Vol. VT-32, pp. 307-320, Nov. 1984.

[231] M. K. Simon and D. Divsalar, "Open loop frequency synchronization of MDPSK with Doppler", Proc. of International Conference on Communications (ICC'87), pp. 7.7.1 – 6, June 1987.

[232] M. K. Simon and D. Divsalar, "Doppler-corrected differential detection of MPSK", IEEE Trans. on Comm., Vol. COM-37, pp. 99-109, Feb. 1989.

[233] M. K. Simon and D. Divsalar, "The Performance of Trellis Coded Multilevel DPSK on a Fading Mobile Satellite Channel", IEEE Trans. on Vehicular Tech., Vol. VT-37, pp. 78-91, May 1988.

[234] M. K. Simon and D. Divsalar, "The Performance of Trellis Coded Multilevel DPSK on a Fading Mobile Satellite Channel", Proc. of International Conference on Communications (ICC'87), pp. 732-738, June 1987.

[235] M. K. Simon, "Double Symbol Error Rates for Differential Detection of Narrow-Band FM", IEEE Trans. on Comm., Vol. COM-33, No. 5, pp. 394-398, May 1985.

[236] M. R. Spiegel, "*MATHEMATICAL HANDBOOK of Formulas and Tables*", Information Theory Series, Prentice-Hall Inc, Enclewood Cliffs, NJ, 1977.

[237] J. J. Spilker, "*Digital Communications by Satellite*", McGraw-Hill Book Inc., 1983.

[238] J. E. Stjernvall and J. Uddenfent, "Gaussian MSK with Differential Demodulation and Channel Coding for Mobile Telephony", IEEE Trans. on Comm., Vol. COM-30, pp. 196-1116, May 1982.

[239] E. Sousa and S. Pasupathy, "Enhanced Receivers for Nonoptimally Allocated Filtering", IEEE Trans. on Comm., Vol. COM-31, No. 7, pp. 879-885, July 1983.

[240] C.-E. Sundberg, "Continuous Phase Modulation", IEEE Communications Magazine, Vol. 24, pp. 210-225, March 1981.

[241] R. Steele, "Deploying Personal Communication Networks", IEEE Communications Magazine, Vol. 28, pp. 12-15, Sept. 1990.

[242] M. Schwartz, W. R. Bennett and S. Stein, "*Communication Systems and Techniques*", McGraw-Hill, 1966.

[243] R. S. Swain and D. W. Holmes, "The Digital cordless telecommunications common air interface", British Telecom Technical Journal, Vol. 8, No. 1, 99. 12-18, Jan. 1990.

[244] D. P. Taylor and P. R. Hardmann, "Telecommunications by microwave digital radio", IEEE Communications Magazine, Vol. 24, pp. 11-16, Aug. 1986.

[245] E. L. Toric, "FMX stereo broadcasting ; FMX system implementation at station", IEEE Trans. on Broadcasting, Vol.35, No. 2, pp. 70-73, March 1989.

[246] E.K. Tsang and R. Douvile, "A Potential 21st century satellite communications application: Personal Communications", Space Communications, Vol. 7, pp.133-138, July 1990.

[247] T. T. Tjhung et al., "Error Performance of Binary FSK with Discriminator detection in Land Mobile radio channels", Proc. of Telecommunications Conference (TENCON'81), Aug. 1981.

[248] Technical Staff, American Telephone and Telegraph Company, Bell Telephone Companies and Bell Telephone Laboratories, "*Telecommunications Transmission Engineering*", Bell System for Technical Education, Winston-Salem, N.C., 1977.

[249] Y. Tunca, D. Makrakis and A. Yongacoglu, "Improved Block-Coded Non-Coherent Schemes", Canadian Conference on Elect. & Comp. Eng., Sept. 1990, Ottawa Ont., pp. 12.3.1-4.

[250] Y. Tunca, "*Partially Coherent Detection of PSK Signals in Rician Channels* ", M.A.Sc Thesis Dissertation, Department of Electrical Engineering, University of Ottawa, Oct. 1991.

[251] G. Ungerboeck, "Channel Coding with Multilevel/Phase Signals", IEEE Trans. on Information Theory, Vol. IT-28, pp. 55-67, Jan. 1982.

[252] G. Ungerboeck, "Trellis Coded Modulation with Redundant Signal Sets Part I: Introduction", IEEE Communications Magazine, Vol. 25, pp. 5-11, Feb. 1987.

[253] G. Ungerboeck, "Trellis Coded modulation with Redundant Signal Sets Part II: State of the Art", IEEE Communications Magazine, Vol. 25, pp. 12-21, Feb. 1987.

[254] H. L. van Trees, "*Detection, Estimation and Modulation Theory*", Wiley and Sons, New York, U.S.A., 1968.

[255] V. K. Varma and S . C. Gupta, "Partial response continuous phase modulation and DPCM coding for speech transmission in cellular mobile radio systems", IEEE Trans. on Vehicular Tech., Vol. VT-35, pp. 100-105, Aug. 1986.

[256] A. J. Viterbi and J. K. Omura, "*Principles of Digital Communication and Coding*", McGraw-Hill Book Inc., 1979.

[257] A. J. Viterbi, "Very Low Rate Convolutional Codes for Maximum Theoretical Performance of Spread Spectrum Multiple-Access Channels", IEEE Jour. on Selected Areas in Comm.,Vol. SAC-8, pp. 641-649, May 1989.

[258] A. J. Viterbi, "Wireless digital communications: A view based on three lessons learned", IEEE Communications Magazine, Vol. 29, pp. 33-36, Sept. 1991.

[259] W. J. Weber et al., "A Bandwidth Compressive Modulation System using Multi-Amplitude Minimum Shift Keying (MAMSK)", IEEE Trans. on Comm., Vol. COM-26, No. 5, May 1978.

[260] R. Wells, "SSB for VHF Mobile Radio at 5 KHz Channel Spacing", IERE Conference Proceedings Radio Receivers and Associated Systems, Southampton, pp. 29-36, July 1978.

[261] L. H. Will, "New Jersey Public Television System Conversion to MTS stereo generation", IEEE Trans. on Broadcasting, Vol.34, No. 2, pp. 58-62, March 1988.

[262] J.H. Winters, "Differential Detection with intersymbol interference and frequency uncertainty", IEEE Trans. on Comm., Vol. COM-32, No. 1, pp. 25-33, Jan. 1984.

[263] J.H. Winters, " Differential Detection of M-ary DPSK with Intersymbol Interference and Noise Correlation", Proc. of International Conference on Communications (ICC'84), pp. 1151-1555, May 1984.

[264] J.H. Winters, "Differential Detection of M-ary DPSK with Intersymbol Interference and Noise Correlation", IEEE Trans. on Comm., Vol. COM-35, No. 1, pp. 117-119, Jan. 1987.

[265] W. C. Wong and T. T. Tjhung, "Error Performance of Discriminator Detection in Fast Fading Channels", Proc. of IEEE International Conference on Communication Systems (ICCCS'88), pp. 714-718, Oct.1988.

[266] D. P. C. Wong and P. T. Mathiopoulos, "Nonredundant error correction analysis and evaluation of differentially detected $\pi/4$-shift DQPSK systems in a combined CCI and AWGN environment", IEEE Trans. on Vehicular Tech., Vol. VT-41, pp. 35-48, Feb. 1992.

[267] J. M. Wozencraft and I.M. Jacobs, "*Principles of Communication Engineering*", Wiley and Sons, New York, 1965.

[268] K. R. Wu, N. Morinaga and T. Namekawa, "Error rate performance of binary DPSK systems with multiple co-channel interference in land mobile radio channels", IEEE Trans. on Vehicular Tech., Vol. VT-33, pp. 23-31, Feb. 1984.

[269] L. F. Wui, "Rotationally Invariant Convolutional Channel Coding with Expanded Signal Space–Part I:180°", IEEE Jour. on Selected Areas in Comm.,Vol. SAC-2, pp. 959-671, Sept. 1984.

[270] L. F. Wui, "Rotationally Invariant Convolutional Channel Coding with Expanded Signal Space–Part II : Nonlinear Codes", IEEE Jour. on Selected Areas in Comm.,Vol. SAC-2, pp. 672-683, Sept. 1984.

[271] L. F. Wui, "Rotationally Invariant Trellis Coded Modulations with Mutidimensional M-PSK", IEEE Jour. on Selected Areas in Comm.,Vol. SAC-7, pp. 1281-1295, Dec. 1989.

[272] M. Yokoyama, "Single-Sideband Transmissions for Land Mobile Radio", IEEE Trans. on Vehicular Tech., Vol. VT-34, pp. 35-40, Feb. 1985.

[273] R. E. Ziemer and W. H. Trander, "*Principles of Communications*", Houghton-Mifflin Inc., Boston, 1976.

[274] A. Lender, "Correlative level coding for binary-data transmission", *IEEE Spectrum*, Vol. 3, Feb. 1966, pp. 104-115.